https://ntrs.nasa.gov/search.jsp?R=19790003913 2020-03-22T00:50:08+00:00Z

NASA CR-135396
PWA-5500-18

NASA

ENERGY EFFICIENT ENGINE
PRELIMINARY DESIGN AND INTEGRATION STUDIES

by

D. E. Gray, et al

UNITED TECHNOLOGIES CORPORATION
Pratt & Whitney Aircraft Group
Commercial Products Division

Prepared for
NATIONAL AERONAUTICS AND SPACE ADMINISTRATION
NASA-Lewis Research Center
Contract NAS3-20628

LIBRARY COPY
RETURN TO
GLENN LIBRARY
CLEVELAND, OHIO

1. Report No.	2. Government Accession No.	3. Recipient's Catalog No.
NASA CR-135396		

4. Title and Subtitle	5. Report Date
ENERGY EFFICIENT ENGINE PRELIMINARY DESIGN AND INTEGRATION STUDIES	November 1978
	6. Performing Organization Code

7. Author(s)	8. Performing Organization Report No.
D. E. Gray etal	PWA-5500-18
	10. Work Unit No.

9. Performing Organization Name and Address	11. Contract or Grant No.
UNITED TECHNOLOGIES CORPORATION Pratt & Whitney Aircraft Group Commercial Products Division - East Hartford, CT 06108	NAS3-20628
	13. Type of Report and Period Covered

12. Sponsoring Agency Name and Address	13. Type of Report and Period Covered
NATIONAL AERONAUTICS AND SPACE ADMINISTRATION Lewis Research Center 21000 Brookpark Road, Cleveland, OH 44135	Contractors Report
	14. Sponsoring Agency Code

15. Supplementary Notes

Project Manager, Mr. N. T. Saunders, NASA-Lewis Research Center
Cleveland, Ohio

16. Abstract

The objective of this study was to obtain in-depth understanding of the technology and configurational requirements of an all new 1990's energy efficient turbofan engine in order to initiate component technology development. Specific design goals for thrust specific fuel consumption, direct-operating cost, exhaust emissions, noise, thrust growth, and performance retention were established by NASA to assure attractive economics and improved environmental quality in addition to performance improvement.

The configuration selected from this study was a twin spool arrangement with a directly coupled fan and low-pressure turbine, a mixed exhaust nacelle, and a high 38.6:1 overall pressure ratio. Major advanced technology design features required to provide the overall benefits were a high pressure ratio compression system, a thermally actuated advanced clearance control system, lightweight shroudless fan blades, a low maintenance cost one-stage high pressure turbine, a short efficient mixer, and structurally integrated engine and nacelle.

The study consisted of a conceptual design analysis followed by integration and performance analyses of geared and direct-drive fan engines with separate or mixed exhaust nacelles to refine the engine cycles defined in previous studies. Preliminary design and more detailed engine-aircraft integration analysis were then conducted on the more promising configurations. Boeing, Douglas, and Lockheed conducted engine and aircraft sizing, fuel burned, and airframe noise studies on projected 1990's domestic and international aircraft. These studies produced sufficient definition of configurational and advanced technology requirements to allow immediate initiation of component technology development.

17. Key Words (Suggested by Author(s))	18. Distribution Statement
Aircraft Turbine Engines Energy Conservation Design Studies	Unclassified - Unlimited

19. Security Classif. (of this report)	20. Security Classif. (of this page)	21. No. of Pages	22. Price*
Unclassified	Unclassified	355	

* For sale by the National Technical Information Service, Springfield, Virginia 22151

FOREWORD

This report describes the work performed by the Pratt & Whitney Aircraft Group, Commercial Products Division of United Technologies Corporation, for the National Aeronautics and Space Administration, Lewis Research Center, under Contract NAS3-20628. Dr. David J. Poferl, the initial NASA Program Manager, was succeeded by Mr. Neal T. Saunders. Mr. Gerald Kraft served as the NASA Project Engineer responsible for monitoring the detailed progress for these studies. This report was prepared by Mr. David E. Gray, Pratt & Whitney Aircraft Program Manager, with the assistance of Messrs. Charles D. Dunn, John W. Bisset, and Robert E. Owens. The technical data presented herein were compiled with the cooperation of a wide segment of Engineering personnel. This report has been assigned Commercial Products Division, Pratt & Whitney Aircraft Group internal Report Number PWA-5500-18.

TABLE OF CONTENTS

TABLE OF CONTENTS (Cont'd)

LIST OF ILLUSTRATIONS

LIST OF ILLUSTRATIONS

LIST OF TABLES

LIST OF TABLES (Cont'd)

1.0 SUMMARY

The objective of this study was to obtain an in-depth understanding of the technology and configurational requirements for an all new 1990's energy efficient turbofan engine in order to permit initiation of advanced component technology development. Specific design goals for thrust specific fuel consumption, direct-operating cost, exhaust emissions, noise, thrust growth, and performance retention were established by NASA to assure attractive economics and improved environmental quality in addition to performance improvement.

The configuration selected from this study was a twin spool arrangement with a directly coupled fan and low-pressure turbine, a mixed exhaust nacelle, and a high (38.6:1) overall pressure ratio. Cruise thrust specific fuel consumption (10,700 m, M 0.8) was estimated to be 15.3 percent lower than the JT9D-7A reference engine, which surpassed NASA's design goal of a minimum of 12 percent. Direct operating cost reductions of 6 percent for domestic aircraft and 10 percent for more fuel sensitive international aircraft were estimated which fully met NASA's design goal of a minimum of 5 percent reduction relative to the JT9D-7A. A two-stage, vortex burning and mixing (Vorbix) combustor was included in the preliminary design to reduce exhaust emissions by 43 to 96 percent from current production levels. An integrated, composite nacelle, fully lined with acoustic treatment, was used to minimize noise and enhance performance retention over the engine operating life.

Major advanced technology design features required to provide the overall benefits were a high pressure ratio compression system, a thermally actuated advanced clearance control system, lightweight shroudless fan blades, a low maintenance cost one-stage high-pressure turbine, a short efficient mixer, and structurally intergrated engine and nacelle.

The study consisted of a conceptual design analysis, followed by integration and performance analyses of geared and direct-drive fan engines with separate or mixed exhaust nacelles, to refine the engine cycles defined in previous studies. Preliminary design and more detailed engine-aircraft integration analysis were then conducted on the more promising configurations. Boeing, Douglas, and Lockheed conducted engine and aircraft sizing, fuel burned, and airframe noise studies on projected 1990's domestic and international aircraft with nine of the study engines. The study results with four of these engines were involved directly in the selection of the final engine configuration.

Two airlines, Eastern Airlines and Pan American World Airways, were contracted by NASA to monitor and critique these studies.

These studies produced sufficient definition of configurational and advanced technology requirements to allow immediate initiation of component technology development. The realization of the Energy Efficient Engine potential is keyed to the successful development of many advancements in the state-of-the-art in fuel savings concepts included in the preliminary design. Critical areas include advanced structural concepts for tighter running clearances, advanced internal aerodynamics, a forced exhaust mixer, higher pressure ratio, advanced materials, an electronic fuel control, acoustically lined lightweight nacelle, and a low emissions combustor. Intensive technology development efforts in these areas can provide needed technology by the mid 1980's to produce significant fuel savings in future commercial turbofan engines of the 1990's.

2.0 INTRODUCTION

The National Aeronautics and Space Administration's Aircraft Energy Efficiency (ACEE) Program has the objective of improving the energy efficiency of future United States aircraft so that substantial savings in domestic fuel use can be realized. One of the elements of the technology plan for implementing this program is the Energy Efficient Engine. Through evolutionary extension of the current technology base the Energy Efficient Engine Program is to develop and demonstrate the technology for achieving higher thermodynamic and propulsion efficiencies in future turbofan engines. It is estimated that these improvements in turbofan engines will result in ten to fifteen percent lower specific fuel consumption as compared to the most efficient current engines.

The Energy Efficiency Preliminary Design and Integration Study was the initial effort in this Energy Efficiency Engine Program and consisted of five technical tasks:

- Task I - Determined the most promising turbofan engine types for further study.
- Task II - Refined the engine cycle(s) based upon engine/airframe integration.
- Task III - Conducted a preliminary engine design analysis to verify feasibility and to provide a base for hardware and technology development programs.

  Established ultimate benefits for the engine/airframe system.
- Task IV - Assessed sensitivity of program goals with respect to the probability of achieving individual technology goals to enable more efficient structuring of the follow-on technology programs.
- Task V - Aerodynamically designed resulting high-pressure compressor to enable an early go-ahead for a compressor test program.

Tasks II and III involved support from three airframe subcontractors, (Boeing, Douglas, and Lockheed).

An earlier NASA sponsored exploratory analytical effort conducted in 1974 and 1975 – The Study of Turbofan Engines Designed for Low Energy Consumption (NASA CR-135002) – indicated that over a 15 percent fuel savings was possible through using projected 1985 technology. The estimation of this potential assumed major improvements in component efficiencies, availability of advanced materials, and structural innovation. Four turbofan design configurations – direct drive and geared fan engines with separate and mixed exhausts – were estimated to provide, within 2 percent, the same fuel savings potential. This closeness made it impossible to clearly segregate a preferred configuration and to ascertain the necessary unique technology advancements. More detailed study of the four candidate configurations, including detailed airframe-engine system evaluation, was needed before a choice could be made.

The Energy Efficient Engine Preliminary Design and Integration Studies provided the additional information necessary for engine configuration selection and established vital technology development requirements prior to starting subsequent technology demonstration and proof testing.

Section 3.0 outlines the general procedures followed in conducting this study. Section 4.0 describes the major program results including the engine configuration selected for continued analysis and the technology advances required to develop this engine configuration. Section 5.0 contains the concluding remarks. Appendices A through E discuss the various aspects of the program in detail.

3.0 STUDY PROCEDURES

3.1 GENERAL APPROACH

This study focused on two major efforts – Energy Efficient Engine configuration/cycle definition and propulsion system preliminary design. The intent was to provide additional substantiation of the fuel savings potential of candidate engine configurations, more detailed component and engine preliminary design analysis, and more in-depth study of engine-aircraft integration than previous NASA sponsored exploratory studies. With this approach, the selection of a preferred engine configuration and cycle from among advanced mixed exhaust and separate exhaust, direct-drive and geared fan turbofans became possible.

The program consisted of the five technical tasks shown in Figure 1. The candidate engine configurations were initially screened by Pratt & Whitney Aircraft (Task I) in an attempt to identify a clearly superior engine configuration at an early stage. Because of the closeness of capabilities of all four configurations screened, engine-aircraft integration and performance evaluations by Pratt & Whitney Aircraft, Boeing Commercial Airplane Company (BCAC), Douglas Aircraft Company (DAC), and Lockheed - California Company (LCC) in Task II were necessary. These evaluations provided sufficient data to select the mixed exhaust installation. In Task III, preliminary design analyses were directed toward key areas of technical concern for direct-drive and geared fan, mixed-exhaust engine configurations with one- and two-stage high pressure turbines (HPT). By emphasizing analysis on the critical engine areas, initial feasibility and more accurate comparisons of the engines could be made. Task IV risk assessments were also conducted on the advanced technology features in order to permit thrust specific fuel consumption (TSFC) and direct operating cost (DOC) comparisons at the manufacturers also conducted more detailed investigations with direct-drive and geared fan, one-stage HPT engines. The Task III/IV evaluations resulted in the selection of the direct-drive fan, one-stage HPT engine configuration as the proposed energy efficient engine. An initial aerodynamic design of the selected engine high pressure-compressor (HPC) configuration (Task V) was included in the study program to expedite the initiation of a follow-on technology development program.

Throughout the program, seven main technical figures-of-merit were considered in selecting engine thermodynamic cycles and in comparing the configurational capabilities: cruise TSFC, fuel burned, DOC, noise, exhaust emissions, thrust growth potential and performance deterioration.

Achievement goals, listed in Table I, were established by NASA for six of the figures-of-merit. The JT9D-7A, the most widely used operational high bypass ratio engine, was used as the reference point. The TSFC goal includes the effects of isolated nacelle drag at a 10,700 m (35,000 ft.), Mach 0.8 cruise condition. The DOC reduction goal encompasses, in addition to fuel costs, the effects of propulsion system weight, price, and maintenance costs. As such, it penalizes weight and cost increases that could otherwise negate the operating economy attendant with TSFC reduction. Stringent environmental goals required incorporation of technological concepts and design features aimed at substantial reductions in exhaust emissions and noise. Goals for performance deterioration with operating time and for thrust growth allowance assured that the design provided for fuel savings over the lifetime of the engine family. In combination, the study goals directed attention to expected requirements of future commercial transport engines of the 1990's.

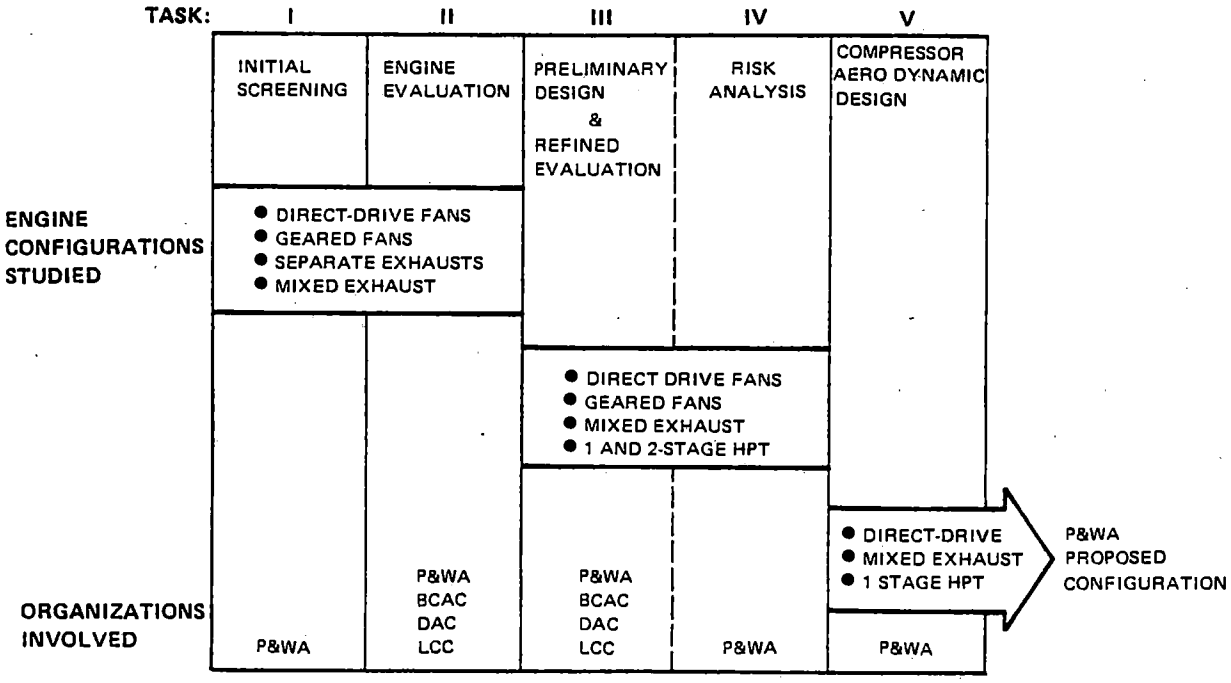

Figure 1 Program Tasks - The program was conducted in five technical tasks.

TABLE I

GOALS FOR ENERGY EFFICIENT ENGINE CAPABILITIES

Cruise TSFC	-12% Minimum (JT9D-7A Reference)
DOC	-5% Minimum (JT9D-7A Reference)
Noise	FAR Part 36 (1969) Minus 10 EPNdB
Exhaust Emissions	1981 EPA Standards
Thrust Growth	Capability Without Compromising Other Goals
Performance Deterioration	Improved (JT9D-7A Reference)

3.2 TASK I – INITIAL CONFIGURATION SCREENING

The exploratory Study of Turbofan Engines Designed for Low Energy Consumption (STEDLEC) program (NASA CR-135002) identified the basic engine concepts evaluated in this study. The four cycle concepts were:

- Separate Flow Exhausts, Direct Drive Fan
- Separate Flow Exhausts, Geared Drive Fan
- Mixed Flow Exhaust, Direct Drive Fan
- Mixed Flow Exhaust, Geared Drive Fan.

Engine cycles were initially defined using STEDLEC TSFC and DOC/ROI trends and more recent mixed flow exhaust study results. Bypass ratio, fan pressure ratio, overall

pressure ratio, and turbine temperature were selected to maximum TSFC and DOC benefits.

The relative ability to meet program goals was to be the basis for screening from four down to two engine configurations for further refinement. Calculation procedures used to quantify the engine capabilities for screening are outlined in the following paragraphs.

3.2.1 Thrust Specific Fuel Consumption

Component aerodynamic definition including updated technology projections were generated to complete the four study engine cycle definitions. Bare engine TSFC was estimated using the State-of-the-Art Performance Program (SOAPP). Isolated nacelle drag was built up from estimates of fan cowl friction drag, pylon and afterbody jet scrubbing drag, plug scrubbing drag, and pressure drag. The friction and scrubbing drag estimates included the effects of wetted area, dynamic pressure, and surface roughness. Fan cowl pressure drag was set proportional to friction drag. Drag was then subtracted from the bare engine thrust to determine installed engine cruise TSFC at the 10,700 m (35,000 ft.) Mach 0.8 design point.

3.2.2 Economics

The economic evaluation was performed by Pratt & Whitney Aircraft using NASA approved DOC, indirect operating cost (IOC), and return on investment (ROI) methods. Ground rules used in the preparation of these parameters are summarized in Tables II, III, and IV for DOC, IOC, and ROI respectively.

3.2.3 Engine Noise

Acoustic requirements were considered during the engine configuration definition. Blade passing frequency concerns influenced the axial spacing and number of fan and low-pressure turbine (LPT) airfoils. Fan inlet and exit, and turbine exhaust treatment lengths and depths were specifically tailored to match the noise frequencies being attenuated.

Engine noise estimates were predicted for the four engine concepts at FAR Part 36 (1969) takeoff, approach, and sideline conditions. Fan noise, turbine noise, and core noise estimates, which rely heavily on engine test data, were based on empirical methods developed at Pratt & Whitney Aircraft. Jet noise, the modification of jet noise due to coaxial flow, the effects of airplane forward speed on jet noise, extrapolation procedures, and engine number were based on SAE A-31 committee procedures. Foreward flight effects, ground plane reflections, doppler shift, and noise attenuation due to treatment were based on Pratt & Whitney Aircraft developed procedures. Effective perceived noise levels (EPNL) were calculated per FAR-36 using 1/3 octave band spectra.

Two levels of engine acoustic technology were evaluated: current and advanced. Advanced acoustic technology was projected for the 1990's time period, which reduced fan, turbine, and jet noise. Advanced low noise fan blades and advanced liners were projected which reduced buzz saw, blade passing, and broadband noise by 1 to 3 dB. Nacelle recontouring and increased understanding of flight velocity effects were projected to have a 1.4 dB jet noise reduction potential at takeoff and side line measuring points. Attenuated turbine noise reductions of up to 4 dB were projected for acoustic tailoring of turbine geometry and advanced technology treatment. Resultant total noise levels were reduced by approximately 2 to 3 EPNdB with application of these advanced acoustic technologies.

TABLE II

FACTORS USED IN CALCULATION OF DIRECT OPERATING COST
MID-1977 DOLLARS

Crew Cost	Domestic	International
2 man crew	$11.987\ (V_{cr} \times TOGW/10^5)^{0.3} + 28.754$	$12.986\ (V_{cr} \times TOGW/10^5)^{0.3} + 95.82$
3 man crew	$16.293\ (V_{cr} \times TOGW/10^5)^{0.3} + 40.695$	$17.652\ (V_{cr} \times TOGW/10^5)^{0.3} + 64.55$

Fuel: 9.2¢/liter (35¢/gal) Domestic
11.9¢/liter (45¢/gal) International
Increased 2% for non-revenue flying.

Insurance: 1% of flyaway price, per year.

Airframe maintenance labor: \$9.90 per manhour; direct labor MH/flight = $9.378 \log_{10} (W_{AF} - 14.848$; direct labor MH/FH = $5.7 \log_{10} (W_A) - 7.651$.

Airframe maintenance materials: maintenance materials cost/flight = $2.411\ (C_A/10^6) + 2.103$; maintenance materials cost/FH = $2.015\ (C_A/10^6) - 0.998$.

Engine maintenance labor: \$9.90 per manhour, manhours per FH utilizes procedures and equations in NASA CR-134645, modified as required to take into account advanced technology features and other provisions (e.g., reduction gearbox).

Engine maintenance materials: Function of engine design, size and average flight time: method consistent with NASA CR-134645, modified (for reasons stated above).

Maintenance burden: Equal to 200% of sum of airframe and engine maintenance labor cost.

Depreciation: 15 years to 0 residual value, includes 6% airframe spares and 30% engine spares.

Where:

Airframe price, millions of mid-1977 dollars.

$$C_A = [0.272W_A^{0.87}\ (Q/250)^{-0.42} + (11.29/Q)W_A^{0.89}] \times (1.0 + 0.012WR) + 0.00396S + 0.79$$

W_{AF} is airframe weight = owe less bare engine weight in kilograms divided by 453.6 (or lbm divided by 1000)

W_A is the AMPR weight in kilograms divided by 453.6 (or AMPR weight in lbm divided by 1000)

MH = manhours

TABLE II (Cont'd)

Q = quantity of airplanes = 300

FH = flight hours

S = number of seats per airplane

V_{CR} = speed factor = 715 (Mach) - 75 (Mach)^4

ATA formula for utilization: Block hours per year = 4275 (BT + 0.3)/(BT + 1.3) + 475

BT = block time = flight time + 0.25 hours

WR = % weight reduction of composite aircraft structure relative to aluminum

Revenue load factor: 55 percent

TOGW = maximum takeoff gross weight in kilograms divided by 45,360

Typical mission stage length: 3700 km (2000 naut. mi.) International
1295 km (700 naut. mi.) Domestic

TABLE III

FACTORS USED IN CALCULATION OF INDIRECT OPERATING COST
MID-1977 DOLLARS

Cabin Attendant, dollars per block hour Wide body aircraft	25.8 *S/27 + 30.14
Aircraft Servicing, dollars per flight	
Fueling and cleaning	W_L * 1.001, Dom., *2.442, Int'l.
Landing fee	W_L *2.02, Dom., *$.95, Int'l.
Aircraft control	W_L *48.95, Dom., *119.9, Int'l.
Ground Equipment and Facilities, dollars per flight	
Maintenance and burden	W_L *0.559, Dom., *1.067, Int'l.
Depreciation and amortization	W_L *0.616, Dom., *1.177, Int'l.

General and Administrative

Costs are assumed to be 6 percent of the total of DOC, cabin attendant, aircraft servicing, and ground equipment and facilities cost.

Definition of Symbols

S is the number of seats per aircraft

W_L is the maximum landing weight in kilograms divided by 453.6 (or max. landing weight in lbm divided by 1000).

TABLE IV

FACTORS USED IN CALCULATION OF RETURN ON INVESTMENT

Basic ROI formula, mid-1977 dollars:

$$\frac{\text{ROI}}{1-(1+\text{ROI})^{-15}} = \frac{\text{Annual Cash Flow}}{\text{Initial Investment}}$$

Annual Cash Flow = Revenue + Depreciation – DOC – IOC – Taxes

Initial Investment = (1.06 × airframe cost) + (1.3 × number of engines × engine price)

Initial Investment Terms: 100 percent purchase at delivery with 6 percent airframe spares and 30 percent engine spares.

Revenue: Dollars per passenger - Kilometer (mile): First class: Dom. = 0.0528 (0.085); Int'l. = 0.848 (0.1365); Tourist: Dom. = 0.432 (0.0695); Int'l. = 0.05058 (0.0814).

Taxes, Income and other taxes equal to 50 percent of net earnings, with no investment tax credit

3.2.4 Exhaust Emissions

Exhaust emissions estimates included unburned fuel (UHC), partially oxidized carbon (CO), oxides of nitrogen (NO_X), and very small carbon particles (smoke). EPA parameter (EPAP) predictions were utilized to quantify the engine emissions. EPAP is a summation of total pounds of pollutant per 1000 pounds of thrust per simulated landing takeoff (LTO) cycle as defined in Figure 2. The emissions indices (EI) used in the calculations were derived from correlations against burner fuel-to-air weight ratio which were obtained from JT9D low emissions burner testing conducted in the Experimental Clean Combustor Program. Using these correlations, differences in burner operating pressure, temperature, and fuel-to-air ratio between the JT9D and advanced engines were taken into account to arrive at the nominal emissions level estimates. Margins to account for a 3 sigma variation in production tolerance, operational deterioration, and development were superimposed on the nominal levels to obtain the final predictions. Inclusion of these margins increased emissions of NO_X by 27 percent, CO by 47 percent, and UHC by 71 percent above nominal values.

EPAP IS A TOTAL LBS. OF POLLUTANT PER 1000 LBS. OF THRUST-HOURS PER SIMULATED LANDING/TAKEOFF (LTO) CYCLE:

$$EPAP = \sum^{N=5} (EI)_N \ (W_F)_N \ (TIM)_N \ / \sum^{N=5} (F)_N \ (TIM)_N$$

EI = EMISSIONS INDEX (LBS. POLLUTANT/1000 LBS. FUEL)

W_F = FUEL FLOW

W_F = FUEL FLOW (LBS/HR.)

WHERE

TIM = TIME IN MODE (HR.)

F = THRUST (LBS.)

AND

THE SIMULATED LANDING/TAKEOFF CYCLE IS

N	MODE	% TAKEOFF THRUST	TIME IN MODE (HR.)
1	TAXI/IDLE (OUT)	ASSIGNED (MFG).	0.317
2	TAKEOFF	100	0.012
3	CLIMB OUT	85	0.037
4	APPROACH	30	0.067
5	TAXI/IDLE (IN.)	ASSIGNED (MFG.)	0.117

Figure 2 EPA Parameter Definition - The EPAP is computed for a simulated landing/takeoff cycle.

3.2.5 Thrust Growth

Thrust growth studies were conducted and evaluated against the program goal of not compromising the other goals. Two approaches were analyzed: constant nacelle diameter to reflect near term commonality requirements; and constant fan pressure ratio, to limit noise increases with growth. In both approaches, fan corrected flow per unit of annulus area (W/A) was increased by 3-5 percent; a low-pressure-compressor (LPC) supercharging stage was added; and turbine temperature was increased as necessary to produce the required thrust. To maintain a constant nacelle diameter, fan pressure ratio was increased with turbine temperature. To hold noise more nearly constant with thrust growth, fan diameter was increased with fan pressure ratio held at a constant value.

Component performance estimates for the growth cycles were obtained from parametric trend data to incorporate the effects of increasing fan specific flow, increasing fan pressure ratio, and increasing turbine temperature. LPC polytropic efficiency and LPT adiabatic efficiency were held constant. Engine TSFC, noise, and exhaust emissions were evaluated.

3.2.6 Performance Deterioration

Performance deterioration was addressed by a design approach that emphasized attaining and maintaining tight component clearances to minimize TSFC deterioration. Design features included seven main bearings and four main support structures; stiff rotors to minimize rotor deflections under thrust, gravitational, or gyroscopic loads; a load sharing nacelle to minimize engine backbone bending; and an active clearance control system to provide tight cruise clearances.

3.3 TASK II – ENGINE-AIRCRAFT INTEGRATION AND PERFORMANCE

In this task a wide range of cycles were evaluated in order to refine each engine type selected during Task I. These evaluations were conducted with the assistance of three airplane manufacturer subcontractors: Boeing, Douglas, and Lockheed. Table V and Figure 3 show the range of cycles considered and the method of analysis.

Seven specific cycles, representing variations in exhaust type and nacelle size were chosen by Pratt & Whitney Aircraft to be evaluated by the airplane manufacturers. For these cycles, plus for the JT9D-7A reference engine, Pratt & Whitney Aircraft supplied fully installed (including customer bleed, horsepower extraction, and external isolated nacelle drag) engine performance data along with engine and nacelle weights, dimensions, and scaling curves.

TABLE V

TASK II STUDY ENGINE CYCLE RANGES

Direct - Drive Fan, Separate Flow Exhausts	6 - 9 BPR
Direct - Direct Fan, Mixed Flow Exhaust	7 - 8 BPR
Geared - Drive Fan, Separate Flow Exhausts	7 - 11 BPR
Geared - Drive Fan, Mixed Flow Exhaust	9 - 11 BPR
OPR*	33 - 45:1
Design RIT*	1120 - 1290°C (2050 - 2370°F)

*At the cruise aerodynamic design point of 10,700 m (35,000 ft.), Mach 0.8.

Trade factors were generated for converting TSFC, weight, and cost into DOC. Projected characteristics and technological improvements for domestic and international range aircraft by the 1990's were assumed for trade factor generation.

Conceptual propulsion system cross-sections of the four engine configurations were drawn-up and used to estimate weight, price and maintenance cost. Weight and price estimates were made by component. Each component was related to previously designed parts. The effects of speed, material, flowpath, blading, and construction differences on weight and manufacturing costs were built up to a total engine estimate. Maintenance cost estimates consisted of a two part procedure. Material replacement costs were estimated by a scrap life method that considered spare parts prices and scrap life estimates for key engine parts. Mainten-

ance labor costs were estimated by a design features method which included estimates of manhours per repair and mean time between repair by module and key part.

Twenty-two additional engine cycles were analyzed by Pratt & Whitney Aircraft. Some of these were eliminated by inspection of their performance, while others were carried through a fuel burned and economic evaluation using trade factors. Results obtained in this manner were used to complete the cycle refinement.

Analytical procedures used in the Task I studies were carried into Task II as applicable.

3.3.1 Boeing, Douglas and Lockheed Aircraft Integration Studies

The three airplane manufacturers evaluated each engine in two advanced aircraft, one do-

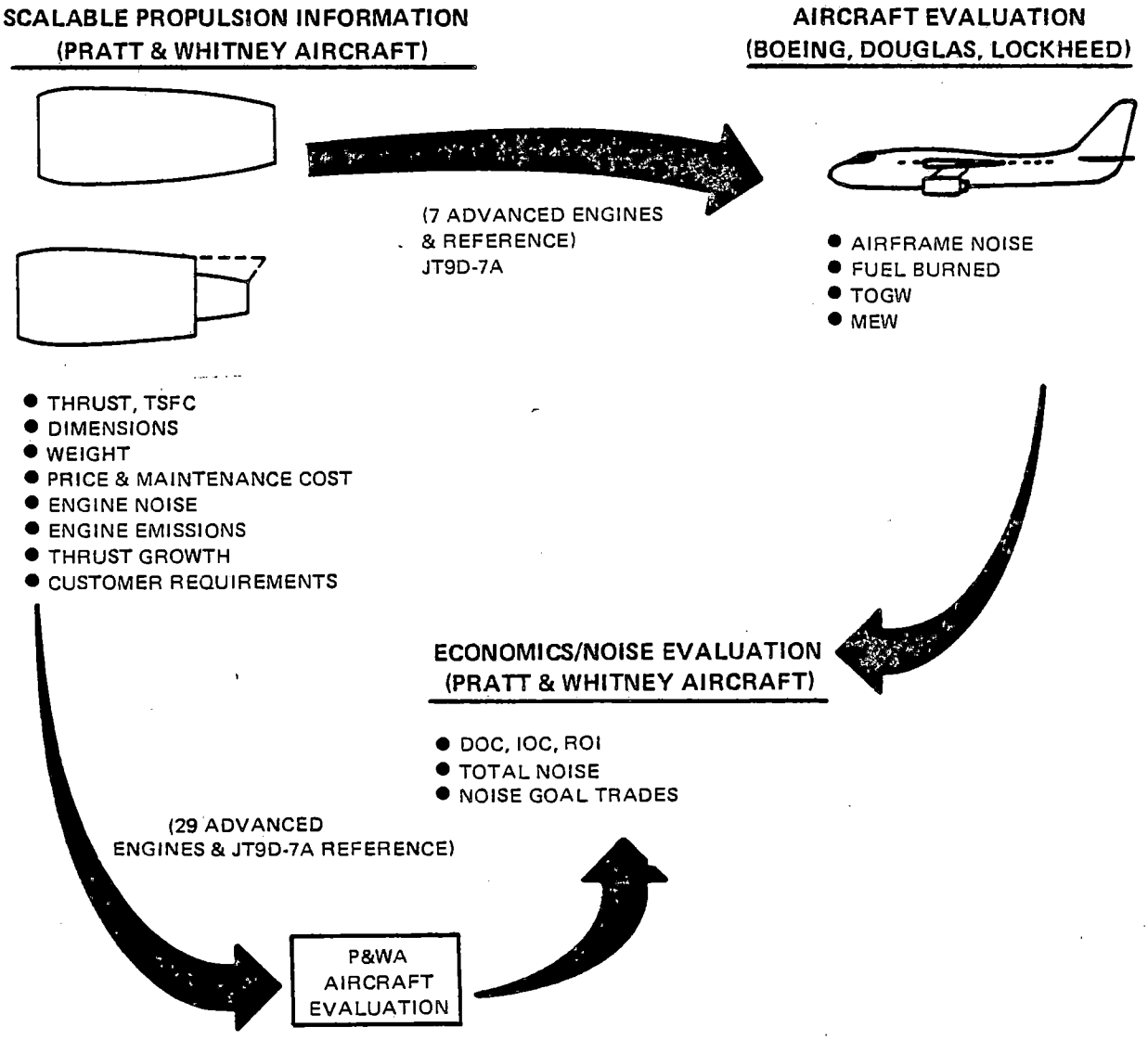

Figure 3 Cycle Refinement - Method of analysis involved P&WA and three airframe company subcontractors.

mestic and one international, which they had selected as suitable for 1990's operation. Advanced technology wide body aircraft selected, illustrated in Figure 4, ranged from a Boeing 86, 300Kg (250,000 lb.) domestic twinjet to a Douglas 210,000 Kg (600,000 lb.) international tri-jet. Correspondingly, engine thrust requirements ranged from a Boeing 89,000 N (20,000 lb.) international quad-jet to near 222,400 N (50,000 lb.) with the Douglas international tri-jet. Technological aircraft advancements included improved wing/airfoil design, composite materials for secondary and primary structures, and active controls.

For each of the study aircraft, the airplane manufacturers conducted integration studies to size engines, determined installation effects, and defined aircraft performance characteristics. A most important integration consideration was the potential for high interference

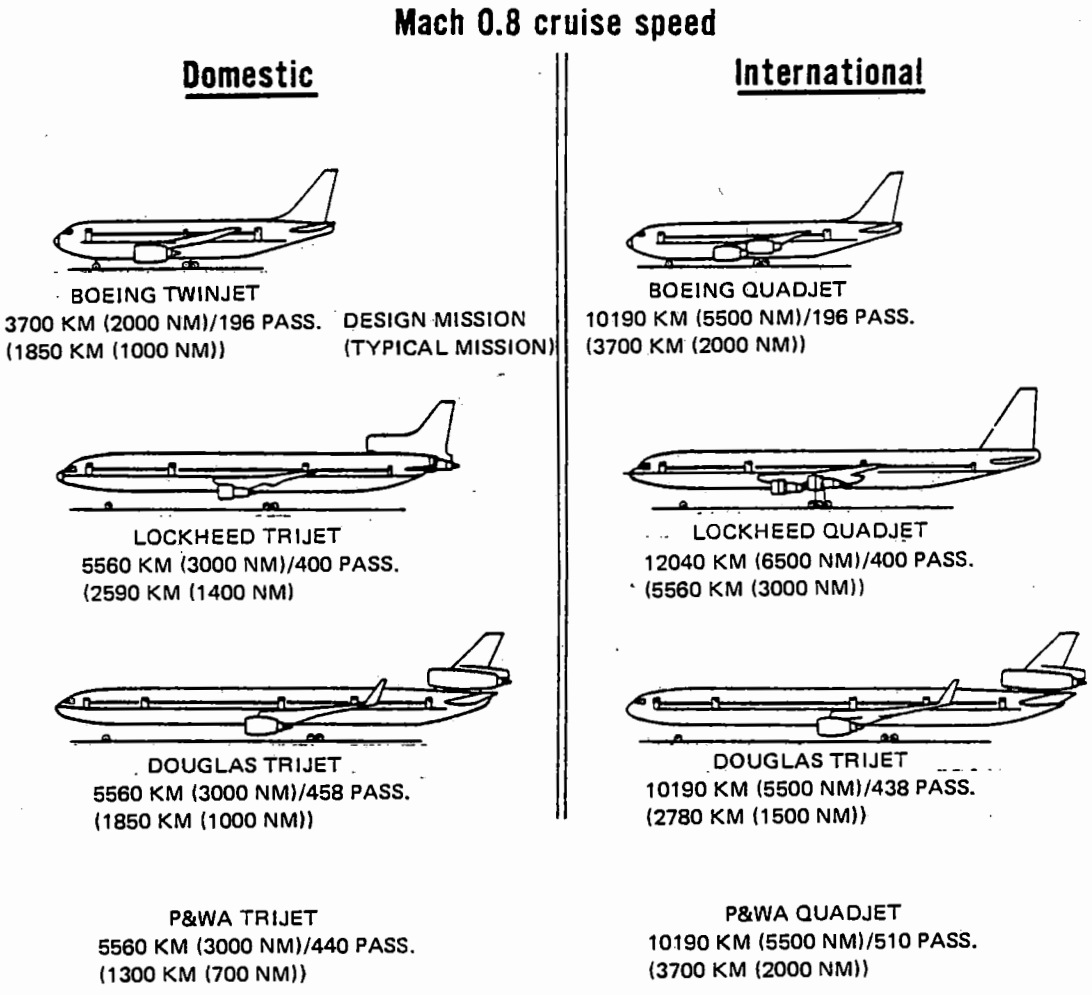

Figure 4 Advanced Study Aircraft - Advanced domestic and international range aircraft suitable for 1990's operation were selected for study.

drag with long, acoustically treated nacelles. This problem was addressed in under-the-wing installations by applying minimum drag nacelle-to-wing positioning criteria based on the aerodynamic development and testing of current high bypass ratio engine installations. Tail engine installations were positioned to maintain present high bypass ratio engine installation interference drag levels and to provide necessary nacelle-to-ground clearance during takeoff rotation. The airplane manufacturers supplied Pratt & Whitney Aircraft with airplane performance, fuel burned, weights, airframe noise, and FAR 36 flight conditions.

3.3.2 Economics

Airplane manufacturer supplied fuel burned and weight information was combined with Pratt & Whitney Aircraft propulsion system cost information to calculate DOC, IOC, and ROI. The calculation procedures outlined in Section 3.2.2 for Task I were retained for use in the Task II studies.

3.3.3 Total Noise

Boeing, Douglas and Lockheed provided Pratt & Whitney Aircraft with airframe noise data for the majority of their mission sized study aircraft. They were in the form of sound pressure levels for discrete octave bands at various selected angles from a reference line, so that airframe noise could be readily combined with Pratt & Whitney Aircraft's engine noise estimates.

The engine noise estimates were based on SOAPP simulations of the engine cycles at the FAR measurement points and power settings specified by the airplane manufacturers. A similar noise evaluation was made for four of the study engines (one for each configuration) in the Pratt & Whitney Aircraft defined international aircraft to serve as a reference point against which the other noise estimates were checked. As part of Task II, a study was conducted to determine the fuel burned and DOC impacts of lowering engine noise through nacelle variations for these four engine cycles. This was done to identify the cycle parameters which provided a fuel optimum condition at each noise reduction level. The study utilized Pratt & Whitney Aircraft's international airplane.

The two levels of engine acoustic technology defined in Section 3.2.3 were included in all of these studies.

3.3.4 Exhaust Emissions, Thrust Growth, and Performance Deterioration

Exhaust emissions estimates were expanded relative to the Task I effort to include examination of the effects of turbine rotor inlet temperature and overall pressure ratio. Estimates were made through the application of emissions indicies over a LTO cycle as outlined in Section 3.2.4.

Thrust growth results of Task I were checked and found to remain applicable to the Task II engine cycles. This permitted the selection of overall pressure ratios and turbine inlet temperature levels for more refined growth engine analysis in Task III.

The same features defined under Task I to minimize performance deterioration were also assumed for the Task II engine cycle studies.

3.4 TASK III – INITIAL PRELIMINARY DESIGN; REFINED ENGINE-AIRCRAFT INTEGRATION AND PERFORMANCE

Preliminary design analyses, conducted in Task III, investigated areas of technical concern for direct drive and geared drive mixed-

exhaust engines. Study emphasis was placed on the engine areas critical to establishing design feasibility and on those where more information was needed for precise configurational comparison. To this point, all of the engine configurations included two-stage HPT's. However, the resulting DOC reductions with advanced engine powered domestic aircraft were small. This prompted the additional consideration of a one-stage HPT for its potential cost savings. As a result, four mixed flow exhaust engines were analyzed in this task:

- One Stage HPT, Direct Drive Fan
- Two Stage HPT, Direct Drive Fan
- One Stage HPT, Geared Drive Fan
- Two Stage HPT, Geared Drive Fan.

3.4.1 Preliminary Design and Analysis

Inputs to the preliminary design process consisted of component aerodynamic and mechanical parameters, updated technology projections, materials projections, and engine design tables. Preliminary design analyses produced component, engine, and nacelle flowpaths and performance. Aerodynamic, structural, and mechanical analyses were concentrated on the key areas summarized in Table VI.

Examples of preliminary design analyses follow:

- Parametric screening studies of the HPC and HPT were conducted to determine the optimum design configuration. Variations in rotor speed, flowpath diameter, throughflow velocity, airfoil numbers, and stage numbers were investigated. Nacelle impacts resulting from component dimensional changes were integrated into the system performance and economic evaluations. Low spool fan, LPC, and LPT evaluations were conducted on a similar, but more limited basis.

- Design simplifications of the combustor configuration from the NASA Experimental Clean Combustor Program (ECCP) were made to reduce cost and weight and to improve durability. Modifications included reducing fuel injector density, clustering pilot and main zone fuel injectors, eliminating the combustor throat, and reducing combustion zone length.

- Three secondary flow systems were evaluated to determine the optimum means of supplying HPT blade cooling air. These were a mini-disk tangential on-board injection (TOBI) system, a pressure balanced TOBI system, and a bore feed-HPC drum bleed. Turbine blade cooling leakage and airflow required to avoid disk windage heatup and prevent hot gas ingestion were examined. Performance, weight, and structural risk were evaluated for each system.

- Structural feasibility of the high speed, tip-shrouded LPT blades for the geared drive fan engines was questioned. The critical last stage was analyzed to determine its vibration and stress characteristics. Of particular concern, from a structural standpoint, were the high level of airfoil root P/A stress and the high low-rotor speeds.

Outputs from the preliminary design analyses included high and low spool definitions, refined propulsion system cross sections and performance, weight, price, and maintenance estimates.

TABLE VI

KEY AREAS OF CONCENTRATED PRELIMINARY DESIGN ANALYSES IN TASK III

Analysis	Reason
HPC Parametric Study	Select Optimum Designs
HPT Parametric Study	Select Optimum Designs
Combustor Study	Define Simplified Low Emissions Configuration
Secondary Flow System Study	Select Minimum Bleed/Leakage Systems
HPC Rotor Study	Assure Structural Feasibility of High Temperature/ Speed Rear Stages
Clearance Control Study	Select Passive/Active System to Minimize Operating Tip Clearances
HPT Structural Study	Optimize Performance in High Temperature/Speed Environment
Hollow Fan Blade Study	Establish Initial Structural Feasibility of Low Weight, Shroudless Design
Fan Reduction Gear Study	Define Feasible Gearbox/Heat Exchanger Systems
Low Spool Parametric Study	Select Preliminary Optimum Fan, LPC, and LPT
LPT Structural Study	Establish Structural Feasibility of LPT in Geared Engine
Rotor Dynamics Study	Define Main Bearing and Support Structures Arrangements for Minimum Deflections
Gear/Bearings Lubrication Study	Define Heat Load/Cooling Requirement with High Power Low Rotor Gearbox
Materials/Construction Study	Define Minimum Weight/Cost Configuration
Stability Audit	Establish Component Surge Margin Requirements
Nacelle Study	Establish Preliminary Contours/Arrangement

3.4.2 Performance Deterioration

Performance deterioration was estimated considering the following: increased airfoil tip clearances, erosion, turbine airfoil creep and distortion, and air seal and joint leakages. Experience, particularly with the JT9D engine, formed the basis for this evaluation. Component clearance changes were obtained by the use of an analytical rotor-frame system model of the engine and nacelle which allowed the study of thermal and centrifugal growth, in-plane ovalization, and transverse bending. The magnitude of the gravitational, gyroscopic, and wind gust loads which were simulated with the model was calibrated to JT9D rub data. The impact of the deterioration factors on component efficiencies and engine matching was evaluated. Cruise TSFC deterioration was predicted at 1000 and 4000 hours of operation.

3.4.3 Thrust Growth

A potential thrust growth requirement of up to 25% was indicated to be desirable by the airframe manufacturers. Thrust growth trends were re-examined for the two methods of growth studied in Task I. Component flowpaths and performance, row-by-row turbine cooling requirements, and optimized cooling schemes were defined for the direct and geared drive fan thrust growth cycles with one and two-stage HPT's. Engine performance and noise were estimated and evaluated.

3.4.4 Engine-Aircraft Integration and Performance

The refined engine designs were re-evaluated in conjunction with the three airplane manufacturers. Investigation of the engine/aircraft integration included engine sizing, thrust reverser design and directivity, customer bleed temperature and pressure requirements and limitations, nacelle aerodynamics and materials, engine-wing geometric and performance interactions, and aircraft characteristics. Boeing's domestic airplane analysis included a wing flutter investigation. Beam representations for the wing, pylon, and fuselage were synthesized. Unsteady aerodynamic forces were analyzed using strip theory modified by experimentally determined section life coefficients and aerodynamic center data for both the wing and nacelles.

The airplane manufacturers also estimated airframe noise, fuel burned, and aircraft weight which were used as inputs into Pratt & Whitney Aircraft DOC, IOC, ROI, and noise comparisons. The techniques were the same as for Task II.

3.5 TASK IV – RISK ANALYSIS

A risk assessment of each engine's technology features was conducted to permit TSFC and DOC comparisons on an equal probability of achievement basis. The risk assessment entailed a Delphi analysis approach in determining the probability of achieving each individual propulsion system technology advancement included in each preliminary design. Then the individual probabilities were statistically summed to arrive at an overall engine configuration probability curve for reducing TSFC. Similar analyses were made for weight, price, and maintenance cost. Trade factors were applied to these results to arrive at a DOC reduction probability distribution for the Task III engine configurations. The results of this risk assessment were factored into the Task III performance predictions to aid in the selection of the final engine configuration.

A program risk assessment was also conducted as part of the Task IV effort in order to identify potential problems which would affect

technology development scheduling or funding and the magnitude of the impact on an overall experimental program. Each potential problem area was categorized as having a minimal, moderate, or large impact on the experimental program schedule or budget. Fall-back positions were identified for each of the potential problems. Program elements were also emphasized to relate the ultimate engine benefits to program cost.

3.6 TASK V – COMPRESSOR AERODYNAMIC DESIGN

Aerodynamic design analyses were conducted to refine the Task III core compressor flowpath and blading shapes prior to finalizing the preliminary compressor design. Aerodynamic assessments included meanline and streamline analyses which considered the effects of interstage airbleeds, boundary layer flow blockage, and aerodynamic loading limits on compressor geometry. First pass stage vibrational analyses were conducted to determine structural design feasibility.

3.6.1 Aerodynamic Analysis

Airfoil axial gapping estimates, bleed locations, and bleed flows were determined during the flowfield definition. With meanline analysis techniques, the effects of boundary layer blockage on the flowfield were also taken into account.

A streamline analysis computer program was used to establish full-span aerodynamics. This streamline analysis program defined velocity vectors and flow conditions by means of an axisymmetric compressible flow solution of the continuity, energy, and radial equlibrium equations. The spanwise and stagewise loading distributions were optimized by adjustments in flowpath shape, radial total pressure slopes, axial pressure distributions, and radial reactions.

Once the flowfield aerodynamics had been optimized, preliminary blading was selected. Radial chord distributions (taper ratio) were selected to maintain loading limits where required. Blading in the subsonic Mach number region was selected using the Pratt & Whitney Aircraft cascade system which was incorporated in the streamline analysis program. For blading selection in the supersonic Mach number regime, correlations of loss and turning data acquired from extensive high tip speed fan tests were employed in conjunction with channel flow calculations to determine blade section shapes.

3.6.2 Vibrational Analysis

The blading, which met the aerodynamic criteria, was subjected to structural analysis. Airfoils were analyzed for flutter stability, a two excitations per revolution (2E) frequency margin, blade tip mode resonance, and foreign object damage resistance.

Bending and torsional flutter stability calculations for all rotors and stators were compared with Pratt & Whitney Aircraft experience curves. Airfoils which violated the experience criteria were modified in either thickness or chord length.

The first stage blade-alone first mode resonant frequency was calculated to assure that the 2E resonance could be designed out of the operating range. Blade resonance calculations were also made for the chordwise bending tip modes.

To conclude the technical effort, the ratio of the minimum axis bending stresses between the maximum airfoil thickness location and the airfoil leading and trailing edges was controlled to limit the stress levels at the leading and trailing edges, where airfoils are most susceptible to foreign object damage.

4.0 PROGRAM RESULTS

4.1 OVERVIEW

The selected engine will be described in detail in this section by major feature and technical advancement. The basis for cycle selection and the evaluations that led directly to engine choice will be discussed.

Three study elements contributed directly to the Pratt & Whitney Aircraft engine configuration selection: (1) assessments against study goals; (2) probabilities of achieving thrust specific fuel consumption (TSFC) and direct operating cost (DOC) study goals; and (3) preliminary engine design analysis.

An assessment against study goals, directly involving three Task II engine configurations, was sufficient to choose a mixed exhaust system. Mixing, assuming 1985 technology, provided TSFC, fuel burned, and DOC reductions combined with a lower noise potential. More detailed study of four Task III/IV mixed exhaust engines, involving all three study elements, led to the selection of a one-stage high-pressure turbine (HPT) and direct-drive fan. The deciding factors in these selections were DOC, relative mechanical simplicity, and inherent operational safety.

This engine has been given Pratt & Whitney Aircraft study designation STF505M-7. Results of the evaluation of this engine are given in Table VII. They show the ability of the engine to meet all the program goals except NO_X. To meet the NO_X goals would require emissions technology beyond that demonstrated in the Experimental Clean Combustor Program which, with production margins added, was used as a baseline for the studies.

4.2 ENGINE DESCRIPTION AND TECHNOLOGY REQUIREMENTS

Figure 5 is the preliminary design cross-section of the Energy Efficient Engine. The engine configuration is illustrated along with the main design features. Also shown are the advanced technologies that are incorporated in the design. This section will discuss the engine cycle characteristics, the major engine components, and the advanced technology areas requiring further development.

4.2.1 Engine Cycle

The Energy Efficient Engine design cycle, compared to the reference JT9D-7A in Table VIII, achieves the fuel consumption goal through utilization of a mixed flow exhaust system, high overall pressure ratio, moderate turbine temperature, and a bypass ratio/fan pressure ratio combination which results in the best balance of DOC and fuel burned improvements. The nominal sea level static takeoff thrust is 174,590 N (39,250 pounds). The aircraft evaluations included in this study required thrusts ranging from 88,965 to 222,410 N (20,000 to 50,000 pounds).

TABLE VII

SUMMARY OF PREDICTED CAPABILITIES FOR THE RECOMMENDED ENGINE (STF 505M-7)

	Boeing	Douglas	Lockheed	Pratt & Whitney Aircraft	Study Goals
Percent Cruise TSFC Reduction[1]	–	–	–	15.3	⩾12
Percent DOC Reductions[1]					⩾5
Domestic	2.8	12.4	8.2	6.2	
International	9.3	13.1	11.2	10.3	
Percent Fuel Burned Reduction[1]					
Domestic	10.5	21.7	18.9	16.0	(none
International	16.5	21.3	20.4	18.1	specified)
EPA Parameters					EPA 1981
CO	–	–	–	2.0	3.0
THC	–	–	–	0.3	0.4
NO_x	–	–	–	4.3	3.0
EPNdB Noise Reduction From FAR (1969)[2]					
Domestic	−7.7	−11.0	–	−9.6	−10
International	−7.8	−10.6	–	−8.9	−10
Percent 4000 hr. TSFC Deterioration	–	–	–	1.5	< 2.8
Percent Thrust Growth	–	–	–	> 20 with NO_x increase	without compromising other goals

Notes: (1) Relative to JT9D-7A except Douglas DOC and fuel burned trends which are relative to JT9D-20; all typical stage length operation.
(2) Maximum noise untraded and without cut-back at takeoff.

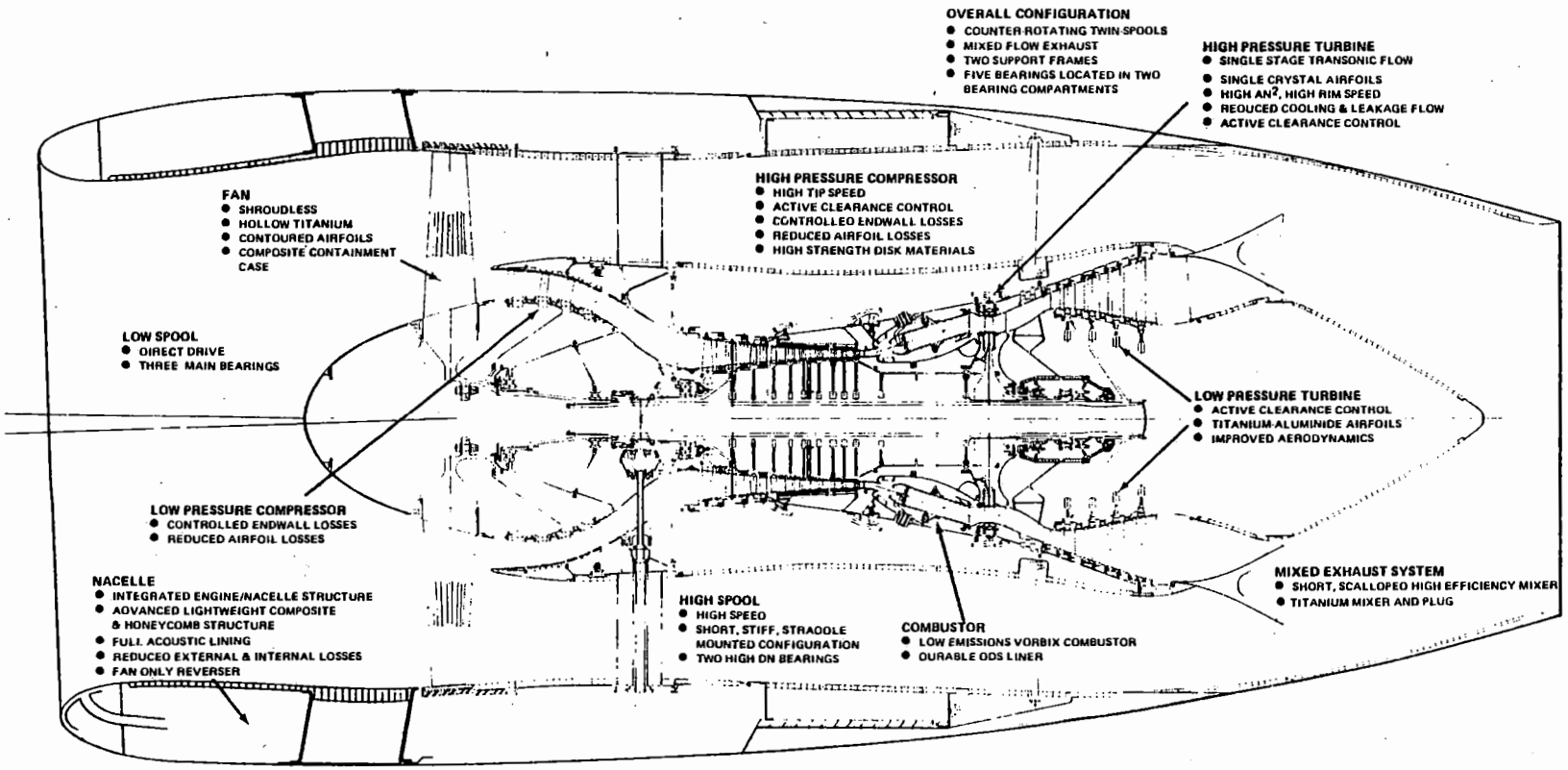

Figure 5 *Preliminary Energy Efficient Engine Cross Section – Major technology and design features are shown.*

TABLE VIII

COMPARISON OF ENERGY EFFICIENT ENGINE AND JT9D-7A CYCLES
(Maximum Cruise, Mach 0.8/10, 700 m (35,000 feet) standard day - unless noted)

	Energy Efficient Engine	Reference JT9D-7A
Bypass Ratio	6.55	5.1
Fan O.D. Pressure Ratio	1.74	1.58
Fan I.D. Pressure Ratio	1.56	1.59
LPC Pressure Ratio (excluding Fan I.D.)	1.77	1.59
HPC Pressure Ratio	14.0	10.0
Overall Pressure Ratio	38.6	25.4
HPT Expansion Ratio	4.0	3.9
LPT Expansion Ratio	5.7	4.0
HPT Rotor Inlet Temperature		
• Maximum Cruise - Std. Day	1204°C (2200°F)	1087°C (1990°F)
• Hot Day Take-off	1343°C (2450°F)	1252°C (2285°F)
Fan Corrected Airflow - kg/sec	642	776
lb/sec	1415	1711
HPC Corrected Airflow - kg/sec	36	59
lb/sec	80	130
Exhaust System	Mixed Flow	Separate Flow
SLS Uninstalled Take-off Thrust ~ N	174,590	205,290
lb	39,250	46,150

- **Overall Pressure Ratio**

The design overall pressure ratio of 38.6:1 at the cruise design point offers a 3 to 4 percent fuel consumption improvement relative to current generation high bypass engines and results in near minimum DOC for the domestic and international aircraft as shown in Figure 6. This overall pressure ratio of 38.6 was selected to allow for engine thrust growth configurations to 45:1, which represents a maximum level which can be projected for the Energy Efficient Engine time period based on mechanical and material considerations. Although higher pressure ratio engines offer further improvement in fuel consumption without severely affecting DOC, thermal/structural analysis of the rear of the compressor section and the HPT indicates that the selected overall pressure ratio level of 38.6 represents an aggressive design limit when considering disk thermal control, maintaining tight rotor clearances, sealing of leakage paths, and especially thrust growth.

The improved component performance levels of the Energy Efficient Engine make possible this benefit in cycle thermodynamic efficiency with increased overall pressure ratio.

The 38.6 overall design pressure ratio is split between the high and low spools such that the high-pressure compressor (HPC) pressure ratio is 14:1 and the low-pressure compressor (LPC), including the fan root section, is 2.76. Increasing the HPC pressure ratio from the JT9D-7A level of 10:1 toward higher values,

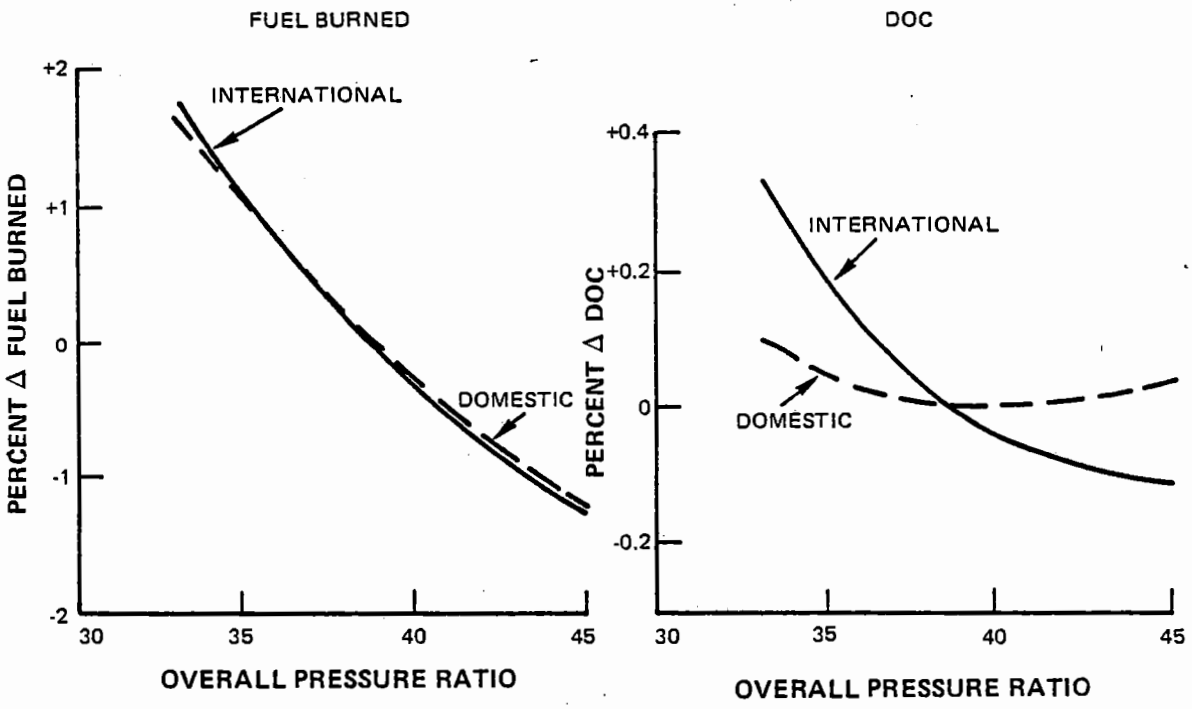

Figure 6 Effects of Overall Pressure Ratio - Relationship of fuel burned and direct operating cost to overall pressure ratio is shown.

and thereby reducing the LPC pressure ratio, results in fewer compressor stages and airfoils, a smaller diameter low-pressure turbine (LPT), and less bleed air for cooling the LPT. These changes translate into lower engine weight, lower price, and lower maintenance costs. However, due to a lower HPT efficiency achievable with a highly loaded one-stage design, a slightly higher TSFC results. The net effect is an improving DOC as the HPC pressure ratio is increased from 10 to 14.

A further increase in pressure ratio to 18:1 could provide an additional 0.3 percent reduction in DOC. However, additional concerns to be considered as HPC pressure ratio is increased are higher HPT aerodynamic risk, a longer core rotor with more difficult clearance control, more difficult compressor stability management, and more difficult engine starting. The 14:1 pressure ratio HPC was selected as a balance among these concerns, TSFC, and DOC trends.

- **Turbine Inlet Temperature**

The Energy Efficient Engine design (maximum cruise rating) turbine rotor inlet temperature of 1204°C (2200°F) minimized fuel consumption while leaving margin for substantial growth in engine thrust which may require increasing maximum temperature by as much as 111°C (200°F). At higher temperatures, engine weight reductions are offset by increased TSFC so that fuel burned remains constant over a large temperature range as shown in Figure 7. DOC is adversely affected at higher temperatures, as shown, because of the required increase in the number of high cost, cooled turbine parts, and decrease in hot section part lives.

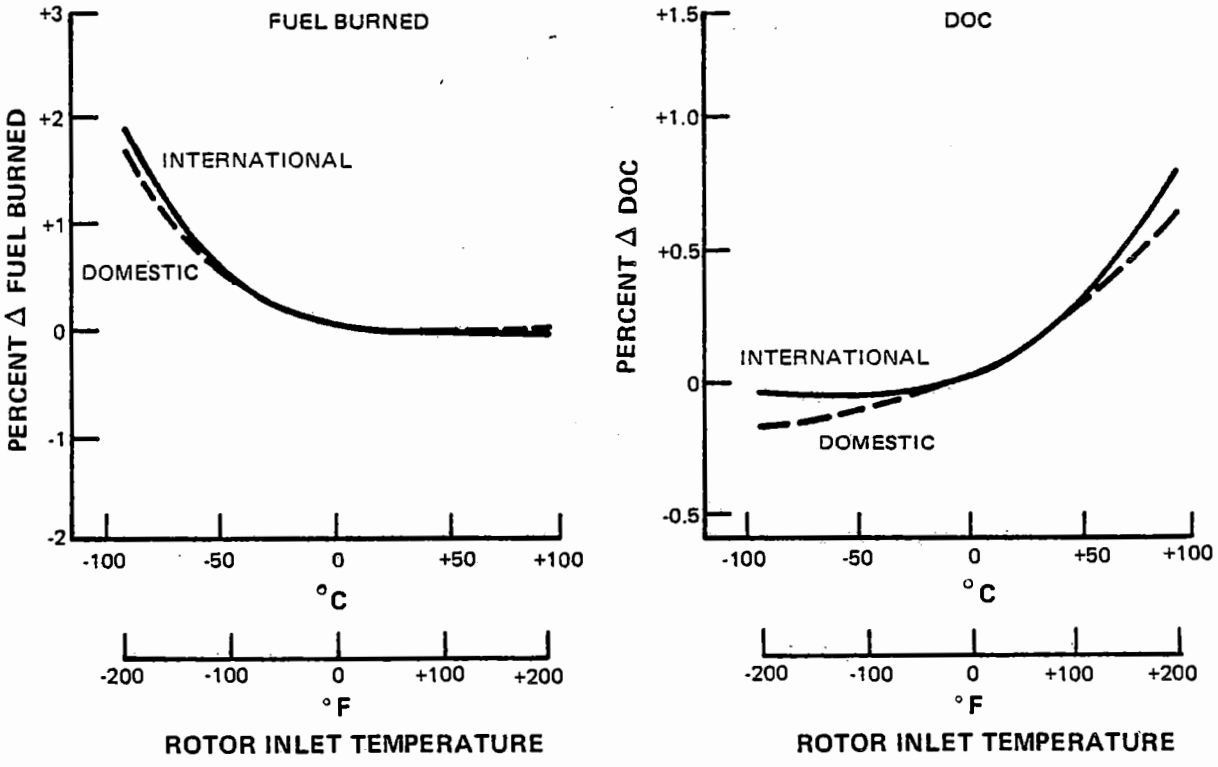

Figure 7 Effects of Rotor Inlet Temperature - Fuel burned remains constant over a large temperature range.

- **Bypass Ratio/Fan Pressure Ratio**

The improved component efficiencies also result in greatly increased available energy that can be converted to propulsive power by increasing bypass ratio. The DOC and fuel burned trends with bypass ratio are shown in Figure 8. As bypass ratio is increased, fan pressure ratio is decreased to maintain approximately equal core and fan stream exhaust total pressure required for a mixed flow configuration with optimum propulsive efficiency. As shown in Figure 8, DOC minimizes at low bypass ratios (approximately 6) for each of the aircraft. As bypass ratio is increased beyond 6, the effects of lower TSFC are offset by increases in the number of LPC and LPT stages, increased fan diameter, and increased nacelle size, with resultant increases in engine and nacelle weight and costs, as well as increased nacelle drag. This results in the shallow fuel burned trend with bypass ratio and a DOC penalty as bypass ratio is increased. The effects of the improved TSFC of the higher bypass ratio engines is more pronounced for the more fuel intensive international aircraft. The selected bypass ratio of 6.5 provides the best combination of improved DOC and fuel burned. The fan pressure ratio of 1.74 was selected to equalize core and fan stream exhaust pressures for efficient mixing.

4.2.2 Engine Components

The design parameters and performance of the major components are discussed in detail in this section. They are summarized in Table IX.

- **Fan**

A hollow titanium shroudless fan blade design with a 472 m/sec (1550 ft/sec) corrected tip speed eliminates the significant performance penalty associated with inter-blade shrouds which are customarily required for aeroelastic stability. The hollow titanium construction reduces the weight penalty of either a tip-shroud configuration or the solid low aspect ratio airfoil needed to solve the aeroelastic stability requirement. Contoured fan airfoil designs provide an additional efficiency improvement relative to current technology multiple circular arc (MCA) fan airfoil shapes.

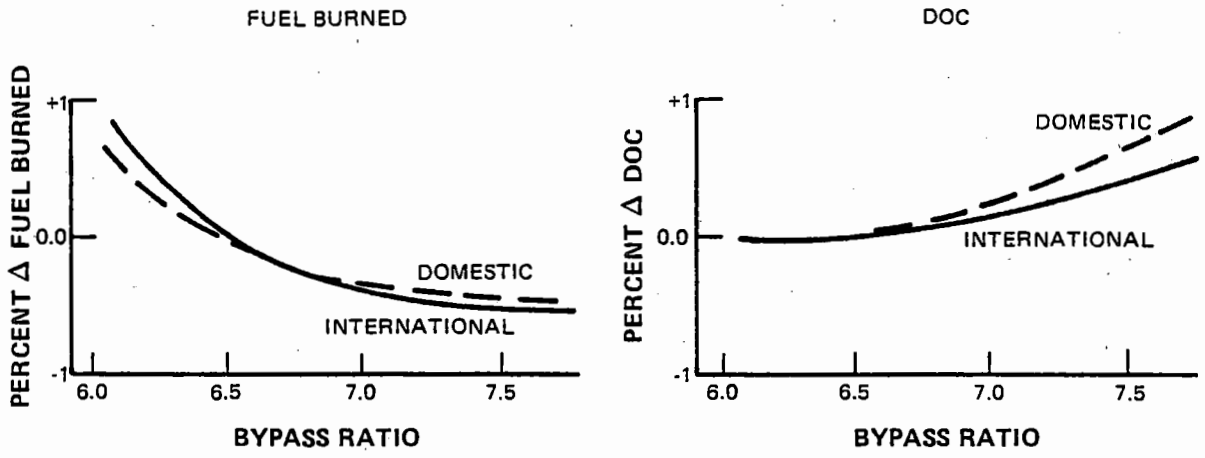

Figure 8 Effects of Bypass Ratio - Direct operating cost minimized at low bypass ratios.

TABLE IX

ENERGY EFFICIENT ENGINE COMPONENT DESIGN
PARAMETERS AND PERFORMANCE
(Maximum Cruise Power, Mach 0.80, 10,700 m (35,000 ft.), unless noted)

Fan	
No. of Blades/Exit Vanes	28/58
Corrected Tip Speed	472 m/sec (1550 ft/sec)
Aspect Ratio	2.7
Shrouds	0
Efficiency ~ O.D. ~ %	87.7
Low Pressure Compressor	
No. of Stages	4
No. of Blades/Vanes	757
Corrected Tip Speed	241 m/sec (790 ft/sec)
Aspect Ratio - Average	2.4
Cx/U	0.7
Efficiency ~ (including fan root) - %	88.3
High Pressure Compressor	
No. of Stages	10
No. of Blades/Vanes	1229
Corrected Tip Speed	405 m/sec (1325 ft/sec)
Aspect Ratio ~ Average	1.7
Efficiency ~ %	88.6
Combustor	
Efficiency ~ %	100
$\Delta P/P$ ~ %	5.5
High Pressure Turbine	
No. of Stages	1
No. of Blades/Vanes	78
Mean Velocity Ratio	0.56
Maximum Rim Speed	527 m/sec (1730 ft/sec)
Maximum AN^2	$3.1X10^7$ m^2Xrpm^2 ($4.8X10^{10}$ in^2Xrpm^2)
Efficiency ~ %	88.2
Turbine Cooling Air ~ % (including LPT)	12.7
Blade Maximum Root Stress	$3.45X10^8$ N/m^2 (50,000 psi)

TABLE IX (Cont'd)

Low Pressure Turbine	
No. of Stages	759
No. or Blades/Vanes	4
Mean Velocity Ratio	0.45
Efficiency ~ %	91.2
ΔP/P Exit Guide Vane ~ %	0.9
ΔP/P Turbine Transition Duct ~ %	0.7
Forced Mixer	
No. of Lobes	12
Efficiency ~ %	85
ΔP/P Hot Side ~ %	0.21
ΔP/P Cold Side ~ %	0.13
Nacelle	
Length-to-Maximum Diameter Ratio	2.27
Highlight Dia.-to-Maximum Diameter Ratio	0.83
Thrust Reverser	Cascade, Fan only
ΔP/P DUCTS ~ %	0.47
ΔP/P Tailpipe ~ %	0.26

- **Low-Pressure Compressor**

The LPC is a four stage design incorporating controlled endwall loss concepts, low-loss airfoils, and increased aerodynamic loadings to provide a large efficiency improvement and fewer numbers of airfoils, while producing more pressure ratio, relative to the JT9D-7A.

- **High-Pressure Compressor**

The HPC is a high 405 m/sec (1325 ft/sec) corrected tip speed, 10 stage design with moderate, 1.7 average aspect ratio blading. The major technology concepts consist of: (a) controlled endwall losses with active clearance control, improved stator cavity design, and grooved endwalls, (b) low-loss airfoil designs, (c) improved performance retention airfoil designs and (d) reduced number of stages via higher tip speeds and increased aerodynamic loading levels. High strength titanium and MERL 76 disk materials permit high rotor speeds and increased compressor exit temperature associated with high overall pressure ratio. Using approximately one-half the number of airfoils and one less stage, this HPC design produces a 3½ point efficiency improvement over the JT9D-7A and produces a 40 percent greater pressure ratio.

- **Combustor**

The combustor is a low emissions, two-stage

Vorbix (vortex burning and mixing) design based on the NASA Experimental Clean Combustor Program, ECCP (NASA CR-135253), and is simplified for improved durability as required for commercial application. An oxide dispersion strengthened (ODS) film cooled louvered liner provides durability at the increased compressor discharge temperatures and pressures associated with a high overall pressure ratio cycle. Thin, aerodynamic diffuser case support struts, located downstream of the diffuser dump, reduce pressure losses and improve combustor durability, relative to a conventional bearing compartment support strut arrangement.

- **High-Pressure Turbine**

The HPT features a one stage design, for large reductions in engine maintenance costs in this high maintenance component, and a high efficiency level made possible with high annulus area, high rotor and rim speeds, active clearance control, and reduced cooling and leakage flows. The HPT is designed for a 0.56 mean velocity ratio, which results in a maximum rim speed of 527 m/sec (1730 ft/sec). A high strength disk material (MERL 76) permits large increases in AN^2 and high aerodynamic efficiency levels. Single crystal airfoil materials, improved effectiveness airfoil cooling, thermal barrier coatings, ceramic outer air seals, improved sealing, and the one stage configuration itself contribute to a greater than 40 percent reduction in total cooling air relative to the JT9D-7A.

- **Low-Pressure Turbine**

The LPT is a 0.45 mean velocity ratio, four-stage design which employs counter-rotation relative to the high spool, reduced Cx/U, low loss airfoils, reduced endwall losses, reduced leakages, and active clearance control for improved performance.

- **Forced Mixer**

The Energy Efficient Engine forced mixer is a convoluted design which consists of 12 lobes arranged around a central plug. The lobes are cut out, or scalloped, on their sides to increase the degree of mixing. The mixer is lightweight titanium, possibly formed in one piece, using a superplastic forming/diffusion bonding process to minimize fabrication cost. The mixer design will also accommodate LPT exit swirl thereby reducing turbine guide vane camber angles and associated turning pressure losses.

The mixed flow exhaust configuration offers both a fuel consumption and DOC benefit, relative to a separate flow exhaust configuration. These benefits are made possible by utilizing a short (0.5 L/D), scalloped mixer with resulting low pressure loss and high mixing efficiency (85 percent), a lightweight mixer design achieved with a high temperature titanium structure, and lightweight composite and honeycomb nacelle structure which minimizes the cowl weight penalty for the longer mixed flow nacelle.

- **Nacelle**

The Energy Efficient Engine nacelle is configured as a long cowl, common exhaust arrangement to accommodate the forced mixer. It is recontoured from current nacelles to reduce drag. Structural nacelle ducts share the engine back-bone bending loads to minimize engine case deflections. "D" shaped ducts, hinged at the top pylon and latched at the bottom, provide complete accessibility to the internal engine components. The nacelle consists of advanced lightweight composite and honeycomb structures and is integrated with the engine structure to reduce weight and engine performance deterioration.

Careful attention to the duct flowpath design reduces nacelle air leakage and duct surface irregularities, and advanced, smooth acoustic treatment is used to reduce wall friction while providing superior noise attenuation

Thrust reverse capability is provided by fan air diverter cascades which are targeted around the nacelle to avoid exhaust gas reingestion by the fan or exhaust flow impingement on adjacent airplane surfaces. The configuration is designed for 50 percent reverser effectiveness which can provide over 35 percent of sea level static take-off thrust within a reverse envelope of 50 to 150 knots.

4.2.3 Technology Requirements

The realization of the Energy Efficient Engine potential is keyed to successful development of the many state-of-the-art advancements in fuel saving concepts included in the preliminary design. Based on preliminary design analysis, critical propulsion technology areas have been identified which need to be translated into acceptable hardware before the fuel savings promise can be realized. These technology areas are discussed along with related benefits in the following paragraphs.

- **Active Clearance Control and Nacelle Load Sharing**

Rotor blades and the engine cases have different rates of thermal expansion which can create large rotor tip-to-case clearances during cruise operation where up to 90 percent of the fuel is consumed. Cruise efficiency can be improved if these clearances, and the resultant leakage, are reduced. The thermal active clearance control system bathes the compressor and turbine cases with hot or cool air to precisely match the case diameter to the rotor tip diameter during cruise while providing sufficient tip clearance to avoid rubs during take-off roll, rotation and climb-out. The result is up to 55 percent reduced blade tip clearance during cruise. The benefit is over a 1.5 percent imporvement in compressor and turbine efficiencies (Figure 9).

Active clearance control is already being introduced into the turbine sections of current operational high bypass ratio turbofan engines as knowledge of case thermal response increases with operational experience. Computerized finite element thermal and structural modeling techniques are being developed for the engine rotor system, engine static structure, and nacelle. Use of these models permits the full use of active clearance control in the compressor and turbine sections for a 3 percent fuel savings.

The Energy Efficient Engine is being designed with short, stiff rotors to minimize rotor deflections under thrust, gravitational, or gyroscopic loads. A load sharing nacelle is included to minimize engine backbone bending which has been identified as a major cause of engine performance deterioration from rub induced blade tip wear.

Load sharing is achieved by utilizing the fan duct walls as structural "beams" in parallel with the engine case "beam." The larger diameter fan ducts are inherently stiffer than the engine cases and will reduce the bending load on the engine cases to keep deflections low.

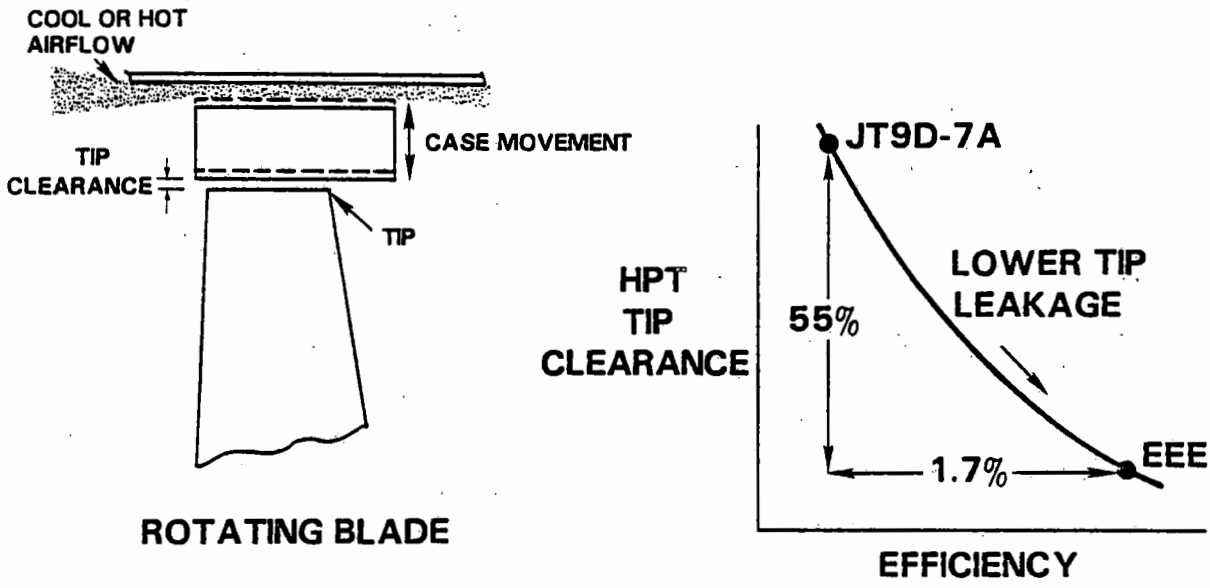

Figure 9 *Active Clearance Control - Reduced blade tip clearances in compressor and turbine can provide a 3 percent fuel savings.*

Ceramic HPT outer air seals, in combination with abrasive blade tips, offer additional protection against rub induced performance loss. In the event of local rubbing, the ceramic seals can wear rapidly with little wear of the treated tip. The predominance of seal wear provides a significantly lower performance penalty for the same degree of interaction as with a non-abradable metal system, which wears off the blade tips.

Testing has demonstrated that an abradable ceramic seal and abrasive blade tip system can withstand a turbine blade rub with the ratio of blade-to-seal volume wear of the ceramic system being significantly less than that of current metallic outer airseal systems. As an example, for a 0.061 cm (0.024 in.) eccentric rub interaction, the actual wear tests show that effectively a 0.033 cm. (0.013 in.) increase in clearance could be expected for a metallic system without abrasive blades. With an abradable ceramic seal and an abrasive blade tip, the effective increase in clearance would only be 0.013 cm (0.005 in.). In addition, because of the insulating characteristics of the ceramic, outer airseal cooling can be reduced to provide a further performance improvement.

Abradable outer airseals are also being developed for the HPC and LPT. A nickel-chrome-polyester system, having performance and durability characteristics comparable to current sintered systems in HPC's, has been successfully sprayed, while a high temperature nickel-chrome-aluminum-Bentonite system has shown considerable performance potential for the LPT. These sprayed abradable systems additionally offer considerable cost advantages over conventional sintered seal systems, while having attractive maintainability features.

In conjunction with active clearance control and improvements in airfoil erosion, distor-

tion and creep and seal and joint leakages, the rigid rotor systems and load sharing are projected to reduce the long term 4000 hour TSFC deterioration to approximately half that of current high bypass ratio engines (Figure 10). The results of this study indicate that these two technologies, via their impact on controlling blade tip clearances, are the largest contributors to reduced deterioration of all the influencing factors. (Engine performance deterioration is described in detail in Appendix C of this report.) Analyses leading to this projected improvement were based on JT9D operational tip clearance experience that has been correlated with configurational characteristics of the JT9D to determine the magnitude of flight loads in the take-off and cruise modes.

An analytical rotor-frame configurational model of the Energy Efficient Engine was subjected to these operational flight loads to estimate tip clearance deterioration effects with time. This model accounted for the improvements projected in cowl load sharing, stiff rotor construction, and stiff cases and frames. These calculated clearance effects were then combined with clearance changes estimated for known additional phenomena (e.g. tolerances, bearing clearances, etc.) and judged for unanticipated problems (e.g. compressor surges, etc.). The sum of these three categories then represents the net clearance deterioration relative to the initial goal clearances. Active clearance control was used in these analyses to provide the initial opened-

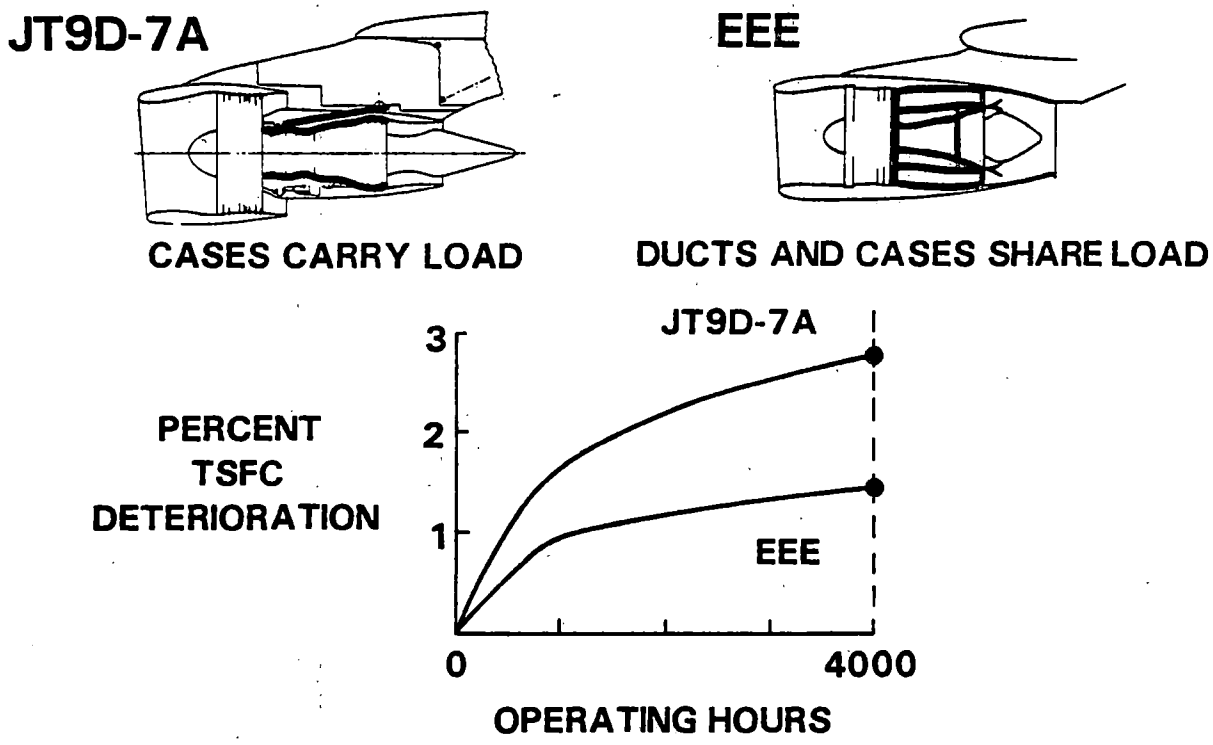

Figure 10 Load Sharing Nacelle - Nacelle load sharing design retains fuel savings over long-term operation.

up goal clearances in the takeoff and climb modes and the closed-down goal clearances for cruise operation. The impacts of net tip clearance deterioration on component efficiency and flow capacity were estimated, and the resulting increase in fuel consumption was determined to be only 0.8% for the selected engine configuration after 4000 hours of operation.

- **Advanced Internal Aerodynamics**

Many new aerodynamic concepts have recently been analytically or empirically identified which, in total, can produce major component efficiency improvements. The improvements involve both better airfoil performance and lower losses in the endwall regions of the gaspath.

Titanium fan blades on operational high bypass ratio turbofan engines require interblade shrouds to limit blade vibration stress to an acceptable level. Shrouds reduce fan efficiency by upsetting the airflow through the fan. Fan efficiency can be increased over 2 percent by eliminating shroud induced aerodynamic losses shown in Figure 11. Vibration can be controlled in shroudless blades by elongating blade chord 50 percent, but this increases the fan assembly weight. One way to reduce weight is to hollow-out the titanium blades.

Superplastic forming manufacturing techniques have recently been developed to mold titanium into complex shapes, at low cost. Superplastic forming is especially suitable to

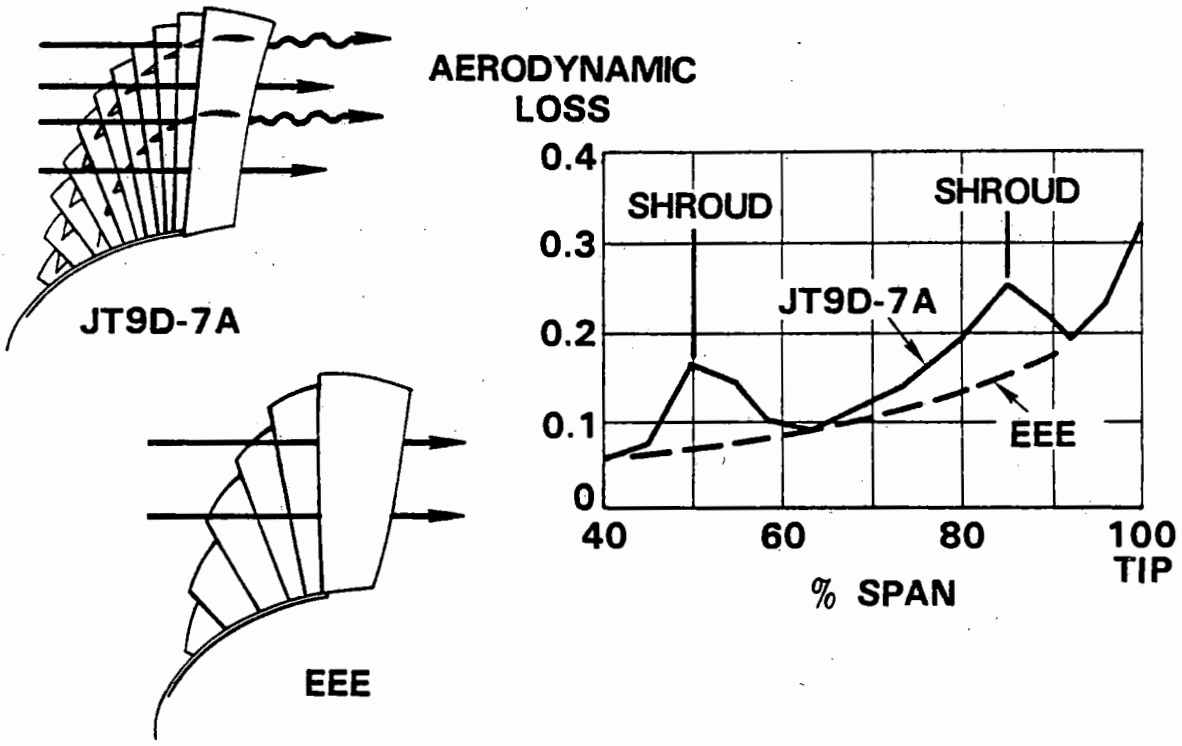

Figure 11 Shroudless Fan Blades - Shroudless fan blades have the potential for a 2 percent efficiency improvement.

titanium, which has the capability of being elongated 300 percent without local thinning under controlled temperature and strain rate. Superplastic forming can be combined with diffusion bonding techniques so that two titanium pieces can be mated along their edges in a heated and pressurized die. The pieces simultaneously bond along their edges and expand into the die to complete the fabrication process.

Through recent developments in computer analysis techniques, increased freedom in compressor airfoil shape selection is also being exploited. Multiple-arc and supercritical compressor airfoil contours have been identified which operate transonically at 15 percent higher relative air Mach numbers than the JT9D-7A with the same efficiency. The airfoils are also capable of carrying higher aerodynamic loads at peak efficiency. This ability is being used to reduce compressor and turbine airfoil count and to reduce the through-flow gas velocity to improve efficiency.

Compressor and turbine research tests have identified a significant efficiency loss caused by flowpath air recirculating into and out of inner engine cavities beneath blade and vane root shrouds. In the turbine, vane inner shroud forward projections overlapped by blade shrouds were tested to isolate these cavities from the flowpath. Efficiency capability increased by 1.0 percent. Compressor rig testing has shown both cavity size and shape to significantly impact compressor efficiency. As a result of the tests, small, smooth, low leakage cavity designs with the potential for improving compressor efficiency by 0.5 percent are becoming possible.

These aerodynamic improvements, taken together, were estimated to reduce the amount of fuel burned by 5 percent.

- **Forced Exhaust Mixer**

It has long been realized that engine thrust output could theoretically be increased without burning more fuel. This output is achieved by forcefully mixing the fan discharge air with the turbine exhaust gases prior to discharge through a common nozzle. This approach could provide substantial fuel savings but has not been used in the past because the theoretical gains were offset by parasitic losses and weight associated with forced mixing.

Mixing now appears more attractive for conserving fuel as a result of recent tests of forced mixers that successfully combined high mixing efficiency, low parasitic loss, and short length. These tests include model and full scale tests of JT8D mixers and model tests of high bypass ratio (5 to 7) mixers. The results of these tests were used to arrive at the Energy Efficient Engine mixer predictions. A portion of the JT8D mixer model test results from the FAA sponsored "Internal Mixer Investigation for JT8D Engine Jet Noise Reduction" program was also available (FAA RD-77-132).

Much remains to be accomplished before deciding on the exact mixer geometry and its ultimate performance potential. Model tests of various candidate geometries are required as an important step before finalizing a design approach and deciding on the mixer application to future powerplants. Integration of the long nacelle with the aircraft without incurring increased interference drag is also a big step in realizing the 3 percent fuel savings potential identified in this study program (Figure 12) and discussed in Appendix B, Section 5).

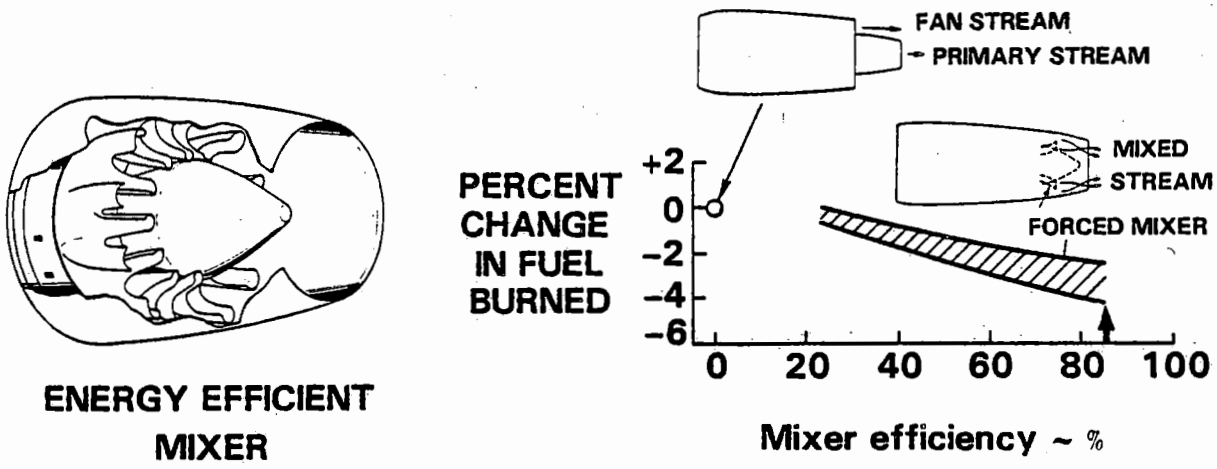

Figure 12 Advanced Exhaust Mixer - Shorter mixer, possible with advanced technology, reduces losses and weight for a 3 percent fuel savings potential.

- **High Pressure Ratio**

In order to take full advantage of the potential 15 percent in fuel savings technology, a compression system pressure ratio which is 50 percent higher than that of the JT9D-7A will be required (Figure 13). Higher pressure ratio was shown to provide significant fuel savings potential in the low energy consumption turbofan study. The question became how to produce the additional pressure with the same number of stages as the JT9D-7A to hold down cost. The straightforward solution was to use 25 percent higher compressor average diffusion factor combined with 28 percent higher compressor blade speeds than the JT9D-7A.

The higher airfoil loading capability derives from increased understanding of compressor design variables. Higher rotor speeds permit higher airfoil loadings. With a given compressor geometry, the peak pressure ratio increases with wheel speed. However, if the number of compressor blades is reduced, the achievable pressure ratio is also reduced. Thus higher speed can be traded for increased stage pressure ratio, or alternatively, for reduced airfoil count. The Energy Efficient Engine HPC, compared with the JT9D-7A in Figure 14, represents a balance between increased stage pressure ratio and lower airfoil count. The lower compressor blade count can give a 12 percent reduction in compressor module maintenance cost.

- **Advanced Materials**

The high pressure ratio and high speed, high spool rotor system dictated the use of advanced, higher strength titanium and nickel base alloy compressor and turbine disks, single crystal high pressure turbine airfoils, and a higher temperature combustor liner. High-strength blade and disk alloys are presently being developed to permit safe operation at the higher speeds and temperatures of the Energy Efficient Engine. A single crystal nickel superalloy (MERL 200) for blades and a nickel superalloy (MERL 76) for the disk permit a 55 percent higher turbine rim speed. This higher speed permits the use of a single stage turbine with an attendant 80 percent total blade and vane count reduction in relation to the 2-stage JT9D-7A turbine (Figure 15). This parts reduction can result in a 30 percent lower turbine maintenance cost which is a major contributor to the overall engine maintenance cost.

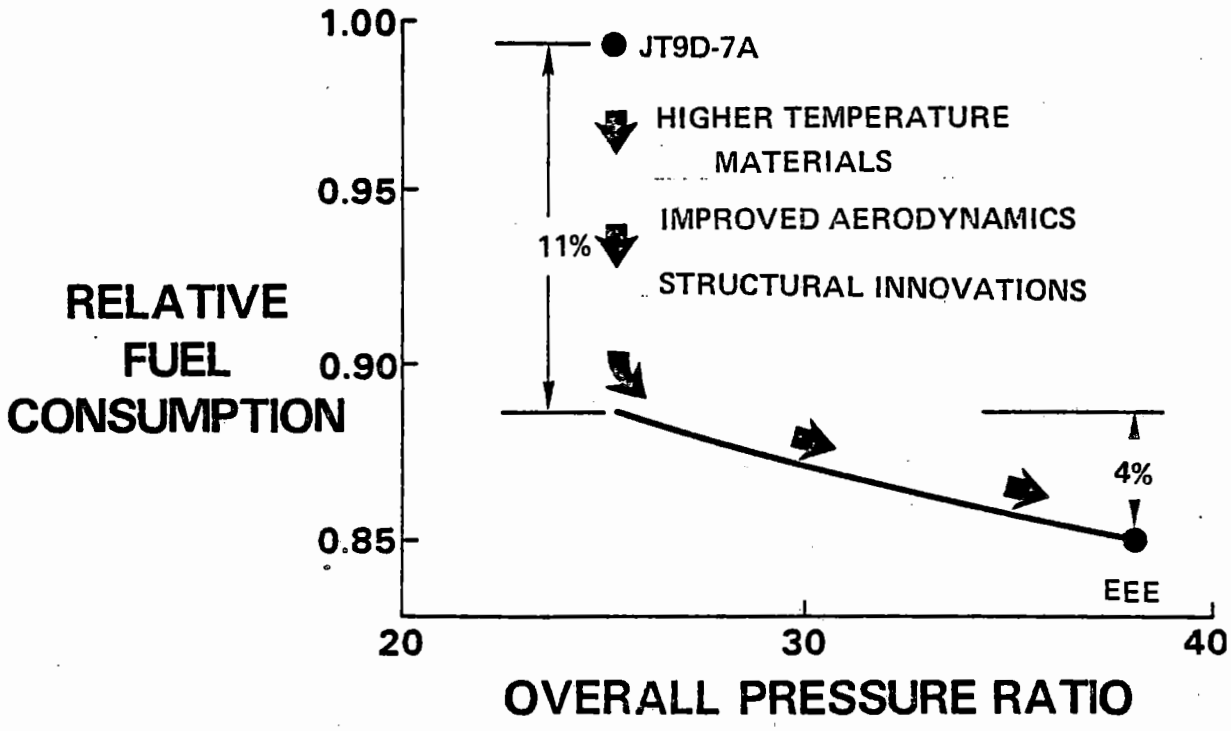

Figure 13 High Overall Pressure Ratio - High pressure ratio made possible by advanced technology provides an additional 4 percent fuel savings potential.

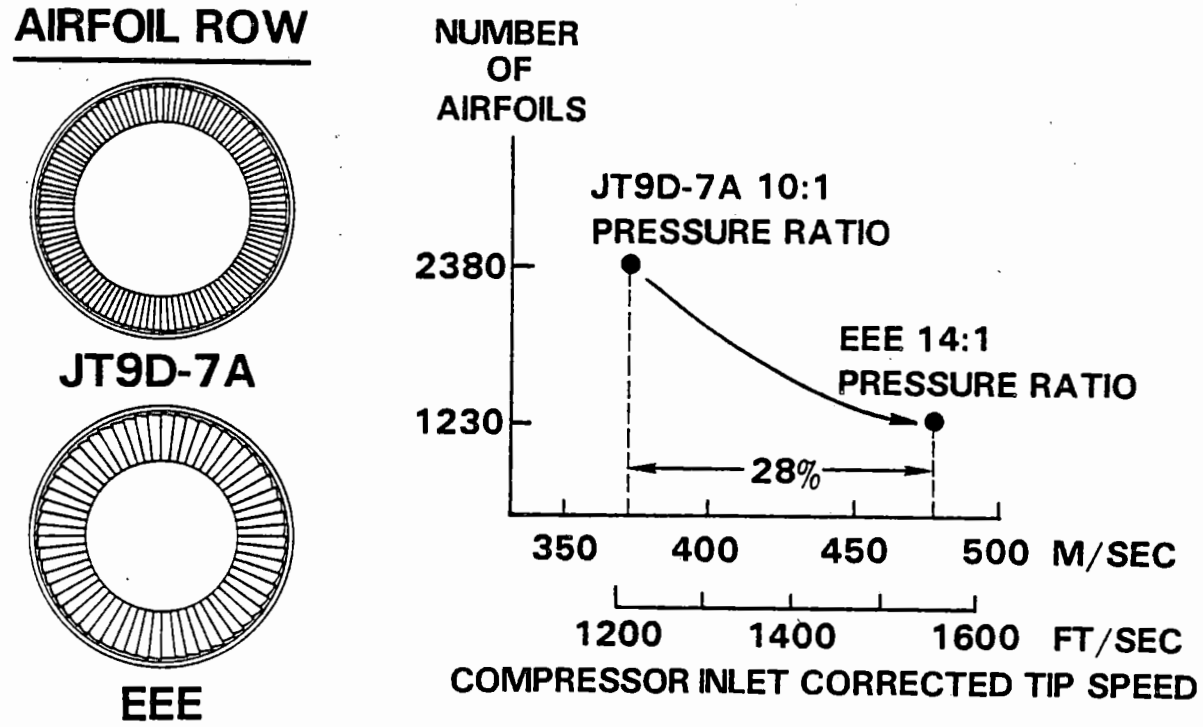

Figure 14 High Speed Compressor - 48 percent fewer airfoils result in a 12 percent lower compressor maintenance cost.

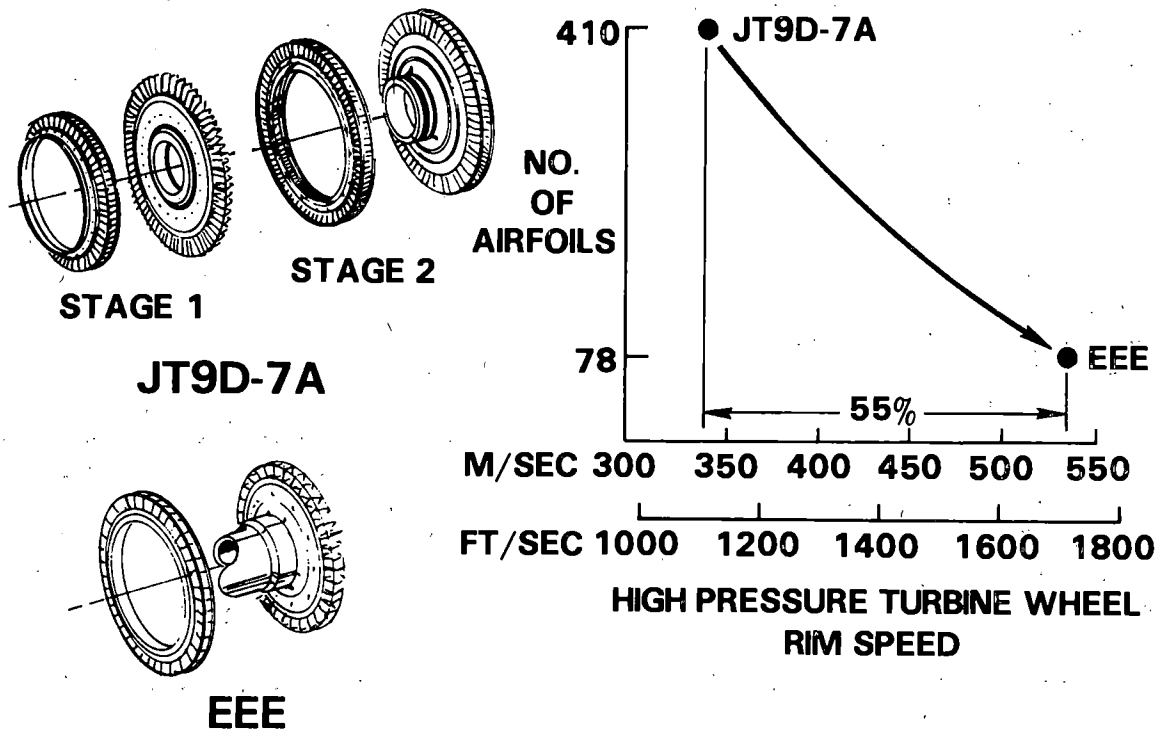

Figure 15 High Work Turbine - High speed, single stage high pressure turbine, with 80 percent fewer blades and vanes, has potential for a 30 percent lower module maintenance cost.

The HPT will also capitalize on improved, higher strength blade and disk materials by including design changes relative to current configurations that will increase aerodynamic efficiency to the point where a single stage is economically more desirable than a two-stage configuration. Past studies on single stage turbines have shown that the best performance can be achieved in a configuration with a high rim speed and long blades (high AN^2) for low through flow gas velocity. These aerodynamic requirements translate directly into the structural parameters of blade stress and blade attachment stress. With advanced materials, the aerodynamic advancements can improve HPT efficiency by 1.0 percent.

High temperature titanium mid-stage disks and MERL 76 aft stage disks also allow operation at the higher speeds and increased temperature levels that are required with the high overall pressure ratio in the compressor.

Current burner liners presently operate at about a 870°C (1600°F) maximum metal temperature. The Energy Efficient Engine burner liner was calculated to require a metal temperature capability of 1040°C (1900°F) to permit 65 percent of the inlet air to be used for emissions and exit temperature profile control, leaving a maximum of 35 percent for liner cooling. An advanced oxide dispersion-strengthened (ODS) material, which has the required operating temperature capability, is being considered as the primary design approach for the Energy Efficient Engine.

Advanced materials also offer benefits in the cooler sections. Various Pratt & Whitney Aircraft engine studies have shown significant weight advantage for the use of titanium alloys for LPT airfoils resulting from a 47 percent lower density compared with conventional nickel based turbine alloys. However, existing titanium alloys have inadequate creep or rupture strengths (even with the stress reduction attendent with the reduced density) to produce commercial airfoil lives in the high stress/high temperature environment which exists in LPT's.

Titanium-aluminide, however, has creep and rupture strengths which are increased relative to the strengths of conventional titanium airfoil alloys, such as PWA 1209 or 1214, in the operating temperature range of the LPT. Titanium-aluminide, as projected, has adequate strength for use in the third and fourth LPT stages. The use of titanium-aluminide there could reduce engine weight by 57 kg (125 lbs).

- **Electronic Fuel Control**

Current hydromechanical engine fuel controls are bulky. The JT9D-7A requires five control components to manage engine operation. Advances in digital electronic technology now make electronic fuel controls a practical alternative. An advanced, full authority digital electronic control, consisting of only two major components, a computer and a flow metering unit, will perform all of the necessary functions (Figure 16). This control will perform 60 percent more functions than the current hydromechanical controls. This additional capability can be used to have the unit continuously monitor the condition of the engine and give early warning of problems or situations which require maintenance action.

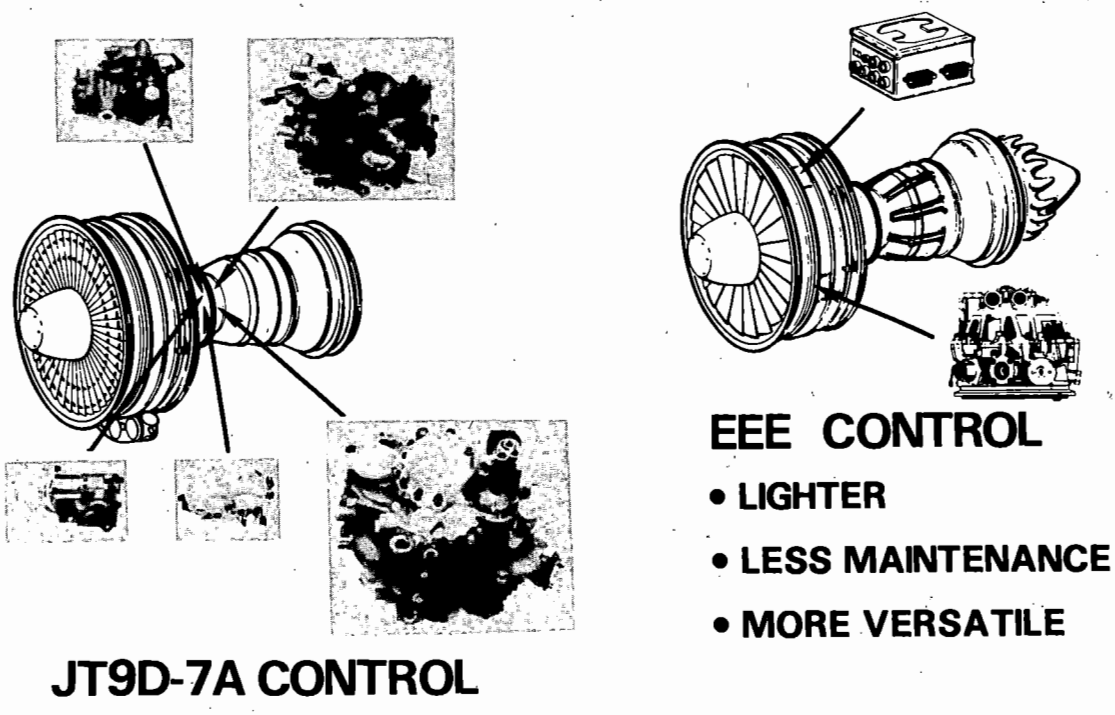

Figure 16 Electronic Fuel Control - 2 major electronic control units are equivalent to 5 hydromechanical components.

The payoff is a 33 percent reduction in control system weight and a 44 percent reduction in control maintenance cost. In-flight shutdowns due to control problems can be reduced by 80 percent. This control approach may also save fuel by eliminating the need for periodic ground run trimming of the engine and control.

- **Acoustically Treated Lightweight Nacelle**

The nacelle of the future will require the latest lightweight composite materials and lightweight structures to reduce weight by 15 percent relative to current configurations (Figure 17). Materials for the various applications within the nacelle will be selected from filament materials (boron, graphite, Kevlar and glass), matrix materials (epoxy, polyimide and aluminum), and composite honeycomb.

Stricter noise rules can be expected in future years. A noise goal of FAR 36 (1969) minus 10 EPNdB was established by NASA for this study. A fully treated nacelle, fan noise 3 EPNdB lower than present, and advanced (presently undefined) acoustical treatment to attenuate fan noise by an additional 2 EPNdB are needed to meet this goal. The required noise reduction might be achieved by 1990 by directing acoustic research to-

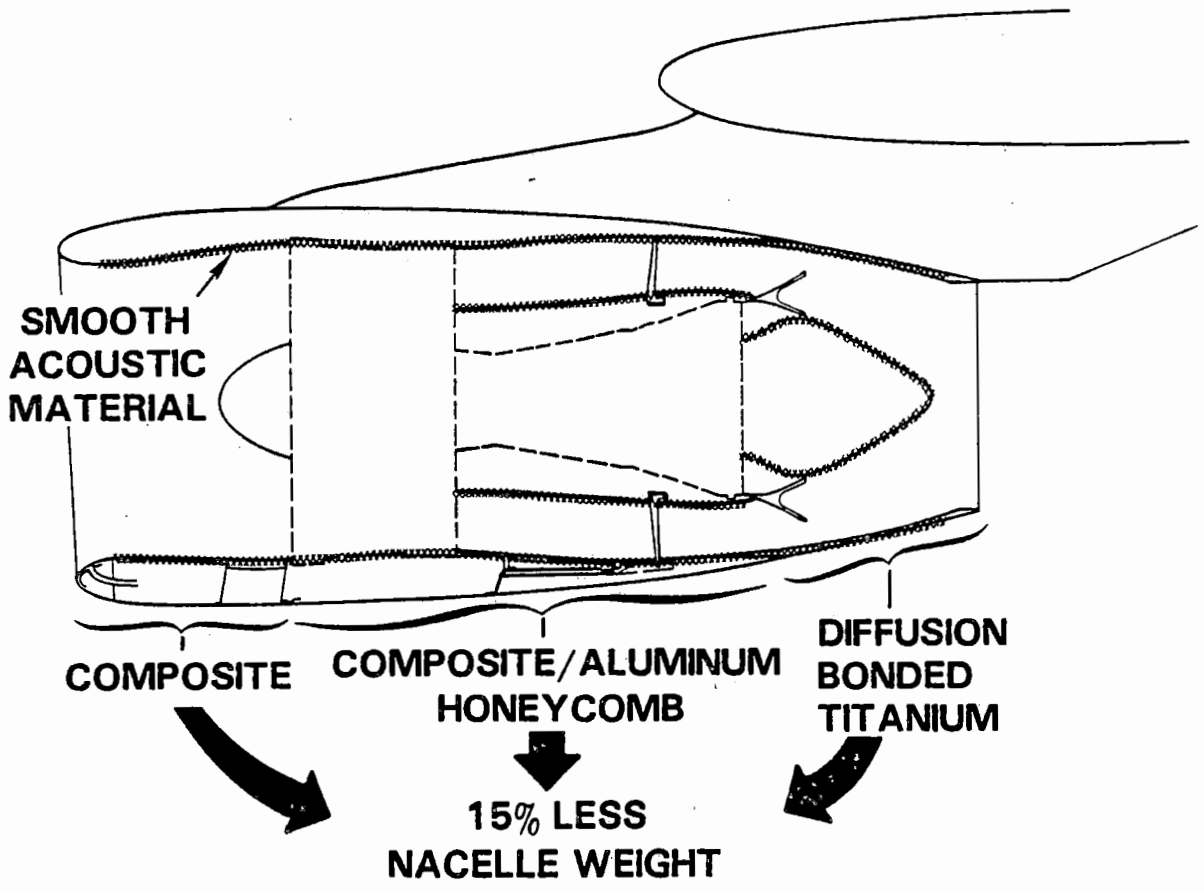

Figure 17 Acoustically Treated Lightweight Nacelle - 15 percent less weight and FAR 36(1969)-10 EPNdB noise may be possible through use of composites and improved acoustical technology.

ward the definition of improved, low noise fan blading shapes, and by developing segmented liners with improved tone and broadband noise attenuation capabilities.

The results of this study indicate that the more recent FAR 36 (amended 1977) rules can be fully met with currently available acoustic technology.

- **Vorbix Combustor**

The low emissions design derives from a combustor developed in the NASA-sponsored Experimental Clean Combustor Program (ECCP) which demonstrated significant reductions in exhaust emissions. It represents a major departure from conventional combustors in commercial engines. Two in-line burning zones are used. The front, or primary zone, is designed to the specific requirements of reduced carbon monoxide and unburned hydrocarbon emissions at very low power settings near idle. The aft, secondary zone is designed to control NO_x. Swirlers are used to thoroughly mix the fuel and air (leading to the acronym Vorbix for vortex burning and mixing). The short length of the secondary zone minimizes the residence time at high temperature to cut NO_x generation in half at the higher power settings.

The Vorbix concept has been tested in the JT9D as experimental hardware. The Energy Efficient Engine emissions predictions were derived from the results of these tests by using emissions indices which correct for the different burner thermodynamic conditions with the higher pressure ratio cycle. Development margin and production tolerances were included in the estimates. The estimated EPA parameters are compared with the current JT9D-7A production combustor and the 1981 regulations in Figure 18. Low power emissions were estimated to meet the regulations. NO_x generation, estimated to be 43 percent lower than the JT9D-7A, needs to be reduced by an additional 30 percent to meet 1981 regulations. A technique to provide the additional reduction has not yet been identified.

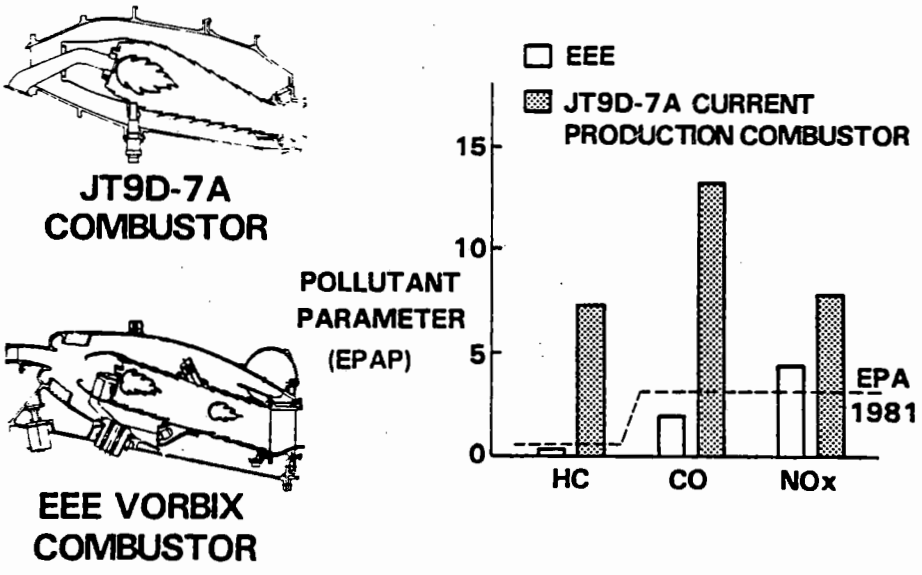

Figure 18 Vorbix Combustor - Emissions reductions from 43 to 96 percent are projected with the two-stage vorbix combustor concept.

The Energy Efficient Engine combustor design concept is simplified substantially from the Experimental Clean Combustor Program configurations. The throat between the two zones was removed and replaced with less costly and more maintainable straight inner and outer wall sections. The number of fuel nozzles were reduced 20 percent and clustered in groups of three to limit fuel supply tube case penetrations to 24 circumferential locations. Substantial additional development work is needed to verify the emissions characteristics of this more practical burner before it can be considered for commercial service.

4.3 ENERGY EFFICIENT ENGINE CONFIGURATION SELECTION

The seven engines directly involved in the configurational selection are listed in Table X by study designation, major cycle parameters, and installation type. Overall pressure ratio

TABLE X

ENGINES INCLUDED IN CONFIGURATION SELECTION PROCESS

Configuration	Study Designation	BPR/FPR/OPR/RIT °C/RIT °F*
Task I/II Studies leading to choice of mixed exhaust.		
• Mixed exhaust, direct drive fan, 2 stg HPT	STF505M-1	7/1.65/38.6/1210./2210.
• Separate exhausts, ¾ length fan cowl, dir. drive fan, 2 stg HPT	STF505-1 (¾)	7/1.74/38.6/1210./2210
• Separate, short fan cowl, dir. drive fan, 2 stg HPT	STF505-1 (short)	7/1.74/38.6/1210./2210.
Task III/IV Studies leading to choice of direct-drive fan and one-stage HPT.		
• Direct drive fan, 1 stage HPT	STF505M-7	6.5/1.74/38.6/1204./2200.
• Direct drive fan, 2 stg HPT	STF505M-9	6.5/1.74/38.6/1204./2200.
• Geared fan, 1 stg HPT	STF495M-4	9/1.52/38.6/1204./2200.
• Geared fan, 2 stg HPT	STF495M-5	9/1.52/38.6/1204./2200.

*Bypass ratio/fan pressure ratio/overall pressure ratio/turbine rotor inlet temperature °C/turbine rotor inlet temperature °F @ 10,700M (35,000 ft.), Mach 0.8 Cruise design point.

and turbine rotor inlet temperature were held constant in order to isolate the effects of low pressure spool parameters. The fan pressure ratio and bypass ratio chosen for each of the engines considered trades that exist between increased propulsion efficiency and higher propulsion system weight and cost associated with larger diameter, higher bypass ratio fans. These trades differed for direct-drive and geared fans, which accounts for the differences between their respective bypass ratios.

4.3.1 Considerations Leading to Mixed Exhaust Configurations Selection

Comparison of a mixed exhaust engine, a low noise separate exhaust engine, and a lightweight separate exhaust engine provided sufficient information to permit selection of the mixed exhaust configuration. Conceptual propulsion system cross-sections of the mixed (STF505M-1) and low noise separate exhaust (STF505-1(¾)) engine configurations are included at the rear of this report as fold-out drawings (Figures 24 and 25).

Both engines consisted of the same high spool components which were defined through regression analysis of many different configurations, followed by more refined analysis of several attractive approaches. A ten-stage HPC was selected to produce an 18:1 pressure ratio at a 445 m/sec (1460 ft/sec) inlet corrected tip speed. The combustor was conceptually designed with two combustion zones for low emissions. A two-stage HPT with a loading coefficient of only 1.2, was selected for high efficiency.

The STF505-1 engine low-pressure spool consisted of a 7 bypass ratio, 1.74 pressure ratio fan rotating at 472 m/sec (1550 ft/sec) tip speed and a three-stage LPC driven by a 2.5 loading coefficient, low speed, 5-stage LPT.

With the STF505M-1 mixed exhaust engine, fan pressure ratio was decreased to 1.65 to equalize turbine exhaust and fan exhaust total pressures for efficient mixing. The rotors were supported by seven main bearings housed in four compartments as a first-pass approach to minimizing rotor deflections and rubs under flight induced loads.

Geometrically similar, 0.55 length-to-maximum diameter ratio inlets and forward fan cowl sections were used for all of the installations. The two separate exhaust engines differed in aft fan cowl length to evaluate performance, weight, cost, and noise trades. The three-quarter length fan cowl extended aft to the turbine exhaust case flange plane to produce a fan discharge duct length-to-height ratio of 6 for low noise. The short, lightweight fan cowl installation provided a fan discharge duct length-to-height ratio of approximately 2. Full acoustical treatment was added to each of the installations to maximize the noise absorption area.

The STF505M-1 and STF505-1 (¾) engines were evaluated by Boeing, Douglas, Lockheed and Pratt & Whitney Aircraft. The STF505-1 (short) was also included in the Pratt & Whitney Aircraft studies. The study results indicated that cruise TSFC, fuel burned, DOC, and noise (listed in Table XI) were the important considerations in choosing the engine exhaust system. The mixed exhaust engine was found to be superior to both of the separate exhaust configurations in each of the evaluations. The engine characteristics which were responsible for these trends are related to TSFC, fuel burned, DOC, and noise in the following paragraphs.

TABLE XI

CONSIDERATIONS LEADING TO MIXED EXHAUST SELECTION

			Mixed Exhaust	Separate Exhausts	
Engine Study Designation			STF505M-1	STF505-1 (¾)	STF505-1 (Short)
Fan Cowl Configuration			Full Length	¾ Length	Short
Installed Cruise TSFC kg/hr/N(lb_m/hr/lb_f) (10,700m/35,000 ft/MO.8)			0.0567 (0.555)	0.0588 (0.576)	0.0585 (0.573)
Average Stage Length Fuel Burned ~ kg					
Boeing	–	Domestic	7850.	8023.	--
	–	International	16562.	17098.	--
Douglas	–	Domestic	15283.	15846.	--
	–	International	22948.	23905.	--
Lockheed	–	Domestic	16231.	16702.	--
	–	International	37432.	38961.	--
P&WA	–	Domestic	9305.	9717.	9560.
	–	International	31058.	32549.	31940.
Relative Average Mission DOC (9.2 ¢/l, 35¢/gal. domestic fuel; 11.9¢/l, 45¢/gal. international fuel)					
Boeing	–	Domestic	1.000	1.004	--
	–	International	1.000	1.015	--
Douglas	–	Domestic	1.000	1.014	--
	–	International	1.000	1.019	--
Lockheed	–	Domestic	1.000	1.010	--
	–	International	1.000	1.022	--
P&WA	–	Domestic	1.000	1.016	1.001
	–	International	1.000	1.023	1.006
Total Maximum Noise rel. to FAR (1969) - ΔEPNdB (untraded & W/O cutback)					
Boeing	–	Domestic	-8.3	-7.9	--
	–	International	-8.1	-7.6	--

TABLE XI (Cont.'d)

			Mixed Exhaust	Separate Exhausts	
Douglas	–	Domestic	-11.5	-11.0	--
	–	International	-11.4	-10.9	--
Lockheed	–	Domestic	-10.8	-9.8	--
	–	International	-11.6	-10.5	--
P&WA	–	Domestic	--	--	--
	–	International	-9.8	-9.2	-8.4

4.3.1.1 Thrust Specific Fuel Consumption (TSFC)

Examination of the TSFC differences identified the three primary causes shown in Table XII. The TSFC advantage of the short nacelle was the result entirely of the reduced pressure loss in the shorter fan duct. The mixed exhaust engine total TSFC advantage, although equal in magnitude to the mixing benefit alone, consisted of two other counter-balancing differences. Internal engine changes, including the lower fan pressure ratio and modified ducting, increased TSFC by 0.6 percent exclusive of the mixing benefit. An unexpected trend in isolated nacelle drag among the three configurations then became important in determining the relative TSFC's.

TABLE XII

CAUSES FOR TSFC DIFFERENCES BETWEEN SEPARATE AND MIXED EXHAUSTS

Configurational Differences	TSFC Effect % STF505M-1	STF505-1 (¾)	STF505-1 (short)
Internal Changes (FPR, efficiences, press. losses)	+0.6	Baseline	-0.5
Isolated Nacelle Drag	-0.6		0
85% Efficient Mixing	-3.6		0
TOTAL	-3.6	Baseline	-0.5

The long mixed exhaust nacelle friction drag was estimated to be approximately 17 percent lower than either the short or ¾-length nacelles. The friction drag build-up was broken down into the individual nacelle components, as shown in Figure 19, to understand the drag differences. The drag predictions shown in the figure were based on the standard techniques of multiplying dynamic pressure, a friction coefficient, and a wetted area together. The friction coefficient, C_F, accounts for Reynolds number effects and surface roughness. Examination of the drag elements indicated that although the fan cowl drag of the separate exhaust configuration was substantially lower than the mixed exhaust cowl, high scrubbing jet velocities on the afterbody, pylon, and plug caused a build-up to a total drag level substantially above the mixed exhaust system. A similar anlaysis of short and three-quarter length fan cowl nacelles showed friction drag to trade-off exactly with pylon and afterbody scrubbing, so that total drag remained unchanged.

The sensitivity of the mixed exhaust engine TSFC to mixer efficiency is compared with the two separate exhaust engines in Figure 20. On an isolated nacelle basis, only a 10 percent mixing efficiency is needed for the mixed exhaust engine TSFC to surpass both of the separate exhaust configuration capabilities.

4.3.1.2 Fuel Burned

Fuel burned is affected principally by TSFC and, to a lesser extent, propulsion system

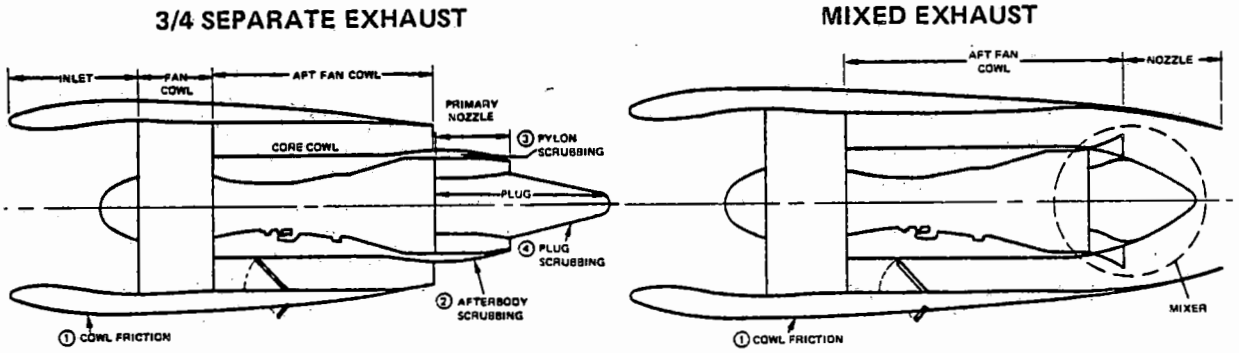

$DRAG = Q \times C_F \times A_{WETTED}$

SEPARATE EXHAUST DRAG ELEMENT:	①	②	③	④	TOTAL
Q/Q MIXED REF.	1.00	2.38	2.38	1.55	--
C_F/C_F MIXED REF.	1.04	1.12	1.12	1.27	--
A_{WETTED}/A_{WETTED} MIXED REF.	0.805	0.077	0.018	0.039	--
DRAG/DRAG MIXED REF.	0.837	0.205	0.048	0.077	1.167

Figure 19 Nacelle Friction Drag Build-up - Mixed exhaust and 75 percent length separate exhaust nacelles.

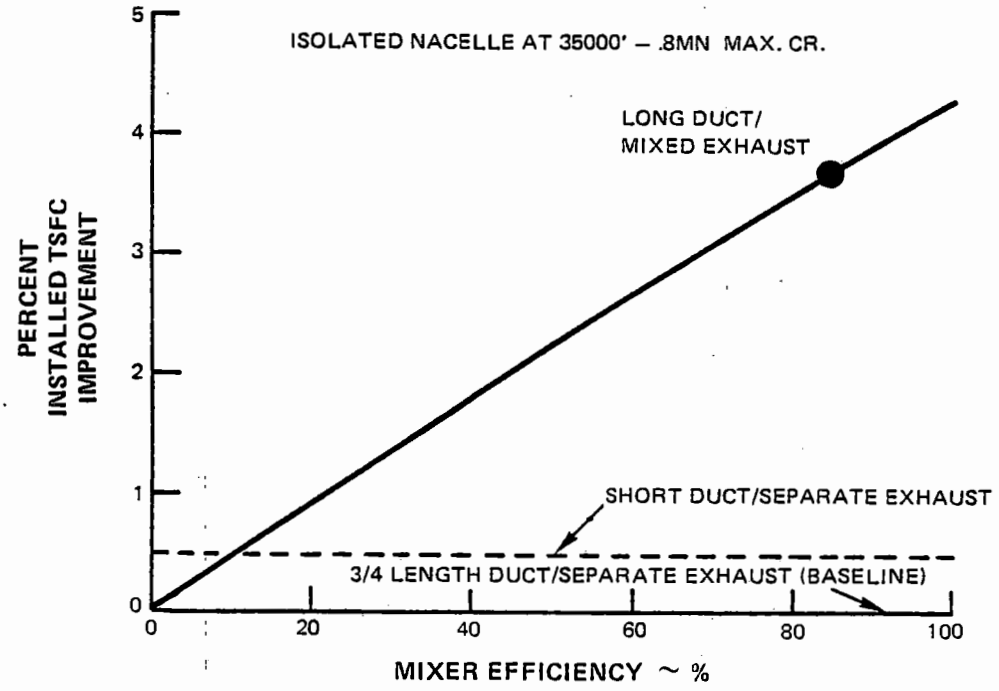

Figure 20 Sensitivity of Thrust Specific Fuel Consumption to Mixer Efficiency

weight. However, the weight differences among the separate and mixed exhaust engines were large enough to become a significant factor in establishing fuel burned trends. The Pratt & Whitney Aircraft study results for the three engines, illustrating these effects, are shown in Table XIII[1]. Examination of the table shows that weight differences between the two long cowl installations and the short, separate exhaust installation accounted for approximately 1 percent in fuel burned.

The weight breakdowns for the three nacelles, listed in Table XIV, were scaled to the same nacelle diameter to show where the weight differences occurred. The mixed exhaust and ¾-length nacelles weighed the same exclusive of the mixer. This similarity is a result of assuming advanced lightweight materials in the nacelles. The mixed exhaust nacelle section was assumed to be of titanium honeycomb structure weighing 5.13 kg/m² (10.5 lbm/ft²), while the separate exhaust system's hot core discharge temperatures dictated steel primary nozzles and plugs which weighed 18.6 kg/m² (3.8 lbm/ft²). The mixer was also assumed to be fabricated from advanced, high temperature titanium. Clearly, the fuel savings potential shown with mixing relied heavily on the availability of advanced nacelle and mixer materials.

4.3.1.3 Direct Operating Cost

Aircraft DOC's with the three configurations reflected the fuel burned trends. The only major additional effect resulted from differences in nacelle prices which were set at $284/kg ($129/lb) for each of the installations. The effects of TSFC, weight, and nacelle price are related with DOC in Table XV.

(1) Study results in Table XIII, XIV, and XV are based on Pratt & Whitney Aircraft trade factors for advanced aircraft. Different aircraft definitions could result in appreciable variations in engine weight and drag effects.

TABLE XIII

RESULTS OF FUEL BURNED STUDIES – SEPARATE AND MIXED EXHAUSTS[2]

	STF505-1 (¾)	STF505-1 (short)	STF505M-1
Installed Cruise TSFC - kg/hr/N (lbm/hr/lb_f)	0.0588 (0.576)	0.0585 (0.573)	0.0567 (0.555)
Propulsion System Weight[1] - kg	5226.	4735.	5252.
Domestic Airplane - Average Mission			
TSFC effect	0.	-0.69	-4.29
Weight effect	0.	-0.92	+0.05
TOTAL FUEL EFFECT		-1.61	-4.24
International Airplane - Average Mission			
TSFC effect	0.	-0.74	-4.64
Weight effect	0.	-1.13	+0.06
TOTAL FUEL EFFECT		-1.87	-4.58

(1) Cruise Thrust = 38,000 N (8520 lb_f)
(2) Results based on P&WA aircraft trade factors

TABLE XIV

NACELLE COMPONENT WEIGHT BREAKDOWN – SEPARATE AND MIXED EXHAUSTS

	STF505M-1	STF505-1(3/4)	STF505-1(short)
Maximum Nacelle Diamter cm(in)	272. (107.)	272. (107.)	272. (107.)
Cruise Thrust - N (lb)	35,000 (7825.)	34,000 (7616.)	34,200 (7661.)
Nacelle Component Weight - kg			
Inlet	281.	281.	281.
Fan Cowl & Fan Nozzle	834.	641.	233.
Core Cowl & Primary Nozzle	61.	201.	201.
Primary Nozzle Plug	–	58.	58.
Fan Thrust Reverser	293.	293.	293.
Mixer	68.	–	–
TOTAL NACELLE WEIGHT	1537.	1474.	1066.

TABLE XV

RESULTS OF DOC STUDY – SEPARATE AND MIXED EXHAUSTS (2)

	STF505-1 (3/4)	STF505-1 (short)	STF505M-1
Installed Cruise TSFC - kg/hr/N	0.0588 (0.576)	0.0585 (0.573)	0.0567 (0.555)
Propulsion System Weight(1) - kg	5226	4735	5252
Nacelle Price(1) - M$	0.472	0.339	0.457
Δ DOC - % (Average Mission)			
Domestic Airplane (9.2c/1, 35c/gal. fuel)			
TSFC effect	0	−0.24	−1.48
P.S. weight & price effect	0	−1.21	−0.13
Other	0	−0.07	+0.03
TOTAL	0	−1.52	−1.58
International Airplane (11.9c/1, 45c/gal. fuel)			
TSFC effect	0	−0.36	−2.25
P.S. weight & price effect	0	−1.27	−0.14
Other	0	−0.06	+0.07
TOTAL	0	−1.69	−2.32

(1) Cruise Thrust = 38,000 N (8520 lbs)
(2) Results based on Pratt & Whitney Aircraft trade factors

DOC reduction with the short fan cowl installation was almost entirely a result of the lighter, less expensive nacelle. The DOC benefit with mixing was almost entirely a result of the lower TSFC. Differences in base engine weight, price and maintenance costs affected the DOC comparison by less than 0.1 percent because of the similarity of construction and design details for all three engines.

4.3.1.4 Noise

Maximum noise levels of all three engines were estimated to be the same within 1.5 EPNdB. Engine noise alone ranged over a broader EPNL range, but the increasing dominancy of airframe noise at approach caused this measurement station both to become more critical than takeoff and to narrow the

EPNL spread. This can be seen in Table XVI which summarizes the Pratt and Whitney Aircraft noise study in the three engines.

These results indicate that engine noise reduction capability is reaching the point where airframe noise is becoming the limiting source at approach. In terms of engine noise, the additional aft fan noise attenuation possible with the 3/4-length fan cowl was estimated to provide about a 1 EPNdB lower noise. The mixed exhaust lower pressure ratio, lower tip speed fan emitted an additional 0.8 EPNdB lower noise at approach.

At takeoff, jet noise became dominant for the long nacelle installations causing both to

TABLE XVI

RESULTS OF INTERNATIONAL AIRCRAFT NOISE STUDY – SEPARATE AND MIXED EXHAUSTS

	STF505M-1	STF505-1 (3/4)	STF505-1 (short)
FAR (1969) Measurement Station			
Approach			
Engine Power Setting ~ % Takeoff	29	29	29
Engine EPNdB	96.7	97.5	98.5
Airframe EPNdB(1)	93.0	93.0	93.0
Total EPNdB	98.2	98.8	99.6
FAR (1969) EPNdB	108.0	108.0	108.0
Takeoff (w/o cutback)			
Altitude m (ft)	289 (950)	289 (950)	289 (950)
Engine EPNdB	97.8	97.8	98.6
Airframe EPNdB(2)	0	0	0
Total EPNdB	97.8	97.8	98.6
FAR (1969) EPNdB	108.0	108.0	108.0

(1) Average of airplane company predicted noise.

(2) Set at zero because of negligible noise contribution.

converge toward the short nacelle noise level. Although the noise trades differ in detail between take-off and approach, this study indicates that the mixed exhaust engine can be designed with equivalent or lower noise than separate exhaust systems.

4.3.1.5 Synopsis of Mixed Exhaust Selection

From Pratt & Whitney Aircraft evaluations, the mixed exhaust engine was calculated to offer advantages in TSFC, fuel burned, DOC, and possibly noise. These studies were based on isolated nacelle characteristics, and did not include the effects of nacelle-to-wing integration and interference effects. Boeing, Douglas and Lockheed studies, which included the effects of nacelle placement to minimize interference drag, also estimated a fuel burned advantage ranging from 2 to 4 percent with the mixed exhaust study engine. DOC reductions of ½ to over 2 percent were estimated for mixed exhaust engine powered aircraft. The noise advantage over a ¾-length duct configuration ranged from 0.4 to 1.1 EPNdB.

These results indicate that mixing has high potential for improved performance in future higher bypass ratio engines. The advanced mixer configuration was, therefore, selected for the Energy Efficient Engine and proposed by Pratt & Whitney Aircraft as a key element in the Energy Efficient Engine Component Development and Integration Program.

4.3.2 Considerations Leading to One-Stage HPT, Direct-Drive Fan Configuration

Refined engine-aircraft integration and performance, TSFC and DOC probabilities of achievement, and propulsion system preliminary design analyses were conducted for direct-drive (d) and geared (g) fan engines with one- or two-stage (1s or 2s) HPT's to arrive at the final configurational choice. Preliminary propulsion cross-sections of the four engines (STF505M-7 (d-1s), STF505M-9 (d-2s), STF495M-4 (g-1s), and STF495M-5 (g-2s) are included at the rear of the main body of this report (Figures 26, 27, 28 and 29).

Direct-Drive Engines: The STF505M-7 was selected as the preferred configuration from these evaluations. It is described in detail in Section 4.2. A summary description is also included here in context with the other candidate configurations. The fan of this direct-drive engine is a shroudless, one stage, hollow titanium design with a pressure ratio of 1.74:1 and a corrected tip speed of 472 m/sec (1550 ft/sec). The four-stage LPC incorporates controlled endwall loss concepts, low loss airfoils, and increased aerodynamic loading. The HPC is a high inlet corrected tip speed (405 m/sec, 1325 ft/sec), ten stage design with 1.7:1 average aspect ratio airfoils. HPC pressure ratio is 14:1. High strength titanium and an advanced high strength nickel base alloy (MERL 76) disk materials are used in the rear HPC section to permit the higher rotor speeds and increased temperatures associated with high overall pressure ratio. The HPC has active clearance control, controlled loss endwalls, and reduced loss airfoil concepts to raise efficiency levels.

A two-stage, Vorbix combustor is used for low emissions. This combustor is conceptually derived from the NASA Experimental Clean Combustor Program. Design changes were conceived relative to the experimental burner to make it commercially more practical without sacrificing low emissions characteristics. An oxide-dispersion strengthened alloy, film-cooled, louvered combustion zone liner is incorporated to provide commercial durability at the elevated HPC exit temperatures encountered in the engine.

The one-stage HPT is designed with a low, 1.6 loading coefficient, which requires a high disk rim, red-line speed of 527 m/sec (1730 ft/sec). The disk is of high strength MERL 76. Single crystal alloy blades with at least a 56°C (100°F) higher metal temperature capability than current materials are used to minimize HPC coolant bleed air. The four-stage LPT, designed for a 2.4 loading coefficient, counter-rotates relative to the HPT to minimize inter-turbine gas turning and pressure loss. The LPT uses titanium-aluminide airfoils in the cooler rear stages to save weight. Active clearance control is incorporated in the turbine section to increase efficiency.

The exhaust mixer is a scalloped design of high temperature titanium. A full authority digital electronic control is used to reduce operating cost and to provide efficient engine operation. The nacelle features an integrated engine/nacelle structure to restrain engine deflections caused by thrust and cowl loads.

Rotor-frame analytical modeling of a 5 bearing, 2 compartment rotor support system, in conjunction with nacelle load sharing, active clearance control, and rigid rotor construction, indicated the ability to carry both severe maneuver and cruise flight loads without incurring significant blade tip rubs. This represented a major simplification from the 7 bearing, 4 compartment support system used in the Task II conceptual studies.

The STF505M-9, a two-stage HPT, direct-drive fan engine, was similar in overall construction to the STF505M-7. The fans were identical. The STF505M-9 had one less LPC stage with the same aerodynamic parameters as the M-7. The 18:1 pressure ratio, 445 m/sec (1460 ft/sec) inlet corrected tip speed, ten-stage HPC ran at the same rotor speed as the 14:1 pressure ratio, ten-stage HPC in the M-7.

The combustors differed only in cant angle to accommodate HPC and HPT dimensions.

The smaller diameter two-stage HPT could have a much lower (430 m/sec, 1420 ft/sec) maximum disk rim speed as allowed by the lower power output required from each stage. The HPT annulus was opened up an additional 20 percent from the one-stage design to maximize the efficiency potential. This approach resulted in the same maximum blade root stresses of 3.4×10^8 N/m^2 (50 ksi) and disk lug concentrated stresses of 13.7×10^8 N/m^2 (200 ksi) for both HPT's.

The two-stage HPT to LPT diametrical offset required was 17 percent greater than for the larger diameter one-stage HPT to produce the same loading coefficient in both LPT's.

Geared Engines: The geared-fan engines were configured with the same core components as the direct-drive-fan engines. The freedom to run the fan and LPT at different rotor speeds resulted in major changes to the engine cross-sections. Larger diameter, 360 m/sec (1175 ft/sec) corrected tip speed fans were geared to two-stage, high speed LPC's and three-stage, 1.75 loading coefficient LPT's. A mid-engine bearing compartment containing intershaft and high rotor shaft roller bearings with a burner-diffuser support system became necessary to force a high strain energy, low-rotor-shaft-excited critical speed out of the engine running range.

A star gear system was used with a speed reduction ratio of 2.5. LPT power was input to the sun gear through a quill shaft having splines at both ends to allow for slight misalignment between the low rotor shaft and the gear. The floating sun gear was configured to drive 6 equally spaced pinions, which in turn drove a floating ring gear loosely splined to the fan hub. The pinion bearings and gear assemblies were clamped between flat plates at their

front and rear to form the cage. The cage was fixed to ground through 6 hairspring supports to minimize misalignment. The design was conceived such that loads would be automatically equalized between pinions by holding close tolerances, letting the sun gear float, and utilizing inherent flexibility of the ring gear.

Gear generated heat was rejected in an air/oil cooler supplemented by a fuel/oil heat exchanger as shown in Figure 21. The air/oil cooler was situated between the HPC case and fan inner flowpath to minimize susceptability to damage by foreign objects. The gearbox and engine oil systems were consolidated into a common overall lubrication and cooling system to minimize system component redundancy.

Nacelle lines were drawn consistent with good aerodynamics and low noise. Inlets were geometrically similar with a length-to-maximum-diameter ratio of 0.55. Nacelle length was tailored to individual gas generator and mixer requirements.

Engine-aircraft integration studies were conducted on the direct drive STF505M-7 and the geared-drive STF495M-4 one-stage HPT engines by Boeing, Douglas, Lockheed and P&WA. Only P&WA conducted aircraft integration studies on the direct-drive STF505M-9 and the geared-drive STF495M-5 two-stage HPT engines. Results of these studies are summarized on Table XVII. On the surface, the results of these evaluations were inconclusive.

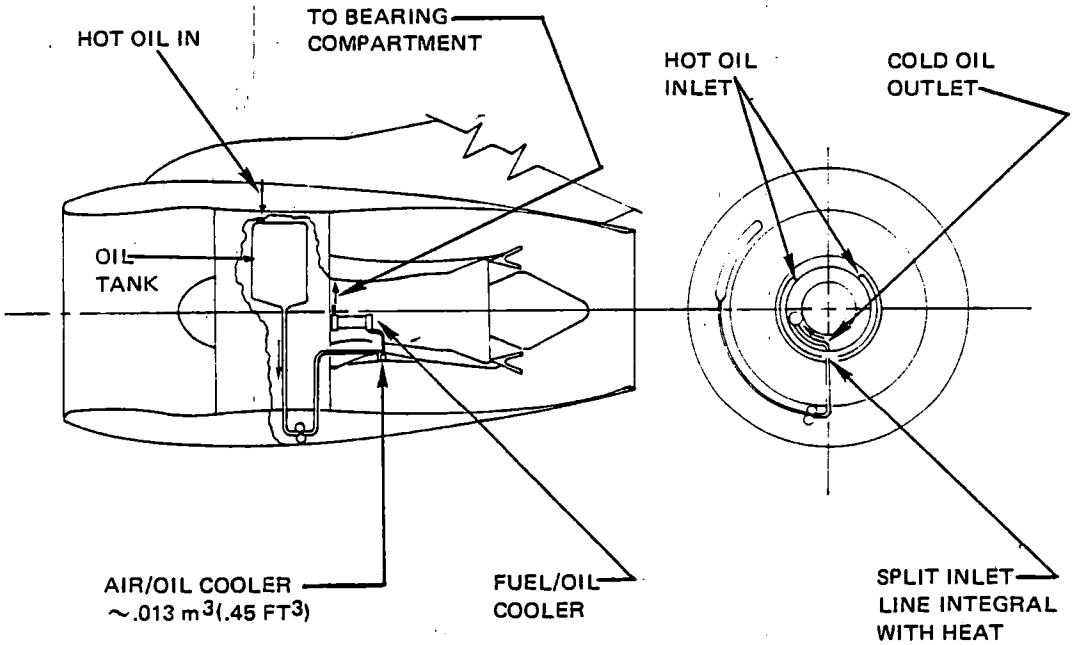

- FAN GEAR BOX USES ~ 284 L/MIN (75 GAL/MIN) OIL
- USED WITH FUEL/OIL COOLER.
- SHARES ENGINE HEAT LOAD.
- USES ADVANCED TECHNOLOGY COMPACT HEAT EXCHANGER.

Figure 21 Fan Gearbox/Oil Cooling System

TABLE XVII

CONSIDERATIONS LEADING TO ONE STAGE HP TURBINE AND DIRECT-DRIVE FAN SELECTIONS

		Direct-Drive Fans		Geared Fans	
Engine Study Designation		STF505M-7	STF505M-9	STF495M-4	STF495M-5
No. of HPT Stages		1	2	1	2
Installed Cruise TSFC kg/hr/N (lbm/hr/lb_f)		0.0585(0.573)	0.0578(0.566)	0.0560(0.549)	0.0552(0.541)
(fan case mounted airframe accessories; 10,700m, 35,000 ft/Mach 0.8)					
Avg. Stage Length Fuel Burned ~ kg					
Boeing	Domestic	8036.	–	7964	–
	International	16685.	–	16349.	–
Douglas	Domestic	14376.	–	13914.	–
	International	21170.	–	19909.	–
Lockheed	Domestic	15070.	–	14666.	–
	International	35437.	–	34047.	–
P&WA	Domestic	9551.	9470.	9295.	9186.
	International	31927.	31605.	30915.	30491.
Avg. Stage Length Energy Efficiency ~ mega joule/seat-km (1000BTU/seat st. mi.)					
Boeing	Domestic	1.754 (2.676)	–	1.739 (2.654)	–
	International	1.821 (2.778)	–	1.785 (2.723)	–
Douglas	Domestic	1.343 (2.049)	–	1.300 (1.983)	–
	International	1.329 (2.104)	–	1.297 (1.978)	–
Lockheed	Domestic	1.151 (1.756)	–	1.121 (1.710)	–
	International	1.264 (1.928)	–	1.214 (1.852)	–
P&WA	Domestic	1.327 (2.024)	1.316 (2.007)	1.291 (1.969)	1.276 (1.946)
	International	1.339 (2.043)	1.326 (2.023)	1.297 (1.978)	1.279 (1.951)
Relative Avg. Stage Length DOC (9.2¢/1, 35¢/gal. domestic; 11.9¢/1, 45¢/gal. international fuel)					
Boeing	Domestic	1.000	–	1.005	–
	International	1.000	–	0.996	–
Douglas	Domestic	1.000	–	0.990	–
	International	1.000	–	0.975	–

TABLE XVII (Cont.'d)

CONSIDERATIONS LEADING TO ONE STAGE HP TURBINE AND DIRECT-DRIVE FAN SELECTIONS

		Direct-Drive Fans		Geared Fans	
Lockheed -	Domestic	1.000	–	0.993	–
	International	1.000	–	0.984	–
P&WA -	Domestic(1)	1.000	1.016	1.012	1.028
	International(1)	1.010	1.012	1.007	1.019

(1) Equal probability of achievement estimates based on Pratt & Whitney Aircraft Task IV Risk Analysis results.

Total Maximum Noise Relative to FAR 36 (1969) - Δ EPNdB (Untraded & without Cut-back)

Boeing -	Domestic	– 7.7	–	– 9.6	–
	International	– 7.8	–	–10.3	–
Douglas -	Domestic	–11.0	–	–	–
	International	–10.6	–	–	–
Lockheed -	Domestic	–	–	–	–
	International	–	–	–	–
P&WA -	Domestic	– 9.3	– 9.3	–11.7	–11.7
	International	– 8.9	– 8.9	–11.3	–11.3

Preliminary Design Analysis

No. of Main Bearings	5	5	8	8
No. of Main Bearing Compartments	2	2	3	3
Last LPT Stage Blade Root Max. Pull Stress N/m^2 (ksi)	1.4×10^8 (20.)	1.4×10^8 (20.)	4.5×10^8 (65.)	4.5×10^8 (65.)
Gearbox failure effects	–	–	Rapid LPT rotor de-energizing required.	

Geared fan engines were estimated to have additional fuel savings potential. Geared engine preliminary design analysis uncovered several unique areas of concern in the low spool system requiring increased mechanical complexity for solution. Two-stage HPT engines were estimated to offer additional fuel savings but lower DOC reductions than one-stage HPT engines. The interpretation of these results leading to the selection of the direct-drive fan, one-stage HPT engine required a closer look at each of the evaluation parameters as discussed in the following sections.

4.3.2.1 TSFC

The TSFC effects of configurational differences are summarized in Table XVIII. Turbine efficiency had a major effect on one- versus two-stage HPT engine TSFC differences. Overall compressor efficiency was slightly higher with the lower corrected tip speed, 14:1 pressure ratio HPC of the one-stage HPT engine. Shorter overall length of the one-stage HPT engine also resulted in less nacelle drag for a small TSFC reduction. Therefore, the efficiency predictions used for the one- and two-stage HPT's were examined more closely to assure consistency in the predicted levels.

TABLE XVIII

CAUSES FOR TSFC DIFFERENCES – ONE- AND TWO-STAGE HPT DIRECT-DRIVE AND GEARED FANS

	TSFC Effect - %		
Configurational Differences	STF505M-7	STF505M-9 (1 to 2 stg HPT)	STF495M-4 (direct-drive to geared fan)
FPR/BPR	Baseline		– 4.3
Fan Efficiency			– 1.2
Overall Compressor Efficiency		+ 0.2	+ 1.0
HPT Efficiency		–1.7	
LPT Efficiency			– 1.2
Gear Efficiency			+ 0.8
Mixer Efficiency			+ 0.4
Nacelle Drag		+ 0.2	+ 0.3
Other		+ 0.1	0
Subtotal		– 1.2	– 4.2
Equal Probability of Achievement(1)		0	+ 1.4
TOTAL		– 1.2	– 2.8

(1) Pratt & Whitney Aircraft estimates based on results of Task IV Risk Analysis

The predicted HPT efficiencies were substantiated by combining the results of previous rig tests with efficiency improvements estimated for advanced design concepts. Results for both HPT's are summarized in Table XIX. Pratt & Whitney Aircraft has no operational engines with high work, one-stage turbines of the EEE type. An uncooled research turbine rig with similar expansion ratio and loading coefficient to the STF505M-7 turbine design was used as the current technology baseline for the one-stage turbine.

TABLE XIX

ONE- AND TWO-STAGE HPT EFFICIENCY PREDICTIONS

	Efficiency in Percent	
	One-stage HPT	Two-stage HPT
Efficiency Base	89.6 (Uncooled)	90.8 (uncooled JT9D-7 rig)
Δ for advanced technology	+ 1.4	+ 1.9
Δ for cooling	− 2.4	− 1.4
TOTAL	88.6	91.3

Uncooled JT9D-7 turbine rig test results were used to substantiate two-stage turbine efficiency. Studies have historically shown an efficiency improvement potential by increasing turbine annular flow area to decrease through-flow gas velocity. Flowpath optimization studies were conducted on both HPT designs, considering the effects of annulus area, disk rim speed, advanced blading shapes, low loss coolant flow injection techniques, and reduced blade tip running clearances. Annulus area increase was limited for the one-stage HPT by blade attachment stresses and minimum vane exit angle considerations. The lower rim speed, two-stage HPT annulus area could be increased 20 percent further to reach the same blade attachment stress levels. As a result, advancing the aerodynamic technology could prove to be more beneficial to a two-stage HPT.

The efficiency penalty associated with cooling also favored the two-stage HPT, although the one-stage HPT had substantially fewer cooled parts and leakage paths. Total cooling flow and leakage was estimated to be only 68 percent of the two-stage HPT level. However, the mainstream gas pressure loss caused by coolant flow injection was predicted to be higher with the transonic flow, one-stage HPT. The resultant efficiency losses associated with cooling correlated directly with the square of the entry point gaspath Mach number in accordance with classical loss equations.

Resultant built-up efficiency predictions were compared with analytical meanline predictions. Both efficiencies for the two-stage HPT were the same; the 0.4% lower level of 88.2 percent predicted by the meanline analysis was selected for the one stage HPT. On this basis, both HPT's were projected to have equal probabilities of achieving their respective cooled efficiencies. Therefore, TSFC comparisons also represented the same probability of achievement for one- and two-stage HPT engines.

The geared engine TSFC reduction potential of Table XVIII was the result of cycle and component efficiency differences from the direct-drive fan engines. Independence of fan and LPT rotor speeds permitted the application of low fan tip speed and high LPT speed for high component efficiency. These benefits were zeroed out by (1) a loss in the compres-

sion system efficiency caused by an additional stator row behind the fan to help turn the airflow into the counter-rotating LPC and the higher blade relative Mach numbers in the high speed LPC, (2) gear power loss, (3) reduced mixer efficiency in the higher bypass ratio, increased diameter fan engine, and (4) higher drag of the larger nacelle. As a result, the increased bypass ratio alone accounted for the geared engine TSFC advantage.

At an equal probability of achievement, the geared engine TSFC advantage was estimated to be slightly under 3 percent. Results of the TSFC probability for direct-drive and geared fan engines are compared in Figure 22. The geared-fan engine baseline Task III TSFC was estimated to have a 30 percent lower probability of achievement than the direct-drive fan engine baseline level. Optimism in gear and LPC efficiency predictions, and a change in airframe accessory location accounted for the very low geared engine TSFC probability of achievement.

The predicted gear efficiency of 98.8% cruise/ 99.2% take-off was assessed to be optimistic by about 0.3%, considering that a flight weight gearbox of this type and horsepower transmission level has yet to be designed and developed. The low speed LPC in the direct-drive fan engine represented a modest advancement beyond JT9D technology; conversely, the geared fan engine high speed LPC required the aerodynamic characteristics and achievement risk associated with mid stages of the HPC. At equal probabilities of achievement, the geared fan engine LPC efficiency was calculated to decrease 1.8 percentage points. The baseline TSFC levels also included nacelle drag effects with fan case mounted engine and airframe accessories which required local nacelle bulging to clear the accessories. The bottom mounted accessories were required on the Douglas center engine installation to avoid interference with engine support structure. Therefore, the Task III engine TSFC's were all estimated with that installation. In assessing probability of achievement, the airframe accessories were moved to the pylon to minimize TSFC. The direct-drive engine, with its smaller nacelle, responded faster to bulge size reduction. A significantly larger portion of the nacelle was affected, resulting in larger drag and attendent TSFC reductions. The cumulative effect of these changes was a 1.4 percent relative increase in geared-fan engine TSFC.

4.3.2.2 Fuel Burned

Before using engine TSFC in fuel burned calculations, the effects of customer bleed and horsepower extractions were included in the estimates. The customer requirements were an average of Boeing, Douglas, and Lockheed estimates normalized against thrust size as shown in Table XX.

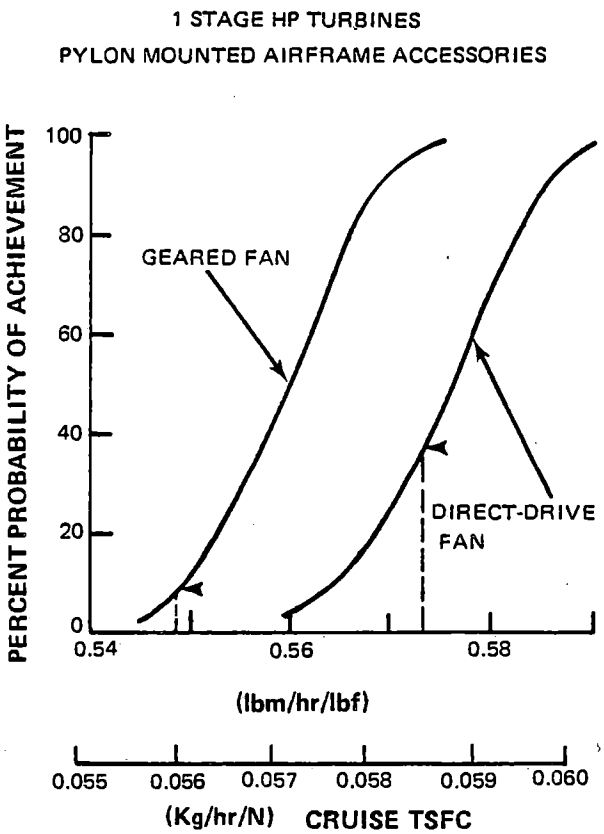

Figure 22 TSFC Probability of Achievement

TABLE XX

TSFC PENALTY WITH CUSTOMER BLEED AND HORSEPOWER EXTRACTION

$$\text{Horsepower Extraction (HPX)} = \frac{\text{sea level takeoff thrust}}{1700\ \text{N/KW}\ (285\ \text{lb}_f/\text{HP})}$$

$$\text{Bleed Extraction (BL)} = \frac{\text{sea level takeoff thrust}}{132{,}500\ \text{NKg/sec}\ (13500\ \text{lb}_f/\text{lb}_m/\text{sec})}$$

Engine Designation	Installed TSFC (w/o HPX & BL) kg/hr/N(lb/hr/lb$_f$)	Installed TSFC[1] (w HPX & BL) kg/hr/N(lb$_m$/hr/lb$_f$)	Percentage Change
Direct-drive Fans			
STF505M-7	0.0585(0.573)	0.0613(0.601)	+ 4.9
STF 505M-9	0.0578(0.566)	0.0606(0.594)	+ 4.9
Geared Fans			
STF495M-4	0.0560(0.549)	0.0593(0.581)	+ 5.8
STF495M-5	0.0552(0.541)	0.0585(0.573)	+ 5.9

(1) Used in Fuel Burned and DOC Evaluations

The inclusion of customer requirements increased direct-drive engine cruise TSFC by about 5 percent and the smaller core size geared engine TSFC by nearly 6 percent.

The higher TSFC's, exclusive of the probabilities of achievement results, were combined with propulsion system weight estimates in arriving at the fuel burned comparison. The Pratt & Whitney Aircraft trade factor study results shown in Table XXI illustrate the importance of both TSFC and weight in establishing the fuel burned trends.

Examination of the weight trends identified HPT and inter-turbine support case weight as primary differences between the one- and two-stage HPT. For the geared engines, heavier, large diameter fans, the gearbox, and the mid-engine bearing compartment were partially compensated for by 23 percent lighter LPT's for a net propulsion system weight increase of about 10 percent relative to the direct-drive engines.

TABLE XXI

PROPULSION SYSTEM WEIGHT AND RESULTS OF P&WA FUEL BURNED STUDY – – ONE- AND TWO-STAGE HPT'S : DIRECT-DRIVE AND GEARED FANS

	STF505M-7	STF505M-9	STF495M-4	STF495M-5
Propulsion System Weight[1] kg (lb_m)	4400(9702)	4655(10258)	4875(10744)	5105(11255)
	ΔFuel Burned[2] ~ % (Average Mission)			
Domestic Airplane				
TSFC Effect	0.0	– 1.39	– 3.69	– 5.32
Weight Effect	0.0	+ 0.54	+ 1.01	+ 1.50
TOTAL	0.0	– 0.85	– 2.68	– 3.82
International Airplane				
TSFC Effect	0.0	– 1.61	– 4.28	– 6.16
Weight Effect	0.0	+ 0.60	+ 1.11	+ 1.66
TOTAL	0.0	– 1.01	– 3.17	– 4.50

(1) Cruise thrust = 36430N (8190 lb_f)

(2) Exclusive of Probability of Achievement Analysis

Bottom-line fuel burned trends typified airplane company evaluation results which showed geared engine advantages ranging from 1 percent for the Boeing domestic twinjet to 6 percent for the Douglas international airplane. If the geared engine TSFC's were increased by 1.4 percent to provide the same probability of achievement as the direct-drive engine, using Pratt & Whitney Aircraft trade factors, it was estimated that the fuel burned would increase by 1.6 percent for the domestic aircraft and by 1.8 percent for the international aircraft. Based on all of the fuel burned studies, high efficiency two-stage HPT's would appear to have an added fuel savings potential of up to 1 percent over single stage HPT's. Gearing may improve fuel economy by an additional 1 to 1½ percent beyond direct-drive engines.

4.3.2.3 Direct Operating Cost

DOC trends for the four engines reflected TSFC, weight, acquisition and maintenance costs, and probability of achievement results. DOC results of the Pratt & Whitney Aircraft evaluation were normalized to the STF505M-7 in Table XXII to obtain an indication of the trend drivers. In addition to TSFC and weight,

discussed previously, maintenance cost was important in establishing differences between one- and two-stage HPT engines. With the geared engines, apparent performance or cost optimism had a significant effect on DOC reduction potential.

Examination of these two areas helped to discover the full impact of differences among the four configurations.

Maintenance costs are compared in Table XXIII for key parts and modules which differed significantly between one- and two-stage HPT engines (STF505M-7 and M-9). Using the procedures outlined in Section 3.0, a $8.39 lower one-stage HPT maintenance cost was estimated. Average turbine blade scrap life projections included the effects of creep/fatigue failures, sulfidation/oxidation/erosion, and impact damage. Pratt & Whitney Aircraft projections indicate dominancy of impact damage as the life limiting failure mode in mature engines. The higher speed blades of the one-stage HPT were more susceptible to impact damage, thus the lower scrap life and mean time between repair. The one-stage HPT required only 54 blades against 80 for the

TABLE XXII
PRATT AND WHITNEY AIRCRAFT DOC STUDY RESULT

	STF505M-7	STF505M-9	STF495M-4	STF495M-5
ΔDOC % (Average Mission)				
Domestic Airplane (9.2¢/liter (35¢/gal) fuel)				
TSFC effect	0.0	– 0.43	– 1.14	– 1.64
Weight effect	0.0	+ 0.47	+ 0.91	+ 1.32
Acquisition Cost Effect	0.0	+ 0.24	+ 0.27	+ 0.57
Maintenance Cost Effect	0.0	+ 1.33	+ 0.01	+ 1.56
Equal P.O.A.(1) Effect	0.0	0.0	+ 1.1	+ 1.0
TOTAL	0.0	+ 1.61	+ 1.2	+ 2.8
International Airplane (11.9¢ /liter (45¢ /gal) fuel)				
TSFC Effect	0.0	– 0.78	– 2.07	– 2.98
Weight Effect	0.0	+ 0.51	+ 0.99	+ 1.44
Acquisition Cost Effect	0.0	+ 0.24	+ 0.26	+ 0.56
Maintenance Cost Effect	0.0	+ 1.21	+ 0.01	+ 1.42
Equal P.O.A.(1) Effect	0.0	0.0	+ 1.5	+ 1.5
TOTAL	0.0	+ 1.18	+ 0.7	+ 1.9

(1) Probability of Achievement

two-stage HPT. A disk, its sideplates, an outer air seal, a vane row, and interstage seals were also eliminated to have higher maintenance costs in two areas. An advanced single crystal alloy for the first row of LPT vanes was needed for the one-stage HPT engine to allow operation at the higher gas temperatures without resorting to cooled airfoils. Also, disassembly and reassembly of the larger diameter combustor and HPT vane sections were estimated to require an additional 52 hours of labor per shop visit. The overall results were substantial parts replacement and labor reductions with the one-stage turbine.

The Task III DOC advantages of the geared engines were reversed by the probability of achievement analysis. The factors involved and their DOC effects are shown in Table XXIV. The optimism in TSFC, discussed previously, accounted for 0.9% in DOC. Another major contributor was optimism in gear replacement rate identified by reliability analysis. The average running time to failure of a new gearbox, without preventative maintenance, was estimated at 8200 hours. This would eventually lead to an engine failure rate in excess of 125 x 10^{-6} failures/hour. In order to bring the failure rate down to a

TABLE XXIII

COMPARISON OF ONE- AND TWO-STAGE HPT ENGINE MAINTENANCE COSTS

Key Parts/Modules	Scrap Lives[1] 1 Stg./2 Stg.	MH/Repair[2] 1 Stg./2 Stg.	MTBR[3] 1 Stg./2 Stg.	Maintenance[4] Cost Advantage for 1 stg. HPT $/EFH
	MATERIAL			
HPT Blades	8000 Hr./8500 Hr.			5.91
HPT Disks, Seals, Sideplates	15000 Cyc./15000 Cyc.			2.55
LPT Airfoils	16000 Hr./17000 Hr.			– 1.08
	LABOR			
HPT		215/362	2750/2850	1.47
Combustor/1st Turbine Vanes		410/358	3100/3100	– 0.46
TOTAL				8.39

(1) Mature engine combined mode average life projections
(2) Manhours per module repair
(3) Mean time between repair in engine flight hours
(4) Based on 3.5 hour flight duration

more realistic 50 x 10^{-6} failures/hour, preventative maintenance was estimated to be required every 6000 hours. To assure non-degradation of gearbox life, 100 percent of the gearbox bearings and 50 percent of the gears were assumed to be replaced at each overhaul. The scrappage of all the bearings did not significantly impact maintenance material cost since they comprised only 14 percent of the total cost. The gears were more significant since they represented 60 percent of the cost. The initial assumption had been a 25 percent gear replacement level. As a result of the replacement increase, maintenance cost went up, causing a 0.4 percent higher DOC. All together, the evaluation resulted in a 1.5 percent loss in geared engine DOC reduction potential.

The direct-drive fan, one-stage HPT engine, with a minimum number of costly turbine parts and reliable straight-through low spool power transfer, offered improved economics over both alternate configurations.

4.3.2.4 Noise

One- and two-stage HPT engines had identical acoustic engine parameters and, therefore, equal noise. Differences in low spool components did result in significant noise differences between the direct-drive and geared engines.

Noise characteristics are compared for direct-drive and geared engines by source in Table XXV. Using Pratt & Whitney Aircraft noise correlations, the geared fan perceived noise level was lower because of the lower pressure ratio and tip speed. The Pratt & Whitney Aircraft noise correlation, which relates maximum one-third octave band sound pressure level against last stage tip speed, exhibits a sharp fall-off in noise with increasing LPT speed. Jet noise reduction reflects the lower geared engine jet velocity. Geared engine core noise is also predicted lower because of the smaller core size required with the high bypass ratio engine to meet aircraft thrust

TABLE XXIV

DETAILS OF PROBABILITY OF ACHIEVEMENT ANALYSIS EFFECTS ON GEARED ENGINE DOC

Engine Variable		Δ DOC(1) %
TSFC	+1.4% to obtain same P.O.A.(2) as direct-drive	+0.9
Gearbox maintenance	Gear replacement rate increased from 25% to 50% per repair	+0.4
Other		+0.2
TOTAL		+1.5

(1) International aircraft – (average mission)
(2) Probability of Achievement

TABLE XXV

DIRECT-DRIVE AND GEARED ENGINE NOISE BREAKDOWN BY SOURCE

EPNL-dB

	Fan	Turbine	Jet	Core	Total Engine	Total Incl. Aircraft[2]
Direct Drive Fan (STF505M-7)						
Takeoff[1]	93.3	83.7	95.3	88.5	98.4	98.4
Approach	94.9	89.3	83.0	85.4	97.9	99.1
Sideline	84.0	63.1	89.7	82.2	91.5	91.5
Geared Fan (STF495-4)						
Takeoff	93.0	78.5	90.8	87.7	96.0	96.0
Approach	86.6	85.3	79.9	85.0	94.3	96.7
Sideline	83.7	60.9	85.1	81.4	89.3	89.3

(1) @ FAR 36 (1969) measurement stations; takeoff altitude = 290 m (950 ft.); approach power setting = 29% of take-off thrust
(2) P&WA International Airplane

requirements. As a result, geared engine noise was about 3 EPNdB lower than the direct-drive engine at the FAR (1969) measurement stations. With approach airframe noise included in the estimates, geared engines could provide approximately a 2 EPNdB lower noise capability.

4.3.2.5 LPT Dynamic Stress

With the high rotational speed and long blades of the geared engine last LPT stage, a wrought nickel base alloy usually reserved for HPT's (UDIMET 700) was needed to obtain adequate high frequency fatigue durability.

A Goodman diagram relating vibrational and steady stresses, used in the analysis, is shown in Figure 23. In the absence of test data, a straight-line correlation between the maximum notched specimen fatigue strength (vibratory stress) and the ultimate tensile strength (steady stress) for the material is ordinarily used to deliniate between safe and unsafe operation. Steady stress analysis of the geared engine LPT last stage blades resulted in a blade pull induced root stress of 4.5×10^2 N/m^2 (65 ksi). Gas bending stresses were cancelled by tilting the blades in such a manner to produce counteracting centrifugal loads. Vibratory stresses included resonance effects such as pulses induced by adjacent vane rows. Assuming the maximum level of current Pratt & Whitney Aircraft LPT (Inconel 713C) vibrational stress experience, of current Pratt & Whitney Aircraft LPT (Inconel 713C) vibrational stress experience, the conventional LPT blade cast nickel base alloy was inadequate for safe operation. The higher ultimate strength wrought, age hardened nickel base alloy provided sufficient safety margin.

On the basis of this analysis, it was found that the improved material was required in the second-to-last LPT stage as well. The cost increase per airfoil was 75 percent for an overall 50 percent increase in LPT airfoils cost in the highly stressed design. Thus, a geared engine would be expected to have approximately a one percent increase in engine cost associated with

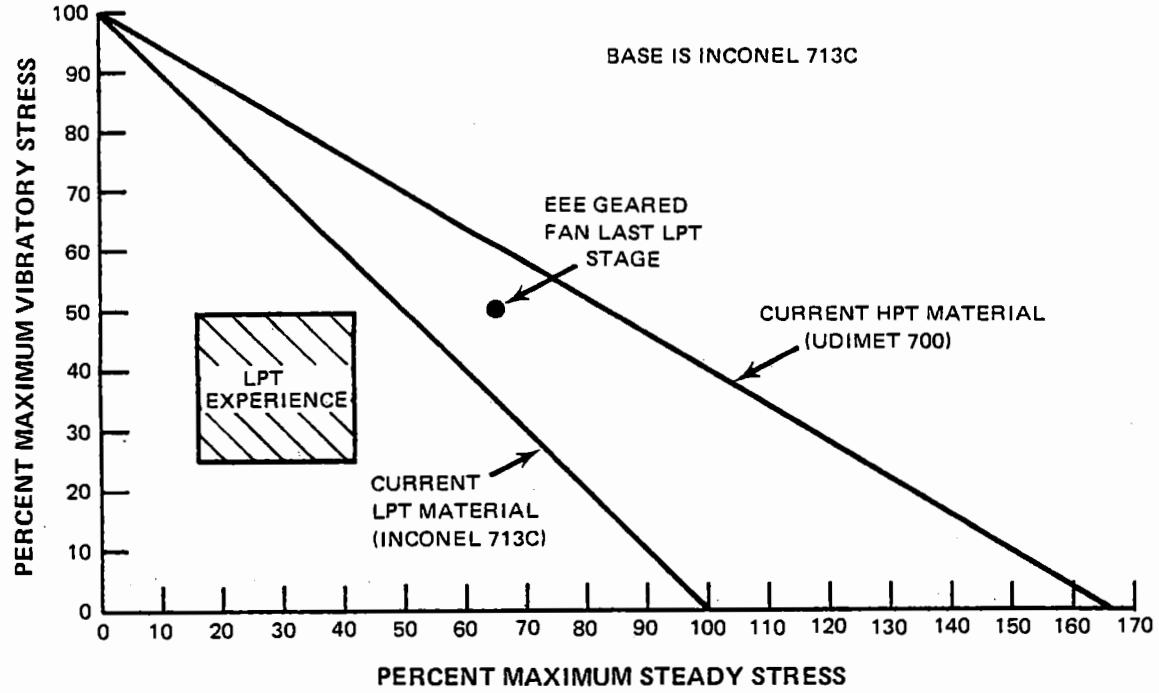

Figure 23 Geared Fan Engine Last Stage Low-Pressure Turbine Goodman Diagram

the more stringent materials required in the LPT.

4.3.2.6 Gearbox Failure Mode Effects

Decoupling of the fan and LPT, in the event of a gearbox failure and no corrective action, would likely result in catastrophic engine failure originated by turbine run-away. If a failure occurred at take-off conditions, the gas flow through the LPT was estimated to cause an acceleration rate of 205.7 revolutions per second^2. This amounts to a 12,340 rpm increase per second.

Two approaches to de-energize the decoupled LPT rotor were analyzed: blade shedding and gas blow-off.

Blade shedding designs are commonly used on free turbine ground installations where weight is non-critical. The disks are designed with sufficient burst margin so that the blades fail first and permit the disk to safely decelerate. Analysis of the first and second stage geared engine LPT disks indicated that at least a 37 percent higher design burst margin was required for a first stage disk capable of carrying the loads necessary to assure blade-first tensile failure. Disk weight was estimated to increase by approximately 68 percent. The conclusion was that over-design of the disks for blade-shedding was impractical in this engine design.

The gas blow-off concept would include a control sensing mechanism and actuator which would open valved passages from the front of the LPT to the fan duct in the event of a gear failure. A control reaction time of 0.25 seconds was estimated with advanced electronic control logic (0.07 seconds sensing lag time). This response time, while not adequate to de-energize the turbine rotor by direct fuel shut-off, was fast enough to activate valves and divert the gas away from the turbine blades.

The gas blow-off system would appear to be the most practical solution to flight safety in the geared engine.

4.3.2.7 Synopsis of the Selection of the One Stage HPT and Direct Drive Fan

Sufficient preliminary design analyses were performed to provide confidence in the cost reductions estimated with one-stage HPT's and direct-drive fan configurations. Reduced acquisition cost, maintenance cost, and DOC attendent with parts count reduction from two-stage HPT and geared engines were all established by the analyses.

Engines with two-stage HPT's and geared-fans were both indicated to burn less fuel than engines with one-stage HPT's and direct-drive fans. The additional fuel savings potential of the two-stage HPT engine was considered to be small in relation to its higher operating cost, leading to the selection of the one-stage HPT configuration. Geared engine fuel burned advantage, originally estimated to be large, diminished rapidly upon careful consideration of the probability of achieving the initially estimated TSFC level. The fuel savings potential was also tempered by the increased mechanical complexity needed to accommodate the gear and to provide flight safety. The success of the geared engine clearly relied on the gear system. The fan, LPC, and LPT would not be applicable to a direct-drive fan if the gear development program were unsuccessful.

Thus, we conclude that the fuel savings potential of the geared engines does not warrant the associated higher technical risks. Pratt & Whitney Aircraft, therefore, chose the direct-drive fan, one-stage HPT, mixed-exhaust configuration as the basis for further technology development.

5.0 CONCLUDING REMARKS

The NASA sponsored Energy Efficient Engine Preliminary Design and Integration Studies were successful in defining a fuel conservative turbofan configuration which could substantially reduce fuel demand, cut operating cost, and meet more stringent environmental regulations in future commercial aircraft.

A direct-drive fan, mixed-exhaust, one-stage high-pressure turbine turbofan configuration, with the potential for operating in the 1990's was estimated to have a 15.3 percent lower cruise thrust specific fuel consumption than the JT9D-7A which resulted in a 16 to 18 percent lower direct operating cost (depending on the selection of aircraft and flight mission).

Many advanced technological concepts were included in the preliminary engine design definition to increase engine operating efficiency and reduce both acquisition and maintenance costs. Key concepts included nacelle load sharing, active clearance control, and rigid rotor support to minimize blade tip running clearances; advanced materials to permit a major parts count reduction in the high pressure compressor and one-stage high-pressure turbine, together with a 50 percent higher cycle pressure ratio; shroudless fan blades for higher efficiency; and an advanced exhaust mixer for increased propulsive efficiency. A Vorbix, two-stage combustor and a fully acoustic lined nacelle were included to address future exhaust emissions and noise requirements.

An all new energy efficient engine is possible in the late 1980's or early 1990's. The NASA sponsored Energy Efficient Engine Component Development and Integration Program has already been initiated by Pratt & Whitney Aircraft with the objectives of developing the required turbomachinery and mixer technology advancements identified in this study to meet these time frames.

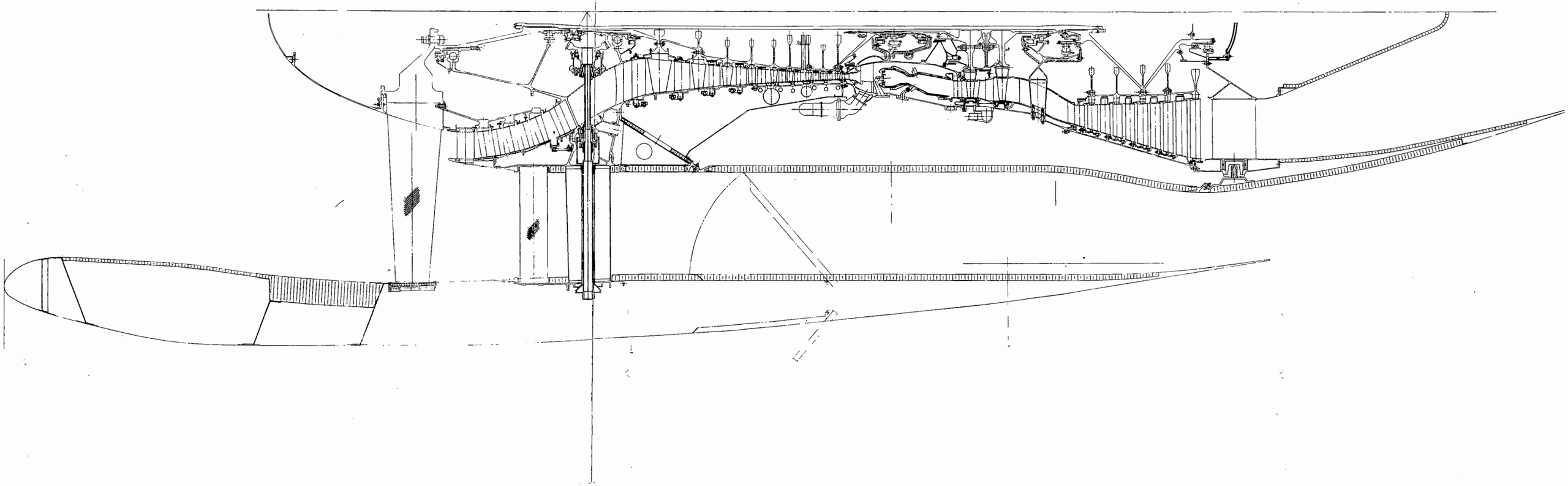

Figure 24 Engine Cross Section, STF505-1

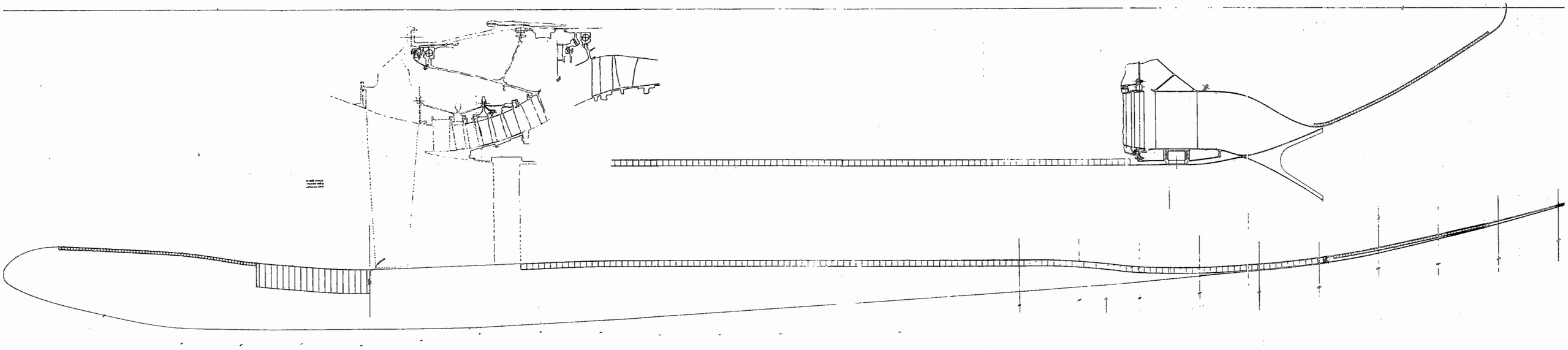

Figure 25 Engine Cross Section, STF505M-1

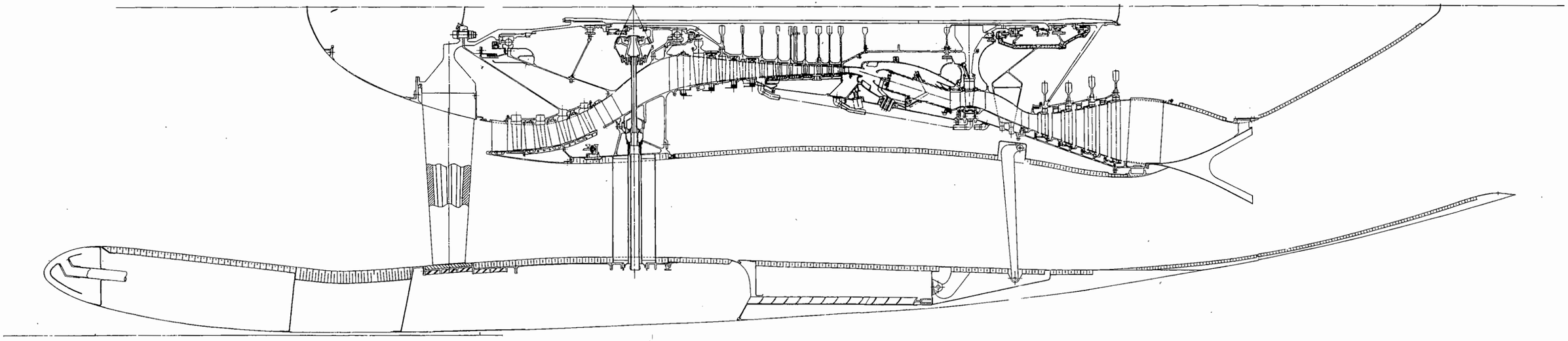

Figure 26 Engine Cross Section, STF505M-7

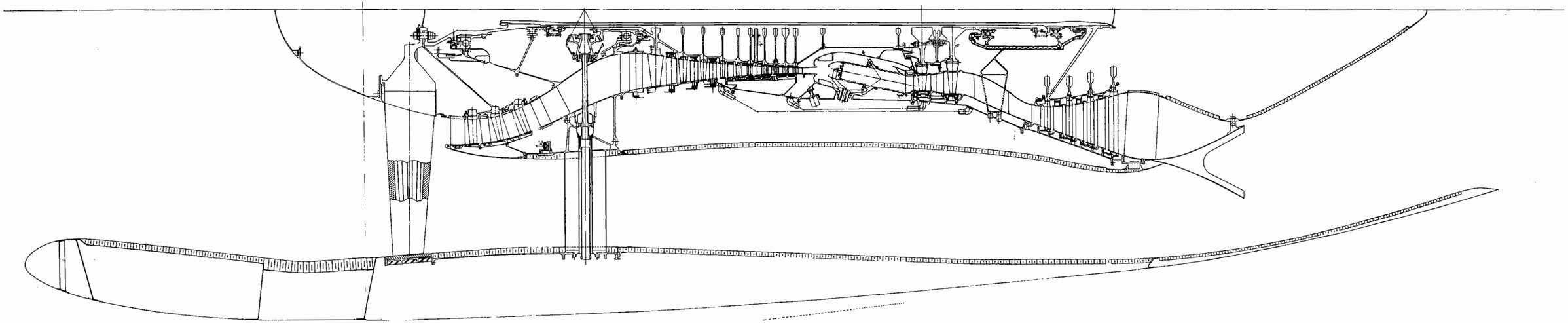

Figure 27 Engine Cross Section, STF505M-9

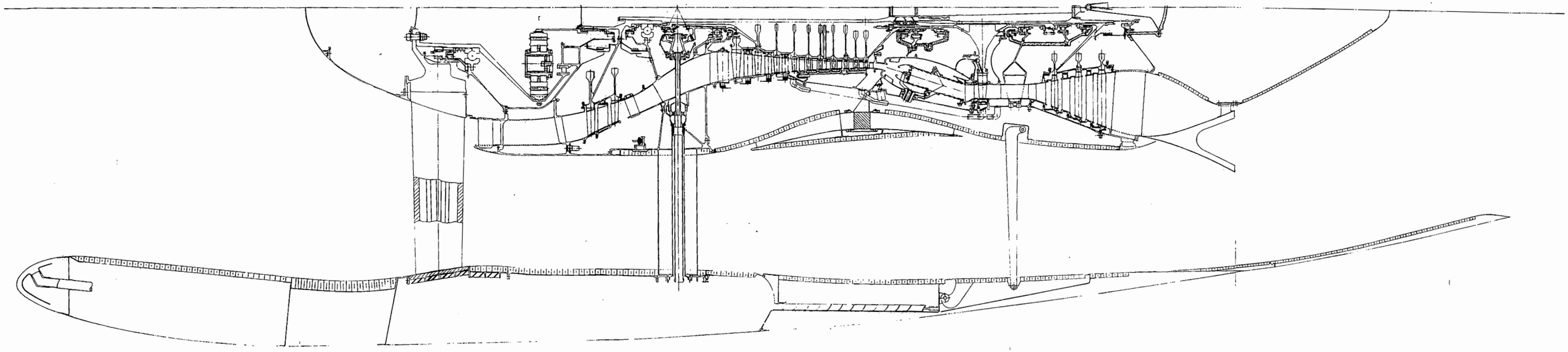

Figure 28 Engine Cross Section, STF495M-4

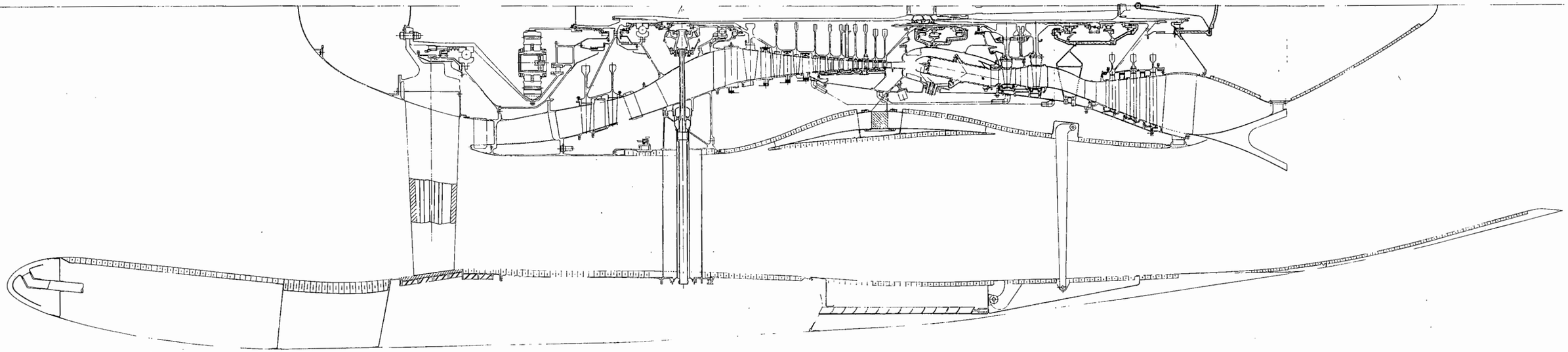

Figure 29 Engine Cross Section, STF495M-5

APPENDIX A

ENGINE CYCLE DEFINITION – TASK I

LIST OF ILLUSTRATIONS
APPENDIX A

APPENDIX A

LIST OF TABLES

APPENDIX A

ENGINE CYCLE DEFINITION – TASK I

1.0 INTRODUCTION

Task I consisted of the evaluation of four engine types, representative of mid-1985 technology, relative to a reference current engine (JT9D-7A) and the Energy Efficient Engine Program goals using the procedure outlined in Section 3.2 of the main body of this report.

The engine types considered were:

- Separate flow exhaust, direct drive fan
- Separate flow exhaust, geared drive fan
- Mixed flow exhaust, direct drive fan
- Mixed flow exhaust, geared drive fan.

The objective of this evaluation was to determine which of these engine types should be carried into the Task II, Cycle Refinement and Aircraft Integration, for further analysis.

The Task I evaluation process was broken down into cycle selection and propulsion technology evaluation. This process is outlined below and discussed in more detail in the succeeding sections.

Fan pressure ratio (FPR), bypass ratio (BPR), overall pressure ratio (OPR) and turbine rotor inlet temperature (RIT) were selected for the four engine types using the results of "Study of Turbofan Engines Designed for Low Energy Consumption" (NASA Contract NAS3-19132) and more recent cycle studies conducted in-house at Pratt & Whitney Aircraft. Inherent in cycle parameter selection were the following:

- trades between minimum thrust specific fuel consumption (TSFC) and minimum direct operating cost (DOC);
- limitations on RIT and OPR imposed by future thrust growth allowances; and
- trades among noise, exhaust emissions, and fuel consumption.

The engine turbomachinery components were analyzed using Pratt & Whitney Aircraft's meanline design system to:

- incorporate advanced technology assumptions;
- refine efficiency estimates;
- select rotor speeds;
- establish flowpath shapes; and
- provide initial definitions for obtaining weight, price, and maintenance cost estimates.

Fan drive reduction gear systems were also reviewed and updated to provide performance, weight, price, and maintenance cost estimates.

Installation technology assumptions were reviewed with respect to acoustics (source noise generation and attenuation with advanced technology treatment), nacelle geometry, performance, and weight.

Propulsion technology levels established in Task I were also used directly in Task II.

After base cycles had been selected for each

engine type, and component technologies had been determined, the four advanced engines were evaluated against the JT9D-7A reference engine and the NASA goals. This evaluation was performed in-house by Pratt & Whitney Aircraft using isolated nacelle performance with no consideration of installation or interference effects. Cruise TSFC, DOC, noise, and exhaust emissions were determined for each engine type and compared with the reference engine and NASA goals.

The results of these evaluations indicated that all four engine types were sufficiently close in overall merit to warrant further study, so all were carried into Task II for refinement and aircraft integration evaluation.

2.0 CYCLE SELECTION

The cycle parameters shown in Table A-I were selected as a result of the tradeoff studies. Maximum cruise thrust at 10,700 m (35,000 ft), Mach 0.8 was the cycle design point. The choice of initial OPR and RIT provided for growth margin by supercharging to a 45:1 overall pressure ratio and increasing rotor inlet temperature approximately 110°C (200°F). The following cycle parameters were considered.

TABLE A-I

TASK I ENGINE CYCLES

Engine Designation Fan Drive Exhaust Type	STF 505-1 Direct Separate	STF 505M-1 Direct Mixed	STF 495-1 Geared Separate	STF 495M-1 Geared Mixed
Max. Cruise Design [10,700 m (35,000 ft) - 0.8M]				
BPR	1.74	1.66	1.58	1.52
FPR overall pressure ratio	7.0	7.0	9.1	9.1
OPR	38.6	38.6	38.6	38.6
RIT, °C	1210	1210	1210	1210
(°F)	(2210)	(2210)	(2210)	(2210)
Max. Climb [10,700 m (35,00 ft) - 0.8M]				
OPR	41.8	41.8	41.7	41.6
Hot Day RIT, °C	1343	1340	1351	1346
(°F)	(2450)	(2445)	(2465)	(2455)
Sea Level Take-Off				
OPR	31.3	31.8	30.2	30.7
Hot Day RIT, °C	1340	1340	1312	1312
(°F)	(2445)	(2445)	(2395)	(2395)

- **Fan Pressure Ratio**

FPR selections for the unmixed exhaust engine cycles were based on the trades that exist between improved propulsive efficiency and the higher weight and price associated with the larger, low FPR engines. For example, although improved propulsive efficiency minimizes installed cruise point TSFC at FPR's below 1.5, the best fuel burned was obtained in the "Low Energy Consumption" studies for a higher FPR cycle. Best DOC was obtained at even higher FPR's because of the resulting trend toward smaller, less expensive engines and nacelles.

For the geared fan, unmixed exhaust engine, the initially selected level of FPR was taken from the "Low Energy Consumption" parametric studies. The higher FPR for the direct-driven fan was initially selected at the level of the STF 477 direct-drive fan Low Energy Consumption study engine. In the course of finalizing preliminary engine component definition, both the geared and direct-drive FPR's were revised slightly to the final values shown in Figure A-1.

- **Jet Velocity Ratio**

Jet velocity ratio defines the portion of core energy that is extracted to pressurize the duct stream. Variations can be achieved by changing BPR at constant FPR. Selection of jet velocity ratio implied a trade between best installed TSFC, which tended to result in a heavier, high BPR engine, and best economics which favored a lighter, smaller diameter, low BPR engine at a slight expense in TSFC. The selected cruise design point jet velocity ratio of 0.74 duct/engine for the unmixed cycles corresponded to the minimum fuel burned (Figure A-2). This level was close to minimum thrust specific fuel consumption and maximum return on investment. Historically, this level of jet velocity ratio has also been found to give balanced core and fan stream jet noise at the FAR 36 (1969) measurement stations.

- **Overall Pressure Ratio**

The OPR selection of 38.6 to 1 at the cruise design point offers a 3 to 4 percent fuel consumption improvement relative to current generation high bypass engines and tends to

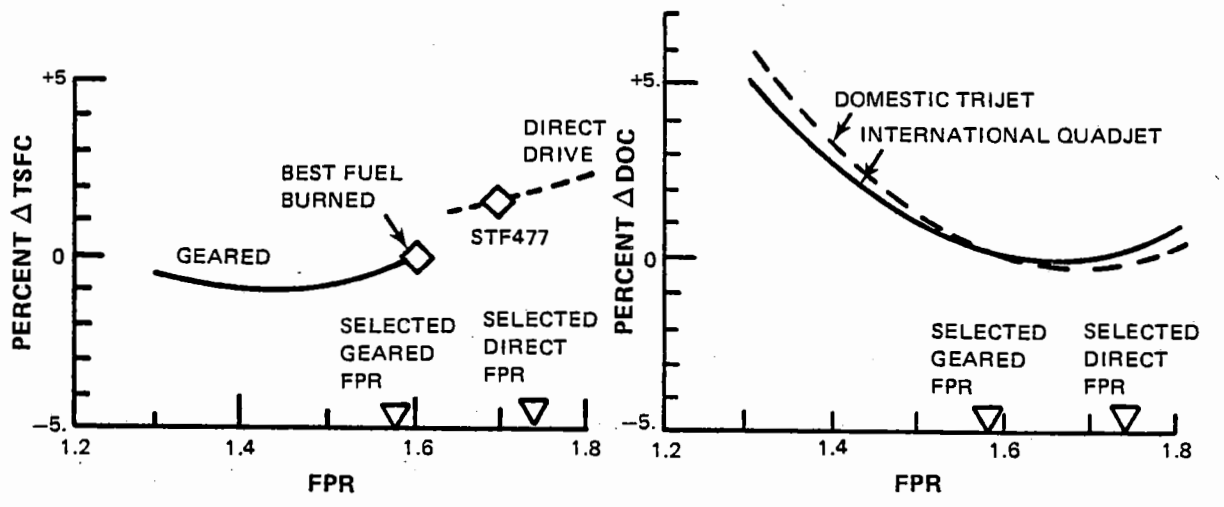

Figure A-1 Task I Fan Pressure Ratio Selection - Separate Exhaust Engine

optimize DOC for the domestic and international range aircraft as shown in Figure A-3. Even higher pressure ratio engines offer still further improvement in fuel consumption without severely affecting DOC since the increasing procurement and maintenance cost effects are counteracted by lower fuel consumption. However, preliminary thermal/structural analysis of the rear of the HPC section and the HPT has indicated the 39:1 OPR level to represent a substantial challenge in disk thermal control, especially when considering thrust growth which usually requires increased pressure ratios. In addition, achieving tight running clearances and sealing of leak paths become progressively more difficult. At the high pressure ratios, NO_x emissions also increase.

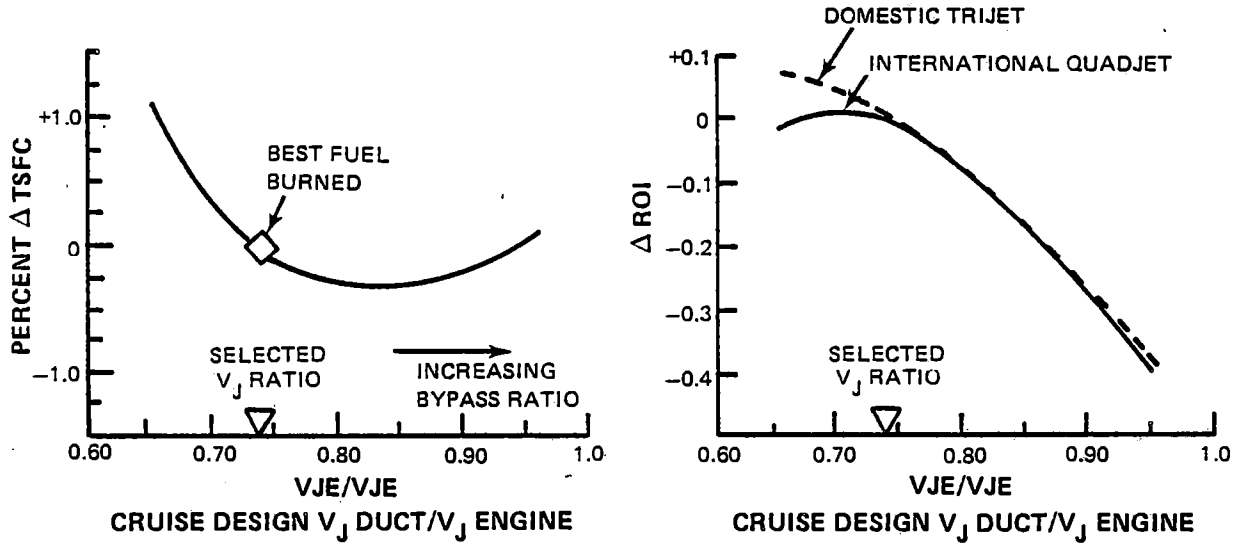

Figure A-2 *Task I Jet Velocity Ratio Selection – Separate Exhaust Engines*

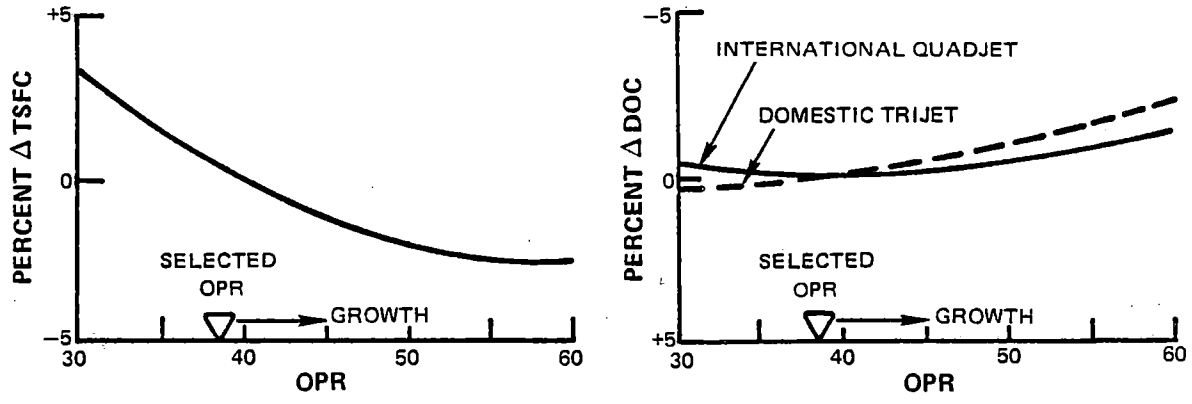

Figure A-3 *Task I Overall Pressure Ratio Selection– Separate Exhaust Engines*

- **Combustor Exit Temperature**

The selected maximum combustor exit temperature (CET) of 1400°C (2550°F) for the baseline Task I engines (Figure A-4) nearly minimized fuel consumption while leaving margin for thrust growth. Growth may require temperature levels as much as 110°C (200°F) higher than the base line, without penalizing either the fuel use or DOC.

Another way of indicating engine operating temperature is HPT RIT. This temperature is measured at the entrance to the first rotating stage of the HPT and, thus, reflects the operating environment of this critical component. It differs from CET in that it includes the effects of passing through one stage of cooled stationary vanes. The actual temperature difference between RIT and CET depends on a number of factors, the primary one being the cooling air assumptions applied to this row of vanes. Both levels of temperatures are quoted in this report.

- **Mixed Engine Cycle Selection**

The benefits of exhaust stream mixing were reviewed using the same OPR and RIT as selected for the unmixed engine, and an assumed mixing efficiency of 85 percent. The FPR and BPR were both simultaneously varied to maintain a mixer duct-to-engine total pressure ratio of 1.0.

- **Mixing Plane Total Pressure Ratio**

Selection of mixing plane total pressure ratio (P_{TD}/P_{TE}) required maximization of mixed total pressure for optimal fuel consumption. Theoretically, with complete mixing (100 percent mixing) the optimum occurred at a P_{TD}/P_{TE} ratio of 1.0 (Figure A-5). The assumption of 85 percent mixing, however, caused the optimum to shift to the right in Figure A-5 in the direction of the optimum unmixed engine P_{TD}/P_{TE}. As shown, when the fan diameter (or BPR) was held constant and FPR varied, optimum fuel consumption

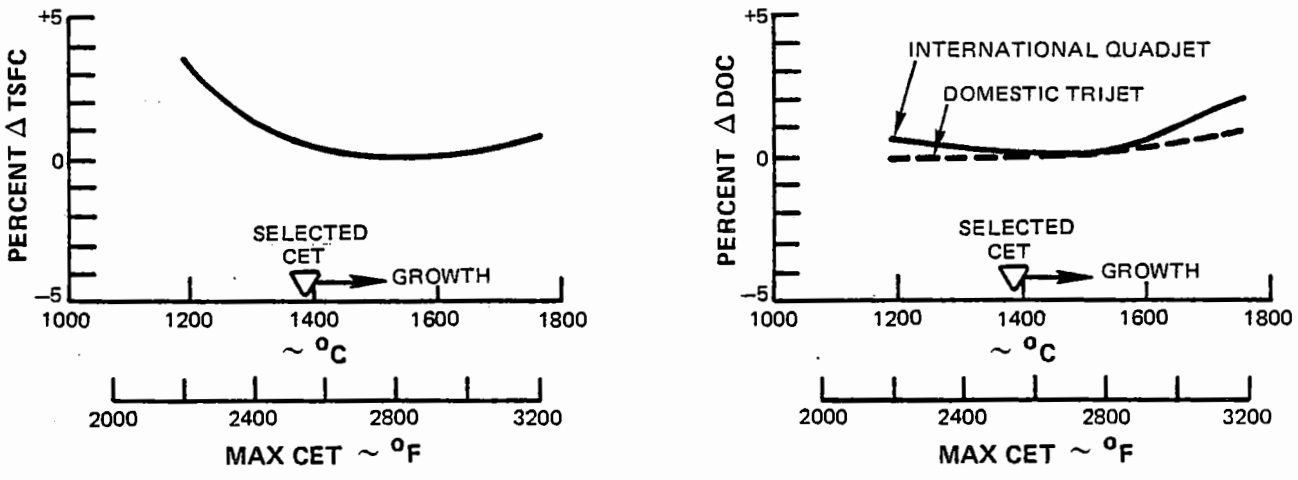

Figure A-4 *Maximum Combustor Exit Temperature Selection – Separate Exhaust Engines*

was in the region of 1 to 1.1 P_{TD}/P_{TE}, and the trend was flat. Therefore, a P_{TD}/P_{TE} of 1.0 was chosen for the basic Task I study.

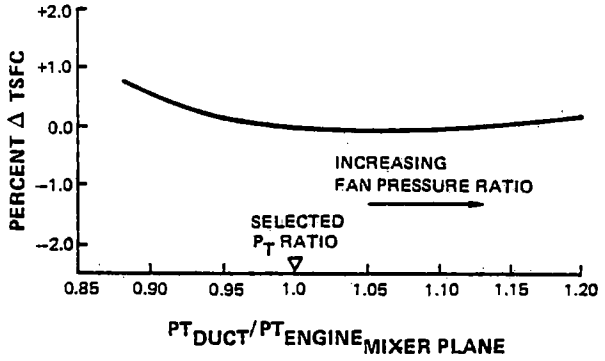

Figure A-5 Task I Mixing Plane Pressure Ratio Selection – Mixed Exhaust Engines

The results of this review were then compared against fan diameter at constant cruise thrust leading to the decision to hold mixed flow engine BPR at the level of the unmixed engines to produce essentially the same diameter (Figure A-6).

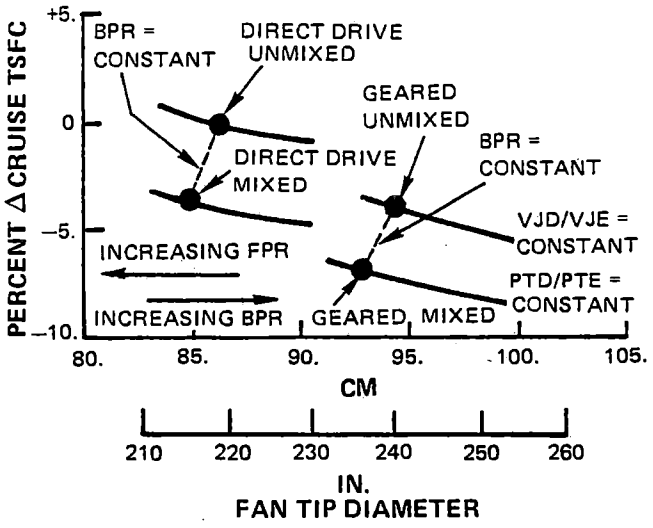

Figure A-6 Task I Fan Diameter Selection – Constant Cruise Thrust

A constant fan diameter comparison was desirable since it provided substantial insight into the overall mixed versus unmixed engine characteristics. Since the trends of TSFC against fan diameter were similar for both types, any substantial difference in final selected diameter on the basis of fuel use or DOC would have had to reflect differences in weight trends, cost trends, or installation effects (such as interference drags with the aircraft). With the exception of the installation, these trends were not expected to differ substantially between the two types. The differences in the installation effects were to be determined during Task II by varying the low pressure spool cycle characteristics for both the unmixed and mixed exhaust engines.

- Nacelle Geometry

Nacelle lines were obtained for the four engines through an iterative process of varying the nacelle design parameters parametically to search for the best combination to minimize drag, duct pressure losses, and weight within engine and acoustic requirement constraints. Drag analysis consisted of analytical skin friction calculations combined with statistically derived data correlations of nacelle pressure drag developed from parametric wind tunnel testing of small-scale powered nacelle simulators. Ducting pressure calculations accounted for the standard effects of hydraulic radius, surface roughness, and flow velocity. Weight estimating procedures reflected the use of lightweight materials and mechanical properties projected to the late 1980's time frame.

Acoustic design constraints included inlet and aft fan cowl (separate exhaust engines) length minima to allow acoustic liners which had the potential for attenuating engine noise to FAR (1969) minus 10EPNdB. This resulted in an inlet treatment length-to-fan diameter ratio of 0.55 and aft fan cowls which extended to the

rear turbine flanges (3/4 length nacelles) on the separate exhaust systems.

Within these constraints, the highlight-to-maximum diameter ratio, axial location of maximum diameter, and cowl and afterbody boat-tail angles were iterated to arrive at the final nacelle contours for the engines. The resultant nacelle lines are shown in Figure A-7 for the four engines.

3.0 PROPULSION TECHNOLOGY EVALUATIONS

The engine turbomachinery components were analyzed utilizing Pratt & Whitney Aircraft's mean-line design system to:

- refine efficiency estimates,
- incorporate advanced technology assumptions,
- select rotor speeds,
- establish flowpath shapes, and
- provide initial definitions to estimate weight, price and maintenance cost.

Fan-drive reduction gear systems were also reviewed and updated to provide weight, price,

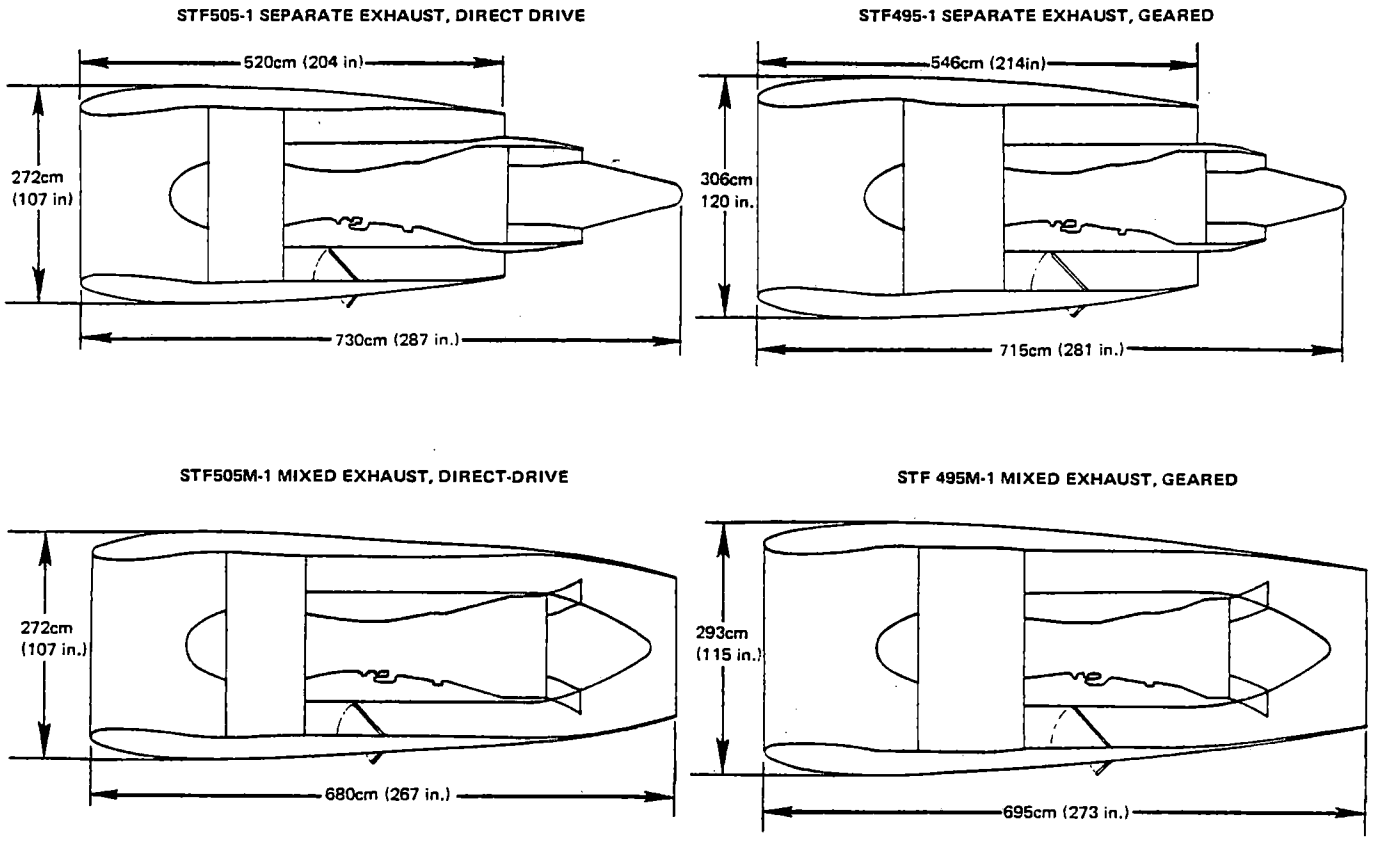

Figure A-7. Task I Nacelle Lines

and maintenance cost estimates for the evaluation against study goals.

Installation assumptions and technologies were reviewed with respect to acoustics (source noise generation and attenuation with advanced technology treatment), nacelle geometries, and acoustic nacelle performance needed to meet the noise goal of FAR 36 (1964) minus 10 EPNdB.

Resultant components are described in the following sections.

3.1 TURBOMACHINERY DESIGN PARAMETERS AND PERFORMANCE

3.1.1 High-Pressure Spool

A common high-pressure spool definition taken from the "Study of Turbofan Engines Designed for Low Energy Consumption" conducted under NASA Contract NAS3-19132 was used for all four engine types. The high-pressure spool features an 18:1 pressure ratio compressor and a 2-stage turbine. Table A-II summarizes the design parameters and performance of these components.

TABLE A-II

TASK I – HIGH-PRESSURE SPOOL COMPONENT DESIGN PARAMETERS

Compressor		Turbine	
Number of Stages	9	Number of Stages	2
Pressure Ratio	18:1	Pressure Ratio	4.3:1
Corrected Tip Speed, m/sec	449	Load Factor, $\frac{GJ\Delta h}{U_m^2}$	1.22
(ft/sec)	(1475)		
Corrected Inlet Flow, Kg/sec	43	Maximum Rim Speed, m/sec	427
(lb/sec)	(94.6)	(ft/sec)	(1400)
Average Aspect Ratio	1.2	Turbine Cooling Air, %Wae	14.2
Inlet Hub/Tip Diameter Ratio	0.593	Cooled Efficiency, %	91.2
Efficiency, %	88.5		

The compressor conceptual design included advanced technologies projected to be available for demonstration in the early 1980's and available for service in the 1990's. They are:

- Improved clearance control to reduce operational airfoil tip clearance at the cruise flight condition to an average of 0.033 cm (0.013 in.)
- High subsonic, low-loss airfoils less sensitive to tip clearance.

The turbine conceptual design shown in Figure A-8 included advanced technologies such as:

- Low through-flow gas velocity,

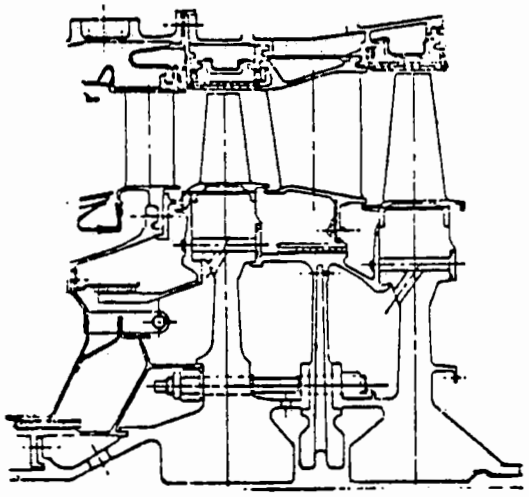

1398°C (2550°F) MAX. COMBUSTOR EXIT TEMPERATURE

1343°C (2450°F) MAX. ROTOR INLET TEMPERATURE

COOLING & SECONDARY AIRFLOW

= 14.2% OF COMPRESSOR EXIT AIRFLOW

	FIRST VANE	FIRST BLADE	FIRST BLADE OUTER AIRSEAL	SECOND VANE	SECOND BLADE	SECOND BLADE OUTER AIRSEAL
MATERIAL	ADV. SINGLE CRYSTAL*	ADV. SINGLE CRYSTAL	GRADED CERAMIC	ADV. SINGLE CRYSTAL	ADV SINGLE CRYSTAL	GRADED CERAMIC
TYPE OF COOLING	SHOWER-HEAD/ FILM COOLING	SHOWER-HEAD MULTI-PASS	NONE	IMPINGEMENT TE DISCHARGE	MULTI-PASS	NONE
COOLING AIR SOURCE	HPC DISCHARGE	HPC DISCHARGE /TOBI	–	MID HPC	MID HPC DISK PUMP	–
PERCENTAGE AIRFLOW	6.6	4.0	0.3	2.0	1.1	0.2

*THERMAL BARRIER COATINGS ON PLATFORMS

Figure A-8 *High-Pressure Turbine Advanced Cooling System*

- Improved clearance control to reduce operational clearances at the cruise flight condition to an average of 0.051 cm (0.020 in.),

- Improved turbine airfoil materials which allow higher metal temperatures with commercial life, graded ceramic rotor tip seals, and thermal barrier coatings on the vane shrouds to reduce cooling requirements, and

- Improved seals to reduce leakage of secondary and cooling airflows.

The low emissions Vorbix combustor concept was assumed to minimize exhaust emissions. It was based on technology proven in the NASA Experimental Clean Combustor Program (ECCP). An attempt was made to simplify the ECCP design for use in the Energy Efficient Engine while retaining the low emissions potential. The configuration is compared with the ECCP concept in Figure A-9.

The Vorbix combustor design included a separate pilot burner optimized for idle power to minimize CO and THC emissions, and rapid vaporization and mixing in the secondary combustion zone to reduce NO_x emissions, at higher power settings.

Since the Energy Efficient Engine burner liner was calculated to require a metal temperature about 170°C above current liner operating temperatures (to permit 65% of the inlet air to be used for emissions and exit temperature profile control, leaving only 35 percent for liner cooling), an advanced oxide dispersion strengthed (ODS) material was selected as the primary design approach for its combustor.

3.1.2 Low-Pressure Spool

The selection of design parameters for the low-pressure spool components is dependent on the rotor speed selected. In the case of the direct-drive engines where the fan and LPT rotate on the same shaft, speed selection is dependent on trades between the fan and LPT efficiencies.

Figure A-10 shows that increased fan corrected tip speed (through increased rotor speed) penalized fan efficiency; however, the increased

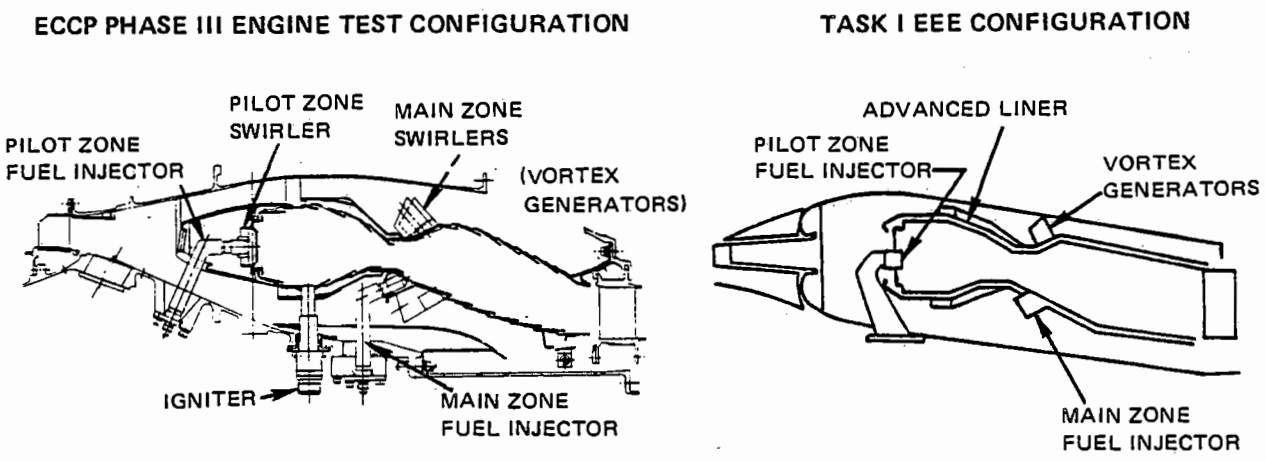

Figure A-9 Energy Efficient Engine Low Emissions Combustor

wheel speed on the LPT reduced loading and improved LPT efficiency.

Another means of increasing the LPT wheel speed to decrease loading and improve efficiency is to increase turbine diameter. This raises wheel speed at constant rotor speed. Increased turbine elevation, however, increases the weight and drag of the isolated nacelle and must be traded against the turbine efficiency.

The low-pressure spool selected for the direct-drive engine types is near optimum fan speed and LPT diameter as shown in Figure A-11.

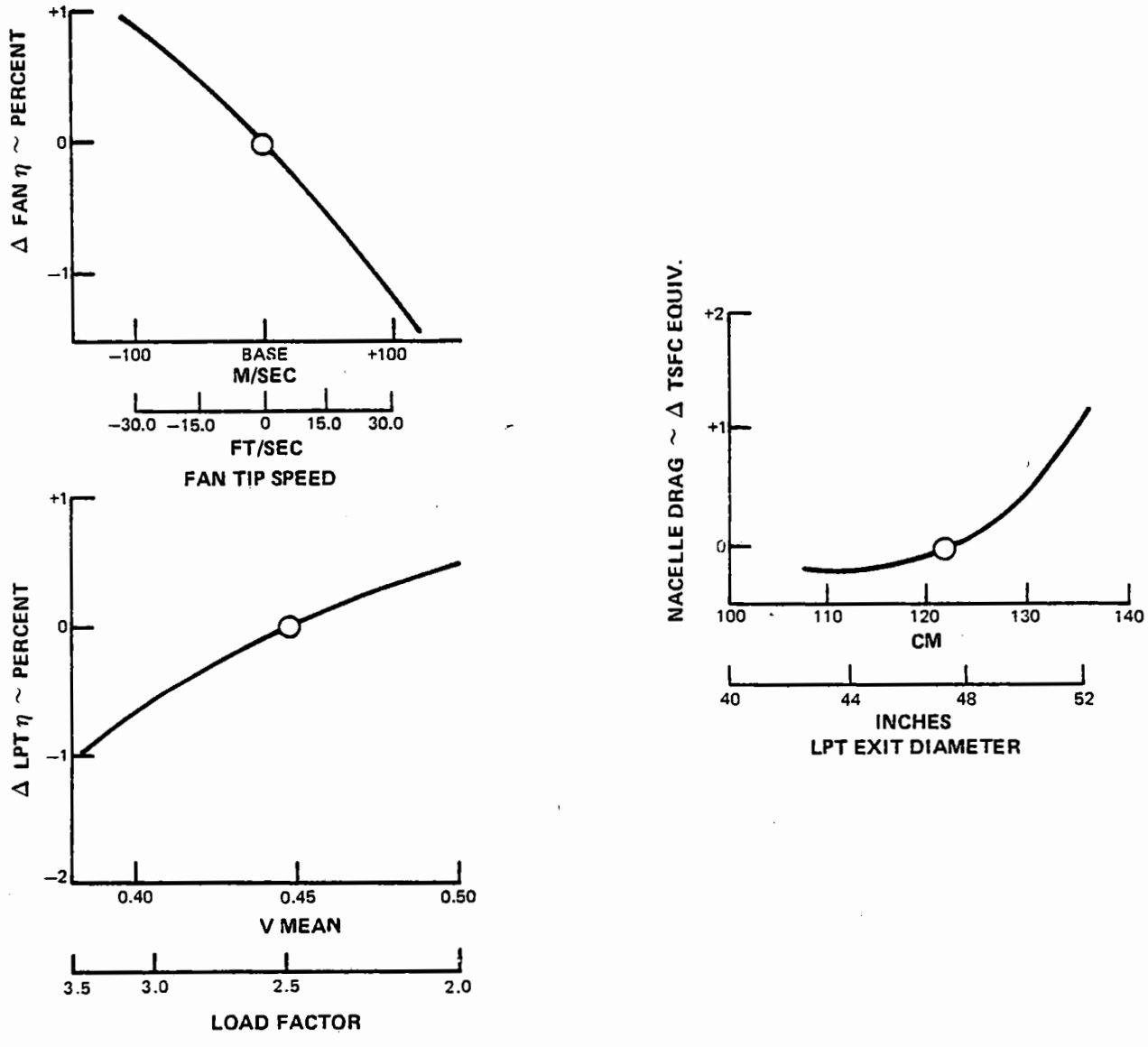

Figure A-10 Task I Low Rotor Trade Study - Constant Fan Pressure Ratio

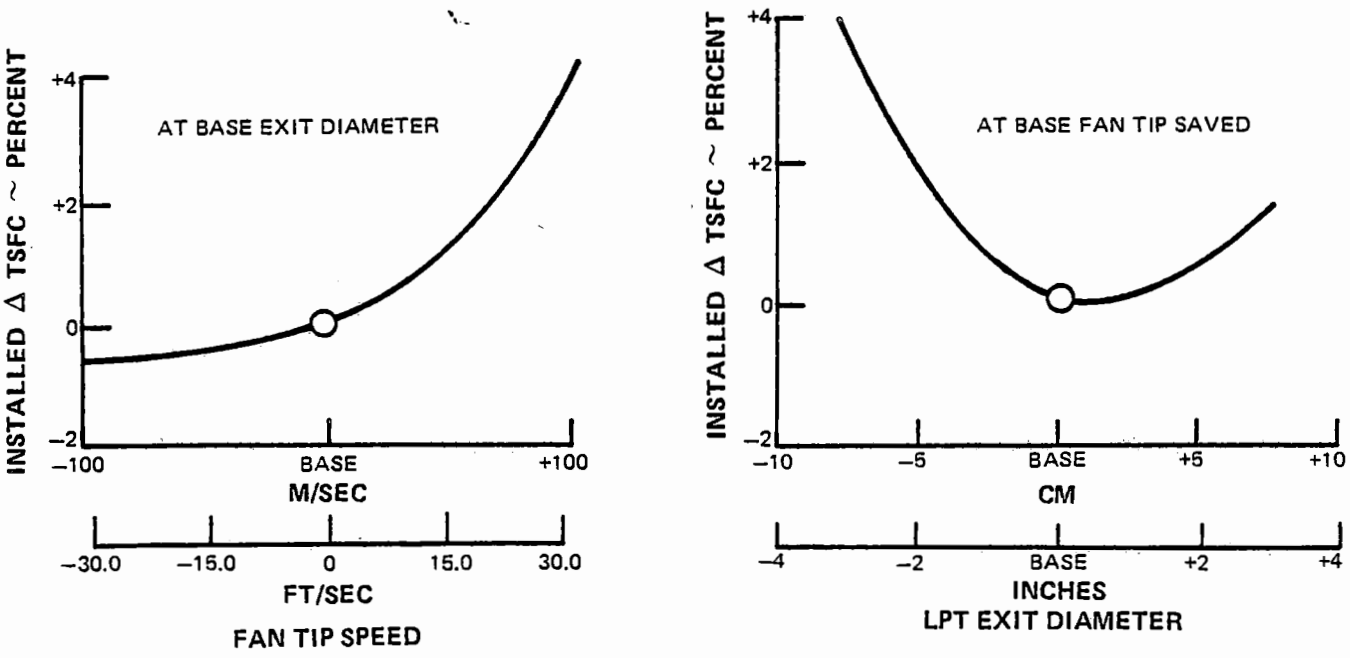

Figure A-11 Task I Low Rotor Speed and Low-Pressure Turbine Diameter Selection

A similar trade was performed for the geared engine types except that only turbine diameter optimization was considered as the reduction gear allows both the LPT and fan to rotate at their respective optimal speeds.

The fan design parameters for the four engines are given in Table A-III. The use of a low aspect ratio, shroudless blade enables an improvement in efficiency because of the elimination of inter-blade shrouds.

The LPC design parameters for the four engine types are given in Table A-IV. The increased speed of the geared LPC's enables elimination of one stage, but the addition of support struts through the gas path to support the reduction gear causes a reduction in compressor efficiency.

The LPT design parameters for the four engine types are given in Table A-V. The LPT's are preceeded by a transition duct which also serves as a bearing support frame which partially supports both the high and low-pressure rotors. This transition duct also provides a radial offset between the turbines and enables the LPT to achieve the optimum elevation, based on the rotor speed, elevation, and nacelle drag trades, independent of the HPT gaspath radius.

The direct-drive LPT requires 5-stages to achieve the desired moderate load factor. The higher rotational speed of the geared turbine provides a low load factor for higher efficiency, and enables the elimination of two stages.

TABLE A-III

TASK I FAN DESIGN PARAMETERS

	STF505-1	STF505M-1	STF495-1	STF495M-1
No. Stages	1	1	1	1
Pressure Ratio*, O.D.	1.74	1.66	1.58	1.52
Corrected Tip Speed, m/sec (ft/sec)	472. (1550)	427 (1400)	381 (1250)	358 (1175)
Tip Diameter, cm (inches)	218.9 (86.2)	218.9 (86.2)	242.8 (95.6)	242.8 (95.6)
Total Corrected Flow, kg/sec (lb/sec)	650.9 (1435)	650.9 (1435)	821.9 (1812)	821.9 (1812)
Avg. Aspect Ratio	2.85	2.85	2.90	2.90
Inlet Hub/Tip Diam. Ratio	0.38	0.38	0.35	0.35
Efficiency* O.D., %	87.2	88.0	89.4	89.8
Gear Ratio	–	–	2.5	2.5

*Includes Exit Guide Vanes

TABLE A-IV

TASK I LOW-PRESSURE COMPRESSOR DESIGN PARAMETERS

	STF505-1	STF505M-1	STF495-1	STF495M-1
No. Stages	1 + 3	1 + 3	1 + 2	1 + 2
Pressure Ratio	2.14	2.14	2.14	2.14
Corrected Tip Speed, m/sec (ft/sec)	230.1 (755)	209.4 (687)	401.1 (1316)	402.9 (1322)
Avg. Aspect Ratio	2.2	1.8	2.0	2.0
Efficiency, %	88.6	88.3	85.3	85.1

TABLE A-V

TASK I LOW-PRESSURE TURBINE DESIGN PARAMETERS

	STF505-1	STF505M-1	STF495-1	STF495M-1
No. Stages	5	5	3	3
Pressure Ratio	6.2	5.1	6.7	5.6
Mean Velocity Ratio	0.45	0.45	0.57	0.57
Load Factor, $\frac{GJ\,\Delta h}{U_M^2}$	2.47	2.47	1.54	1.54
Avg. Flow Coefficient, C_x/U_M	0.88	0.89	0.56	0.62
HPT-LPT Offset Ratio, (LPT Avg. Inlet Diam./HPT Avg. Exit Diam. Ratio)	1.34	1.41	1.14	1.25
Turbine Cooling Air, % W_{AE}	1.4	1.4	1.7	1.7
Efficiency, %	91.2	91.2	92.1	92.1

3.1.3 Mainshaft Speed Reduction Gear

The three candidate gear systems considered are shown in Figure A-12. The conceptual configuration studies indicated that a 2.5 to 1 gear ratio was desired with a goal efficiency of 99 percent.

The planetary gear system was found to be inapplicable since, with this system, the relatively low gear ratio required resulted in excessively small pinions and pinion bearings which would preclude adequate service life.

The layshaft gear system has a load sharing feature which reduces the axial force on the fan rotor bearing. This force is shared by the gears and the gearbox support structure. Although the weight of the layshaft system is comparable to the star system, the layshaft gearbox would be longer and contain one extra pinion and 75 percent more pinion bearings. In addition, the layshaft gear system has a predicted efficiency of 98.5 percent at cruise compared to 98.8 percent for the star gear system.

The star gear system was selected for use in the geared Energy Efficient Engine types based on consultation with other United Technologies Corporation divisions (Hamilton Standard, Sikorsky, Pratt & Whitney Aircraft of Canada) and also for the reasons outlined below:

- Higher efficiency potential of the star

gear system yielded better fuel consumption and reduced the size of the oil cooler.

- Fewer parts in the star gear system provided higher reliability and reduced maintenance costs.

- Short axial gearbox length reduced engine length.

The resulting star gear system configuration was evaluated using projected reduction gear technologies. The star gear design parameters are given in Table A-VI.

Oil cooling systems were reviewed to provide adequate heat rejection for both the reduction gear and the engine rotor bearings. An air/oil cooler in series with the fuel/oil cooler, and a common lubrication system were adequate for the configurations studied.

3.1.4 Advanced Installation Technology

Installation losses, defined in Figure A-13, reflected predicted advances in nacelle technology, such as reduced leakage (of fan duct air), elimination of internal flow path steps and gaps, and use of low pressure loss acoustic treatment material. The use of advanced lightweight materials (composites, honeycombs, titanium) was assumed for the nacelle, allowing a reduction in total weight of 15 percent compared to conventional nacelle materials.

The advanced technology forced mixer used in the mixed exhaust engines was a short, scalloped design with a mixing length about 29 percent shorter than current designs. This short mixing length offered potential for lower internal pressure loss, lower external nacelle drag, and reduced nacelle weight. Based on JT8D experience and on high BPR mixer model tests, a mixing efficiency of 85 percent was predicted for the Energy Efficient Engine design concept.

A summary of the installation losses and drags are given in Table A-VII.

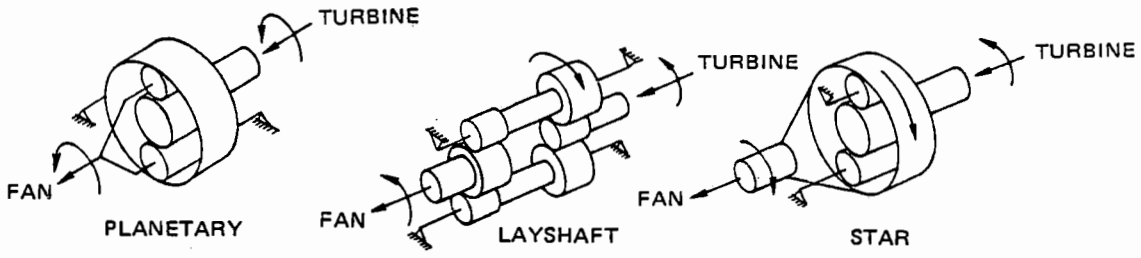

- GEAR RATIO ≈ 2.5
- GOAL EFFICIENCY = 99%

Figure A-12 Candidate Gear Systems

TABLE A-VI

TASK I STAR GEAR DESIGN PARAMETERS

Gear Ratio	2.5:1
Horsepower @ Maximum Cruise	20,000 (14.9×10^6 watts)
@ Takeoff	40,000 (29.8×10^6 watts)
Torque, inch pounds	400,000 (0.0126 Kwhr)
Number of Pinions	6
Number of Bearings	12
Diameter, inches	32 (81.3 cm)
Length, inches	5.5 (14.0 cm)
Efficiency @ Maximum Cruise %	98.8
@ Takeoff, %	99.1

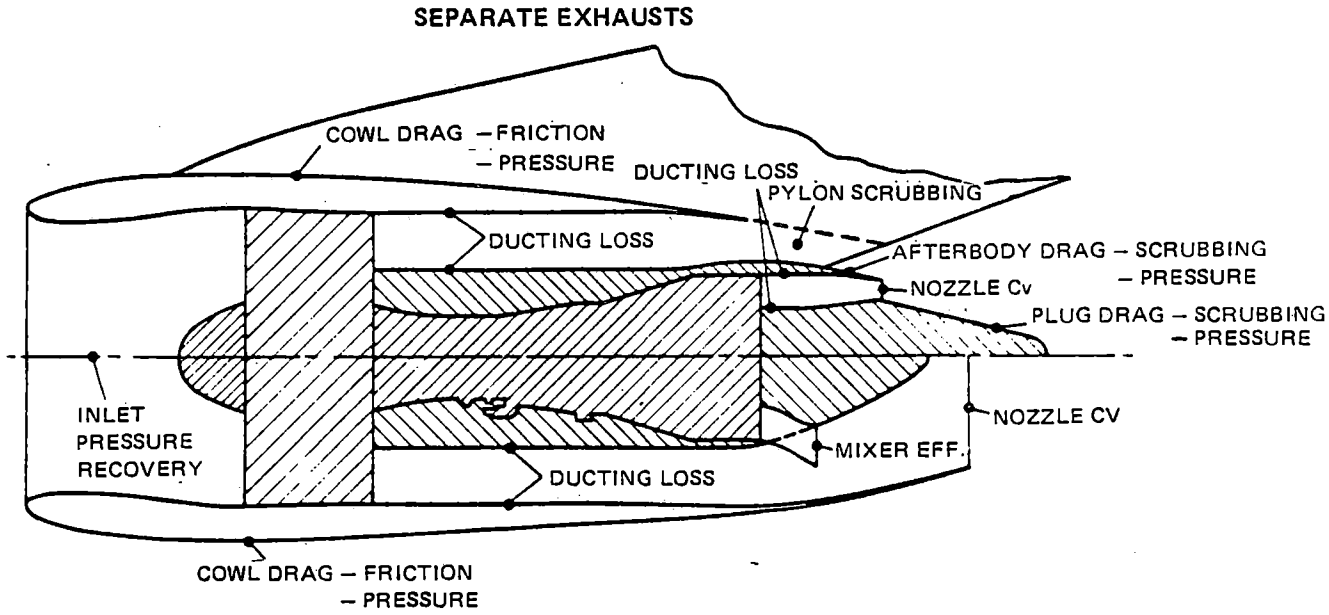

Figure A-13 Energy Efficient Engine Installation Analysis

TABLE A-VII

TASK I ENERGY EFFICIENT ENGINE INSTALLATION ANALYSIS SUMMARY
35,000 FT., 0.80 MN, MAX. CRUISE RATING

	STF495 Non-Mixed	STF505 Non-Mixed	STF495 Mixed	STF505 Mixed
Inlet Total Pressure Recovery	0.9966	0.9966	0.9966	0.9966
Ducting Pressure Losses - $\Delta P_T/P_T$				
Fan Duct	0.0109	0.0125	0.0061	0.0067
Tailpipe	0.0090	0.0130	0.0024	0.0025
Mixer				
Efficiency	–	–	85%	85%
Pressure Loss $\Delta P_T/P_T$				
Duct Lobes	–	–	0.0010	0.0010
Primary Lobes	–	–	0.0018	0.0020
Nozzle Cv	0.998	0.998	0.998	0.998
Nacelle Drag-to-Thrust$_{uninst.}$ Ratio				
Fan Cowl	4.18%	3.72%	4.81%	4.34%
Pylon/Afterbody Scrubbing	0.65	0.95	–	–
Plug Scrubbing	0.18%	0.33%	–	–

3.2 COMPARISONS OF ENGINE CAPABILITIES RELATIVE TO THE REFERENCE ENGINE

The reference engine for establishing benefits of the Energy Efficient Engine cycles was the JT9D-7A engine serial number P-686089 installed in a B747-200 nacelle. Over 1600 JT9D engines have been delivered, representing 18 million flight hours. The JT9D-7A can be considered representative of current technology high BPR turbofans since the JT9D-7A/-20/CN series is the largest portion of current (greater than 1300) and potential future engine sales.

Comparisons of the advanced engines to the reference engine in Task I were done by Pratt & Whitney Aircraft usingisolated nacelle trade factors (Table A-VIII) developed for both domestic and international range advanced airplanes. The aircraft configurations used in developing these factors are given in Table A-IX. The comparisons were based on engines scaled to equal maximum cruise thrust at 10,700 m (35,000 ft), Mach 0.8, with TSFC also being evaluated at that condition.

Engine and nacelle weights, prices, and maintenance costs were assessed for each of the four candidate engine types. The engine and

nacelle weights scaled to fit the international aircraft are shown in Table A-X, while Figure A-14 presents relative prices and maintenance costs.

All four engine types studied in the Task I Engine Cycle Definition exceeded the 12 percent minimum TSFC reduction goal. As shown in Figure A-15, both mixing and reduction gears indicate additional TSFC savings potential on the basis of an isolated nacelle. The DOC improvement relative to the scaled JT9D-7A for all engine types exceeded the goal for an international range aircraft. This level was checked for the less fuel sensitive domestic trijet with the direct-drive, unmixed engine and the goal DOC was still surpassed.

The results of the Task I first pass analysis, summarized in Table A-XI, indicated that all four advanced engine types could meet or surpass the study goals (except for NO_x emissions, which none of the cycles met). Since this evaluation did not include interference and other airplane integration effects, the decision was made to carry all four engine types into the Task II Cycle Refinement/Aircraft Integration Evaluation, where these effects would be assessed with the assistance of Boeing, Douglas, and Lockheed as subcontractors. The cycle of each engine type would also be further optimized in Task II so that a more accurate comparison could become possible.

TABLE A-VIII

TASK I DOC TRADE FACTORS
Typical Mission Base Fuel Prices
Installed Thrust @ 10,700 m (35,000 ft) Mach 0.8 = (9456 Lbs.) 42080 N

	Medium Range Domestic	Long Range International
1% DOC =		
% Δ TSFC	2.38	1.56
Engine Weight ~ kg	771.	644.
~ (lbs)	1700	1420
Nacelle Weight ~ kg	386	372
~ (lbs)	850	820
Engine Price ~ $1000	296	309
Maint. Cost ~ $/Eng. Hr.	8.20	7.35

TABLE A-IX

TASK I AIRCRAFT

	Medium Range Domestic	Long Range International
Design Range ~ km	5,560	10,190
~ (n.m)	3,000	5,500
Passengers • (6 A/B first, 9A/B tourist)	440	510
Cruise MN	0.80	0.80
No. of Engines	3	4
Nominal TOGW ~ kg	231,340	344,740
~ (lbs)	510,000	760,000
Nominal Engine Thrust Class ~ N	186,820	186,820
~ (lbs)	42,000	42,000
Aspect Ratio	12	12
Aerodynamics	Supercritical	
Structure	Advanced Composite	

TABLE A-X

TASK I CYCLES VS. JT9D-7A
PROPULSION SYSTEM CHARACTERISTICS
Engines Sized for International Aircraft Design Mission

	JT9D-7A	STF505	STF505M	STF495	STF495M
Engine Type	Dir. Dr. Sep. Flow	Dir. Dr. Sep. Flow	Dir. Dr. Mixed Flow	Geared Sep. Flow	Geared Mixed Flow
Thrust ~ SLS, Unin. ~ N ~ (lbs.)	212,440 (47,760)	187,080 (42,060)	183,660 (41,290)	189,490 (42,600)	186,590 (41,950)
Engine Weight ~ kg ~ (lbs)	4,060 (8,940)	3,570 (7,860)	3,550 (7,820)	3,650 (8,050)	3,530 (7,790)
Nacelle Weight ~ kg ~(lbs)	1,090 (2,410)	1,660 (3,660)	1,570 (3,460)	1,680 (3,710)	1,640 (3,610)
Total Pod Weight ~ kg ~ (lbs)	5,150 (11,350)	5,230 (11,520)	5,120 (11,280)	5,330 (11,760)	5,170 (11,400)
Nacelle Cowl Length ~ cm ~ (in.)	290 (114)	533 (210)	676 (266)	546 (215)	688 (271)
Nacelle Max. Diameter ~ cm ~ (in.)	269 (106)	284 (112)	279 (110)	305 (120)	297 (117)

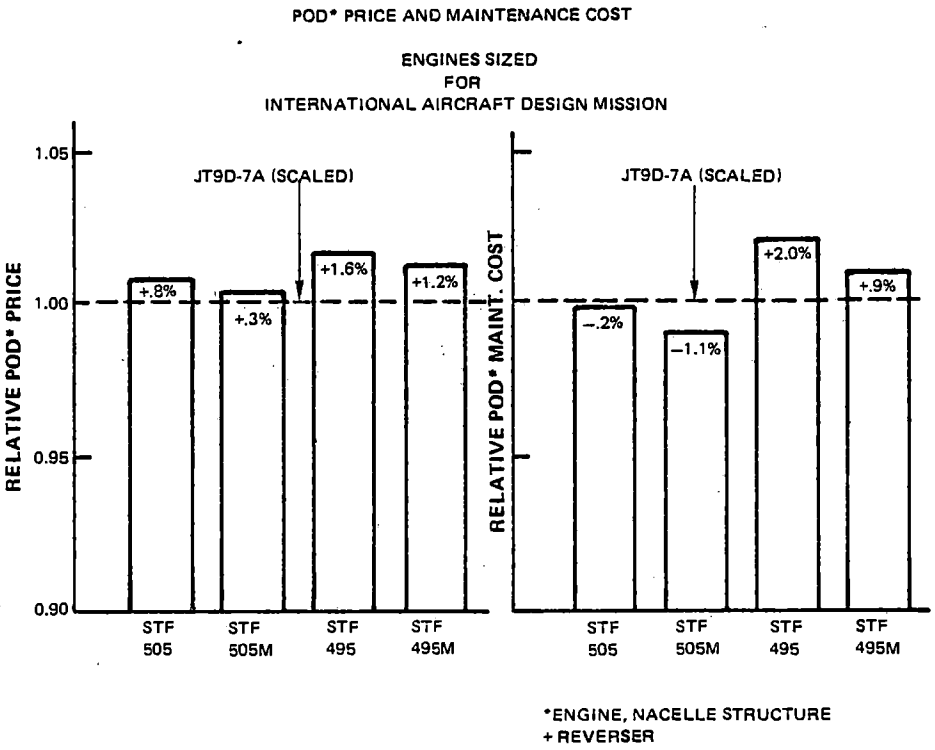

Figure A-14 *Energy Efficient Engine Cycles Versus JT9D-7A - Relative price and maintenance cost for engines sized for long range aircraft design mission.*

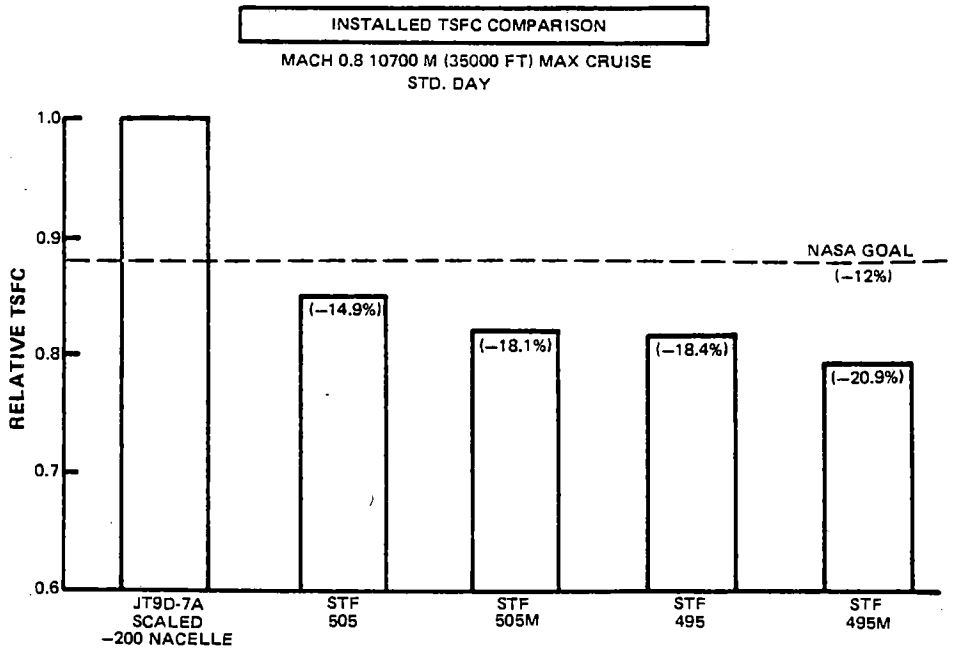

Figure A-15 *Energy Efficient Engine Versus JT9D-7A – Comparison of installed TSFC with NASA goal shown.*

TABLE A-XI

TASK I CYCLE BENEFITS

		Engine				
			Direct Drive		Geared	
	Goal	Reference JT9D-7A	Non-mixed STF505-1	Mixed STF505M-1	Non-mixed STF495-1	Mixed STF495M-1
Installed cruise TSFC	−12%	Base	−15%	−18%	−18%	−21%
Direct operating cost (DOC)	−5%	Base	Better than 5% reduction			
Emissions	1981 EPA	–	Meets 1981 THC and CO, exceeds NO_x			
Engine noise	FAR 36-10 EPNdB	–	Meets FAR 36-10 EPNdB			
Thrust growth	No compromising other goals	–	Supercharging and increased turbine temperature increases NO_x			
Deterioration		Base	Improved			

APPENDIX B

ENGINE-AIRFRAME INTEGRATION – TASK II
(Engine Cycle Refinement)

LIST OF ILLUSTRATIONS
APPENDIX B

LIST OF ILLUSTRATIONS
APPENDIX B

LIST OF ILLUSTRATIONS
APPENDIX B

APPENDIX B

LIST OF TABLES

APPENDIX B
ENGINE–AIRFRAME INTEGRATION–
TASK II
(ENGINE CYCLE REFINEMENT)

1.0 INTRODUCTION

The engine cycles that had been chosen during Task I were refined during Task II, and high- and low-spool configurations were selected for further analysis to be performed during Task III. The cycles chosen during Task I were evaluated over a wide range of perturbations (see Table B-I below). From this assessment, twenty-nine specific advanced-engine types were selected for airplane performance analysis. The method of analysis is explained in Section 3.3 of the main body of the report.

TABLE B-I
TASK II ENGINE STUDY CYCLE RANGE

Bypass Ratio (BPR)	6 to 9 (Direct Drive Nonmixed Cycle) 7 to 8 (Direct Drive Mixed Cycle) 7 to 11 (Geared Nonmixed Cycle) 9 to 11 (Geared Mixed Cycle)
Overall Pressure Ratio (OPR)	33:1 to 45:1
Design Rotor Inlet Temp. (RIT)	1120°C to 1290°C (2050°F to 2360°F)

All twenty-nine engines were evaluated by Pratt & Whitney Aircraft, and seven of the twenty-nine, representing variations in parameters that have the greatest effect on engine-aircraft integration, were evaluated by three airplane companies: Boeing, Douglas, and Lockheed. All three evaluated the same seven engines. The JT9D-7A engine was also analyzed by Pratt & Whitney Aircraft and the airplane companies for use as a reference baseline. For the eight engines evaluated by the airplane companies, Pratt & Whitney Aircraft provided fully installed – including customer bleed, horsepower extraction, external isolated nacelle drag, engine performance data, engine and nacelle weights, dimensions, and scaling curves. Each company evaluated the engines in two airplanes: a domestic route airplane and an intercontinental route airplane. The airplanes were selected independently by each company as being suitable for operation in the 1990's.

Based on their evaluations, the airplane companies provided Pratt & Whitney Aircraft with airplane performance, fuel burned, weights, airframe noise, and FAR 36 flight conditions. Pratt & Whitney Aircraft combined this information with propulsion system prices, maintenance costs, and engine noise; and calculated airline operating costs, ROI, and total noise for each engine-airplane system. Pratt & Whitney Aircraft also assessed exhaust emissions levels and engine growth potentials.

Of the twenty-nine engines analyzed by Pratt & Whitney Aircraft, some were eliminated by inspection of their performance, while the remainder were carried through a fuel-burned and economic evaluation, using Pratt & Whitney Aircraft generated trade factors. The results obtained in this manner agreed well with the airplane company evaluations and were used to complete the cycle refinement.

A summary of the Task II refined cycle benefits relative to the JT9D-7A reference engine is shown in Table B-II. Mixed exhaust engines showed a clear advantage in both fuel burned (2% to 4% additional savings) and DOC (0.5% to 2.5% reduction) relative to separate exhaust engines and, as a result, mixed-exhaust engines

in both direct-drive and geared configurations were chosen for further analysis in Task III. All Task I and II engines had two-stage HPT's as does the JT9D-7A engine. At the end of Task II, it was decided to also consider a single-stage HPT configuration which offered a number of economic advantages as a result of mechanical simplicity and reduced maintenance cost.

TABLE B-II
TASK II E^3 STUDY CYCLE BENEFITS
(Two-Stage, High-Pressure Turbine)

	Goal	Reference JT9D-7A	Direct Drive		Geared	
			Separate	Mixed	Separate	Mixed
Bypass Ratio			6.5	6.5	9	9
Installed Cruise TSFC ~ %	-12	Base	-14	-17.5	-19	-21
Direct Operating Cost (DOC) ~ %	-5					
Domestic Aircraft (Ave.) ~ %		Base	-5	-6	-5	-5
International Aircraft (Ave.) ~ %		Base	-8	-10	-9.5	-11.5
Emissions	1981 EPA	–	Meets 1981 THC and CO, exceeds NO_x			
Total Noise (w/curr. tech.)[a]	FAR 36 (1969) – 10 EPNdB	–	-6	-7	-8	-9
(w/adv. tech.)			-9	-10	-10	-11
Thrust Growth	No compromising other goals	–	Goals uncompromised except for NO_x			

Note: (a) All engines meet FAR 36 (Amended 1977)

2.0 AIRCRAFT AND MISSION SELECTION

This section describes the airplane and mission definitions, the technology assumptions, and marketing rationale used by each of the airplane companies in arriving at their Energy Efficient Engine airplane definitions.

2.1 BOEING AIRCRAFT

2.1.1 Market Considerations and Design Constraints

Boeing's examination of the 1990's market suggested that future airline requirements will be similar to those existing today. This prediction was based on the assumption that the air traveling community of the 1990's would be approximately the same percentage of the total population as today, with a small annual growth rate of 4 percent to 6 percent. Air cargo growth will also be similar unless a large dedicated air freighter is developed, which might increase the growth rate.

Many current, narrow-body aircraft will probably be retired from service by the major airlines in the late 1980's. These include about 750 international range B707 and DC8 series airplanes, and over 1000 B727 domestic range airplanes. There should, therefore, be a market in the late 1980's for a large number of 180 to 220 passenger aircraft with domestic or international range capability. Accordingly, the design missions and sizing constraints selected by Boeing for the study are given in Table B-III.

TABLE B-III

BOEING - MISSIONS AND SIZING CONSTRAINTS

	Domestic Airplane	International Airplane
Design Range, km (naut. mi.)	3710 (2000)	10,190 (5500)
Passengers (15/85 split)	196	196
Cruise Mach No.	0.80	0.80
Takeoff Field Length, m (ft)	2290 (7500)	3350 (11,000)
Approach Velocity m/sec (knot)	65 (125)	70 (135)
Initial Cruise Alt., m (ft)	10,100 (33,000)	10,100 (33,000)
Typical mission for economic evaluation:		
Range, km (naut. mi.)	1850 (1000)	3710 (2000)
Passengers (15/85 split)	108	108
Cruise Mach No.	0.80	0.80

A four wing mounted engine configuration was chosen over a three engine configuration for the international airplane to simplify engine installation problems and to provide wing-bending relief and flutter suppression. Because passengers have shown a preference for double-aisle seating on long flights (over 10 hours), a wide body airplane with a seven abreast, two-aisle seating arrangement was chosen. The fuselage diameter determined by this seating will accommodate 17 LD-3 containers side by side in the cargo hold.

The domestic airplane configuration was selected for high commonality with the international airplane; hence, it has the same body seating and cargo arrangement with two wing mounted engines.

2.1.2 Advanced Technology Features

Boeing reviewed each technology area, and identified the following advanced technology features expected to be available for a 1986 program start and an early 1990's in-service date.

The advanced aerodynamic features included improved wing-airfoil design, wing-nacelle-strut design for minimum interference, and tailoring of the empennage to the wing body flowfield. These features were included in both airplanes, resulting in a 2 percent reduction in cruise drag. In addition, the low speed (takeoff and landing) lift/drag of the domestic airplane was increased 5 percent through incorporation of sealed leading-edge flaps, seal between nacelle struts and lateral edges of leading edge flaps, and aileron droop. Improvements in low speed aerodynamics were not assumed for the international airplane.

Advanced structural features (see Table B-IV) include the use of advanced aluminum alloys, high-strength titanium, and composites.

Advanced flight control technology features incorporated in both airplane designs were:

1) all axes handing qualities stability augmentation systems, 2) all flying tail, and 3) double-hinged control surfaces.

Systems technology advancements applied to each design consisted of cabin air reconstitution and recirculation, integration of anti-icing with environmental control system, carbon brakes, and limited slip braking system.

TABLE B–IV
BOEING–ADVANCED AIRFRAME STRUCTURE

Current Technology	New Technology		
Material	Material	Structural Component	Weight Saving % of Component Weight
Standard Aluminum Alloys (Current B747)	Advanced Aluminum Alloys	Wing Box	6
		Fuselage	4
		Empennage Box	6
Conventional Aluminum Construction	Advanced Composite Structure (Graphite)	Control Surfaces Landing Gear Doors	25
	Carbon	Main Landing Gear Brakes	40
Titanium Fittings		Landing Gear Support	20
		Side of Body Rib	
		Empennage Body Attach	
		Engine Strut Attach Flap Support	

Typical design selection charts for international and domestic airplanes are shown in Figures B-1 and B-2, respectively. The wing loading of the international airplane was selected as a

compromise between block fuel, takeoff gross weight, fuel volume, and growth C_L buffet. Thrust loading was determined by the 10,100 m (33,000 ft) initial cruise altitude requirement. For the domestic airplane, wing loading was chosen to minimize takeoff gross weight and block fuel while the 2290 m (7500 ft) takeoff field length set thrust loading.

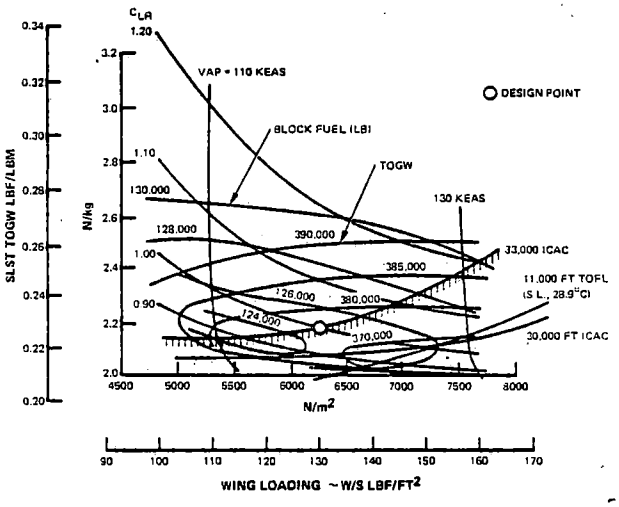

Figure B-1 Boeing International Airplane Design Selection Chart (Mach No. = 0.80, 196 Pass./5500 N. Mi. Still Air Range). The intercontinental airplane was selected as a compromise between block fuel, takeoff gross weight, fuel volume, and growth C_L buffet.

Configuration drawings of international and domestic airplanes are shown respectively in Figures B-3 and B-4.

2.2 DOUGLAS AIRCRAFT

2.2.1 Market Considerations and Design Constraints

Douglas believes that normal progress of development and traffic growth indicates the

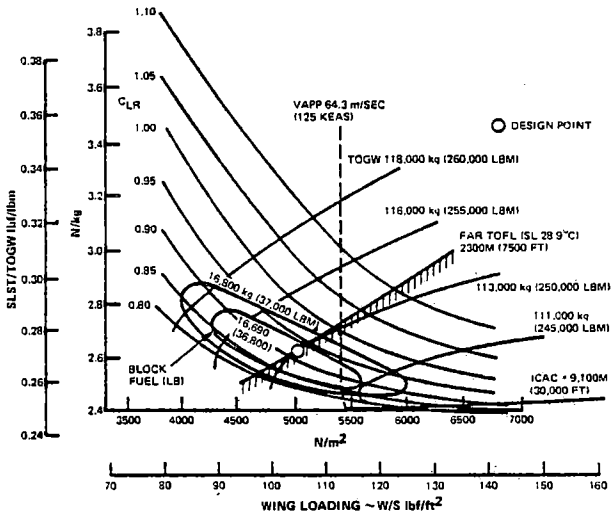

Figure B-2 Boeing Domestic Airplane Design Selection Chart (Mach No. = 0.80, 196 Pass./ 2000 N. Mi. Still Air Range). The domestic airplane was selected based on a wing loading chosen to minimize takeoff gross weight and block fuel; the 2290 m takeoff field length set thrust loading.

most likely new airplane program that could be initiated in the 1990's is a growth airplane (450 to 500 passengers). While this program could be developed for an all new airplane, an improved technology derivative of a current wide body transport appears to be more likely. This airplane would probably have a domestic and an international version, similar to the DC10 series practice.

Although a new aircraft to replace DC8's and B707's in domestic operations is clearly needed, this need is expected to be fulfilled by the DCX-200 and/or B7X7 aircraft, which should be in its production peak in the mid-to-late 1980's. Thus a replacement would not be needed for these aircraft in the early 1990's.

Similarly, the current wide-body transports should continue in production through the 1980's, with stretched versions based on the

current wing being introduced in the early 1980's. If there is a technical breakthrough in laminar-flow technology in the early 1980's, an airplane sized to replace the existing wide-body fleet would be a logical development, since this fleet would be the largest users of aviation fuel. Such a high technology airplane would then be available for the 1990-1995 time period.

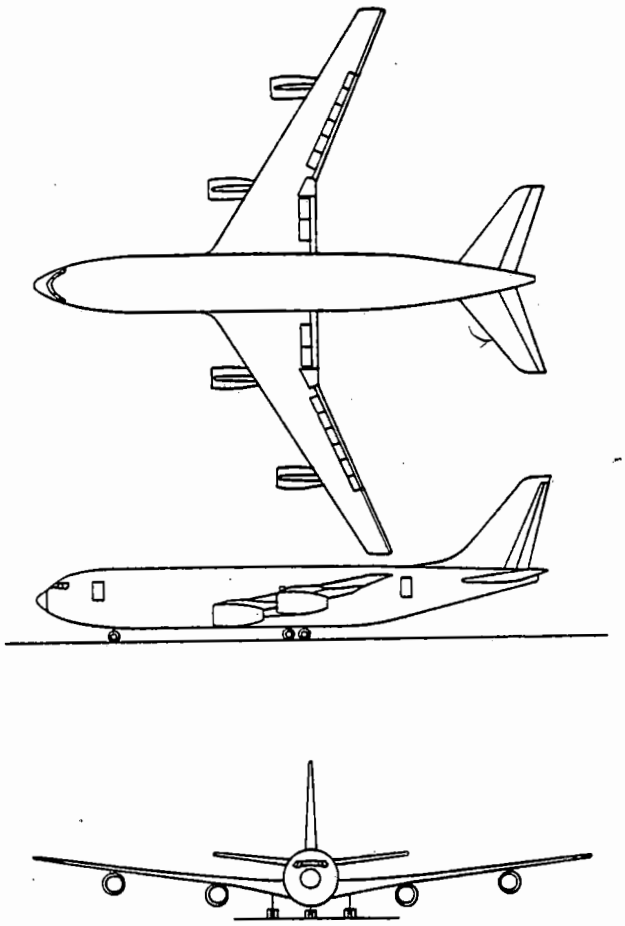

Figure B-3 *Boeing International Airplane. Selection for the international airplane was a four wing mounted engine configuration.*

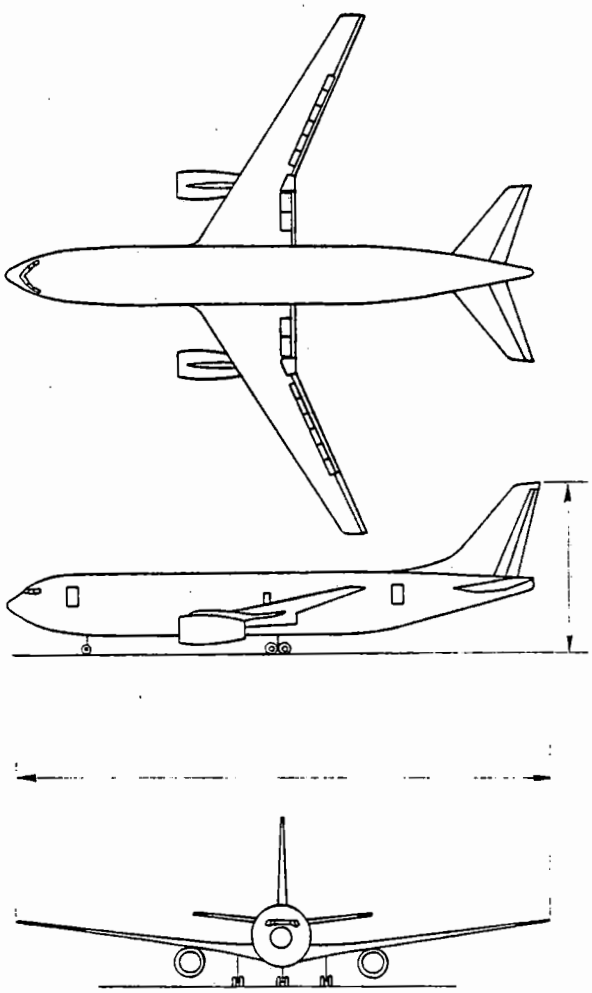

Figure B-4 *Boeing Domestic Airplane. Domestic airplane selection based on high commonality with the intercontinental airplane; the domestic airplane has two wing-mounted engines.*

Based on these marketing projections and on the assumption that aircraft development will proceed along normal trend lines without a major technical breakthrough, the Douglas airplanes were based on a DC10 trijet derivative with stretched fuselage and all new wing. Aircraft sizing and mission criteria are presented in Table B-V.

TABLE B-V

DOUGLAS - MISSIONS AND SIZING CONSTRAINTS

	Domestic Airplane	International Airplane
Design Range, km (naut. mi.)	5560 (3000)	10190 (5500)
Passenger (10/90)	438	438
Cruise Mach No.	0.80	0.80
Takeoff Field Length, m (ft)	2440 (8000)	3350 (11000)
Approach Velocity m/sec (knots)	65 (125)	70 (135)
Initial Cruise Alt., m (ft)	10100 (33000)	9500 (31000)
Typical mission for economic evaluation:		
Range, km (naut. mi.)	1850 (1000)	2780 (1500)
Passengers	252	241
Cruise Mach No.	0.80	0.80

Externally, the domestic and international airplanes are similar—having the same wing, fuselage, and empennage—but have different thrust requirements. Interior arrangements are also different: the domestic airplane has a lower galley, allowing more seating but less cargo space (40 vs 50 LD-3 containers) than the upper galley interior configuration of the international airplane. Engine placement and fuselage diameter are the same as in the current DC10 series aircraft, but the fuselage has been stretched 18.3 meters (60 ft) in length.

2.2.2 Advanced Technology Features

A review of the various technology areas by Douglas indicated that the following advanced features should be available for an early 1990's configuration:

Advanced aerodynamic features included a thick supercritical, high aspect ratio wing, winglets, and an advanced high lift system. The advantages of a supercritical wing of increased thickness—such as that now flying on the YC-15—include less weight, reduced drag, and improved C_L buffet. Increasing wing aspect ratio from the 6 to 8-1/2 level of current transports to 10 to 12 will reduce induced drag which will reduce engine size and fuel consumption. Although winglet design technology is not expected to be ready for the next generation of aircraft, it should have advanced sufficiently for inclusion in an early 1990's airplane. The advanced high lift system, consisting of a variable camber Krueger leading edge and a translating flap, will provide improved C_L max and lift/drag.

Composite materials should be ready for application in the next generation of transport aircraft in such areas as control surfaces, floor beams, fairings, and landing gear doors. Design, fabrication, and repair techniques should be sufficiently advanced by the early 1990's to permit essentially full-composite wings and empennage. The fuselage pressure shell, however, would still be of metal construction.

In the area of advanced controls, a longitudinal stability augmentation system would be incorporated to reduce empennage area and trim drag.

Advanced systems features would include digital avionics, reduced-bleed requirement air conditioning, advanced APU, and advanced cockpit displays.

2.2.3 Aircraft Design Point Selection

Douglas chose to use the same wing for both domestic and international airplanes. The procedure that led to this decision is illustrated in Figure B-5. The DOC penalty for this compromise wing is small. Thrust loading was determined from the initial cruise altitude for both airplanes, using the Task II baseline advanced engine, STF505-1. A general arrangement drawing applicable to both airplanes is presented in Figure B-6.

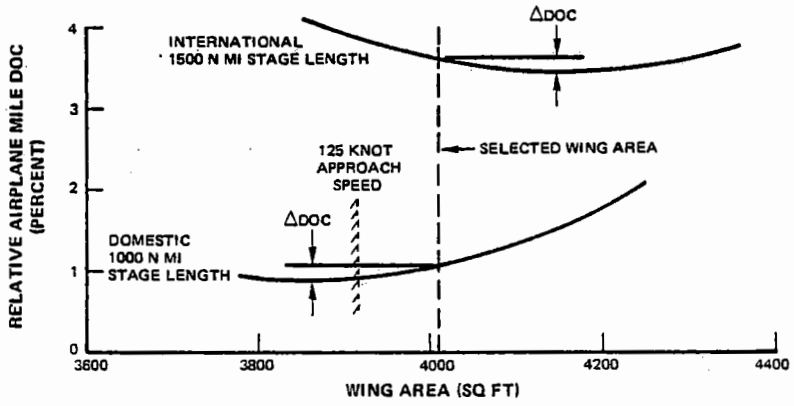

Figure B-5 Douglas Wing Loading Selection Procedure. Douglas chose to use the same wing for both the domestic and inter-continental aircraft.

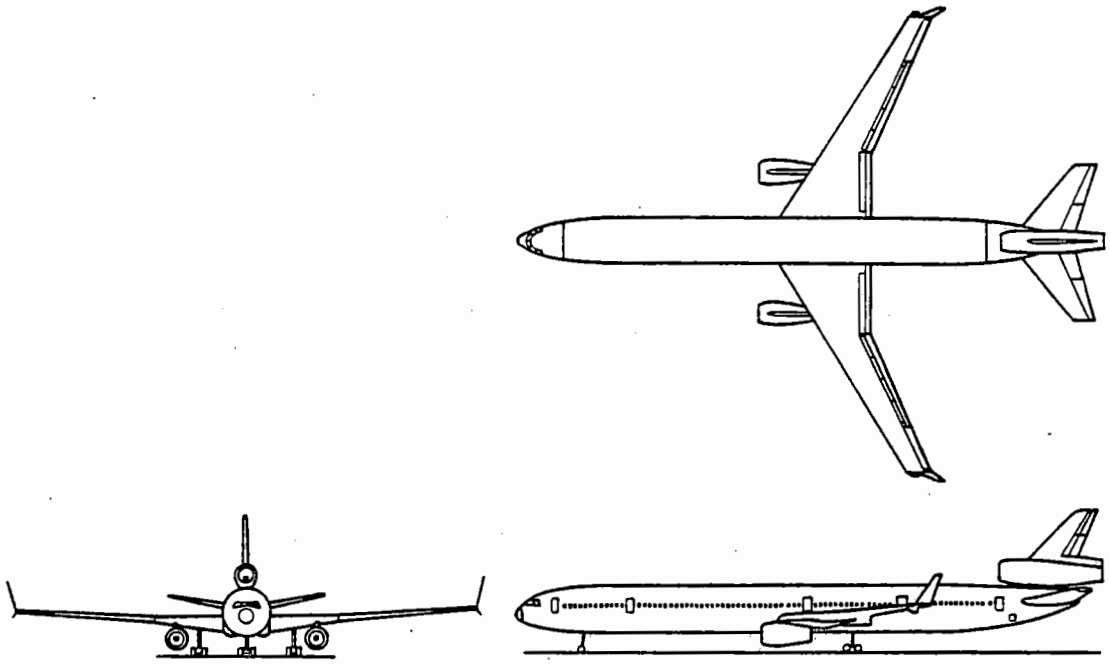

Figure B-6 Douglas General Arrangement Applicable to Both Domestic and International Airplane. Advanced aerodynamic features included are a thick supercritical high aspect ratio wing, winglets, and an advanced high lift system.

2.3 LOCKHEED AIRCRAFT

2.3.1 Market Considerations and Design Constraints

Lockheed market projections to the year 2000 were used to establish total world-traffic demand (Table B-VI). Traffic distribution patterns were studied to establish range requirements for both domestic and international airplane designs. Combining the world traffic forecast with traffic distribution provided an estimate of the number of aircraft, by seating capacity, that would be required to accommodate the market (Table B-VII). From this data, the aircraft design range was established as 5560 km (3000 naut. mi.) for the domestic mission and 12,050 km (6500 naut. mi.) for the international mission. These design ranges encompass all domestic routes and 93 percent of the total long-range traffic projected for the year 2000. Based on considerations of seat-distance costs, airport congestion, scheduling flexibility, frequency of service, and number of aircraft required, an aircraft size of 400 passengers was selected for both domestic and international missions.

Market projections and airline preference indicate a cruise speed of Mach 0.85, especially for the longer-range mission. Previous studies by Lockheed, however, showed that lowest operating costs and optimum fuel utilization in a high fuel-cost environment are attained at a cruise speed of Mach 0.8. A cruise speed of Mach 0.8 was therefore selected. A summary of the mission and aircraft design criteria is presented in Table B-VIII.

TABLE B-VI

LOCKHEED TRAFFIC FORECAST

(Major Long-Haul Markets – Over 4800 km – One-Way Daily Average Passengers)

Market	1975*	1990	Avg. Annual Growth Rate ~ %	2000	Avg. Annual Growth Rate ~ %
No. America–Europe	16,986	34,979	4.9	51,777	4.0
Europe–Asia/Oceania	4,071	15,864	9.5	28,410	6.0
No. America–Asia/Oceania	3,425	14,668	10.2	28,850	7.0
Europe–Africa	2,328	11,222	11.1	22,078	7.0
Europe–So. America	1,644	8,025	11.1	15,787	7.0
No. America–Latin/So. America	1,506	6,303	10.0	12,398	7.0
Group Total	29,960	91,061	7.7	159,394	5.8

*Lockheed Estimate

TABLE B-VII

LOCKHEED PROJECTION OF TOTAL LONG-HAUL AIRCRAFT REQUIREMENTS BY YEAR 2000

(Based on Daily Service 60% Load Factor)

	Aircraft Seating Capacity				
Distance Block ~ km (mi)	200	300	400	500	600
4,800 - 6,440 (3,000 - 4,000)	448	298	222	176	146
6,400 - 8,100 (4,000 - 5,000)	395	259	195	152	126
8,100 - 9,700 (5,000 - 6,000)	374	246	186	145	120
9,700 - 11,300 (6,000 - 7,000)	245	161	119	93	78
11,300 - 12,900 (7,000 - 8,000)	26	15	7	7	6
12,900 - 14,500 (8,000 - 9,000)	21	13	8	6	5
14,500 - 16,100 (9,000 - 10,000)	27	17	13	10	8
16,100 - 17,700 (10,000 - 11,000)	20	13	10	8	7
Total	1,556	1,022	760	597	496

TABLE B-VIII

LOCKHEED - MISSIONS AND SIZING CONSTRAINTS

	Domestic Airplane	International Airplane
Design Range, km (naut. mi.)	5560 (3000)	12,050 (6500)
Passengers	400	400
Cruise Mach No.	0.80	0.80
Takeoff Field Length, m (ft)	2135 (7000)	2895 (9500)
Approach Velocity, m/sec (knots)	69 (135)	69 (135)
Initial Cruise Altitude, m (ft)	10,700 (35,000)	10,200 (35,000)
Typical mission for economic evaluation:		
Range, km (naut. mi.)	2595 (1400)	5560 (3000)
Passengers	220	220
Cruise Mach No.	0.80	0.80

A three-engine configuration similar to the L1011 was chosen for the domestic airplane, and a four wing-mounted engine configuration was chosen for the international airplane Passenger accommodations follow the L1011 practices with a fuselage of similar diameter stretched in length to accommodate the additional passengers.

2.3.2 Advanced Technology Features

The levels of advanced technology appropriate for incorporation into the airframe design for the early 1990's time frame as projected by Lockheed are discussed in the following paragraphs.

The primary advanced aerodynamic technology feature incorporated in the design was a high aspect ratio, supercritical wing. The refined supercritical airfoil as used in this wing is compared with a current L1011 wing airfoil in Figure B-7.

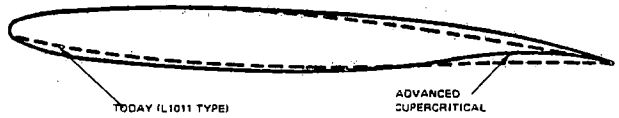

SUPERCRITICAL AIRFOILS FEATURE:
MORE ROUNDED NOSE
MORE CAMBERED TRAILING EDGE

PERMIT:
HIGHER CRUISE SPEEDS
REDUCED WING SWEEP
THICKER AIRFOILS

Figure B-7 Lockheed's Refined Supercritical Wing Compared With Current Technology L1011 Wing. The primary advanced aerodynamic technology features incorporated in the Lockheed design is a high aspect ratio, supercritical wing.

An advanced active control system was incorporated in the Energy Efficient Engine airplane design. This system, currently under development for use in the L1011, will provide load relief and relaxed static stability. Wing-load relief will be accomplished through the use of computer controlled active ailerons to redistribute wing loadings, resulting in reduced bending moments and, hence, reduced wing and body structural weights. Relaxation of static stability will result in a smaller horizontal tail. The effects of these active controls on aircraft configurations in this study are 5.5

percent wing and 1.0 percent body weight reductions resulting from wing load-relief and a 28 percent tail size reduction from relaxed static stability.

Advanced composites will be utilized for internal and external secondary structures and for a significant portion of the primary structures. Specific applications of composites will be:

1) Floor supports, beams, posts, dividers, doors, fuel tank baffles (Internal Secondary Structure);
2) Flaps, slats, spoilers, gear doors (External Secondary Structure); and
3) Vertical fin, horizontal stabilizers, wing, fuselage, engine nacelle (Primary Structure).

The effect of composite structure on aircraft empty weight is shown in Table B-IX.

TABLE B-IX

LOCKHEED - ADVANCED COMPOSITES EFFECT

Component	ΔWt %	
Wing	23	
Tail	20	
Body	7	
Landing Gear	4	
Nacelles	19	
Air Induction	19	
Surface Controls	5	
Furnishings	0	
	Domestic	International
Total reduction in manufacturing empty weight	8.7%	9.2%

2.3.3 Aircraft Design Point Selection

The Lockheed Asset Synthesis Program was used to conduct parametric sizing studies to establish design points for domestic and international airplanes. The results of these studies are shown in Figures B-8 and B-9. Wing loading and thrust loading were chosen to minimize DOC – for the domestic airplane, takeoff distance was limiting; for the international airplane takeoff distance was limiting for wing loading and cruise altitude was limiting for thrust loadings.

Drawings of the domestic and international airplane designs are shown in Figures B-10 and B-11.

2.4 STUDY AIRCRAFT SUMMARY

Summaries of the domestic and international airplane configurations are presented in Tables B-X and B-XI for each airplane company. The data provided is for airplanes with STF505-1 engines. Airplane configurations defined by Pratt & Whitney Aircraft for in-house evaluations have been included for comparison.

3.0 TASK II ENGINE CYCLE PERTURBATIONS

The Task II screening established base cycles for each of four engine types. Pratt & Whitney Aircraft, with the assistance of Boeing, Douglas, and Lockheed, redefined these cycles during Task II. This section describes the range of cycles parameters examined in Task II and discusses their effects on engine performance.

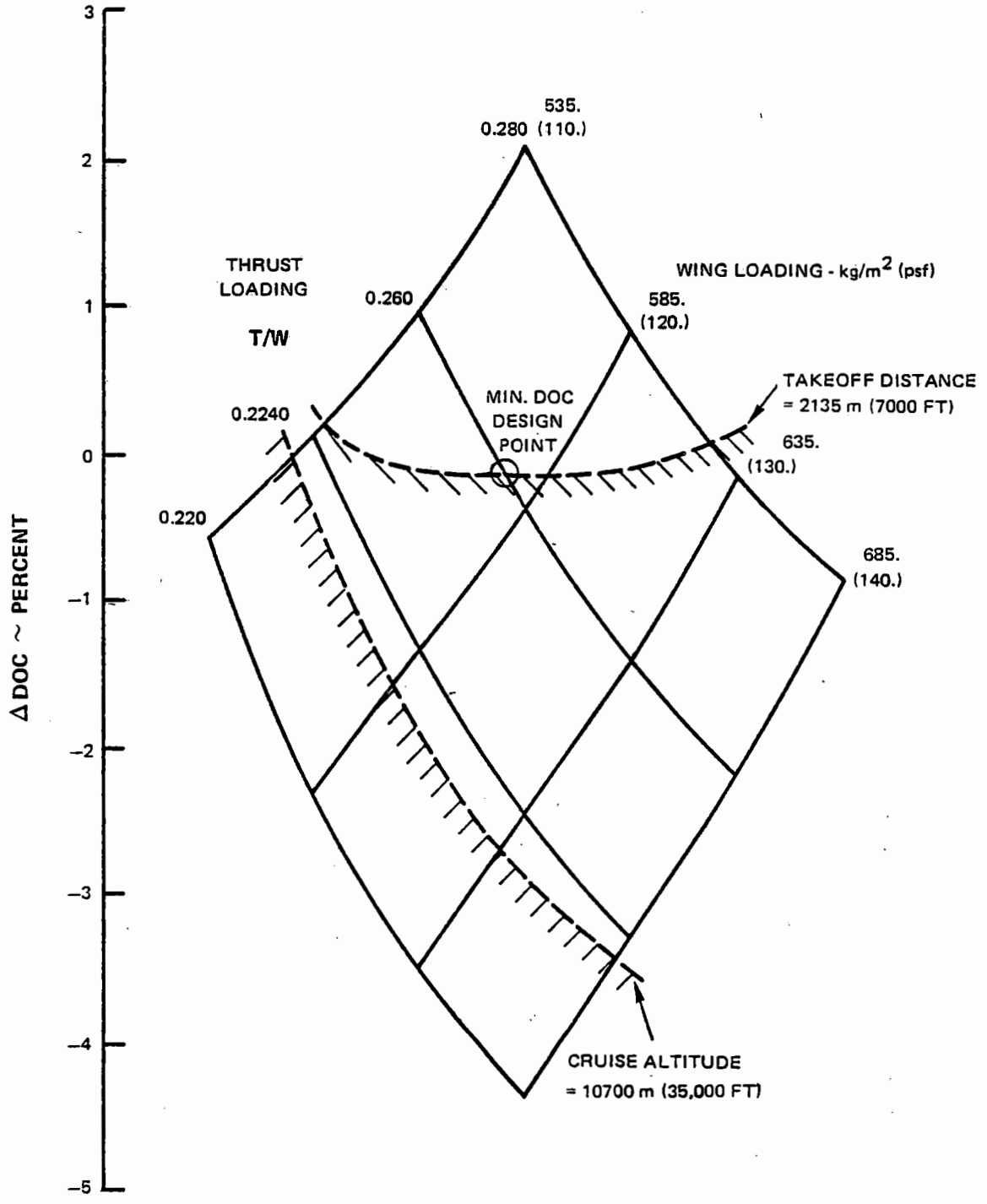

Figure B-8 Results of Lockheed Parametric Studies to Establish Design Points for Domestic Airplane. Wing loading and thrust loading was chosen to minimize DOC; takeoff distance was limiting.

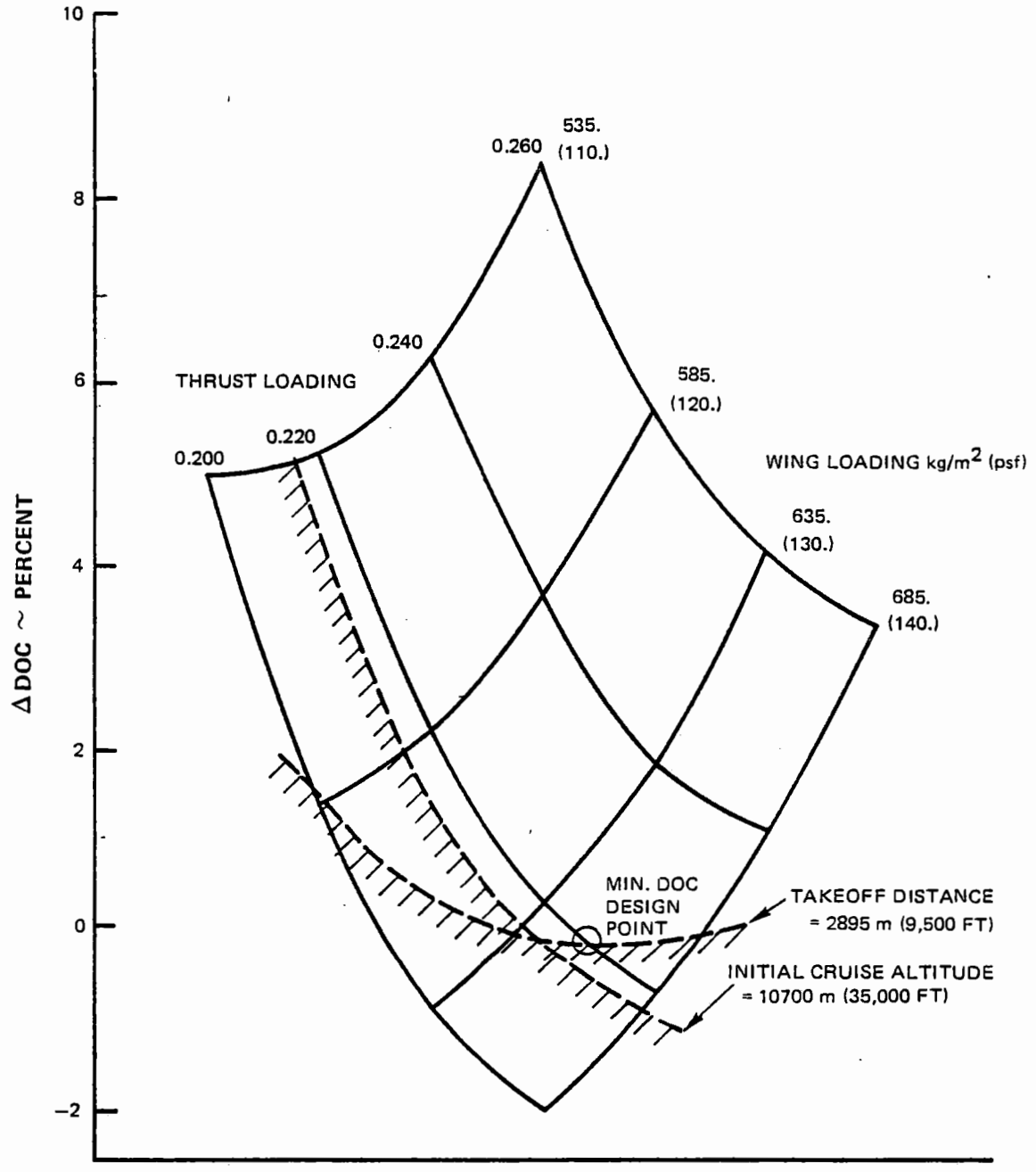

Figure B-9 Results of Lockheed Parametric Studies to Establish Design Points for International Airplane. Wing loading and thrust loading was chosen to minimize DOC; takeoff distance was limiting.

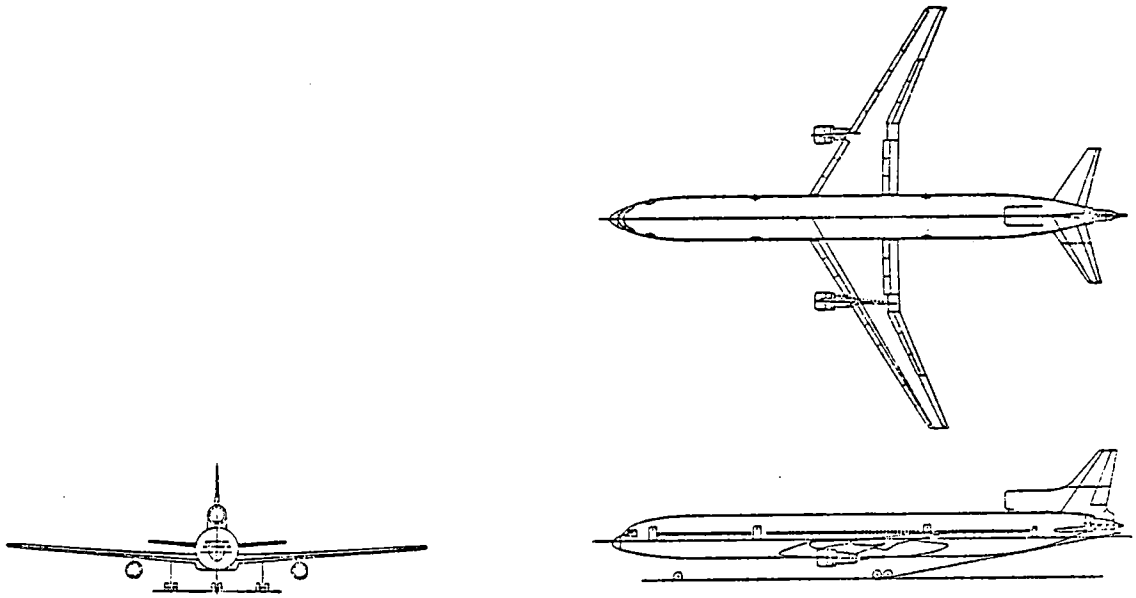

Figure B-10 Lockheed Domestic Airplane Design. The three-engine configuration is similar to L1011 airplane.

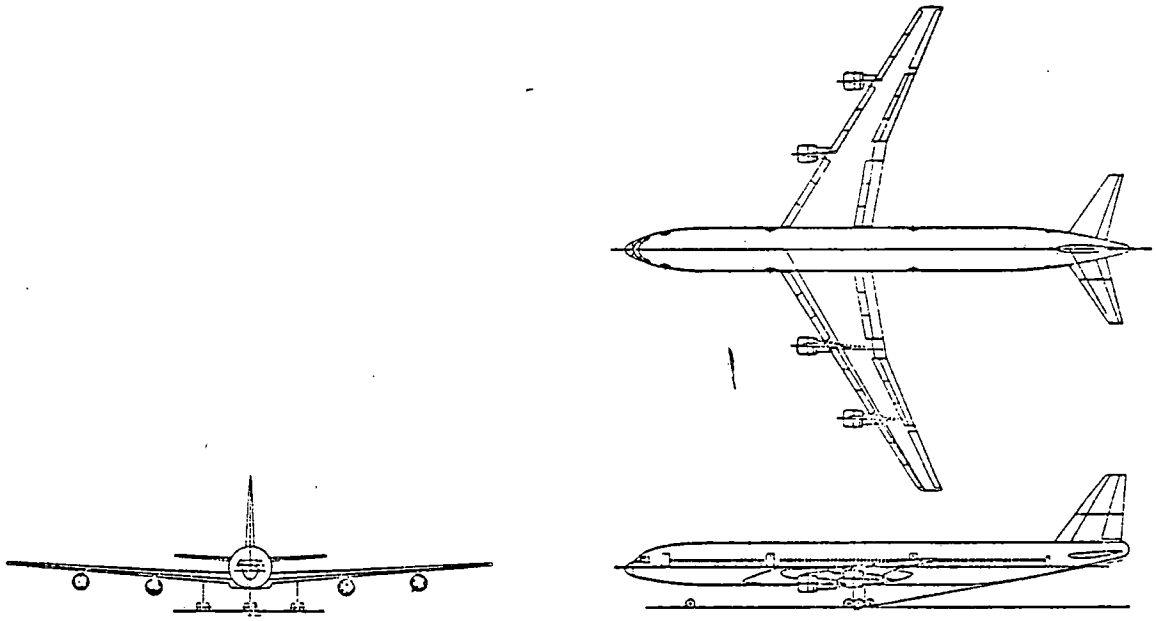

Figure B-11 Lockheed International Airplane Design. Passenger accommodations for both domestic and international airplanes follow L1011 practice with a fuselage of similar diameter stretched in length to accommodate the additional passengers.

TABLE B-X

DOMESTIC AIRPLANE SUMMARY
(With Separate Exhaust, Direct-Drive
STF505-1 Engine)

	Boeing	Douglas	Lockheed	P&WA
Passengers	196	458	400	440
Design Range, km (naut. mi.)	3710 (2000)	5560 (3000)	5560	5560
Typical Mission Range, km (naut. mi.)	1850 (1000)	1850	2595 (1400)	1295 700
Engines	2	3	3	3
Cruise Speed, Mn	0.8	0.8	0.8	0.8
Field Length, m (ft)	2290 (7500)	2260 (7400)	2135 (7000)	2320 (7600)
Initial Cruise Altitude, m (ft)	11300 (37000)	10100 (33000)	11300 (37000)	11700 (35000)
Aspect Ratio	10.24	10	10	12
Sweep (.25c)	30°	30°	30°	25°
Wing Loading - kg/m^2 (lbm/ft^2)	513 (105)	615 (126)	575 (118)	571 (117)
TOGW, kg (lbm)	114000 (251000)	229000 (504000)	185000 (408000)	233000 (514000)
OEW, kg (lbm)	73000 (161000)	131000 (289000)	106000 (233000)	137000 (301000)
Thrust/engine, SLS Inst., kn (lbf)	149.9 (33700)	175.7 (39500)	156.6 (35200)	177.0 (39800)
Airframe noise @ Approach, EPNdB	94	94	92	93

TABLE B-XI

INTERNATIONAL AIRPLANE SUMMARY
(With Separate Exhaust, Direct-Drive
STF505-1 Engine)

	Boeing	Douglas	Lockheed	P&WA
Passengers	196	438	400	510
Design Range km	10190	10190	12050	10190
(naut. mi.)	(5500)		(6500)	
Typical Mission Range~ km	3710	2780	5560	3705
(naut. mi.)	(2000)	(1500)	(3000)	
Engines	4	3	4	4
Cruise Speed M_N	0.8	0.8	0.8	0.8
Field Length m	2620	3110	2895	2775
(ft)	(8600)	(10200)	(9500)	(9100)
Initial Cruise Altitude m	10100	9500	10700	10100
(ft)	(33000)	(31000)	(35000)	
Aspect Ratio	10.24	10	10	12
Sweep (.25C)	30°	30°	30°	25°
Wing Loading kg/m^2	635	776	655	674
(lbm/ft^2)	(130)	(159)	(134)	(138)
TOGW, kg	170,000	289,000	264,000	345,000
(lbm)	(374000)	(638000)	(583000)	(760000)
OEW, kg	85,000	139,000	121,000	170,000
(lbm)	(187000	(306000)	(266000)	(375000)
Thrust/engine SLS Inst., kn	91.2	208.2	142.6	177.0
(lbf)	(20500)	(46800)	(32070)	(39800)
Airframe Noise				
Approach EPNdB	95	95	90	93

3.1 ENGINE STUDY MATRIX

The range of cycle variations considered in Task II is shown in Table B-I. Perturbations of fan tip speed and jet velocity ratio were also evaluated in the refinement process. The matrix of specific engines studied in Task II is presented in Table B-XII. Engines noted as "(c)" were evaluated by the airplane companies. These engines represented perturbations in BPR, nacelle length, and exhaust system type which could significantly affect engine-airplane integration. Full data packages containing installation sketches, engine and nacelle weights, and installed isolated nacelle-engine performance for typical transport aircraft flight conditions were prepared for each of these engines. The other engines were analyzed by Pratt & Whitney Aircraft based on isolated nacelle engine Mn 0.8, 10,700 m cruise performance and parametric weight and cost trends.

TABLE B-XII
TASK II ENGINE MATRIX

Engine	Type	Nacelle	Cruise[a] TSFC kg/hr/N	TSFC lbm/hr/lbf	Fan Press. Ratio	Bypass Ratio	Overall Press. Ratio	RIT[b], °C	°F
JT9D-7A[c]	Direct Drive	Short Duct	0.0690	0.677	1.58	5.1	38.6	1082	1980
STF505 -1[c]		3/4 Duct	0.0587	0.576	1.74	7.0	38.6	1210	2210
-2			0.0584	0.573	1.68	7.6	38.6	1210	2210
-3			0.0582	0.571	1.58	8.8	38.6	1210	2210
-4[c]			0.0575	0.564	1.58	9.0	38.6	1210	2210
-5			0.0596	0.584	1.74	7.4	33.0	1210	2210
-6			0.0581	0.570	1.74	6.6	45.0	1210	2210
-7			0.0589	0.578	1.74	7.8	38.6	2360	2360
-8			0.0592	0.581	1.80	6.5	38.6	1210	2210
-9			0.0591	0.580	1.74	6.9	38.6	1210	2210
-10			0.0605	0.593	1.74	6.1	38.6	1210	2210
-11			0.0595	0.583	1.74	6.6	38.6	1210	2210
-12			0.0584	0.573	1.74	7.6	38.6	1210	2210
-13			0.0594	0.582	1.74	5.9	38.6	1121	2050
STF505M-1[c]		Mixed Flow	0.0566	0.555	1.65	7.0	38.6	1210	2210
M-2[c]			0.0561	0.550	1.60	7.7	38.6	1210	2210
M-3			0.0563	0.552	1.65	7.4	38.6	1210	2210
M-4			0.0568	0.557	1.65	7.8	38.6	1210	2210
M-5			0.0566	0.555	1.69	7.0	38.6	1293	2360
M-6			0.0577	0.566	1.74	6.1	38.6	1210	2210
M-8[c]			0.0572	0.561	1.65	5.9	38.6	1121	2050
STF495 -1[c]	Geared	3/4 Duct	0.0563	0.552	1.58	9.1	38.6	1210	2210
-2[c]		Short Duct	0.0560	0.549	1.58	9.1	38.6	1210	2210
-3		3/4 Duct	0.0560	0.549	1.58	9.8	38.6	1210	2210
-4			0.0555	0.544	1.50	10.5	38.6	1210	2210
-5			0.0586	0.575	1.74	6.9	38.6	1210	2210
-6			0.0566	0.555	1.58	10.0	38.6	1293	2360
STF495M-1[c]		Mixed Flow	0.0547	0.536	1.52	9.1	38.6	1210	2210
-2			0.0538	0.528	1.45	10.7	38.6	1210	2210
-3			0.0559	0.548	1.60	7.8	38.6	1210	2210

Notes: (a) Installed, no bleed or HPX, 10,700 m (35,000 ft), Mn = 0.8
(b) RIT = Turbine rotor inlet temperature
(c) Engine evaluated by airplane company

Engine and nacelle technology assumptions of Task II were the same as in Task I. Nacelles designs of both tasks reflected the use of advanced composite structure technology, which reduced nacelle total weights by about 15 percent compared with conventional structures, and the use of a split gearbox which allows separation of airplane and engine accessories. In a split gearbox arrangement, with airplane accessories mounted on top of the fan case in the pylon and with engine accessories mounted on the bottom quadrant of the fan case, the accessory "bump" could be eliminated from the nacelle, thus reducing nacelle drag and weight.

A two-stage HPT high-spool configuration was assumed for all cycles in the Task II matrix.

3.2 CYCLE TRENDS

The Task II installed cruise TSFC trends is presented in Figures B-12 and B-13. The figures, which show percent change in TSFC as a function of specific thrust, include the effects of fan cowl drag, afterbody and plug skin friction and pressure drags, and the drag of that portion of the pylon wetted by the fan stream. Interference drag and customer bleed or horsepower extraction effects are not included.

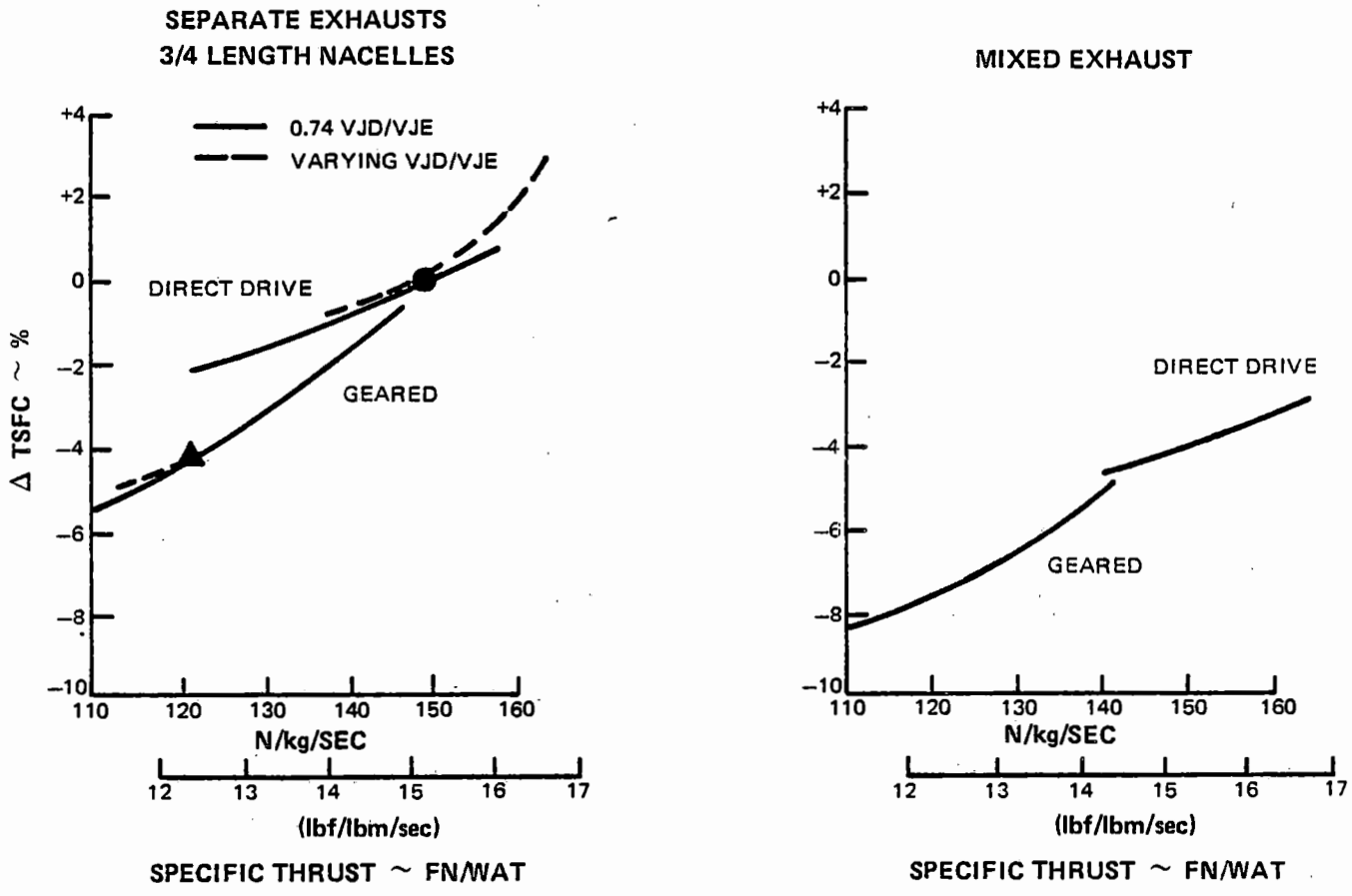

Figure B-12 Task II Isolated Nacelle Cruise Performance (10,700 m, MN max cruise = 0.8, OPR = 38.6:1, Design RIT = 1210°C).

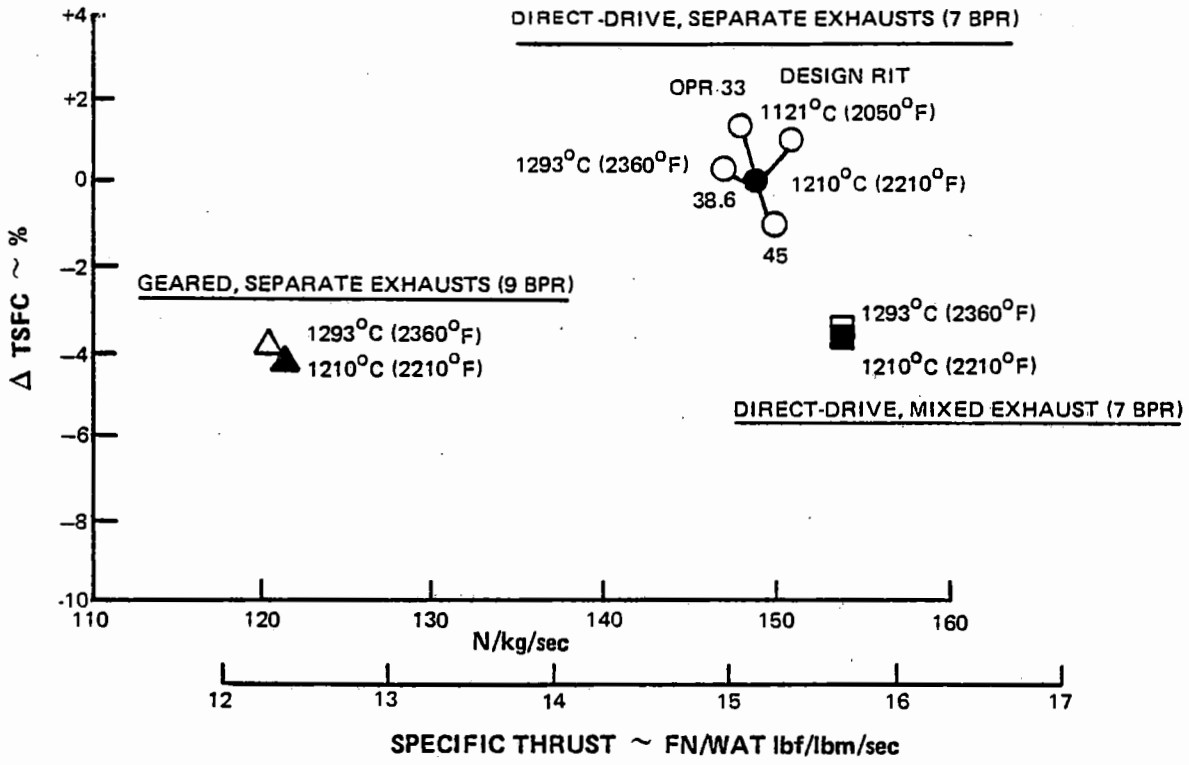

Figure B-13 Task II Isolated Nacelle Cruise Performance Effects on RIT and OPR (10,700 m, 0.8 Mn max. cruise). The trends presented in the figure indicated that for both mixed and separate exhaust, 1210°C RIT is optimum for TSFC and fuel consumption is improved by increasing OPR to 45.

Specific thrust, which varies inversely with BPR was used because it has proven to be a good correlating parameter for cycle performance. The dotted lines in Figure B-12 show a jet velocity ratio (fan duct jet velocity/engine jet velocity) variation about the baseline value. This study indicated that the chosen jet velocity ratio was optimum for installed TSFC at the specific thrust level of the baseline engine.

The effects of RIT and OPR on TSFC are shown in Figure B-13. The trends, both for mixed-exhaust and for separate-exhaust, indicate that 1210°C (2210°F) RIT is optimum for TSFC and that fuel consumption is improved by increasing OPR to 45.

The total engine and nacelle weight trends (i.e., engine plus nacelle), see Figure B-14, indicate a significant weight penalty for increasing BPR. This is particularly true for direct-drive engines. When fan diameter is increased to accommodate the higher BPR – thus causing nacelle weight to increase – the diameter of the LPT of a direct-drive engine must also be increased to maintain turbine performance at the lower rotational speeds required by the increased diameter fan. Because the fan and LPT of geared engines can be operated at different rotational speeds, the impact on total engine and nacelle weight of increased BPR is less severe than with direct-drive engines.

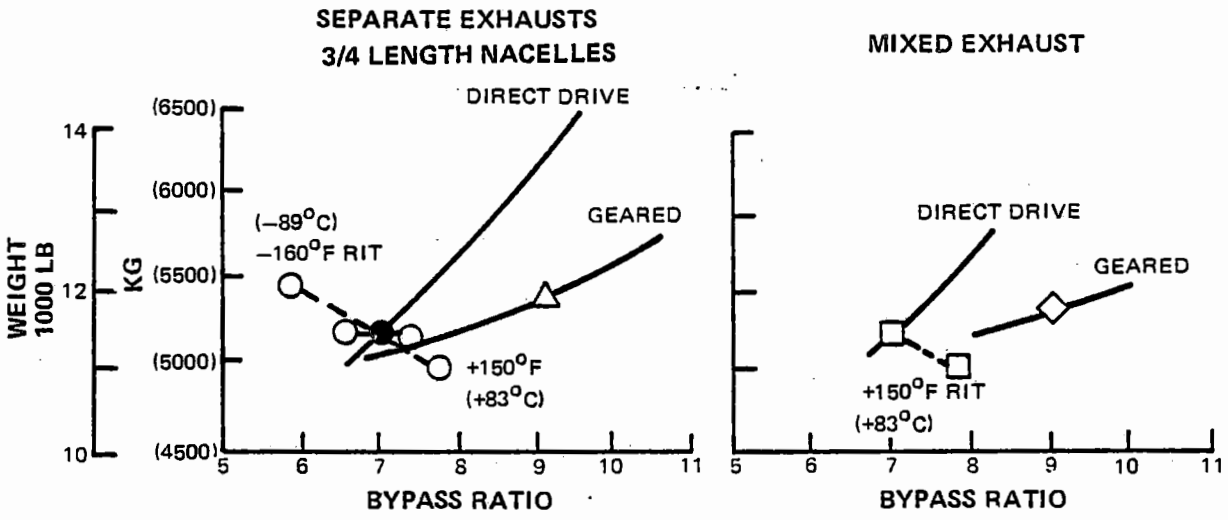

Figure B-14 *Task II Total Engine and Nacelle Weight Trends (Max. Cruise Thrust = 42.1 kN, OPR = 38.6, RIT = 1210°C). Total engine and nacelle weight trends indicate a significant weight penalty for increasing bypass ratio.*

Total engine and nacelle price trends (Figure B-15) were similar to weight trends. Figure B-16 shows the strong influence RIT has on maintenance cost relative to BPR variations.

The engine information thus far in this section does not include the effects of customer bleed and horsepower extraction. The data submitted to the airplane companies (Boeing, Douglas, and Lockheed) and the data used by Pratt & Whitney Aircraft for fuel-burned and economic calculations included the (Table B-XIII) bleed and power extraction levels (per engine):

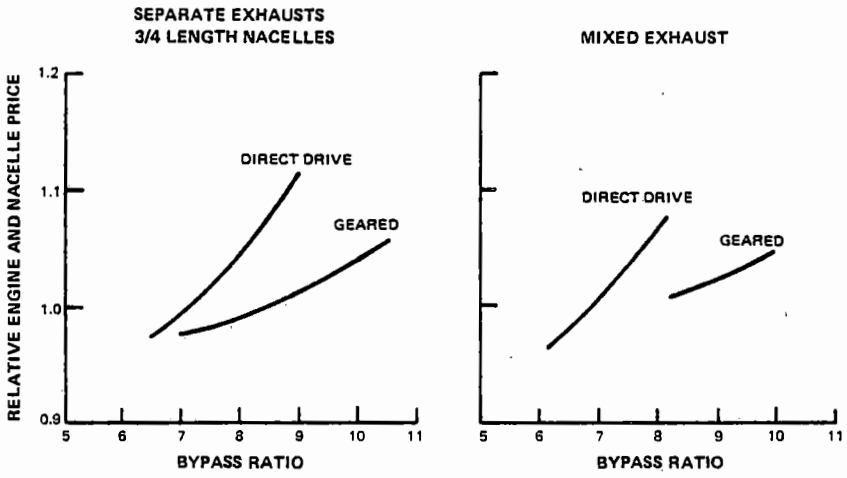

Figure B-15 *Task II Total Engine and Nacelle Price Trends (Max. Cruise Thrust = 42.1 kN, OPR = 38.6, RIT = 1210°C). Price trends were similar to weight trends.*

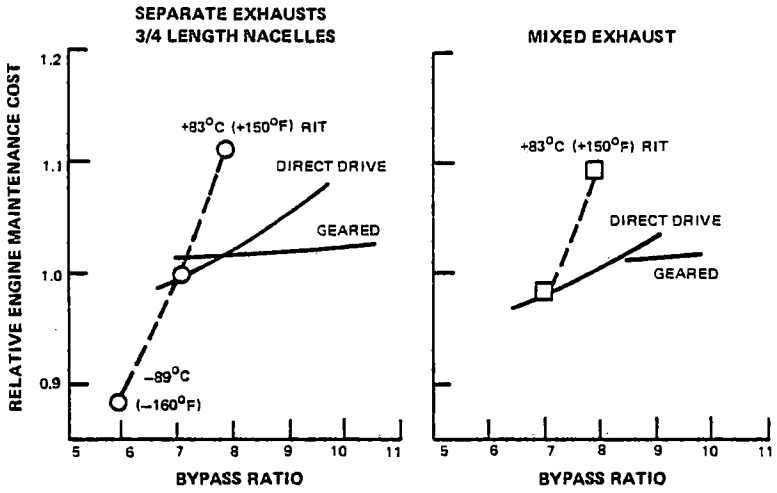

Figure B-16 Task II Engine Maintenance Cost Trends (Max. Cruise Thrust = 42.1 KN, OPR = 38.6, RIT = 1210°C). RIT has a strong influence on maintenance cost.

TABLE B-XIII

CUSTOMER BLEED AND POWER EXTRACTION REQUIREMENTS ASSUMED BY P&WA

Customer bleed flow (kg/sec)	=	(7.8×10^{-6}) x SLTO thrust (in newtons)
Power extraction (kW)	=	(5.9×10^{-4}) x SLTO thrust (in newtons)

TYPICAL VALUES

SLTO thrust	=	165,000 N (37,000 lbf)
Bleed flow	=	1.3 kg/sec (2.8 lbm/sec)
Power extraction	=	98 kW/engine (132 hp/engine)

The effects of these levels on engine performance are shown in Figure B-17. The bleed flow became a larger portion of the total engine core flow as BPR increased (core size decreased); and, as a result, the performance loss became greater.

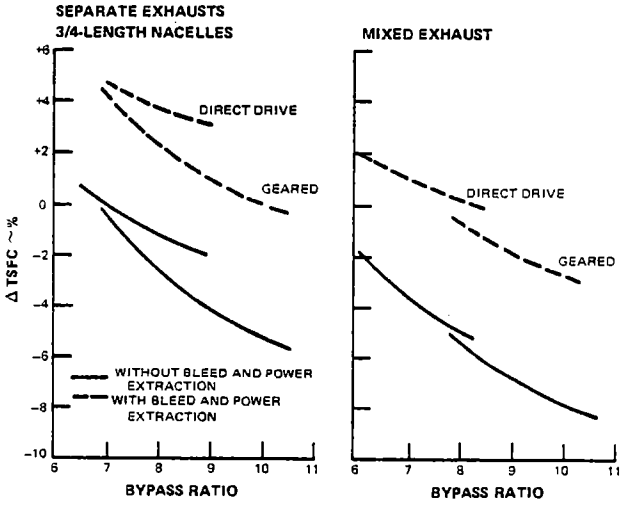

Figure B-17 Effect of Customer Bleed and Extraction on Task II Isolated Nacelle Cruise Performance Trends (10,700 m, 0.8 Mn, OPR = 38.6, RIT = 1210°C). Bleed flow became a larger portion of the total engine core flow as bypass ratio increased.

4.0 EVALUATION AND CYCLE REFINEMENT

This section discusses 1) the ground rules used in the airplane-performance evaluation of the thirty selected engines (see Sections 1.0 and 2.0 of this appendix), 2) the results of the evaluation, and 3) the cycle refinements.

4.1 Evaluation Ground Rules

Each airplane company developed installation ground rules to determine the placement of each study engine. An example of these ground rules – as developed by Boeing for its airplanes – is shown in Figure B-18. With combination of the ground rules with airplane geometry guide lines – see Figure B-19 also from Boeing – the impact of engine dimensions variations (length, diameter, exhaust type) on the airplane design was determined. An example of the influence of engine dimensions on airplane design is shown in Figure B-20. The landing gear length increments – shown for the Boeing domestic airplane – are a direct result of the engine placement and airplane geometry guide lines and are reflected in the structure weights of each engine-airplane combination.

After the effects of engine installation had been assessed, each engine was run through the missions. The engine performance used included bleed and power extraction losses. Douglas and Lockheed used Pratt & Whitney Aircraft supplied levels; while Boeing, using sensitivities supplied by Pratt & Whitney Aircraft with each engine data pack, incorporated its own bleed and power extraction levels.

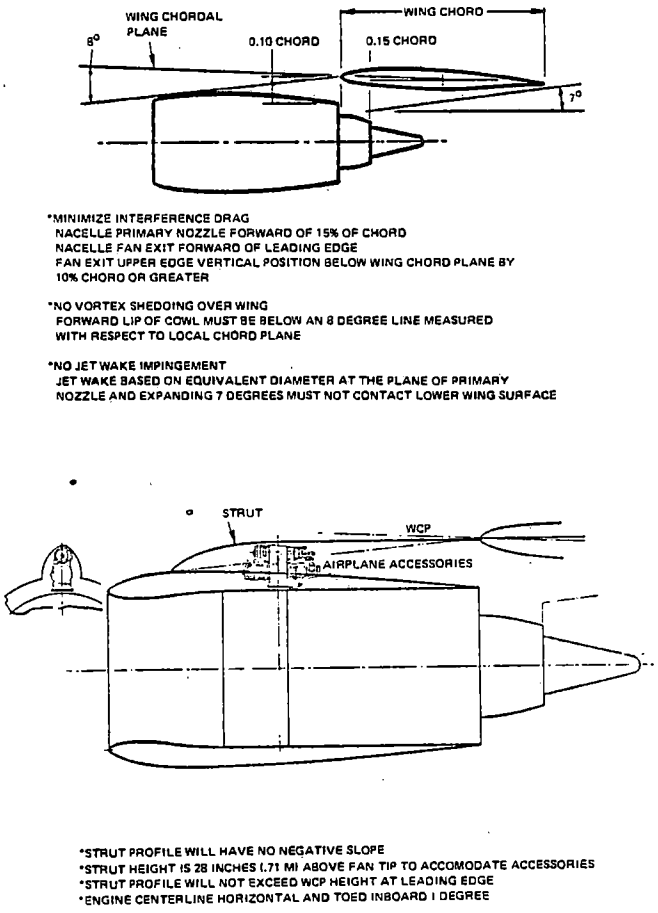

Figure B-18 Example of Engine Installation Ground Rules as Developed by Boeing. Each aircraft company developed ground rules to determine placement of engine.

The Pratt & Whitney Aircraft evaluation used the trade factors shown in Table B-XIV. These factors were developed about the Pratt & Whitney Aircraft airplanes. Isolated nacelle performance data (including bleed and power extraction at the Mach 0.8, 10,200 m maximum cruise condition were used along with nacelle and engine weights in this evaluation. Engines in both airplanes were sized by initial cruise altitude requirements.

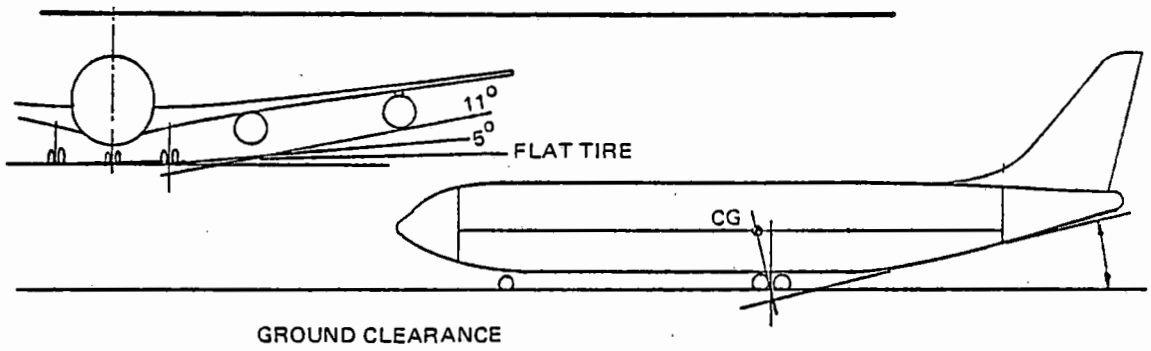

*TAKEOFF ROTATION
15.5 DEGREES DOMESTIC
13.5 DEGREES INTERCONTINENTAL
*TOUCH DOWN
ROLL CLEARANCE ANGLE 11 DEGREES WITH GEAR EXTENDED
*TAXI
ROLL CLEARANCE ANGLE 5 DEGREES WITH OLEO COMPRESSED
*NO GROUND CONTACT WITH FLAT TIRE AND COLLAPSED OLEO

Figure B-19 Example of Engine Installation Ground Rules Combined With Airplane Geometry Guide Lines as Developed by Boeing. The impact of engine dimension variations on airplane design was determined by combining engine installation ground rules with airplane geometry guide lines.

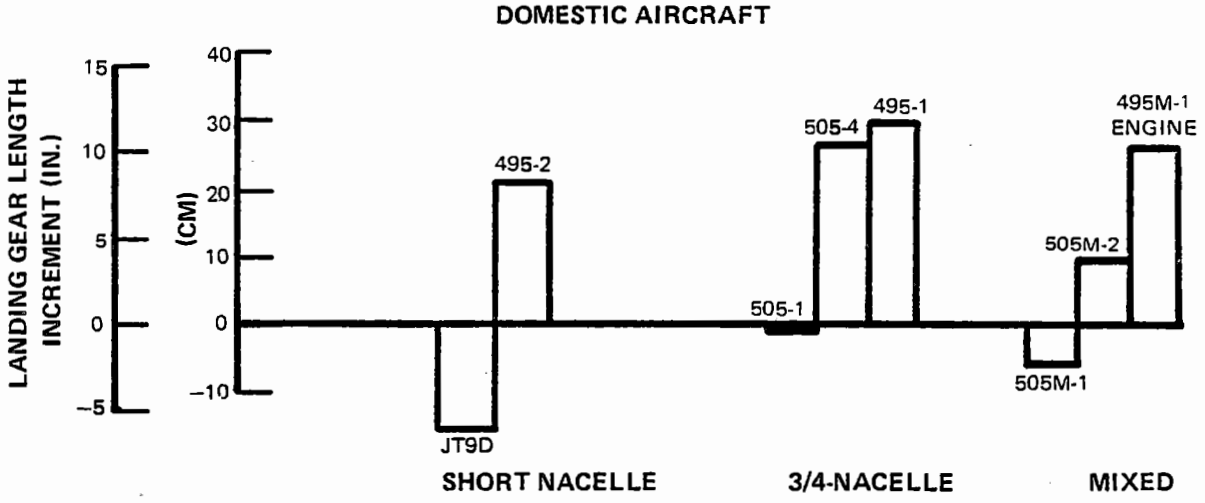

Figure B-20 Examples of Influence of Engine Dimensions on Landing Gear Length for Boeing Domestic Airplane. Changes in airplane geometry affect airplane structural weight.

TABLE B-XIV

TASK II REFINED TRADE FACTORS
(Engines Sized for P&WA Airplanes)

Airplane	International				Domestic			
Mission Range ~ km (nm)	10190 (5500)		3710 (2000)		5560 (3000)		1295 (700)	
Fuel Price ~ ¢/liter	11.9	14.5	11.9	14.5	9.2	11.9	9.2	11.9
~ ¢/gal.	45	55	45	55	35	45	35	45
% Δ DOC Due to:								
1% TSFC	0.75	0.81	0.64	0.69	0.50	0.56	0.35	0.40
500 kg Engine Weight	0.77	0.79	0.78	0.80	0.68	0.70	0.67	0.68
500 kg Nacelle Weight	1.26	1.24	1.35	1.34	1.26	1.23	1.31	1.29
100,000 $ Engine Price	0.28	0.26	0.32	0.30	0.30	0.28	0.33	0.31
10 $/EFH Engine Maintenance	1.31	1.20	1.36	1.26	1.33	1.21	1.19	1.12
% Δ Fuel Burned Due to:								
1% TSFC	1.41	1.41	1.32	1.32	1.21	1.21	1.14	1.14
500 kg Engine Weight	1.05	1.05	1.15	1.15	0.89	0.89	1.04	1.04
500 kg Nacelle Weight	1.05	1.05	1.15	1.15	0.89	0.89	1.04	1.04

4.2 Evaluation Results

4.2.1 Fuel Burned and DOC

Domestic typical-mission fuel-burned trends with BPR are shown in Figure B-21 for advanced engines relative to the JT9D-7A reference engine. All advanced engines on this plot have a baseline OPR of 38.6 and a RIT of 1210°C (2210°F). The lines on the plot are for the Pratt & Whitney Aircraft evaluation and the points are for each airplane company evaluation. The trends with BPR and the relationships between advanced engine types are similar in most cases; the notable exception is Boeing's assessment of mixed engines, where a second segment engine-out takeoff and climb limitation penalized high BPR engines because of their higher windmilling drag. Fuel-burned levels relative to the JT9D-7A reflect difference in airplanes and missions. The Boeing airplane, designed for a shorter range (3710 km vs 5560 km) and fewer passengers (196 vs 400 to 458) than the other airplanes, tended to be less sensitive to the TSFC reductions with the advanced engines.

The overall advantages of advanced engines relative to the JT9D-7A were greater for the long range international airplanes, as shown in Figure B-22. Again the trends were similar among the different airplanes. Lockheed showed the largest advantage for advanced engines, primarily because the design range of their airplane was longer (12050 km vs 10190 km) than those of the other airplanes.

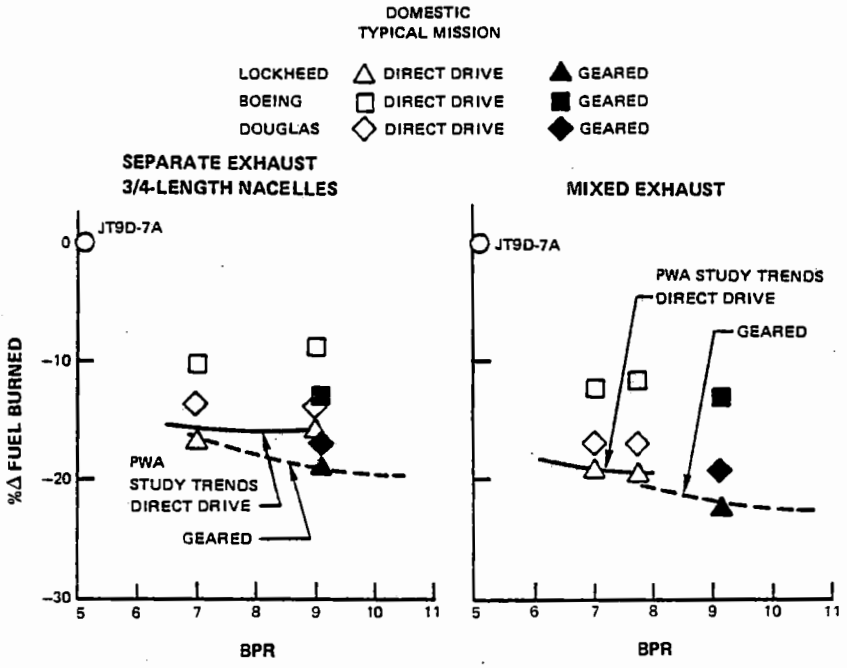

Figure B-21 Task II Fuel Burned as a Function of Bypass Ratio for a Typical Domestic Mission (RIT = 1210°C, OPR = 38.6). The fuel-burned with bypass ratio was similar for most airplanes.

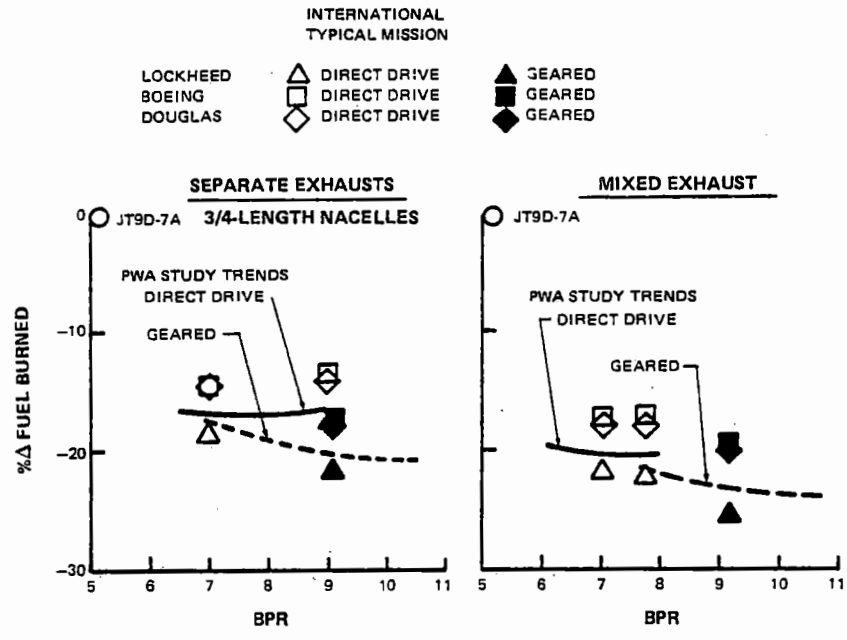

Figure B-22 Task II Fuel Burned as a Function of Bypass Ratio for a Typical International Mission. The overall advantages for increased bypass ratio were greater for the long range international airplanes.

While the fuel-burned trends indicated, in general, an advantage for increasing BPR, the DOC trends of Figure B-23 and B-24 indicate a disadvantage for increasing BPR in the direct drive engines, and little or no advantage for increasing BPR past about 9 to 9.5 in the geared engine. The fuel-burned advantages of higher BPR's were largely offset by higher engine and nacelle weights and costs in DOC. Installation penalties usually associated with larger nacelle diameters—such as landing gear length that increased airframe cost and hence, DOC—also tended to favor lower BPR engines.

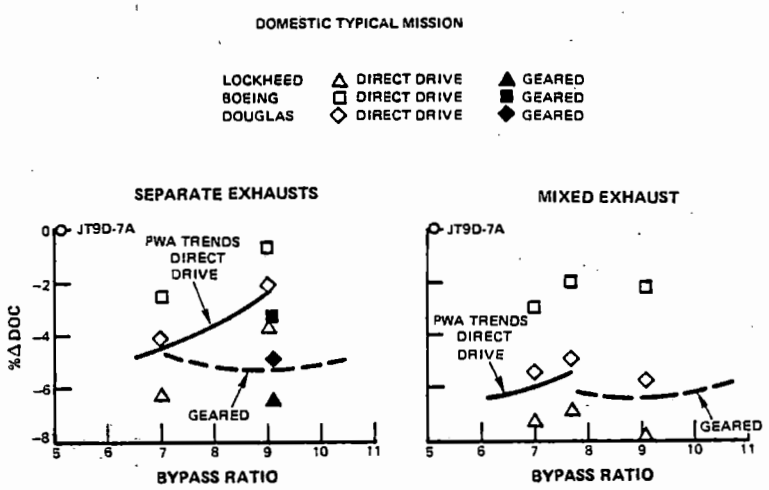

Figure B-23 *Task II Direct Operating Cost as a Function of Bypass Ratio for a Typical Domestic Mission. DOC trends indicate a disadvantage for increasing bypass ratio of direct-drive engines and no advantage for geared engines for bypass ratios greater than 9.*

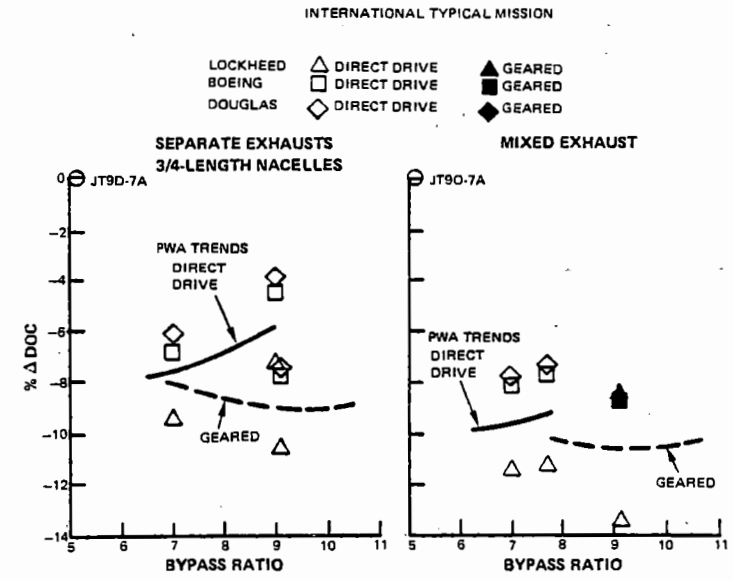

Figure B-24 *Task II Direct Operating Cost as a Function of Bypass Ratio for a Typical International Mission. DOC trends indicate a disadvantage for direct-drive engine and no advantage for geared engines for bypass ratios greater than 9.5.*

The Boeing 3710 km (2000 naut. mi.) domestic airplane showed the least DOC advantage for advanced engines and the Lockheed 12050 km (6500 naut. mi.) international airplane showed the most, for essentially the same reasons as stated for fuel burned.

DOC trends with BPR were quite similar for the four evaluations, except that the Boeing domestic airplane consistently indicated less advantage for the higher BPR, mixed geared engine. Comparison of separate and mixed engines showed that the Boeing domestic airplane was again atypical, having the least advantage for mixing, even at lower BPR's.

ROI was also calculated during the evluation. A comparison of ROI and DOC results for the Pratt & Whitney Aircraft domestic airplane is presented in Figure B-25. Since both parameters gave essentially similar trends and since DOC was an easier parameter to understand, it was chosen for presentation of results.

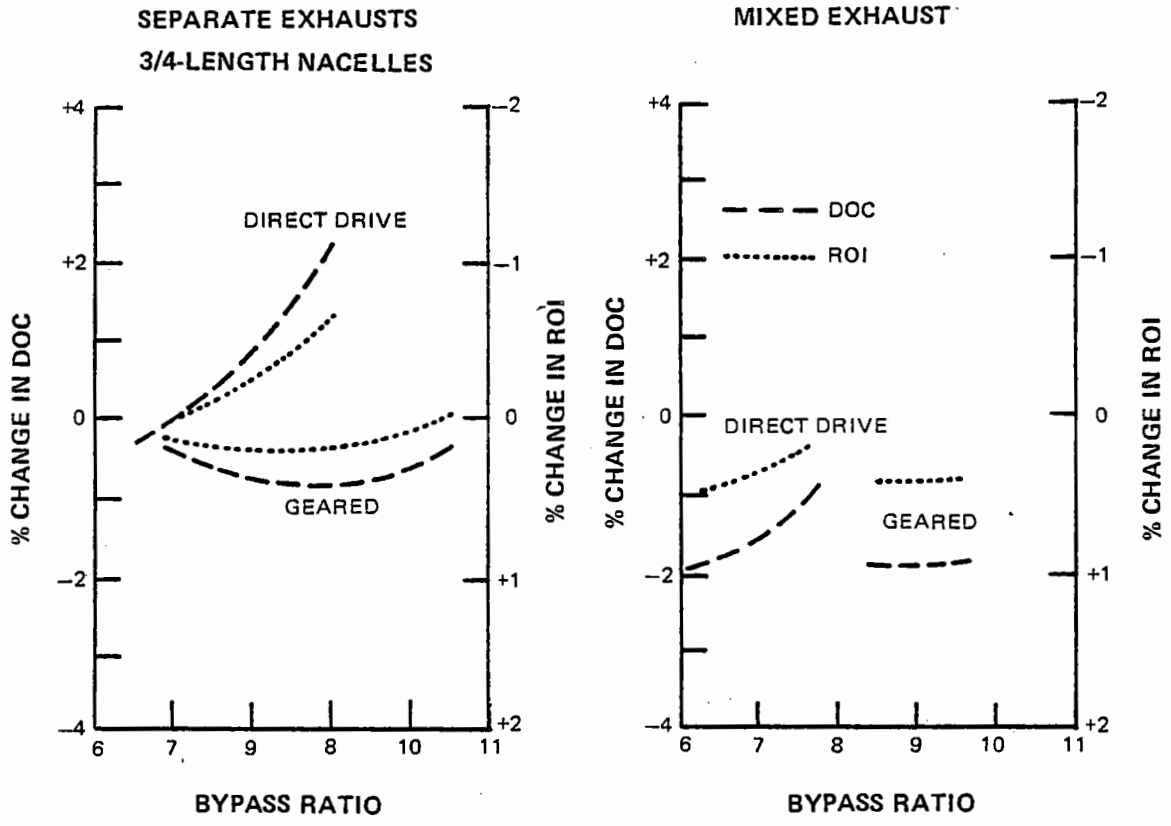

Figure B-25 Task II Comparison of ROI and DOC Trends for the Pratt & Whitney Aircraft Domestic Airplane. The trends for ROI and DOC with BPR were similar.

The effect of increased fuel price on DOC trends is shown in Figure B-26 for the Pratt & Whitney Aircraft domestic airplane. Adding 2.64¢ /l (10¢ /gal) to the fuel price did not change major trends. Results were similar with the international airplane.

The results of the evaluation of OPR and RIT are shown in Figures B-27 and B-28. These evaluations were performed in-house using Pratt & Whitney Aircraft domestic and international airplane influence coefficients and engine trends obtained by perturbing the STF505-1 separate exhaust, direct-drive engine cycle. Fuel burned showed benefits for increased OPR for both airplanes primarily because of TSFC reduction. DOC was considerably less sensitive to TSFC than was fuel burned, and, as a result, showed little advantage for increasing OPR over the baseline value of 38.6.

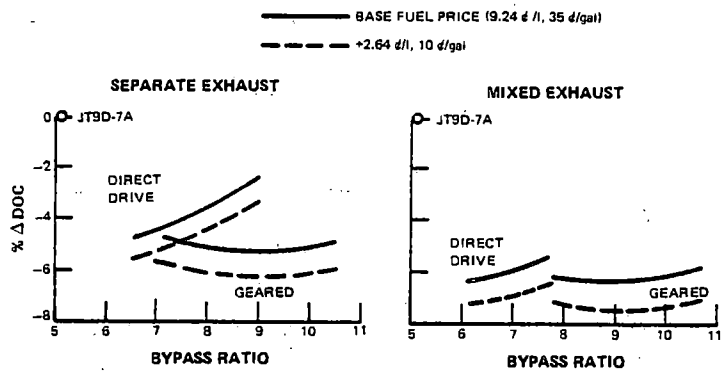

Figure B-26 *Task II Effect of Increased Fuel Price on DOC for Typical Domestic Mission. Major trends were not affected. The effects on international missions were similar to those shown for the domestic mission.*

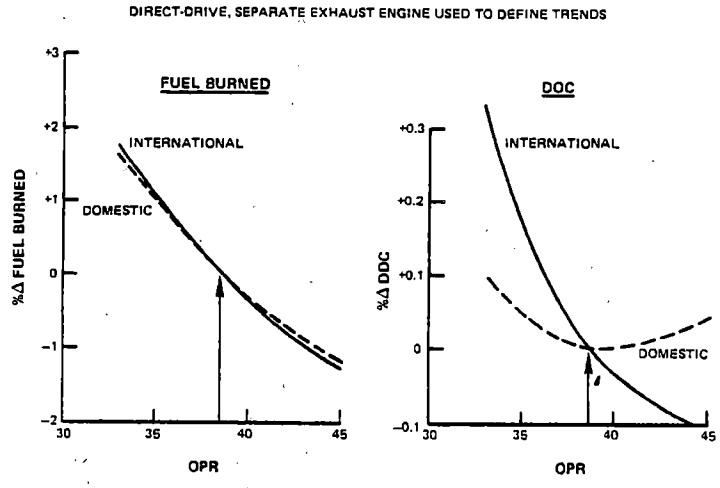

Figure B-27 *Task II Effects of OPR on Fuel Burned and DOC for Typical Domestic and International Missions. Fuel burned benefitted with increased OPR because TSFC was reduced.*

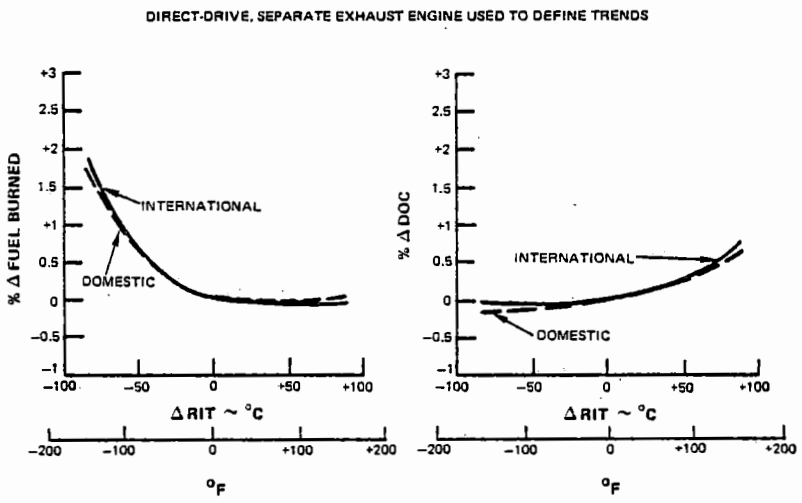

Figure B-28 *Task II Effects of Rotor Inlet Temperature on Fuel Burned and DOC for Typical Domestic and International Missions. Increasing rotor inlet temperature beyond the baseline of 1210°C (2210°F) showed flat fuel-burned trend because of increased TSFC trading with lower engine weight; however, there were penalties in DOC because of the increased maintenance cost.*

Decreasing RIT below the baseline value of 1210°C (2210°F) showed definite fuel-burned penalties because of the increased TSFC and engine weight. But there was no penalty in DOC because decreased maintenance cost associated with lower RIT more than offset the performance and weight disadvantages. Increasing RIT above baseline did not provide any additional fuel-burned benefits and had a detrimental effect on DOC.

4.2.2 Environmental Parameters

A summary of Boeing, Douglas, and Lockheed airframe noise estimates is shown in Figure B-29. FAR 36 lines refer to the 1969 regulations to which the Energy Efficient Engine goal of FAR 36-10 EPNdB applied.

A summary of the ranges of total airplane plus engine noise including Boeing, Douglas, and Lockheed airplanes is presented in Table B-XV for representative engine cycles of each type. The wide range of noise in each case was caused as much by the variation of FAR 36 (1969) regulation with gross weight, as shown in Figure B-29, as by differences in actual noise levels between airplanes. In each case the smallest airplane showed the least noise reduction from FAR 36 (1969).

A comparison of advanced and current acoustic technology effects on total noise for the Pratt & Whitney Aircraft international aircraft was made to quantify the benefits of advancing the acoustic technology. Results are shown in Table B-XVI. The new FAR 36 (1977) noise levels are included on this chart for reference. The critical noise condition for each engine is identified. In most cases the same noise condition was critical for both old and new regulations. However, for the geared, separate exhaust engine with current technology acoustics, takeoff was critical under the old regulation and approach, for the new regulation.

TABLE B-XV

TASK II TOTAL ENGINE PLUS AIRFRAME NOISE (BOEING, DOUGLAS, AND LOCKHEED AIRCRAFT) EPNdB RELATIVE TO FAR 36 (1969)

Engine	BPR		Domestic Aircraft	International Aircraft
Direct Drive, Separate Exhausts	7.0	Approach	-8 to -11	-8 to -11
		Takeoff*	-12 to -13	-8 to -11
Direct Drive, Mixed Exhaust	7.0	Approach	-8 to -11	-8 to -11
		Takeoff*	-12 to -13	-8 to -11
Geared, Separate Exhausts	9.1	Approach	-9 to -12	-9 to -11
		Takeoff*	-12 to -13	-8 to -11
Geared, Mixed Exhaust	9.1	Approach	-9 to -12	-9 to -12
		Takeoff*	-13 to -14	-10 to -12

*Without cutback

Notes: 1) Engine noise based on "advanced acoustics" as defined in Section 3.2 of the main body of the report.
2) Range in noise levels reflects differences in study airplane characteristics.

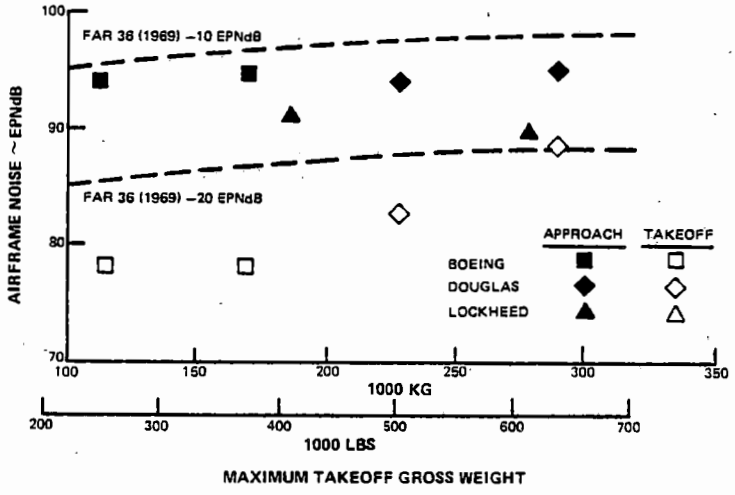

Figure B-29 Predicted Airframe Noise. The wide range of noise was caused as much by the variation of FAR 36 (1969) with gross weight as to differences in actual noise levels.

TABLE B-XVI

TASK II TOTAL NOISE SUMMARY
(P&WA International Airplane - EPNL (a))

	Direct Drive		Geared		Noise Rule	
	Separate	Mixed	Separate	Mixed	1969	1977
BPR	7.0	7.0	9.1	9.1		
Advanced Acoustics Prediction						
Takeoff	97.8	97.8	97.8 (b)	96.2	108	105.2
Approach	98.8 (b)	98.2 (b)	96.8	96.5 (b)	108	104.5
Current Acoustics Prediction						
Takeoff	100.4	100.4	100.4 (b)	98.8	108	105.2
Approach	102.1 (b)	101.4 (b)	100.0 (b)	99.0 (b)	108	104.5

Note: (a) Includes 93 dB Airframe Noise at Approach
(b) Critical Noise Condition

Nacelle geometry and/or acoustic treatment was varied for these four engines to establish trades between noise and TSFC/DOC. The variations examined are shown in Figure B-30. This figure serves as a key for Figures B-31, B-32, B-33 and B-34, which present the results of the noise-impact study. Noise levels include airframe noise of 93 dB at approach.

The results of the study indicate that there are severe penalties, especially in DOC, associated with providing rings and splitters to reduce noise. In addition to performance and economic penalties, there are other problems such as de-icing and maintenance associated with inlet rings which were not assessed in this study. Removing wall treatment from the nacelles has little effect on performance since the use of structural acoustic material with low-pressure loss characteristics was assumed for both levels of technology. No difference in price was assumed for acoustic duct material versus non-acoustic duct material.

With advanced technology acoustics, all engine types except the separate-exhaust, direct drive engine met the FAR 36 – 10 EPNdB (1969) goal in their baseline nacelle configurations. With current technology acoustics, none of the engine types can meet that goal with baseline nacelles. All engine types in baseline nacelles can meet the new FAR 36 (1977) noise rules, however, with current acoustic technology.

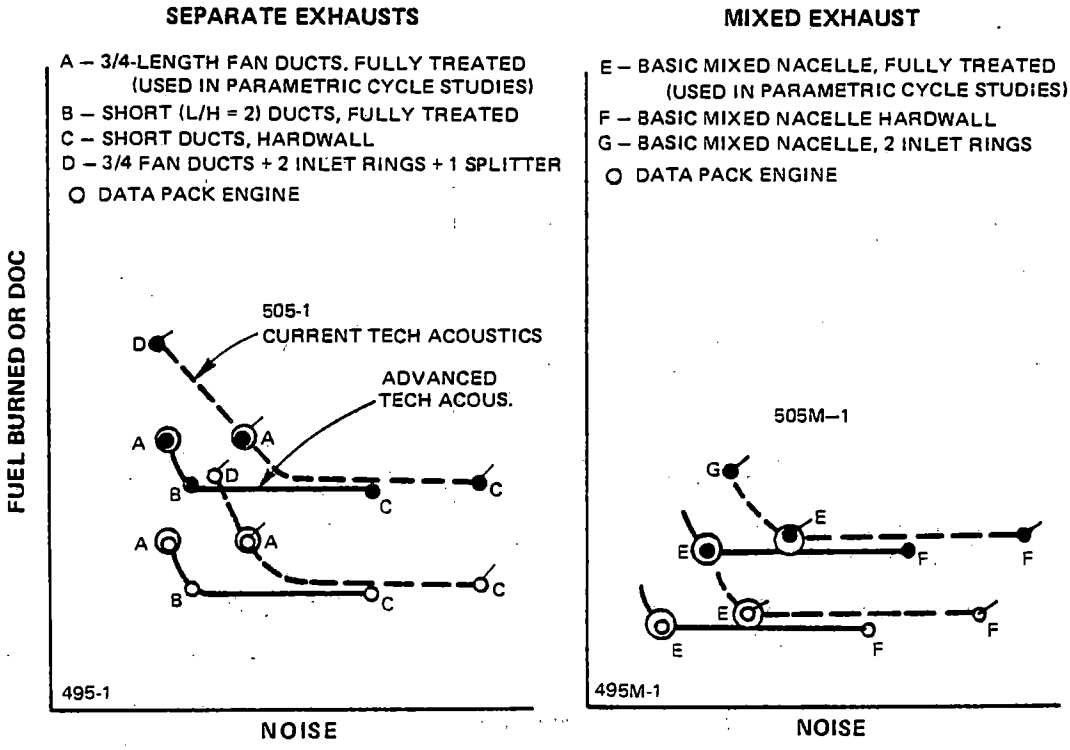

Figure B-30 *Key to Task II Noise/Cycle Impact Plots. This figure serves as a key to Figures B-31, B-32, B-33, and B-34.*

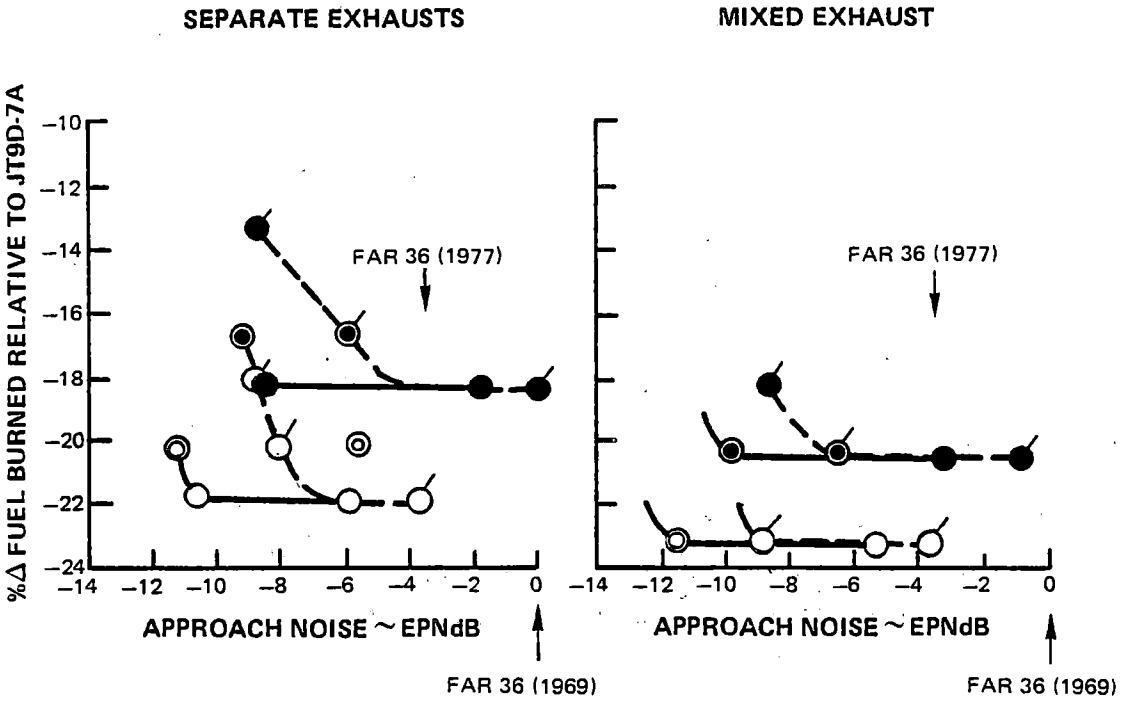

Figure B-31 *Impact of Approach Noise on Fuel Burned*

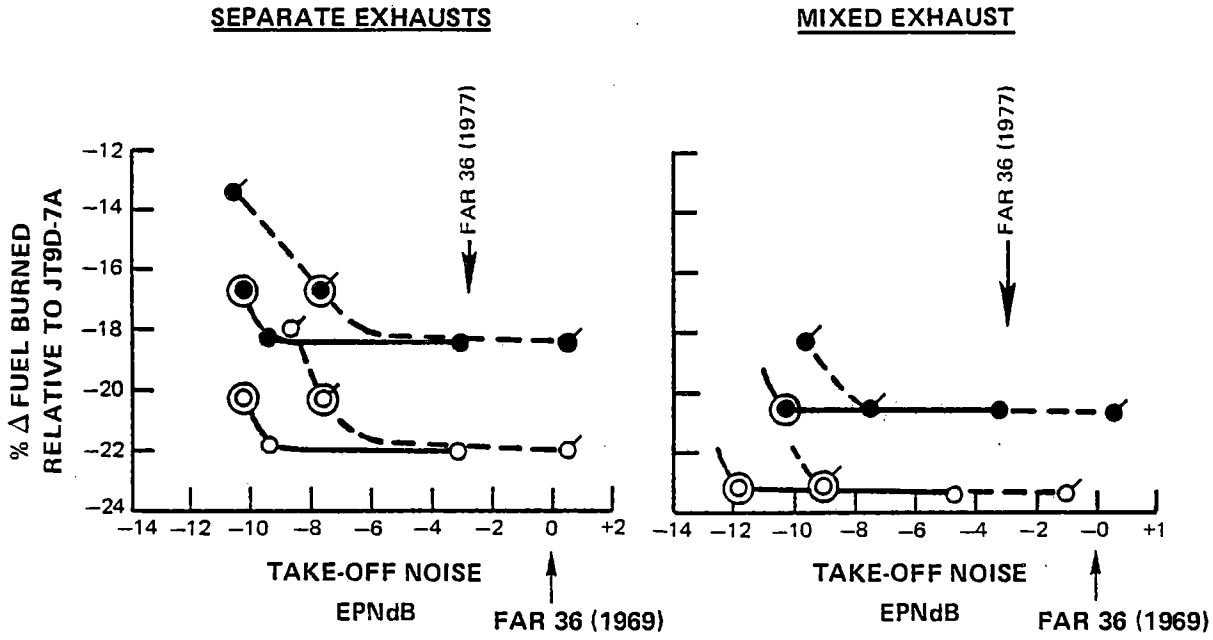

Figure B-32 Impact of Take-Off Noise on Fuel Burned

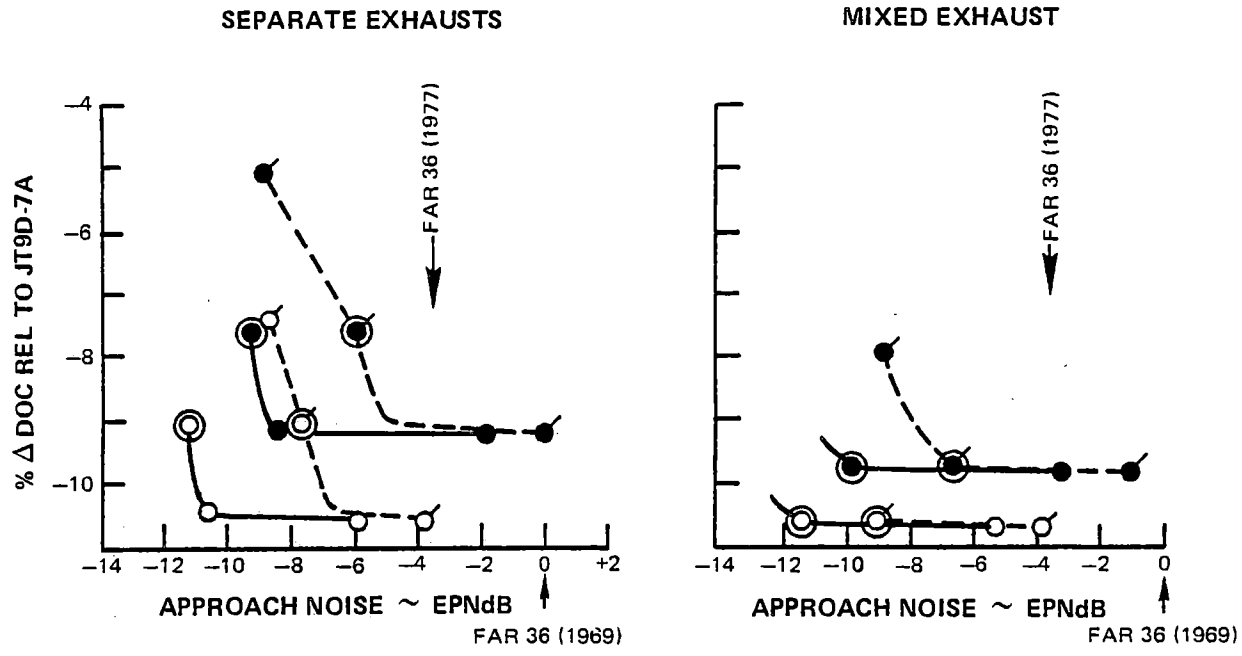

Figure B-33 Impact of Approach Noise on Direct Operating Cost

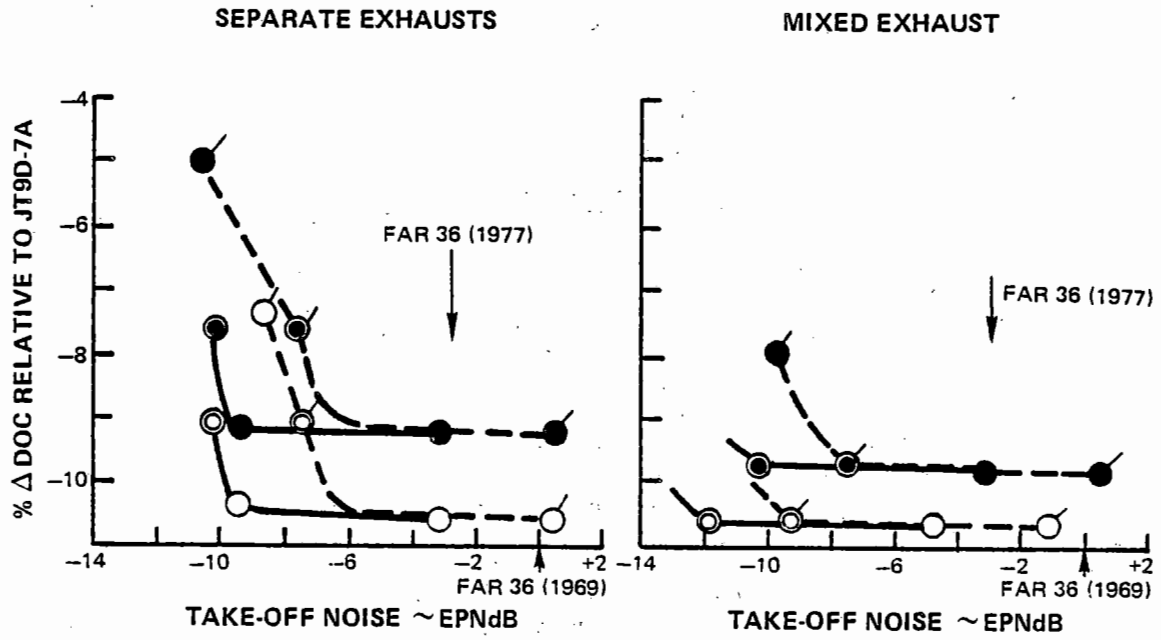

Figure B-34 Impact of Takeoff Noise on Direct Operating Cost

Figure B-35 shows predicted emissions in terms of EPA parameter for Task II engines. The effect of OPR on emissions is shown because it has the greatest effect of any of the cycle parameters. Reduction of OPR to meet the NO_x rule requires both significant engine performance penalties (see Figure B-27) and rapid increases in CO and THC emissions.

4.3 CYCLE REFINEMENT

The results of Task II evaluations were used to refine the cycle parameters of each of the four engine types. The evaluations indicated that a design RIT of 1210°C (2210°F) is a good compromise between fuel burned and DOC (Figure B-28) and is low enough to allow a reasonable growth potential. A 1210°C (2210°F) design level was therefore chosen for the refined cycles.

The choice of an OPR for the refined cycles was not as straightforward as was RIT. Fuel burned and DOC continued to improve as OPR was increased, except that the DOC of the domestic airplane bottomed at an OPR around 38 to 40 (Figure B-27). The domestic airplane DOC was less sensitive to fuel consumption than the international airplane, and as a result the fuel-burned advantages of higher OPR were outweighed by the higher price and maintenance costs associated with it. Thrust growth considerations suggest a lower OPR, leaving margin for increasing thrust by raising the ratio. Based on this thrust growth allowance and on the operating cost trend of the domestic airplane, an OPR of 38.6 was retained at the design level.

Selection of BPR for the refined cycles is illustrated in Figure B-36. For direct-drive, separate-exhaust engines, there was no fuel-burned advantage for BPR's higher than 7, while DOC increased at BPR's above 6. This DOC advantage at lower BPR's was also evident in mixed-exhaust, direct-drive engines, although there was a fuel-burned advantage in the international airplane for BPR's higher than 7. A BPR of 6.5 was picked as a reasonable compromise between fuel-burned and DOC for direct-drive refined cycles.

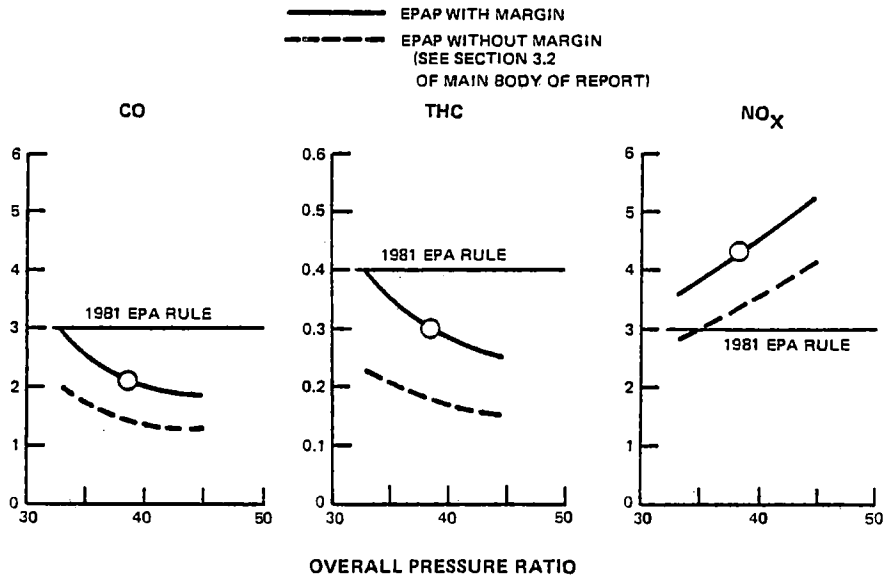

Figure B-35 Predicted Emissions in Terms of EPA Parameter. The NO_x rule appears to be unobtainable without both significant performance penalties and increases in CO and THC emissions.

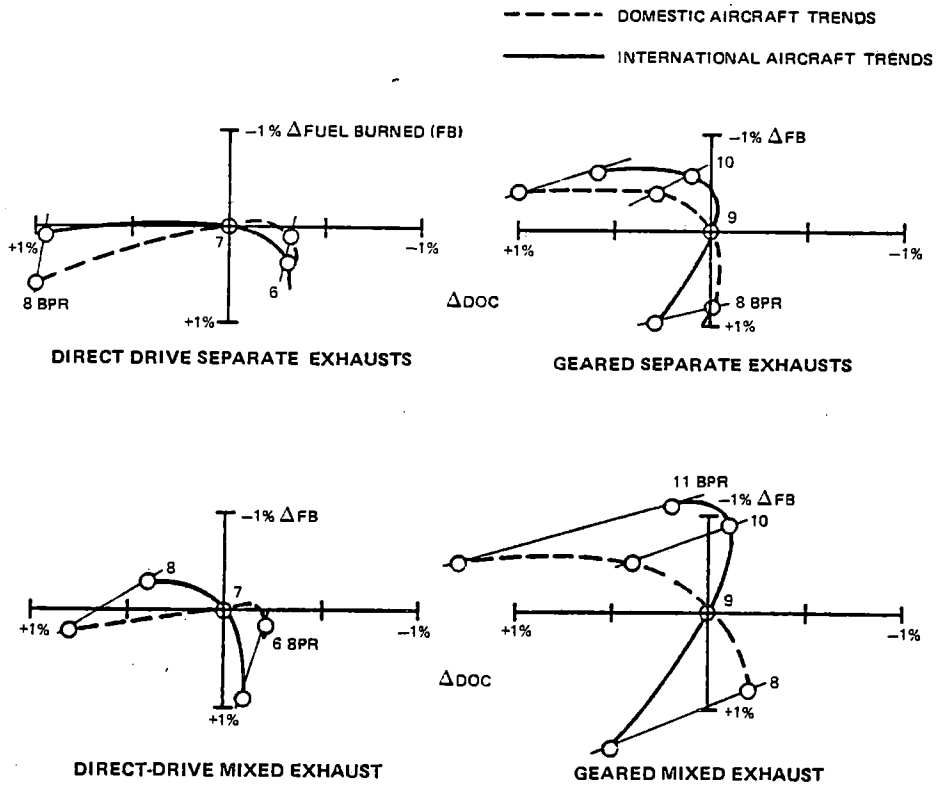

Figure B-36 Task II Refined Cycle Bypass Ratio Trends

Geared engines exhibited fuel-burned improvements up to a BPR of about 10.5 for all cases. DOC, however, optimized in the 8 to 10 BPR range. As a result, a BPR of 9.1 was chosen as overall best for geared refined cycles. The refined cycles for each engine type, as determined in Task II, are presented in Table B-XVII.

5.0 CYCLE SELECTION FOR TASK III

Figures B-37 and B-38 summarize the airplane manufacturer evaluations of the Task II engines that most resembled the refined cycles. Averaging the advantage of mixed over separate exhaust engines for Boeing, Douglas, and Lockheed in both airplanes and engine types showed a 2.5 percent advantage in fuel burned and a 1.1 percent advantage in DOC. Fuel burned and DOC advantages for gearing were estimated at 2.7 percent and 0.7 percent, respectively.

A breakout of the fuel and DOC savings for mixed exhaust is shown in Figure B-39 for each airplane company. The figure also shows the mixer assumptions and an indication of the difference between Energy Efficient Engine and current mixer technology. On the basis of these analyses, mixed-exhaust engines were chosen for further study in Task III.

Although there were reservations about the increased development risk, unique mechanical requirements, and reliability of the geared engines, the mixed-flow geared engine was included for additional analysis in Task III on the strength of the predicted fuel burned and DOC benefits.

Although most of Task II was devoted to the study of various low-spool configurations, an attractive alternate to the baseline, two-stage HPT was introduced for consideration during the later stages of the task. This alternate is a one-stage HPT, which has a distinct advantage in mechanical simplicity over the two-stage configuration, as illustrated below:

	1 Stage HPT	2 Stage HPT	JT9D HPT
Number of foils	78	129	410
Number of disks	1	2	2
Number of rotor seals	1	3	3
Number of outer air seals	1	2	2

TABLE B-XVII

TASK II REFINED ENGINE CYCLES

	Direct-Drive Separate Exhausts	Direct-Drive Mixed Exhaust	Geared Separate Exhausts	Geared Mixed Exhaust
Max. Cruise Design (10.7 km - 0.8 Mn)				
Bypass Ratio	6.5	6.5	9.1	9.1
Fan Pressure Ratio	1.8	1.74	1.58	1.52
Overall Pressure Ratio	38.6	38.6	38.6	38.6
Turbine Rotor Inlet Temp., °C	1210	1210	1210	1210
(°F)	(2210)	(2210)	(2210)	(2210)

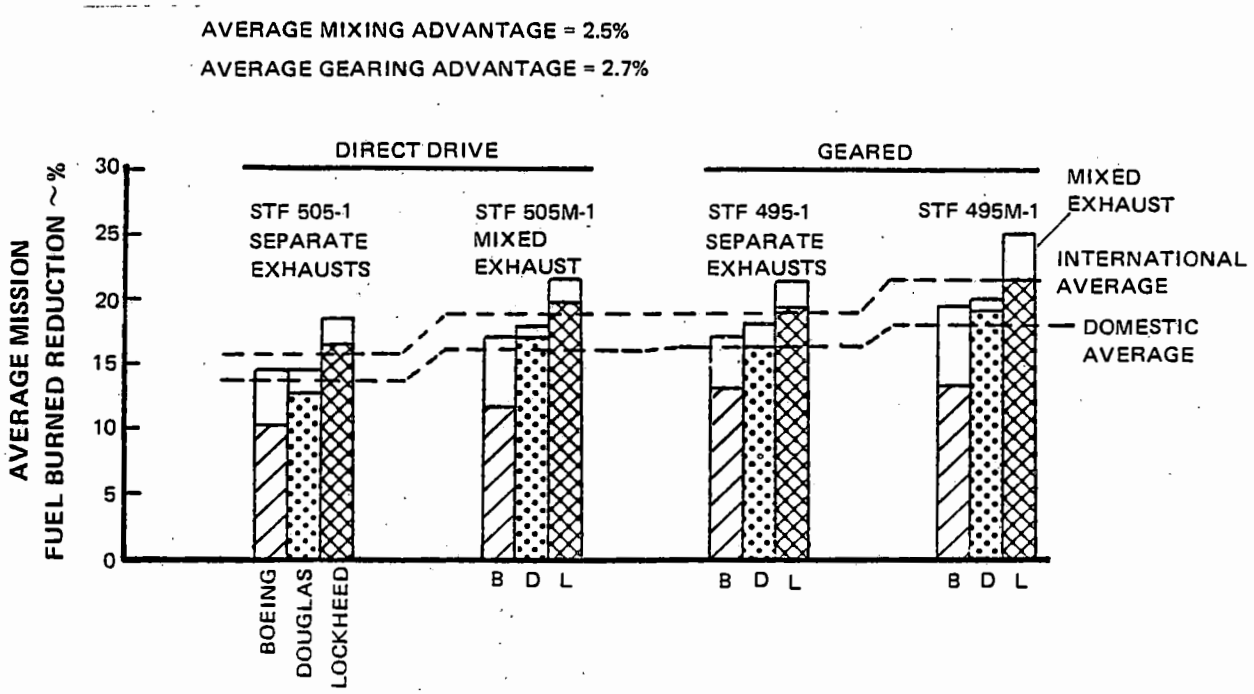

Figure B-37 Reduction in Average Mission Fuel Burned for Advanced Turbofans (Two-Stage High-Pressure Turbine) per airframe manufacturer studies.

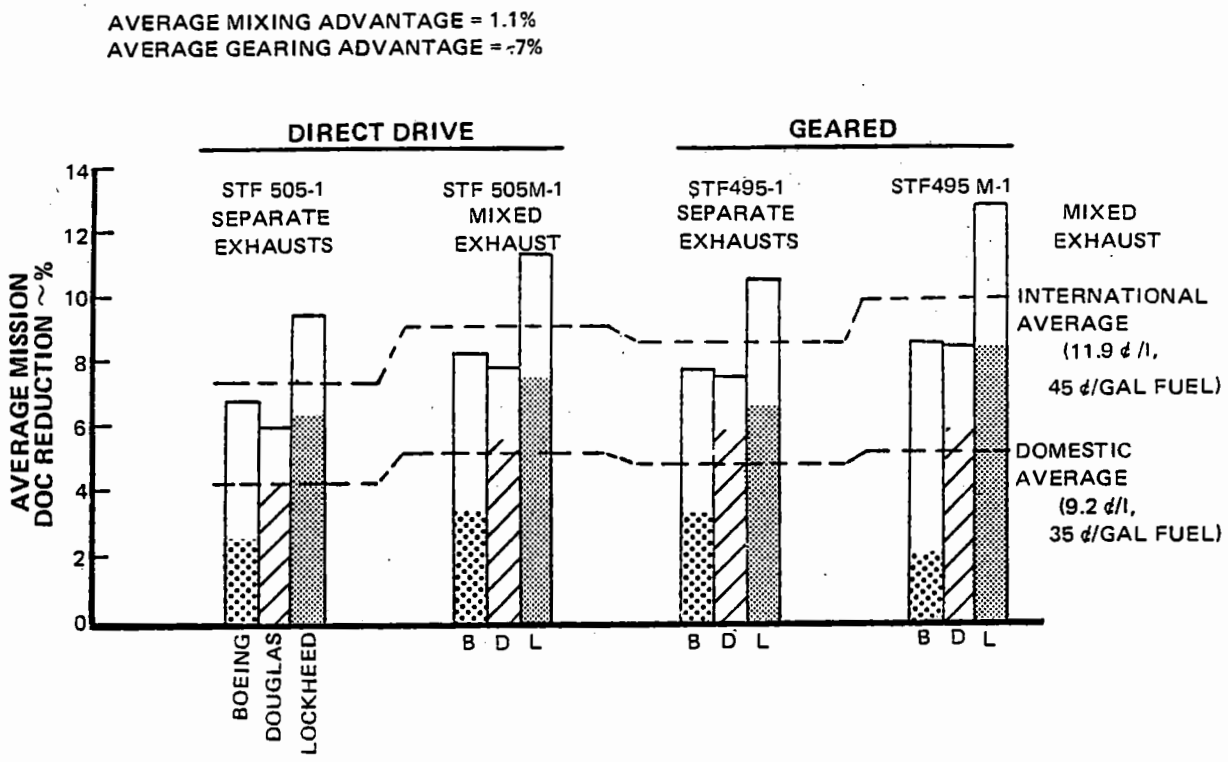

Figure B-38 Reduction in Average Mission DOC for Advanced Turbofans (Two-Stage High-Pressure Turbine) for Airframe Manufacturers Study Airplanes

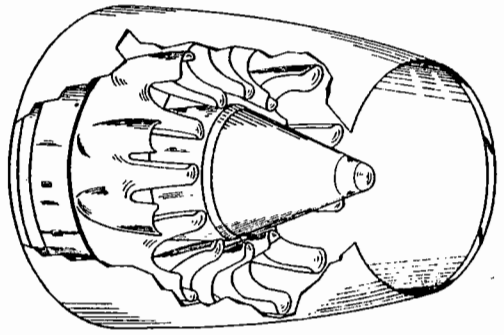

MIXER EFFICIENCY = 85%
MIXER PRESSURE LOSS = 0.4%
MIXING LENGTH TO
DIAMETER RATIO = 0.5

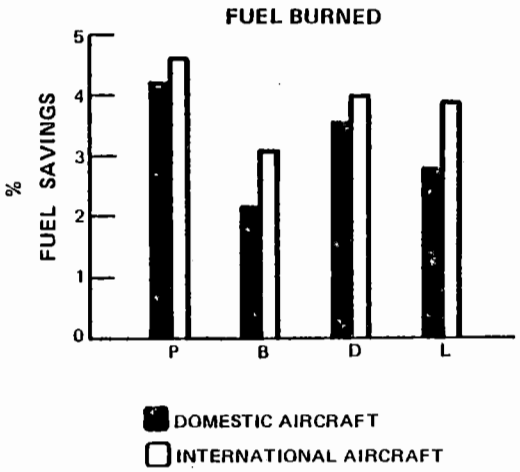

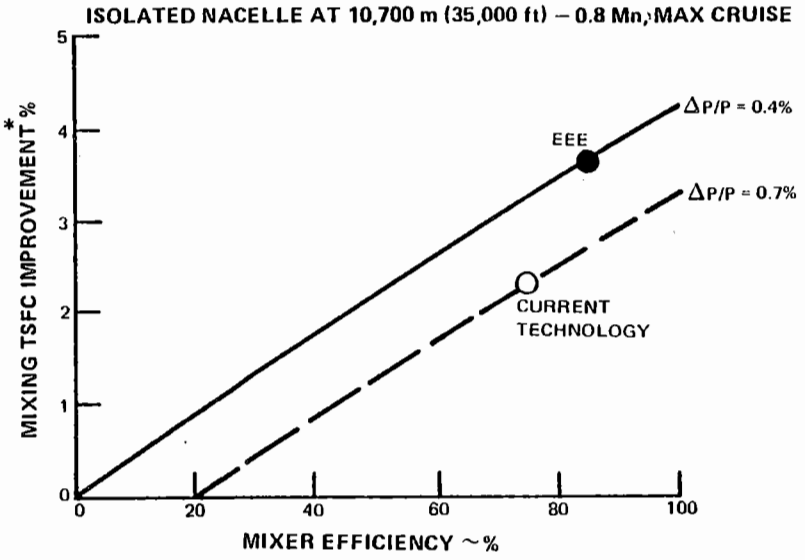

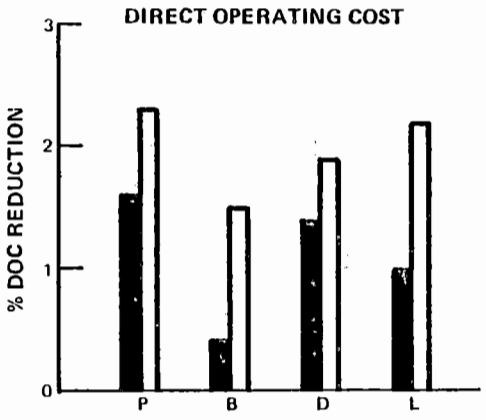

*RELATIVE TO THREE-QUARTER LENGTH SEPARATE-EXHAUST SYSTEM

Figure B-39 Fuel Burned and DOC Savings for Mixed Exhaust Engine - Average Missions

Since these mechanical-simplicity advantages could reduce maintenance cost, as well as engine weight and cost, the single-stage turbine configuration was included for further study in Task III.

Four engines were therefore carried into Task III: one and two stage HPT versions of direct drive and geared engines, all withmixed exhausts. These engine cycles are defined in Table B-XVIII.

TABLE B-XVIII

TASK III ENGINE MATRIX
(All Mixed-Flow Nacelles)

Engine[a]	Type	HP Turbine No. of Stages	Cruise[b] TSFC	Fan Pres. Ratio	Bypass Ratio
STF505M-7[c]	Direct	1	0.573	1.74	6.55
STF505M-9	Direct	2	0.566	1.74	6.52
STF495M-4[c]	Geared	1	0.549	1.52	9.12
STF495M-5	Geared	2	0.541	1.52	9.12

Notes: (a) For all four engines, overall pressure ratio equals 38.6 and rotor inlet temperatures equals 1204°C (2200°F).

(b) Installed, No Bld. or HPX, 10,700m (35,000 ft), Mn = 0.8

(c) Engine evaluated by airplane companies

APPENDIX C

INITIAL PRELIMINARY DESIGN – TASK III

APPENDIX C (Cont'd)

LIST OF ILLUSTRATIONS
APPENDIX C

LIST OF ILLUSTRATIONS
APPENDIX C

LIST OF ILLUSTRATIONS
APPENDIX C

LIST OF ILLUSTRATIONS
APPENDIX C

LIST OF ILLUSTRATIONS
APPENDIX C

LIST OF ILLUSTRATIONS
APPENDIX C

APPENDIX C

LIST OF TABLES

LIST OF TABLES (Cont'd)

LIST OF TABLES (Cont'd)

LIST OF TABLES (Cont'd)

LIST OF TABLES (Cont'd)

APPENDIX C

INITIAL PRELIMINARY DESIGN – TASK III

1.0 Introduction

Evaluation of four engine preliminary designs, in combination with Task IV risk analyses, resulted in the selection of the direct-drive fan, one-stage HPT engine configuration.

Preliminary design analyses, conducted in Task III, investigated the key areas of concern for direct-drive and geared fan, mixed exhaust engines having one- and two-stage HPT's. Intrinsic design feasibility was established for the four engine configurations. These analyses resulted in designing two bearing compartments and five mainshaft bearings to support the two rotor systems in the direct-drive engines. The need for a third main bearing compartment with a roller bearing and an additional high rotor roller bearing was established for the geared engines. Geared fan and LPT-induced vibration decoupling necessitated the relocation of the rear gear support roller bearing from the Task I intershaft position to the gearbox supporting structure. This relocation resulted in an 18.8 cm (7.4 in.) engine length increase. Analysis on failure mode effects indicated the need for an innovative solution to prevent low spool runaway and catastrophic LPT bursting in the event of an internal gearbox failure. One possible solution consisted of sophisticated gearbox containment and fast acting LPT gas blow-off devices to arrest rapid turbine rotor acceleration. Analyses also indicated that the one- and two-stage HPT's were equally aggressive aerodynamically, structurally, and mechanically.

The resulting engine designs were evaluated against the established program goals. Un-installed and installed capabilities were estimated for performance, weight, costs, fuel burned, DOC, ROI, emissions, noise, thrust growth, and deterioration. A change to bottom-mounted accessories, because of airframe preference, increased the relative TSFC advantage of the geared engine compared to Task II results. Fuel burned and DOC comparisons between the geared and direct-drive fan engines showed very similar results to those in Task II. The one-stage HPT engine configuration was found to have a 1.4 percent DOC advantage over the two-stage HPT, but suffered a relative fuel burned penalty of 1.1 percent. Relative to program goals, the selected direct-drive, one-stage HPT mixed exhaust engine:

- Surpassed the minimum 12 percent TSFC goal by 3.3 percent
- Surpassed the minimum 5 percent DOC reduction goal by one percent and five percent, respectively, for the domestic and international airplane missions
- Met the 1981 EPA emissions for CO and THC, but exceeded the NO_x goal by 43 percent
- Met the FAR 36 (1969) - 10 EPNdB engine noise goal with advanced acoustics
- Had a capability for greater than 20 percent thrust growth without severely affecting the other goals
- Had an estimated TSFC deterioration one-half that of the JT9D-7A rate for over 4000 operating hours.

2.0 Preliminary Design Analyses

Figure C-1 shows the major elements of the general preliminary design process used in this task. Inputs to this process consisted of key

initial component aerodynamic and mechanical parameters and updated technology projections, materials updates, and initial engine design tables. The preliminary design process defined performance, engine/nacelle contours, and component and sub-system configurations. Aerodynamic, structural, and mechanical analyses concentrated on the key areas summarized in Table C-I.

Outputs of the preliminary design analyses were spool definitions and propulsion system drawings, performance, weights, prices, and maintenance costs.

2.1 Preliminary Design Analyses Inputs

2.1.1 General Design Criteria

Current developmental engine design criteria were reviewed and evaluated relative to the projected Energy Efficient Engine requirements

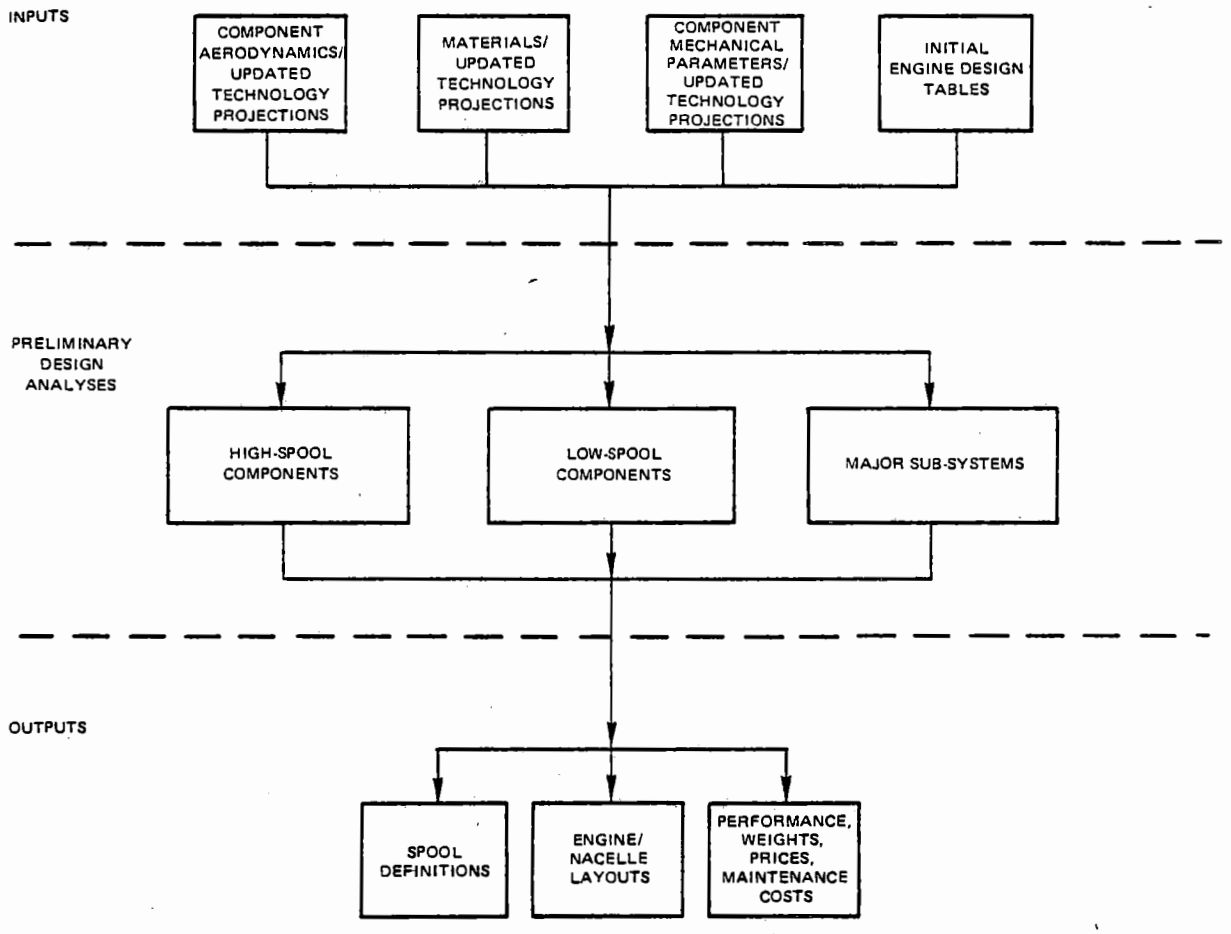

Figure C-1 Task III Flow Diagram – Inputs and outputs of the preliminary design process are shown.

TABLE C-I

KEY AREAS OF TASK III PRELIMINARY DESIGN ANALYSES

Analysis	Reason
High-Spool Components:	
HPC Parametric Study	Select optimum feasible designs
HPC Rotor Study	Structural concern for high temperature/speed rear stages
Combustor Study	Define simplified low emission configuration
HPT Parametric Study	Select optimum feasible designs
HPT Structural Study	Concern to optimize performance in high temperature/speed environment
Low-Spool Components:	
Low-Spool Parametric Study	Select preliminary optimum components
Hollow Fan Blade Study	Establish initial structural feasibility of low weight, shroudless design
LPT Structural Study	Concern for high speed in geared engine
Fan Reduction Gear Study	Define gearbox/heat exchanger systems
Major Sub-Systems:	
Stability Audit	Establish component requirements
Secondary Flow System Study	Selection minimum bleed/leakage systems
Clearance Control Study	Select passive/active system to minimize operating tip clearances
Rotor Dynamics Study	Define bearing arrangements for minimum deflections
Gear/Bearings/Lubrication Study	Define heat load/cooling requirement with high power gearbox
Nacelle Study	Establish preliminary contours/arrangement
Materials/Construction Study	Define minimum weight/cost configuration

and goals. Both domestic and international type aircraft missions were considered. In addition, technological advancements projected in materials/fabrication were factored into the establishment of these criteria. The decision was to use the current criteria with minimal changes to account for the two missions. In the area of rotor dynamics, current critical speed margins and allowable strain energy criteria were selected. Airfoil dynamics criteria for resonance and flutter were also kept the same as current. Allowable stresses for airfoils, disks, and vanes were set based on the selected materials, disks, shafts, bearings, and combustion liners were established based on consideration of future application for both missions.

2.1.2 Initial Component Aerodynamic Parameters/Updated Technology Projections

Task I engine component efficiency and pressure loss technology projections were reviewed, and values were re-estimated for use in preparing initial engine design tables. These projections are presented at the cruise design point of 10,700 m (35,000 ft.), Mach 0.8, and are discussed in the following paragraphs.

2.1.2.1 Fan

Projected performance levels for the direct drive and geared fans are presented in Table C-II.

TABLE C-II

TASK III INITIALLY PROJECTED FAN PERFORMANCE

Fan Type	Direct-Drive	Geared
Efficiency (O.D.) – (%)	87.7	89.5
Efficiency (I.D.) – (%)	88.3	81.0
Pressure Loss (Exit Case) – (%)	0.23	0.23

The fan efficiency and pressure loss predictions were based on the preliminary Task I evaluation, first-pass low-spool geometry optimization, and on a more thorough assessment of technological concepts. The current technology fan base had two part span shrouds for flutter control. Advanced concepts selected for the Energy Efficient Engine study were shroudless, hollow titanium blades; design contour blades; supercritical stators; and blade tip grooves.

2.1.2.2 Low Pressure Compressor (LPC)

Performance levels projected for the direct drive and geared fan and 1 and 2 stage HPT engine LPC's were also based on Task I evaluations, a spool/pressure ratio split study, and updated technological concept assessments. Results are summarized in Table C-III.

TABLE C-III

TASK III INITIALLY PROJECTED LPC PERFORMANCE

Engine Type	One-Stage HPT, Direct-Drive	Two-Stage HPT, Direct-Drive
Efficiency –(%)	89.7	89.5

	One-Stage HPT, Geared	Two-Stage HPT, Geared
	88.5	89.6

Four advanced technology concepts identified as enhancing the performance of the LPC were improved stator endwall cavity design, blade tip grooves, low loss airfoils, and high stage loading. The low loss airfoil concept was estimated to improve in-service performance through an improved durability design.

2.1.2.3 High Pressure Compressor (HPC)

Performance levels projected for the one- and two-stage HPT engine HPC's are shown in Table C-IV. These efficiencies were estimated from preliminary Task I evaluations, the spool pressure ratio split study, and reassessment of technology projections for the time period.

TABLE C-IV

TASK III INITIALLY PROJECTED HPC PERFORMANCE

Engine Type	One-Stage HPT	Two-Stage HPT
Efficiency (%)	88.6	87.9

Advanced concept categories applicable to the HPC were controlled endwall loss, reduced airfoil loss, performance retention, and increased stage loading.

2.1.2.4 Combustor

The combustor concept selected for the Energy Efficient Engine was a simplified Vorbix configuration based on Pratt & Whitney Aircraft's NASA sponsored Experimental Clean Combustor Program. Performance and emissions goals are presented in Table C-V.

TABLE C-V

TASK III INITIAL COMBUSTOR PERFORMANCE/EMISSIONS GOALS

	Goal
Performance:	
Pattern Factor	0.37
Section Pressure Loss	5.5%
Emissions:	
THC (EPAP)	0.4
CO (EPAP)	3.0
NO_X (EPAP)	3.0
Smoke (SAE No.)	21

Advanced concepts for the combustor included an ODS alloy cooling liner, curved wall strutless dump diffuser, two-stage combustion, and vortex burning and mixing. Incorporation of the ODS liner permits operation in the higher temperature and pressure environment without an increase in liner cooling flow. The curved wall diffuser was projected to reduce section pressure loss by 0.15 percent, to improve airflow and pressure distribution within the combustor, and to enhance general durability. Staging was estimated to reduce EPAP's by factors of 3.3:1 for CO and 20:1 for THC. A 2.5:1 NO_X EPAP reduction was projected for vortex burning and mixing.

2.1.2.5 High-Pressure Turbine (HPT)

Performance levels projected for the one- and two-stage HPT's are shown in Table C-VI.

TABLE C-VI

TASK III INITIALLY PROJECTED HPT PERFORMANCE

Engine Type	One-Stage HPT	Two-Stage HPT
Efficiency (%)	88.2	91.3

Efficiency for the one-stage HPT was projected, based on Pratt and Whitney current technology one-stage uncooled turbine rig testing and applicable technology advances. Two-stage HPT efficiency projection was predicted on Task I preliminary evaluation and reassessed in the technology application.

Advanced technology concepts applied to the one-stage HPT were:

- Aerodynamic concepts that included large annulus area and high rim speed, contoured vane endwalls, swirled coolant flow injection, reduced tip loss configurations, and active clearance control.

- Reduced coolant flow and leakage concepts that included single staging, improved airfoil cooling effectiveness, single crystal airfoil materials, thermal barrier platform coatings, efficient coolant supply system, low windage, reduced leakage length, improved gap sealing, and improved rim sealing.

Abradable ceramic outer airseals and abrasive blade tips were included in the design to retain in-operation performance.

Two-stage HPT concept projections were similar in nature to those for the one-stage HPT.

2.1.2.6 Low-Pressure Turbine (LPT)

The LPT efficiency and pressure loss predictions were based on the Task I evaluations, the first-pass low-spool optimization, and updated technology assessment. Resulting values projected for the four engine configurations are presented in Table C-VII.

Advanced technology concepts considered appropriate for LPT application were:

- Aerodynamic concepts that included low Cx/U ratio and low loss airfoils, reduced secondary flow losses, optimum radial velocity triangle distribution, counter-rotation, and an aerodynamically optimized EGV.
- Reduced leakage concepts that included active clearance control and wide channel seals.

2.1.2.7 Mixer/Nacelle

Task I and II installation component pressure losses, drag, and mixing efficiency technology projections were reviewed and updated as inputs into the initial engine design tables and installed performance calculations. Resulting projected values are presented and discussed in the following paragraphs.

Inlet

Based on Task I and II results, nacelle inlet cruise efficiency was projected to be 99.66% for all four engine configurations. Advanced, low loss acoustical wall treatment (Dyna Rohr) was included in this estimate.

Fan Duct

Performance for the long mixed flow fan duct was projected from Task I evaluations and updated technology assessments. A summary of these projections is presented for the four engines in Table C-VIII.

TABLE C-VII

TASK III INITIALLY PROJECTED LPT PERFORMANCE

Engine Type	One Stage HPT Direct-Drive	Two-Stage HPT Direct-Drive	One-Stage HPT Geared	Two-Stage HPT Geared
Efficiency – (%)	91.2	91.2	92.6	92.6

TABLE C-VIII

TASK III INITIALLY PROJECTED FAN DUCT PRESSURE LOSSES

Engine Type	One-Stage HPT Direct-Drive	Two-Stage HPT Direct-Drive	One-Stage HPT Geared	Two-Stage HPT Geared
Pressure Loss (Internal) – (%)	0.47	0.55	0.33	0.41

Duct technology advancements included low loss acoustical wall treatment and improved contouring and sealing of joints to reduce aerodynamic losses and leakage.

External Nacelle

Task I and II evaluations and technology reassessment resulted in the total drag predictions for the four engines shown in Table C-IX.

External nacelle technology improvement was projected to result from external recontouring of the inlet lip, fan cowl,and aft cowl.

Exhaust Mixer/Nozzle System

Task I evaluation and reassessed technology projections resulted in the system pressure losses, mixing efficiency, and nozzle thrust coefficients shown for the four engines in Table C-X.

TABLE C-IX

TASK III INITIALLY PROJECTED EXTERNAL NACELLE DRAG

Engine Type	One-Stage HPT Direct Drive	Two-Stage HPT Direct Drive	One-Stage HPT Geared	Two-Stage HPT Geared
Total Drag – N (lbs)	1990 (447)	2070 (465)	2145 (482)	2225 (500)

TABLE C-X

TASK III INITIALLY PROJECTED EXHAUST MIXER/NOZZLE PERFORMANCE

Engine Type	One-Stage HPT Direct Drive	Two-Stage HPT Direct Drive	One-Stage HPT Geared	Two-Stage HPT Geared
Pressure Loss (Fan Mixer) - %	0.13	0.13	0.07	0.07
Pressure Loss (Engine Mixer) - %	0.21	0.21	0.23	0.23
Efficiency (Mixer) - %	85	85	75	75
Pressure Loss (Tailpipe) - %	0.26	0.26	0.21	0.21
Thrust Coefficient - %	99.58	99.58	99.60	99.60

Projected system technology improvements included a short scalloped, convoluted mixer configuration; low-loss exhaust nozzle acoustical treatment; and mixer acceptance of LPT exit airflow residual swirl to reduce LPT exit guide vane loading and loss.

2.1.3 Initial Materials/Updated Technology Projections

Task I materials and fabrication technique projections were reviewed relative to latest technology state-of-the-art. Generally, selections and property goals of the advanced technologies were unchanged. The most significant technology updates are shown in Table C-XI.

Hollow titanium was selected for the fan blade approach because of continuing major concern about the foreign object damage capability of composites. Indications that the property characteristics of titanium-aluminide were not required in the rear stages of the HPC resulted in its being eliminated to reduce cost with minimal weight impact. MERL 76 was chosen for the one-stage HPT disk because, with higher rim speed, its cooler rim did not require the dual properties provided by MERL 85 for the two-stage HPT. The HPT-LPT transition duct strut was changed to single crystal material to reduce cooling airflow requirements and to improve performance. MERL 76 rotors and disks were incorporated for the LPT for weight reduction purposes. Titanium-aluminide was eliminated from the front two LPT stages because projected properties were deemed inadequate for the higher temperature environment.

Table C-XII presents a summary of the significant advanced materials technologies projected for use in these analyses:

TABLE C-XI

SIGNIFICANT CHANGES IN SELECTED MATERALS TECHNOLOGIES FROM TASK I TO TASK III

Component	From Task I	To Task III
Fan Blades	Superhybrid Composite	Hollow Titanium
HPC Blades (Rear)	Titanium-Aluminide	Current Steel (PWA 1003)
HPT Disk (1 Stage HPT) (2 Stage HPT)	(Not Applicable) MERL 85	MERL 76 (No Change)
Turb. Transition Duct Strut	Cobalt Base Alloy (MAR-M509)	Single Crystal Alloy
LPT Rotor/Disks	Current Steel (PWA 1003/1029)	MERL 76
LPT Blades	Titanium-Aluminide	Front Stages Current Steel (PWA 663/655)

TABLE C-XII

ADVANCED MATERIALS TECHNOLOGIES PROJECTED FOR ENGINE APPLICATION

Technology	Property Projection	Benefit
Composite Fan Vanes	High strength-to-density ratio	Weight reduction
Advanced Titanium Alloys (MERL 102, MERL 103)	High creep and tensile strength	Weight reduction
Advanced Nickel Alloys (MERL 76)	High strength-to-density ratio	Cost and weight reduction
Single Crystal Turbine Airfoils (MERL 200 Blade, MERL 220 Vane)	High temperature capability	TSFC improvement
ODS Burner Liner	High temp. creep resistance	TSFC improvement
Titanium-Aluminide LPT Airfoils and Exhaust System	High creep strength	Weight reduction
Ceramic Outer Airseal	Low thermal conductivity	TSFC improvement
Thermal Barrier Coatings	Low thermal conductivity	TSFC improvement

2.1.4 Initial Component Mechanical Parameters/Updated Technology Projections

Task I component mechanical parameters and technologies were reviewed in detail. Results of these reassessments are discussed in the following paragraphs.

2.1.4.1 Low Clearance Rotors

Component blade tip clearance goals were established, based on projected rotor-case deflection behavior with a number of advanced mechanical and structural features. Advanced technology features included:

- Abradable gaspath seals in all components.
- Active clearance control in the middle and rear stages of the HPC, the HPT, and the LPT.
- Fan duct-engine case (cowl) load sharing.
- Stiff rotor construction with high rotor supported fore and aft.
- Stiff cases and frames.
- Improved thermal matching design system.

Resulting clearance goal projections are given in Table C-XIII.

TABLE C-XIII

TASK III BLADE TIP CLEARANCE GOALS AT CRUISE

Component	Average Goal - mm (inches)
Fan	1.9 (0.076)
LPC	0.5 (0.020)
HPC	0.3 (0.013)
HPT	0.5 (0.020)
LPT	0.5 (0.020)

2.1.4.2 Mainshaft Bearings/Seals

Based on technological projections in the areas of bearings and shaft sealing, parameter projections were made. Table C-XIV summarizes the selected mechanical levels.

TABLE C-XIV

TASK III BEARINGS/SEALS TECHNOLOGICAL CONCEPTS AND GOALS

Concept	Goal
High Speed Ball Bearings	2.7 X 10^6 DN
High Speed Roller Bearings	2.7 X 10^6 DN
High Speed Carbon Face Seals	160 m/sec (525 ft/sec.)

2.1.4.3 Mainshaft Speed Reduction Gearbox

Current operational experience was investigated to establish a firm current technology base for both the gearbox and its lubrication system. Trends in technology were then projected, and those most appropriate for the fan speed reduction gear system were selected. These projected goals are presented by Table C-XV.

Advanced technology concepts projected to accomplish these goals were

- Improved gear tooth geometry
- Use of advanced materials and lubricant
- Better oil distribution management
- New roller bearing concepts
- Advanced shafting techniques.

2.1.5 Initial Engine Design Tables

All pertinent component performance and mechanical projections made for the four engine types were input to the State-of-the-Art Performance-Program (SOAPP) for assessment and refinement. Cycle refinements with SOAPP were accomplished by analyzing the design point inlet, engine component, and nozzle performance characteristics. The resulting internal engine airflows, pressures, temperatures, speed, etc. as well as the thrust and fuel flow, comprised the aerodynamic design point (ADP) engine design table at the 10,700 m (35,000 ft), Mach 0.8 maximum cruise rating.

Off-design performance was then run using the ADP engine and the appropriate SOAPP system library of component maps. This procedure established engine design tables at portions of the commercial engine flight spectrum found from experience to be critical to the engine.

TABLE C-XV

TASK III REDUCTION GEARBOX TECHNOLOGICAL GOALS

Parameter	Goals
Efficiency (cruise/takeoff) – %	98.8/99.1
Pitch Line Velocity – m/min (ft/min)	7,620 (25,000)
Scoring Limit – kg/m (lb/in.)	53,570 (3,000)
Contact Stress – N/m^2 (psi)	12.4×10^8 (180,000)
Bending Stress – N/m^2 (psi)	5.5×10^8 (80,000)
Lubricant	Advanced Type II
Maximum Horsepower – Watts (hp)	29.8×10^6 (40,000)

Initial engine design tables were prepared for each of the engines at the flight conditions indicated in Table C-XVI. A summary of ADP data for each engine configuration is given in Table C-XVII.

2.2 Preliminary Design Analyses

2.2.1 High-Spool Component Analysis

2.2.1.1 Spool Pressure Ratio Split Selection for the One-Stage HPT Engines

A study was undertaken to select the low- versus high-spool pressure ratio (PR) split for the one-stage HPT engines. (The choice of 18:1 HPC PR with a 2.14:1 fan root-LPC pressure ratio for the two-stage HPT engines had been made before initiation of this contract, using the same study techniques.)

A range of HPC PR from 10:1 to 18:1 was established by holding the overall cycle pressure ratio (OPR) at 38.6:1. Increasing the HPC PR from 10:1 decreased the total number of compressor stages and airfoils, and reduced the LPT diameter and cooling requirements. These changes resulted in lower engine weight, lower price, and lower maintenance cost. However, HPT loading and consequent efficiency loss caused a TSFC penalty. The net effect was an improvement in DOC. DOC improved greatly in the PR range of 10:1 to 14:1 and improved only slightly in the 14:1 to 18:1 range. These results are summarized in Table C-XVIII.

Other things considered as HPC PR was increased were:

- Increases in HPT aerodynamic risk.
- Increases in high-spool rotor length and clearance control concerns.
- Reductions in low speed HPC surge margin.
- Requirements for engine-starting surge bleed.

TABLE C-XVI

CRITICAL FLIGHT CONDITIONS FOR TASK III INITIAL ENGINE DESIGN TABLES

Altitude m (ft)	Mn/Speed	Atmosphere	Rating
10700 (35,000)	0.80	Standard	Max. Cruise (ADP)
10700 (35,000)	0.80	Std. + 10°C (18°F)	Max. Climb
0	85 km/hr (100 kts.)	Std. + 14°C (25°F)	Takeoff
0	0	Std. + 14°C (25°F)	Takeoff

TABLE C-XVII

SUMMARY OF AERODYNAMIC DESIGN POINT DATA FOR TASK III ENGINES
10,700 m (35,000 FT.) MACH 0.80, MAX. CRUISE

Engine Type	One-Stage HPT Direct-Drive	Two-Stage HPT Direct-Drive	One-Stage HPT Geared	Two-Stage HPT Geared
Total Corrected Airflow – kg/sec (lb/sec)	643(1415)	640(1409)	859(1889)	860(1892)
Fan Pressure Ratio	1.74	1.74	1.52	1.52
Bypass Ratio	6.5	6.5	9.1	9.1
Overall Pressure Ratio	38.6	38.6	38.6	38.6
Turbine Rotor Inlet Temp. – °C (°F)	1204(2200)	1204 (2200)	1204 (2200)	1204 (2200)
Turbine Cooling Airbleed – %	12.7	15.0	12.9	15.2
Mixing – %	85	85	75	75
Total Thrust – N (lb)				
Uninstalled	43150(9700)	42550(9570)	44600(10,030)	44250(9945)
Installed	40850(9180)	40150(9030)	42100(9,460)	41650(9360)
TSFC – kg/hr/N (lb/hr/lb)				
Uninstalled	0.056(0.544)	0.055(0.536)	0.054(0.520)	0.053(0.511)
Installed	0.059(0.573)	0.058(0.566)	0.057(0.549)	0.056(0.541)

TABLE C-XVIII

SELECTION OF SPOOL PRESSURE RATIO SPLIT FOR ONE STAGE HPT ENGINES

HPC Pressure Ratio	10:1	14:1	18:1
Fan Root – LPC PR	3.86	2.76	2.14
HPT PR	3.5	4.0	4.4
BPR	6.5	6.5	6.5
OPR	38.6	38.6	38.6
Number of Stages			
Fan	1	1	1
LPC	6	4	3
HPC	8	9	9
HPT	1	1	1
LPT	5	5	5
Δ TSFC – %	-0.4	Base	+0.3
Δ Weight – %	+7.0	Base	-1.7
Δ Price – %	+4.2	Base	-2.1
Δ Maintenance Cost – %	+3.3	Base	-2.3
Δ DOC – %	+0.7	Base	-0.3

Based on these considerations and on the study evaluation results, the 14:1 PR HPC was selected as the best balanced choice.

2.2.1.2 High Pressure Compressor Analyses

2.2.1.2.1 Stability Audit

Before initiating the aerodynamic preliminary design analyses of the HPC's for the four engine types, a stability audit was made to establish surge margin requirements. The general approach taken to define the preliminary design surge margin requirements was as follows:

A stability audit, reflecting current technology, was performed for the HPC at potentially critical flight conditions. An engine currently under development was used as this technology base. The Energy Efficient Engine HPC audit was then established by applying the projected technology improvements to the current

technology base. Surge margin requirements derived from the advanced technology audit were combined with the estimated HPC operating lines and surge line lapse rates to establish the surge margin requirement at the ADP's of each HPC.

Results of this stability audit that set surge margin and surge bleed flow requirements are presented in Tables C-XIX and C-XX for the 14:1 (one-stage HPT) and 18:1 (two-stage HPT) pressure ratio HPC's.

TABLE C-XIX

STABILITY AUDIT FOR 14:1 PRESSURE RATIO HPC'S

	Direct-Drive	Geared
Flight Condition: Maximum Climb		
% ADP Airflow	100.8	101.5
Required Surge Margin – %	13.4*	13.4*
Available Surge Margin – %	13.4	13.4
Required Surge Bleed – %	0	0
Flight Condition: Sea Level Static Idle**		
% ADP Airflow	32.3	30.7
Required Surge Margin – %	18.6	18.6
Available Surge Margin – %	18.6	18.6
Required Surge Bleed – %	9.5	11.3

*Result set ADP surge margin requirements
**Condition set maximum surge bleed flow requirement

TABLE C-XX

STABILITY AUDIT FOR 18:1 PRESSURE RATIO HPC'S

	Direct-Drive	Geared
Flight Condition: Maximum Climb		
% ADP Airflow	100.9	101.9
Required Surge Margin – %	13.4*	13.4
Available Surge Margin – %	13.4	14.0
Required Surge Bleed – %	0	0
Flight Condition: Takeoff/Reverse		
% ADP Airflow	94.5	91.5
Required Surge Margin – %	15.0	15.0*
Available Surge Margin – %	15.7	15.0
Required Surge Bleed – %	0	0
Flight Condition: Sea Level Static Idle**		
% ADP Airflow	26.5	26.5
Required Surge Margin – %	18.6	18.6
Available Surge Margin – %	18.6	18.6
Required Surge Bleed – %	16.0	15.6

*Result set ADP surge margin requirement
**Condition set maximum surge bleed flow requirement

Results further indicated that ADP surge margin requirements for both 14:1 and 18:1 HPC's were nearly the same, showing a range of 13.4 to 14.4 percent. Maximum surge bleed requirements for the 14:1 HPC ranged from 9.5 percent for the direct-drive turbofan engine to 11.3 percent for the geared engine. However, bleed flow requirements for the 18:1 HPC were found to be 16.0 percent. The lower bleed flow requirements for the 14:1 HPC were a result of a higher HPC airflow rate at idle power which in turn resulted in less bleeds closed surge margin deficit than the 18:1 HPC.

Because of the inability to account for active clearance control stability effects at this stage of the initial preliminary design effort, a HPC surge margin design goal of 20 percent was set at the ADP.

2.2.1.2.2 Aerodynamic Parameter Selection Study

A study was undertaken to select the best HPC aerodynamic parameters for the one- and two-stage HPT engines. The specific purpose of this analysis was to identify combinations of parameters that would provide designs optimized for good efficiency and low DOC. The general approach taken was to conduct a statistical parametric study for the two-stage HPT 18:1 PR HPC, leading to selection of an optimum configuration. An optimized HPC for the one-stage HPT's 14:1 PR HPC was then established by examining several near-optimum HPC's obtained from a re-examination of the parametric study trends and results.

18:1 Pressure Ratio HPC Optimization

HPC aerodynamic design parameters and their desired ranges of interest were identified for meanline analysis as shown in Table C-XXI.

In order to use a statistical evaluation procedure to seek an optimum design, a matrix was established representing the eight design parameters and their ranges of interest. The necessary statistical pattern of HPC combinations was then selected from this matrix for purposes of analysis (see Figure C-2).

TABLE C-XXI

18:1 PR HPC PARAMETRIC STUDY VARIABLES

	Meanline Analysis Range
Speed	*Base ±5%
Flowpath Shape**	0.25 to 0.75
Inlet Hub/Tip	0.45 to 0.70
Exit Axial Mach No.	0.22 to 0.46
Avg. Aspect Ratio	0.8 to 1.6
Δ Loading ($\Delta \frac{\Delta P}{Po-P}$)	0 to 0.04
Inlet Specific Flow – $\frac{lb/sec}{ft^2}$	36 to 40
Solidity	0.8 to 1.2

*Base high-rotor speed was established by a study optimizing the HPT
**As given here, the span fraction from the inner diameter which has a constant diameter for all rows

These HPC's were next evaluated using the meanline design system. Variables in this matrix defined the basic HPC configuration and speed, but not the number of stages. Assumptions were made on stagewise distributions of the average design parameters and on the number of stages needed to satisfy the loading limit and surge margin requirements. Meanline evaluation was conducted at surge. The wall loading($\frac{\Delta P}{Po-P}$) at surge for 20 percent margin was checked by the system against the loading limit incorporated in the program, and the actual surge margin was determined. If this surge margin was significantly off-target, a stage was added (or deleted), and the new compressor was re-evaluated. Once the number of stages was established, the exact loading to achieve 20 percent surge margin was obtained by varying the HPC diameter. This iterative procedure affected only one matrix parameter, inlet hub-tip ratio.

INLET CORRECTED AIRFLOW = 42.9 kg/sec (94.6 lbs/sec)
PR = 18.
P_{T3} = 2101 N/mm^2 (2116 PSFA)
T_{T3} = 15°C (518.7°R)
BASE INLET CORRECTED SPEED = 12625 RPM

POINTS (1) ON MATRIX YIELD LINEAR EFFECTS
POINTS (2) ON MATRIX YIELD INTERACTIONS
POINTS (X) ON MATRIX YIELD QUADRATIC EFFECTS

ΔSPEED					-5%									BASE							+5%								
FLOWPATH					.5	.25				.75				.25	.5				.75		.25				.75				.5
INLET HUB/TIP RATIO					.55	.5		.6		.5		.6		.55	.45	.55			.7	.55	.5		.6		.5		.6		.55
EXIT MACH NO.					.3	.26	.38	.26	.38	.26	.38	.26	.33	.3	.3	.22	.3	.46	.3	.3	.26	.38	.26	.38	.26	.38	.26	.38	.3
COLUMN					1	2	3	4	5	6	7	8	9	10	11	12	13	14	15	16	17	18	19	20	21	22	23	24	25
0.8	2%	186	1.0	A													X												
1.0	0%	176	0.9	B		(1)																						(2)	
			1.1	C						(2)													(1)					
		195	0.9	D				(2)																		(1)			
			1.1	E								(1)										(2)							
	4%	176	0.9	F									(1)								(2)								
			1.1	G					(2)																(1)				
		195	0.9	H							(2)												(1)						
			1.1	I			(1)																				(2)		
1.2	0%	186	1.0	J													X												
	2%	176	1.0	K													X												
		186	0.8	L													X												
			1.0	M	X									X	X	X	X	X	X	X									X
			1.2	N													X												
		195	1.0	O													X												
	4%	195	1.0	P													X												
1.4	0%	176	0.9	Q			(2)																				(1)		
			1.1	R							(1)												(2)						
		195	0.9	S					(1)															(2)					
			1.1	T									(2)								(1)								
	4%	176	0.9	U								(2)										(1)							
			1.1	V				(1)																		(2)			
		195	0.9	W						(1)														(2)					
			1.1	X		(2)																						(1)	
1.6	2%	186	1.0	Y													X												

ASPECT RATIO	LOADING	W/A $\frac{kg/sec}{m^2}$	SOLIDITY	ROW

Figure C-2 *High-Pressure Compressor Aerodynamic Parameter Study – Shows statistical pattern of high-pressure compressor combinations.*

Since, in this analysis, surge was set by the wall loading parameter $\frac{\Delta P}{P_{O-P}}$, and since D-factor is considered to be a better indicator of airfoil loading capability, the maximum allowable D-factor at surge was observed as a limit in the design system. When the D-factor limit was exceeded, the solidity was increased and the surge margin re-calculated.

These analyses also ensured general structural adequacy. Aspect ratio distributions were made

from front-to-rear using flutter criteria developed for preliminary configurations from detailed studies and testing. A first blade chordal taper ratio, shown acceptable regarding vibratory considerations, was used for this analysis.

Other factors in the aerodynamic meanline analysis included a uniform clearance for all airfoils equivalent to the 0.013 in. average goal clearance at the ADP with active clearance control. Based on past study results, a single reaction distribution was used for all HPC's. Improved airfoil durability was ensured by using a minimum nominal leading edge radius limit in conjunction with surface recontouring to minimize the resultant potential losses. Calculations also included erosion resistant coatings that reduced surface roughness.

Statistical models representing mathematical expressions for HPC efficiency, number of stages, axial length, and number of airfoils established the initial evaluation of the HPC's in the matrix. HPC integration with the other engine components was considered in order to arrive at the engine TSFC and DOC parameters.

The change in TSFC for various HPC configurations was made a function of HPC efficiency, HPT-LPT transition duct loss, and engine nacelle cowl drag. Diffuser loss was made a function of HPC exit axial Mach number. HPT efficiency and turbine transition duct losses were dependent primarily on HPC speed. The maximum nacelle diameter was assumed to be unaffected by the HPC, so cowl drag changed only with changes in HPC axial length.

Based on similar past studies, DOC was made a function of the primary aerodynamic variables, maintenance costs for the HPC and HPT, and engine TSFC. Maintenance costs and TSFC were made functions of the two airplane configurations/missions, Pratt & Whitney Aircraft domestic trijet and international quadjet.

Maintenance cost estimates were determined based on the projected part life and replacement cost. The major effects on maintenance costs were number of HPC blades and vanes, airfoil chords, speed, and number of stages. Front stage chords were significant contributors to cost because of their effect on airfoil life in an area highly susceptible to impact damage.

Several major considerations affecting HPC selection were apparent from this evaluation. Many combinations of parameters resulted in high efficiency predictions. Parameters which showed strong consistent trends were number of stages, inlet hub/tip ratio, and loading. At constant aspect ratio, an increase in number of stages improved efficiency, reduced the number of airfoils, but increased length. Figure C-3 shows these results. Since the increased length with additional stages makes it more difficult to maintain tip clearances, the effect of increasing aspect ratio to minimize length impact was investigated. As shown in Figure C-4, this approach resulted in increased efficiency with no DOC penalty. Lower inlet hub/tip ratio showed efficiency improvement, but bearing/support mechanical considerations and vibratory limitations on the first blade dictated a restriction on a minimum value. Increased surge loading (technology) levels were shown to have adverse effects on both efficiency and DOC, as seen in Figure C-5.

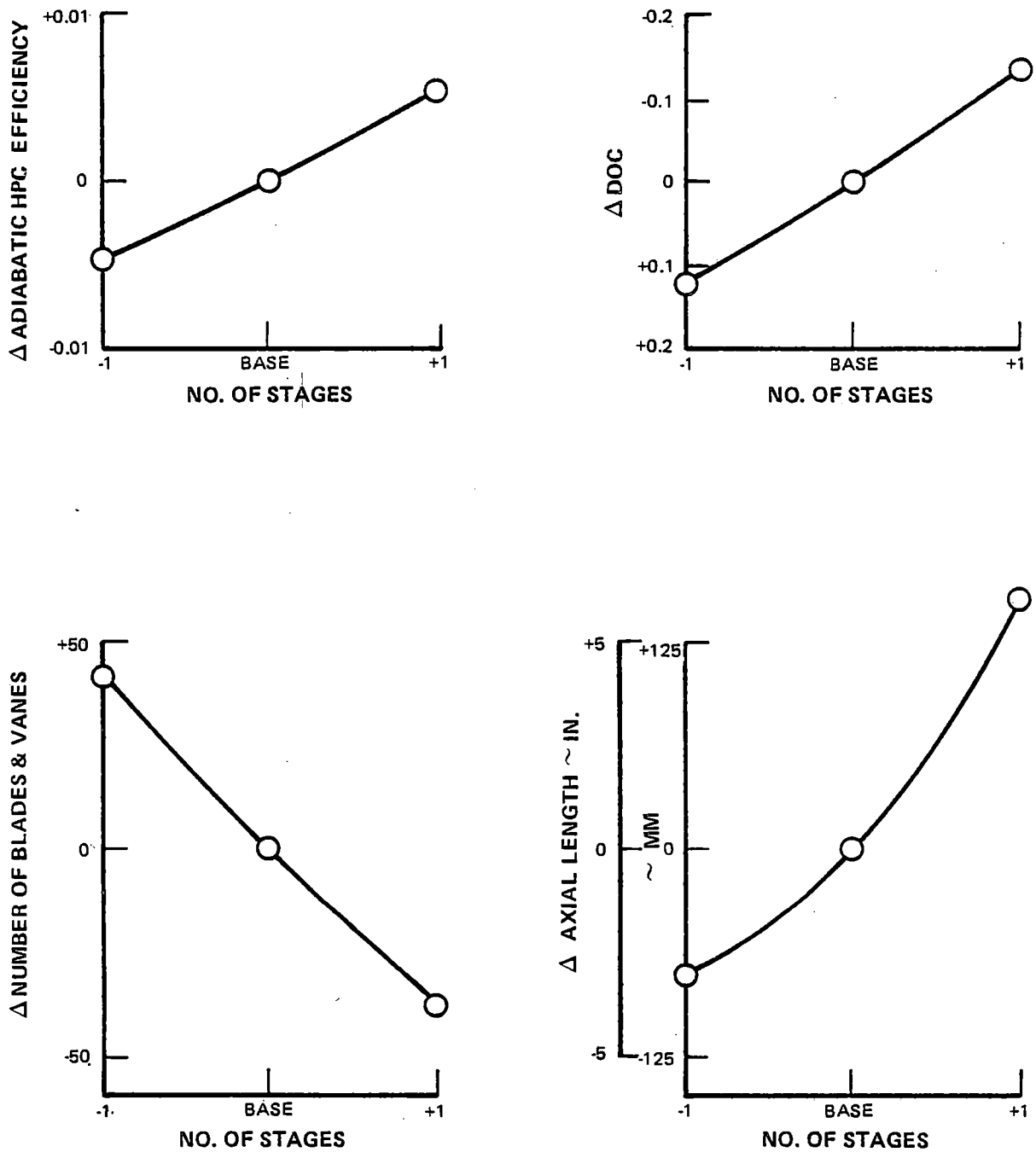

Figure C-3 *Effect of the Number of High-Pressure Compressor Stages at Constant Aspect Ratio – Shows the relationship of the number of stages to efficiency, direct operating cost, number of blades and vanes, and axial length.*

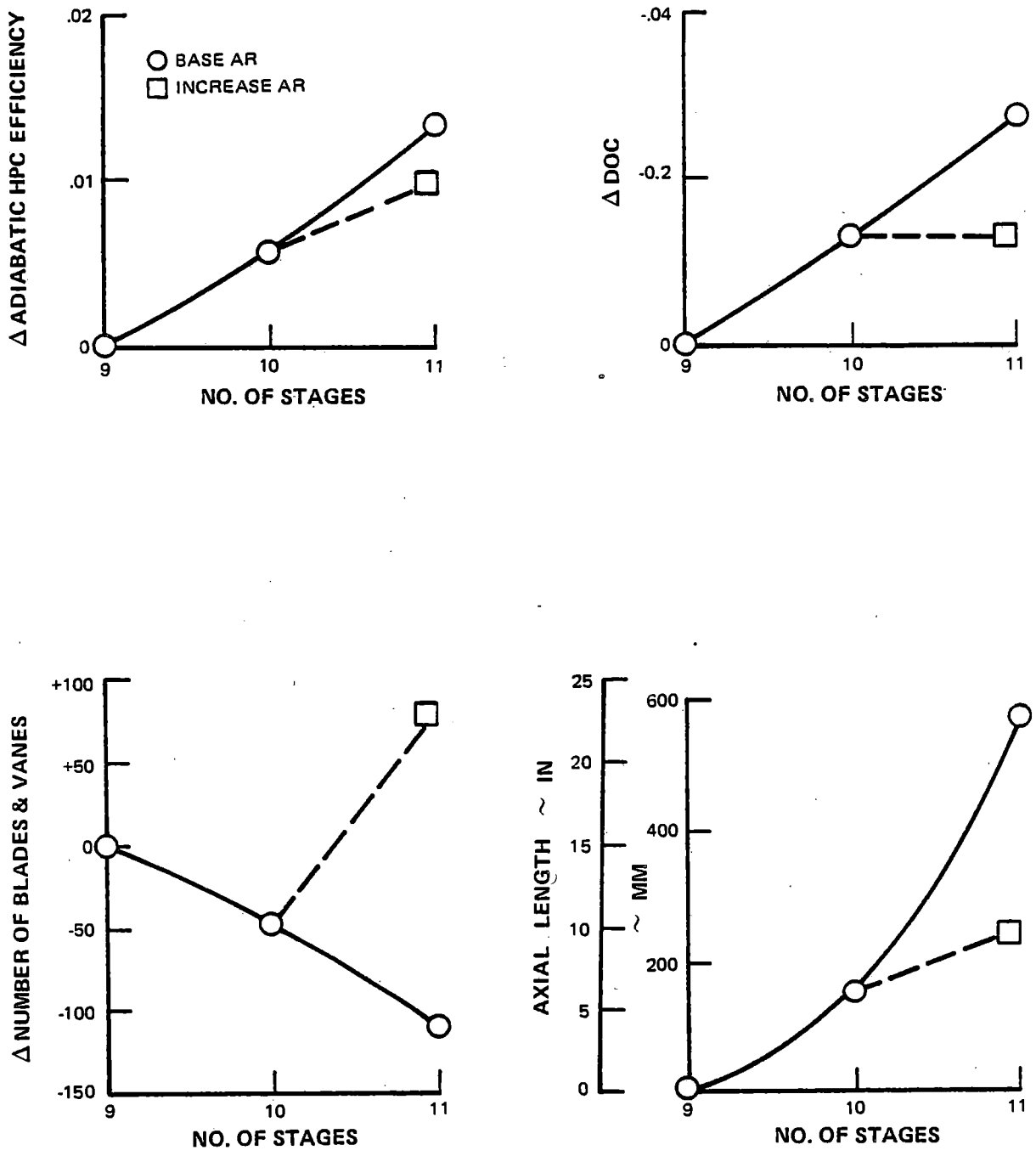

Figure C-4 *Effect of the Number of High-Pressure Compressor Stages at Increased Aspect Ratio – Shows the relationship of the number of stages to efficiency, direct operating cost, number of blades and vanes, and axial length for an increased aspect ratio.*

Figure C-5 *Effect of Increased HPC Loading Limit at Constant Aspect Ratio – Shows the relationship of efficiency and direct operating cost to increased surge loading limits.*

Based on the parametric regression results, the more promising 9-, 10-, and 11-stage HPC configurations were selected for specific meanline analysis and further evaluation. Table C-XXII summarizes these results. Meanline analysis results showed the two 9-stage HPC's (Configuration Nos. 3 and 5) to have significant efficiency deficits relative to the 10- and 11-stage HPC's. In addition, configuration No. 3 showed a relatively large 6.6 cm (2.6 in.) length penalty relative to the base HPC (Configuration No. 1), which was selected from the regression analyses as potentially the best 18:1 PR configuration. Design mechanical analyses indicated that this length increase could preclude the ability to maintain tip clearances and rotor stiffness with the two-bearing high spool support configuration selected for the direct-drive fan engine (see Section 2.2.3.4) of this appendix).

Because of the problems that might arise from the length penalty, Configurations No. 3 and 5 were eliminated from further consideration. Despite a 0.53 percent efficiency advantage over the base HPC, configuration No. 4 was eliminated because its 9.6 cm (3.8 in.) length increase was unacceptable for the desired two-bearing high spool. The 11-stage HPC (Configuration No. 6) was still promising and was therefore evaluated further. Results of this evaluation showed this HPC to offer a small fuel consumption advantage relative to the base HPC, but its DOC was worse. Therefore, the base Configuration No. 1 was selected for the 18:1 PR component since it offered the best DOC within the high spool length constraints.

14:1 Pressure Ratio HPC Optimization

Based on the 18:1 PR HPC optimization study results, a number of 14:1 PR HPC's were evaluated with the meanline design system. Considered as variables were speed, number of stages, inlet hub-tip ratio and specific flow, aspect ratio, and exit axial Mach number. This array of HPC's is shown in Table C-XXIII. Configuration Nos. 1 to 16 were included for verification of the 18:1 PR HPC parameter regression trends. Configuration Nos. 17 to 26 were defined in order to concentrate on the areas offering an apparent optimum combination of aerodynamic parameters.

TABLE C-XXII

STUDY RESULTS FOR MORE PROMISING 18:1 PRESSURE RATIO HPC'S

Configuration No.	1	3	4	5	6
No. Stages	10	9	11	9	11
Avg. Aspect Ratio	1.68	1.30	1.68	1.40	1.97
Inlet Hub-Tip Ratio	.577	.577	.577	.625	.577
% Base Rotor Speed	100	100	100	100	100
Inlet Specific Flow kg/sec/cm^2 (lb/sec/ft^2)	18.5 x 10^{-3} (38)	18.5 x 10^{-3} (38)	18.5 x 10^{-3} (38)	18.5 x 10^{-3} (38)	18.5 x 10^{-3} (38)
Exit Mn	.30	.30	.30	.30	.30
Δ Axial Length cm (in.)	Base	+6.6 (+2.6)	+9.6 (3.8)	−.8 (−.3)	0 (0)
Δ Adiabatic Efficiency %	Base	−.64	+.53	−.97	+.35
Δ Weight kg (lb.)	Base	*	* *	*	−17.3 (−37)
Δ Cost $	Base	*	* *	*	+8000
Δ Maint. Cost $/EFH	Base	*	* *	*	+2.12
Δ TSFC %	Base	*	* *	*	−.19
Δ DOC					
International Airplane	Base	*	* *	*	+.124
Domestic Airplane	Base Selected HPC	*	* *	*	+.139

*Not evaluated further because of efficiency deficit.
**Not evaluated further because of excessive length.

TABLE C-XXIII

14:1 PR HPC PARAMETRIC STUDY MATRIX

Inlet corrected flow = 44.7 kg/sec (98.4 lb/sec)
Inlet corrected rotor speed = 10,652 rpm

Comp. No.	% Base Rotor Speed	No. of Stages	Inlet Hub-Tip Ratio	Aspect Ratio	Inlet Specific Flow $Kg/sec/cm^2$ ($lb/sec/ft^2$)	Exit Mn	Δ Axial Length cm (in.)	Δ Adiabatic HPC Efficiency %
1 (Base)	100	9	.63	1.3	18.5×10^{-3} (38)	.30	Base	Base
2	105	9	.63	1.3	18.5×10^{-3} (38)	.30	+2.0 (+0.8)	−.01
3	105	8	.63	1.3	18.5×10^{-3} (38)	.30	−10.4 (−4.1)	−.71
4	100	9	.63	1.3	19.5×10^{-3} (40)	.30	−1.8 (−0.7)	−.24
4A	100	9	.63	1.3	18.5×10^{-3} (38)	.36	0	−.42
5	100	9	.63	1.45	19.5×10^{-3} (40)	.30	−9.4 (−3.7)	−.26
6	100	8	.63	1.15	18.5×10^{-3} (38)	.30	−4.1 (−1.6)	−.77
8	100	9	.54	1.3	18.5×10^{-3} (38)	.30	+3.1 (+1.2)	+.43
9	105	9	.54	1.3	18.5×10^{-3} (38)	.30	+5.1 (+2.0)	+.47
10	100	10	.63	1.3	18.5×10^{-3} (38)	.30	+12.5 (+4.9)	+.51
11	105	10	.50	1.3	18.5×10^{-3} (38)	.30	+21.4 (+8.4)	+1.18
12	105	10	.54	1.3	18.5×10^{-3} (38)	.30	+19.6 (+7.7)	+1.01
13	100	10	.50	1.3	18.5×10^{-3} (38)	.30	+18.1 (+7.1)	+1.12
14	100	10	.54	1.3	18.5×10^{-3} (38)	.30	+17.1 (+6.7)	+.99
15	105	10	.54	1.7	18.5×10^{-3} (38)	.30	−3.1 (−1.2)	+.98
16	105	10	.54	1.6	18.5×10^{-3} (38)	.30	+1.3 (+0.5)	+1.00
17	100	9	.63	1.4	18.5×10^{-3} (38)	.30	−5.3 (−2.1)	+.01
18	100	9	.67	1.3	18.5×10^{-3} (38)	.30	−1.8 (−0.7)	−.31
19	100	9	.67	1.5	18.5×10^{-3} (38)	.30	−11.7 (−4.6)	−.31
20	100	10	.63	1.7	18.5×10^{-3} (38)	.30	−7.9 (−3.1)	+.42
21	100	10	.565	1.57	18.5×10^{-3} (38)	.30	+0.8 (+0.3)	+.84
22	100	9	.617	1.3	18.5×10^{-3} (38)	.31	+2.0 (+0.8)	−.12
25	100	10	.61	1.62	18.5×10^{-3} (38)	.30	−3.8 (−1.5)	+.58
26	100	9	.61	1.31	18.5×10^{-3} (38)	.30	0	+.11

Fourteen of the more promising HPC's were selected from this array for TSFC and DOC evaluation. Results are shown in Table C-XXIV.

In order to magnify the differences between the most competitive 9- and 10-stage HPC's from the matrix, a more in-depth analysis was conducted for six of the fourteen with regard to nacelle impact, structural and mechanical limitations, and length-clearance effects on efficiency. For these six HPC's, the thrust bearing location, engine length, stagewise clearance distribution, and spool critical speed became major considerations. Increased axial length became especially troublesome because of the increased difficulty to maintain tip clearances and high-spool rotor stiffness.

From these candidates, Configuration No. 20 was selected for the 14:1 PR HPC. The 8-stage configurations were eliminated primarily on the basis of their reduced efficiency potential which reflected in increased fuel consumption. Generally, the 9-stage HPC's were found to have lower aspect ratio (fewer airfoils) and lower efficiency than the 10-stage HPC's. Typically, however, lengths for both 9- and 10-stage HPC's were comparable because of the higher aspect ratios of the 10-stage HPC's The results showed that, although maintenance cost is higher for the high aspect ratio configurations, the efficiency benefit derived from the additional stage more than compensates and clearly points to the choice of a 10-stage HPC. From these candidates, Configuration No. 20 was selected since it offered engine and nacelle performance improvement and length and weight reduction advantages relative to the other 10-stage HPC's

TABLE C-XXIV

STUDY RESULTS FOR MORE PROMISING 14:1 PRESSURE RATIO HPC'S

Configuration No.	1*	2	8	9	10	12	15	3	6	17*	26*	20*	25*	21*
No. Stages	9	9	9	9	10	10	10	8	8	9	9	10	10	10
Avg. Aspect Ratio	1.3	1.3	1.3	1.3	1.3	1.3	1.7	1.3	1.15	1.4	1.31	1.7	1.62	1.57
Inlet Hub-Tip Ratio	0.63	0.63	0.54	0.54	0.63	0.54	0.54	0.63	0.63	0.63	0.61	0.63	0.61	0.565
% Base Rotor Speed	100	105	100	105	100	105	105	105	100	100	100	100	100	100
Engine: Δ HPC Length - cm	Base	+2.0	+3.1	+5.1	+12.5	+19.6	-3.1	-10.4	-4.1	-5.3	0	-7.9	-3.8	+0.81
(in)	Base	(+0.8)	(+1.2)	(+2.0)	(+4.9)	(+7.7)	(-1.2)	(-4.1)	(-1.6)	(-2.1)	(0)	(-3.1)	(-1.5)	(+0.3)
Δ Adiab. HPC Efficiency - %	Base	-0.01	+0.43	+0.47	+0.51	+1.01	+0.98	-0.71	-0.77	+0.15	+0.11	+0.63	+0.68	+8.1
Δ Weight - Kg	Base	-21	-29	+3	-9	-6	-44	-7	+34	-10	+6	-46	-36	-24
(lb)	Base	(-47)	(+63)	(+6)	(-20)	(-13)	(-96)	(-15)	(+75)	(-21)	(+14)	(-102)	(-80)	(-54)
Δ Cost - $	Base	-6100	-200	-5300	-700	-5400	-4400	-4000	+1000	+200	-45	+600	-100	-1400
Δ Maint. Cost - $/EFH	Base	-0.39	-0.76	-1.10	-0.63	-1.45	+0.90	-0.66	-1.19	+0.86	-0.17	+2.22	+1.60	+0.57
Δ TSFC - %	Base	+0.006	-0.236	-0.258	-0.280	-0.556	-0.539	+0.391	+0.424	-0.083	-0.061	-0.346	-0.374	-0.446
Nacelle: Δ Length - cm	Base	–	–	–	–	–	–	–	–	-5.3	+1.0	-7.9	-2.8	+3.8
(in)	Base	–	–	–	–	–	–	–	–	(-2.1)	(+0.4)	(-3.1)	(-1.1)	(+1.5)
Δ TSFC - %	Base	–	–	–	–	–	–	–	–	-0.036	+0.017	-0.053	-0.024	+0.026
Δ Weight - Kg	Base	–	–	–	–	–	–	–	–	-14	+3	-20	-7	+10
(lb)	Base	–	–	–	–	–	–	–	–	(-30)	(+6)	(-45)	(-16)	(+22)
Δ DOC: International Aircraft	Base	-0.10	-0.13	-0.25	-0.16	-0.38	-0.31	+0.07	+0.16	-0.02	-0.03	-0.12	-0.15	-0.21
Domestic Aircraft	Base	-0.09	-0.09	-0.19	-0.12	-0.28	-0.20	+0.03	+0.08	0	-0.02	-0.05	-0.08	-0.13
												Selected HPC		

*Configurations analyzed in more depth in terms of structural and mechanical limitations, length effects on clearance and performance, and nacelle impact.

2.2.1.2.3 18:1 Pressure Ratio HPC Rear Stages Structural Analysis

Because of the high overall cycle pressure ratio (temperature) and higher than current speed environment imposed on the HPC rear stages, a structural study was conducted for the 18:1 PR configuration. Although the study was performed for the base 38.1:1 cycle, consideration was also given to ultimate future thrust growth incorporating 45:1 OPR.

Ground rules for this analysis were as follows:

The established mechanical design parameters, design criteria, and material property projections were used. The domestic airplane mission was assumed for cyclic life analysis. Local environmental estimates are summarized in Table C-XXV.

TABLE C-XXV

ENVIRONMENTAL GROUND RULES FOR HPC REAR STAGE STRUCTURAL STUDY

	9th Stage	10th Stage
Rotor Speed - rpm		
ADP	13200	13200
Max.	14450	14450
Temperatures (Max. Steady State)		
Avg. Airfoil - °C (°F)	570 (1060)	625 (1160)
Attachment - °C (°F)	595 (1100)	645 (1190)
Avg. Disk - °C (°F)	490 (910)	510 (950)
Materials:		
Disk	MERL 76	MERL 76
Blade	Incoloy 901 (PWA 1003)	Incoloy 901 (PWA 1003)

A general shell analysis was used to permit analysis of the last stage disk snaploads, which were found to be of great significance. Disks were rough sized using the initially calculated loads. Loads and temperatures were then corrected and reassessed to correspond to refined disk shapes. Results of these analyses are summarized in Table C-XXVI.

With the proper detailed design, the HPC rear configuration is feasible, providing the advanced material, MERL 76, is used in the final three disks. Also, since blade load was found to constitute only a small percentage of total disk loading, the potential for realizing significant weight reduction through the use of low density titanium-aluminide blades would be minimal.

2.2.1.2.4 HPC Configuration Summary

A summary of the aerodynamic design parameters of the 14:1 and 18:1 PR HPC's is given in Table C-XXVII.

Cross sections of the two HPC's are shown in Figure C-6.

TABLE C-XXVI

RESULTS OF STRUCTURAL ANALYSIS OF REAR STAGES OF 18:1 PRESSURE RATIO HPC

	Stage	Disk Weight kg (lbs)	Burst Margin	Max. Avg. Temp. °C (°F)	Bore Fracture Mechanics Life ~ Cycles	In-Plane LCF Life ~ Cycles Bore	Rim	Bolt Circle	Web
Initial Design	9	13.5 (29.8)	20%	445 (830)	500	6,500	–	–	10^5
	10	14.8 (32.7)	19%	465 (870)	500	4,000	–	$>10^5$	30,000
Refined Design	9	14.7 (32.6)	39%	445 (830)	$>10^5$	25,000	–	–	–
	10	19.1 (42.2)	34%	465 (870)	$>10^5$	20,000	>50,000	21,000	25,000

TABLE C-XXVII

TASK III HPC AERODYNAMIC SUMMARY
(AERODYNAMIC DESIGN POINT)

Pressure Ratio	14	18
Number of Stages	10	10
Average Aspect Ratio	1.70	1.68
Rotor Speed-rpm	13000	13000
Corrected Tip Speed m/sec (ft/sec)	403 (1322)	445 (1459)
Inlet Hub/Tip Ratio	0.63	0.577
Exit Hub/Tip Ratio	0.919	0.924
Average Solidity	0.958	0.998
Average Cx/U	0.524	0.497
Average Wall Loading	0.402	0.417
Average Airfoil Loading	0.504	0.509
Exit Axial Mach No.	0.30	0.30
Adiabatic Efficiency - %	88.6	87.9
No. of Airfoils (w/o IGV)	1231	1223
Axial Length (w/o IGV) - cm (in.)	67.4 (26.5)	66.3 (26.1)
Flowpath Shape	CMD	CMD
Inlet Specific Flow $\frac{kg/sec}{m^2}\left(\frac{lb/sec}{ft^2}\right)$	185 (38.0)	185 (38.0)
Surge Margin - %	20	20

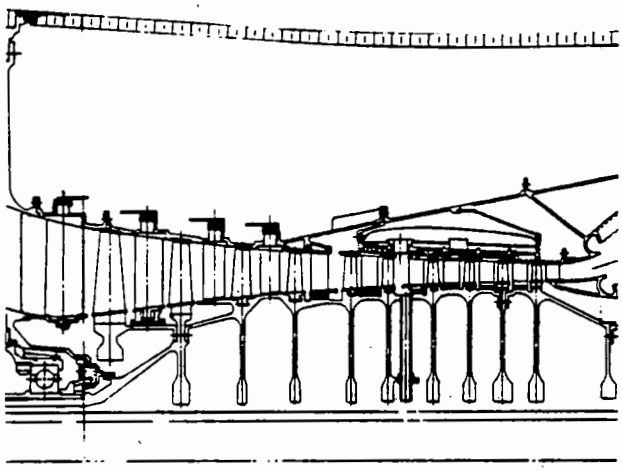

ONE-STAGE HPT ENGINE

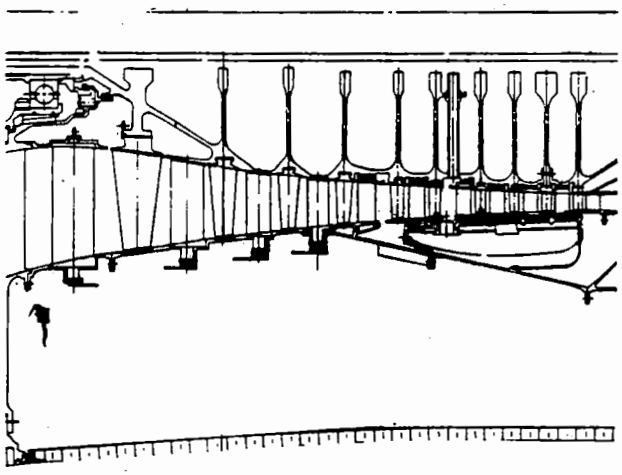

TWO-STAGE HPT ENGINE

Figure C-6 Task III Selected High-Pressure Compressor Cross Sections

2.2.1.3 Diffuser/Combustor Analyses

2.2.1.3.1 Diffuser Analysis

In order to select a diffuser configuration that had the best combination of pressure loss and length, a comparison study of three concepts was conducted. These concepts, shown in Figure C-7, were:

- A short axial flow diffuser with struts located in a downstream dump section
- A boundary layer bleed diffuser
- A highly canted diffuser utilizing HPC exit swirl.

Each of these diffuser concepts were evaluated as described next.

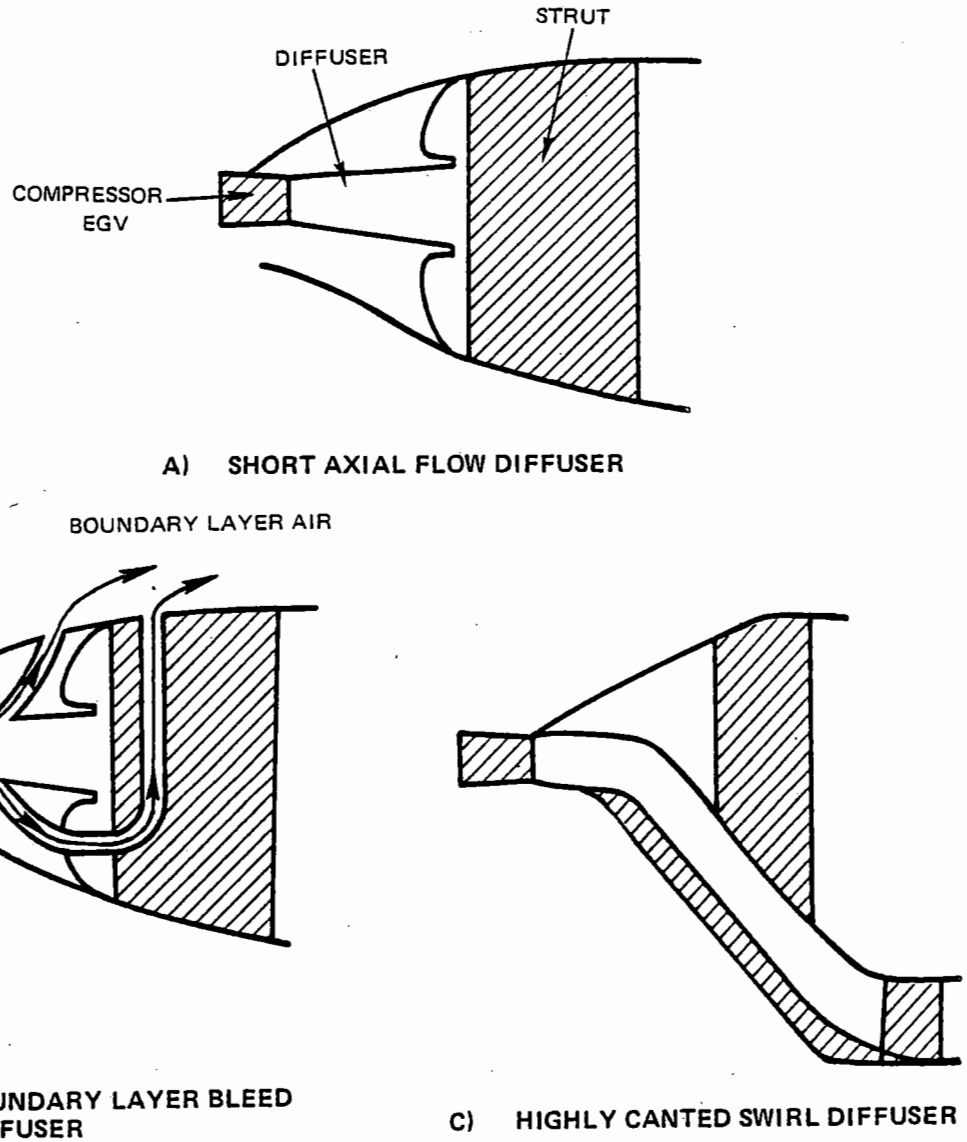

Figure C-7 Candidate Task III Diffuser Concepts

2.2.1.3.2 Axial Flow Diffuser Analysis

The short axial flow diffuser concept was configured using the diffuser-combustor interaction design system. A burner dome was defined to provide adequate back pressure to the diffuser to prevent incipient separation with the aggressive diffusion angle. The struts were located in the dump section to minimize aerodynamic impact. Aerodynamic analysis to estimate pressure loss started with a theoretical, isolated diffuser loss, and then added HPC distortion and strut effects with an allowance for burner pattern factor development. The resulting loss levels for two HPC exit Mach numbers as a function of length to inlet height of the diffuser are shown by Figure C-8.

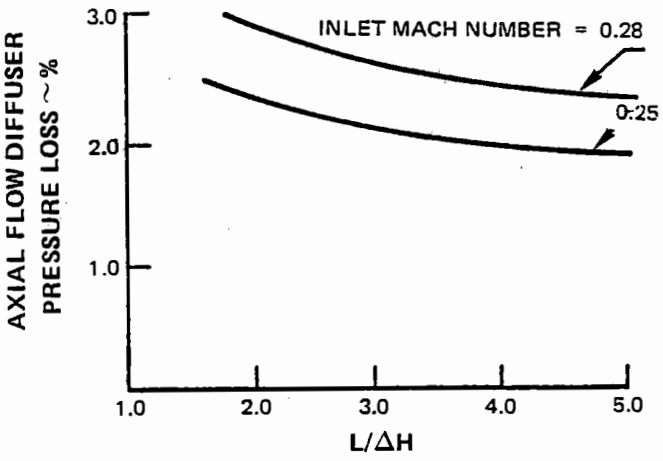

Figure C-8 Axial Flow Diffuser Pressure Loss Versus Length–Shows loss levels for two high-pressure compressor exit Mach numbers as a function of length to inlet height of the diffuser.

2.2.1.3.3 Bleed Diffuser Analysis

Figure C-9 shows estimated axial flow diffuser pressure loss reduction as boundary layer bleed is drawn off. Utilization of this bleed air was then assessed. The two uses considered were first HPT vane cooling and then HPT blade cooling. Vane cooling was rejected because of marginal feed supply pressure, so use in the blade cooling supply system was selected as the only viable approach.

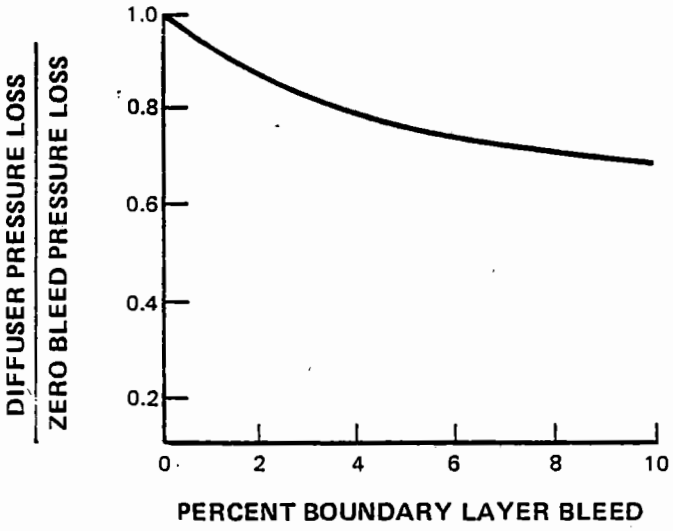

Figure C-9 Diffuser Pressure Loss With Diffuser Boundary Layer Bleed–Shows estimated axial flow diffuser pressure loss reduction as boundary layer is bled-off.

Performance weight, and cost of this approach were estimated for two levels of diffuser inlet Mach number and bleed. Results in terms of equivalent TSFC are shown in Table C-XXVIII.

2.2.1.3.4 Canted Diffuser Analysis

Pressure loss for the highly canted diffuser concept was assessed at 1.6 to 2.0 percent for a diffuser inlet Mach number of 0.25. This estimate included a benefit of 0.3 percent associated with unloading the HPC exit vanes, since they were no longer required to remove flow swirl. Very little pressure loss trade with length was found in this concept because the burner front end overlaps the diffuser.

TABLE C-XXVIII

BLEED DIFFUSER ANALYSIS RESULTS (EQUIVALENT TSFC)

Inlet Mach Number/Bleed:	0.25/3.7%	0.25/5.5%	0.28/5.5%
Diffuser Pressure Loss Reduction	-0.121	-0.168	-0.210
Cooling Air Penalty	+ 0.010	+0.015	+0.015
Weight Penalty	+0.045	+0.045	+0.045
Cost Penalty	+0.020	+0.020	+0.020
Net Equivalent TSFC:	-0.046%	-0.088%	-0.130%

2.2.1.3.5 Diffuser Configuration Selection

The small performance advantage offered by the bleed diffuser is not of sufficient magnitude to justify the required technology development. The highly canted diffuser scheme offers the lowest system loss, but it significantly adds to the complexity, weight, and cost of the combustion system.

Therefore, the short flow diffuser was selected for good performance and minimal development risk. This diffuser provided reasonable pressure loss and length reductions relative to current technology diffusers, and its shortness permitted the burner front end to be located in a position to force stable diffuser flow at more aggressive diffusion angles.

2.2.1.3.6 Combustor Analysis

Because of the stringent emissions requirements for the Energy Efficient Engine, the utilized combustor was based on the potentially successful Vorbix design developed by Pratt & Whitney Aircraft in the NASA Experimental Clean Combustor Program (ECCP), NAS3-18544. The major goal was to establish a more commercially viable version of this combustor while retaining its low emissions characteristics.

2.2.1.3.7 Combustion Analysis

In order to meet the emissions goals, the two pertinent major features of the ECCP combustor were two-stage combustion vortex burning and mixing.

Two axially separated burning zones or stages were configured, a pilot zone and a main zone, each independently fueled and each optimized for one extreme of the engine operating range. Separating both air and fuel introduction into two district stages allowed the pilot zone to be designed for the high efficiency required for low power CO and UHC emissions, while optimizing the main zone for low NOx emissions. The pilot zone was designed as a conventional swirl-stabilized bulkhead type combustor with fuel injected directly into the combustion zone.

The Vorbix concept was applied to the combustor design in order to optimize the main zone to minimize formation of NOx during high power operation while retaining high combustion efficiency. The main zone was configured so that fuel is injected into the hot gases at the exit of the pilot zone to provide partial mixing and pre-evaporization prior to entering the main zone. This fuel preparation was found to be essential to achieve complete combustion with the rapid mixing in-

duced by main zone combustion air introduced through swirlers designed into the inner and outer liners.

Based on utilization of these emissions reduction concepts, emissions levels were estimated. These estimates were calculated based on extrapolations of ECCP test results to the higher pressure and temperature environment imposed by the advanced cycle using the techniques discussed in Section 3.0 of the main body of the report. Emissions levels thus determined are summarized in Table C-XXIX for direct-drive and geared engines. Differences between separate and mixed exhaust engines were negligible.

TABLE C-XXIX

ESTIMATED TASK III ENGINE EMISSIONS LEVELS

	EPA Parameter	
Pollutant	Direct-Drive	Geared
HC	0.3	0.3
CO	2.0	2.0
NOx	4.3	3.8

Combustion zone sizing was accomplished by scaling the ECCP Vorbix design. The pilot zone was sized to provide a heat release rate consistent with high combustion efficiency (low CO and HC emissions) at the low pressures and temperatures associated with idle operation. This sizing also considered the provision for long residence time of combustion products before quenching by dilution air to help minimize CO and HC emissions.

Sizing of the main zone was based on the extremely delicate balance of the time and temperature in the burning and mixing zones. This sizing considered the fact that to achieve low levels of NOx, relatively short residence times in a low temperature environment are required. Alternatively, long reaction times at high temperature are required to obtain low levels of CO and HC. In addition, the sizing had to account for proper fuel penetration and stable combustion operation.

Relative to the ECCP burner, it was felt that weight, cost, and complexity improvements were required in order to achieve a commercially viable burner design. A design study was undertaken to accomplish this.

Twenty-four pilot zone fuel injectors and forty-eight main zone fuel injectors were estimated to be capable of providing acceptable performance. A design arrangement was then conceived whereby one pilot and two main zone injector supports would be cast into a clustered arrangement on a common base. The support bases were then configured to protrude through the outer wall of the diffuser case. This design approach can reduce injector weight and cost, and improve the structural integrity of the case as a result of fewer wall penetrations.

Casting approaches were conceived to cluster other main and pilot zone components for fabrication simplicity. Included were eight cast members in the pilot zone, each containing the support flanges for three fuel injector swirlers and one combustor mount lug, and forty-eight main zone fuel injector ports, and Vorbix swirlers cast in clusters.

A construction technique was devised that reduces weight and cost and improves performance (reduced leakage) by welding the rear outer section of the diffuser case to the front outer wall, thereby eliminating a flange.

To simplify burner liner construction and to permit removal of the combustor from the engine with the fuel injectors installed for improved maintenance, the Vorbix throat section of the ECCP was eliminated from the outer liner. The verification of this concept will require further burner development and proof testing.

2.2.1.3.8 Cooling Liner Analysis

Because of the more severe temperature and pressure environment of the Energy Efficient Engine combustor relative to current technology, liner durability and cooling configuration were of a major concern. Therefore, a preliminary study was conducted to assess durability and fabrication potentials of several configurations and to select a concept for the engine.

A preliminary liner life analysis was made for three potential materials: Hastelloy X, MERL 72, and Oxide Dispersion Strengthened (ODS) alloy. The same analysis was made for four liner configurations (Figure C-10): Impingement-Transpiration, Counterflow Film Cooled (CFFC), Transpiration Film, and Conventional Louvered. In performing these analyses, both low cycle fatigue (LCF), which is the dominant failure mode for the typical domestic airplane mission, and creep buckling and oxidation, the dominant failure modes for the international mission, were addressed.

A consistent strain model accounting for both hoop and axial components was used for each configuration. Constant liner pressure drop, hot streak temperature, and liner cooling flow were assumed for the study. Thermal boundary conditions were also made consistent in each configuration. Relative liner lives were calculated and absolute levels were established based on current operational experience.

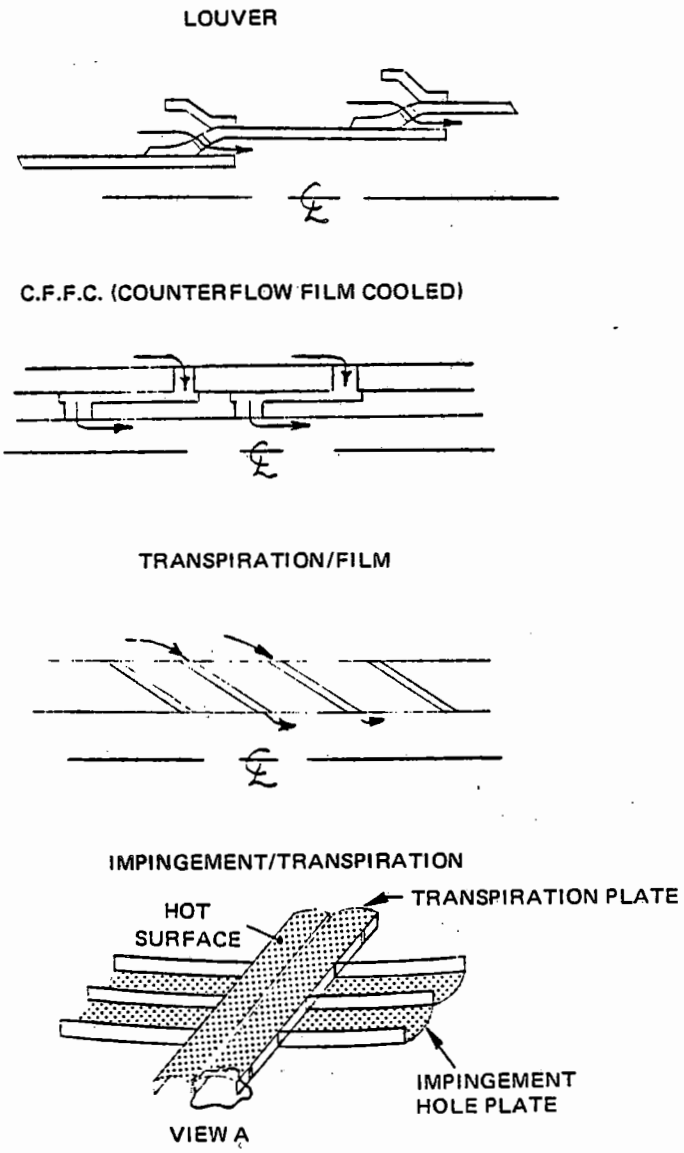

Figure C-10 Candidate Combustion Liner Cooling Schemes – Shows four liner cooling configurations.

Table C-XXX summarixes the predicted lives for the four candidate cooling configurations.

TABLE C-XXX

COMBUSTOR LINER DURABILITY/LIFE ANALYSIS RESULTS

Cooling Configuration	Hastelloy X		MERL 72	
	Cycles	Hours	Cycles	Hours
Impingement-Transpiration	2,500	10,000	4,900	19,600
Counterflow Film Cooled	550	2,200	1,000	4,000
Transpiration	490	1,960	800	3,200
Louver	320	1,280	490	1,960

Note: Liner life with ODS material was not calculated in-depth when it became apparent, based on a property comparison, that ODS had a lower LCF life than Hastelloy X.

The initial general conclusion drawn from this durability study was that only the impingement-transpiration cooling concept in either Hastelloy X or MERL 72 met the liner life goal. However, considerable concern existed over erosion damage to the liner caused by dirt particles impinging on the metal surfaces with this concept

Along with the durability analysis, a fabrication design study was conducted. Conceptual layouts were drawn for each basic liner configuration. Analysis included details pertaining to liner hole or slot size and quantity, wall thicknesses and contours, and materials and joining requirements. The layouts were then reviewed with regard to manufacturing methodology. Results of this review were used to make a preliminary cost comparison.

Relative costs for the several liner configurations studied are given in Table C-XXXI.

TABLE C-XXXI

COMBUSTOR LINER FABRICATION/COST ANALYSIS RESULTS

Configuration	Material	Δ Cost – $
Louver	ODS/Hast-X	Base
Impingement-Transpiration	Hast-X/MERL 72	+3,500 to 4,500
Counterflow Film Cooled	MERL 72	+6,000 to 13,000

In the more severe environment of the Energy Efficient Engine, the ODS alloy's 300°F higher metal temperature capability was needed to permit liner cooling airflow levels below the 35% limit established in the ECCP as being the upper limit for good emissions and pattern factor. On the other hand, Hastelloy X was estimated to exceed this cooling limit by 15% and MERL 72 to be marginal enough not to provide the necessary developmental capability required in the Energy Efficient Engine.

After carefully considering all aspects, the ODS louvered liner was selected as the prime candidate for the Energy Efficient Engine. This choice was made primarily on the basis of ODS's 300°F higher temperature capability than Hastelloy X and on the relative low cost and simplicity of the louver concept. The remaining problem, low ODS cyclic life was felt to be solvable with further design-fabrication work, such as that offered by the NASA MATE III Program. The Impingement-Transpiration and Transpiration configurations were rejected because of concerns about erosion, complexity, cost, and the amount of technology development required. Despite its apparently higher cost, the CFFC concept offered potentially good life relative to the transpiration configurations and was felt to be a worthy alternate to the selected configuration.

2.2.1.3.9 Combustor Configuration Summary

A summary of the combustor design parameters for the one- and two-stage HPT engines is given in Table C-XXXII.

TABLE C-XXXII

TASK III COMBUSTOR DESIGN SUMMARY
(Aerodynamic Design Point)

Configuration:	One-Stage HPT Engine	Two-Stage HPT Engine
Fuel/Air Ratio	0.0244	0.0244
Heat Release Rate – $\frac{KW}{atm \cdot cm^3}$	0.078	0.078
$\frac{BTU}{hr\text{-}atm\text{-}ft^3}$	(7.5×10^6)	(7.5×10^6)
Volume – m^3 (ft^3)	0.028 (1.0)	0.028 (1.0)
Burning Length – m (in.)	0.27 (10.7)	0.28 (11.2)
Section Length – m (in.)	0.42 (16.7)	0.45 (17.9)
Avg. Radius - m (in.)	0.33 (12.9)	0.30 (11.7)
No. Nozzles		
Pilot Zone	24	24
Main Zone	48	48
Nozzle Type		
Pilot Zone	Aerating	Aerating
Main Zone	Pressure Atomize	Pressure Atomize
Nozzle Spacing/Height		
Pilot Zone	1.18	0.93
Primary Zone	0.73	0.60

Cross sections of the two combustors are shown in Figure C-11.

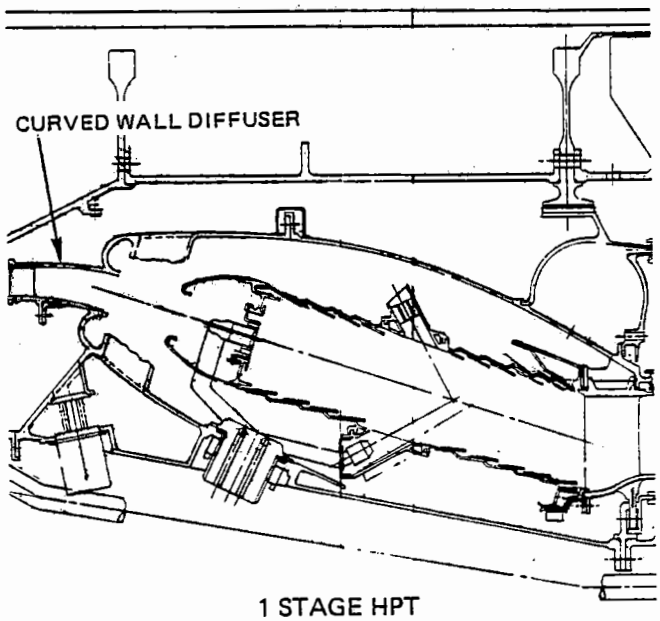

Figure C-11 Task III Selected Combustor Cross Sections

2.2.1.4 High-Pressure Turbine Analysis

Preliminary design analysis was conducted to optimize one- and two-stage definitions. Parametric aerodynamic, structural, and mechanical study evaluations were made to select basic designs. The critical aspects of these designs were then investigated to ensure basic feasibility.

2.2.1.4.1 Parametric Optimization Studies

Parametric optimization studies evaluated changes in annulus area, rotor speed, and rim speed in the case of the one-stage HPT and annulus area, velocity ratio, and rotor speed for the two-stage HPT. These parameters were varied, in the context of the projected aerodynamic, structural, and materials technologies, to define discrete, apparently feasible designs. These designs were then evaluated to determine their performance and economics. Results, including structural and mechanical risks, were then assessed to lead to configurational selection.

The parametric aerodynamic study was conducted using the meanline design system to define flowpaths, velocity triangles, and performance so that promising candidates could be selected for more detailed design. Aerodynamic constraints were first vane exit angles, blade tip and root Zwiefel loading coefficients, and first blade mean turning limits.

Airfoil cooling estimates were made using the durability design system considering the given mission and life criteria. Allowable metal temperatures were calculated using takeoff, climb, and cruise performance. Flowpath gas temperatures were estimated from the meanline analysis. Cooling airflow temperatures were defined from the engine secondary flow system map. Cooling flows were calculated using previously established effectiveness data and assumed cooling schemes. Stress limits, wall thicknesses, and airfoil numbers were determined by means of iterations with the mechanical design analyses. Cooling design modes for blades and vanes were creep and oxidation, respectively.

Resulting parametric aerodynamic trends for the one-stage HPT are shown in Figure C-12. Configurations D1, D2, and D3 were selected for further, more detailed study from these trends to explore high rotor speed, rim speed, and efficiency designs. Table C-XXXIII shows design parameters for these selected configurations.

Parametric aerodynamic trend results for the two-stage HPT are presented by Figure C-13. Configurations B1, B2, and C were selected from these trends to further investigate increased annulus area and rotor speed with high efficiency designs. A design parameter summary of these selected configurations is given in Table C-XXXIV.

2.2.1.4.2 Mechanical Analysis

Mechanical analyses were conducted on the candidate HPT configurations to evaluate their structural and mechanical feasibility. Airfoil and attachment stresses and lives were calculated to define airfoil numbers and wall thicknesses. Blade pulls were estimated to size and evaluate disks. Finally, airfoil-disk resonances were evaluated.

In performing these analyses, coated, single crystal blade materials were used in conjunction with an optimized four-tooth firtree attachment based on platform overhang criteria defined in previous Pratt & Whitney Aircraft studies. Disk and attachment temperatures

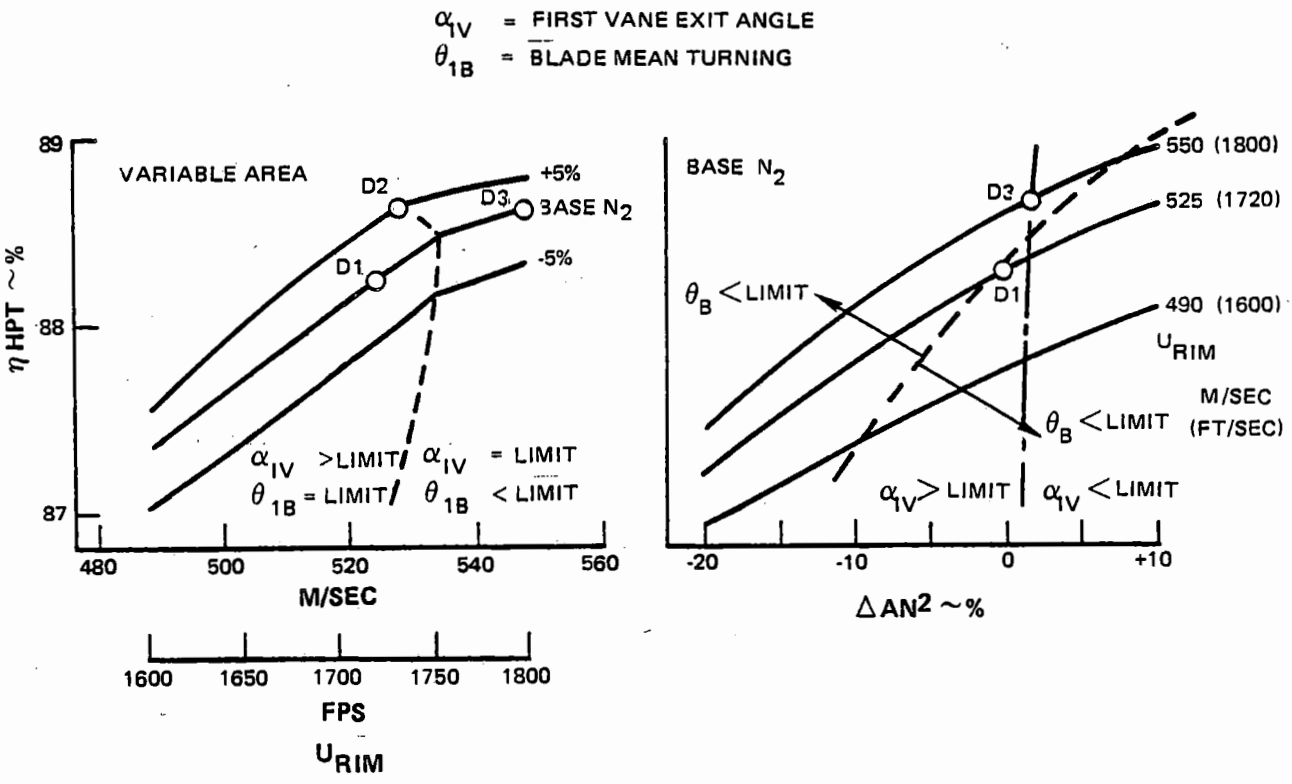

Figure C-12 One-Stage High-Pressure Turbine Efficiency Trends – Shows parametric trends.

TABLE C-XXXIII

TASK III CANDIDATE ONE-STAGE HPT CONFIGURATIONS

	D-1	D-2	D-3
N_2 (Redline)	Base	+5%	Base
Annulus Area	Base	Base	Base
U_{rim} - m/sec (ft/sec)	525 (1720)	525 (1720)	550 (1800)
Turbine Efficiency	88.2%	88.6%	88.5%

were established from secondary flow system studies which indicated MERL 76 and MERL 85 material requirements for the one- and two-stage HPT's, respectively.

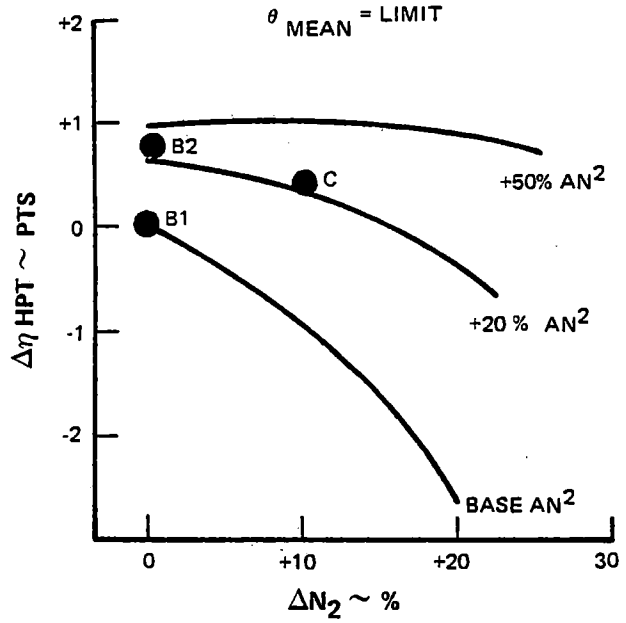

Figure C-13 Two-Stage High-Pressure Turbine Efficiency Trends – Shows parametric aerodynamic trends.

Table C-XXXV summarizes the results of the mechanical analysis for the one-stage HPT's. Configuration D1 was established by blade trailing edge overhang and disk vibration limits. It had the lowest number of blades of the three configurations. The highest rotor speed configuration, D2, also had the greatest number of blades. D2 was configured by attachment stress limits and blade vibration considerations. D3 (highest rim speed) was defined by disk size limitations. D3 was the heaviest configuration, but it also had relatively few blades.

Conclusions resulting from these analyses were:

- Increased rotor speed capability is quite sensitive to blade wall thickness and attachment stress capabilities.
- Increased rim speed capability is limited by attachment leakage restricting side-plate feasibility and disk size.
- Minimum blade number capability is sensitive to blade trailing edge platform overhang stress limitations.

TABLE C-XXXIV

TASK III CANDIDATE TWO-STAGE HPT CONFIGURATIONS

	B-1	B-2	C
N_2	Base	Base	+10%
Annulus Area	Base	+25%	+25%
U_{rim} - m/sec (ft/sec)			
1st Stage	400 (1310)	430 (1410)	395 (1290)
2nd Stage	380 (1250)	410 (1350)	375 (1230)
Turbine Efficiency	90.4%	91.3%	90.7%

TABLE C-XXXV

RESULTS OF MECHANICAL ANALYSIS OF CANDIDATE TASK III ONE-STAGE HPT

	D-1	D-2	D-3
Number of Blades	48	72	54
Mechanical Limit	T.E. O/H Disk Vib.	Attach Stress Blade Vib.	Disk Size
Total HPT Weight - kg (lbs)	Base	-14 (-31)	+22 (+48)
Disk Bore Width - m (in)	0.14 (5.6)	0.13 (5.2)	0.15 (6.1)
T. E. Overhand Parameter	0.72	0.47	0.62
Aspect Ratio	1.36	2.24	1.46

Two-stage HPT mechanical analysis results are summarized in Table C-XXXVI. The primary limitation leading to the B1 configuration was found to be blade trailing edge overhang. This configuration resulted in the minimum number of blades and almost the lightest weight. Disk bore thickness limits and blade vibration considerations defined the highest annulus area B2 configuration. B2 was found to be the heaviest configuration with more blades than B1. The highest rotor speed configuration, C, was set by disk size and shape

TABLE C-XXXVI

RESULTS OF MECHANICAL ANALYSIS OF TASK III CANDIDATE TWO-STAGE HPT

	B-1		B-2		C	
	1st	2nd	1st	2nd	1st	2nd
No. of Blades	34	36	38	42	48	54
Mechanical Limit	• T.E. O/H		• Disk Bore Thk. • Blade Vibration with S/C Blades		• Disk Shape • Blade Vibration with Non-S/C Blades	
Total Rotor Weight - kg (lbs)	Base		41 (+90)		-45 (-10)	
Disk Bore Width - m (in)	0.07 (2.8)	0.08 (3.2)	0.09 (3.8)	0.10 (3.9)	0.08 (3.0)	0.085 (3.4)
T.E. Overhand Parameter	0.65	0.50	0.58	0.52	0.43	0.33
Aspect Ratio	1.10	1.42	1.55	1.65	1.56	2.33

limitations and blade vibration considerations which required that the second stage blade material be changed from single crystal to an equiaxed alloy. Although C was the lightest configuration, it also had the highest number of airfoils.

Conclusions reached for the two-stage HPT were:

- Increased rotor speed capability is restricted by disk shape and size limitations and airfoil vibration characteristics.
- Minimum blade number capability is sensitive to blade trailing edge overhand stress limitations.

2.2.1.4.3 Performance/Economic Evaluation

A performance and economic comparison was made of the candidates to aid in the selection of final configurations. Weight and performance estimates had been established in the process of conducting the aerodynamic and mechanical analyses. Price and maintenance cost estimates were made for each configuration using standard analytical procedures. DOC was then calculated for the Pratt & Whitney Aircraft defined domestic and international aircraft. Evaluation results are summarized in Table C-XXXVII.

For the one-stage HPT matrix, configuration D1 was found to have the best economics despite slightly lower efficiency, primarily because of its low number of airfoils and consequent lowest price and maintenance cost. Configuration D2, with the best performance, had poor economics because of its large number of blades. D3 suffered economically because of the high weight and cost associated with its increased diameter.

TABLE C-XXXVII

TASK III HPT PERFORMANCE AND ECONOMIC STUDY RESULTS

	One-Stage HPT			Two-Stage HPT		
Configuration	D1	D2	D3	B1	B2	C
Δ Rotor Speed - %	Base	+5	Base	Base	Base	+10
Maximum Rim Speed - m/sec	525	525	550	400	430	390
(ft/sec)	(1720)	(1720)	(1800)	(1310)	(1410)	(1290)
Δ Annulus Area - %	Base	Base	Base	Base	+25	+5
No. of Blades	48	72	54	70	80	102
Efficiency – %	Base	+0.4	+0.3	Base	+0.9	+0.3
Δ DOC						
Domestic - %	Base	+0.11	+0.12	Base	-0.19	-0.11
International - %	Base	+0.08	+0.10	Base	-0.25	-0.07

Configuration B2 from the two-stage HPT matrix had the best economics because it had high performance and a moderate number of airfoils. Configuration C was also found to have good economics, despite high blade numbers, because of its equiaxed second stage airfoil material which was lower cost than higher strength single crystal. Its weight and case cost were low because of a small diameter, and it had reasonably good performance. B1's economics were the poorest primarily because of inferior performance.

2.2.1.4.4 HPT Configuration Selection (One- and Two-Stages)

Selection of final configurations was based on evaluation results and mechanical considerations. Configurations selected were D1 for the one-stage HPT and B2 for the two-stage HPT.

Configuration D1 was chosen because of its best economics and the structural/mechanical recommendation that base rotor speed and rim speed be used for most acceptable risk. Because of blade trailing edge overhand stress risk concerns, the number of airfoils was increased to 54 for the final configuration.

The B2 configuration was selected on the basis of best performance and economics. It also met the most acceptable structural/mechanical risk recommendation of base rotor speed and +25 percent of base annulus area.

2.2.1.4.5 Additional Design Feasibility Analyses

Preliminary design analyses of the selected one- and two-stage HPT's were continued in those key areas required to complete the establishment of basic feasibility. The aerodynamic and mechanical studies discussed in the following paragraphs were

- Increased airfoil turning (two-stage HPT)
- First vane exit angle (one- and two-stage HPT's)
- Stage work split (two-stage HPT)
- Airfoil cooling schemes (one- and two-stage HPT's)
- Blade attachment (one- and two-stage HPT's)
- Vane leakage (one-stage HPT)
- Rotor analysis (one- and two-stage HPT's)

2.2.1.4.6 Increased Airfoil Turning Analysis

To probe the significance of the mean blade turning limit utilized in the two-stage HPT parametric study, increases of 10 degrees for both stages were considered to evaluate the impact on the critical second stage. Numbers of blades and axial chords were held constant for this study. Blade loading was found to decrease slightly because of the change in gas angles, and the flowpath was moved inward 8 percent in mean diameter with a resulting 8 percent increase in blade span to maintain annulus area constant. Mean velocity ratio was reduced from 0.64 to 0.59 in the process.

This aerodynamic definition was then analyzed structurally and mechanically. The maximum attachment stress was calculated (constant disk rim width) and found to be increased 13 percent relative to the base mean turning case, primarily because of the smaller diameter. A disk was configured and found to have a poorer shape because of reduced radial room. Vibration estimates indicated inadequate margin because of the span increase. The stage was weighed and found to be 17 percent lighter.

Increased turning was rejected from further consideration at this point because solving the identified problems required more blades and weight. A reduced weight advantage and increased cost were not worth the increased aerodynamic risk associated with lack of experience.

2.2.1.4.7 First Vane Exit Angle Analysis

Concern over low first vane exit angles prompted studies to evaluate first blade sensitivities to changes in vane angle. Table C-XXXVIII summarizes the sensitivities for both HPT's.

TABLE C-XXXVIII

FIRST BLADE SENSITIVITY TO VANE EXIT ANGLE

	One-Stage HPT	Two-Stage HPT
Base 1st Vane Exit Angle (α_1) – deg.	10.2	11.7
Base 1st Blade Inlet Angle (β_1) – deg.	34.1	54.0
$\Delta\beta_1$ for +1 deg. $\Delta\alpha_1$ – deg.	11.5	16.5

Blade root sections were then designed for various incidences, and no adverse effects on pressure distributions were found.

2.2.1.4.8 Stage Work Split Analysis

An analysis was made to evaluate the choice of a base 48.5 to 51.5 percent stage work split in the two-stage HPT. The meanline system results are shown in Figure C-14. A small performance improvement was found in HPT efficiency for shifting first stage work to the second stage. However, HPT exit Mach number increased in the process and caused increasing HPT-LPT transition duct losses. Because of these offsetting influences, the base stage work split was retained at this point in the design process.

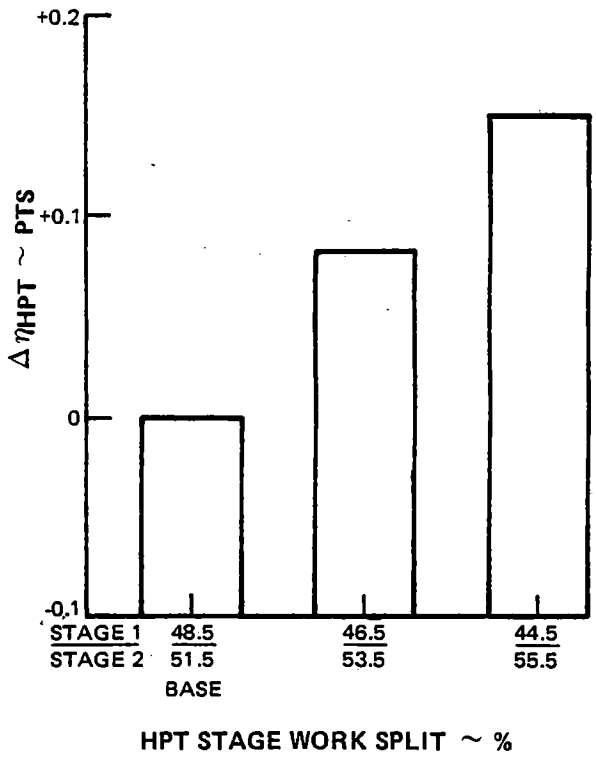

Figure C-14 Work Split Variation for Two-Stage High-Pressure Turbine – Shows meanline system efficiency results.

2.2.1.4.9 Airfoil Cooling Schemes

Airfoil durability analyses conducted during the parametric study were extended to better establish cooling configurations and flows that met the designated life criteria.

Review of the two-stage HPT airfoil cooling schemes resulted in no basic change to the concepts assumed in the parametric study. The final preliminary concepts are shown in Figure C-15. The first vane was defined with a single rib, two cavity configuration using internal impingement in conjunction with showerhead and pressure side film holes and pedestal trailing edge release. A three rib, four cavity convective configuration with showerhead and trailing edge releases was the approach taken for the first blade. The resulting second vane and blade were single cavity internal impingement and three cavity multipass convective, respectively, both with pedestal trailing edge release. Thermal barrier coatings were used on vane platforms to minimize cooling requirements. The first vane platform was impingement film cooled.

The review of the one-stage HPT vane indicated that the previously assumed suction side film cooling holes were not needed. The revised configuration then was as shown in Figure C-16. A two rib, three cavity concept with internal impingement, showerhead leading edge, pressure side film cooling, and pedestal trailing edge release resulted.

For the one-stage HPT blade, a short study was conducted to compare a preliminary multipass impingement cooled concept with the previously assumed multipass with showerhead leading edge concept because of the impingement concept's better performance potential. Results of this comparison are shown in Table C-XXXIX.

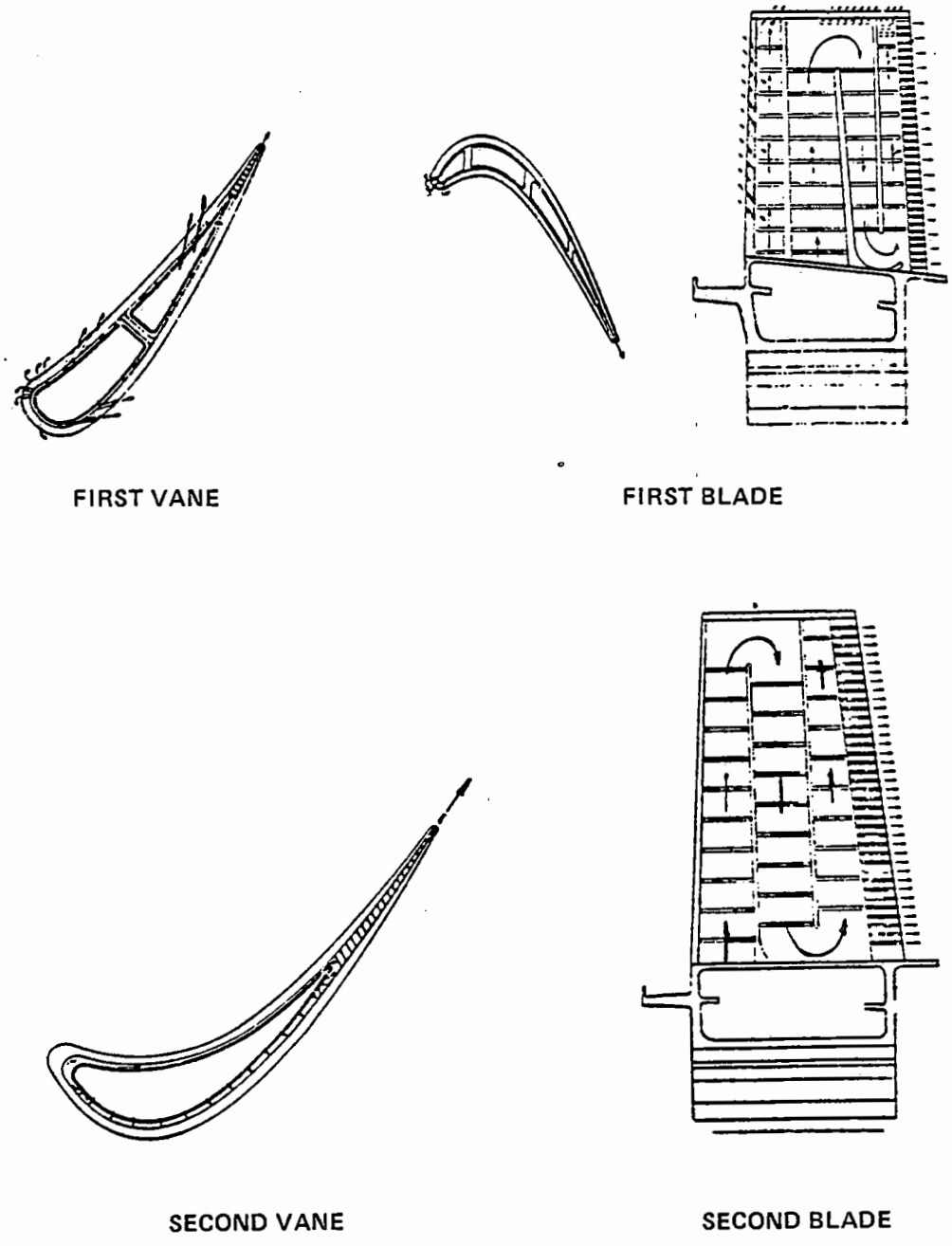

Figure C-15 Two Stage Turbine Airfoil Cooling Scheme – Shows airfoil cooling configuration

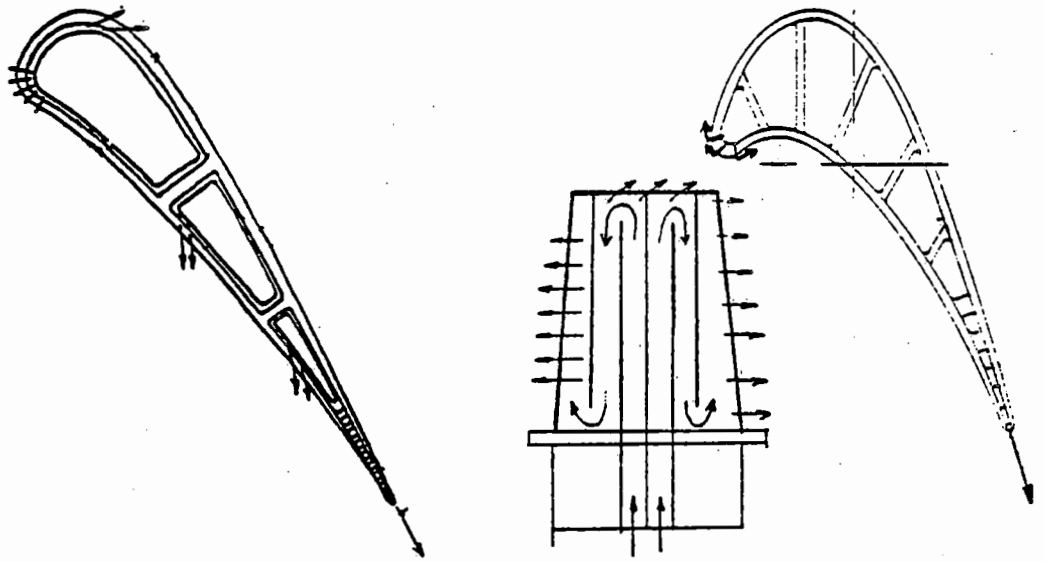

Figure C-16 One-Stage Turbine Airfoil Cooling Scheme – Shows airfoil cooling configuration

TABLE C-XXXIX

IMPINGEMENT VS. SHOWERHEAD COOLING CONCEPT PARAMETERS FOR 1 STAGE HPT BLADE

Cooling Concept:	Impingement	Showerhead
Pressure:		
Supply (TOBI) – % HPC exit	40	40
Blade Rivet – % HPC exit	40	48
Temperature		
Blade Rivet – °C (°F)	525(975)	565(1050)
Blade Metal Avg. – °C (°F)	955 (1750)	880 (1615)
Blade Metal Max. – °C (°F)	990(1810)	1010 (1850)
Blade Cooling Airflow – %	1.25 to 1.50	1.75

These results showed the impingement concept to have a potential performance advantage both in terms of less cooling air required and the fact that without showerhead flow and lack of gaspath disturbance, the blade efficiency may be higher. Furthermore, elimination of the disk-pumping hole associated with the higher pressure requirement of the showerhead system simplified the disk design. Because the preliminary analyses indicated the impingement blade to have excessive rib strain range and possible manufacturing difficulties, the showerhead concept was encouraged until more detailed design could be performed on the impingement blade. Additionally, with these high risk concerns, to design the secondary system for the lower supply pressure requirement of the impingement blade would preclude easy fallback to the showerhead concept. The refined selected one-stage HPT blade cooling scheme utilizes five ribs and six cavities for convective cooling, the showerhead for leading edge film cooling, and a pedestal type release for trailing edge cooling (Figure C-16).

Refined cooling flows for the two HPT configurations are presented in Table C-XL.

2.2.1.4.10 Blade Attachment Analysis

Because of the high rim speeds and temperatures of both one- and two-stage HPT's the preliminary attachment designs defined in the parametric studies were reviewed. Primary effort was concentrated on attachment design approach and life estimates.

The first of these studies investigated curved blade attachments and compared them to the straight root design used in the parametric studies. Both stages of the two-stage HPT were evaluated for several numbers of blades to determine the impact on trailing edge overhang. Allowable overhangs for each stage were then used to find the resulting effect on blade number at the allowable concentrated stress level. The advantage of a curved attachment was rejected on the basis that a 4 blade saving was not cost effective relative to the added expense of manufacturing the more complicated disk rim slots and blade roots. Attachment life estimated for both stages in the parametric study was confirmed in this study to be adequate with the 4 toothed firtree.

TABLE C-XL

ONE– AND TWO–STAGE HPT AIRFOIL COOLING AIRFLOW SUMMARY

	One-Stage HPT	Two-Stage HPT
1st Vane:		
Airfoil – %	6.00	6.15
Platform – %	1.30	1.00
1st Blade – %	1.75	2.00
2nd Vane – %	–	0.90
2nd Blade – %	–	0.30
Total	9.05%	10.35

Because of the very high rim speed selected for the one-stage HPT in the parametric study, the attachment area was reassessed to ensure adequate life. Maximum steady state disk lug and blade root temperatures were estimated from secondary airflow system and gaspath conditions. Initial indications were that the attachment area was about 50°F hotter than previously estimated, so an extra cooling flow quantity of 0.1% was introduced to the rim area. Resulting maximum temperatures and the attachment configuration are shown in Figure C-17. A two-dimensional finite element breakup was made of the attachment area, as shown in Figure C-18, and stresses and lives were calculated. Maximum bearing, shear, centrifugal pull, and concentrated fillet stresses in both the blade and disk were calculated to be below the allowables. Disk lug cyclic life was adequate, but blade root life was somewhat less than the goal. Further, more detailed design analysis should result in adequate blade root life.

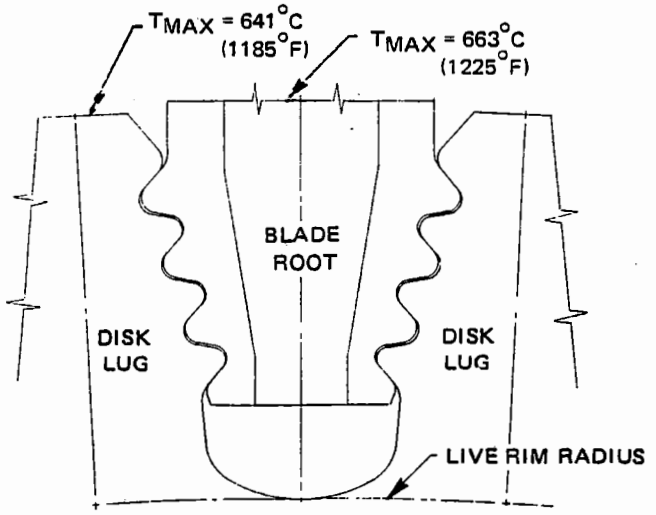

Figure C-17 One Stage High-Pressure Turbine Blade/Disk Attachment Design Temperatures – Shows maximum steady state temperature of the disk lug and blade root.

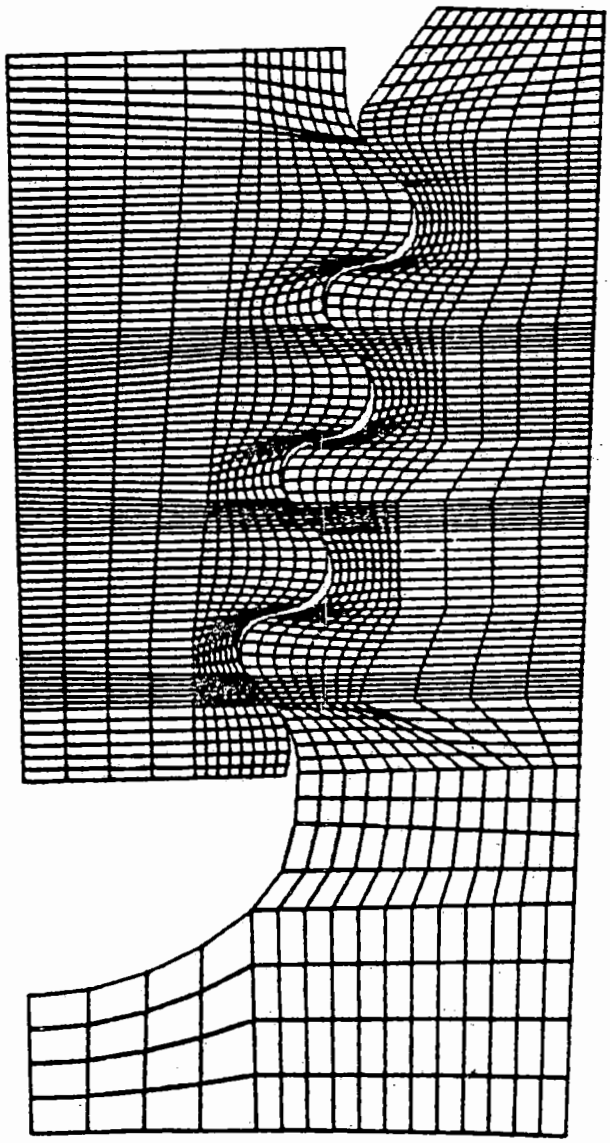

Figure C-18 One-Stage HPT Blade Attachment Design Two-Dimensional Finite Element Analysis Model – Shows blade/disk attachment region finite elements.

2.2.1.4.11 Vane Leakage Analysis

First vane platform leakage minimization is required for best performance, especially in a one-stage HPT design with its long vane chord

and high pressure differentials across the platforms. Preliminary analysis in this regard indicated that a vane incorporating advanced sealing features leaked about 1.8 times the goal flow. Figure C-19 shows the results of this analysis. Looking at the individual leakage sources, the combined I.D. and O.D. platform feather seals area and the vane twist areas at the forward and aft rails each accounted for almost 50% of the total. As a result, effort was concentrated on finding ways of reducing these two sources. More unconventional attachment approaches to control leakage were investigated in an attempt to reduce leakage.

Three general approaches were taken: clustered vane pairs; floating platforms; and full ring-strut-ring.

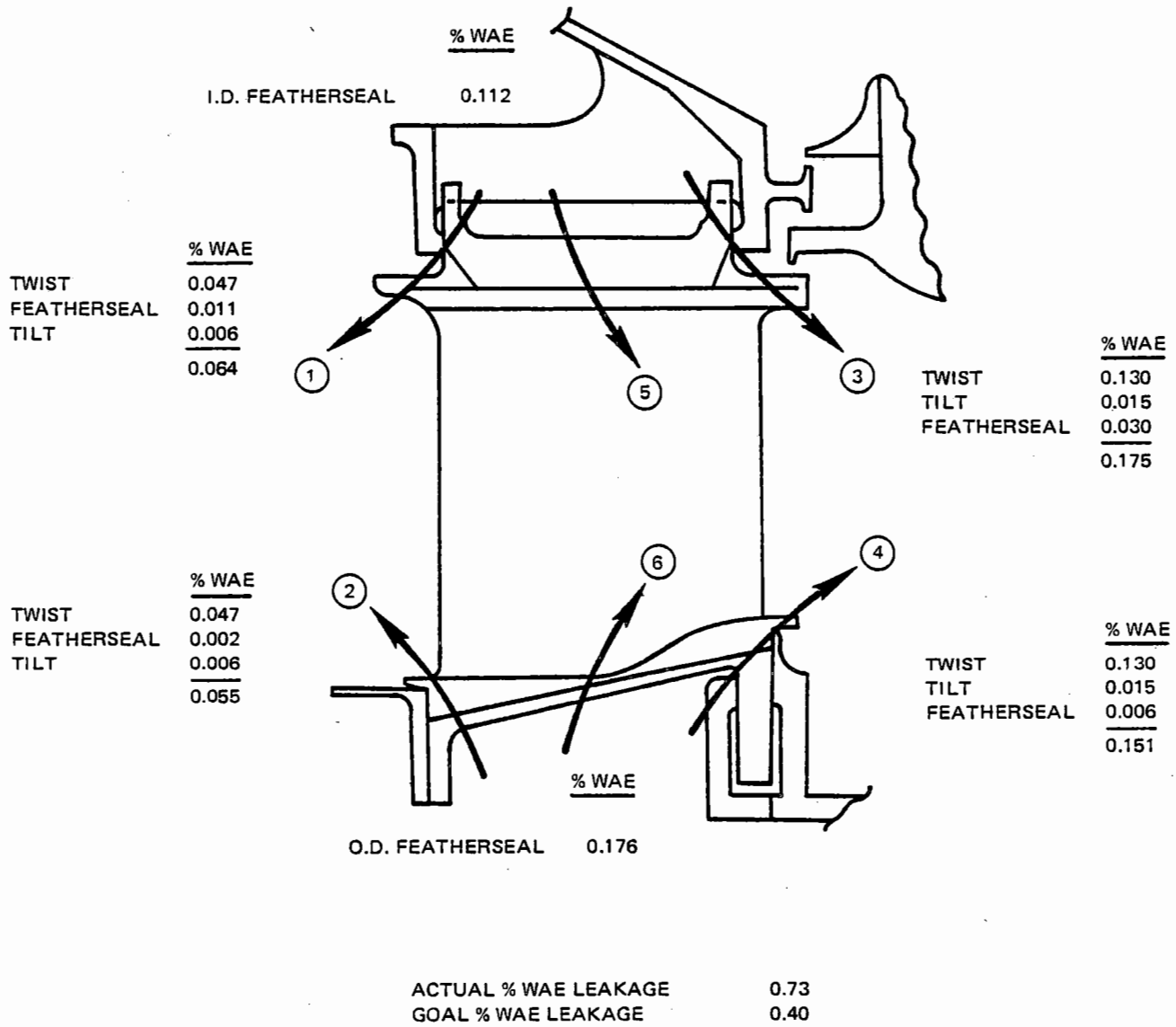

Figure C-19 One-Stage High-Pressure Turbine Vane Leakage Analysis -- Leakage estimates exceeded goal by 83 percent.

Clustering vanes into pairs theoretically eliminates leakage caused by thermal untwist of the airfoil. The floating platform concept allows vane loads to be absorbed by the "rails" rather than the platforms, allowing both the I.D. and O.D. platforms to be continuous over 360 degrees. A backbone supporting supplement to the platforms is provided in the full ring-strut-ring configuration by "locking" the platforms (in the casting process) via integral rail segments on each end of the airfoil. Variations to these basic approaches were also evaluated.

Results of the vane attachment study are shown in Table C-XLI.

These results showed that all the concepts considered have the potential to reduce platform leakage to the 0.40% goal level. However, all of the schemes have, to varying degrees, structural and manufacturing problems which must be solved before the benefits can be viably achieved. The general conclusion reached was that further detailed analysis is required prior to selecting the vane platform configuration.

2.2.1.4.12 Rotor Analysis

Rotor concerns addressed in more detail were in the areas of the HPT disk and sideplate stresses, lives, and vibration. The causes of concerns were the high speeds and temperatures associated with the advanced configuration and cycle. These refined analyses were conducted for both the one- and two-stage HPT's.

The one-stage HPT rotor was thermally analyzed on the basis of the secondary flow system and gaspath conditions. Maximum steady state metal temperatures were defined. The resulting temperatures and the thermal node breakup are shown in Figure C-20.

Disk stress analysis was performed with generalized stress and shell design systems. Both burst and low cycle fatigue (LCF) calculations were made for MERL 76 material. Refinement of the disk size and shape resulted in a structually adequate configuration meeting the designated life goals. The disk stress/life summary is presented in Table C-XLII

TABLE C-XLI

ONE-STAGE HPT VANE ATTACHMENT LEAKAGE STUDY RESULTS

Concept	Leakage Area - mm^2 (in^2)	Leakage Flow - %
Basic Advanced Vane	225(0.345)	0.733
Clustered Pairs with I.D. Fish Hook Seal	85-120(0.13-0.19)	0.27-0.39
Clustered Pairs with 360 deg. I. D. Sheet Metal Seal	70-110(0.11-0.17)	0.22-0.32
Floating Platform with O.D. Ring Support	50-110(0.08-0.17)	0.15-0.34
Floating Platform with O.D. and I.D. Ring Support	50-110(0.08-0.17)	0.15-0.34
Ring-Strut-Ring, Simply Supported	32- 64(0.05-0.10)	0.10-0.19
Ring-Strut-Ring, I.D. Supported	50- 64(0.08-0.10)	0.20-0.25

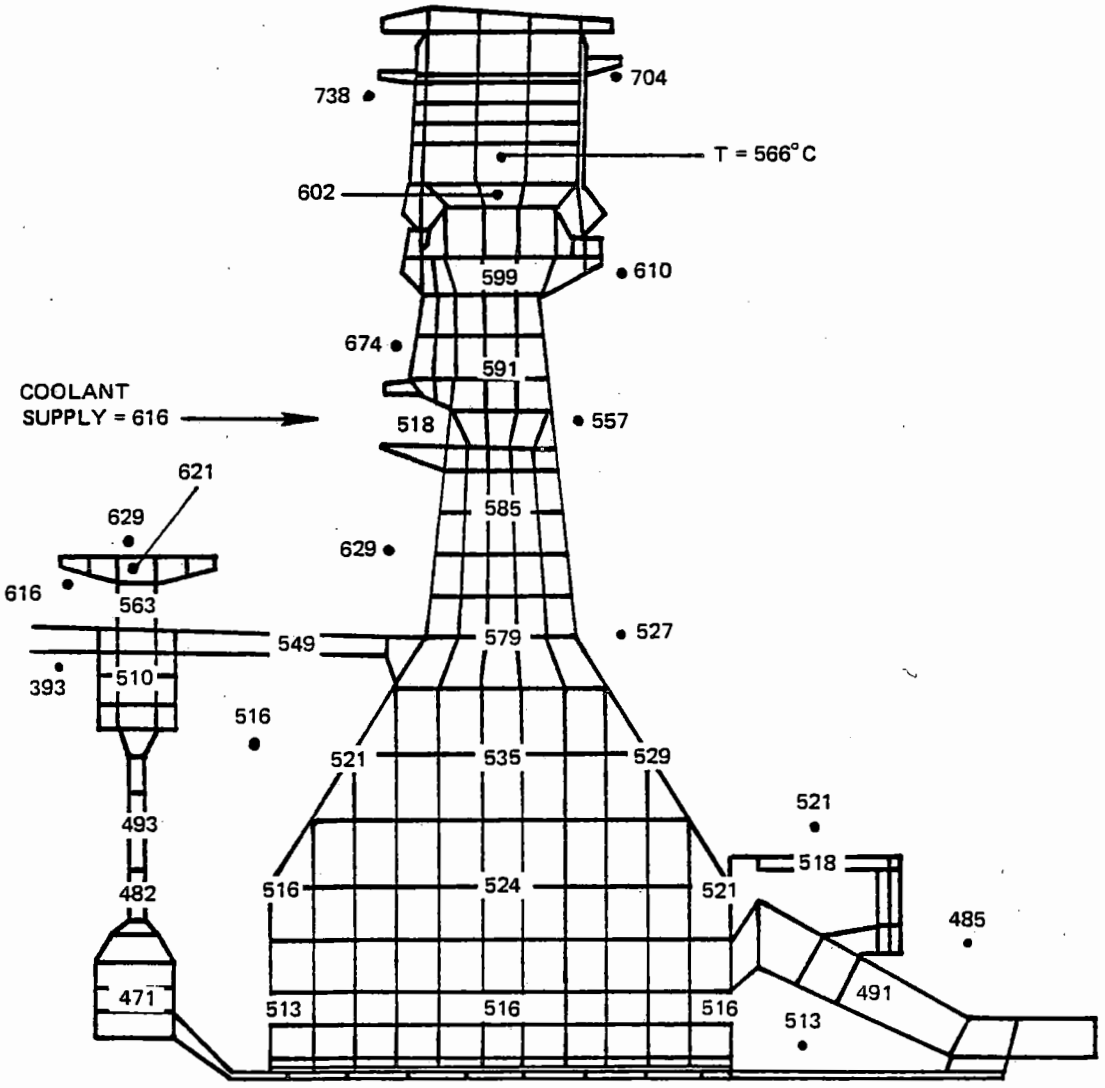

Figure C-20 One-Stage High-Pressure Turbine Rotor Temperatures – Shows maximum steady state metal temperatures and node network.

TABLE C-XLII

ONE STAGE HPT DISK STRESS/LIFE ANALYSIS SUMMARY

Burst Margin - %	26
Bore LCF Life - cycles	10^4
Rim Slot LCF Life - cycles	8×10^4
Cooling Air Hole LCF Life - cycles	10^5

The one-stage HPT full ring for minimum leakage) MERL 76 sideplate, shown in Figure C-21, was analyzed using finite element techniques. The finite element breakup of the sideplate and disk are shown in Figure C-22. Periodic displacement boundary conditions were imposed at all locations where the sideplate tends to grow into the disk. Analytical results showed the sideplate, as configured,

to have adequate LCF life in all areas except the bayonet lug (Figure C-23) where only 8000 cycles were predicted. However, the slight shape modification shown in Figure C-23 by the dashed outline was estimated to result in a minimum 50,000 cycle life for that region.

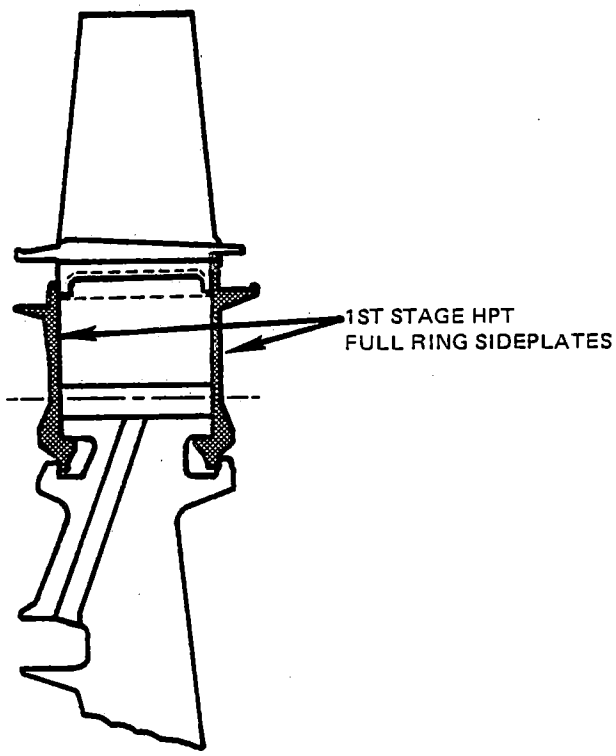

Figure C-21 One-Stage High-Pressure Turbine Sideplates – Shows full ring for minimum leakage.

All predicted structural results are tabulated on the figure.

A refined vibration analysis of the selected one-stage HPT was conducted to determine the resonant and flutter characteristics and to define an acceptable number of diffuser case and HPT – LPT transition duct struts. The analysis assumed a stress limited disk design and single crystal alloy blades. The resulting resonance diagram is presented in Figure C-24. Adequate resonance margin was predicted for all lower vibration orders (2 through 4). As a result, eight diffuser case struts and fifteen transition duct struts were selected to avoid resonance problems. Eight diffuser struts were required to provide sufficient frequency margin at redline rotor speed for first and second mode resonances which would be excited by a higher number of struts. In order to move the first mode resonance low into the engine running range while maintaining adequate 15E second mode frequency margin at redline speed, fifteen transition ducts struts were required. A damper amplitude ratio of 7.1%, adequate to promote efficient damping along the blade surface, was calculated. The blade flutter stability was also checked and found to be within the safe limit for undamped blades.

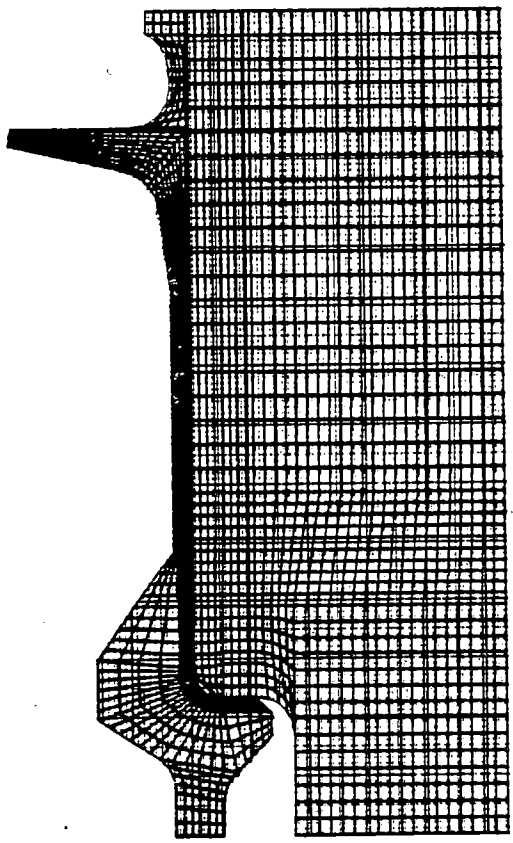

Figure C-22 One-Stage HPT Stress Analysis – Shows finite element breakup of sideplate and disk.

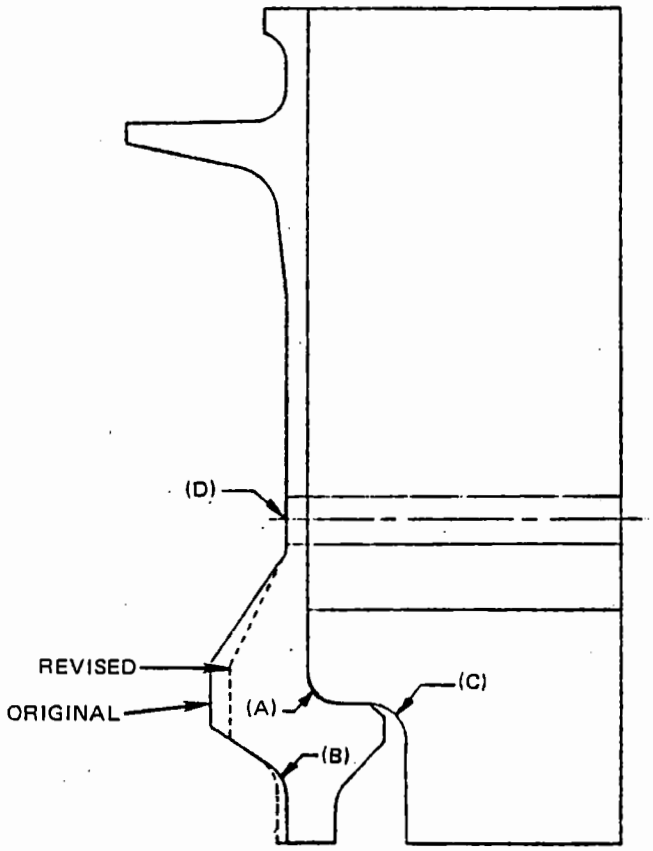

		ORIGINAL DESIGN	REVISED DESIGN
SNAP LOAD		210897 kg (464948 lbs)	203265 kg (448122 lbs)
TOTAL RADIAL FORCE		1.484 x 10^6 kg (3.272 x 10^6 lbs)	1.476 x 10^6 (3.255 x 10^6 lbs)
SIDEPLATE FILLET (A)	STRESS* LIFE*	942 (136.6) $>10^5$	954 (138.3) $> 10^5$
SIDEPLATE LUG (B)	STRESS LIFE	1580 (229.2) 8,000	965 (140.0) $>10^5$
DISK FILLET (C)	STRESS LIFE	1400 (203.0) 23,000	1375 (199.4) 25,000
SIDEPLATE BOLT HOLE (D)	STRESS LIFE	1310 (190.0) > 40,000	1287 (186.7) 50,000

*STRESS ~N/mm^2 (KSI), LIFE ~CYCLES

Figure C-23 One-Stage High-Pressure Turbine Sideplate Low Cycle Fatigue Lives – Shows LCF lives based on sideplate-disk rim temperature gradients.

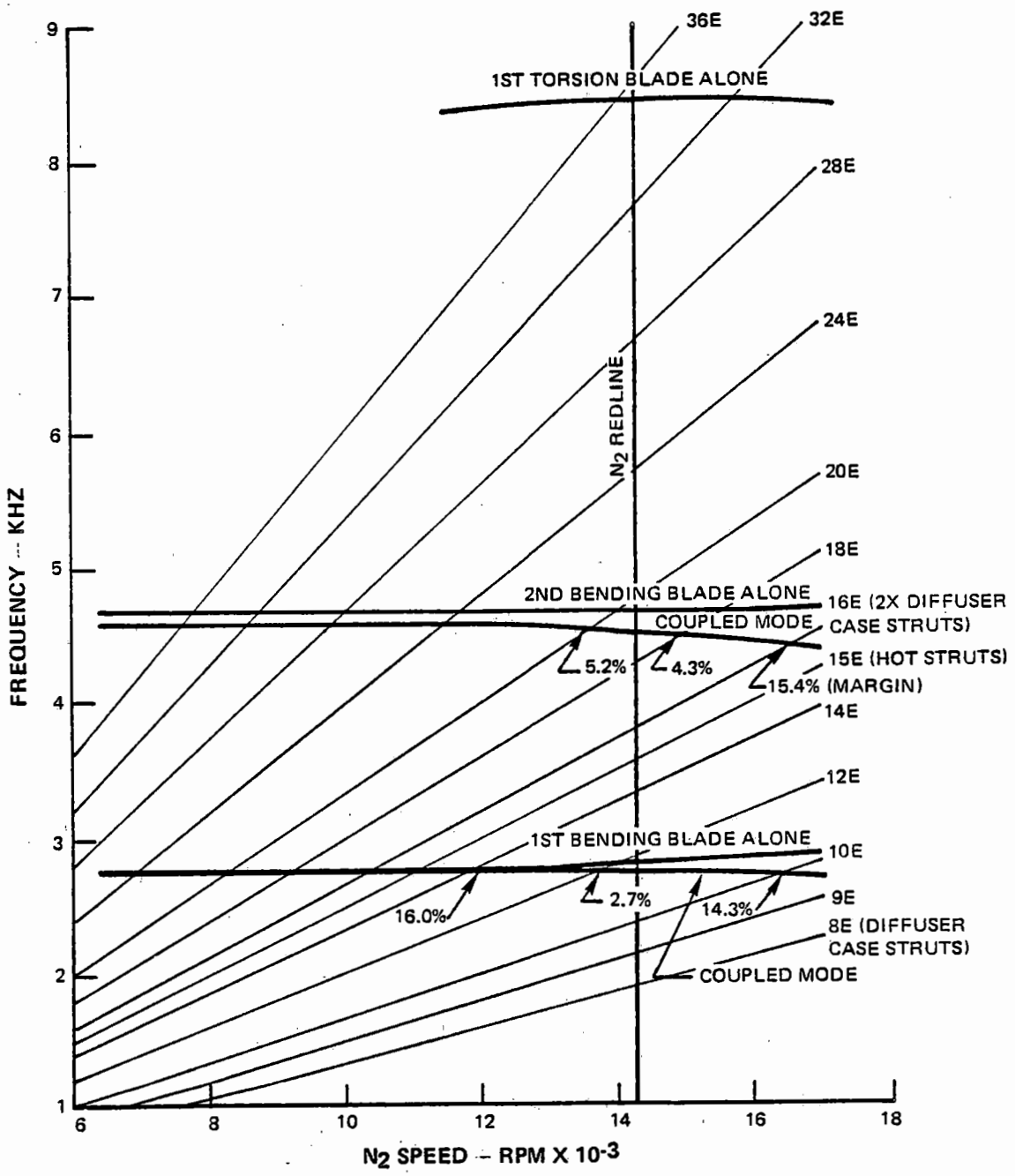

Figure C-24 One-Stage High-Pressure Turbine Resonance Diagram– Shows eight diffuser case struts and fifteen turbine transition duct struts are required for adequate vibration frequency margin.

The two-stage HPT rotor was thermally analyzed in a manner similar to the one-stage HPT. Resulting steady state metal temperatures and the thermal node network are shown in Figures C-25 and C-26 respectively. Generalized stress and shell design system analyses of the disks were conducted. Both disk bores were LCF life limited. Results allowed radial stress to be increased in the first disk bolt circle region while maintaining adequate life so that thickness could be reduced 22% in that area. It was also possible to reduce second disk bore width about 0.64 cm (0.25 in.) without reducing burst margin and life below goal levels. The concept of elliptical cooling hole slots with long axis in the tangential direction was evaluated (versus round holes) and found to reduce the rim stress concentration factor and consequently improve rim life. A summary of the disk stress/life analysis results is given in Table C-XLIII. The general conclusion reached from these refined analyses was that both disks were structurally feasible.

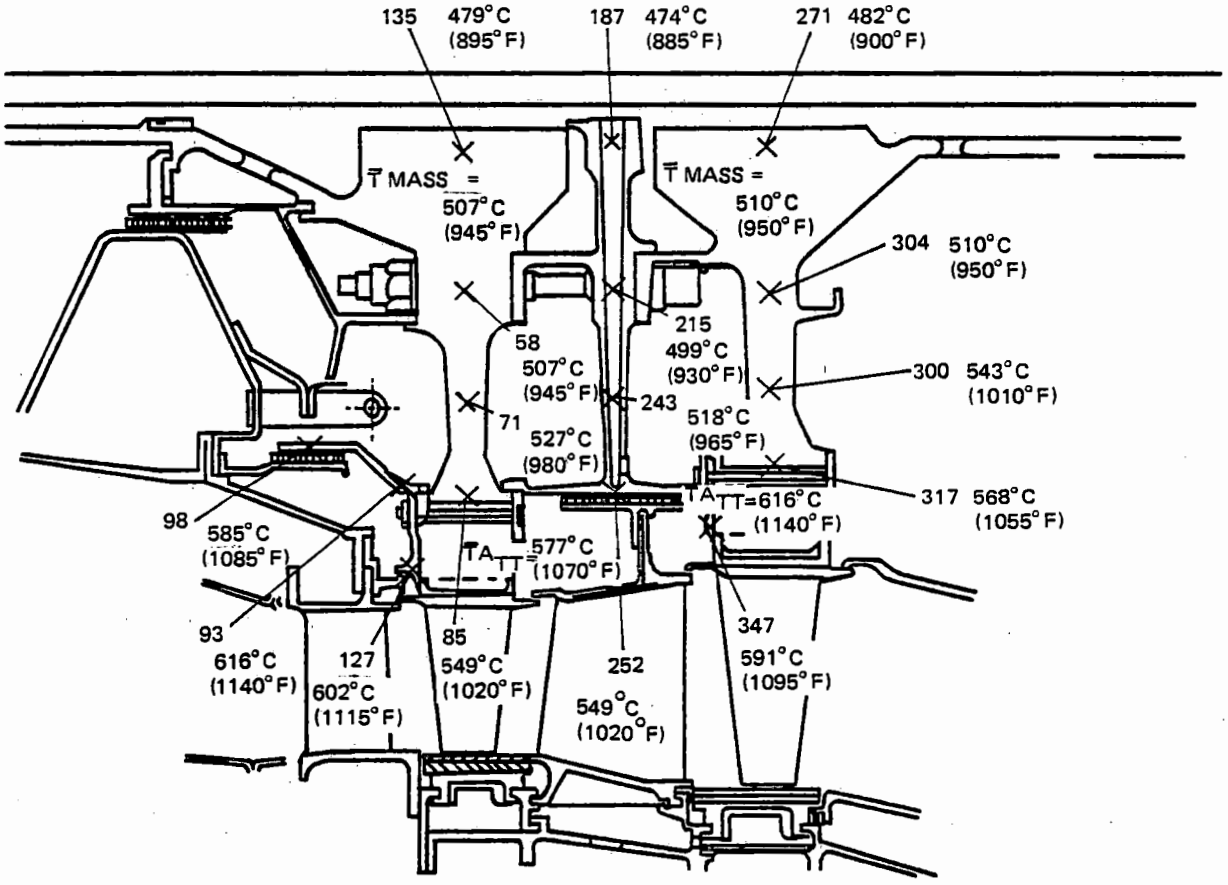

Figure C-25 Two-Stage High-Pressure Turbine Rotor Temperatures – Shows steady state metal temperatures.

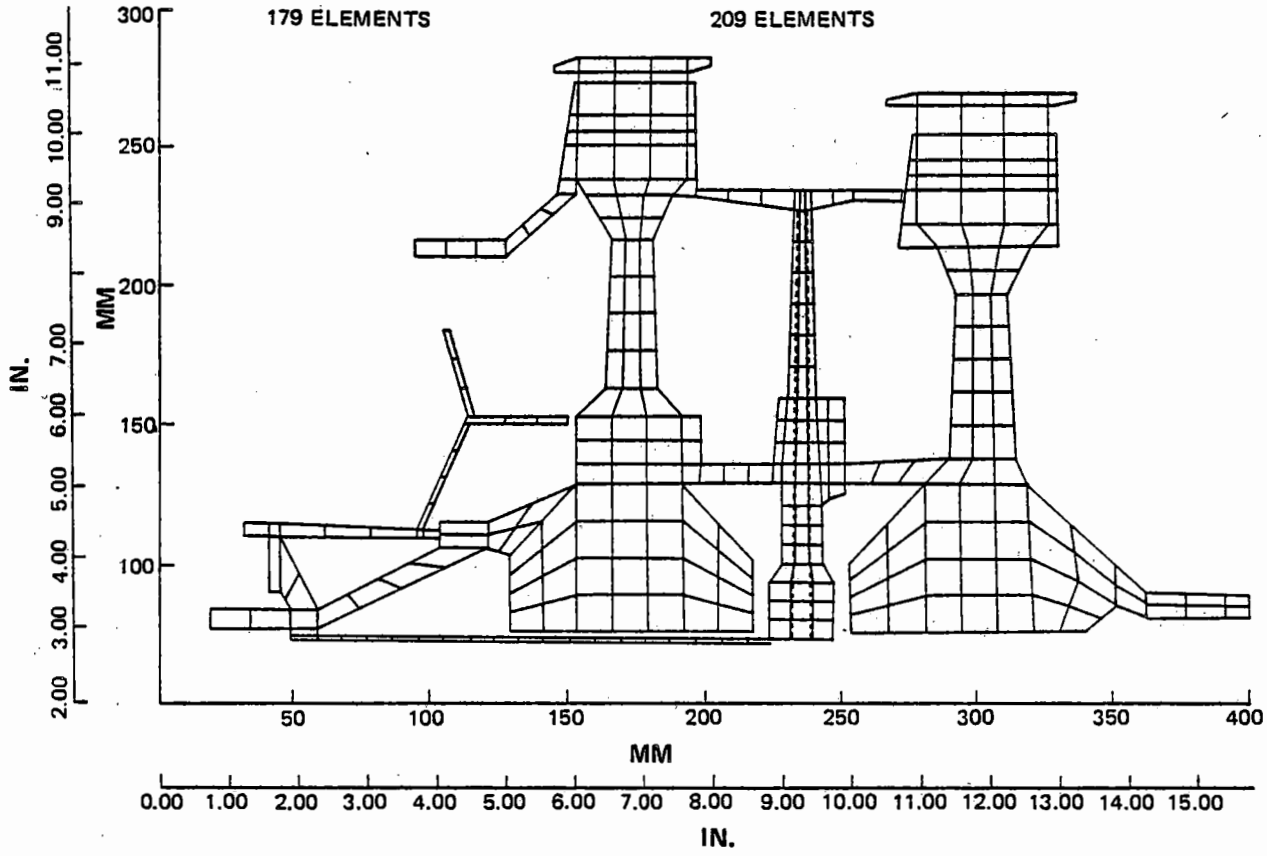

Figure C-26 Two-Stage High-Pressure Turbine Rotor Thermal Node Network

TABLE C-XLIII

TWO STAGE HPT DISK STRESS/LIFE ANALYSIS SUMMARY

	Stage 1	Stage 2
Burst Margin – %	25.6	25.0
Bore LCF Life – cycles	$> 15 \times 10^3$	$> 15 \times 10^3$
Bolt Circle LCF Life – cycles	16×10^3	–
Rim Cooling Air Hole – cycles	$> 5 \times 10^4$	$> 10^5$

Sideplate analyses for both HPT stages were refined. A generalized two-dimensional finite element analysis of the combined outer TOBI seal/first stage sideplate showed the snap to be highly loaded. LCF life was calculated to be 30% below the goal, so the integral seal/sideplate concept was eliminated. LCF life of the revised sideplate design was estimated to be greater than 15,000 cycles, and therefore, adequate. Snap loads on the second disk sideplate were found to be very low throughout the entire flight cycle, so no problem was anticipated with a calculated hook LCF life of greater than 10^5 cycles.

Vibration analysis refinement was undertaken on the two-stage HPT to check the effects of the number of blades selected. Items studied were first mode frequency margin, flutter stability, and damper deflection ratio. Results are shown in Table C-XLIV. Both blades have adequate first mode blade-alone margins for the orders excited by the preliminary choice of diffuser case and transition duct strut numbers. Flutter parameters for both stages were well below the design criteria and, therefore, were acceptable. Damper deflection ratios for both stages were unacceptably low. As a result, neck extensions were lengthened to achieve the desired ratios. Although attachment stresses and first mode frequency margin would be hurt slightly by neck lengthening, the proper balance can be worked out in a detailed design. Therefore, the two-stage HPT configuration was considered to be feasible, as a preliminary design.

2.2.1.5 HPT Design Parameter Summary (One- and Two-Stage Configurations)

A summary of the final preliminary design parameters for the two HPT configurations is given in Table C-XLV.

TABLE C-XLIV

TWO STAGE HPT VIBRATION ANALYSIS SUMMARY

	Stage 1	Stage 2
1st Mode Blade Frequency – cycles	2720	1375
1st Mode Blade Margin	25% 9E	42% 4E
Flutter Parameter	1.06	2.38
Damper Deflection Ratio	4.9	4.3

TABLE C-XLV

TASK III DESIGN SUMMARY – ONE- AND TWO-STAGE HPT'S

(AERODYNAMIC DESIGN POINT UNLESS SPECIFIED)

	One-Stage HPT	Two-Stage HPT
Rotor Speed – rpm	13000	13000
Mean Velocity Ratio	0.565	0.643
Cooling/Leakage – %	11.15	13.50
Efficiency – %	88.2	91.3
Expansion Ratio	4.00	4.27
Flow Coefficient	0.34	0.32
Max. Rim Speed – m/sec (ft/sec)	530(1735)	435(1420)
Number of Airfoils	78	129
Max. Combustor Exit Temperature – °C(°F)	1400(2550)	1400(2550)

Cross sections of the two HPT'S are shown in Figure C-27.

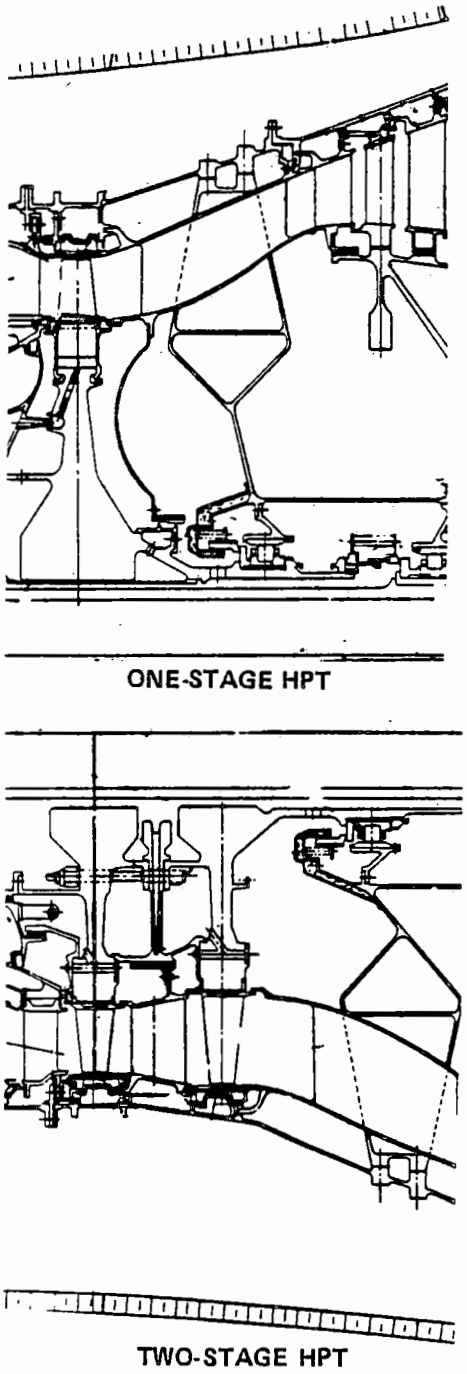

Figure C-27 Task III Selected High-Pressure Turbine Cross Sections

2.2.2 Low-Spool Component Analyses

2.2.2.1 Direct-Drive Engine Low-Spool Configuration Selection

A more in-depth optimization study was conducted to permit a refined selection of low-spool rotor speed and low pressure turbine (LPT) elevation for the direct drive engines relative to the Task I definition. This refinement examined trades among the effects of fan tip speed on fan efficiency, number of low pressure compressor (LPC) stages, number of LPT stages, LPT efficiency, and nacelle drag. The study was done around the one-stage HPT high-spool, but results are applicable to the two-stage HPT engine. Table C-XLVI summarizes the matrix of low-spools analyzed in this optimization.

Preliminary aerodynamic analyses were conducted to define component performance and flowpaths for each low spool in the matrix. A summary of the component performance is given in Table C-XLVII.

Using influence coefficients developed for the purpose, the low spool component performance and nacelle impacts were assessed to determine installed TSFC for each.

Engine and nacelle weight, price, and maintenance cost changes were determined from the flowpath and dimensions using standard estimating procedures. Trends resulting from this evaluation of the low-spool matrix are shown in Figures C-28 through C-31. Basically, the overall loss in TSFC shown with increased fan tip speed is a result of fan efficiency reducing at a faster rate than LPT efficiency improves. Increased fan tip speed did reduce weight and costs by pulling in the LPT diameter. Weight was also decreased, although costs were increased somewhat, by the increased LPC aspect ratio to maintain the required

TABLE C-XLVI

LOW-SPOOL PRELIMINARY OPTIMIZATION STUDY MATRIX

Configuration:	Base	1	2	3	4
Corrected Fan Tip Speed – m/sec (ft/sec)	470(1550)	455 (1500)	455(1500)	495(1620)	495(1620)
LPC Avg. Aspect Ratio	2.4	2.0	2.0	2.8	2.8
LPT No. Stages	4	4	5	4	4
LPT Mean Velocity Ratio	0.455	0.455	0.455	0.475	0.455
Relative LPT Diameter	Base	+	-	Base	-
Relative Rotor Speed	Base	-	-	+	+

TABLE C-XLVII

COMPONENT PERFORMANCE – DIRECT-DRIVE LOW-SPOOL CONDITIONS

Configuration:	Base	1	2	3	4
Fan:					
Δ Efficiency - %	Base	+0.6	+0.6	-1.1	-1.1
LPC:					
Δ Efficiency - %	Base	+0.2	+0.2	-0.5	-0.5
Δ No. Airfoils	Base	-19	-19	+101	+101
LPT:					
Δ Pressure Loss Transition - %	Base	+0.10	+0.07	0	+0.10
Δ Efficiency - %	Base	-0.20			
Δ Pressure Loss Exit Vane - %	Base	-0.04	+0.13	+0.47	+0.18
Δ No. Airfoils	Base	+4	+210	-22	-20
Δ Diameter, Tip - mm (in.)	Base	+25(+1.0)	-50(-2.0)	0	-33(-1.3)
Nacelle:					
Δ Length - mm (in.)	Base	+79(+3.1)	+94(+3.7)	-41(-1.6)	-74(-2.9)
Δ Drag - N (lbs.)	Base	+18(+4.0)	+20(+4.5)	-9(-2.0)	-16(-3.5)

loading level. The trends also showed that an additional LPT stage or increased LPT diameter improved TSFC, but weight and costs increased. The 5 stage LPT was, however, lighter because of its smaller diameter.

Economic trade factors developed for both the domestic and international airplanes were then applied to these evaluation results to obtain trends in fuel burned and DOC, as shown in Figures C-32 and C-33. These figures show that the matrix base provides the minimum DOC and is also at the "knee" of the fuel burned curve. These results occurred because the increased weight associated with reduced fan tip speed negates the TSFC benefit and flattens out the fuel burned trend. Increased LPT diameter (mean velocity ratio) improved TSFC and fuel burned, but slightly increased DOC. An additional LPT stage improved fuel burned but increased DOC more significantly.

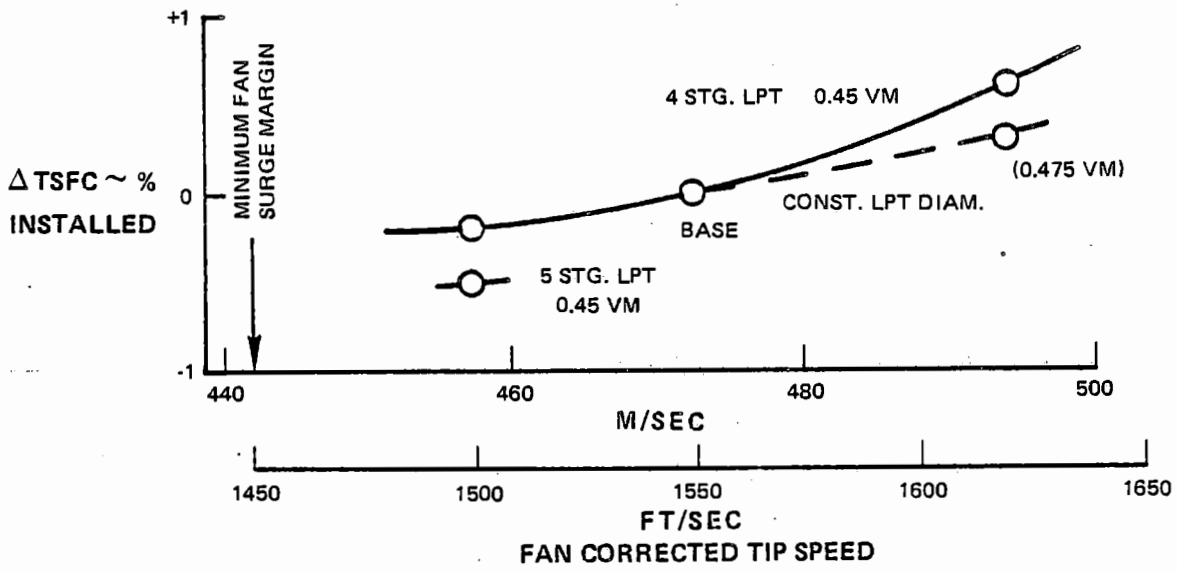

Figure C-28 *Results of Low Spool Evaluation (TSFC) – Shows trends in the relationship of TSFC to fan corrected tip speed.*

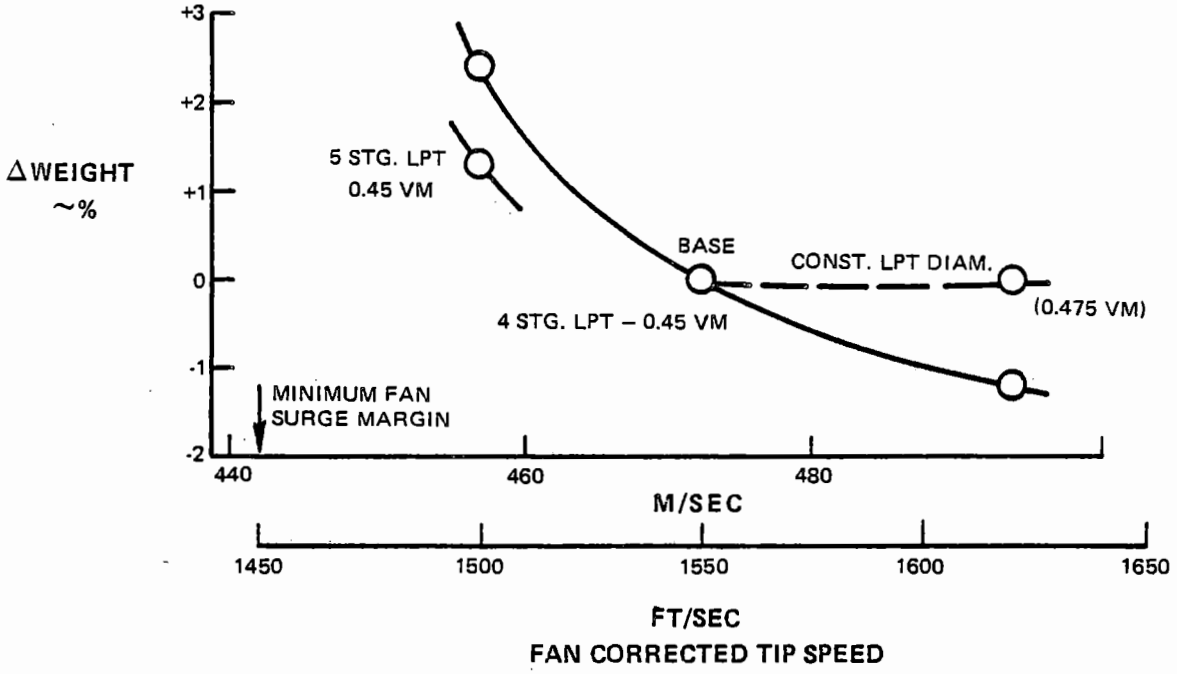

Figure C-29 *Results of Low- Spool Evaluation (Weight) – Shows trends in the relationship of weight to fan corrected tip speed.*

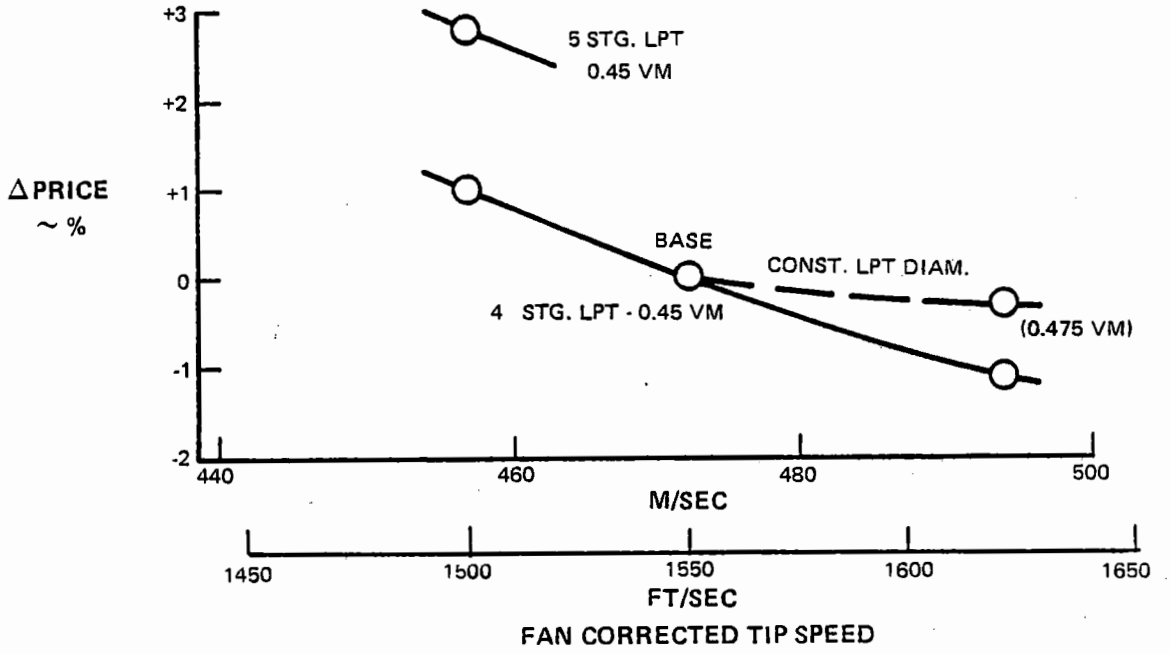

Figure C-30 *Results of Low Spool Evaluation (Price) – Shows trends in the relationship of price to fan corrected tip speed.*

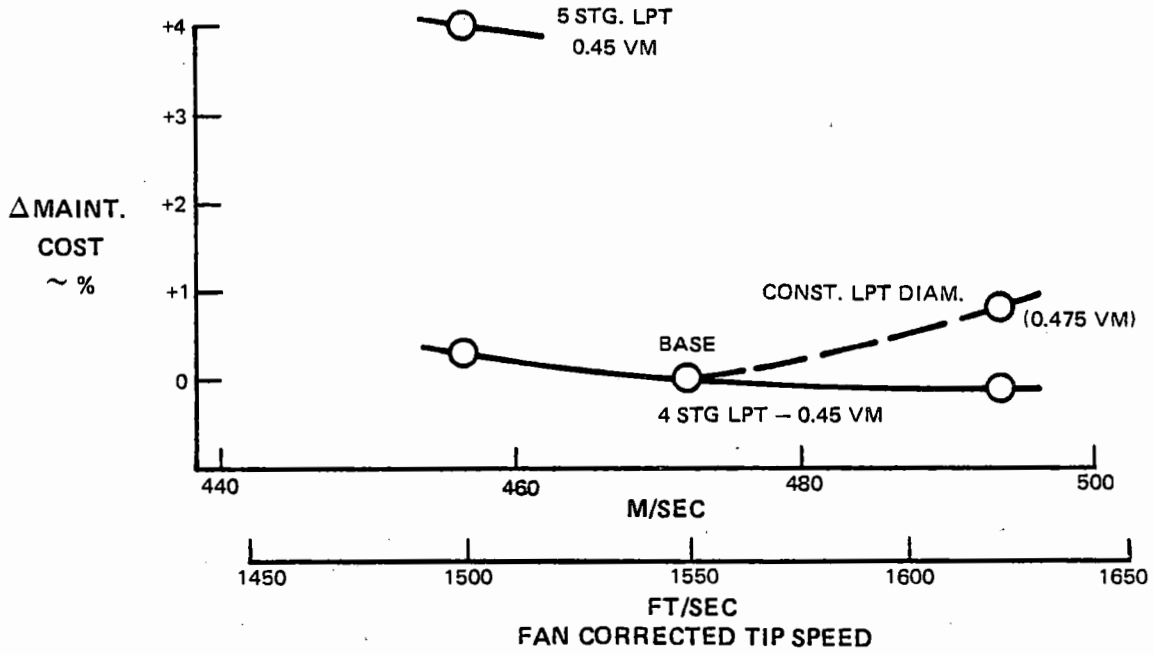

Figure C-31 *Results of Low Spool Evaluation (Maintenance Case) – Shows trends in the relationship of maintenance cost to fan corrected tip speed.*

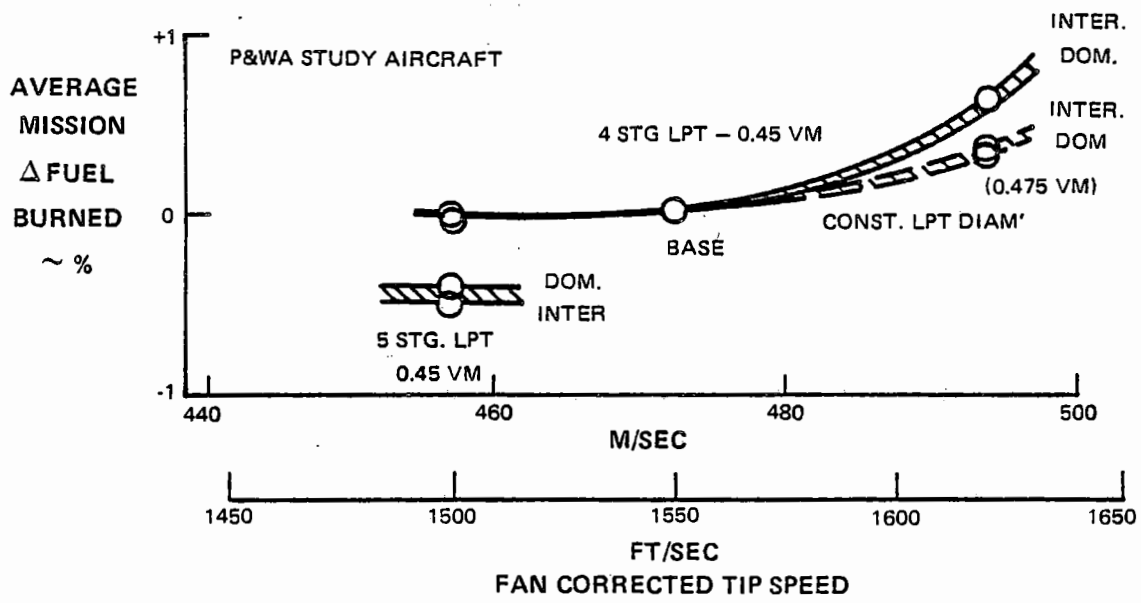

Figure C-32 *Results of Low Spool Evaluation (Fuel Burned) – Shows trends in the relationship of fuel burned to fan corrected tip speed.*

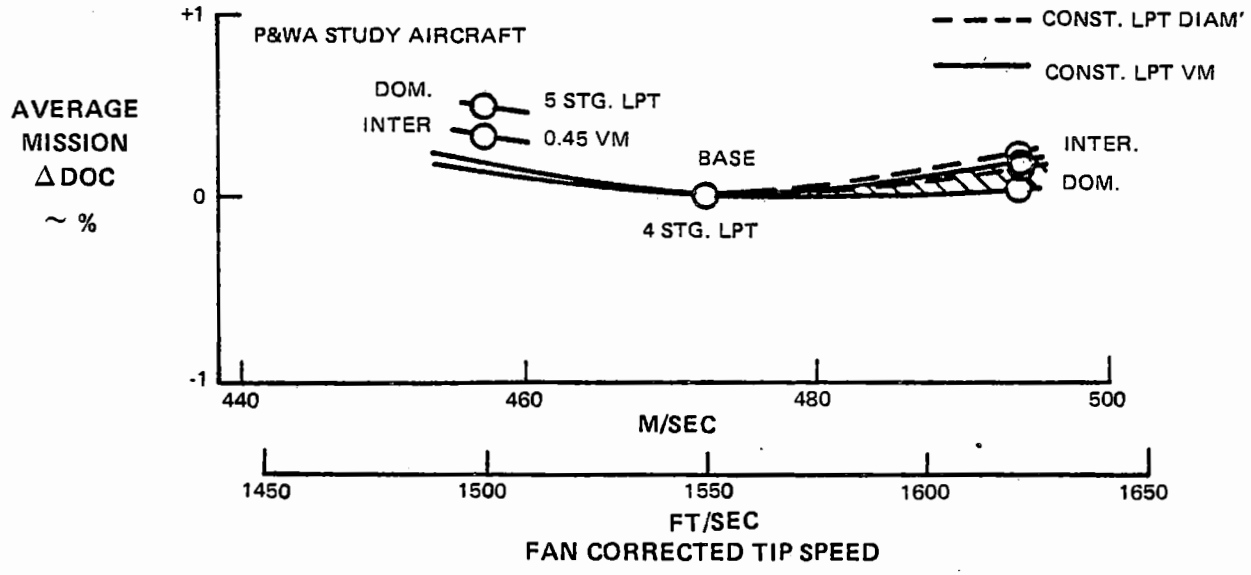

Figure C-33 *Results of Low Spool Evaluation (DOC) – Shows trends in the relationship of DOC to fan corrected tip speed.*

As a result of this parametric study, a 475 m/sec (1550 ft./sec.) corrected fan tip speed and 0.45 mean velocity ratio, 4 stage LPT were selected as the preliminary low pressure spool for the direct-drive fan Task III engines.

2.2.2.2 Fan/Low Pressure Compressor Analyses

2.2.2.2.1 Stability Audit

Prior to initiating the aerodynamic preliminary design analyses of the fans and LPC's for the four engine types, a stability audit was made to establish surge margin requirements. The general approaches taken to define the preliminary design surge margin requirements were as follows.

For the fan, a stability audit reflecting current technology was made at the potentially critical flight conditions. The JT9D-7 was used as this technology base. Fan technology improvements were then assessed to determine their impacts on the base fan requirement. The only accountable improvement resulting from this assessment was for the assumption that the Energy Efficient Engine thrust reverser could be designed without a detrimental exit area mismatch or distortion. No technology improvement impacts were projected for the other critical flight conditions because the destabilizing factors evaluated, with the possible exception of surge line deterioration, appeared to have little effect on surge margin and thereby little improvement potential. A potential for reducing the fan surge margin relative to the JT9D-7 could exist once the deterioration effects of various types of blade tip treatment are defined. Surge margin requirements derived from the audit were combined with the fan operating lines and surge line lapse rates to establish the surge margin requirement at the aerodynamic design point (ADP) of each fan.

Results of this fan stability audit that set surge margin requirements are presented in Table C-XLVIII for the direct drive and geared fans.

Results indicated that ADP surge margin requirements were nearly the same for the two fans, ranging from 8.4% for the direct drive to 9.5% for the geared configuration. To provide for some development capability relative to the assessed requirement, 10% surge margin was established as the minimum goal for both preliminary fan designs.

In a similar manner, a stability audit was conducted for the LPC. No technology improvement impacts were projected relative to the current technology base JT9D-7 LPC because of the following:

TABLE C-XLVIII

STABILITY AUDIT FOR THE DIRECT DRIVE AND GEARED FANS

Flight Condition: Sea Level Static Takeoff*	Direct Drive	Geared
% ADP airflow	89.7	87.5
Required Surge Margin - %	9.5	9.5

*Condition set ADP surge margin requirement

- No reduction in transient excursions were projected for the electronic control system based on experience showing limited success in regulating operating line excursions during deceleration transients.
- The JT9D-7 levels for effects of deterioration and production variations were felt to be small in light of the generally high sensitivity of the LPC operating line to performance levels of other engine components.
- The technology to evaluate LPC design sensitivity to a vortex environment at standing takeoff and reverse conditions was not at hand at the time of the assessment.

Results of the LPC stability audit that set surge margin and surge bleed flow requirements for all direct drive and geared fan engines for standing and rolling takeoffs are summarized in Tables C-XLIX and C-L respectively.

TABLE C-XLIX

STANDING TAKEOFF STABILITY AUDIT FOR GEARED AND DIRECT DRIVE FAN LPC'S

	Direct-Drive 2/1 Stage HPT	Geared 2/1 Stage HPT
Flight Condition: Takeoff*		
% ADP Airflow	86.4/86.4	85.0/85.0
Required Surge Margin - %	23.7/23.7	23.7/23.7
Required Surge Bleed - %	0/0	0/0
Flight Condition: Reverse		
% ADP Airflow	86.4/86.4	85.0/85.0
Required Surge Margin - %	26.7/26.7	26.7/26.7
Required Surge Bleed - %	4.0/ 4.0**	4.0/ 4.0
Flight Condition: Flight Idle		
% ADP Airflow	_	44.0/44.0
Required Surge Margin - %	_	5.1/5.1
Required Surge Bleed - %	_	7.6/11.9**

*Condition set ADP surge margin requirement
**Result set maximum surge bleed flow requirement

TABLE C-L

ROLLING TAKEOFF STABILITY AUDIT FOR
GEARED AND DIRECT DRIVE FAN LPC'S

	Direct Drive 2/1 Stage HPT	Geared 2/1 Stage HPT
Flight Condition: End of Cruise*		
% ADP Airflow	82.0/82.0	82.0/82.0
Required Surge Margin - %	7.3/7.3	7.3/7.3
Required Surge Bleed - %	0/0	0/0
Flight Condition: Reverse**		
% ADP Airflow	86.4/86.4	85.0/85.0
Required Surge Margin - %	26.7/26.7	26.7/26.7
Required Surge Bleed - %	20.8/21.6	20.5/20.3

*Condition set ADP surge margin requirement
**Condition set maximum surge bleed flow requirement

Results indicated that LPC ADP surge margin requirements for the direct drive engines ranged from 11.2 to 12.1% for rolling takeoff to 25.4 to 25.9% for standing takeoff. In addition, a maximum surge bleed flow of about 21% was required to accommodate reverse operation. The geared engine LPC ADP surge margin requirement was found to range from about 15% for rolling takeoff to 29.1 to 29.4% for standing takeoff operation with a maximum bleed requirement of about 20.5% to accommodate reverse.

Because of the extreme ranges of these surge margin results, further investigation was undertaken in order to select a design goal. A 20% LPC surge margin design goal was established as a result. This level was selected based on optimism concerning the rate at which protecting against the LPC vortex threat would be understood. A rolling takeoff was considered to be a logical back-up if this technology was not available in time for actual flight operation of the Energy Efficient Engine.

2.2.2.2.2 Aerodynamic Assessment

The fan–LPC configurations were aerodynamically evaluated using the Pratt and Whitney Aircraft compressor design systems. Preliminary fan configurations for the base direct drive and geared engines established in Task I were refined aerodynamically primarily as a result of structural reassessment and, in the case of the direct drive fan, required bypass ratio adjustments. In addition, a matrix of fans and LPC's was defined for evaluation in the direct drive low spool optimization study discussed in Paragraph 2.2.2.1 of this appendix, using the refined Task I fan-LPC as a base.

The general fan aerodynamic design procedure

utilized is described here. The tip speed–pressure ratio effect on fan efficiency and surge margin was evaluated using the fan efficiency prediction system. Pressure ratio profiles were adjusted to yield reasonable blade loadings consistent with high efficiency. Fan root pressure ratio profiles were adjusted to give root work levels consistent with those of a fan currently under development. Root work was varied with the changes in tip speed, holding loading level and base efficiency constant. The aerodynamic duct exit struts were designed for a 0.45 exit Mach number based on actual areas. The number of struts, 2N + 2, was determined based on acoustic goals. Their chord length was selected consistent with a projected improvement in loading capability. The number of fan root exit vanes was selected on the basis of a midspan gap size that minimizes the occurrence of ice bridges forming between the vanes. Root exit vane chord size was chosen on the basis of aerodynamics. The geared fan and LPC counter-rotate, and therefore, required the design of a strut to provide support for the gearbox and align the fan root exit swirl into the LPC. Axial gapping of this geared fan root exit strut was selected to minimize strut wake interactions with the rotor.

LPC aerodynamic analyses were performed on the meanline design system accounting for counter-rotation between the LPC and HPC (requiring axial discharge from the LPC). The LPC and intermediate case flow paths were contoured to provide a smooth transition into the HPC's. The number of LPC stages was selected to provide the desired pressure ratio at approximately the required 20% surge margin. Within structural limitations, iterations to achieve surge margin were made using primarily aspect ratio and solidity. Since the same fan root-LPC pressure ratio was maintained as fan tip speed was varied for optimization, LPC pressure ratio changed accordingly in these analyses. For the geared fan engine, LPC speed was set by the LPT. The LPC prediction system was used in conjunction with projected technology improvements to obtain efficiency estimates.

Configurational summaries for the fans and and LPC's derived for the low-spool configuration selection study are given in Table C-LI.

2.2.2.2.3 Fan Structural Assessment

Because of its high tip speed and hollow construction, the fan of the direct drive engine was identified as a key area in which to establish basic structural feasibility. As a result, evaluations were made in these areas:

- Airfoil Bird Ingestion Capability
- Blade Static Stress
- Stage Vibration and Flutter
- Blade containment.

General parameters for the blade studied are presented by Table C-LII. The general conclusion made from these analyses was that the high tip speed, hollow titanium fan blade appears to be feasible. These studies are discussed in the following paragraphs.

Airfoil Bird Ingestion Capability

The leading edge bird ingestion capability of the hollow fan blade was assessed by utilizing the Pratt & Whitney Aircraft solid blade analysis with modifications to account for local inertia and shear area changes due to hollowness. This analysis resulted in a blade tip section wall thickness of .13cm (0.050 in.) and a leading edge solid length of 5.1cm (2.0 in.). These requirements were based upon maintaining a leading edge stress parameter that was below the experience level, as shown in Figure C-34. The gross bending bird parameter was calculated and found to be well below the maximum allowable, as seen in Figure C-35.

TABLE C-LI

DIRECT-DRIVE FAN/LPC PARAMETRIC AERODYNAMICS ANALYSIS SUMMARY

Configuration:	Base	1	2	3	4
Fan					
Corrected Tip Speed – m/sec (ft/sec)	470(1550)	455(1500)	455(1500)	495(1620)	495(1620)
Efficiency OD – %	87.7	88.3	88.3	86.6	86.6
Surge Margin – %	15.0	12.5	12.5	18.0	18.0
Hub/Tip Ratio	0.38	0.38	0.38	0.38	0.38
Aspect Ratio	2.7	2.7	2.7	2.7	2.7
Rotor Speed – rpm	3855	3730	3730	4030	4030
Tip Diameter – m (in.)	2.2(85.4)	2.2(85.4)	2.2(85.4)	2.2(85.4)	2.2(85.4)
Pressure Ratio OD	1.74	1.74	1.74	1.74	1.74
Pressure Ratio ID	1.56	1.52	1.52	1.62	1.62
LPC					
Corrected Tip Speed – m/sec (ft/sec)	240(794)	235(778)	235(778)	250(823)	250(823)
Pressure Ratio	1.77	1.81	1.81	1.70	1.70
No. Stages	4	4	4	4	4
Avg. Aspect Ratio	2.4	2.0	2.0	2.8	2.8
Avg. Solidity	1.0	1.18	1.18	1.0	1.0
Surge Margin – %	20	20	20	20	20
Inlet Corrected Airflow kg/sec (lb/sec)	58.6(129.1)	59.9(132.0)	59.9(132.0)	56.7(124.9)	56.7(124.9)
Efficiency —%	89.7	89.9	89.9	89.2	89.2

From these analyses, the bird ingestion capability of the hollow titanium blade was estimated to be acceptable. However, since the analytical procedures used were uncalibrated for hollow blades, impact testing should be conducted to establish final feasibility of the configuration.

Fan Blade Static Stress

Finite element analyses for static stress were made. Assumptions were that hollow blade stresses are the same as solid blade stresses, i.e., no hollowness maldistribution was included, and the attachment area of the blade is solid. This latter assumption thereby reduced stresses by 35%. Stress concentration factors in the attachment fillet area were assumed based on previous analysis of similar solid blades.

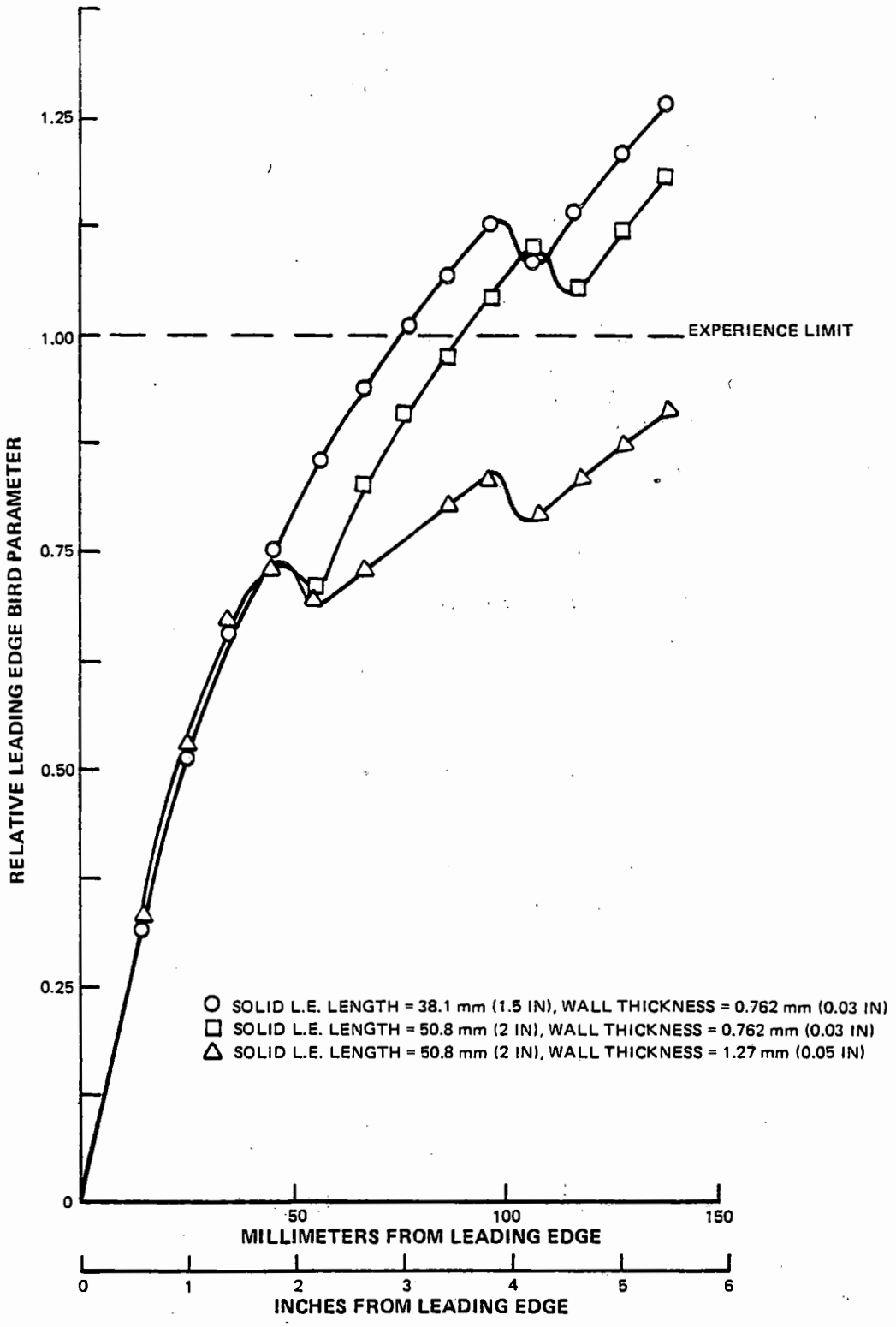

Figure C-34 Direct-Drive Fan Blade Leading Edge Bird Parameters -- Shows fan blade bird ingestion capability for three configurations.

TABLE C-LII

GENERAL GEOMETRIC PARAMETERS DIRECT-DRIVE FAN BLADE

Hub/Tip Ratio	.382 (L.E.) .413 (AVG.)
Aspect Ratio (Avg. Span/ Root Chord)	2.69
Span (AVG.) – m (in.)	0.63(24.92)
Root Radius (AVG.) – m (in.)	0.44(17.52)
Root Chord - m (in.)	0.23 (9.25)
Taper Ratio (Tip Chord/ Root Chord)	1.37
T/B @ Root	.099
T/B @ Tip	.020
Number of Blades	28
Redline Rotor Speed – rpm	4300
Utip @ max. mec – m/sec (ft/sec)	485(1590)
Utip @ ADP – m/sec (ft/sec)	436(1430)

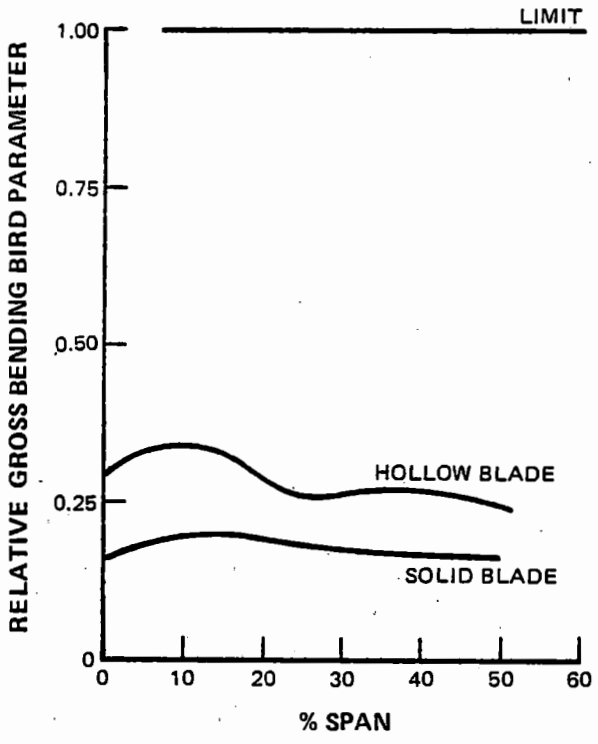

Figure C-35 Direct-Drive Fan Blade Gross Bending Bird Parameters – Shows bending parameters well below maximum allowable limit.

Several attachment configurations were studied, from a conventional dovetail to a tapered curved dovetail with a faired transition region. The conventional root blade was assumed to have a 1.27cm (0.5 in.) platform fillet radius, while other blade roots were assumed to have no attached platform and therefore, no local stress concentration. The tapered curved root design analyzed had acceptable stresses, but was rejected because it complicated engine maintenance by not allowing a damaged blade to be removable from the front of the disk. A constant thickness curved root which would allow front blade removal was found to have unacceptable stresses for both the airfoil and the attachment. A 15° straight broach root with a faired transition region between the attachment and the airfoil was found to have acceptable stresses. A conventional root design analysis showed that airfoil changes would be required to accomplish a 10% reduction in stress at the root 3/4 chord location for acceptability. These results are shown in Figure C-36.

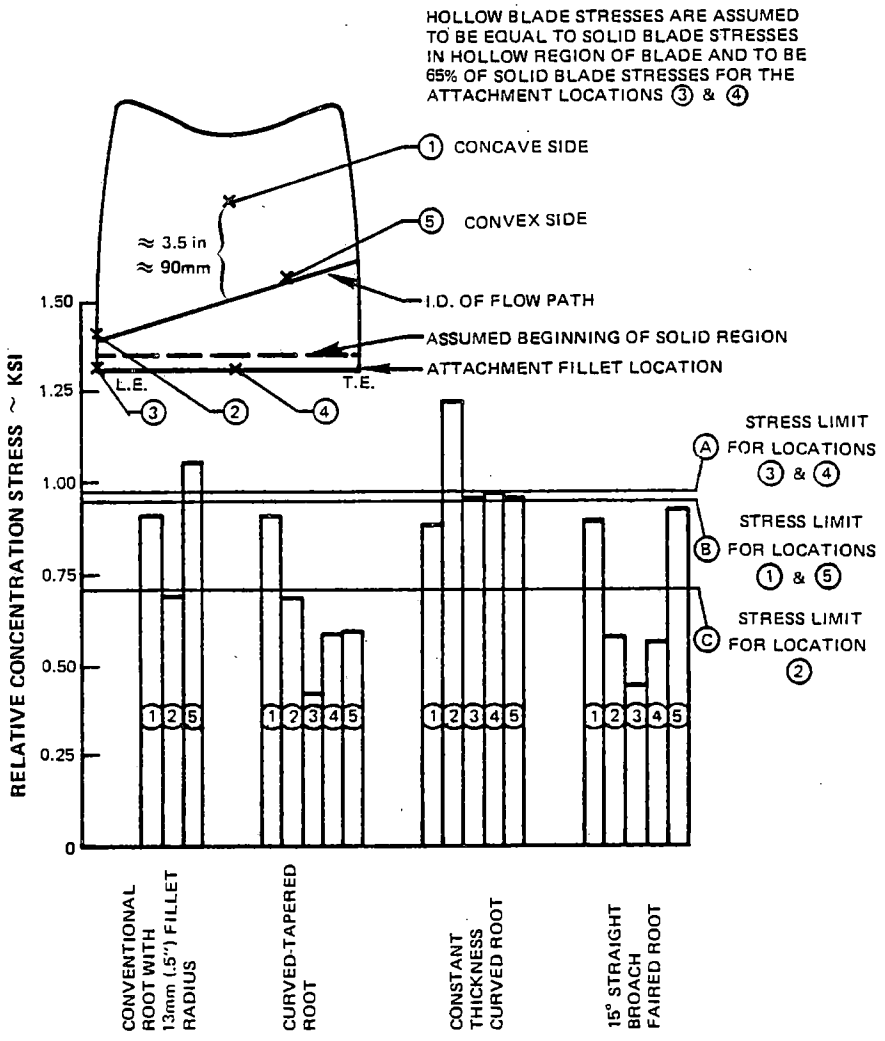

Figure C-36 Hollow Fan Blade Static Stress Summary

Although the static stress for a hollow blade with a straight root with faired transition regions between the airfoil and attachment was found acceptable, several concerns remained. More detailed studies using three dimensional finite element analyses and laboratory testing would be required to evaluate stress maldistribution due to hollowness and interior surface stress levels for accurate cyclic life analysis. In addition, more in-depth analyses would be required to assess the possibility of integral blade platforms with the faired root blades.

Fan Vibration and Flutter

Frequency calculations were made for the hollow shroudless blades using the standard beam analysis. This analysis showed the blade to have a 2E first mode resonance in the operating range between the idle and the minimum cruise rotor speeds. The initial analysis showed the 3E second mode resonance margin to be acceptable, but it could become inadequate with the mass added to the blade tip to meet the bird ingestion criteria. The actual magnitude of the 3E frequency margin could not be quantified at the time of the assessment because of a lack of bending–torsion coupling in the beam analysis. Incorporation of a conventional root configuration was found to provide significant frequency increase for this second mode resonance, while disk stiffness was found to have little effect. These results are shown in Figure C-37.

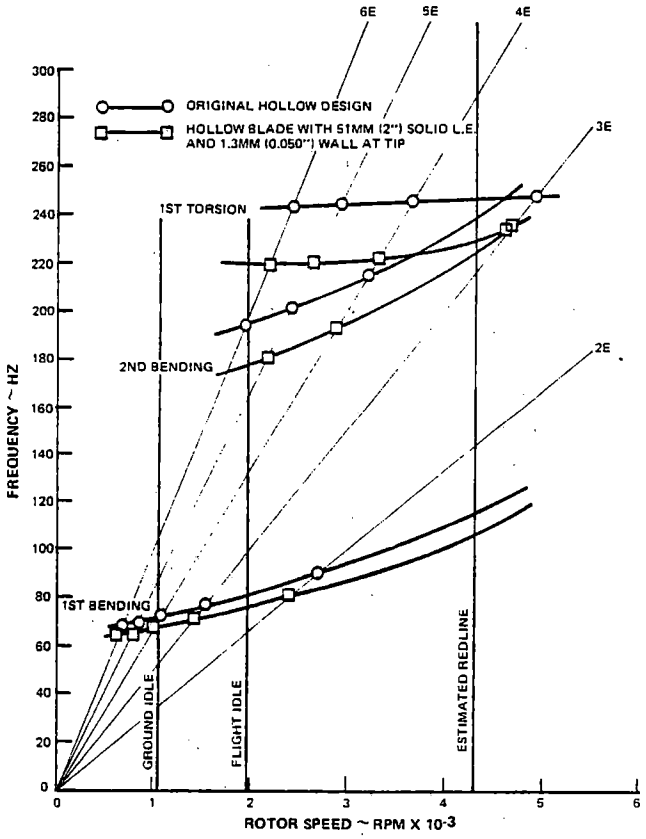

Figure C-37 Fan Stage Resonance Diagram

The supersonic unstalled flutter stability of the hollow blade was evaluated using a mode shape from a coupled bending torsion beam deck. The hollow blade was estimated to be stable in all modes prior to the addition of tip mass for bird ingestion capability, but it is expected to be unstable in the 3rd mode with the added mass. The torsional stall flutter stability did meet the design requirement. Table C-LIII summarizes these results.

As shown by Table C-LIV, vibratory stress ratios were studied and found to be acceptable for the hollow blade with a 15° broach angle, straight dovetail attachment. Stress ratios were found to improve by 10 to 15% with the incorporation of a 2 tooth firtree type attachment.

Although the general conclusion was made that the blade can be made to work from stage vibration and flutter standpoints, several concerns exist. Distortion rig and fatigue testing must be done to determine allowable vibratory stress levels. A vibratory finite element analysis of the blade is required to better assess the aspect ratio or thickness changes required to resolve resonance and flutter problems anticipated to occur because of tip mass increase for bird ingestion.

TABLE C-LIII

DIRECT-DRIVE FAN FLUTTER PARAMETER SUMMARY

		Original Hollow Blade	Hollow Blade With Tip Mass For LESBIP
Torsional stall flutter parameter		1544	1470
Unstalled	1st mode	+.028	NC
Supersonic	2nd mode	+.0028	NC
Flutter (aerodynamic log decrement)	3rd mode	+.0035	NC

LEBIP – Leading edge bird ingestion parameter
NC – Not Calculated

TABLE C-LIV

DIRECT-DRIVE FAN VIBRATORY STRESS RATIOS

	(15° Broach Angle)	
Configuration	1st Mode Stress Ratio	2nd Mode Stress Ratio
Hollow Blade & Dovetail*	3.07	2.68
Hollow Blade & Firtree*	3.53	2.95

*Assumes blade is hollow at airfoil root and solid at attachment fillet.

Fan Blade Containment

A preliminary study was conducted to determine the impact of a hollow bladed fan on case weight requirements for containment. Containment both forward and aft of the fan exit flow splitter was considered (see Figure C-38). A titanium case was assumed. For the purpose of comparison, an equivalent solid fan blade was also assessed. Relative to the solid blade, the case weight savings realized with the hollow blade were estimated to be about 30%, as shown by Table C-LV.

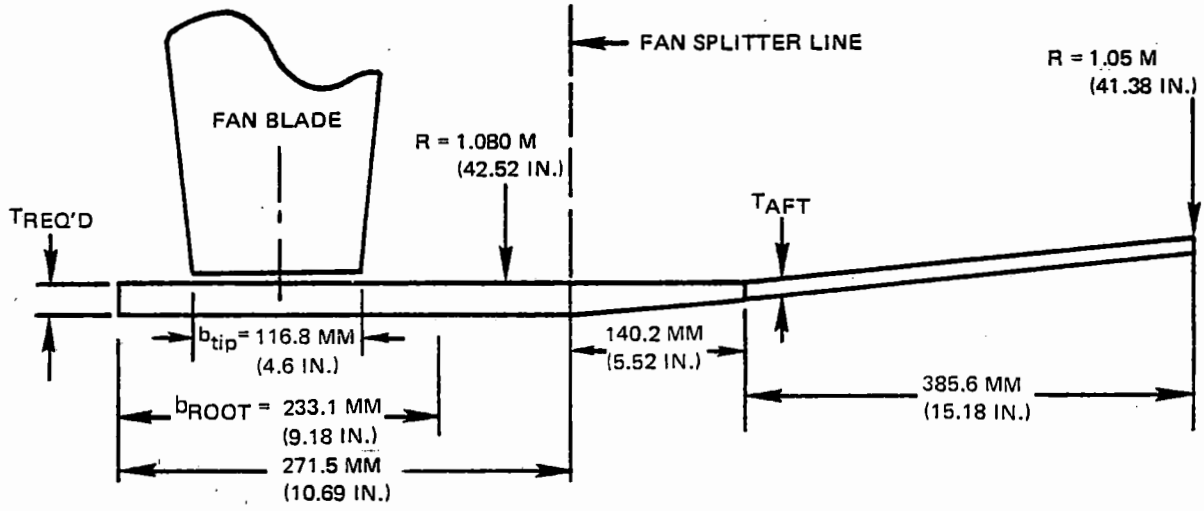

Figure C-38 Direct-Drive Fan Blade Containment Schematic

TABLE C-LV

DIRECT-DRIVE FAN CASE WEIGHTS
FOR CONTAINMENT
(AMS 4928 TITANIUM CASE)

Configuration	Blade Wt. Without Dovetail kg (lbs.)	Required Case Thickness mm (in.)	Required Case Thickness Aft of Splitter mm (in.)	Fan Case Weight Forward of Splitter kg (lbs.)	Fan Case Weight Aft of Splitter kg(lbs)	Total Fan Case Weight kg(lbs)
Hollow Blade	5.2(11.5)	11.8(.466)	3.3(.130)	97.1(214.1)	69.9(154.0)	167(368.1)
Solid Blade	9.7(21.3)	16.6(.655)	4.7(.184)	136.8(301.6)	98.8(217.8)	236(519.4)

Fan/LP Compressor Configuration Summaries

Summaries of the design parameters for the fans and LPC's selected for the four engine types are presented by Tables C-LVI and C-LVII respectively.

TABLE C-LVI

TASK III FAN AERODYNAMIC DESIGN SUMMARY
(AERODYNAMIC DESIGN POINT)

Engine:	1 Stage HPT Direct Drive	2 Stage HPT Direct Drive	1 Stage HPT Geared	2 Stage HPT Geared
Number of Stages	1	1	1	1
Pressure Ratio, Duct	1.74	1.74	1.52	1.52
Efficiency, Duct-%	87.3	87.3	89.1	89.1
Surge Margin-%	15	15	15	15
Corrected Airflow- kg/sec (lb/sec)	641 (1415)	639 (1409)	857 (1889	858 (1892)
Rotor Speed-rpm	3844	3857	2550	2550
Bypass Ratio	6.55	6.55	9.1	9.1
Corrected Tip Speed- m/sec (ft/sec)	470 (1550)	470 (1550)	360 (1175)	360 (1175)
Inlet Specific Flow- $kg/sec/m^2$ ($lb/sec/ft^2$)	205 (41.5)	205 (41.5)	205 (41.5)	205 (41.5)
Inlet Hub/Tip Ratio	0.38	0.38	0.35	0.35
Rotor Aspect Ratio	2.7	2.7	2.65	2.65
Rotor Taper Ratio	1.36	1.36	1.36	1.36
Number Blades	28	28	28	28
No. Duct Exit Vanes	58	58	58	58
No Partspan Shrouds	0	0	0	0

TABLE C-LVII

TASK III LPC AERODYNAMIC DESIGN SUMMARY
(AERODYNAMIC DESIGN POINT)

Engines:	1 Stage HPT Direct Drive	2 Stage HPT Direct Drive	1 Stage HPT Geared	2 Stage HPT Geared
Number of Stages	4	3	2	2
Pressure Ratio	1.77	1.37	2.19	1.71
Efficiency-%	89.7	89.5	88.5	89.6
Surge Margin-%	20	20	20	20
Corrected Inlet Flow- kg/sec (lb/sec)	58 (129)	58 (129)	69 (154)	70 (155)
Rotor Speed-rpm	3844	3857	6364	6160
Inlet Corrected Tip Speed- m/sec (ft/sec)	245 (798)	240 (780)	410 (1350)	390 (1280)
Inlet Specific Flow - $kg/sec/m^2$ ($lb/sec/ft^2$)	160 (32.8)	161 (33.0)	177 (36.2)	172 (35.3)
Inlet Hub/Tip Ratio	0.82	0.82	0.80	0.79
Exit Hub/Tip Ratio	0.84	0.79	0.85	0.81
Exit Mach Number	0.42	0.38	0.46	0.44
Avg. Aspect Ratio	2.4	2.4	1.8	1.9
Avg. Solidity	1.0	1.0	1.18	1.06
Avg. Flow Coefficient	0.70	0.69	0.48	0.49
Number of Airfoils	757	508	372	312

Cross sections of the fans and LPC's for the four engine types are shown in Figure C-39.

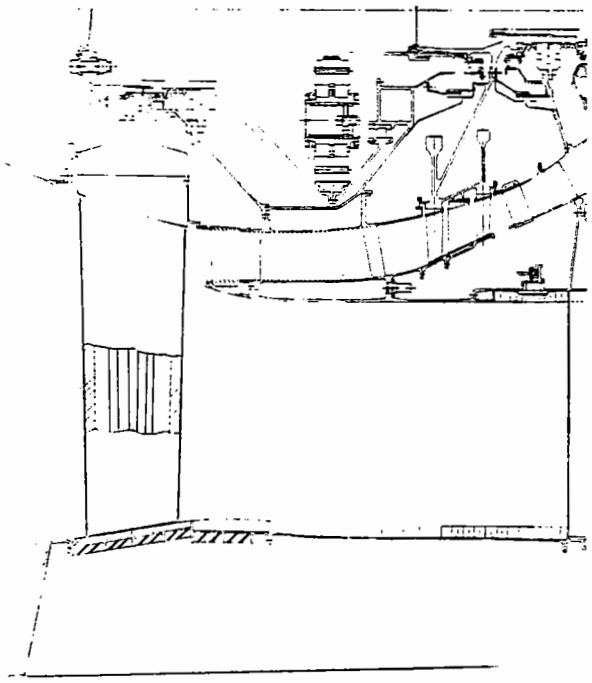

STF 495 M-4

GEARED, 1 STG HPT

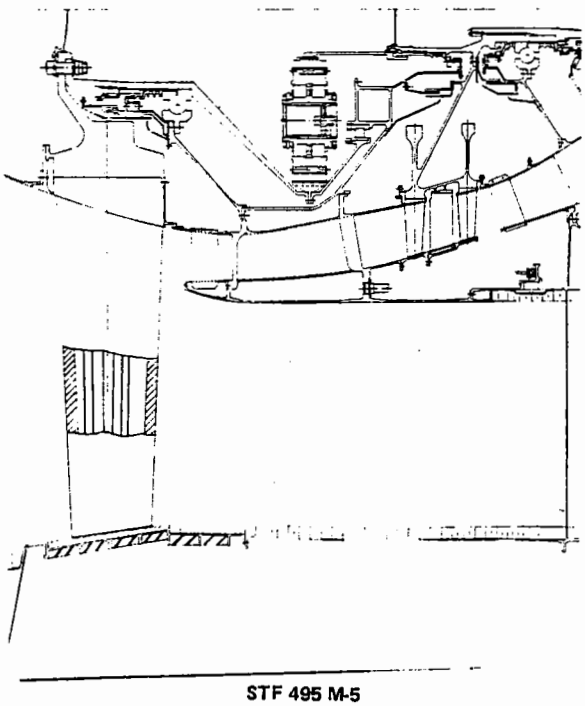

STF 495 M-5

GEARED, 2 STG HPT

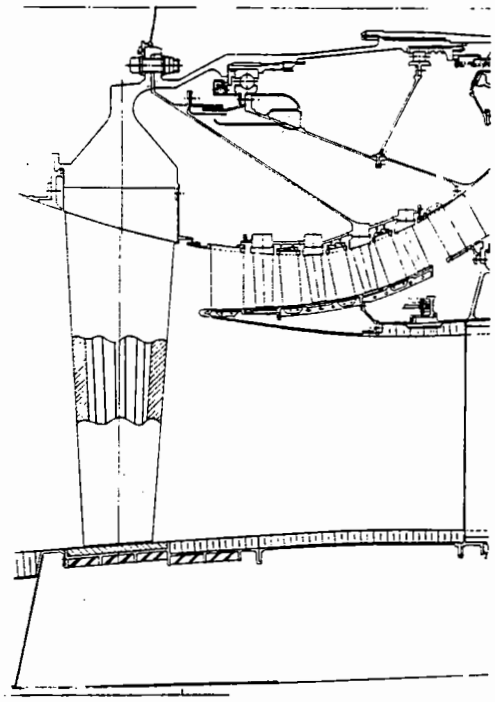

STF 505 M-7

DIRECT-DRIVE, 1 STG HPT

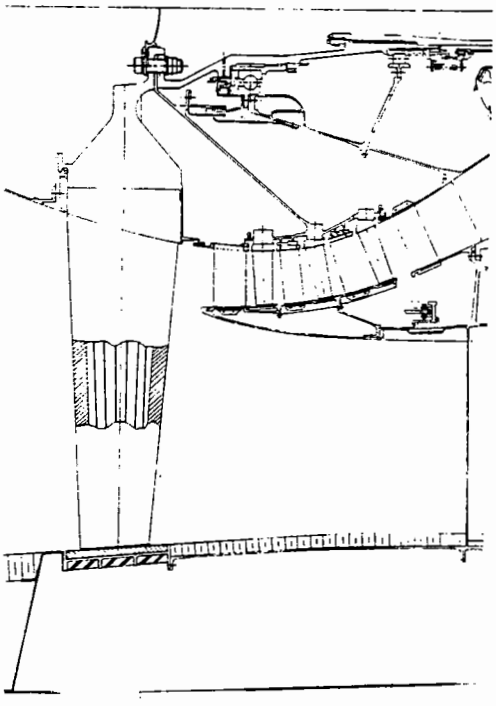

STF 505 M-9

DIRECT-DRIVE, 2 STG HPT

Figure C-39 Cross Sections of the Fans and Low-Pressure Compressors of the Four Task III Engine Types

2.2.2.3 Low Pressure Turbine

2.2.2.3.1 Aerodynamic Assessment

LPT configurations were evaluated aerodynamically using the Pratt & Whitney Aircraft turbine design system. Preliminary configurations for the base direct drive and geared engines established in Task I were refined primarily as a result of decisions to counter-rotate the HPT and LPT of the direct drive engines and to better integrate the LPT with the exhaust mixer. Other refinement of the direct drive engines was necessitated by cycle bypass ratio adjustment. In addition, a matrix of LPT's was defined for evaluation in the direct drive low-spool optimization study discussed in Paragraph 2.2.2.1 of this appendix, using the refined Task I LPT as a base.

General LPT aerodynamic design procedure utilized is described here. Meanline analysis was used to choose the best gas triangles and predict efficiency using empirical and analytical correlations of profile and endwall losses. Flowpaths were based on inlet and exit flow capacity requirements, the desired exit Mach Number, and exit swirl constraints dictated by the exhaust mixer. Chord lengths were set based on aerodynamic and structural guidelines, and airfoil numbers were determined considering projected loading limits and acoustics. In order to minimize losses (optimize flow coefficient), proper mean radius and annulus area distributions were defined consistent with the selected mean velocity ratio level. For the direct drive engines, LPT maximum diameter was set by optimizing resulting efficiency and nacelle drag. In this optimization, care was taken to ensure that minimum mean velocity ratios considered still satisfied criteria for laminar flow airfoils. Final rotor speed for the direct drive engines was selected from the low-spool optimization study, while speed for the geared fan engines was set by LPT structural considerations. The curved wall annular diffuser HPT-LPT transition ducts were configured to minimize losses associated with the bends. Transition duct struts were designed at optimum angles to minimize HPT exit swirl losses.

Summaries for the LPT's derived for the low-spool configurational selection study are given in Table LVIII.

2.2.2.3.2 Nacelle Drag Impact of LPT Flowpath

To help select LPT configurations, the impact of exit diameter on the nacelle was evaluated. Changes in nacelle drag and weight were estimated as functions of LPT exit diameter using standard design procedures. These changes were then put in terms of equivalent TSFC, as shown in Figure C-40. In this form, LPT diameter effects were then traded against efficiency to optimize component performance.

2.2.2.3.3 Structural assessment

Because maximum low-rotor speed for the geared fan engine is set by structural limitations in the last stage of the LPT, this area was identified as a key one in which to establish basic feasibility. Also considered critical was the impact of a potential reduction gearbox failure that decouples the low-spool. As a result, the items studied structurally in the LPT were:

- Stage vibration
- Flutter stability
- Stress ratios
- Dynamic stress allowables
- Shroud curling stress
- Retained shroud tightness
- Shroud bearing stress
- Attachment stress
- Overspeed.

TABLE C-LVIII

LPT PARAMETER STUDY AERODYNAMICS ANALYSIS SUMMARY
(AERODYNAMIC DESIGN POINTS)

	Configuration				
Configuration:	Base	1	2.	3	4
Number of Stages	4	4	5	4	4
Rotor Speed - rpm	3854	3730	3730	4028	4028
Mean Velocity Ratio	0.454	0.453	0.455	0.474	0.455
Efficiency - %	91.2	91.0	91.3	91.7	91.4
Expansion Ratio	5.74	5.76	5.73	5.67	5.71
Flow Coefficient	0.804	0.807	0.864	0.759	0.805
Number of Airfoils	759	763	969	737	739
Radii:					
Inlet Mean m -(in.)	0.48(18.8)	0.49(19.4)	0.44(17.5)	0.48(18.8)	0.45(17.9)
Exit Mean m-(in.)	0.52(20.4)	0.54(21.1)	0.49(19.1)	0.52(20.4)	0.50(19.5)
Exit Maximum m-(in)	0.65(25.6)	0.66(26.1)	0.62(24.6)	0.65(25.6)	0.63(24.9)
HPT-LPT Mean Radial					
Offset - %	24	28	15	24	18
Pressure Loss:					
Transition Duct - %	0.90	1.00	0.97	0.90	1.00
Exit Vane - %	0.90	0.86	0.77	0.72	0.84

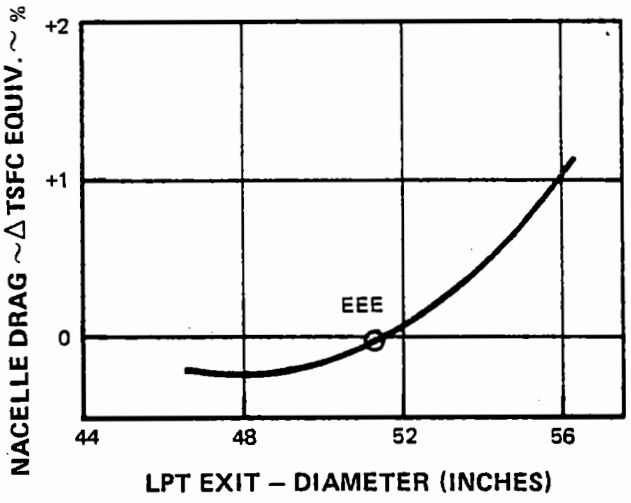

Figure C-40 Low Rotor Trade Study – The effect of low-pressure turbine diameter on nacelle drag is shown.

General parameters for the stage studied are presented by Table C-LIX.

Initial analyses for all these items assumed that the blades and disk were of nickel base alloy materials. Subsequently, the effects of using titanium-aluminide blades and disk were studied for stage resonances and dynamic stresses. Using the airfoil definition, the disk was sized based on burst considerations. A standard three tooth broach configuration was found to fit within the allowed attachment space, and it was used, with modified neck widths, to determine attachment stresses and firtree felxibilities. The shroud was sized based on the airfoil definition. Airfoil and shroud weights were obtained with a procedure incorporated in the meanline design system, and the disk weight was estimated using standard ratioing procedures.

TABLE C-LIX

GEARED ENGINE LAST LPT STAGE GEOMETRIC INFORMATION

Number of Blades	54
Assumed No. of Firtree Teeth	3
Assumed Broach Angle	12°
Root Chord	60mm (2.35″)
Taper Ratio (b_{tip}/b_{root})	1.083
Airfoil Length	244mm (9.6″)
A.R. (length/b_{root})	4.08
Redline Speed	7623 RPM

The general conclusion was that the LPT was structurally feasible at the level of rotor speeds envisioned for the geared fan engines. These studies are discussed in the following paragraphs.

Stage Vibration

A stage vibration analysis was completed for the first three coupled modes. Figure C-41 is a resonance diagram showing the results of this analysis. Included are results for a nickel blade and disk, titanium-aluminide blade and nickel disk, and titanium-aluminide blade and disk. The 2E frequency margins for all configurations were found acceptable.

Flutter Stability

Flutter Stability was checked for the nickel base rotor and was found to be acceptable. Figure C-42, a flutter stability plot for various nodal diameters, shows these results. Although the flutter stability of titanium-aluminide blades was not calculated, it should be acceptable since its stage frequencies are equal to or greater than those of the nickel base blades.

Stress Ratios

Stress ratios were calculated for the first three coupled modes. Figure C-43 shows the results. The lowest predicted stress ratio, 1.35 for the first coupled mode, is well above the minimum criteria which assumes resonances excited by exhaust struts or other known sources of excitation would not be within the operating range. The stress ratios for the second and third modes are also acceptably above their criteria.

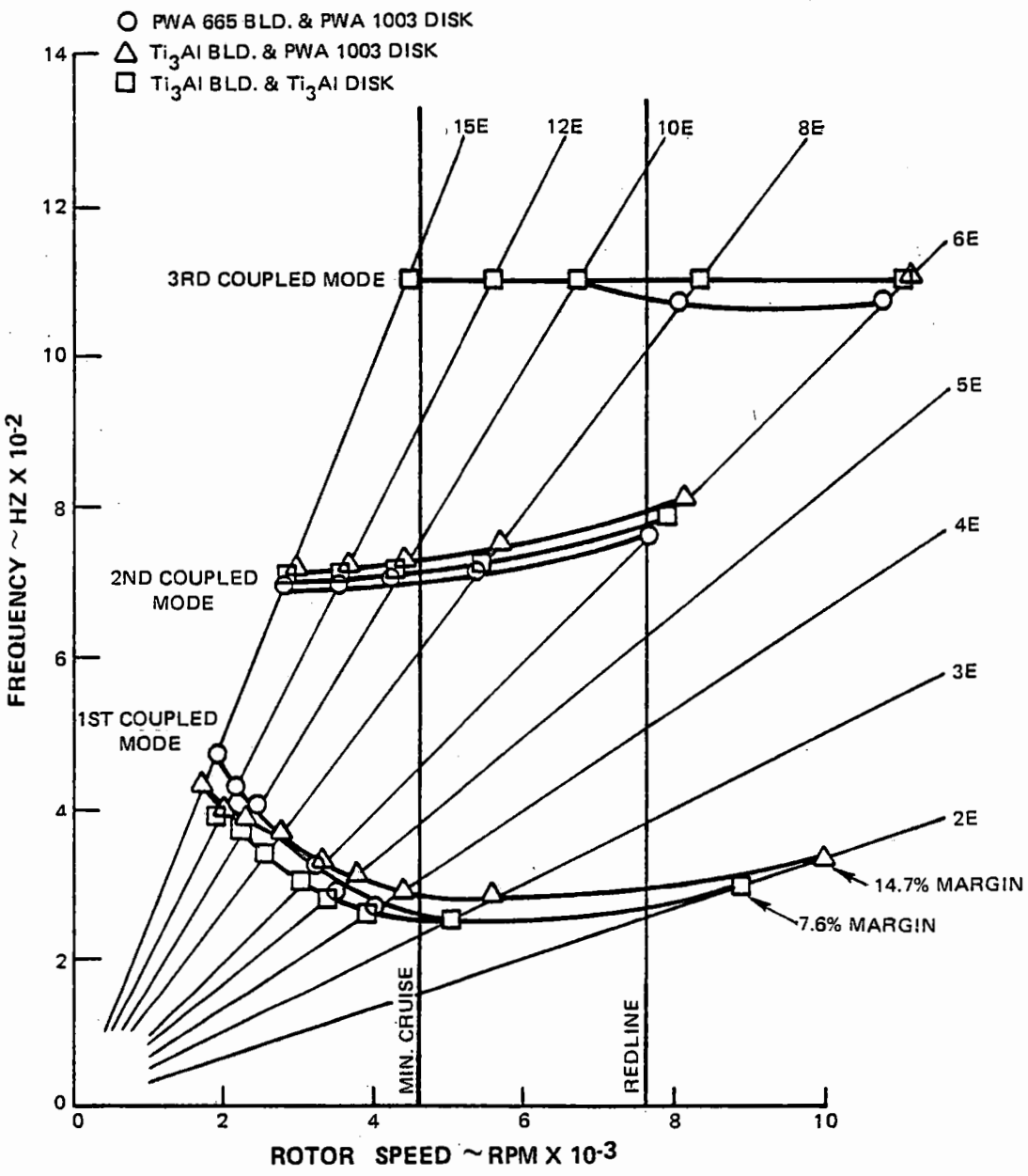

Figure C-41 Geared Engine Last LPT Stage Resonance Diagram

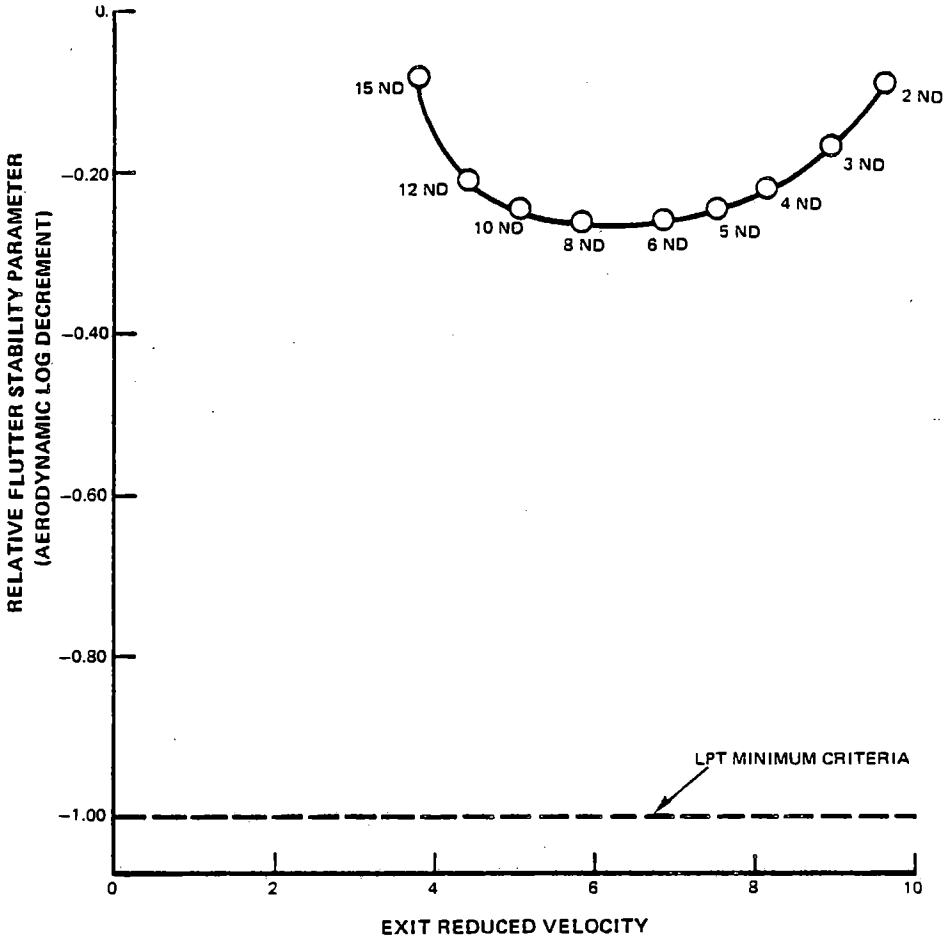

Figure C-42 Geared Engine Last LPT Stage Flutter Stability

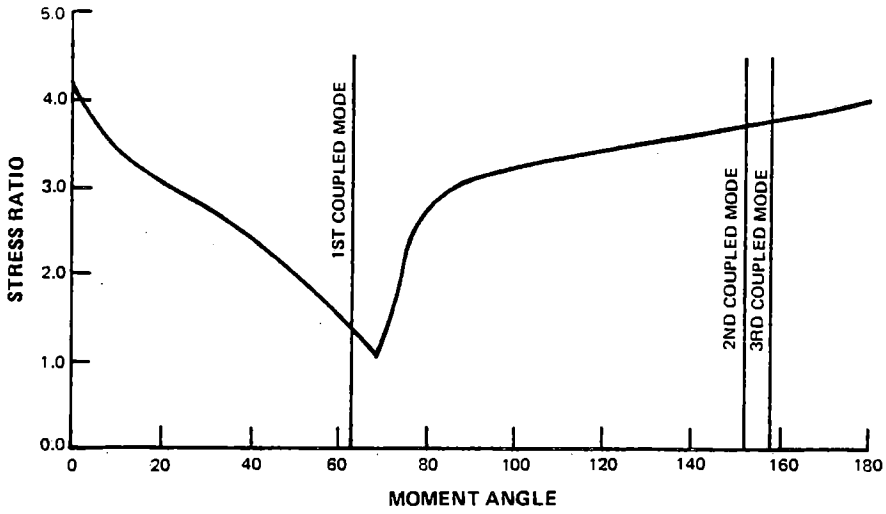

Figure C-43 Geared Engine Last LPT Stage Stress Ratio

Dynamic Stress Allowables

Goodman diagrams were constructed to determine the blade materials required for sufficient high frequency fatigue (HFF) durability at anticipated vibratory stress levels. The nickel base blade diagram, Figure C-44, shows the 448 N/mm^2 (65,000 psi) centrifugal stress level at the blade root to be well above the maximum commercial engine experience level with current LPT materials. This increased static stress level would, as shown, require a material with higher ultimate strength, such as current HPT materials, to obtain sufficient margin between the Goodman line and the expected vibratory stress levels. The projected titanium-aluminide is also shown to have adequate margin.

Shroud Curling Stress

The effects of maximum rotor speed on curling stresses were studied for the preliminary shroud configuration shown in Figure C-45. The maximum calculated stress of 301 N/mm^2 (43,600 psi) is well below the 0.2% yield strengths and 300 hour 1% creep strengths for any of the blade materials considered.

Retained Shroud Tightness

The retained shroud tightness parameter was calculated for the preliminary shroud configuration shown in Figure C-45. The results was a 7.5 parameter for a 1 degree pretwist angle, which exceeds the allowable level. The shroud configuration was changed to that shown by Figure C-46, which reduces the shroud angle to 30 degrees, giving an acceptable tightness parameter. Since curling stresses were not considered a problem, they were not recalculated for the final shroud configuration. However, the final configuration was used for the final vibration analyses discussed above.

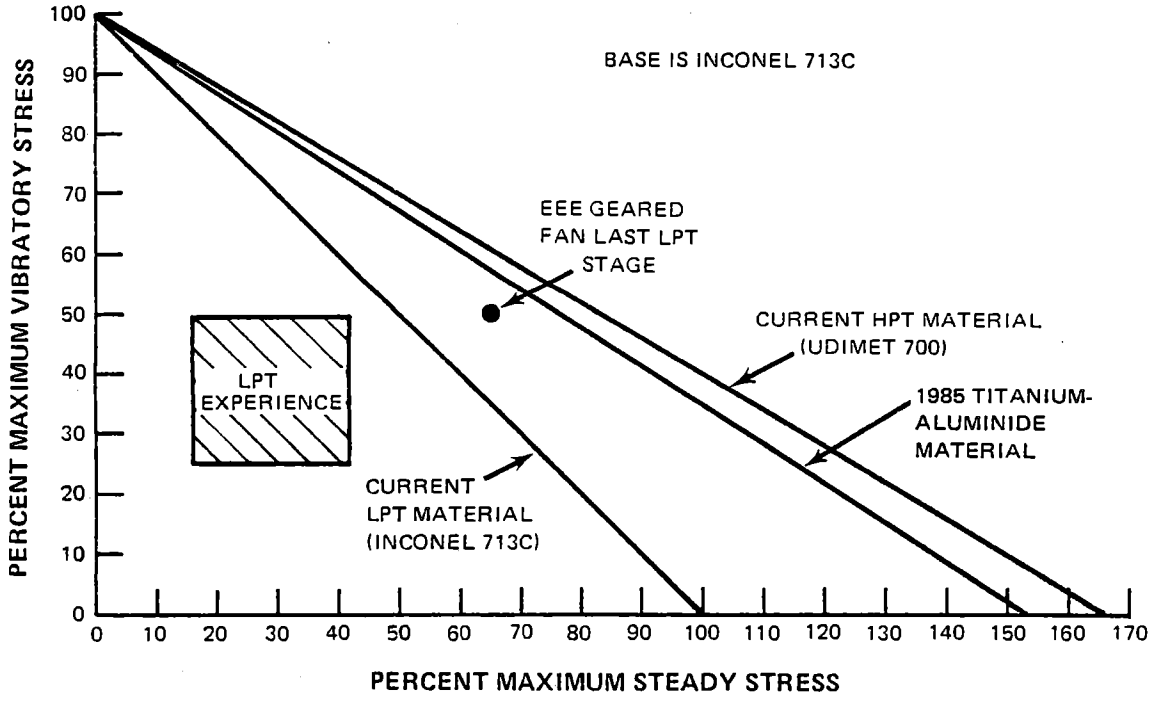

Figure C-44 Geared Fan Engine Last Stage Low–Pressure Turbine Goodman Diagram

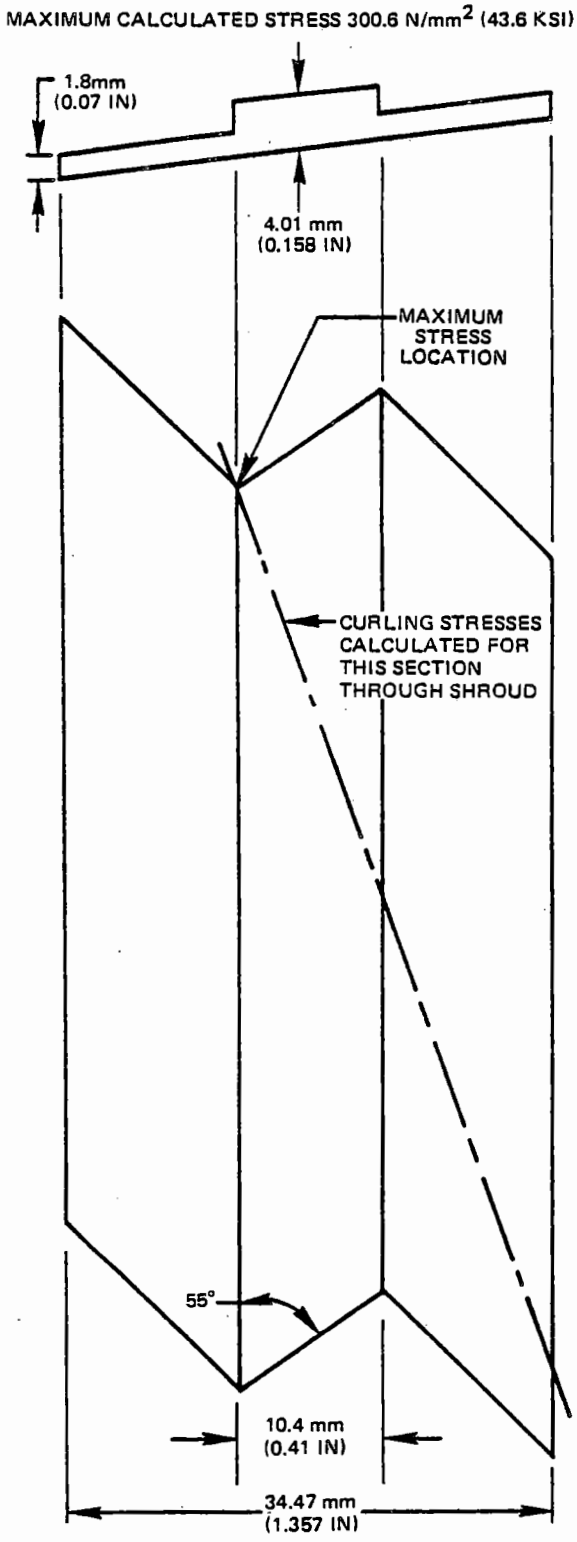

Figure C-45 *Geared Engine Last LPT Stage Curling Stress Calculation Preliminary Shroud*

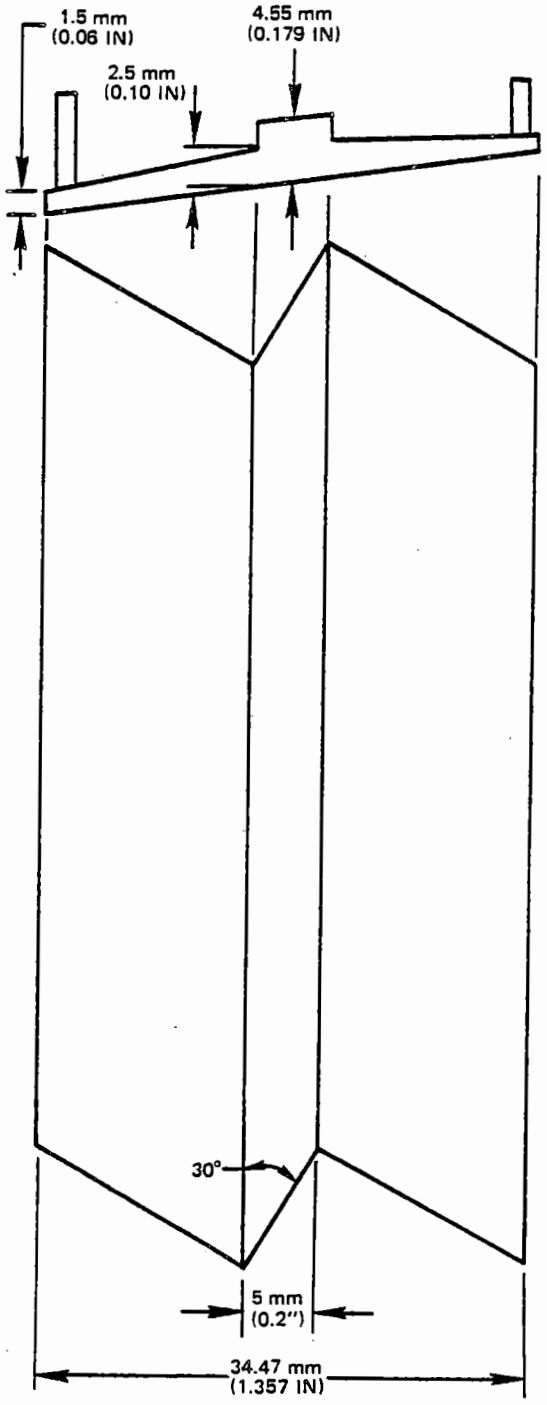

Figure C-46 *Revised Geared Engine Last LPT Stage Shroud Configuration to Meet Tightness Parameter*

Shroud Bearing Stress

Based on the final shroud configuration, bearing stress was calculated. The estimated result of 22.3 N/mm^2 (3300 psi) is well below the allowable level.

Attachment Stress

Attachment stresses were calculated using a 12° broach angle for the nickel alloy blade and disk. Neck widths used for these calculations were obtained by proportioning the outer blade neck width to that of the inner disk lug neck. Maximum stresses calculated for this configuration are summarized in Table C-LX. These stresses are all below the allowable stresses.

TABLE C-LX

GEARED ENGINE LAST LPT STAGE
ATTACHMENT STRESS SUMMARY
12° BROACH ANGLE
PWA 665 BLADE AND PWA 1003 DISK

Stress Type	Max. Calculated Stress N/m^2 (ksi)
Blade Neck Tensile	$2.09X10^8$(30.4)
Blade Tooth Shear	$1.85X10^8$(26.8)
Blade Tooth Bending	$2.08X10^8$(30.2)
Blade Tooth Bearing	$5.82X10^8$(84.4)
Disk Neck Tensile	$2.34X10^8$(33.9)
Disk Tooth Shear	$1.90X10^8$(27.5)
Disk Tooth Bending	$1.91X10^8$(27.7)
Disk Tooth Bearing	$5.82X10^8$(84.4)
Disk Effective Stress	$5.89X10^8$(85.4)

Since the amount of blade trailing edge overhang was also a concern, the impact of a broach angle increase on attachment stresses was investigated. Results indicated that the broach angle could be increased to 16 degrees without exceeding the effective stress or bearing stress allowables. The effect of broach angle changes on the length of trailing edge overhang is shown in Figure 47. Trailing edge overhang for a 16 degree broach angle should not overstress the attachment, based on HPT experience.

Overspeed

Analyses were conducted to determine what the impact of a reduction gearbox failure that decouples the fan from the rest of the low spool would be on the LPT.

The first analysis was to estimate the magnitude of the overspeed and the ability of an advanced fuel control to handle it. Low spool overspeed was estimated at two flight conditions:

- 11050m (36,089 ft.), 0.69 Mach number, Maximum Climb Power
- Sea Level Static, Hot Day, Takeoff power.

Initial rotor speed rate of change resulting from gearbox failure was calculated from the excess LPT work, initial spool speed, and polar moment of inertia of the low spool sans fan. The maximum initial rate was estimated to be 12,340 rpm/sec at the sea level condition because core airflow, and consequently fan and LPT work, were maximum there. Based on a typical 30% LPT disk burst margin, a necessary "time-to-react" of 0.25 sec. was determined. "Reaction time" was estimated, considering advanced electronic fuel control sensing and logic, to be of the order of 0.07 sec. This "reaction time" would be fast enough to slow down the rate of speed

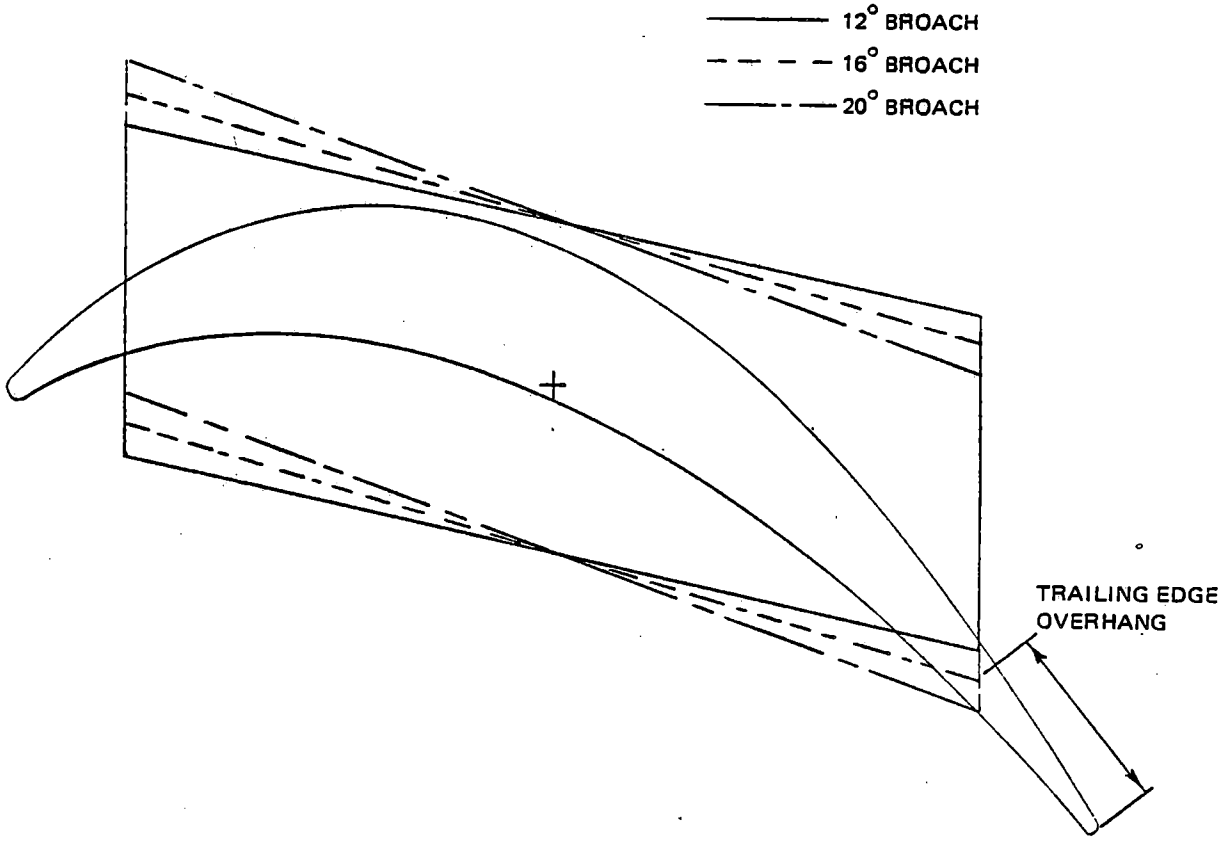

Figure C-47 Geared Engine Last LPT Stage Blade Root and Neck Sections

increase after failure, but the residual LPT gas path energy would continue to accelerate the spool above the burst limit.

As a result of this finding, an analysis was made to approximate the disk burst margin required to allow blade failure (which would be contained or noninjurious to flight safety) in lieu of disk. The first and second disks were arbitrarily resized for 50% burst margin at redline speed using MERL 76 as a material with steel blades (PWA 655). The result, 50% burst margin, was inadequate for failsafe disks. The data were extrapolated to determine that the burst margin of the first stage disk must be at least 67% for the disk to be strong enough to make the minimum strength blades fail in tension. Since this 67% burst disk's size and weight were already unwieldy, no effort was made to determine the burst margin required to ensure that "all" blades fail statistically. The general conclusion was that the LPT could not be reasonably designed to handle overspeeds resulting from gearbox failure.

2.2.2.3.4 Mixer Aerodynamic Integration

LPT aerodynamic design analyses were conducted based on the projection that approximately 20 degrees of exit airflow swirl can be allowed because of the mixed flow configuration. Testing has shown that convoluted mixers have inlet swirl tolerance, as can be seen in Figure C-48 in terms of nozzle thrust coefficient. As a result, the LPT designs took advantage of the mixer's elimination of the need for fully axial exit flow by reducing airfoil loadings on the exit guide vanes.

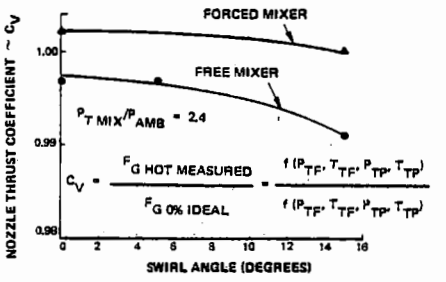

Figure C-48 Effect of Swirl on Exhaust Nozzle Performance – The convoluted forced mixer will accommodate a high degree of flow swirl with negligible effect on performance.

Results of this design approach showed the reduced exit guide vane turning requirements to lower vane aerodynamic loading by 50%. Pressure losses were in turn estimated to be 0.3% lower. It was also estimated that reduced loading would desensitize the vane to incidence variation and allow improved performance at off-design conditions.

2.2.2.3.5 Geared Engine LPT Disk Weight Analysis

Because of the high rotational speed of the geared LPT, significant weight was found to be associated with the conventional LPT material disks. As a result, a weight reduction analysis was conducted to determine the impact of using MERL 76, a higher ultimate strength material, to reduce disk size. Conventional disk design procedures were used to provide the definitions.

This assessment concluded that a total disk weight reduction of 30.5% was accomplished by incorporation MERL 76 disks.

Table C-LXI summarizes these results.

As a result of this study MERL 76 disks were incorporated into the LPT.

2.2.2.3.6 LPT Configuration Summary

A summary of final preliminary LPT designs for each of the four engine configurations is given in Table C-LXII.

Cross sections of the LPT's for the four engines are shown in Figure C-49.

2.2.3 Subsystem Analysis

2.2.3.1 Reduction Gears

The three basic types of reduction gearbox considered in Task I were reviewed in order to select one for the Task III geared fan engines. These were the planetary, star, and layshaft configurations shown schematically in Figure C-50.

2.2.3.1.1 Planetary Gear System Analysis

A planetary system was again considered briefly during the initial phase of the study, but was rejected because the required gear ratio of approximately 2.45:1 resulted in the need for 13 small diameter pinions.

2.2.3.1.2 Star Gear System Analysis

A star system was studied in more detail because of its more reasonable number of larger diameter pinions. A preliminary sketch of the star gear was made based on current technology (Figure C-51). With this concept, power was input to the sun gear through a quill shaft having splines at both ends to account for misalignment between the low-rotor and the gear. The floating sun gear was configured to drive 6 equally spaced pinions, which in turn drove a floating ring gear that was loose splined

to the fan hub. The number of pinions was determined from gear ratio, ring gear diameter, and allowable clearance between pinions. Pinion bearing and gear assemblies were clamped between flat plates at their front and rear to form a cage. The cage was fixed to ground through 6 hairspring supports used to minimize misalignment.

The design permitted loads to be equalized between pinions by depending on the flexibility of the ring gear, by letting the sun gear float, and by holding close tolerances.

TABLE C-LXI

GEARED ENGINE LPT DISK WEIGHT REDUCTION WITH MERL 76

Disk No.	Material	Weight - kg (lbs.)	Material	Weight - kg (lbs.)	Savings - kg (lbs.)
1	PWA 1007	13.5(29.8)	MERL 76	10.8(23.7)	2.8(6.1)
2	PWA 1003	20.0(44.0)	MERL 76	13.5(29.8)	6.4(14.2)
3	PWA 1003	38.8(85.6)	MERL 76	26.0(57.3)	12.8(28.3)

Net Weight Saving = 22 kg (48.6 lbs.)

TABLE C-LXII

TASK III LPT AERODYNAMIC DESIGN SUMMARY
(AERODYNAMIC DESIGN POINT)

Engine:	1 Stage HPT Direct Drive	2 Stage HPT Direct Drive	1 Stage HPT Geared	2 Stage HPT Geared
Number of Stages	4	4	3	3
Rotor Speed – rpm	3844	3852	6365	6156
Mean Velocity Ratio	0.454	0.456	0.530	0.535
Cooling/Leakage – %	1.55	1.45	1.79	1.69
Efficiency – %	91.2	91.2	92.6	92.6
Expansion Ratio	5.70	5.36	5.85	5.52
Flow Coefficient	0.804	0.794	0.625	0.660
Number of Airfoils	759	765	422	462
HPT-LPT Mean Radial Offset–%	24	41	2	23

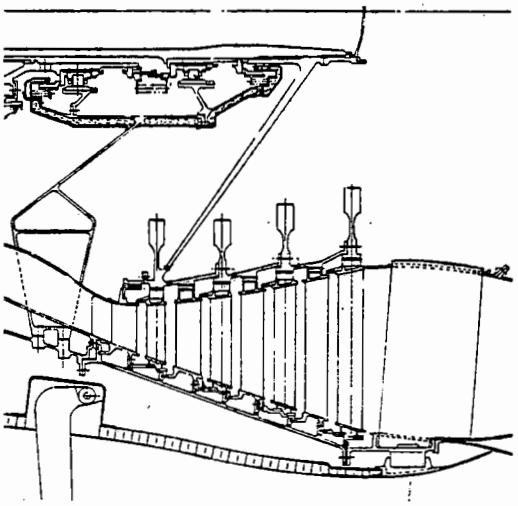

STF 505 M-7
DIRECT-DRIVE, 1 STG HPT

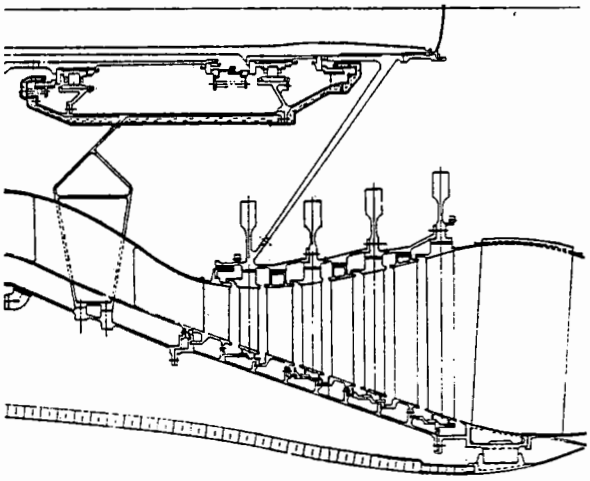

STF 505 M-9
DIRECT-DRIVE, 2 STG HPT

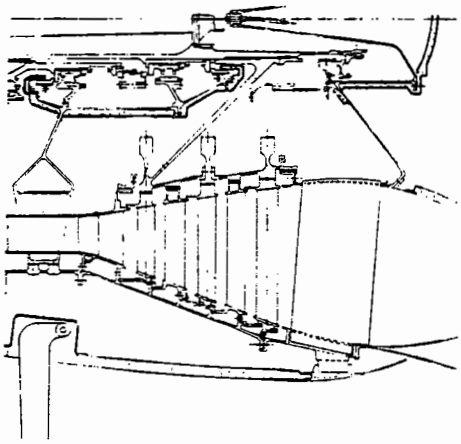

STF 495 M-4
GEARED, 1 STG HPT

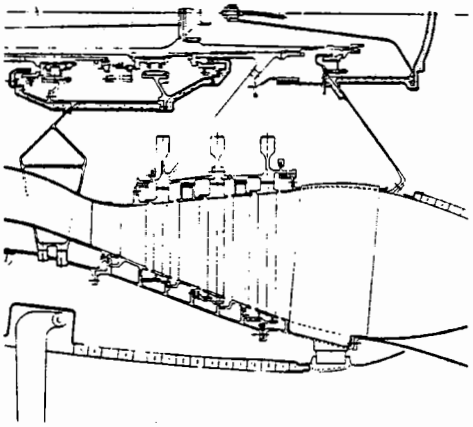

STF 495 M-5
GEARED, 2 STG HPT

Figure C-49 Cross Sections of the Low-Pressure Turbines for the Four Task III Engine Types

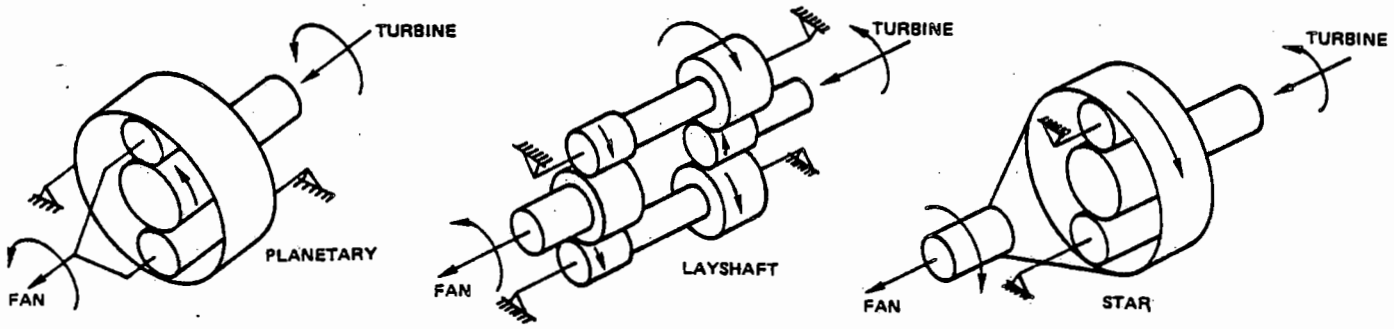

Figure C-50 Candidate Gear System Schematics – The star gear system was selected for Task III preliminary design

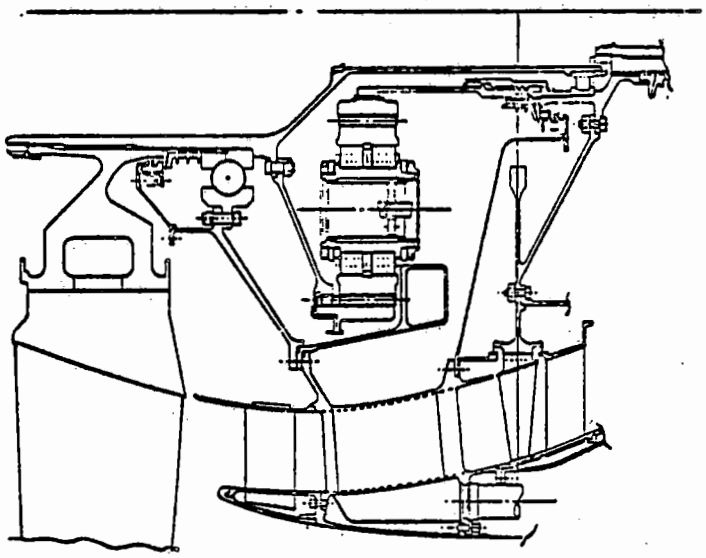

Figure C-51 Preliminary Star Gear System (Current Technology)

Preliminary tooth design was done based on a contract ratio of 2 for smooth operation. Analysis showed face width to be set by tooth bending stress allowables.

The gearbox inlet support case was rough sized based primarily on lubrication and aerodynamic requirements. Unbalanced fan thrust was used to size the fan bearing.

2.2.3.1.3 Layshaft Gear System Analysis

Using current technology, a layshaft system was studied because of Pratt & Whitney's previous experience with the concept shown in Figure C-52.

Three configurations were examined on a preliminary basis. The first configuration has staggered input (sun) gears on the layshaft which resulted in a large overall diameter and length. The subsequent and final configurations increased sun gear diameters such that the staggered arrangement was no longer required. This approach resulted in reduced diameter and length, although the overall length was still greater than the star system.

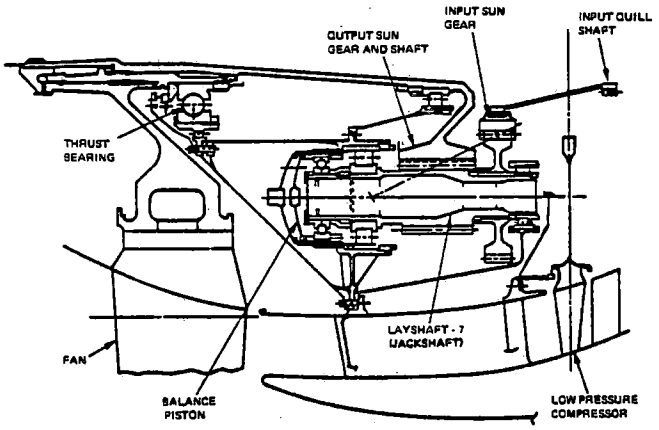

Figure C-52 Preliminary Layshaft Gear System – Load sharing results from use of a unique hydraulic balance system.

The design also featured helical gearing throughout which allowed part of the LPT thrust load to be balanced against the fan thrust. In addition, approximately half of the fan thrust was taken through the gear train balance pistons. As a result of this thrust load sharing feature, a smaller diameter, more conventional fan thrust bearing than the star gear system's could be used. Smaller size allowed the fan bearing to be placed in the plane of the fan disk, thus improving wheelbase. The entire fan support with the layshaft system was estimated to be very stiff.

2.2.3.1.4 Gear Set Evaluation and Selection

Very preliminary performance predictions and weight estimates were made for the star and layshaft gear systems. In addition, both gearboxes were qualitatively assessed on the bases of development risk, production cost, reliability, and packaging. Results are shown in Table C-LXIII.

This comparison led to the selection of the star gear system for incorporation into the Task III Energy Efficient Engine Design. The advantages of the star system in terms of performance, cost, and reliability were felt to outweigh its development risk.

The 0.3 to 0.4% gearbox efficiency advantage estimated for the star system was partially offset by a 1% fan root loss associated with the fan-LPC counterrotation aspect inherent with the concept. However, a net TSFC advantage was estimated for the star system, and the better efficiency significantly reduced heat rejection.

Since the layshaft system was inherently more complex because of its load equalization and fan bearing thrust reduction concepts, penalties were assessed in the areas of reliability and cost. The increased number of layshaft system parts was the cause for a decrease in mature gearbox reliability and a higher production price.

The development risk concern for the star system was associated with the structure of the large diameter ring gear. Large deflections were predicted because of centrifugal loading and localized pinion gear radial and tangential loads. The structure was also estimated to be more susceptible to fan blade loss induced deflections. These concerns were not felt to prevent ultimate success with this gear system.

2.2.3.1.5 Refined Star Gear Analysis

Design of the star gear system was conducted in more detail in order to establish a final preliminary configuration. Additional analyses included an evaluation to assess the impact of advanced technology and a redesign of the fan support system to eliminate estimated critical speed problems.

The preliminary star gear system was reconfigured to projected 1985 technology. Two lubrication oil approaches were assessed, a cold or current technology oil and an advanced hot synthetic oil. Table C-LXIV presents the advancements considered.

TABLE C-LXIII

COMPARISON OF LAYSHAFT AND STAR GEAR MERITS

CONFIGURATION:	LAYSHAFT	STAR
COMPONENTS		
No. Gearbox Brgs.	21	12
No. Engine Brgs.	2	2 (1 Intershaft)
No. Gear Meshes	14	12
SHAFT ROTATION	Co Rotating	Counter-Rotating
MISALIGNMENT COMPENSATION	Yes	Yes
LOAD EQUALIZATION	Base	Somewhat Less
THRUST BALANCE		
Fan Brg.	50%	None
Turbine Brg.	Optional	None
ENGINE WEIGHT		
Ignoring Air/Oil Cooler	Base	+22.7 kg (+50 lb)
With Air/Oil Cooler	Base	−22.7 kg (−50 lb)
MODULAR GEARBOX	O. K.	Difficult-with Intershaft Brg.
DEVELOPMENT RISK	Base	Much Higher
RELIABILITY (MATURE BOX)	Base	Better (Fewer Parts)
COST	Base	Less (Fewer Parts)
PERFORMANCE PREDICTIONS		
Gearbox Efficiency	98.8% T/O/98.4% CR.	99.1% T/O/98.8% CR.
Fan (I. D.) Efficiency	Base	-1.0% (caused by counter-rotation)
Overall TSFC	Base	-0.2%

TABLE C-LXIV

ADVANCED STAR GEARBOX TECHNOLOGY CRITERIA

	Current Technology	Advanced Technology	
		Cold Oil	Hot Oil
Materials Limits			
Contract Stress – N/m^2X10^8 (psi)	Base	+2.0 (+30,000)	Base
Bending Stress – N/m^2 X 10^8 (psi)	Base	+1.0 (+15,000)	+0.34 (+5,000)
Reverse Bending Stress – N/m^2 X 10^8 (psi)	Base	+1.0 (+15,000)	+0.34 (+5,000)
Bearing Life Multification Factor	Base	+10	+10
Lubricant			
Oil Temperature Out – °C (°F)	Base	Base	106 (+190)
Cooler Size	Base	-20%	–80%
Gearbox Failure Goal – hrs.	Base	+20,000	+20,000

The resulting advanced technology gears were both smaller in size and lighter in weight. The cold oil system gear was 67 kg (147 lbs) lighter than the current technology system. However, the hot oil system gear only saved 39 kg (85 lbs) because of bending strength limitations of the gear material at elevated operating temperatures.

Based on these results and on considerations of risk, the decision was made to incorporate the current technology star gearbox system in the Energy Efficient Engine design. The additional risk with advanced technology versus the relatively small system benefits was not justifiable in an already high risk component.

Design modification of the star gearbox system was required relative to the Task I definition as a result of a critical speed problem in the operating range. A redesign of the fan-to-low shaft bearing coupling was found necessary to eliminate this problem. The critical speed was associated with the close coupling of the fan and shaft via the inner roller bearing (see Figure C-51). Decoupling of the fan and shaft raised the shaft frequency to an acceptable margin above the operating range. To accomplish decoupling, the fan shaft bearing was moved to the gearbox support structure as shown in Figure C-53.

This forced the fan hub to be attached through a floating type joint at the ring gear, and also required stiffening of the gearbox supports to minimize fan deflections and control ring gear deflections. Required stiffening resulted in a 18.8 cm (7.4 in.) engine length increase.

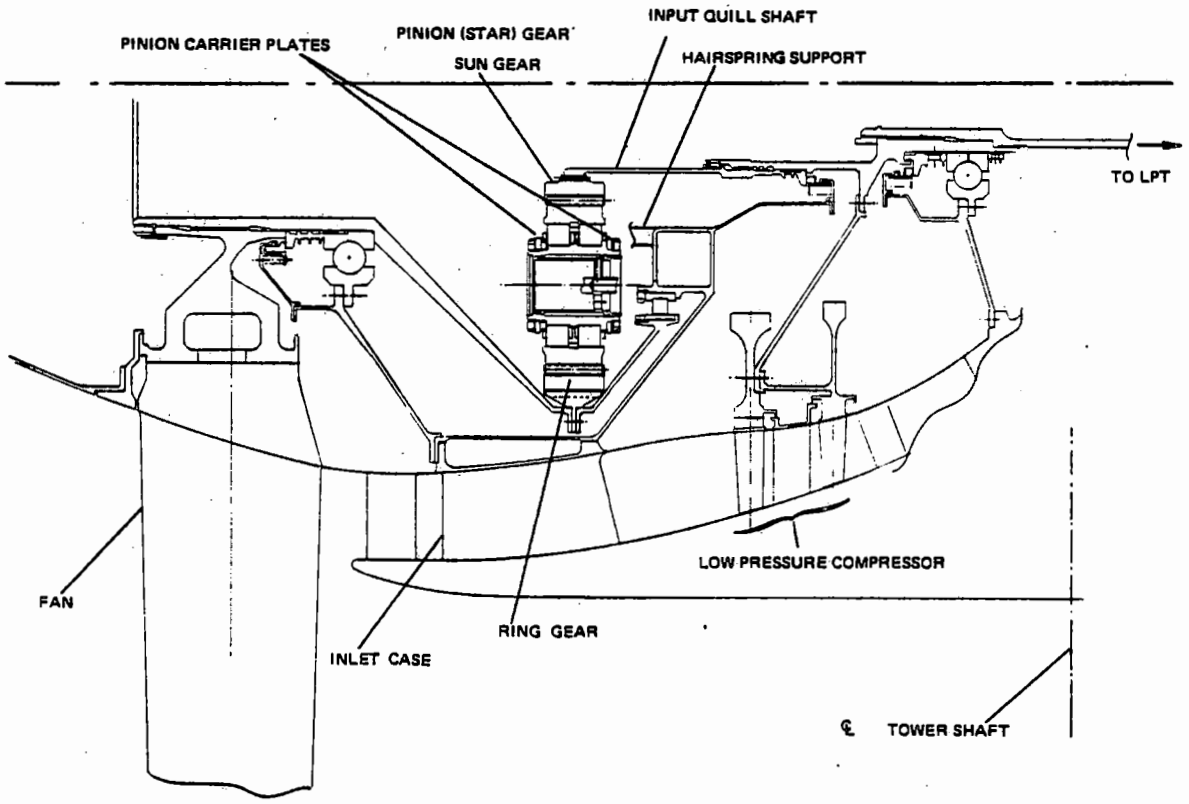

Figure C-53 Refined Star Gear System – Gearbox support structure was revised to raise low shaft natural frequency.

Further review of the gears and bearings showed the same feasible levels of stress and life estimated in the Task I conceptual analysis.

2.2.3.1.6 Star Gear Efficiency Analysis

To better establish gearbox loss levels relative to the preliminary assessments of Task I, a complete review of the nature of gear system loss and the adequacy of the prediction system was conducted. These included gear friction, windage, oil churning, and bearing friction.

A literature search and discussions with other United Technology Corporation Divisions were conducted to examine the power loss analysis.

Methodologies used by the Sikorsky and Hamilton Standard Divisions were found to be based on the work of Buckingham ("Analytical Mechanics of Gears"), while Pratt & Whitney Aircraft Canada used methods based on the Dudley "Gear Handbook". Another method considered was found in an AGMA paper. The first two sources recognized an effect of gear mesh geometry on power loss while the third did not. The Dudley method yielded power loss estimates between the other two methods, and therefore, was selected, together with a more favorable contact ratio assumption, for use in the analysis. A friction coefficient of 0.05 was used at full speed, and the Buckingham speed to the 0.5 power relationship was applied at part speed conditions.

The windage calculation procedure selected followed methods set forth by Dudley with a correction for oil-air mixture viscosity effects. Oil-air mixture volumetric ratio used was 0.015 based on Pratt & Whitney Aircraft Canada practice.

Oil churning calculations were based on Pratt & Whitney Aircraft design procedures. This method considers the power required to accelerate all oil directed at the gear mesh up to wheel speed. The resulting reference point may have to be modified in any future development depending on detailed designs of the oil jets and baffles.

The procedure used to calculate both ball and roller bearing friction losses was a modified version of Harris' ("Roller Bearing Analysis"). Modification accounted for projected improvements in precision and lubrication practice.

Based on the above methodology, gearbox efficiencies at the ADP and Sea Level Static Take-off conditions were estimated to be 98.8% and 99.1% respectively for the star gearbox system.

2.2.3.1.7 Oil Cooler Sizing and Integration

Sizing

Task I configuration analysis identified the need to supplement air cooling of the geared engine's oil with fuel in order to handle the tremendous amount of heat rejected(250% greater than direct-drive engine) from the gearbox and bearings with a reasonable size cooler. In that effort, a cross-flow core made of alternating layers of corrugated and flat sheets was identified as the best general air-oil cooler approach.

To optimize cooler size, a progressive study was undertaken. Core geometries were calculated to meet estimated air and oil flow rates, pressure drop, and heat flux requirements. Results of this study are presented in Table C-LXV.

TABLE C-LXV

TASK III AIR-OIL COOLER SIZING RESULTS

	Scheme	Frontal Area - $m^2(ft^2)$	Volume m^3 (ft^3)
A	Coarse matrix corrugated fin plate, equal plate spacing air and oil, crossflow	0.44 (4.7)	0.10 (3.7)
B	Same as A except size reduced 20% to represent technology development	0.37 (4.0)	0.08 (3.0)
C.	Same as B except heat load reduced 40% by using excess heat capacity of fuel at high power	0.22 (2.4)	0.05 (1.8)
D	Same as C except matrix proportion changed to reduce frontal area	0.17 (1.8)	0.05 (1.8)
E	Application of high density corrugated fins and reduced oil side plate spacing relative to air side to provide same thermal and flow characteristics as D in 75% reduced length	0.17 (1.8)	0.013 (0.45)

An advanced technology air-oil cooler was sized having a 0.047 m^2 (0.5 ft^2) frontal area and a 0.0036m^3 (0.125 ft^3) volume, but was rejected because risk was not felt to be worth the benefit.

The final configuration, Scheme E, was determined to be the best representation of state-of-the-art heat exchanger technology.

Initially, the selected air-oil cooler was located in the nacelle lower bifurcation, and the fuel-oil cooler was located on the inner fan duct. It was immediately recognized that this location of the air-oil cooler made it susceptible to foreign object damage (FOD). The location had been selected primarily to ease maintainability by allowing maximum accessibility to the core engine.

As a result, in Task III alternate locations were considered to better integrate the air-oil cooler. This assessment showed a cooler located between the engine HPC case and the inner fan duct to present a reasonable compromise between possible FOD and maintenance ease. Figure C-54 shows this integration. Fan duct air is centrifuged to remove debris as it is ducted into this configuration.

2.2.3.1.8 Star Reduction Gear Configuration Summary

The resulting star gearbox design from the Task III Analysis is summarized in Table LXVI.

Figure C-55 shows the final gearbox configuration for the geared fan engine.

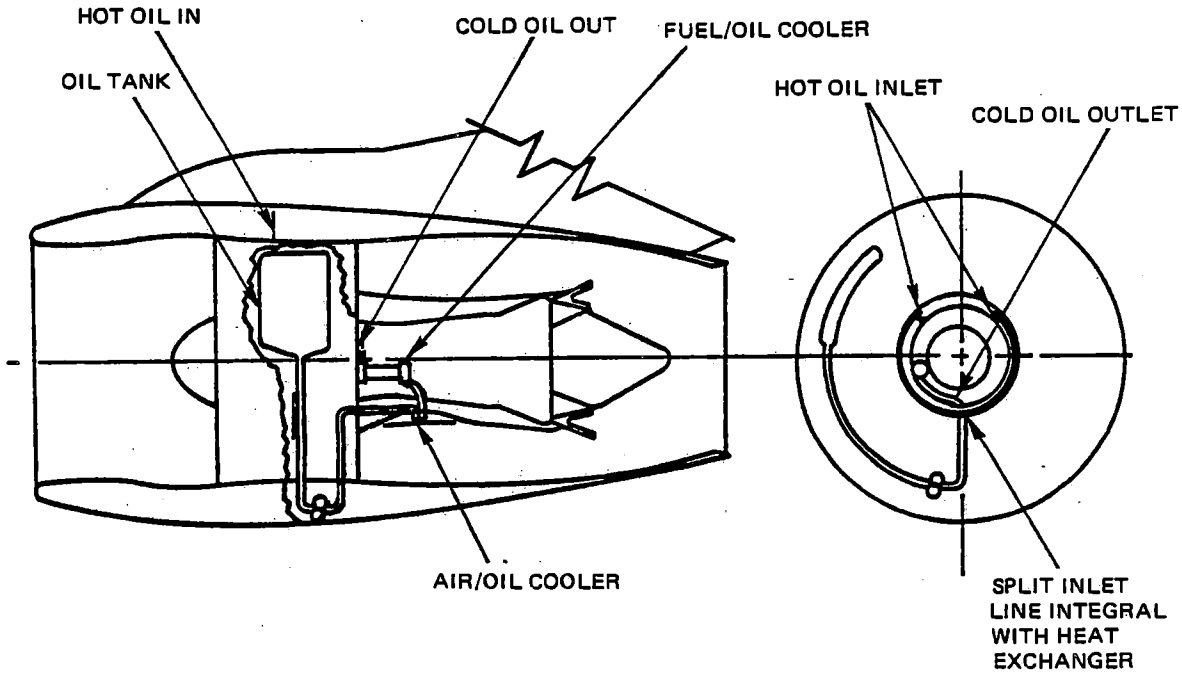

Figure C-54 Fan Gearbox Air-Oil Cooler

TABLE C-LXVI

TASK III GEARBOX/OIL COOLER DESIGN SUMMARY
(AERODYNAMIC DESIGN POINT EXCEPT AS NOTED)

Gear Ratio	2.50
Max. Power Watts x 10^6 (hp) (Takeoff)	29.8 (40,000)
Sun Gear Speed - rpm	6364
Gear Pitch Line Velocity m/min.(ft/min.)	6460 (21,200)
Pinion Gear Speed - rpm	8845
Ring Gear Speed - rpm	2550
Number of Pinions	6
Number of Gear Teeth	
Sun Gear	68
Pinion Gear	49
Ring Gear	166
Efficiency - %	98.8%
Oil Coolers	
Air-Oil:	
Frontal Area - m^2 (ft^2)	0.17 (1.8)
Volume - m^3 (ft^3)	0.013 (0.45)
Heat Rejection ADP/Sea Level Takeoff – joules/sec (BTU/min.)	189,000/169,000 (10,750/9,600)
Fuel-Oil:	
Heat Rejection ADP/Sea Level Takeoff – joules/sec (BTU/min.)	107,000/239,500 (6,100/13,600)

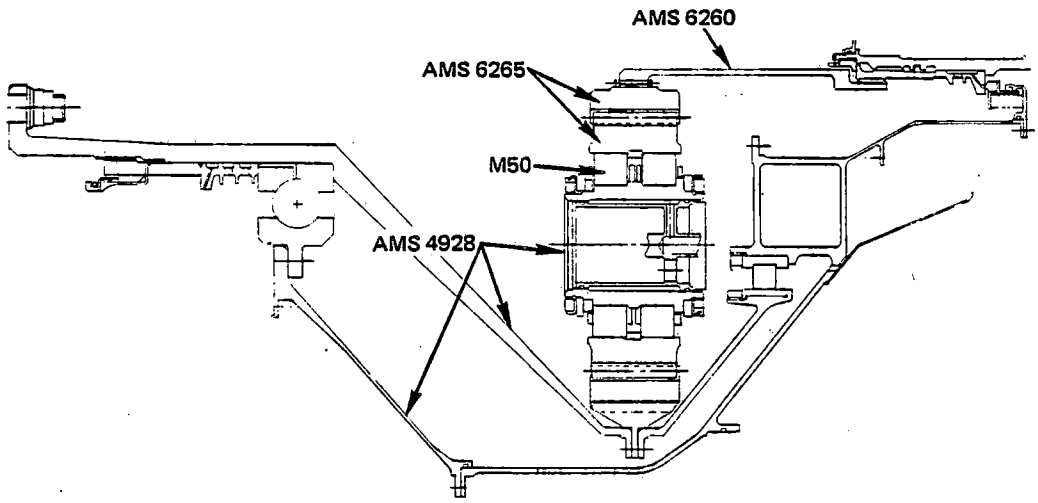

Figure C-55 Final Gearbox Configuration

2.2.3.2 Secondary Flow System/Geared Engine Low Rotor Thrust Balance Analysis

In order to define the preliminary secondary airflow system for the one-stage HPT engine, a parametric study was first done to establish the best manner in which to feed cooling air to the HPT blade. With these results in hand, flow systems for the HPT, transition duct bearing support strut, and LPT were configured.

Since the blade cooling air feed systems for the two-stage HPT had been selected in previous Pratt & Whitney Aircraft in-house preliminary design work, these concepts were simply analyzed for the Task III engine. Flow systems were then defined.

Because of the critical nature of rotor thrust balance in the geared fan engine caused by the gear's axial uncoupling of the fan from the rest of the low-spool, this problem was also analyzed.

2.2.3.2.1 One-Stage HPT Engine-Parametric Blade Cooling Feed Study

To select an HPT blade cooling air feed supply system, three concepts were selected from an initially larger matrix for further evaluation:

- Mini-Disk Tangential On Board Injection (TOBI) (Figure C-56).
- Pressure Balanced TOBI (Figure C-57).
- Bore Feed (Figure C-58).

The Mini-Disk TOBI uses a seal outboard of the TOBI nozzle to prevent excessive leakage into the gas path. Because of the high wheel speed of the seal, it requires a disk for support.

The Pressure-Balanced TOBI balances the pressure in the inner cavity in front of the turbine disk. This eliminates the need for a large diameter seal outboard of the TOBI nozzles.

The Bore Feed system uses the HPT disk to pump air to the blade supply pressure level. It utilizes lower HPC bleed air pressure from the middle stage instead of from the exit stage as required by the other two concepts. The pumping could either be accomplished by a hollow disk that incorporates ribs or holes, or by ribs on the face of the disk as shown in Figure C-58.

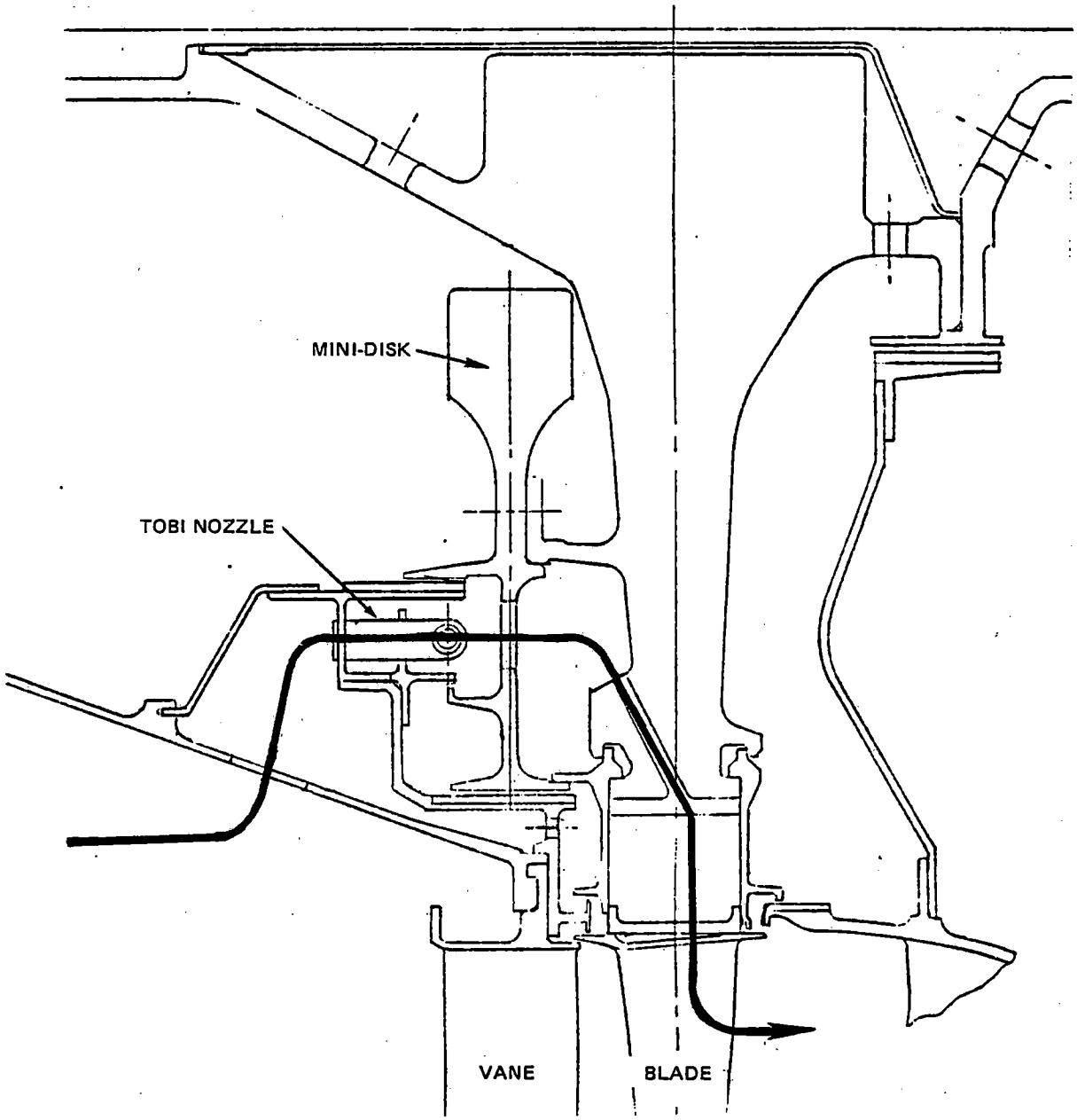

Figure C-56 HPT Blade Cooling Supply System – Mini-disk tangential on board injection.

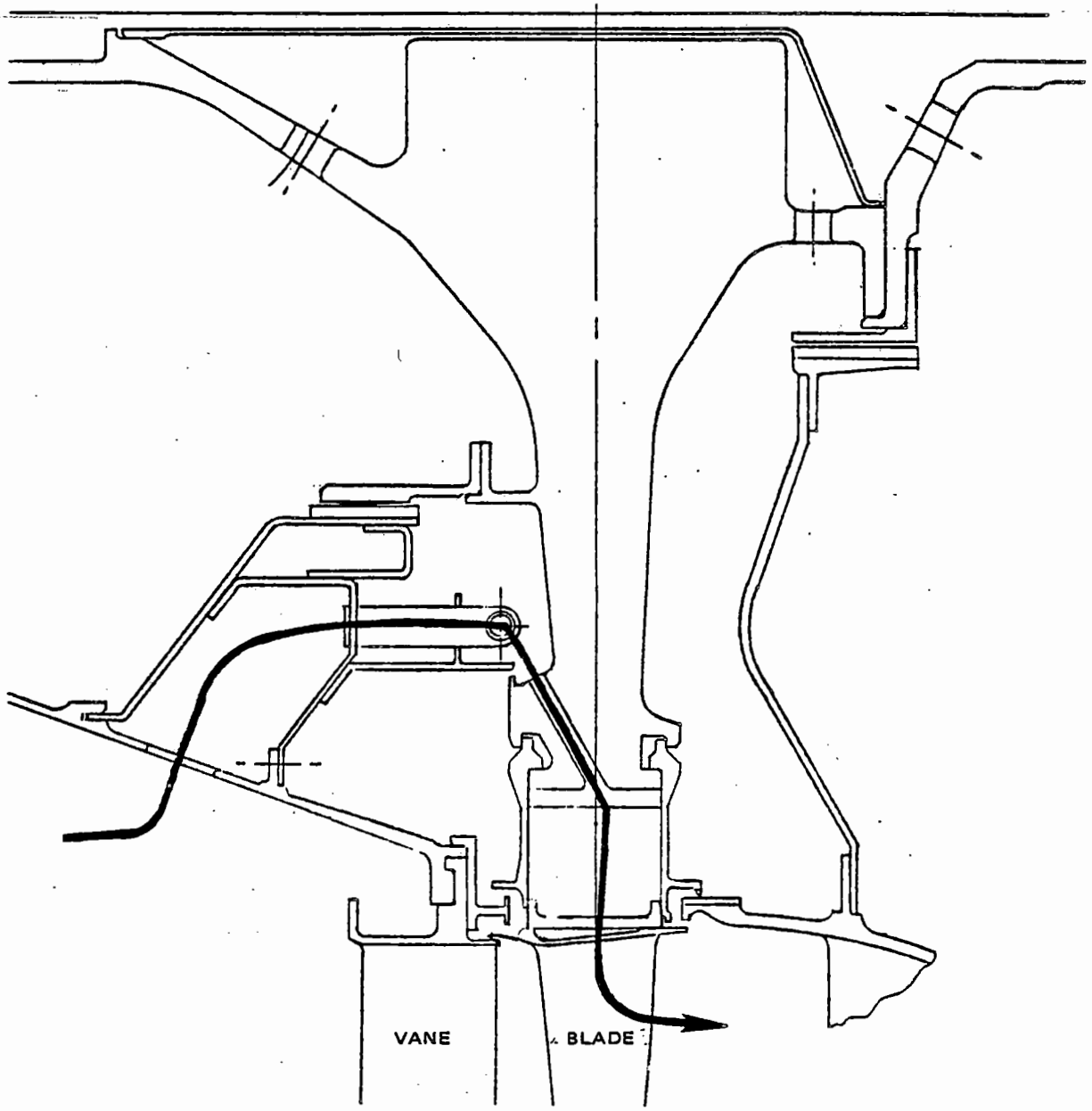

Figure C-57 HPT Blade Cooling Supply System – Pressure balanced tangential on board injection.

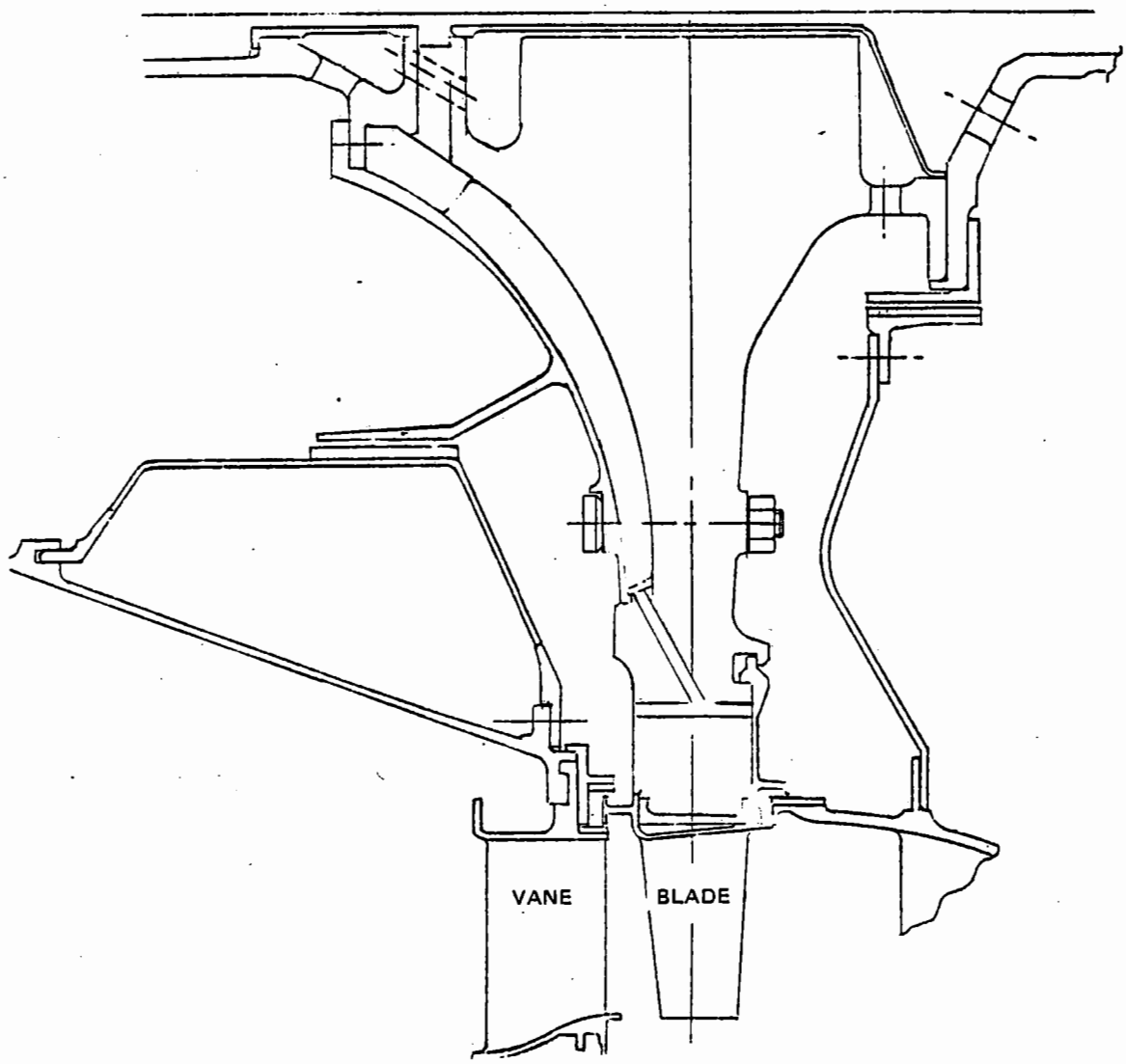

Figure C-58 HPT Blade Cooling Supply System – Bore feed.

Ground rules formulated for the parametric study were that all concepts were designed for:

- +10% of nominal blade flow
- +50% of attachment leakage
- +50% of all seal clearances
- No seal clearance below .051cm (0.02 in.)
- Satisfaction of initial spool thrust balance
- Thrust balance trim capability
- Maximum 704°C (1300°F) front rim cavity temperature
- 482°C (900°F) HPT disk bore temperature
- Blade supply pressure adjustment

- Range of blade supply pressure (48 to 54% HPC discharge)
- With and without supersonic TOBI flow.

Ranges considered were to determine concept sensitivities to detailed design, development, and/or production-caused variations in those parameters.

Flow systems were defined for each concept, and the resulting design configurations were analyzed aerodynamically and thermally. Basic results of these analyses, including performance effects are summarized in Table C-LXVII.

Conclusions were:

- No large performance advantage was offered by any concept
- All concept designs were windage or thrust balance limited
- The supersonic flow TOBI concept was worth only -0.04% TSFC.

In a further attempt to select a concept, a semi-qualitative assessment was made for performance, weight, cost, risk, and tolerance sensitivity. These results are presented in Table C-LXVIII.

Based on this evaluation, the Pressure Balanced TOBI concept was selected for engine incorporation because of its lower weight and reduced risk/complexity.

2.2.3.2.2 One-Stage HPT Engine - Secondary Airflow System

Based on the selection of the Pressure Balanced TOBI, a preliminary secondary airflow system map was configured for the one-stage HPT. This map, as shown in Figure C-59, summarized all secondary flow quantities, air pressures, and air temperatures.

TABLE C-LXVII

ONE STAGE HPT PARAMETRIC BLADE COOLING SYSTEM
AERO/THERMO RESULT

Concept:	Mini-Disk TOBI	Pressure Balanced TOBI	Bore Feed
48% Supply Pressure			
Blade Cooling Air Temp.	-18°C (-32°F)	Base	-3.3 (-6)
Disk Front Leakage - %WAE	-0.10	Base	+0.10
Disk Rear Leakage - %WAE	+0.15	Base	-0.15
TSFC-%	-0.05	Base	Base
54% Supply Pressure			
Blade Cooling Air Temp.	-19°C (-35°F)	Base	-23 (-42)
Disk Front Leakage - %WAE	-0.10	Base	+0.10
Disk Rear Leakage - %WAE	+0.15	Base	-0.06
ΔTSFC-%	-0.05	Base	-0.06

TABLE C-LXVIII

ONE STAGE HPT PARAMETRIC BLADE COOLING SYSTEM
EVALUATION SUMMARY

Concept:	Mini-Disk TOBI	Pressure Balanced TOBI	Bore Feed
Performance	Equal	Equal	Equal
Weight - kg (lbs)	+36 (+80)	Base	— -
Cost - $	—	—	—
Aerodynamic Risk	Medium	Medium	Less
Structural Risk	—	Best	Worse
Tolerance Sensitivity	Good	Adequate	Adequate

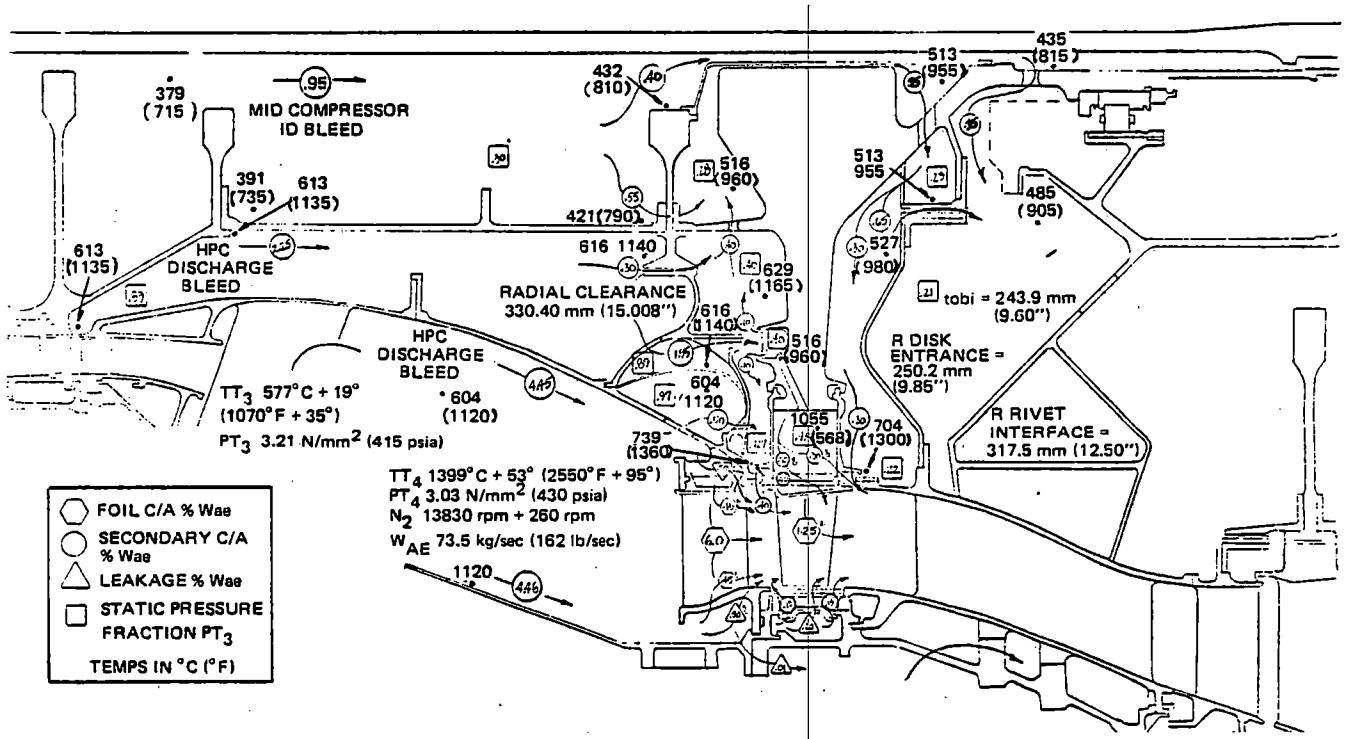

Figure C-59 One-Stage HPT Preliminary Secondary Airflow System Map

Airflow quantities, pressures, and temperatures were also estimated for the turbine transition duct strut and LPT. This analysis identified the need for a HPT rear inner seal. This feature was incorporated to provide a windage shield for the HPT rear disk cavity to reduce static structure drag area. It also maintained lower LPT environmental temperatures by preventing LPT air from mixing with larger amounts of HPT rim cavity air. The seal also provided for potential spool thrust balance trim. The resulting transition-LPT flow map is shown by Figure C-60.

Total resulting secondary system airfoil cooling and leakage flow assessments are tabulated in Table C-LXIX.

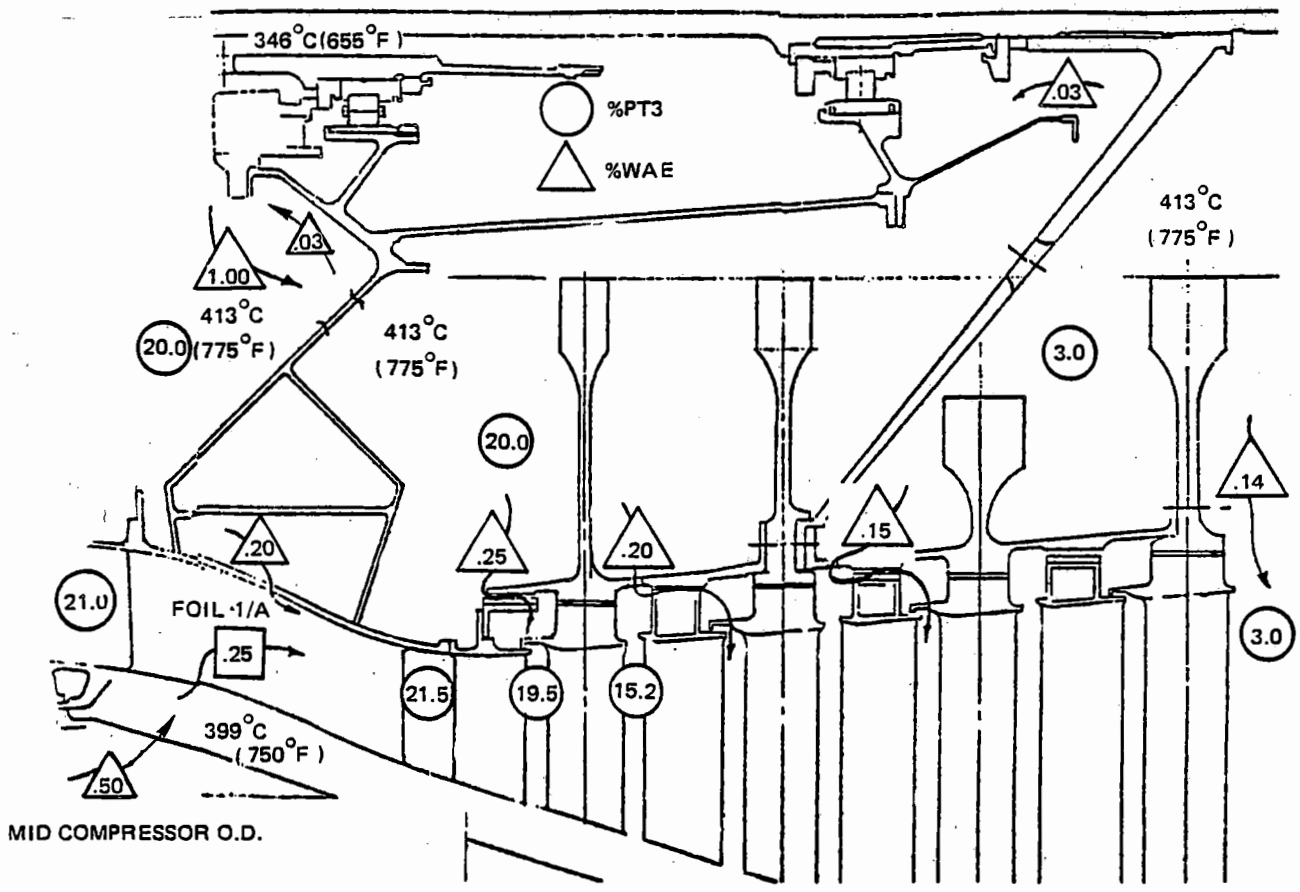

Figure C-60 Direct-Drive, One-Stage HPT Engine LPT/Transition Duct Flow Map

TABLE C-LXIX

ONE-STAGE HPT ENGINE SECONDARY SYSTEM
COOLING AND LEAKAGE SUMMARY

Location	Percentage of Core Airflow
HPT Vane Airfoil Cooling Air	6.00
HPT Vane Platform Cooling Air	0.90
HPT Vane Leakage Air	1.00
HPT Blade Airfoil Cooling Air	1.25
HPT Disk Front Rim Cavity Cooling Air	0.40
HPT Disk Rear Rim Cavity Cooling Air	0.60
HPT Disk Platform Cooling Air	0.40
HPT Outer Airseal Cooling Air	0.30
HPT Outer Airseal Leakage Air	0.20
HPT Case/Flange Leakage Air	0.01
Transition Strut Cooling Air	0.25
Transition Duct Leakage Air	0.20
LPT Inner Leakage Air	0.80
LPT Outer (Case) Leakage Air	0.25
Breathers	0.05
TOTAL	12.61

2.2.3.2.3 Two-Stage HPT Engine – Blade Cooling Feed Assessment

A previously defined "best" two-stage HPT blade cooling feed concept, shown in Figure C-61, was reassessed for the Energy Efficient Engine. This concept utilized a positive vortex TOBI to supply first blade cooling air and a spacer pump located between the two stages to supply second blade air.

A thermal analysis of the complete HPT rotor system was conducted for the Task III engine conditions. Results showed that the initial secondary flow system caused the first disk bore to be hotter by about 50°F than the rim over most of the operating cycle. The second disk maintained a 300°F gradient over most of the operating cycle with no inverse during descent. Also, the blade neck and platform temperatures exceeded desired levels by 300 to 400°F, and rim temperatures were also slightly high.

As a result, the initial secondary flow system was revised to mix mid-HPC and rear HPC bleed air forward of the first HPT disk. Mixed air was allowed to pass over the disk bores and then be pumped to the second stage rim. Rim cooling flow was also increased slightly to achieve the desired level of blade attachment temperature. Mid-HPC air was also used to cool the second stage vane.

Structural feasibility of the critical spacer pump was also reviewed in terms of the engine environment. Bore entry cooling air holes and the assembly bolt holes (See Figure C-61) are the critical portions of this concept. Predicted LCF life for the pump was found adequate in

MERL 76 material, except for the initial bolt circle area. Bolt circle life was reanalyzed as a function of the number of holes. Results are shown in Figure C-62. The conclusion reached was that for satisfactory life, a minimum of 12 tiebolts and 12 shielding holes had to be provided. The first disk bolt circle life was checked with this change in configuration and was found to be acceptable in MERL 85 material.

2.2.3.2.4 Two-Stage HPT – Secondary Airflow System

Based on the reassessment of the critical portions of the two-stage HPT blade cooling feed concept, a preliminary secondary airflow system map for the HPT was configured. This map summarized secondary flow quantities, air pressures, and air temperatures, as shown in Figure C-63.

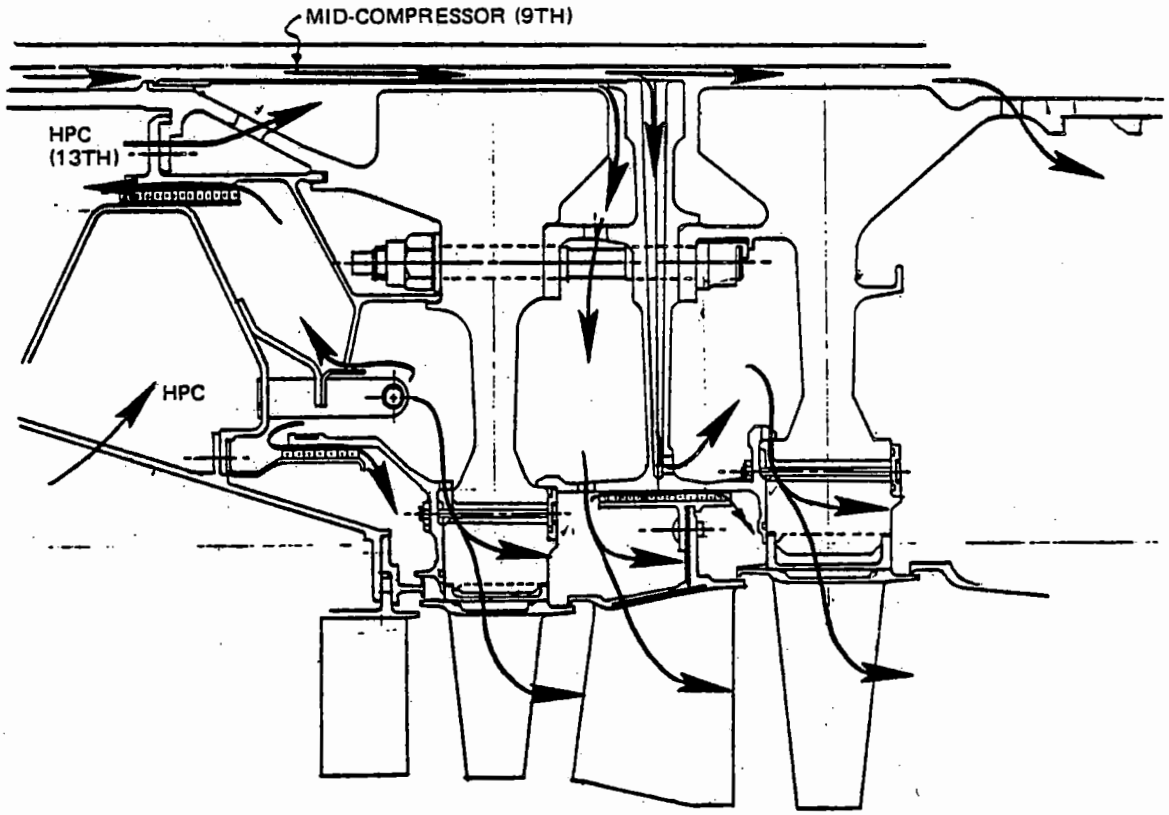

Figure C-61 Two-Stage HPT Blade Cooling Feed Concept

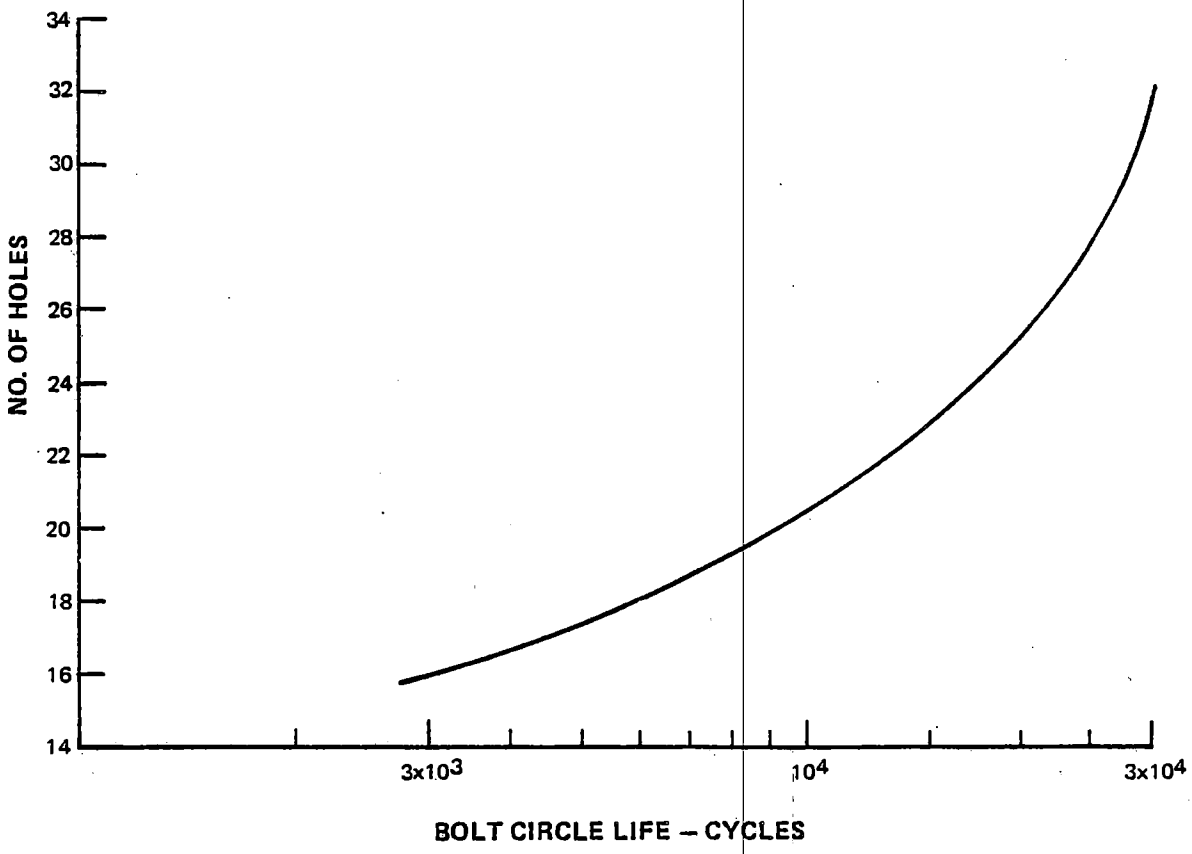

Figure C-62 Two-Stage HPT/Pump Bolt Circle Life Versus Number of Holes

Total secondary system airfoil cooling and leakage flow assessments are presented in Table C-LXX.

2.2.3.2.5 Geared Fan Engine Low-Rotor Thrust Balance Study

Analysis was undertaken to establish the critical low-spool thrust balance for the geared engine resulting from the reduction gear divorcing the traditional forward thrust component of the fan from the rearward component of the LPT. Thrust requirements of the fan were considered in the sizing of the large fan ball bearing in the reduction gearbox assessment. The study described here addressed the thrust balance of the LPC-LPT spool.

The first step taken in the thrust balance was to size the LPC ball (thrust) bearing. A number of bearings were investigated with bore diameters ranging from 15 to 30 cm (6 to 12 in.) and ball diameters from 2.5 to 4.5 cm (1.00 to 1.75 in.). Large bore diameter bearings were found to drop off in capacity because of the centrifugal loading of the balls. Smaller ball diameters were also anticipated to be inadequate.

Potential aerodynamic thrust balance was then assessed by adding wide channel seals at the front and rear of the LPT as shown by Figure C-64. With both seals located at 28.5 cm (11.2 in.) radius, and front and rear seal flows of 0.15 % and 0.32% core airflow, respectively, a minimum thrust load was obtained.

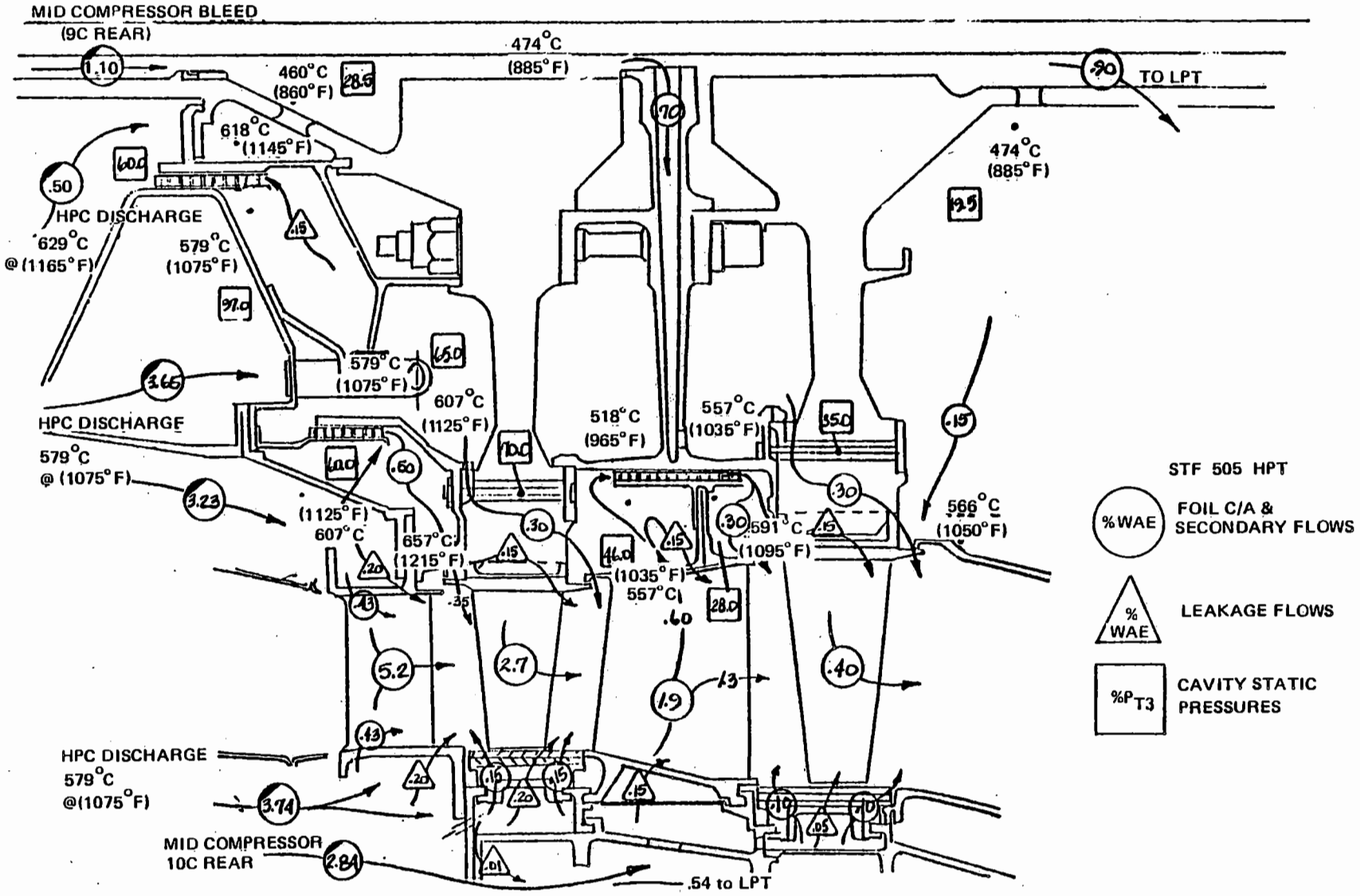

Figure C-63 Two-Stage HPT Preliminary Secondary Airflow System Map

TABLE C-LXX

TWO-STAGE HPT ENGINE SECONDARY SYSTEM
COOLING AND LEAKAGE SUMMARY

Flow Location			$\%W_{AE}$
Air Foils	1st Vane		6.15
	1st Blade		2.00
	2nd Vane		1.50
	2nd Blade		0.30
		Total	9.95
HPT Secondary	1st Vane Platform		1.00
	1st Outer Air Seal		0.30
	2nd Vane Hook		–
	2nd Outer Air Seal		0.20
	1st Disk Front		0.35
	1st Disk Rear		0.30
	2nd Disk Front		–
	2nd Disk Rear		0.45
		Total	2.60
HPT Leakage	1st Vane Platform		0.40
	1st Outer Air Seal		0.20
	1st Blade Platform		0.15
	1st Disk Sideplate		–
	2nd Vane Platform		0.15
	2nd Outer Air Seal		0.05
	2nd Blade Platform		–
	2nd Disk Sideplate		–
		Total	0.95
LPT Secondary	Disks		0.65
	ID EGV		0.14
	Case		0.40
		Total	1.19
LPT Leakage	3rd Vane ID	Total	0.20
O/B	Breathers		0.05
	Flanges		0.01
		Total	0.06
Total Flow Hot Section			14.95

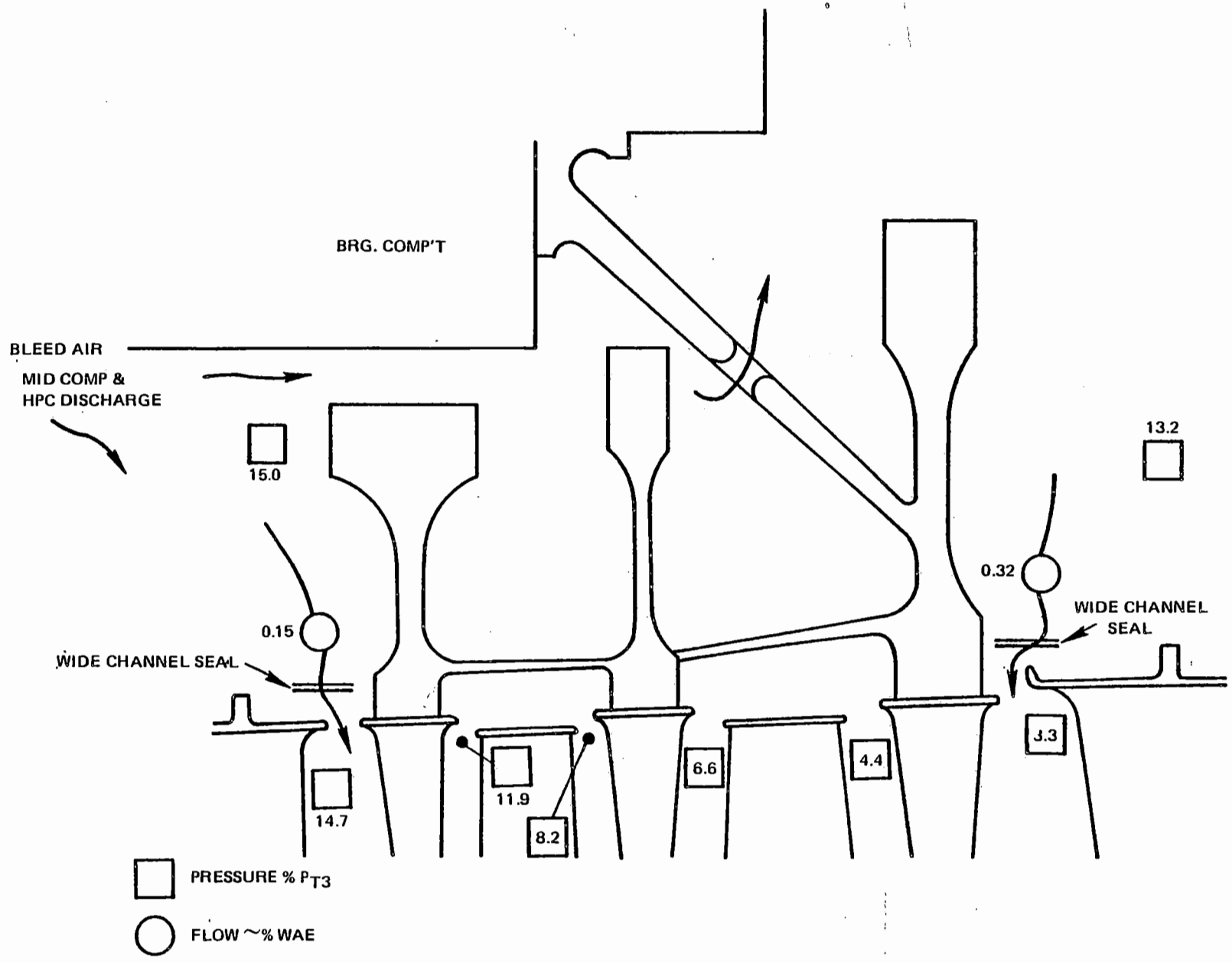

Figure C-64 Geared Engine Low-Pressure Turbine Wide Channel Seals for Thrust Balancing

To adequately balance the calculated low spool thrust load, a feasibly sized LPC ball bearing with 15 cm (6 in.) diameter bore and a 3.8 cm (1.5 in.) diameter ball was selected.

2.2.3.3 Clearance Control Analysis

The overall clearance control approach taken in the Task III preliminary engine design was aimed at achieving and maintaining reduced rotor tip clearances essential to meeting the component efficiency goals. Many advanced clearance control concepts were utilized to make this possible. Major clearance control features incorporated were nacelle duct (cowl) – engine case load sharing, straddle mounted high spool, stiff rotor and case construction, thermal matching of the rotor and case, and active clearance control. These design concepts are discussed in the following paragraphs. A more detailed discussion of the engine bearing arrangement selection is addressed in Paragraph 2.2.3.4.

2.2.3.3.1 Cowl Load Sharing

On current Pratt & Whitney Aircraft engine installations, the thrust reaction and the transverse component of the cowl air loads combine to produce a large bending moment (Ma) on the engine core cases hurting tip clearances. Since this problem is accentuated as bypass ratio increases, it was imperative that the Energy Efficient Engine design significantly reduce this effect. As a result, the concept of load sharing was created. In the design, load sharing was accomplished by providing load paths at the rear of the fan exit case, at the turbine case, and at the pylon hinges. To make this concept totally successful, attention will have to be paid in the final detailed design integration to flight load predictions over the engine operating envelope and to ensure that nacelle latch designs are such that all load paths through the cowl doors are unbroken. Figure C-65 illustrates the load paths with and without cowl load sharing.

Pratt & Whitney's best current experience with nacelle-engine load sharing is the Common Nacelle System (CNS) on the JT9D-59/70 engines which incorporates structural I.D. and O.D. fan ducts, while still providing easy access for maintenance, as shown in Figure C-66.

For substantiation, an analysis was conducted to assess the capability of a structural I.D. duct on the Energy Efficient Engine. A static deflection analysis was used to evaluate the relative load capability and deflections of various sections of the engine and nacelle. The analysis considered cases, rotors, ducts, etc. as beams carrying both bending and shear loads. The principal simulated applied loads were thrust reactions that do not act on the engine centerline and normal (in-flight) cowl air loads. Figure C-67 shows the results as a function of duct face thickness. These results show that a structural I.D. duct alone can be designed to carry up to 70% of the imposed moment. Combining this result with the addition of a structural O.D. duct, and paying careful attention to latching and load paths in the final engine/nacelle/airframe integration resulted in the projection that 90% of the moment could be carried in the Energy Efficient Engine ducting.

A rotor tip clearance study was also conducted to evaluate the benefits of cowl load sharing. In this analysis, both I.D. and O.D structural ducts were simulated. Normal (once per flight) maneuvers and cowl air loads at sea level takeoff were imposed, and the resulting changes in rotor tip-to-component case gap were estimated.

The resulting potential component tip gap reductions due to cowl load sharing are summarized in Table C-LXXI.

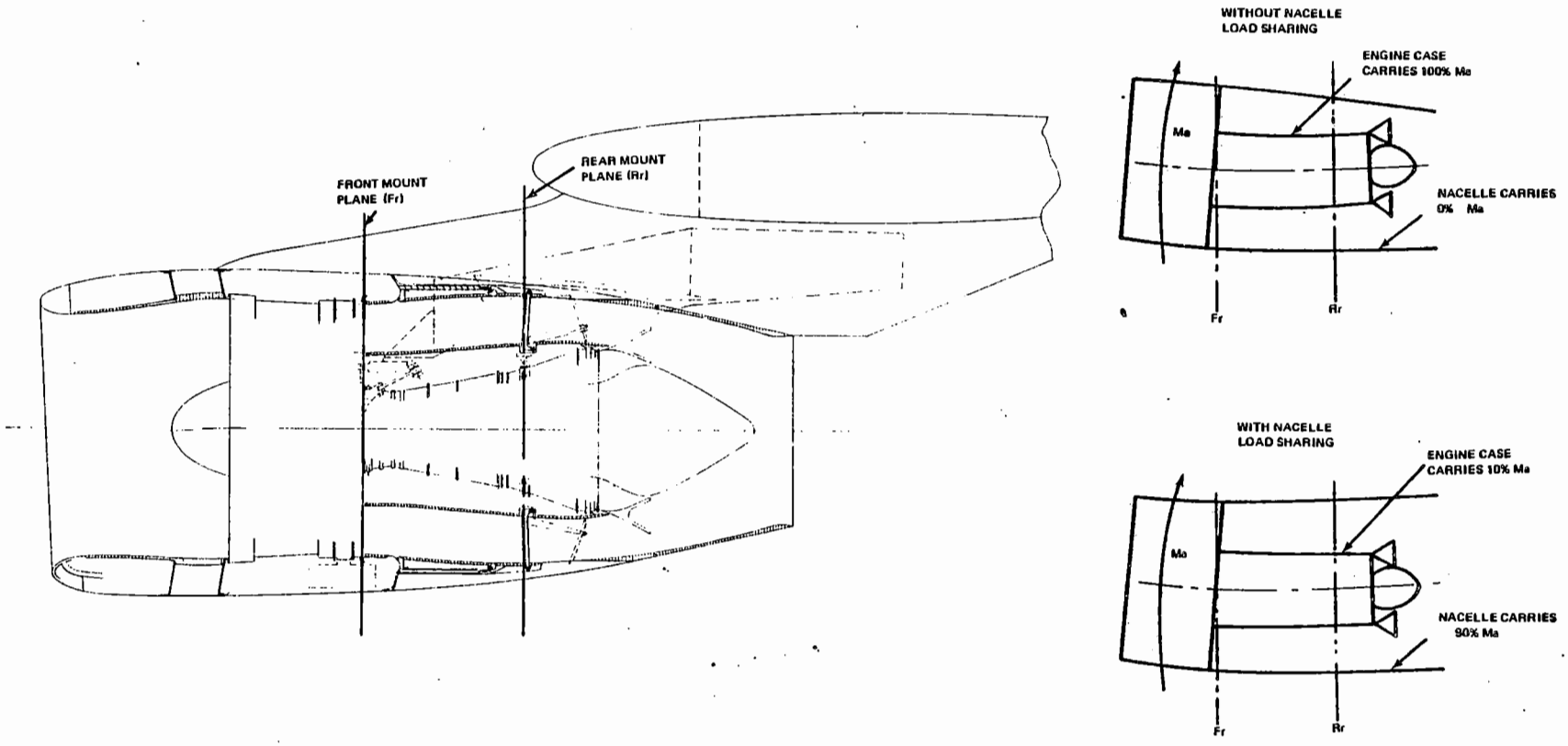

Figure C-65 Benefits of Engine-Nacelle Load Sharing

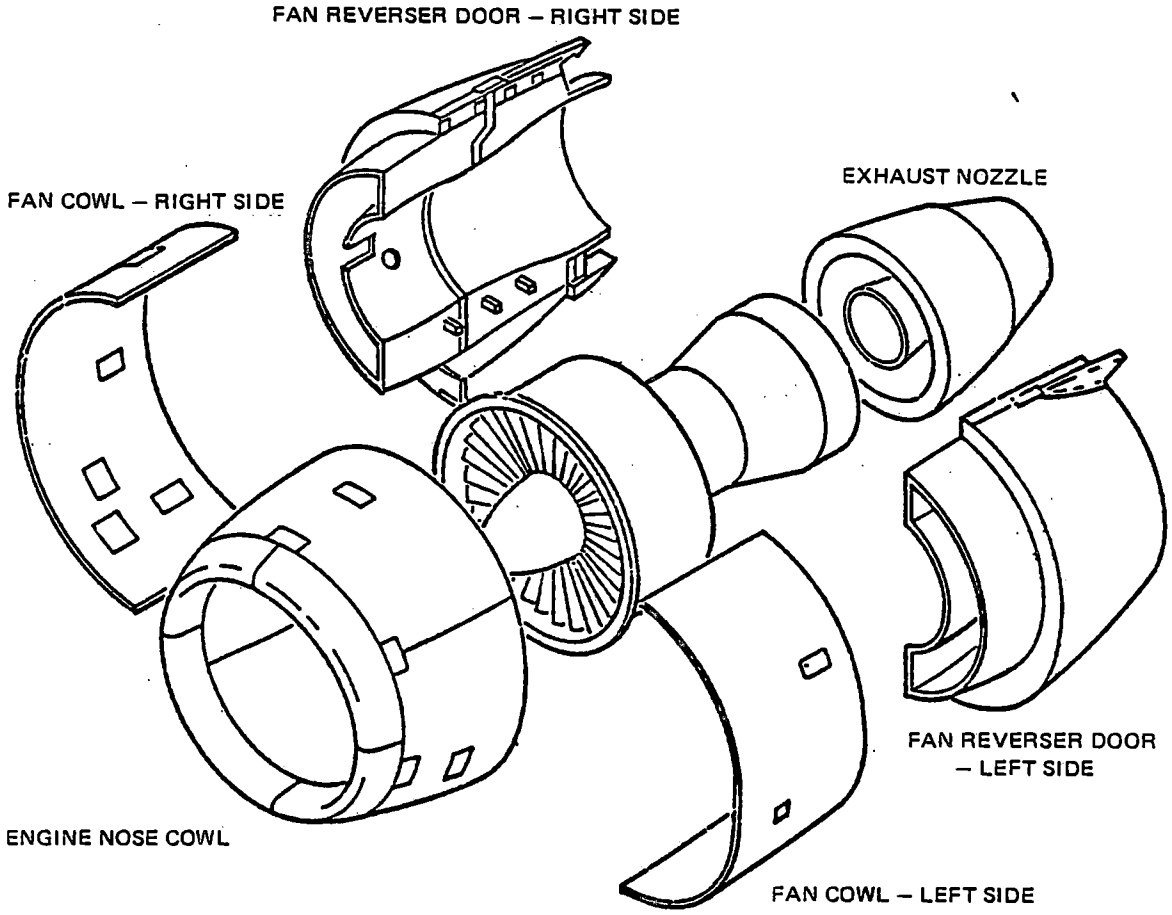

Figure C-66 Common Nacelle System

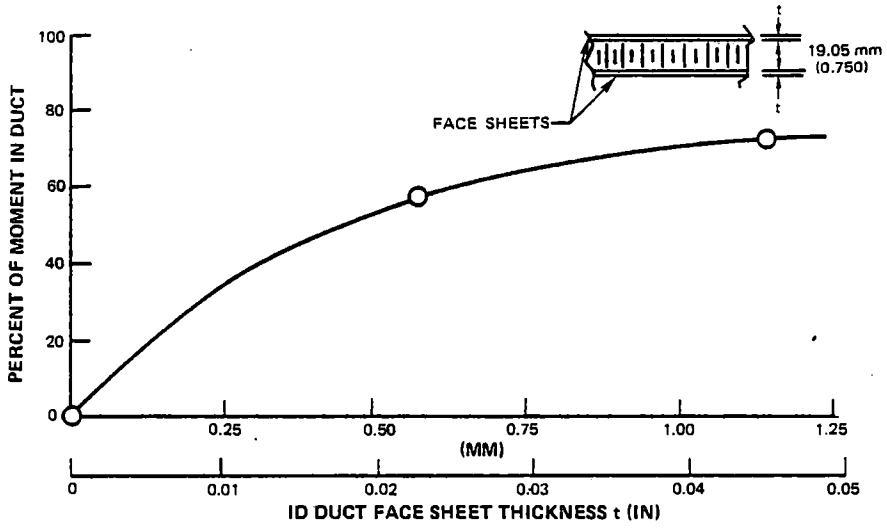

Figure C-67 Results of Static Deflection Analysis of Structural Fan Ducts

TABLE C-LXXI

POTENTIAL TIP GAP REDUCTIONS
WITH COWL LOAD SHARING

(SLTO)

	Tip Gap Reduction mm (Inches)
Fan	1.27 (0.0500)
HPC Front	0.18 (0.0070)
HPC Rear	0.10 (0.0040)
HPT	0.03 (0.0010)
LPT	0.013 (0.0005)

2.2.3.3.2 Stiff Rotor/Case Construction

Component clearance control was also obtained by purposely designing the engine rotors and cases to be stiff. The basic approach taken to accomplish stiffness was to pay particular attention to the overall mechanical arrangement of the components. Short length and proper load paths were the major concerns in determining the mechanical arrangement.

Shortness in the high rotor was achieved by high speed to minimize the number of HPC stages. The parametric HPC studies included consideration of length in the configuration selection process. Moderate HPC aspect ratios were chosen, as a result. Diffuser length was shortened as much as possible with an acceptable pressure loss, and burner length was minimized while maintaining combustion characteristics required for low emissions, high efficiency, and durability. The single stage HPT designs were also found to shorten high spool length considerably.

Low spool shortness was accomplished by utilizing the fan-HPC transition section for the LPC and limiting the LPT to four stages for the direct drive fan engines. In the case of the geared fan engines, high speed was incorporated to further minimize the number of LPC and LPT stages. In addition, the highest feasible aspect ratios were utilized in the LPC's and LPT's.

Additional stiffening of the rotors was achieved by improved rotor support. Straddle mounting of the high rotor with bearings located under the HPC front and HPT rear with bearing supports at these locations provided the desired stiffness.

A two-bearing fan-LPC rotor configuration with large wheelbase provided a stiff support system to minimize deflections of these components. LPT rotor deflection control was achieved by placing the bearing directly underneath. Additionally, maximum shaft diameters were used for stiffness to further minimize deflections.

Stiff case construction resulted directly from the general shortness of the engines. In addition, care was taken in designing the case configurations and flanging to handle the imposed loads.

The stiff rotor and case construction features described here were incorporated into the base engine configuration used in the cowl load sharing analyses discussed above.

2.2.3.3.3 Thermal Matching

Thermal matching of rotors and cases in the engine design was achieved by proper selection and utilization of materials and analysis of rotor-case growths throughout the critical engine operating transients.

Case and rotor materials with compatible coefficients of thermal expansion were selected to ensure similar growth. Also, tip seal designs were configured such that seal and case thermal growths were simultaneous.

Thermal analyses were made to evaluate rotor and case growths and clearances and to determine which components would benefit from the application of active clearance control (ACC). These analyses were conducted by scaling results from previous detailed design analyses, where appropriate, and by using general shell and finite element analyses else-

where. They were done for accelerations from idle to takeoff and decelerations from takeoff to idle to determine rotor-case clearance pinch points. Clearance estimates were also made for the maximum cruise aerodynamic design point. A typical result of the rotor-case thermal response and active clearance control behavior analyses is shown in Figure C-68.

These thermal analyses indicated that ACC should be applied to the rear of the HPC, the HPT, and the front LPT stages. Fan analysis indicated a potential for a 25% reduction in cruise tip clearance equivalent to about 0.1% TSFC reduction, but the complication of ACC was felt not to justify the benefit. Analysis of the LPC indicated excellent rotor-case thermal response as designed, negating a requirement for ACC. HPC results indicated that while all stages could benefit from ACC, the rear stages could achieve the largest gain. As a result, since ACC application to the variable front stages would be difficult, it was decided to consider only the last seven stages. ACC for the HPT was found to be required because of the large clearances estimated to handle the deceleration pinch resulting from the large mass of the high speed disks. LPT analysis showed a deceleration pinch caused by rapid case response associated with it responding to the secondary flow environment rather than that of the gaspath. The resulting requirement for relatively large clearances in the performance-sensitive front stages made the LPT a candidate for ACC.

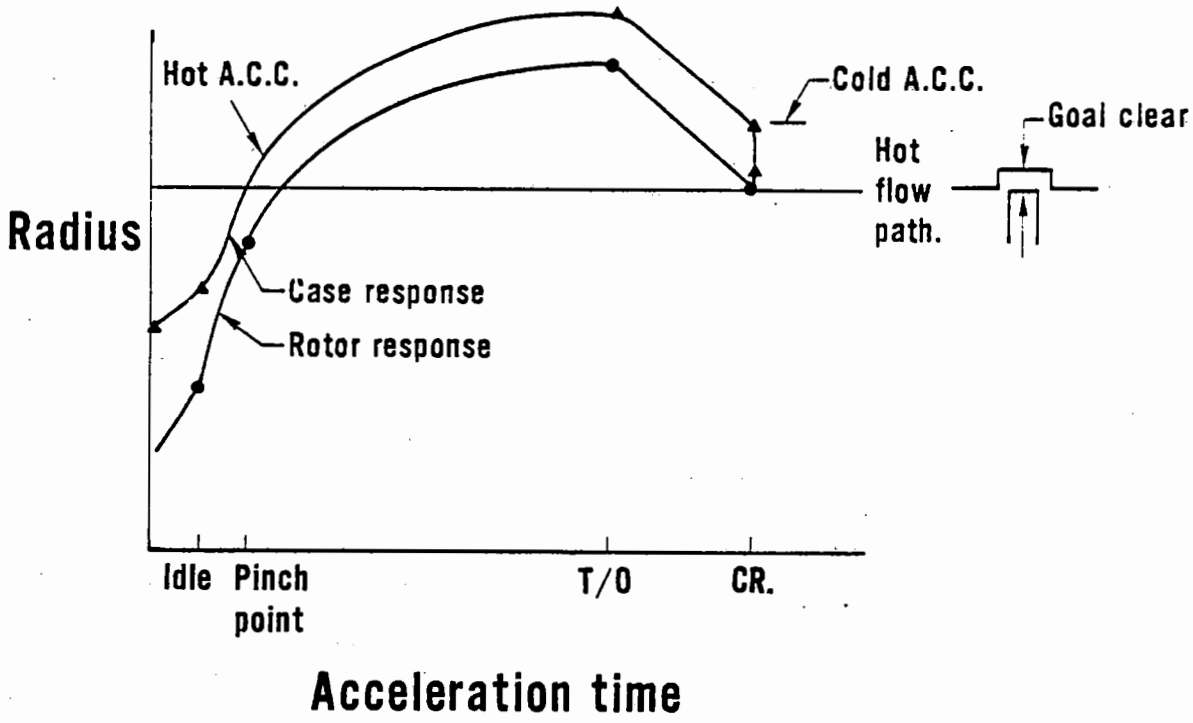

Figure C-68 *High Pressure Compressor Thermal Response and Active Clearance Control Behavior During Acceleration – Shows prevention of pinch point rub by case heating and achievement of cruise clearance goal by case cooling.*

2.2.3.3.4 Active Clearance Control

An initial screening study was made of several ACC concepts in order to select a preliminary approach for the engine. The objective of the systems considered was to provide for minimum tip seal clearances at cruise and adequate clearances at the identified pinch points to prevent excessive rubs and subsequent performance loss. Candidate systems considered were heating the case through transients to takeoff, cooling the case at cruise, and a mechanical case closure at cruise and opening at takeoff. These concepts are shown in Figure C-69 and described in the following paragraph.

The heated system was configured to collect and pipe HPC discharge bleed air to the component and, for the HPC and HPT, impinge the air on the component case to control its temperature. For the LPT, the hot air was discharged internal to the case. The cold system used fan duct airbleed piped to and impinged on the component. The mechanical system, considered and immediately discarded because its complexity was not warranted to achieve the relatively small amounts of closure required, used a pneumatically actuated piston to cause slight rotation of a ring which, in turn, rides up an inclined surface on each component stage to change the circumference and consequently, the diameter of a split case.

The hot and cold systems were evaluated as to their estimated tip clearance change capability and their weight and cost. These results are summarized in Table C-LXXII.

Performance effects of the ACC airbleed were also estimated since the cold system uses fan bleed continuously at cruise and the hot system uses it continuously at takeoff. In addition, fan airbleed was required to vent and maintain a safe temperature limit of 149°C (300°F) in the compartment between the engine case and fan I.D. duct with the hot external systems. These TSFC results are presented in Table C-LXXIII.

TABLE C-LXXIII

PERCENT ACTIVE CLEARANCE CONTROL AIRBLEED TSFC PENALTY SUMMARY

	Cold System		Hot System	
	T. O.	ADP	T. O.	ADP
HPC	0	0.63	0.60	0
HPT	0	0.15	0.94	0
LPT	0	0.39	0.32	0

The general conclusion was that no ACC concept should be selected until a combined hot and cold system was configured and evaluated.

Knowledge gained in the initial ACC screening study was combined to configure a concept felt to be the best baseline system for the engine. It combined the best features of the hot and cold internal systems in terms of simplicity, cost, weight, and overall performance.

TABLE C-LXXII

ACTIVE CLEARANCE CONTROL CONCEPT EVALUATION SUMMARY

	Cold System			Hot System		
	Weight - kg (lb)	Cost-$	Clearance Change	Weight-kg(lb)	Cost-$	Clearance Change
HPC	Base	Base	Goal	-2.3 (-5)	-1000	Goal
HPT	Base	Base	Goal	-0.5 (-1)	- 900	Goal
LPT	Base	Base	Goal+	-7.7 (-17)	-8100	Goal-
Bleed Air Valving	Base	Base	–	-0.5 (-1)	- 400	–

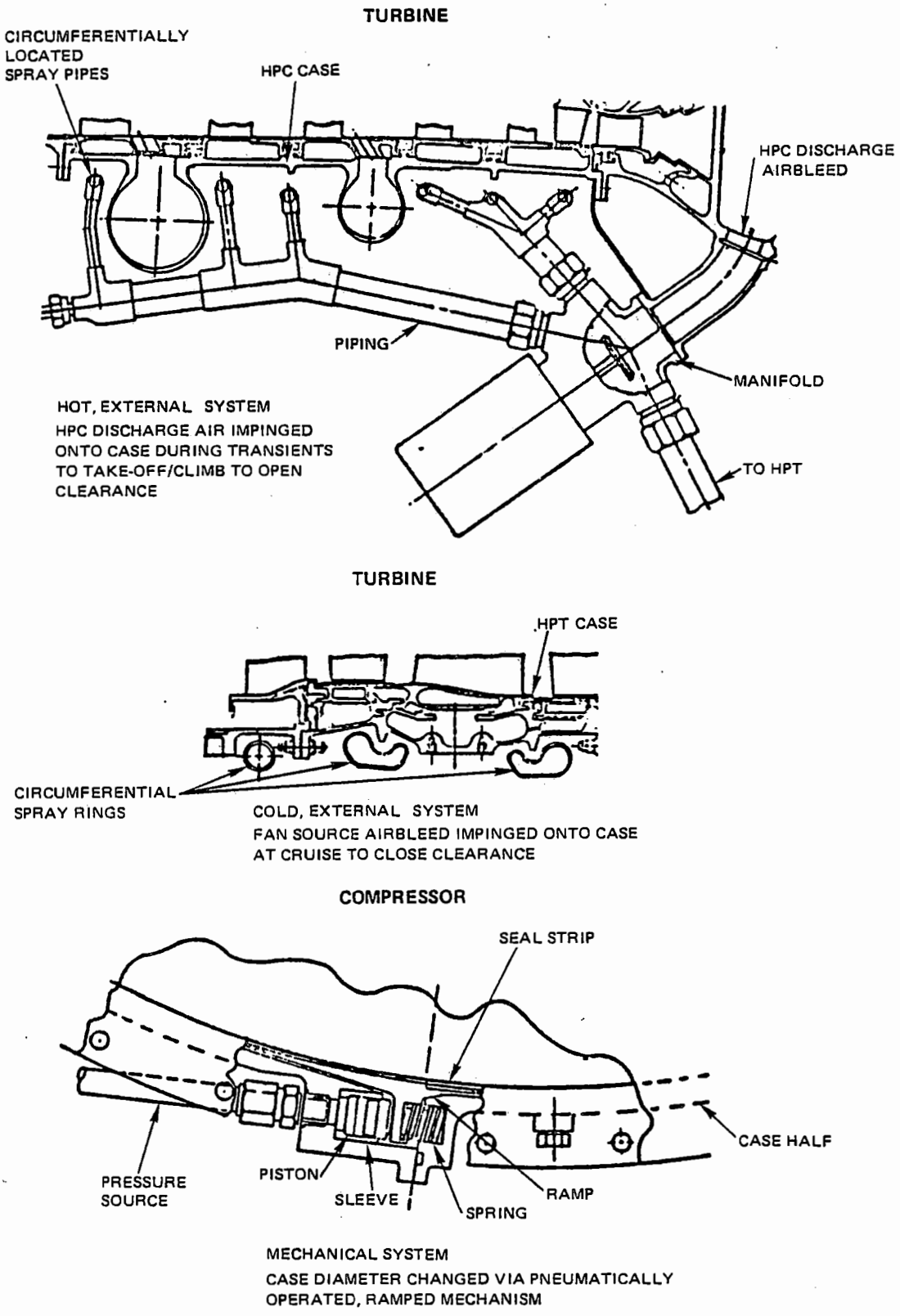

Figure C-69 Active Clearance Control Concepts

The resulting hot/cold ACC system is shown in Figure C-70. At takeoff, the system utilizes HPC hot discharge air which is bled from the diffuser case wall into an internal manifold at the forward end of the case. The discharge air then flows both directly to the turbine section and through an annulus that surrounds the rear stages of the HPC case, and then also through tubular manifolds to the turbine section. The air then flows along the inner surface of the HPT and LPT case walls. The HPC discharge air provides the necessary blade tip-case clearances for transient operation from idle to takeoff and maneuver loading during takeoff and climb. At the cruise condition, the valving shuts off the flow of HPC discharge air allowing cooler, mid-HPC air to flow both directly to the turbine section, and within the HPC rear case and then through the tubular manifolds to the HPT and LPT cases. The mid-HPC air cools the cases, reduces their diameter, and results in decreased tip clearances.

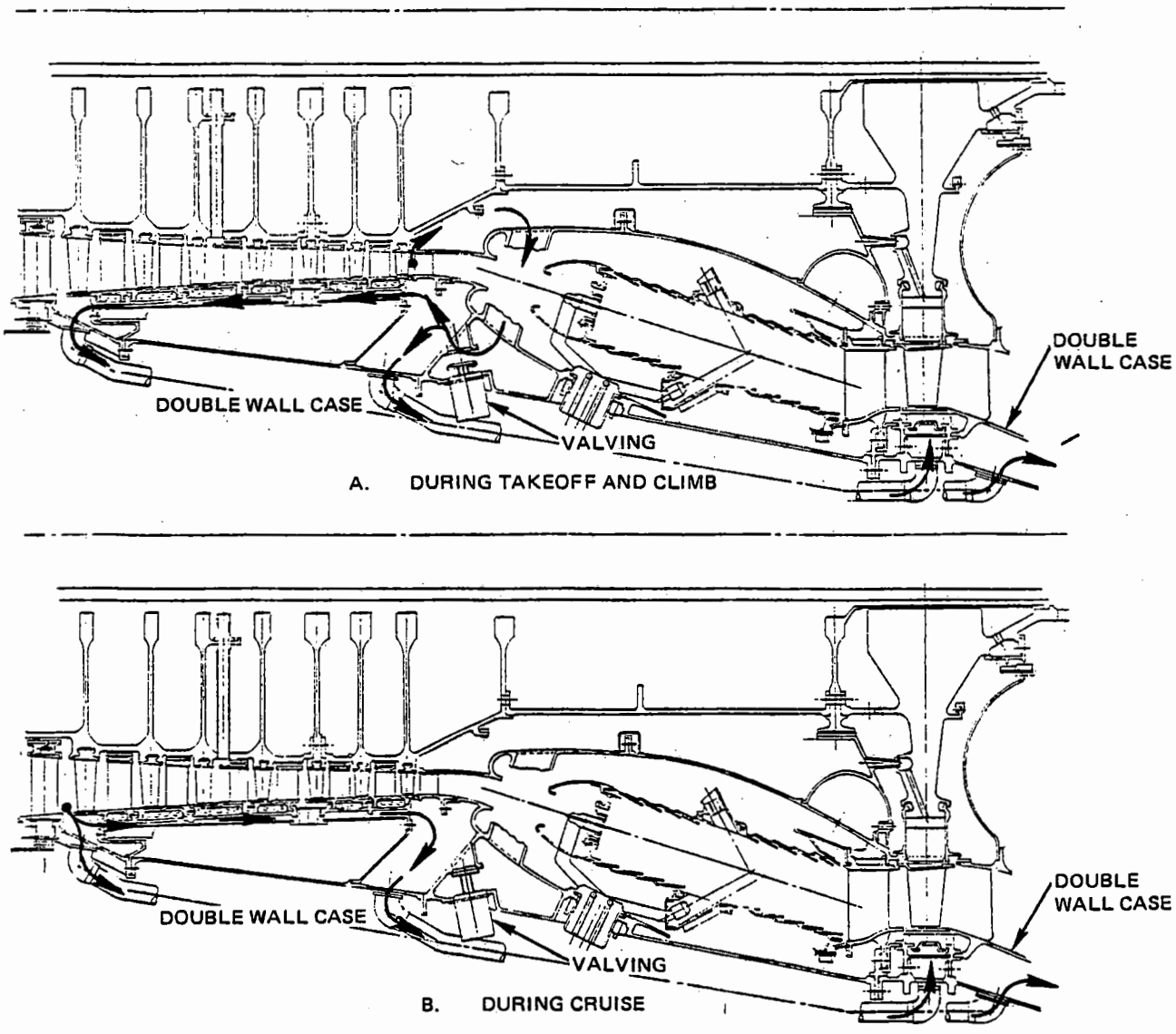

Figure C-70 Selected Baseline ACC System

All valving is done with a single actuator at the diffuser case bleed manifold. Elimination of valving at the mid-HPC location was made possible by designing a controlled ACC air pressure loss into the double-wall HPC case during takeoff and climb-operation. The pressure level of the HPC discharge bleed is reduced so that it will not re-enter the HPC at the mid-location. At the same time, its pressure level is not reduced to the point where air is allowed to escape the HPC at that location.

2.2.3.4 Structural Analysis

Preliminary bearing and bearing support arrangements selected in Task I for the direct-drive and geared fan engines were reviewed in terms of critical speeds and maneuver tip gap reductions. In this process, a major objective was to reduce the number of bearings to a minimum required for good rotor support, because of the high cost and weight penalties associated with the straddle-mounting-of-all-components approach taken in Task I. The major concerns addressed were the differences between one- and two-stage HPT high spools, the number of high spool bearings for the direct-drive engine, and the elimination of a critical low rotor mode in the operating range uncovered for the geared fan engine in Task I analysis.

2.2.3.4.1 Direct-Drive Engine Configuration Analysis

A rotor-frame model of the entire direct-drive engine was prepared to analyze critical speed and tip gap reductions. The model was structured to have the capability to assess bearing placement, rotor length, support spring rate, hub stiffness, and weight. It included nacelle load sharing in its make up. Figure C-71 shows this model.

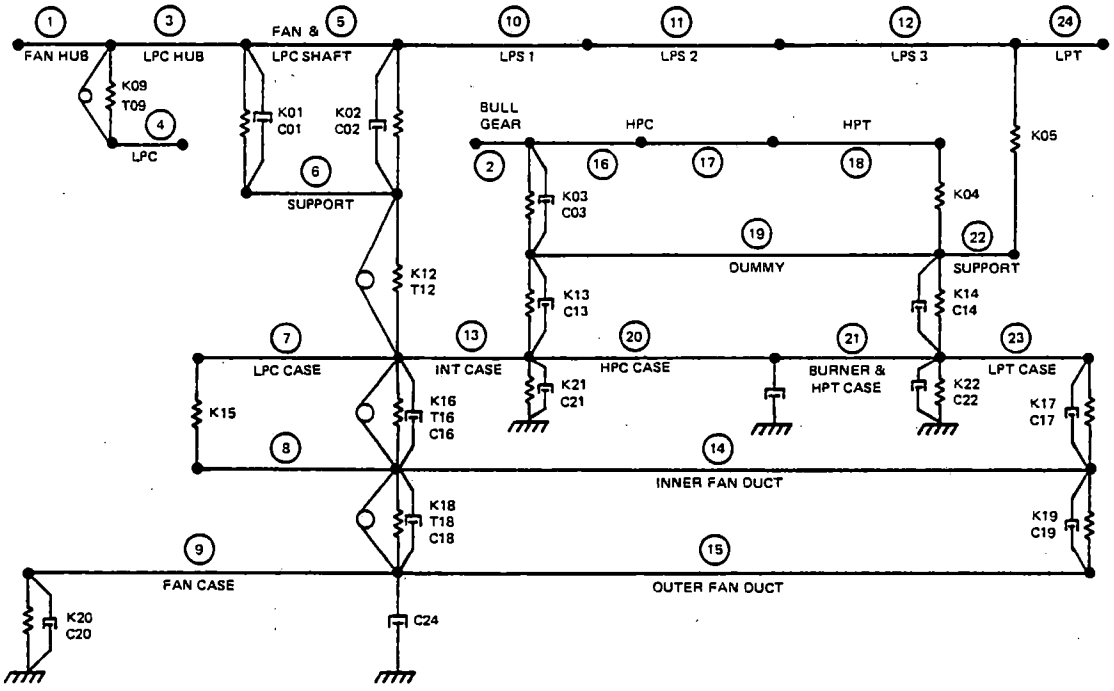

Figure C-71 Direct-Drive Engine Rotor – Frame model

The model was exercised to determine critical speeds. Basic speeds, mode shapes, and strain energies are presented on Figure C-72 for the two high spool bearing/one LPT bearing/one stage HPT configuration. The engine was found to have a high strain energy HPC pitch mode just below redline high spool speed (N_2). It was projected that this mode can be controlled with the incorporation of a viscous damped high rotor thrust bearing. Driving the pitch mode above redline N_2 with desired margin was considered briefly, and rejected when the magnitude of required spool configuration changes became apparent. The high spool was also found to have a high strain energy mode below idle N_2. The engine had no anticipated low rotor mode problems. The HPC pitch mode was also found to be nodal at the diffuser case location. As a result, elimination of the center high spool bearing had little effect on critical speed, or strain energy as shown by Table CLXXIV. Also shown are the results of the exercise to study the effect of one vs. two LPT bearings and one- vs. two-stage HPT's. Removal of the additional LPT bearing was found to have minimal effect on critical speeds. The two-stage HPT resulted in lowering the HPC pitch mode N_2, although it remained in the operating range.

The rotor frame model was used again to calculate tip gap reductions, as functions of imposed normal (once per flight) takeoff and cruise maneuver loadings, for the several engine configuration variations. Results are summarized in Table C-LXXV for the key components.

Maneuver tip gap reductions for the three bearing high spool and the straddle mounted LPT were found to be lower, offering some potential improvement in long-time operational performance. However, the weight and cost reductions associated with the removal of these bearings, e.g., 50 lbs. and $13,500 for the center high spool bearing, are the more significant benefits. As a result, the two bearing high spool and one bearing LPT configurations were selected for the direct-drive fan engine.

The added length associated with a two-stage HPT was observed to have negligible effect on maneuver tip gap reductions.

2.2.3.4.2 Geared Engine Configuration Analysis

The Task I geared fan engine critical speed analysis identified two main problem areas. The requirement for a diffuser case supported intershaft bearing was established at the outset by a high strain energy (82%) low shaft mode at about 4100 rpm N_1. Incorporation of the intershaft bearing was the only manner in which to enable the low rotor to run to its redline speed. In addition, the star reduction gear caused counter rotation of the fan and low spool that introduced a high strain energy (42%) high rotor excited low rotor mode in the normal operation speed range (11,800 rpm) that was considered unacceptable. This problem appeared to be caused by the coupling action of the intershaft bearing located between the rear of the fan and the low shaft.

As a result of these problems, an updated rotor-frame model of the geared engine was prepared to reanalyze critical speed and maneuver tip gap reductions. Figure C-73 shows this model.

LOW ROTOR EXCITED LOW ROTOR MODES

N_1 RPM = 2825*

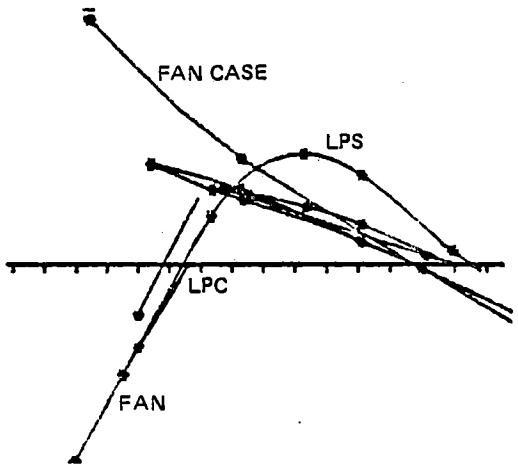

% STRAIN ENERGY

LOW ROTOR	13.14
HIGH ROTOR	0.61
CASES	15.25
SUPPORTS	71.08
K01	17.64 x 10^3 kg/mm (9.88 lb/in)
T12	68.97 x 10^3 kg/mm (38.62 lb/in)
K18	17.48 x 10^3 kg/mm (9.79 lb/in)

HIGH ROTOR EXCITED HIGH ROTOR MODES

N_2 RPM = 5741*

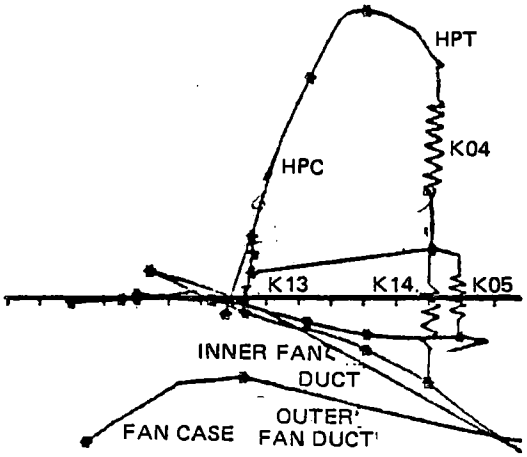

% STRAIN ENERGY

LOW ROTOR	0.66
HIGH ROTOR	19.98
CASES	7.38
SUPPORTS	71.98
K04	62.84 x 10^3 kg/mm (35.19 lb/in)
K14	29.70 x 10^3 kg/mm (16.63 lb/in)
K18	13.34 x 10^3 kg/mm (7.47 lb/in)

N_1 RPM = 3574*

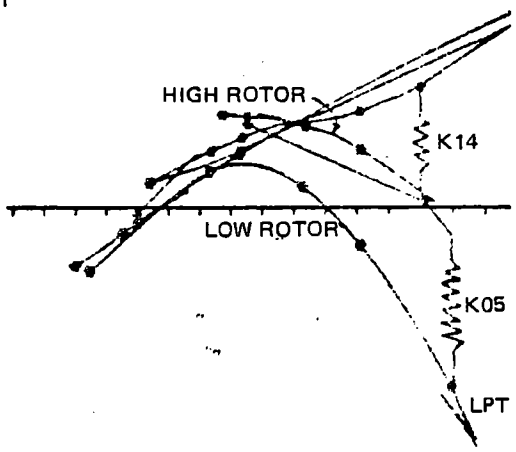

% STRAIN ENERGY

LOW ROTOR	7.82
HIGH ROTOR	1.19
CASES	11.72
SUPPORTS	79.25
K05	67.21 x 10^3 kg/mm (39.97 lb/in)
K14	55.75 x 10^3 kg/mm (31.22 lb/in)

N_2 RPM = 12481*

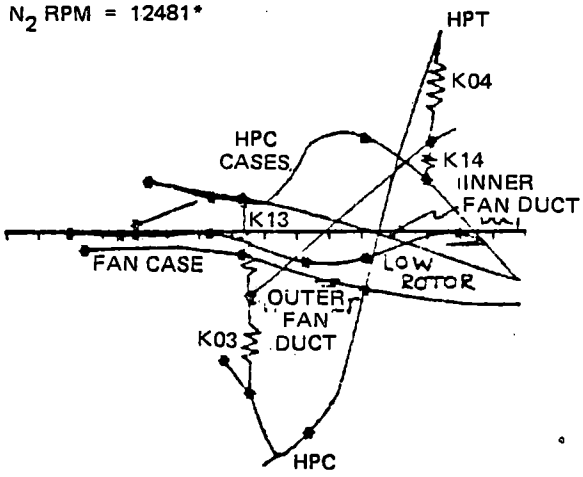

% STRAIN ENERGY

LOW ROTOR	0.89
HIGH ROTOR	32.13
CASES	18.10
SUPPORTS	48.87
K03	30.75 x 10^3 kg/mm (17.22 lb/in)
K13	29.02 x 10^3 kg/mm (16.25 lb/in)

*IDLE: N_1 = 900 RPM, N_2 = 9000 RPM, REDLINE: N_1 = 3710 RPM, N_2 = 12700 RPM

Figure C-72 Direct-Drive Engine Critical Speeds and Mode Shapes

TABLE C-LXXIV

DIRECT-DRIVE ENGINE CONFIGURATION CRITICAL SPEED SUMMARY

Configuration Changes	*Low Rotor Speed N_1 –rpm	Energy–%	*High Rotor Speed N_2 –rpm	Energy–%
Base	2825	13.1	12481	32.1
Three High Spool Bearings	2825	13.1	12816	29.3
Two LPT Bearings	2834	13.6	12481	32.1
Two HPT Stages	–	–	10878	27.6

*Idle: N_1 = 900 rpm, N_2 = 9000 rpm; Redline: N_1 = 3710 rpm, N_2 = 12,700 rpm

TABLE C-LXXV

DIRECT-DRIVE ENGINE CONFIGURATION MANEUVER LOAD
TIP GAP REDUCTION SUMMARY

Configuration Changes	Component	Tip Gap Reductions – mm(inches) Takeoff	Cruise
Base	–	Base	Base
Three High Spool Bearings	HPC Rear	-0.08 (-0.0031)	-0.05 (-0.0021)
Two LPT Bearings	LPT Front*	+0.018 (+0.0007)	-0.03 (-0.0010)
Two HPT Stages	HPT	-0.005 (-0.0002)	-0.003 (-0.0001)

*Tip gap reductions in the rear LPT stages were greater, but rear stage performance is less sensitive to tip clearance and design improvements are anticipated.

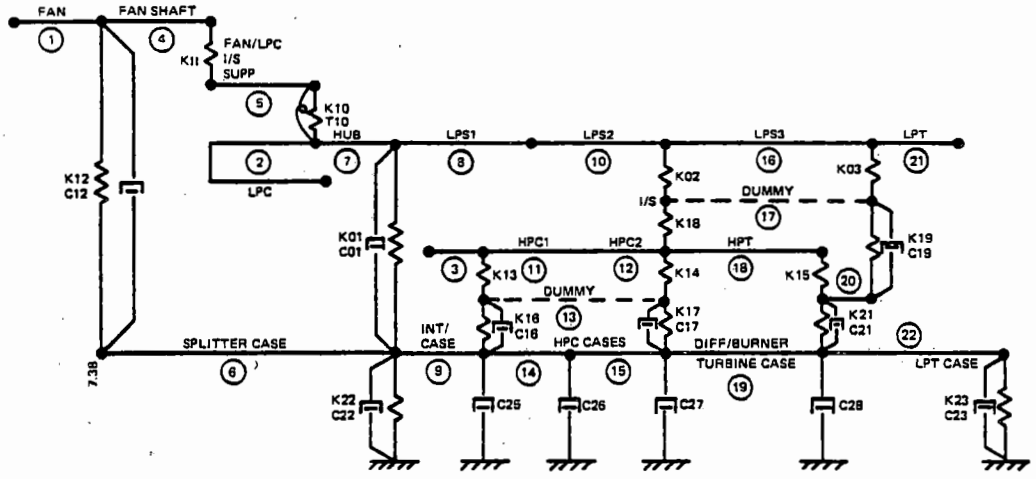

Figure C-73 Updated Geared Engine Rotor Frame Model

This model was used to predict both high and low rotor excited modes for the engine. Resulting critical speeds, mode shapes, and strain energies are shown on Figures C-74 and C-75. The high rotor excited low spool mode identified in the running range at 13654N_2 (Figure C-74) was projected to be controllable by an oil damped bearing. The previously identified high rotor excited low spool mode (Figure C-74) introduced by the counter rotational fan-low spool star gear system was found to occur again at 11813 rpmN_2 with a strain energy in excess of 42%. This problem was resolved by a redesign which eliminated the intershaft bearing between the fan and low shafts, thereby decoupling them. A below idle HPC mode at 9769 rpm N_2 (Figure C-74) was also identified. Strain energies associated with the low rotor excited low rotor modes (Figure C-75) were found to be significant, but within the level allowed and, therefore, acceptable.

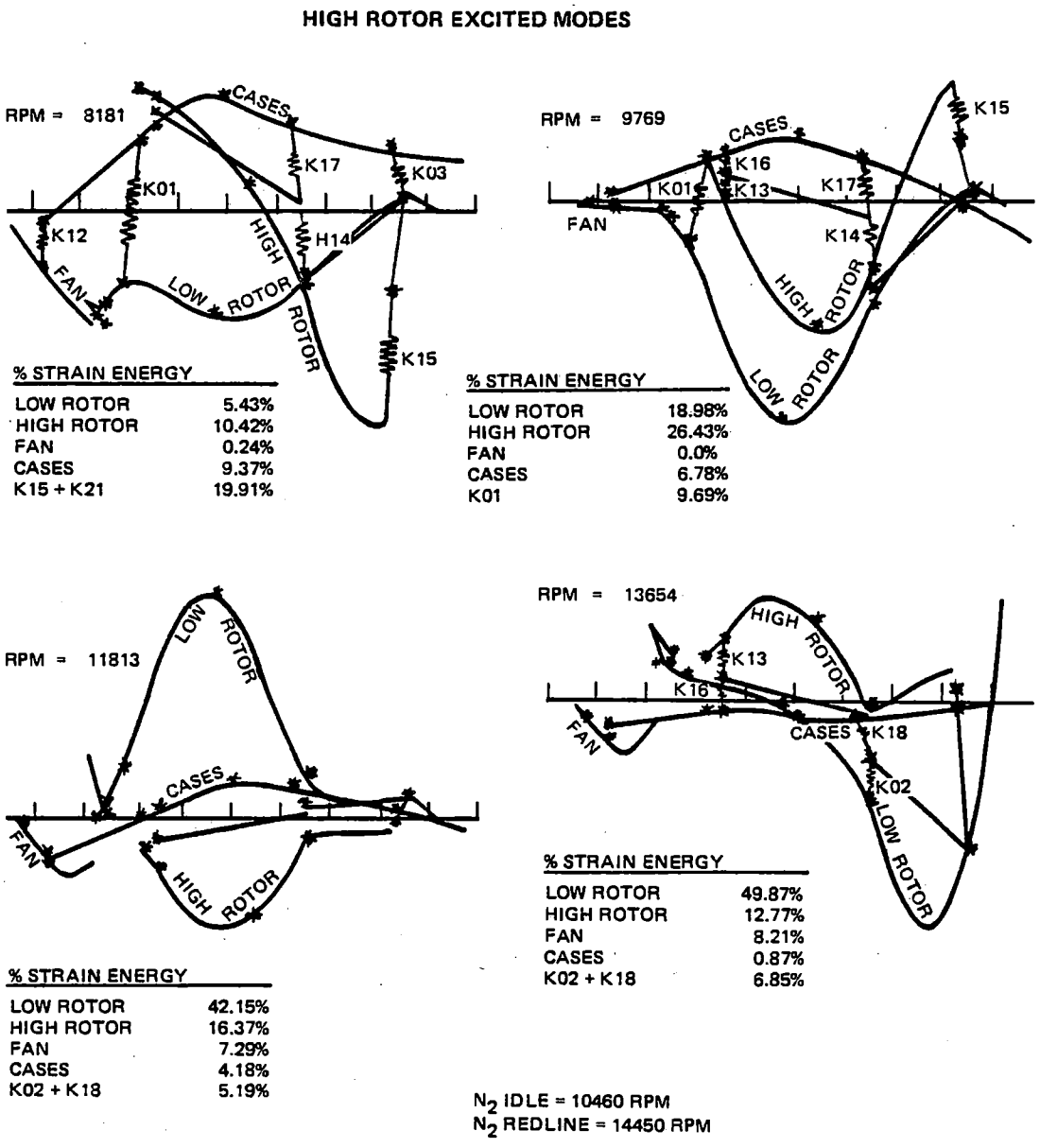

Figure C-74 Updated Geared Engine High Rotor Excited Critical Speeds and Mode Shapes

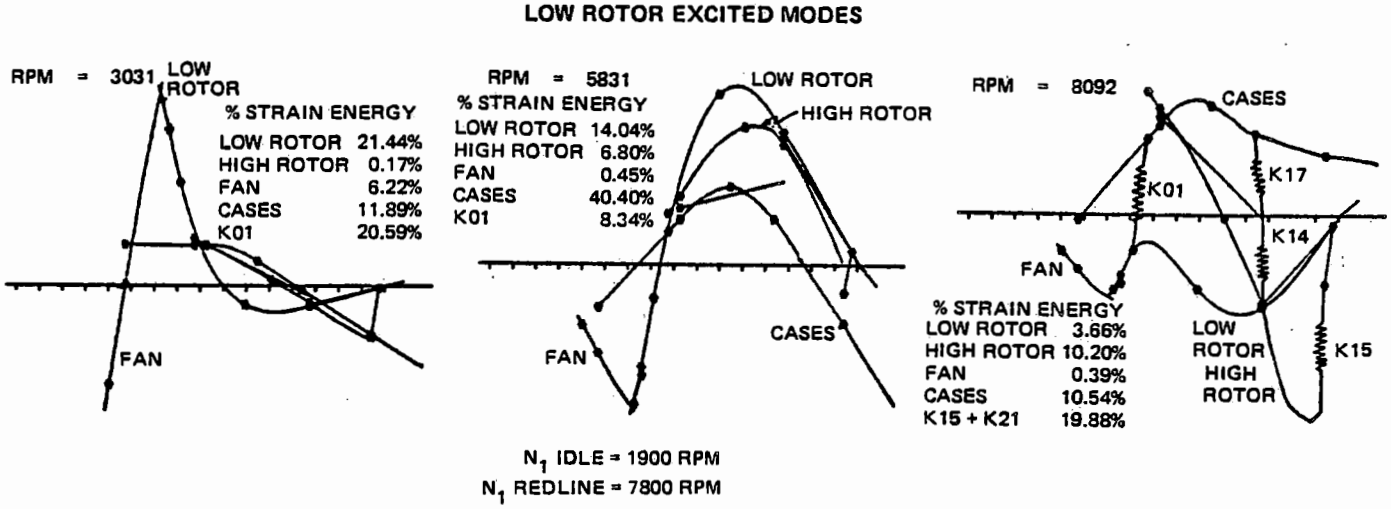

Figure C-75 Updated Geared Engine Low Rotor Excited Critical Speeds and Mode Shapes

Maneuver tip gap reductions were calculated at takeoff and cruise, and found to be generally lower for all components relative to those for the direct drive engine.

The bearing configuration for the geared fan engine was as follows:

- Fan (as in direct-drive case) supported on a ball and a roller bearing
- LPC front supported on a ball bearing
- LPT supported on a roller bearing
- An intershaft bearing in the diffuser location for critical speed control
- HPC front supported on a ball bearing
- HPT rear support on a roller bearing
- A roller bearing to support high spool and intershaft bearing located in the diffuser.

Bearing support frames were located as follows:

- Front support between fan and LPC
- Intermediate support between LPC and HPC
- Center support at diffuser case
- Rear support between HPT and LPT.

2.2.3.5 Fuel/Lubrication/Accessory Systems Analysis

2.2.3.5.1 Fuel System Analysis

The fuel system preliminary design effort was concentrated on simplification of the distribution system for the Vorbix combustor and identification of a basic fuel control concept.

Several trade studies were conducted to evaluate cost effects of fuel injector quantity, fuel manifold shielding methods, and injector supports. The effects of typical combinations of injectors on combustor cost are summarized in Table C-LXXVI. It is apparent from these results that the minimum feasible number of injectors should be used.

TABLE C-LXXVI

COMBUSTOR COST EFFECT OF FUEL INJECTOR QUANTITY

Potential Quantity Combinations		
Pilot Zone Injectors	Main Zone Injectors	Combustor Cost - $
18	18	Base
18	36	+2,000
27	54	+5,400

Individually shielded fuel manifolds were estimated to cost up to $1,000 less than a large diameter shield over the entire manifold system. A potential candidate system consisting of 9 injector supports and distribution points, 18 pilot zone injectors, 36 main zone injectors, and individually shielded manifolds was estimated to cost up to $18,000 less than the combustor developed in the NASA sponsored Experimental Clean Combustor Program.

Cost trades were considered, along with the other combustor requirements, in arriving at the final preliminary combustor configuration.

A full authority digital electronic control was selected for the Energy Efficient Engine because its flexibility permitted incorporation of a number of sophisticated control functions that provide for efficient engine operation and minimize the effects of component deterioration with operating time. Key features incorporated included self trimming and accurate rating control, which reduces maintenance and improves hot section life by ensuring that the engine operates where intended; stator vane control with reset scheduling to anticipate transient operating effects; bleed control with reset to anticipate transients; and capability for closed loop active clearance control to provide design clearances throughout the life of the engine.

2.2.3.5.2 Lubrication System Analysis

The lubrication system of the direct-drive engine was considered to be conventional; however, that of the geared engine was distinct enough to warrant study. The commonality of the main engine system with that of the reduction gearbox and the consequent high heat loads were the primary concerns.

The devised geared engine lubrication system is shown schematically in Figure C-76. The general arrangement is similar to that for the direct-drive engine system except for the addition of two components. One compartment was added between the fan and LPC to house the fan spool bearings and the reduction gearbox, and another compartment was added in the diffuser case location to contain the center high spool bearing and the intershaft bearing between the low and high spool shafts. Oil to these bearings is supplied through the diffuser case to the center bearing and through the LPT exhaust case to the intershaft bearing by means of a center tube in the low spool shaft. Oil scavenging from the two forward compartments is by means of gear pumps. The rear compartments are scavenged by gravity that is assisted by seal leakage airflow through the scavenge lines. Oil de-aeration and filtration are accomplished by the same components as those used in the direct-drive engine. Oil cooling is handled by an enlarged fuel-oil cooler and by an air-oil cooler because of the increased flow rates and heat loads associated with the reduction gearbox.

Lubrication system thermodynamic balances derived to size the system are shown in Figures C-77 and C-78 for takeoff and cruise conditions respectively.

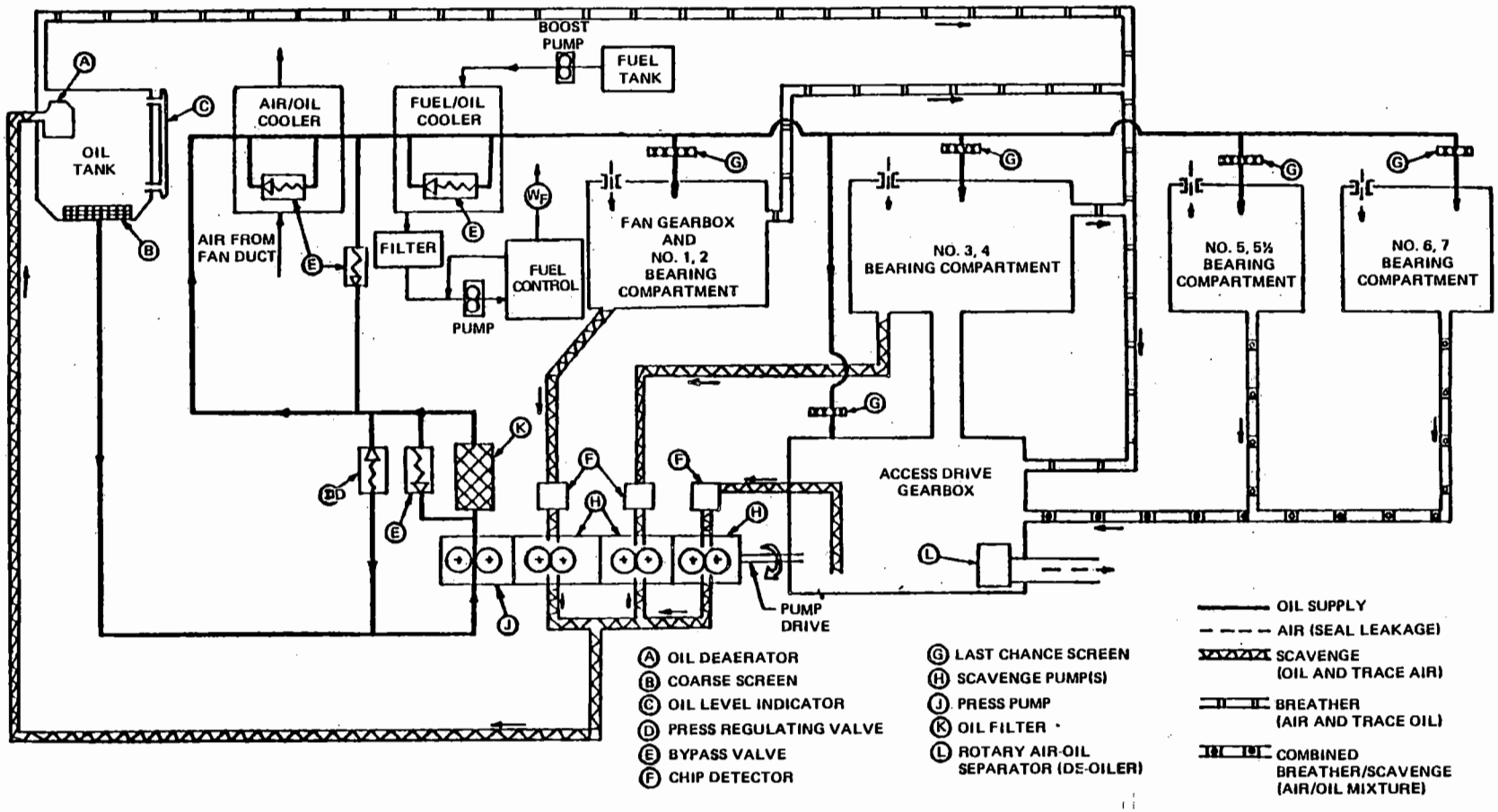

Figure C-76 Oil System Schematic for the Geared Fan Engine

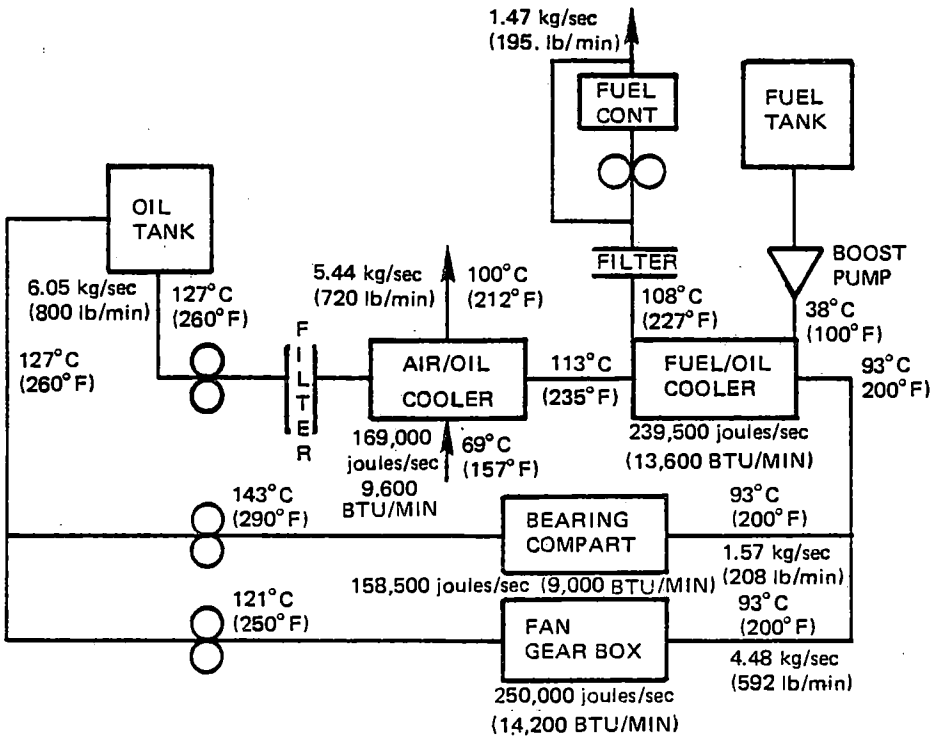

Figure C-77 Geared Engine Lubrication System Conditions – Sea level takeoff

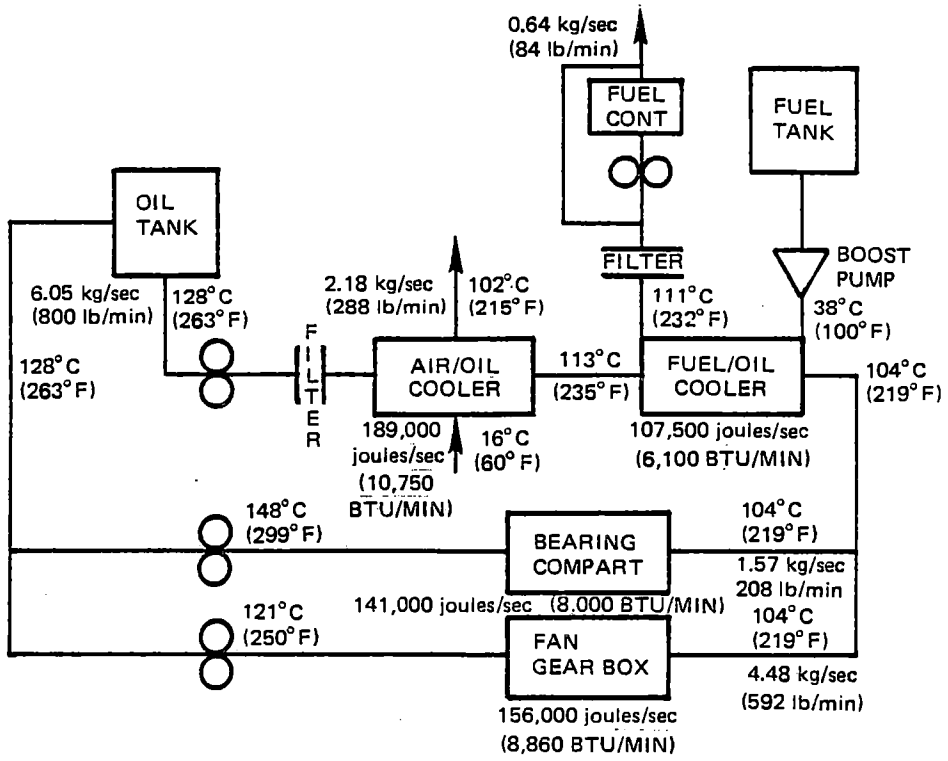

Figure C-78 Geared Engine Lubrication System Conditions – Aerodynamic design point

2.2.3.5.3 Accessories Analysis

All regular engine and aircraft accessories were sized and located on a preliminary basis prior to review by the airframe subcontractors. Two approaches were considered for accessory packaging:

- Bottom mounting of all accessories with single shaft power drive off the forward end of the high spool.

- Bottom mounting of engine accessories with aircraft accessories located in the pylon with two power drive shafts off the front of the high spool.

Realizing that final accessory location selection will depend on airline customer requirements, the bottom location was tentatively selected primarily because of maintenance ease and a Douglas (only subcontractor to state preference) requirement for installation in the center engine position on their trijet aircraft. The full duty gearbox with all engine and airframe accessories was located in a typical position on the outer fan exit case at the bottom dead center of the engine.

2.2.3.6 Nacelle Analysis

Nacelles were aerodynamically and structurally configured on a preliminary basis and initial installation drawings were prepared for assessment and evaluation by the airframe subcontractors. Configurations determined for each of the four engine configurations included consideration of inlets, nacelle shape requirements, thrust reversers, cowl load sharing with the engine, mounting, acoustical treatment, accessory location, and accessibility. Exhaust mixer configurations were also selected. Finally, Nacelle external drags were estimated, as were internal ducting losses and exhaust nozzle performance.

Aerodynamically, the nacelles were defined to minimize external drag and internal losses. Starting with the bare engine dimensional and performance requirements, the nacelle wrap assumptions and procedures developed in Task II, based on improvement of past designs, were utilized. The inlet characteristics derived were the same as Task II except that the inlet throat area was designed to include 8% engine airflow growth capability, as recommended by Task II airframe subcontractors. All surfaces in the inlet and fan and primary exhaust ducts were treated with advanced low loss material to reduce noise. The fan duct was contoured around a Task II airframer type bifurcator/pylon blockage which had a maximum thickness of 51 cm (20 in.) at the top and 31 cm (12 in.) at the bottom and was configured in such a way as to avoid the exhaust mixer. A thrust reverser requirement of 35% of takeoff thrust was used. A convergent-divergent exhaust nozzle with an area ratio of 1.02 was designed.

Utilizing the preliminary aerodynamic analyses, a conceptual nacelle mechanical configuration was defined such as shown in Figure C-79.

The acoustically treated inlet was provided with thermal anti-icing for the inlet tip.

Acoustically treated structural nacelle ducts were selected to share the engine back bone bending loads to minimize engine case deflections. The fan ducts were designed as "D" shaped sections which hinge at the top pylon bifurcation and structurally latch at the lower bifurcation. This approach was taken so that these doors, when opended, provide access to the core of the engine for maintenance. When closed, "V" grooves were utilized at the front and rear joints to provide structural ties to the engine and exhaust nozzle. The inner and outer ducts, to perform their load sharing

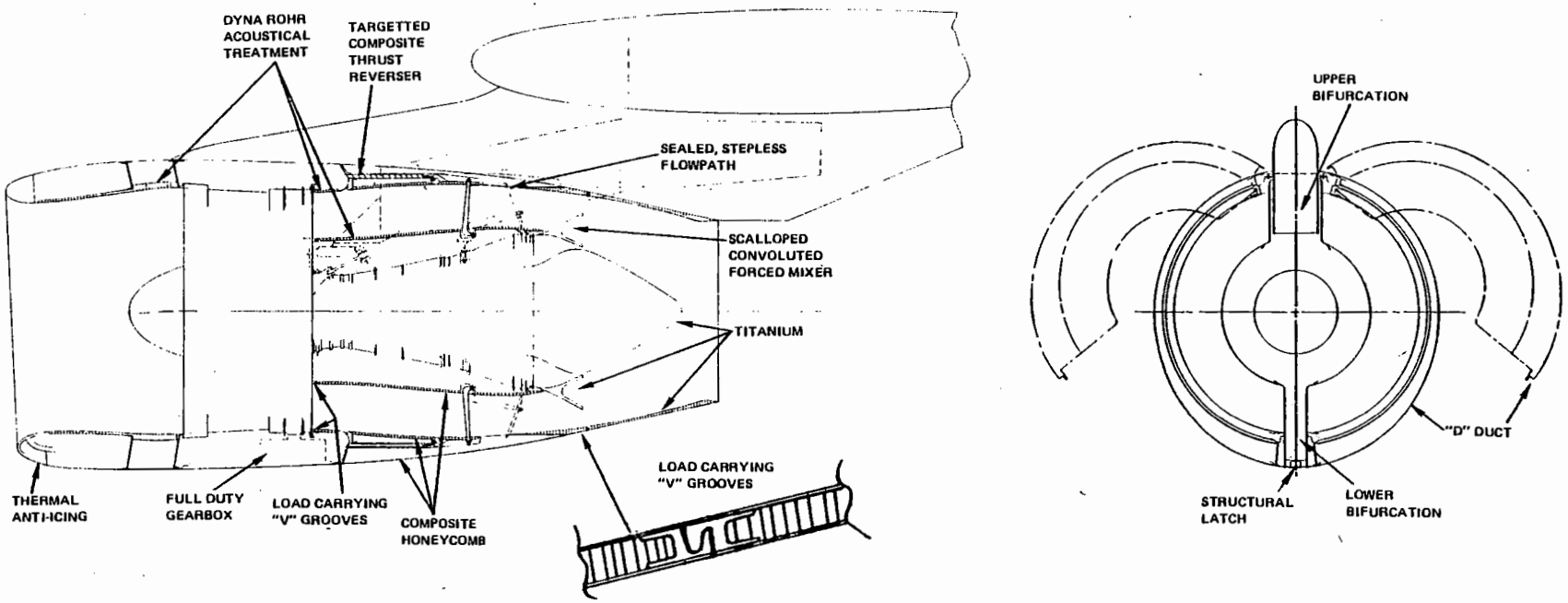

Figure C-79 Nacelle Configuration – The nacelle is designed to provide reduced thrust specific fuel consumption and improve engine performance retention.

function, were configured to carry loads between the fan exit and HPT exit planes. The top and bottom flow path bifurcations were configured to provide room for structural support of the engine and for passage of services between the engine core and the accessory gearbox and accessories. Engine support was provided in two axial planes by the top bifurcations. The front mount at the fan exit case was configured to carry thrust loads at two points 45 degrees from the centerline. Vertical and side loads were also carried by the front mount at the top vertical centerline. The rear mount located between the HPT and LPT was configured to carry vertical, side, and torsional loads through links between the top bifurcation and the turbine case. Structural features of the nacelle were reviewed with the airplane subcontractors and found to be consistent with their nacelle design practices, and therefore, satisfactory.

A cascade type thrust reverser was incorporated on the fan duct based on service experience indicating that it is unnecessary to reverse the primary stream of high bypass ratio engines to achieve the desired amount of reverse thrust. Reverser cascades were configured to be exposed by moving a translating sleeve cover rearward. Internal duct blocker doors were defined to divert the fan air through the cascades. Based on coordination with the subcontractors, the cascades were individually tailored to direct the flow forward over the wing and away from the fuselage, engine inlet, and runway.

Careful attention in the final duct flow path design process was projected to reduce air leakage and duct surface irregularities. Advanced acoustic treatment, called "Dyna Rohr", was selected to reduce wall friction.

To achieve the design goal of 15% structural weight reduction relative to comparable current nacelles, projections were made to use composites and/or honeycomb structure extensively in the final design process. Application of some earlier NASA sponsored activity in this area by airframers confirmed that this weight reduction is possible.

2.2.3.6.1 Nacelle/Mixer/Nozzle Performance

Based on the resultant mechanical configurations for the nacelle, mixer, and nozzle, performance at the aerodynamic design point was estimated for an uninstalled (isolated) situation.

The total external wetted surface areas of the nacelle and the external accessory mounting were the inputs to the drag calculations. Friction drags of the nacelle were computed with a method which includes the effects of compressibility, roughness, and Reynolds number. Fan cowl pressure drag was assumed to be 15% of the fan cowl skin friction drag. Accessory bump drag was derived as a function of relative size.

These procedures and results were reviewed with the airframe subcontractors and found to be sufficiently accurate as this stage of design. Further discussion indicated that no additional performance penalty should be taken for interference effects between the nacelle and the wing, since it was believed that careful tailoring of the nacelle-pylon-wing dimensional interface would minimize additional drag.

Internal inlet, duct, and nozzle frictional losses were calculated based on compressibility, roughness, and Reynolds number considerations. Resulting nacelle, mixer, and nozzle performance at the aerodynamic design point is presented in Table C-LXXVII for the four engine types.

Predicted exhaust nozzle thrust and flow coefficients are shown by Figures C-80 and C-81, respectively.

TABLE C-LXXVII

INSTALLATION PERFORMANCE SUMMARY
(AERODYNAMIC DESIGN POINT)

Engine:	(1 Stage HPT Direct Drive)	(2 Stage HPT Direct Drive)	(1 Stage HPT Geared)	(2 Stage HPT Geared)
Pressure Loss-%				
Inlet	0.0035	0.0035	0.0035	0.0035
Fan Duct	0.0047	0.0047	0.0033	0.0038
Tailpipe	0.0026	0.0026	0.0021	0.0021
Fan Duct Mixer	0.0013	0.0013	0.0007	0.0007
Primary Duct Mixer	0.0021	0.0021	0.0023	0.0023
Duct Air-Oil Cooler	–	–	0.0007	0.0007
Mixer Efficiency-%	85	85	75	75
Total Nacelle Drag-N(lbs)	1990(447)	2070(465)	2220(500)	2290(514)
Nozzle Pressure Ratio	2.56	2.56	2.29	2.29
Nozzle Thrust Coefficient	0.9958	0.9958	0.9960	0.9960

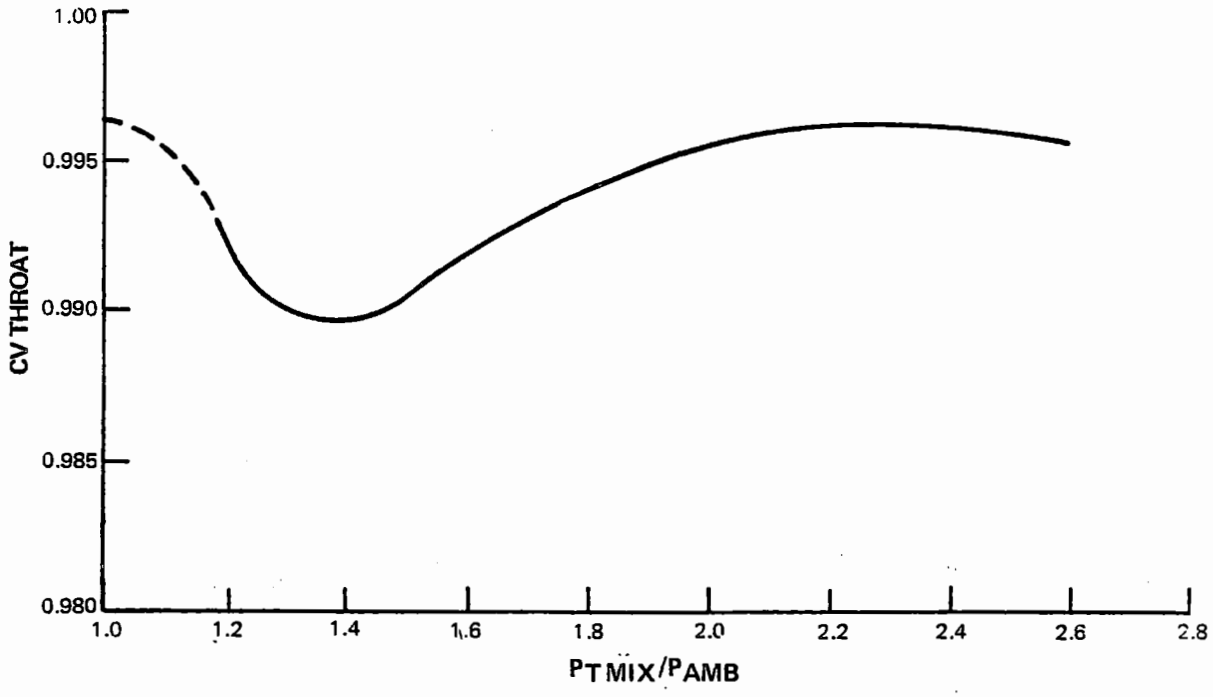

Figure C-80 Nozzle Thrust Coefficie.it

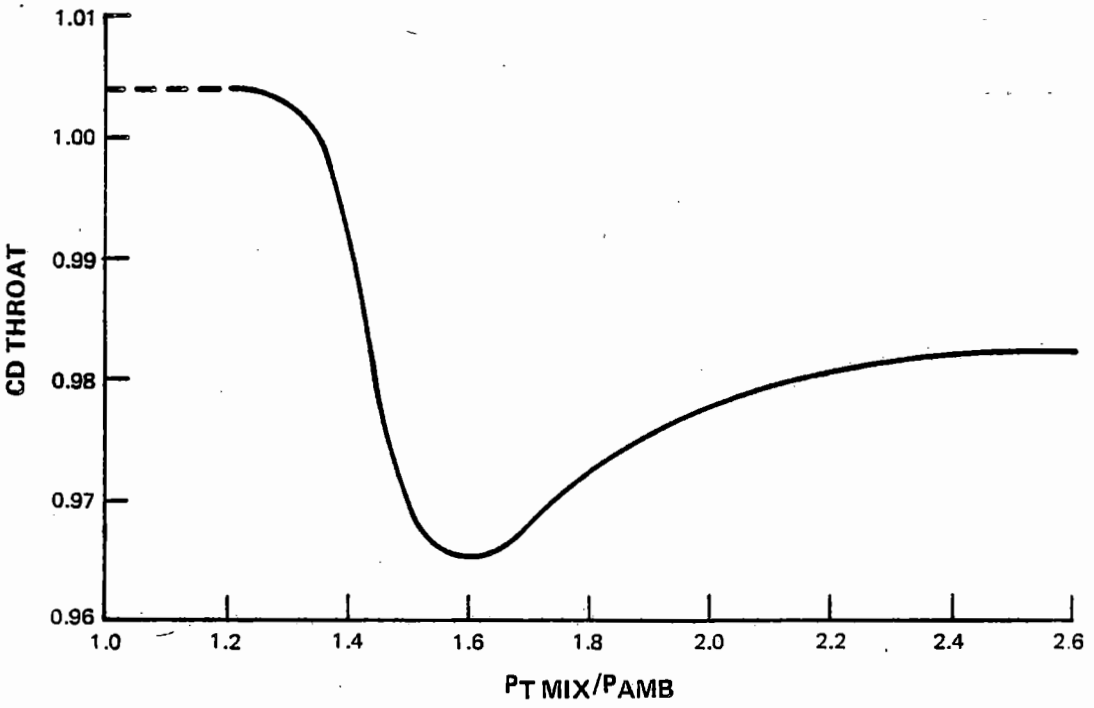

Figure C-81 Nozzle Flow Coefficient

2.3 PRELIMINARY DESIGN OUTPUT

Based on the preliminary engine component and propulsion system preliminary design analyses results, preliminary engine layouts were prepared and evaluated. These layouts for the four engine types are shown as Figures 24 through 29 in the main body of this report. Final evaluations included performance, weight, price, and maintenance cost.

2.3.1 Performance Summary

The State-of-the-Art-Performance Program (SOAPP) cycle and performance analysis computer simulation created at the outset of Task III was updated on the basis of the engine component and nacelle performance analyses conducted in the preliminary design process. This simulation was then exercised to determine final preliminary performance. Resulting TSFC's and thrusts at the critical flight operating conditions for the four engine configurations are summarized in Table C-LXXVIII.

2.3.2 Weight/Price/Maintenance Cost Estimates

Engine weight, price, and maintenance cost estimates were made based on the component and overall propulsion system analytical results from the preliminary design process.

Nacelle weight, price, and maintenance cost were also estimated for the four engine configurations based on modification of past detailed designs to reflect the long "D" duct design and the application of lightweight materials and acoustical treatment.

A summary of these results on a relative basis is presented for the four engine types in Table C-LXXIX.

TABLE C-LXXVIII

ENGINE PERFORMANCE SUMMARY

Engine:	(1 Stage HPT Direct Drive)	(2 Stage HPT Direct Drive)	(1 Stage HPT Geared)	(2 Stage HPT Geared)
Max. Cruise (ADP) - 10,700 m (35,000 ft) 0.8 MN, Standard Day				
Uninstalled TSFC kg/hr/N (lb/hr/lb)	0.056(0.544)	0.055(0.536)	0.053(0.520)	0.052(0.511)
Uninstalled FN N (lb)	43,100(9699)	42,600(9568)	44,600(10,029)	44,200(9945)
Installed TSFC kg/hr/N (lb/hr/lb)	0.059(0.573)	0.058(0.566)	0.0565(0.549)	0.0557(0.541)
Installed FN N (lb)	40,800(9180)	40,200(9032)	42,100(9460)	41,600(9360)
Max. Climb - 10,700 m (35,000 ft) 0.8 MN, Standard + 10°C (18°F) Day				
Uninstalled TSFC kg/hr/N (lb/hr/lb)	0.058(0.570)	0.057(0.561)	0.0562(0.546)	0.0552(0.536)
Uninstalled FN N (lb)	48,100(10,815)	47,500(10,670)	49,800(11,185)	49,300(11,093)
Takeoff - Sea Level, 100 kts, Standard + 13.9°C (25°F) Day				
Uninstalled TSFC kg/hr/N (lb/hr/lb)	0.0386(0.375)	0.038(0.367)	0.034(0.331)	0.033(0.322)
Uninstalled FN N (lb)	149,600(33,623)	148,400(33,371)	159,900(35,938)	158,600(35,651)
Takeoff - Sea Level, Static, Standard + 13.9°C (25°F) Day				
Uninstalled TSFC kg/hr/N (lb/hr/lb)	0.034(0.320)	0.032(0.313)	0.028(0.274)	0.027(0.266)
Uninstalled FN N (lb)	174,700(39,270)	173,500(39,006)	192,100(43,197)	190,900(42,918)

TABLE C-LXXIX

RELATIVE WEIGHT/PRICE/MAINTENANCE COST SUMMARY

Engine:	(1 Stage HPT Direct Drive)	(2 Stage HPT Direct Drive)	(1 Stage HPT Geared)	(2 Stage HPT Geared)
Engine Weight-%	Base	+ 3.33	+12.58	+16.82
Engine Price-%	Base	+ 5.29	+ 8.13	+15.13
Engine Maintenance Cost -%	Base	+11.14	+ 0.76	+14.14
Nacelle Weight-%	Base	+ 4.65	+17.32	+21.15
Nacelle Price-%	Base	+ 4.74	+17.38	+21.05
Nacelle Maintenance Cost-%	Base	0	0	0

To evaluate the four engine configurations in their variety of applications, scaling curves were developed for TSFC, weight, and price.

The variation of TSFC with engine thrust size was obtained from detailed scaling studies which accounted for the following effects:

- Clearance-to-span change effects on compressor/turbine section efficiencies
- Blockage changes in certain component stages relating to structural restraints as they affect efficiency
- Leading/trailing edge radius-to-chord revisions in some component stages which result in airfoil section shape changes and affect efficiency
- Reynolds number changes in compressors and turbines which affect efficiency.

Figure C-82 shows the TSFC scaling function.

Other scaling curves were prepared based on techniques resulting from extensive past studies in which engines were evaluated, in several thrust sizes, in sufficient detail to determine the effects that size has on individual major parts and components. Techniques used involved analysis of each individual component. Total propulsion system scaling was then estimated by a summation of the individual component results. Weight and dimensional scaling curves obtained by this procedure are shown in Figure C-83, price in Figure C-84, and maintenance cost in Figure C-85.

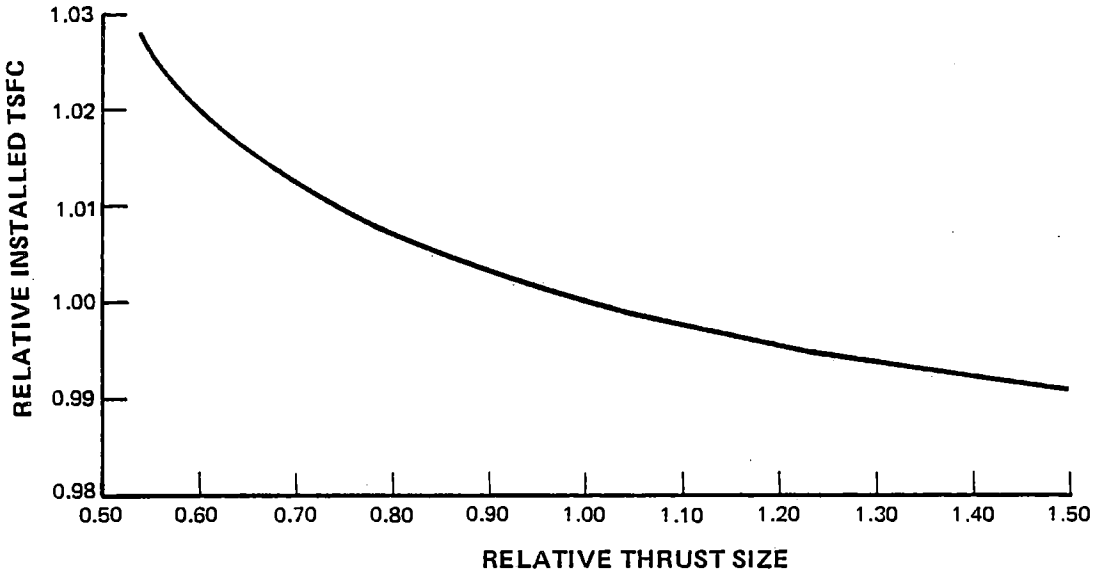

Figure C-82 Engine TSFC Scaling – Relative TSFC versus thrust size

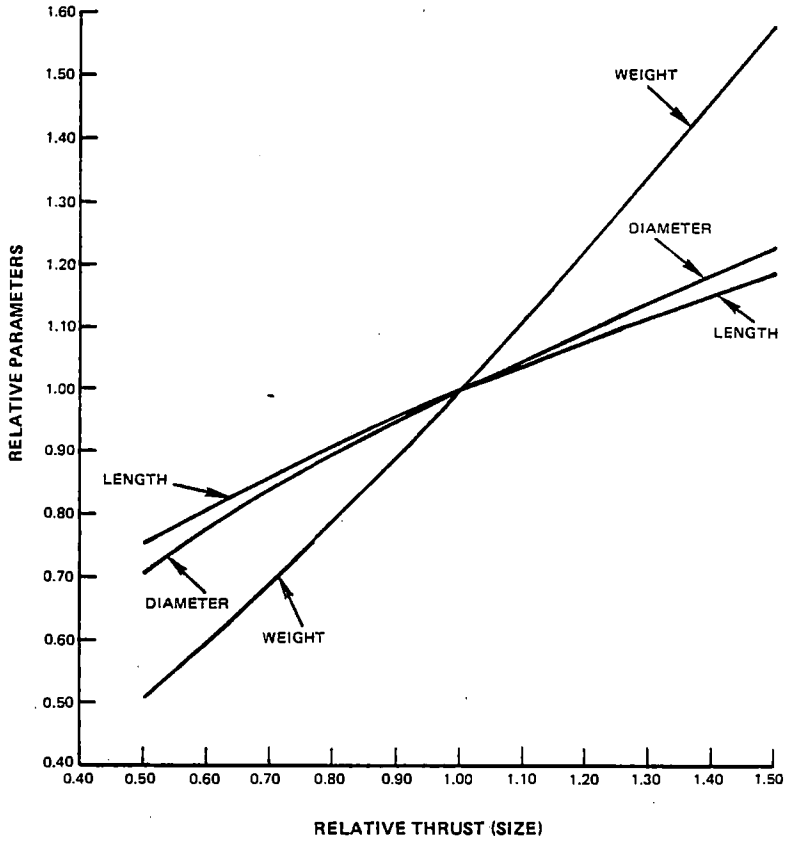

Figure C-83 Engine Weight, Length and Diameter Scaling – Relative parameter versus thrust size.

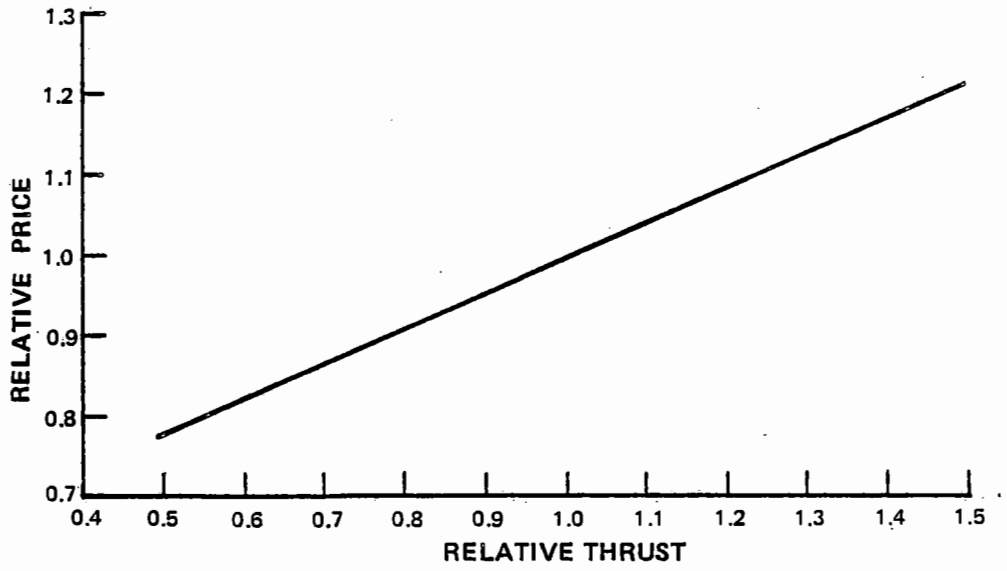

Figure C-84 Engine Price Scaling – Relative price versus thrust size

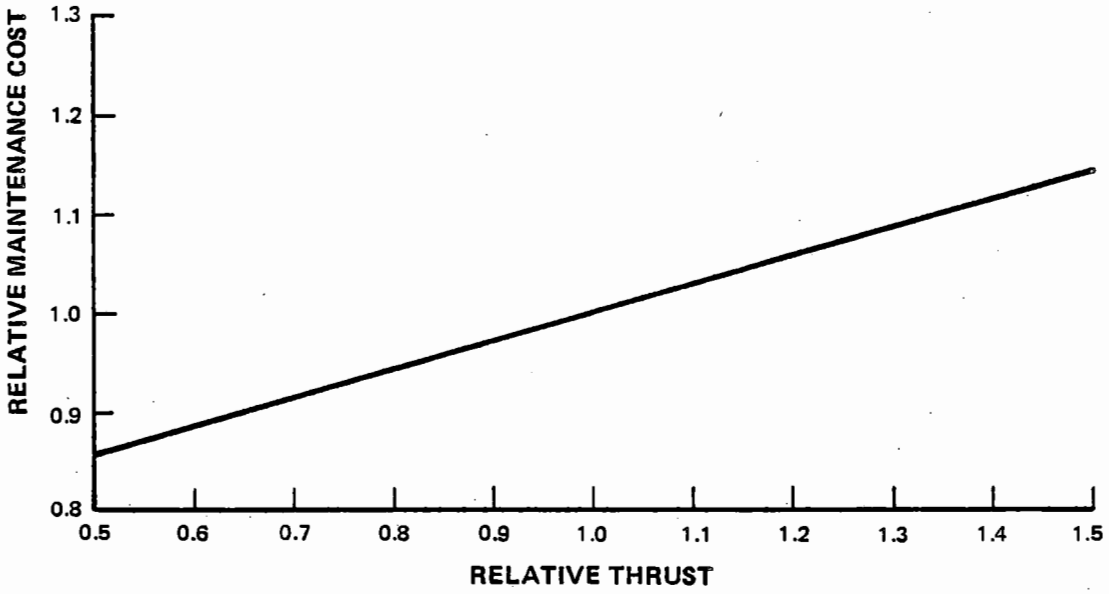

Figure C-85 Engine Maintenance Cost Scaling – Relative Maintenance Cost versus Thrust Size

3.0 SYSTEM EVALUATIONS

3.1 Fuel Burned and DOC Evaluations

Boeing, Douglas, and Lockheed resized their aircraft with the STF505M-7 (direct drive, one-stage HPT) and STF495M-4 (geared, one-stage HPT) study engines scaled to meet individual airplane thrust requirements.

Aircraft weights and engine thrust sizes are summarized in Table C-LXXX. Takeoff thrusts of 89,000 N (20,000 lb) to 222,000 N (50,000 lb) were required to cover the full range of aircraft studied.

Boeing domestic airplane weight estimates included the effect of using flutter weight penalties. Beam representations for the wing, pylons, and fuselage were determined. Unsteady aerodynamic forces were analyzed using strip theory modified by experimentally determined section lift coefficients and aerodynamic center data for both the wing and nacelles. Three fuel conditions (wing full, 80% full, and wing empty) were investigated for both symmetric and antisymmetric flutter.

Material addition required was determined relative to the basic strength-designed wing to reach the desired flutter clearance boundary. The spanwise position of the nacelles was held constant at 35% of the semi-span. Chordwise position of the nacelles was selected according to the guidelines established in Task II. Resultant flutter weight penalties shown on Table C-LXXXI were included in Task III Boeing airplane studies.

Using internally generated trade factors, each of the airplane companies and Pratt & Whitney Aircraft estimated fuel burned over average stage length flights with the advanced engines and with the JT9D-7A. Douglas comparisons were made against the JT9D-20 engine installation which powers the DC10-40. Average mission fuel burned reductions with the advanced engines ranged from 10 percent for the STF505M-7 powered Boeing domestic aircraft to over 25 percent for the STF495M-4 powered Douglas international airplane, as shown in Figure C-86. For the design missions, as shown in Figure C-87, the advanced engines offered fuel burned reductions ranging from just under 14 percent for the STF505M-7 powered Boeing domestic aircraft to 26 percent for the STF495M-4 powered Douglas domestic and international aircraft. On an average basis, gearing provided an additional fuel burned reduction over the direct-drive fan engines of 2.5 and 2.8 percents for the average and design missions, respectively.

Average mission DOC reductions ranging from just over 2 to 15 percent, as shown in Figure C-88, and design mission DOC reductions ranging from 4 to almost 17 percent, as shown in Figure C-89, resulted from the lower fuel burned and the lower maintenance costs of the advanced engines. Gear maintenance costs nearly offset reduced fuel costs with the geared engine for the domestic airplanes resulting in approximately the same DOC as the direct-drive engine. The longer range international airplanes averaged a 1.4 percent lower DOC with geared engines. On an overall average, gearing reduced DOC by an additional 0.7 and 1.1 percents for the average and design missions, respectively. Both the fuel burned and DOC comparison between the direct-drive and geared engines remained unchanged from the Task II results.

Pratt & Whitney Aircraft fuel burned and DOC trade factor evaluations of one and two-stage HPT engines are compared in Table C-LXXXII. The lower TSFC potential of the two-stage HPT engines carried over into an additional one percent fuel savings. The 10 percent lower maintenance costs, produced a net 1.5 percent DOC advantage for the one-stage HPT engines.

TABLE C-LXXX

TASK III AIRPLANE CHARACTERISTICS

	Domestic Airplane			International Airplane		
	JT9D-7A/20	STF505M-7	STF495M-4	JT9D-7A/20	STF505M-7	STF495M-4
Boeing						
TOGW - kg	117,900	115,500	116,300	188,200	166,200	164,500
(lbs)	(260,000)	(254,700)	(256,300)	(415,000)	(366,500)	(362,700)
OEW - kg	73,300	74,700	75,800	88,900	83,100	83,400
(lbs)	(161,600)	(164,700)	(167,200)	(196,000)	(183,100)	(183,800)
Thrust/Engine (Inst) N	153,100	156,000	163,900	99,100	86,900	90,700
(lbs)	(34,420)	(35,060)	(36,840)	(22,280)	(19,540)	(20,380)
Douglas						
TOGW - kg	247,200	220,900	217,700	321,100	277,600	270,800
(lbs)	(545,000)	(487,000)	(480,000)	(708,000)	(612,000)	(597,000)
OEW - kg	136,900	125,500	125,200	145,600	131,800	130,600
(lbs)	(301,900)	(276,700)	(276,000)	(321,000)	(290,600)	(287,900)
Thrust/Engine (Inst) N	191,300	161,500	169,000	222,000	190,400	193,100
(lbs)	(43,000)	(36,300)	(38,000)	(49,900)	(42,800)	(43,400)
Lockheed						
TOGW - kg	195,000	182,100	180,500	296,200	259,900	254,700
(lbs)	(430,000)	(401,500)	(398,000)	(653,000)	(573,000)	(561,500)
OEW - kg	107,500	104,100	104,200	127,000	118,400	117,500
(lbs)	(237,000)	(229,500)	(229,800)	(280,000)	(261,000)	(259,000)
Thrust/Engine (Inst) N	143,700	151,700	153,900	159,700	140,100	142,800
(lbs)	(32,300)	(34,100)	(34,600)	(35,900)	(31,500)	(32,100)

TABLE C-LXXXI

WING FLUTTER ANALYSIS RESULTS – BOEING

Domestic Airplane

Engine:	STF505M-7	STF495M-4	JT9D-7A
Location of Primary Nozzle Exit as Percent of Wing Chord	15	15	15
Flutter OEW Penalty – kg(lb)	2000(4410)	2080(4582)	840(1850)

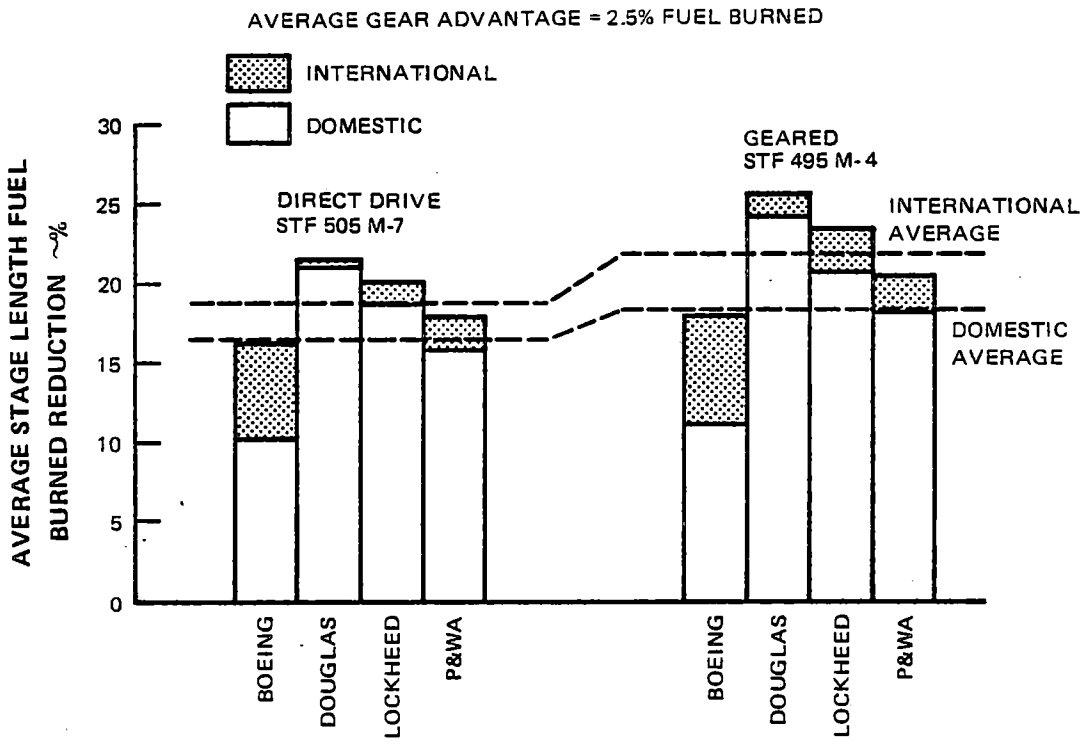

Figure C-86 Task III Average Mission Fuel Savings – Shows savings relative to JT9D-7A

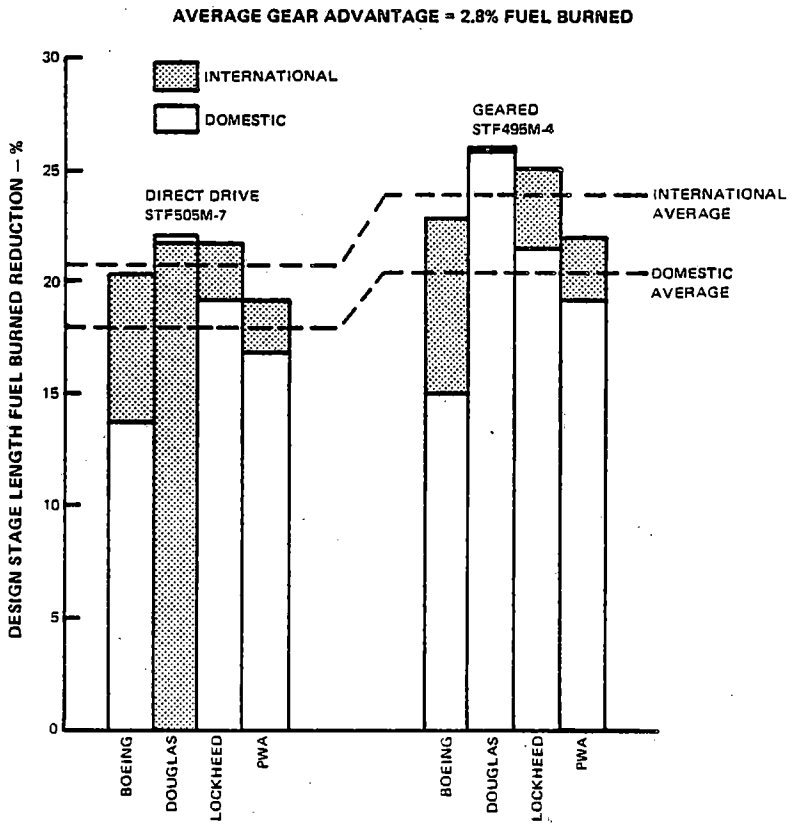

Figure C-87 Task III Design Mission Fuel Savings – Shows savings relative to JT9D-7A

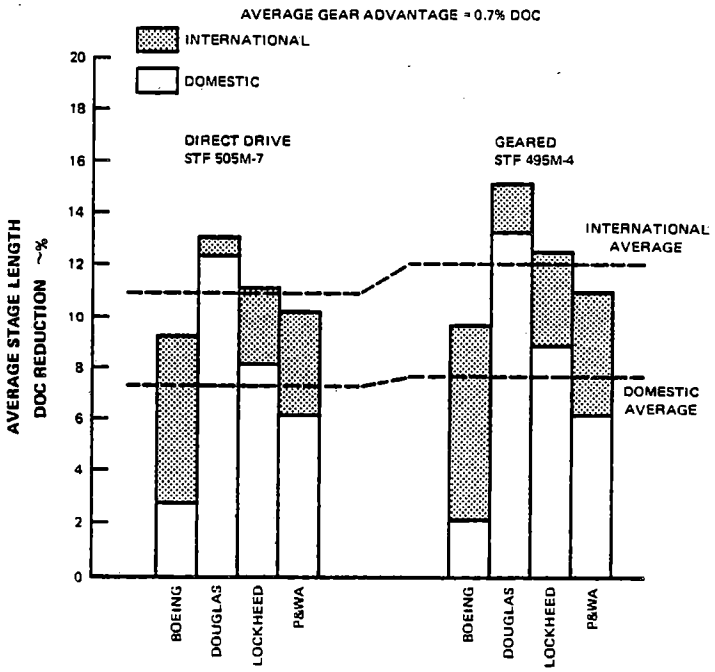

Figure C-88 Task III Average Mission Direct Operating Cost Reductions – Shows reduction relative to the JT9D-7A

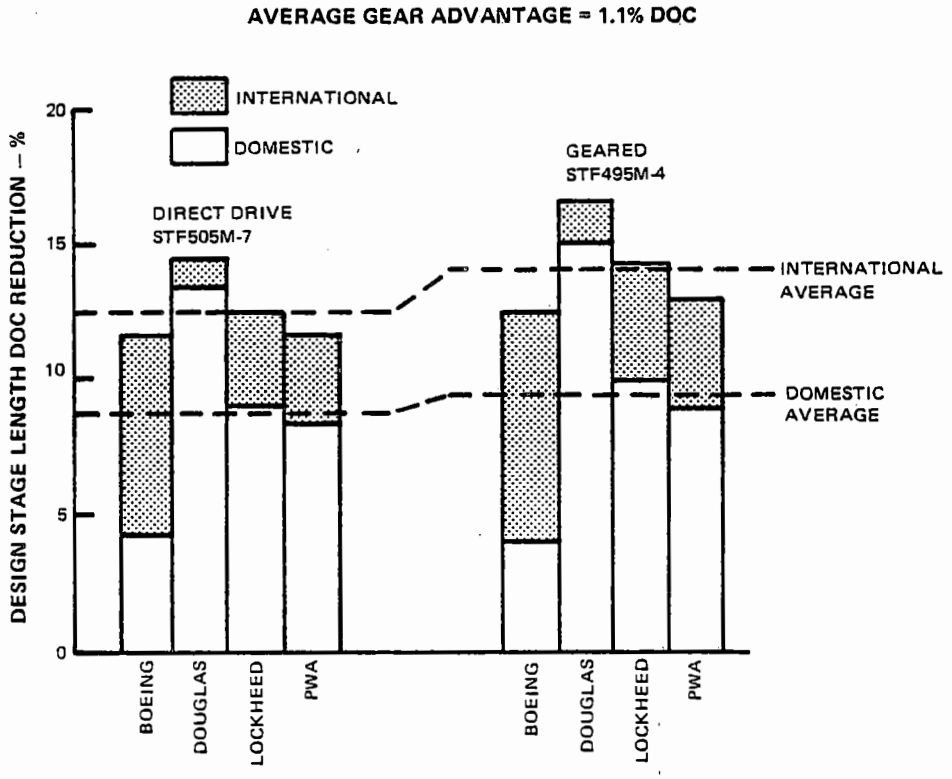

Figure C-89 Task III Design Mission Direct Operating Cost Reductions Shows Reduction Relative to JT9D-7A

TABLE C-LXXXII

P&WA TASK III ENGINE EVALUATION
1- AND 2-STAGE HPT CONFIGURATIONS

	Additional benefits relative to JT9D-7A	
Configuration	One-Stage HPT	Two-Stage HPT
Δ TSFC ~ %:	Base	$-1.1/-1.3^{(1)}$
Δ Fuel Burned ~ %		
Domestic:	Base	$-0.7/-1.0^{(1)}$
International:	Base	$-0.8/-1.1^{(1)}$
Δ DOC ~ %:		
Domestic:	$-1.5/-1.6^{(1)}$	Base
International:	$-1.1/-1.1^{(1)}$	Base

(1) Direct-Drive/Geared

3.2 NOISE EVALUATIONS

Noise estimates were updated using the Task III procedures with the acoustic design features of Figure C-90 engines. Each individual source noise was estimated including attenuation at the FAR Part 36 (1969) measurement points. Current and advanced propulsion acoustical technology effects were identified. Total airplane and propulsive noise levels were estimated for several of the study aircraft. Based on this evaluation, the direct-drive turbofan powered aircraft, with advanced acoustics were estimated to produce noise 10 EPNdB below FAR Part 36 (1969). Geared turbofan powered aircraft were another 2 EPNdB quieter. With currently available propulsion acoustic technology, noise levels three to seven EPNdB lower than FAR 36 (amended 1977) were estimated.

An engine noise breakdown by source is shown in Table C-LXXXIII for direct-drive and geared turbofans. The results apply to either one- or two-stage HPT engines. Fan noise was generally dominant with the single exception of takeoff jet noise with the higher jet velocity direct-drive fan engines. Advanced acoustic technology was projected which reduced fan, turbine, and jet noise. Low noise fan blades and advanced technology liners were projected which reduced buzzsaw, blade passing, and broadband noise 1 to 3 EPNdB. Nacelle reconditioning and increased understanding of forward flight velocity effects were projected to have the potential for a 1.4 EPNdB jet noise reduction at takeoff and sideline measuring stations. Acoustic tailoring of turbine geometry and advanced treatment technology were projected to reduce turbine noise up to 4 EPNdB.

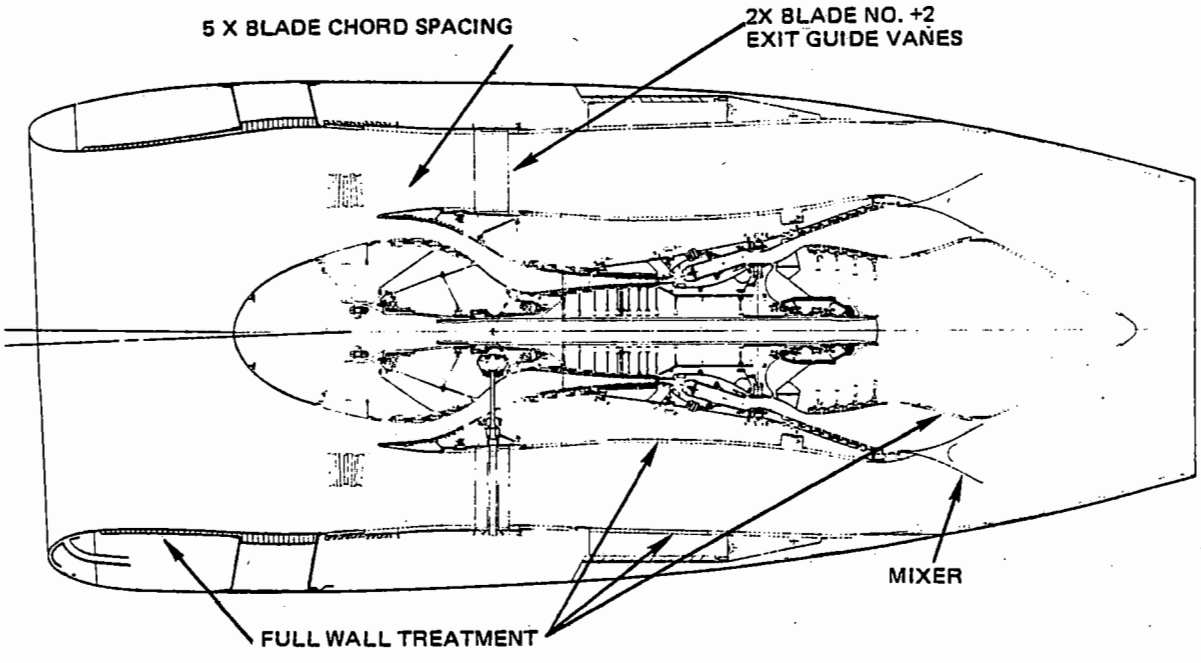

Figure C-90 Task III Acoustic Design Features

TABLE C-LXXXIII

TASK III ENGINE NOISE BREAKDOWN(1)
(P&WA INTERNATIONAL AIRCRAFT)

	Fan	Turbine	EPNdB Jet	Core	Total
Direct-Drive Fan					
Advanced Acoustics					
Takeoff power	93.3	83.7	95.3	88.5	98.4
Approach	94.9	89.3	83.0	85.4	97.9
Sideline	84.0	63.1	89.7	82.2	91.5
Current Acoustics					
Takeoff Power	95.5	87.9	96.7	88.5	100.3
Approach	98.9	92.3	83.0	85.4	101.8
Sideline	86.2	66.1	91.1	82.2	93.1
Geared Fan					
Advanced Acoustics					
Takeoff	93.0	78.5	90.8	87.7	96.0
Approach	89.6	85.3	79.9	85.0	94.3
Sideline	86.2	60.9	85.1	81.4	89.3
Current Acoustics					
Takeoff	95.1	82.5	92.2	87.7	98.2
Approach	92.5	88.3	79.9	85.0	96.1
Sideline	88.3	63.9	86.5	81.4	91.5

(1) @ FAR Part 36 (1969) measurement stations

Total noise levels were reduced by approximately 2 to 3 EPNdB with the full application of advanced acoustic technology possible by the 1990's. Engine noise, with advanced acoustical technology, was combined with airframe noise at the FAR 36 (1969) measurement points for the Pratt & Whitney Aircraft, Boeing, and Douglas aircraft. The noise characteristics were calculated at takeoff, sideline, and approach. The most severe noise condition was isolated, without trading, for comparison. Results are shown in Figure C-91. Total aircraft noise, with direct-drive fan engines ranged from 8 EPNdB to 11.5 EPNdB below FAR 36 (1969). Geared fan engine aircraft produced, on an average, approximately 2 EPNdB lower noise.

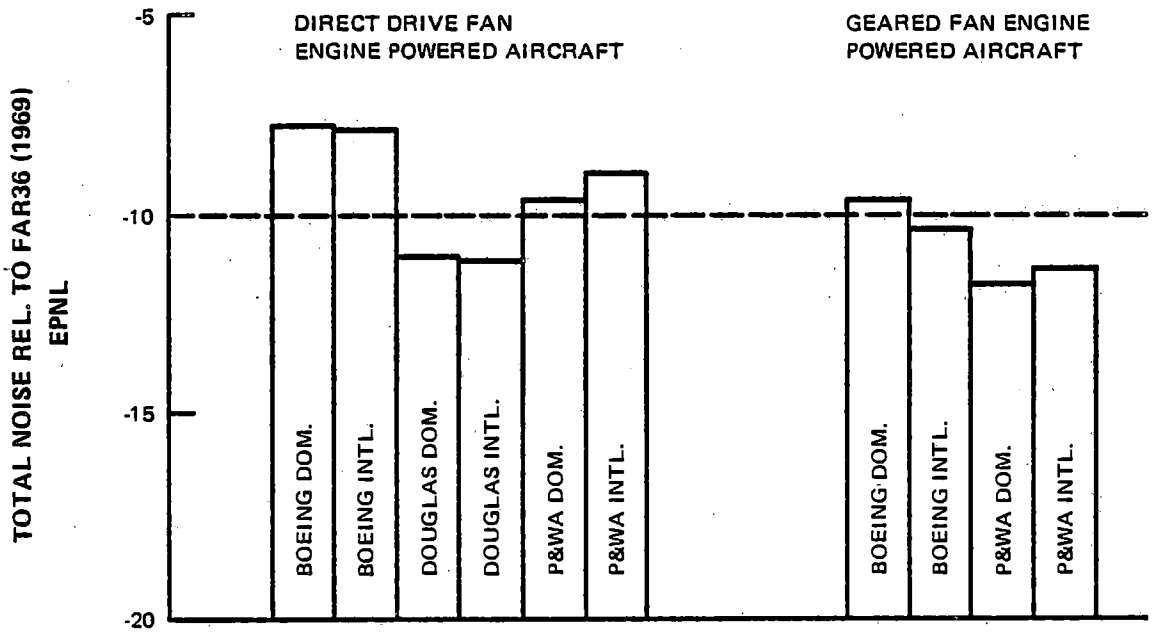

Figure C-91 Task III Total Noise Characteristics

3.3 Engine Performance Deterioration

Another aspect considered in the evaluation of the four engine configurations was the relative performance deterioration characteristics of each. Factors influencing deterioration that were considered were:

- Increased blade tip clearance
- Airfoil and tip seal erosion/foreign and bill of material object damage
- Turbine airfoil distortion and creep
- Increased airseal and mechanical joint leakage.

The general approach taken in these analyses was to use the JT9D operational experience as a basis (both company funded and NASA sponsored efforts under Contract NAS3-20632 Diagnostics Program), to evaluate this experience in terms of the Energy Efficient Engine design features, and to determine the resulting cruise TSFC deterioration. JT9D experience showed the major causes of deterioration to be:

- Fan tip clearance and leading edge erosion
- LPC tip clearance and rub strip erosion
- HPC tip clearance, airfoil dirt, and rub strip erosion
- HPT tip clearance, vane distortion, and seal leakage
- LPT tip clearance.

These then were the factors evaluated in terms of the Energy Efficient Engine as discussed in the following sections.

3.3.1 Running Clearances

In designing the Energy Efficient Engine, the following running clearance philosophy was established as being reasonable, based on operational and design experience. Goal tip clearances exist at the aerodynamic cruise design point after the post production acceptance test. Sufficient tip clearance occurs during the takeoff pinch point operation so that rubbing under normal (in flight) maneuver loads is precluded. Finally, rubbing at cruise under normal loads is minimal.

As discussed in paragraphs 2.2.3.3 and 2.2.3.4 of this appendix, features were incorporated into the engine preliminary designs to meet the established running clearance philosophy. Improved clearance control was achieved through the incorporation of non-eroding abradable tip seals in all components; active clearance control in the HPC, HPT and LPT; cowl load sharing; stiff rotor construction; stiff cases and frames; and improved thermal matching of the rotors and cases. Active clearance control was utilized to prevent rubs during normal operation in the takeoff and climb modes by opening up clearances during these portions of the mission, and then by closing down clearances for cruise operation.

In the assessment of tip clearance deterioration, factors experienced for the JT9D in up to 4000 service hours operation were considered. These included ovalization, "back-bone" bending, and concentric motion of the rotor. Ovalization of the engine cases was produced by reactions to gyroscopic loads imposed by aircraft maneuvers, wind gusts, "G" loads, aircraft maneuvers, wind gusts, and thrust loads. "Back-bone" bending resulted from imposed maneuver "G" loads, gyroscopic effects, gusts, and thrust. Concentric motion of the rotor relative to the cases was affected by speed and temperature. Three categories of deflection were defined for the purposes of these analyses:

- Calculated values
- Judgments and estimates of known phenomenon
- Judgments for unanticipated problems.

In the first category, the effects of thrust, gusts, "G's", and gyro's were included. Known phenomena judgments in the second category involved things not yet analyzed such as parts tolerances, clearances in the bearings, and fan ovalization and turbine intermediate case deflections associated with thrust mounting and thermals. Third category items included were such things as an unanticipated pinch point, surge deflections, and nacelle environment.

The rotor-frame models prepared to analyze critical speed and tip gap reductions for engine configuration selection (Figures C-71 and C-73) were used to assess the "Calculated value" category of tip clearance deterioration. Maximum maneuvers, thrusts, and gusts that had been determined with a comprehensive JT9D-7 analytical model were imposed on the Energy Efficient Engine models. (The JT9D-7 model, developed jointly by Pratt & Whitney Aircraft and the Boeing Commercial Airplane Company, predicts the effects of flight loads on performance degradation by correlating component outer air seal and blade wear with blade tip-airseal interference. It considers a mission profile and the relationships of clearances to temperature and speed. Engine/component cases, frames, etc. responses to these external loads were simulated with a NASTRAN finite-element analysis. The most severe operational maneuvers, gusts, and thrusts were determined on the basis of simulated versus actual tip-gap rub experience with time.) Calibrated rotor and case deflections were determined, and tip clearance impacts were calculated for each component at the takeoff and cruise flight conditions.

Judgments and estimates of tip clearance impacts associated with known phenomena not yet calculated were based primarily on detailed JT9D analyses and test results. These JT9D data were biased, based on experience, to reflect known configurational differences in the Energy Efficient Engine.

The deflections caused by unanticipated problems in past JT9D operation were applied to the engine configuration using the judgment of pertinent experts.

These three categories of tip clearance impact, when added together, defined the greatest possible tip deflections anticipated to occur in 4000 hours of engine operation in the airline environment. Again based on JT9D experience, maximum 1000 hour tip deflection impacts were taken to be 80% of those at 4000 hours. Results showed takeoff deflections to be 2 to 3 times greater than the cruise values. In addition, takeoff was found to set the maximum deteriorated clearances, since the cruise deflections were less than the target clearances, "G's", gyro's, thrust, and gust deflections were estimated to account for approximately 1/4 of the total deflections in the high spool and from 1/4 to 2/3 of those in the low spool. Deflections caused by items in the "known phenomena" category accounted for about 1/2 of the high rotor and LPT deflections and less than 1/3 in the fan and LPC. The "unanticipated problems" category was found to account for roughly 1/5 of the total fan and LPC deflections and 1/4 of the high rotor and LPT totals.

The total tip clearance deterioration impacts were assessed in each of the components for the direct drive and geared engines. Since the expected 4000 hour fan tip clearance of 1.7 mm (0.067 in) is lower than the 1.9 mm (0.076 in) new engine goal, no fan performance deterioration occurs because of tip clearance increase. In the LPC, the 4000 hour clearance was estimated at 0.7 mm (0.028 in) as compared to a goal of 0.5 mm (0.020 in.). Because the TSFC impact of this size difference in LPC tip clearance is almost negligible, it was decided to increase the new engine goal clearance to the 0.7 mm (0.028 in) level to preclude deterioration. This approach will eliminate LPC flow capacity loss, which experience shows is a major cause of increased HPT operating temperature in a deteriorated engine.

The analyses showed expected maximum 2000 and 4000 hour deflections in the other engine components to exceed the new engine goal clearances. The resulting tip clearance deteriorations and performance impacts in these components are presented in Table C-LXXXIV for the direct drive engine configurations and Table C-LXXXV for the geared engines.

Clearance deterioration analysis results showed the expected deflections of the 1 and 2 stage HPT engines to be the same, and those of the geared engines to be less than those of the direct-drive engines, especially in the high spool components. The same deflections occurred with the two HPT configurations because of the stiffness of the high rotor shafts and the rigid rear support provided by the turbine intermediate cases. Geared engine clearance deteriorations were lower because of the additional center spool bearings and bearing support required for critical speed control.

Although clearance deteriorations with time were estimated to be the same for the one- and two-stage HPT engines, the effects on HPT efficiency and flow capacity were found to be different. Flow capacity in the two-stage HPT was affected more because of its lower first vane Mach number. Alternatively, the one-stage HPT's efficiency was debited more because of its greater expansion ratio.

TABLE C-LXXXIV

DIRECT-DRIVE ENGINE CRUISE TIP CLEARANCE DETERIORATION SUMMARY

Engine:		1 Stage HPT			2 Stage HPT	
Operating Time:	0 hrs	1000 hrs	4000 hrs	0 hrs	1000 hrs	4000 hrs
Component/Effect						
HPC						
Clearance-mm(in)	0.33(0.013)	0.41(0.016)	0.43(0.017)	0.33(0.013)	0.41(0.016)	0.43(0.017)
Efficiency-%	Base	-0.40	-0.50	Base	-0.40	-0.50
Flow Capacity-%	Base	-0.30	-0.40	Base	-0.30	-0.40
HPT						
Clearance-mm(in)	0.51(0.020)	0.63(0.025)	0.66(0.026)	0.51(0.020)	0.63(0.025)	0.66(0.026)
Efficiency-%	Base	-0.42	-0.53	Base	-0.33	-0.42
Flow Capacity-%	Base	+0.06	+0.07	Base	+0.18	+0.23
LPT						
Clearance-mm(in)	0.51(0.020)	0.66(0.026)	0.71(0.028)	0.51(0.020)	0.66(0.026)	0.71(0.028)
Efficiency-%	Base	-0.10	-0.12	Base	-0.10	-0.12
Flow Capacity-%	Base	Base	Base	Base	Base	Base

TABLE C-LXXXV

GEARED ENGINE CRUISE TIP CLEARANCE DETERIORATION SUMMARY

Engine		1 Stage HPT			2 Stage HPT	
Operating Time:	0 hrs	1000 hrs	4000 hrs	0 hrs	1000 hrs	4000 hrs
Component/Effect						
HPC						
Clearance - mm	0.33	0.36	0.38	0.33	0.36	0.38
(in)	(0.013)	(0.014)	(0.015)	(0.013)	(0.014)	(0.015)
Efficiency - %	Base	-0.13	-0.24	Base	-0.13	-0.24
Flow Capacity - %	Base	-0.10	-0.20	Base	-0.10	-0.20
HPT						
Clearance - mm	0.51	0.56	0.58	0.51	0.56	0.58
(in)	(0.020)	(0.022)	(0.023)	(0.020)	(0.022)	(0.023)
Efficiency - %	Base	-0.21	-0.26	Base	-0.17	-0.21
Flow Capacity - %	Base	+0.03	+0.04	Base	+0.09	+0.11
LPT						
Clearance - mm	0.5	0.63	0.66	0.5	0.63	0.66
(in)	(0.020)	(0.025)	(0.026)	(0.020)	(0.025)	(0.026)
Efficiency - %	Base	-0.10	-0.12	Base	-0.10	-0.12
Flow Capacity - %	Base	Base	Base	Base	Base	Base

Table C-LXXXVI presents estimated 4000 hour TSFC effects due to these clearance and flow capacity shifts for the four engine configurations.

TSFC deterioration was found to be less for the geared engines because of their additional center high spool bearings.

3.3.2 Erosion/Surface Roughening/Object Damage

Operational experience, in particular the JT9D work performed under Contract NAS3-20632, has helped to sort out the mechanisms and effects of erosion and object damage. Erosion was found to cause performance degradation by increasing surface roughening, changing the airfoil shape with loss of material, and increasing blade tip and seal clearances. Additionally, this work showed that airfoil surface roughness can increase in airline service because of dirt accumulation. Engine-ingested debris is the cause of airfoil leading edge nicks and dents which cause airflow disturbance and increased losses. Finally, turbine blade impact damage from hard carbon particles formed in the combustor has been observed. This experience indicates that erosion, foreign object damage (FOD), and dirt have been deterioration factors only in the compression system. The carbon particle damage (bill of material object damage, BMOD) observed only affects the first stage HPT blading, and, although this erosion required that the blades be replaced more frequently, no significant performance detriment was observed. As a result, the Energy Efficient Engine design was concentrated on concepts applicable to improving compression system durability.

Preliminary designs incorporated thicker leading edge airfoils (with reduced loss contours) and resistant surfaces to slow these mechanisms of compression system performance deterioration. Since it is particularly difficult to quantify the impact of changes in airfoil shape on performance because of lack of basic data, considerable judgment was used to estimate the deterioration improvement (relative to JT9D experience) resulting from thicker leading edges. Conversely, surface roughness loss effects have been successfully correlated with airfoil design parameters, so the deterioration improvements resulting from the use of coatings and surface treatments were readily estimated. Total predicted 4000 hour compression system deterioration associated with these factors was judged to be the equivalent of about +0.3 percent TSFC for the direct drive engines. A slightly less 4000 hour deterioration was predicted for the geared engines because of their lower relative fan speed, 110 m/sec (375 ft/sec) less.

TABLE C-LXXXVI

CRUISE TSFC EFFECTS OF CLEARANCE DETERIORATION AT 4000 HOURS

Engine:	1 Stage HPT Direct-Drive	2 Stage HPT Direct-Drive	1 Stage HPT Geared	2 Stage HPT Geared
Δ Cruise TSFC - %	+0.8	+0.7	+0.4	+0.4

3.3.3 Seal/Mechanical Joint Leakage

During structural and secondary system analyses, seal clearances were set large enough to prevent deterioration. Essentially zero leakage deterioration could be identified, as a result, and no differences between engine configurations could be assessed.

Mechanical joints, again based on JT9D experience, are not a major factor in performance deterioration. Linear leakage evaluation results showed that although the two-stage HPT configuration has more joints than the one-stage, the latter has higher leakage performance penalties because of its greater expansion ratio such that no significant net difference could be determined. Predicted 4000 hr. mechanical joint deterioration was estimated to cause only about +0.1% TSFC effect for all configurations.

3.3.4 Turbine Airfoil Distortion/Creep

HPT vane distortion or bow and blade creep untwist as functions of time were investigated using established design systems. Operational data for bowing in JT9D vanes had been previously correlated, with a simple beam bending analysis, to design parameters to form a base for future predictions. The vane distortions for the Energy Efficient Engine configurations were calculated considering the effects of airfoil span, chord, metal temperature, and gas loads using the same beam analysis. In regard to blade untwist, JT9D experience and experience with other Pratt & Whitney Aircraft long, highly twisted, shroudless turbine blades had been correlated to the rates of torsional and radial creeps to define a method to calculate untwists for other airfoils. Energy Efficient Engine HPT blade creep untwists were calculated using this methodology in combination with specific radial chord angle variation, torsional stiffness, temperature, and centrifugal stress design data.

Results of these analyses are presented in Tables C-LXXXVII and C-LXXXVIII for the direct drive and geared engines respectively. Since the HPT first stage vane design and operating parameters, such as chords, spans, and metal temperatures are similar for the four engine configurations, maximum calculated bows are identical. However, because of the one-stage HPT's higher expansion ratio, its flow capacity increase from first vane bow is twice that of the two-stage HPT. Analysis of the second stage vane of the two stage HPT showed the vane and its attachment to be sufficiently stiff to preclude deflection. Again, because of similar design parameters and operating environments, first stage blade maximum creep untwists calculated were the same for all four engines. The two stage HPT efficiency was estimated to be adversely affected because of the increased blade untwist with time associated with the longer span second stage blade.

Resulting predicted performance deteriorations for the one and two-stage HPT engines at 4000 hours were +0.3 and +0.7 percent respectively.

3.3.5 Overall Deterioration

Overall performance deterioration, considering all causes, was found to be the same for both one- and two-stage HPT engines. The direct drive configurations showed a total of about 1.5 percent increase in cruise TSFC at 4000 hours, while the geared configurations showed about 0.35 percent less deterioration.

TABLE C-LXXXVII

DIRECT DRIVE ENGINE HPT AIRFOIL DISTORTION
CRUISE DETERIORATION SUMMARY

Engine:	1 Stage HPT			2 Stage HPT		
Operating Time:	0 hrs	1000 hrs	4000 hrs	0 hrs	1000 hrs	4000 hrs
Effect						
1st Vane Bow - deg.	0	0.125	0.250	0	0.125	0.250
1st Blade Untwist - deg	0	0.330	0.670	0	0.330	0.670
2nd Blade Untwist - deg	–	–	–	0	0.670	1.340
Efficiency - %	Base	-0.14	-0.40	Base	-0.30	-0.80
Flow Capacity - %	Base	+1.39	+2.79	Base	+0.88	+1.77

TABLE C-LXXXVIII

GEARED ENGINE HPT AIRFOIL DISTORTION
CRUISE DETERIORATION SUMMARY

Engine:	1 Stage HPT			2 Stage HPT		
Operating Time:	0 hrs	1000 hrs	4000 hrs	0 hrs	1000 hrs	4000 hrs
Effect						
1st Vane Bow - deg	0	0.125	0.250	0	0.125	0.250
1st Blade Untwist - deg	0	0.330	0.670	0	0.330	0.670
2nd Blade Untwist - deg	–	–	–	0	0.670	1.340
Efficiency - %	Base	-0.14	-0.40	Base	-0.29	-0.80
Flow Capacity - %	Base	+1.39	+2.79	Base	+0.88	+1.78

3.4 Engine Thrust Growth

The Energy Efficient Engine was designed to accommodate thrust growth for extended airline utilization without significant compromise to fuel consumption, economic, and environmental goals. Cycles and configurations were selected such that the aerodynamics, structures, and materials are capable of providing for increased thrust. Two approaches were taken to evaluate up to 25 percent growth impacts. The first approach retained the base fan diameter, and hence the nacelle, while achieving increased thrust by HPT temperature (RIT) and fan pressure ratio (FPR) increases and a slight increase in fan specific flow. The second method increased fan diameter and RIT while holding FPR constant. Both approaches increased overall pressure ratio (OPR) to 45:1 and gas generator airflow by the incorporation of a LPC supercharging stage.

Component performance and turbine cooling air assessments were made so that configurational impacts and overall engine performance could be evaluated.

FPR, tip speed, and efficiency relationships were predicted using the aerodynamic design system that defined the base fans. The relationships developed are shown in Figure C-92 for the direct drive engine fans and Figure C-93 for the geared fans.

Rated RIT's for growth were set to hold base engine cruise-to-takeoff thrust ratios with the results shown in Figures C-94 to C-97. Turbine airfoil cooling schemes were assessed for the several growth steps, considering both increased combustor exit temperature (CET) and increased cooling air temperatures resulting from the OPR increase. Figures C-98 and C-99 show the resulting turbine cooling configurations at the base and increased thrust levels. Efficiency effects were determined at each growth step considered.

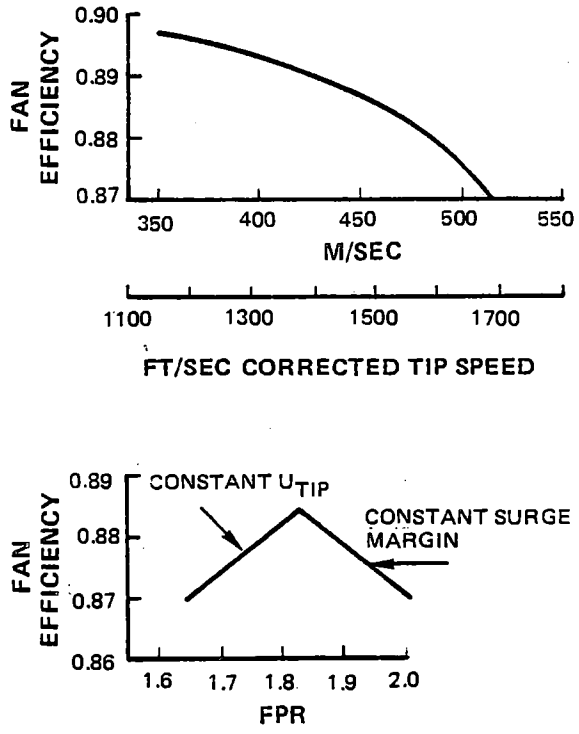

Figure C-92 Direct-Drive Engine Fan Efficiency Trends for Growth

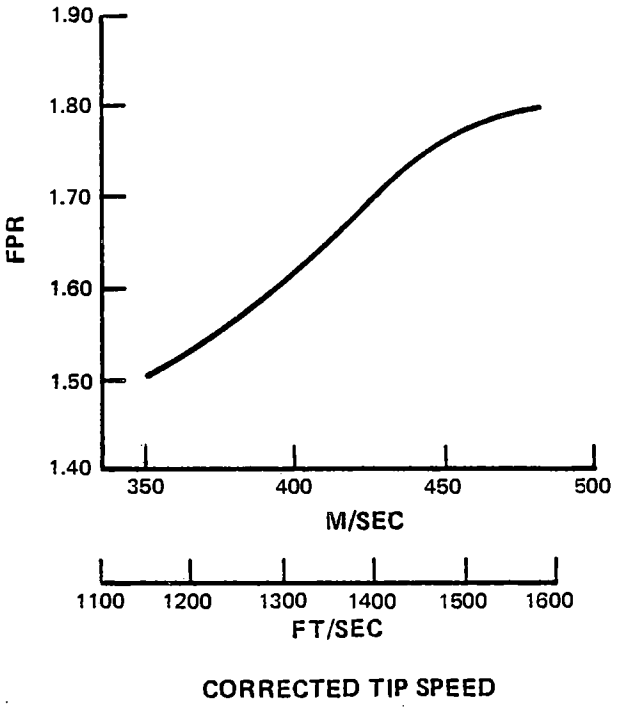

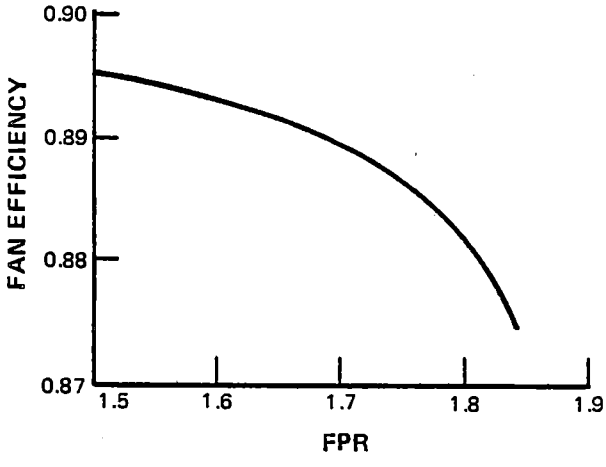

Figure C-93 Geared Engine Fan Efficiency Trends for Growth

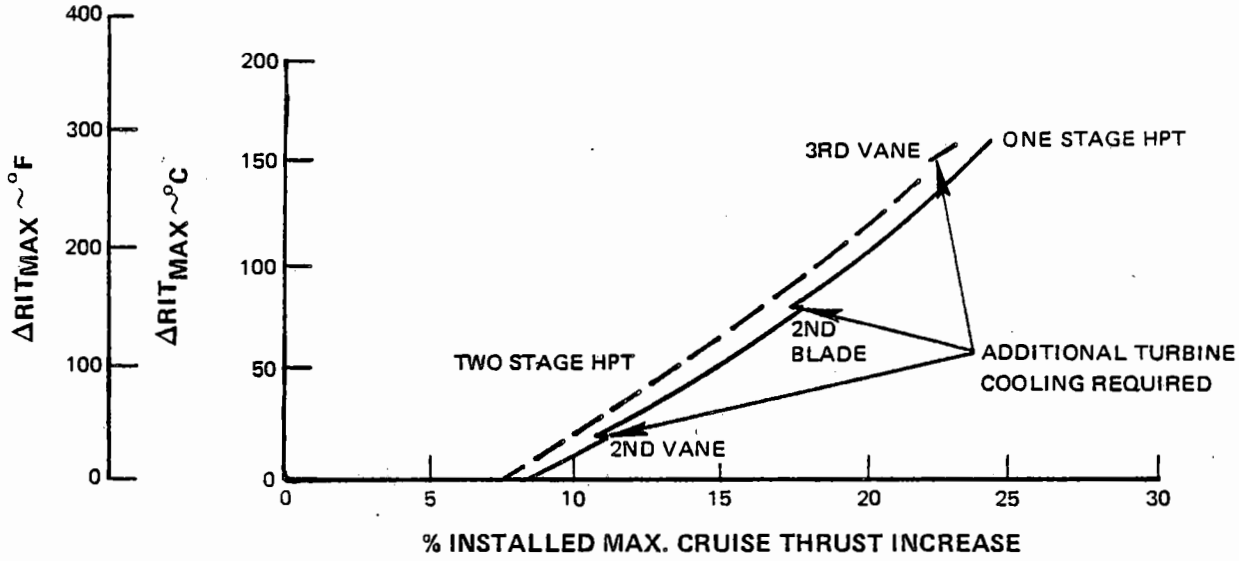

Figure C-94 Direct-Drive Engine Constant Fan Diameter Growth Turbine RIT Trends

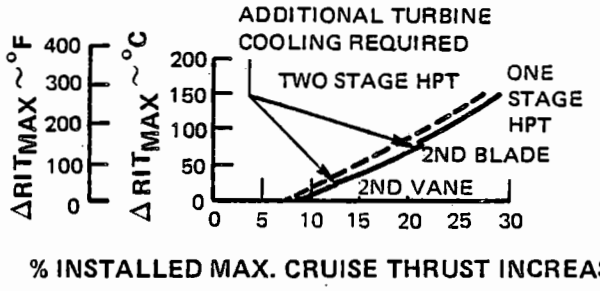

Figure C-95 Direct-Drive Engine Increased Fan Diameter Growth Turbine RIT Trends

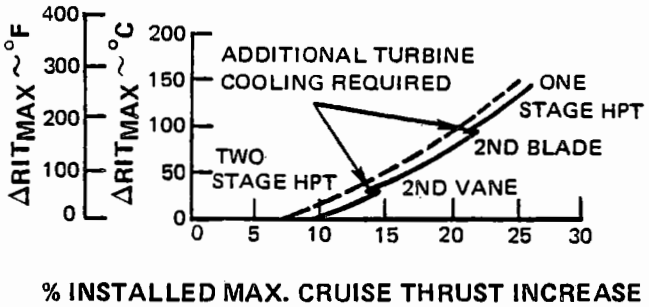

Figure C-96 Geared Engine Constant Fan Diameter Growth Fan RIT Trends

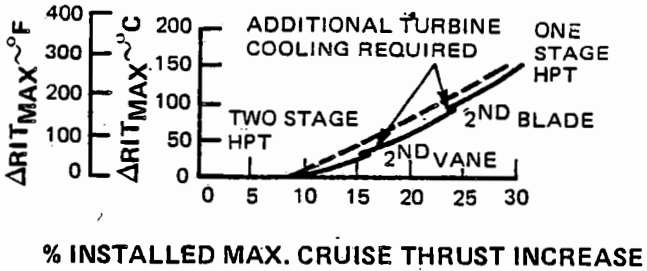

Figure C-97 Geared Engine Increased Fan Diameter Growth Turbine RIT Trends

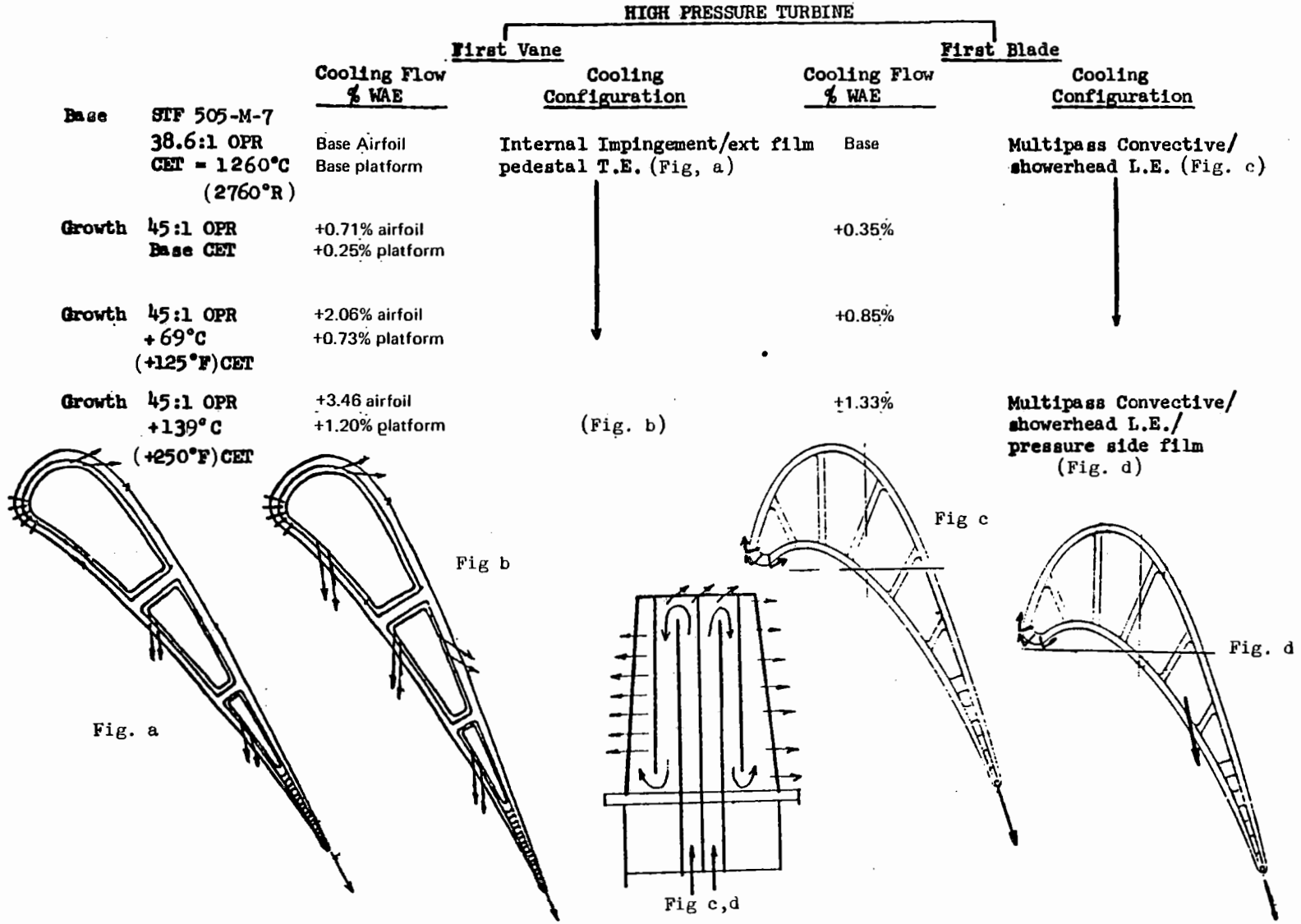

Figure C-98 One Stage High-Pressure Turbine Growth Engine Cooling Configurations

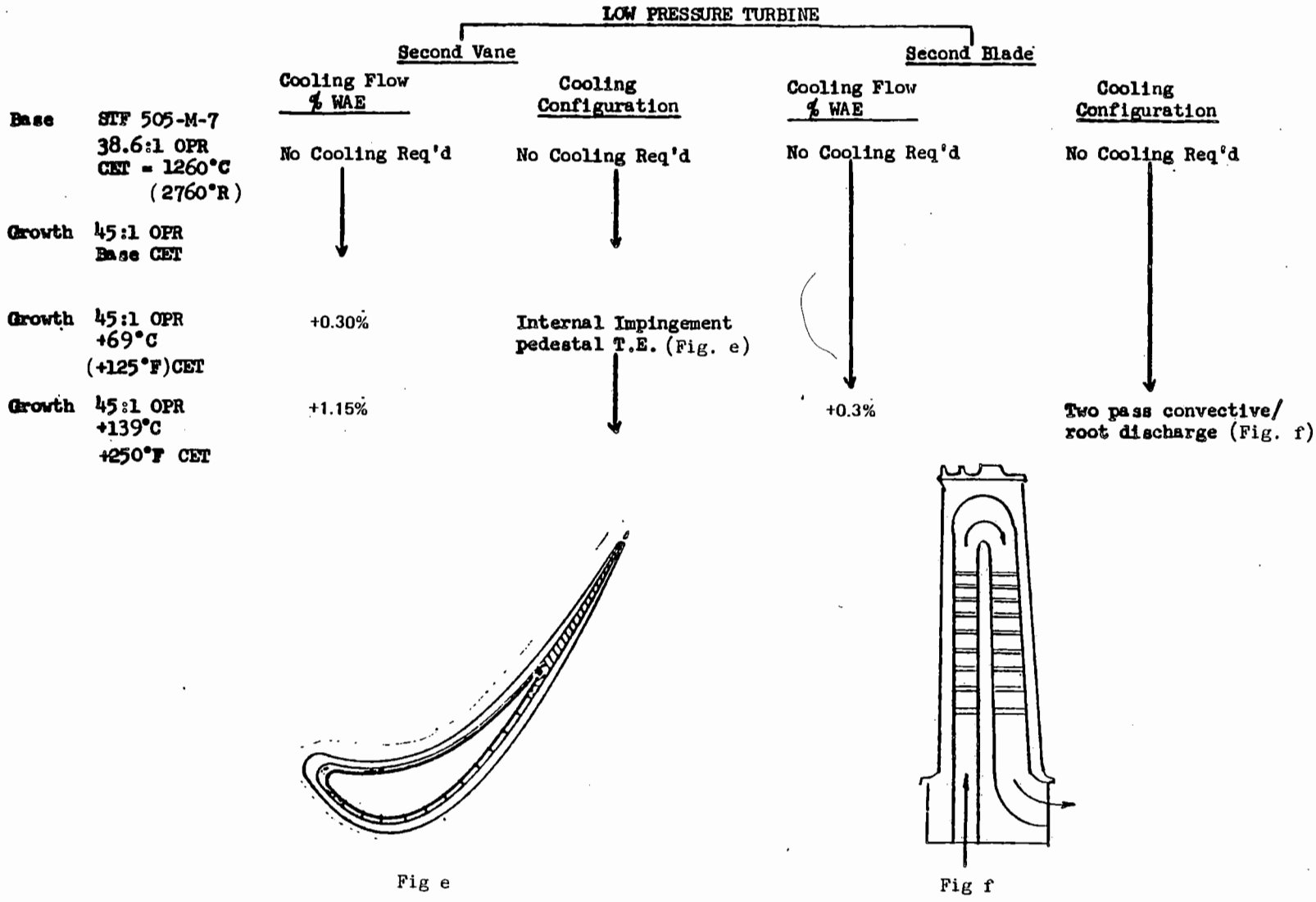

Figure C-98 (Cont'd)

HIGH PRESSURE TURBINE

		First Vane		First Blade	
		Cooling Flow % WAE	Cooling Configuration	Cooling Flow % WAE	Cooling Configuration
Base	STF 505-M-9 38.6:1 OPR CET = 60°C (2760°R)	Base airfoil Base platform	Internal Impingement/ external film pedestal T.E. (Fig, a)	Base	Multipass Convective/ showerhead L.E. (Fig. c)
Growth	45:1 OPR Base CET	+0.50% airfoil +0.52% platform		+0.32%	
Growth	45:1 OPR +69°C (+125°F)CET	+1.83% airfoil +1.00% platform		+0.80%	
Growth	45:1 OPR +139°F CET (+250°F)CET	+3.29% airfoil +1.49% platform	(Fig. b)	+1.31%	Multipass Convective/ showerhead L.E./ pressure side film (Fig, d)

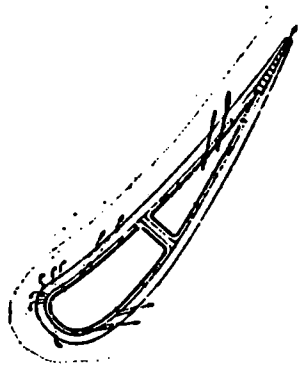

Fig a.

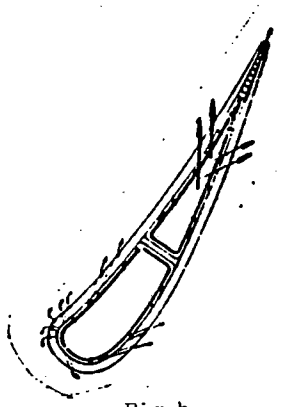

Fig b

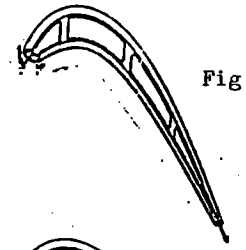

Fig c

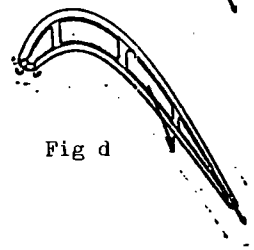

Fig d

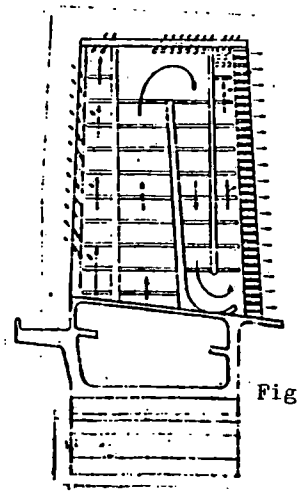

Fig c,d

Figure C-99 Two-Stage High-Pressure Turbine Growth Engine Cooling Configurations

		HIGH PRESSURE TURBINE				LOW PRESSURE TURBINE
		Second Vane		Second Blade		
		Cooling Flow % WAE	Cooling Configuration	Cooling Flow % WAE	Cooling Configuration	
Base	STF 505-M-9 38.6:1 OPR CET = 1260°C (2760°R)	Base	Internal Impingement pedestal T.E. (Fig. e)	Base	Multipass convective/ pedestal T.E. (Fig. g)	No Foil Cooling Required
Growth	45:1 OPR Base CET	+0.78%		+0.06%		
Growth	45:1 OPR +69°C (+125°F)CET	+1.32%		+0.30%		
Growth	45:1 OPR +139°C (+250°F)CET	+1.86%	Internal Impingement showerhead L.E./ pedestal T.E. (Fig. f)	+0.60%		

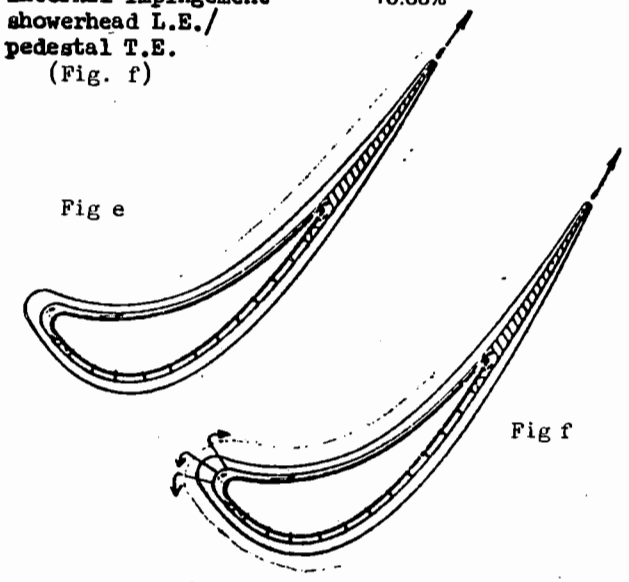

Fig e

Fig f

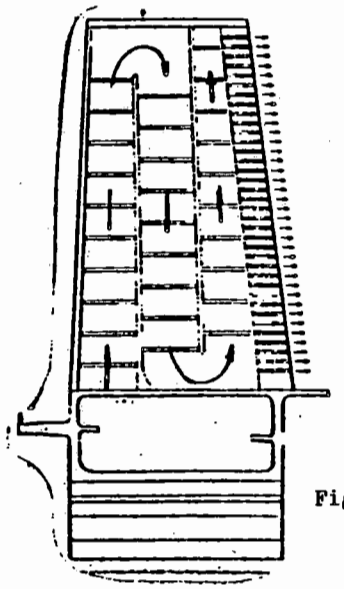

Fig g

Figure C-99 (Cont'd)

Results showed that for all the growth steps, one-stage HPT cooling schemes remained essentially unchanged. As temperature increased, additional flow was obtained in the first vane through an increase in the number and size of the film cooling holes. At roughly +140°C (+250°F), film cooling holes were added to the rear of the vane suction side to facilitate trailing edge cooling. Additional blade cooling flow was obtained by increasing the blade supply pressure and by adding pressure side film holes at about +140°C (+250°F) to limit the supply pressure requirements.

LPT airfoil cooling was found to be required at the higher temperature levels for the one-stage HPT engine. At both +70°C (+125°F) and +140°C (+250°F), inlet vane cooling was required. This cooling was accomplished with an internal impingement and a pedestal trailing edge scheme. At +140°C (+250°F), it was also necessary to convectively cool the first blade.

Two-stage HPT aerodynamic differences resulted in minor changes in the cooling schemes selected with growth.

As in the case of the one-stage HPT, the two-stage first vane and first blade flows were increased by implementing a larger quantity of dense film holes and by increasing the supply pressure, respectively. In the second vane, the temperature of +140°C (+250°F) necessitated additional film holes as well as a showerhead leading edge. The second blade cooling scheme remained unchanged throughout the considered growth steps.

For the two-stage HPT engine, LPT cooling was not required for any of the growth steps because of the higher work requirement of the HPT (18:1 HPC pressure ratio) and the resultant reduced LPT inlet temperature.

Based on the engine component performance and turbine cooling air changes, growth performance for the four engines was calculated using the SOAPP computer model. For the constant fan diameter appraoch, the fan duct-to-engine exhaust pressure ratio was allowed to decrease in the initial supercharging step at constant CET, FPR, and LPC polytropic efficiency. This lower pressure ratio (1.0 vs 1.1) was then held constant with increases in temperature by varying FPR. This approach was taken to minimize FPR increase (efficiency decrease), and thus the TSFC penalty. The increased fan diameter growth appraoch taken held a 1.1 exhaust pressure ratio with increasing temperature by varying bypass ratio (diameter). To obtain installationation effects, base nacelle drags for the constant fan diameter cases were maintained, while for the increased fan diameter appraoch, nacelle drag was scaled proportionally to inlet airflow.

Installed TSFC results presented as functions of installed thrust increase are represented in Figures C-100 through C-103. In general, these results showed that for the constant fan diameter approach, thrust growth is limited to roughly 25% for the maximum temperature increase evaluated. Thrust growth for the two-stage HPT engines for a given temperature increase was slightly less than that of the one stage because of a more rapid increase of turbine cooling air. TSFC trends were similar, although the one-stage HPT engine did not have as significant a fuel consumption improvement for the initial supercharging step because of increased HPT efficiency penalty for expansion ratio increase. Both one- and two-stage HPT engines had significant TSFC increases as thrust was increased beyond the supercharging step because of increased specific thrust and poorer propulsion efficiency.

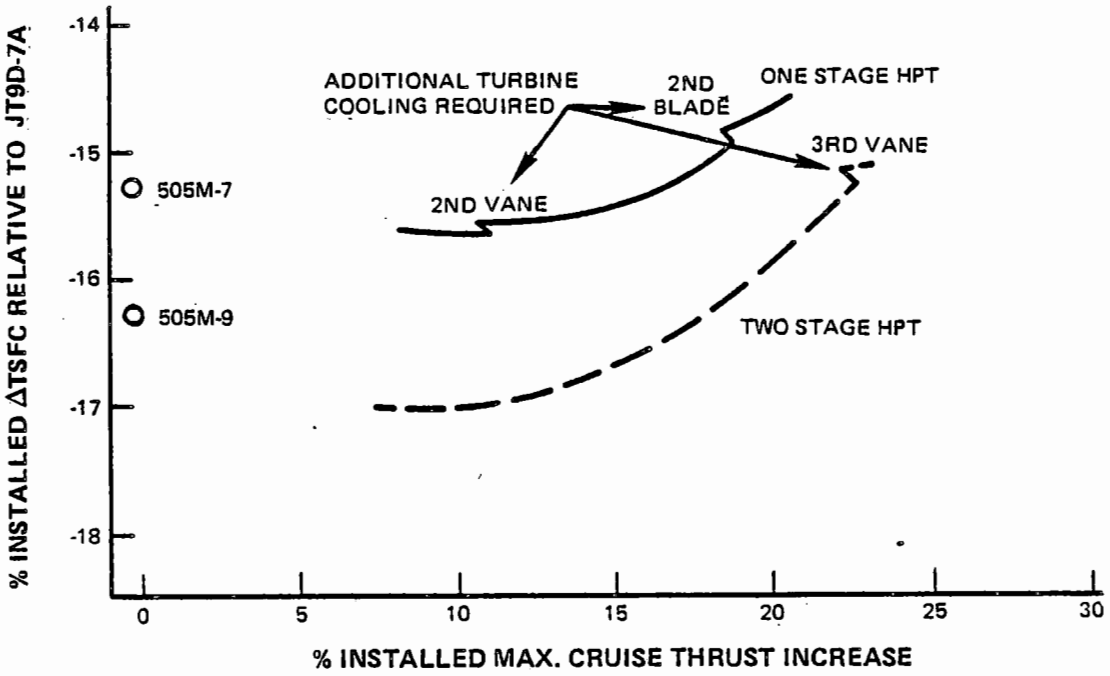

Figure C-100 Direct-Drive Engine Constant Fan Diameter Growth TSFC Trends

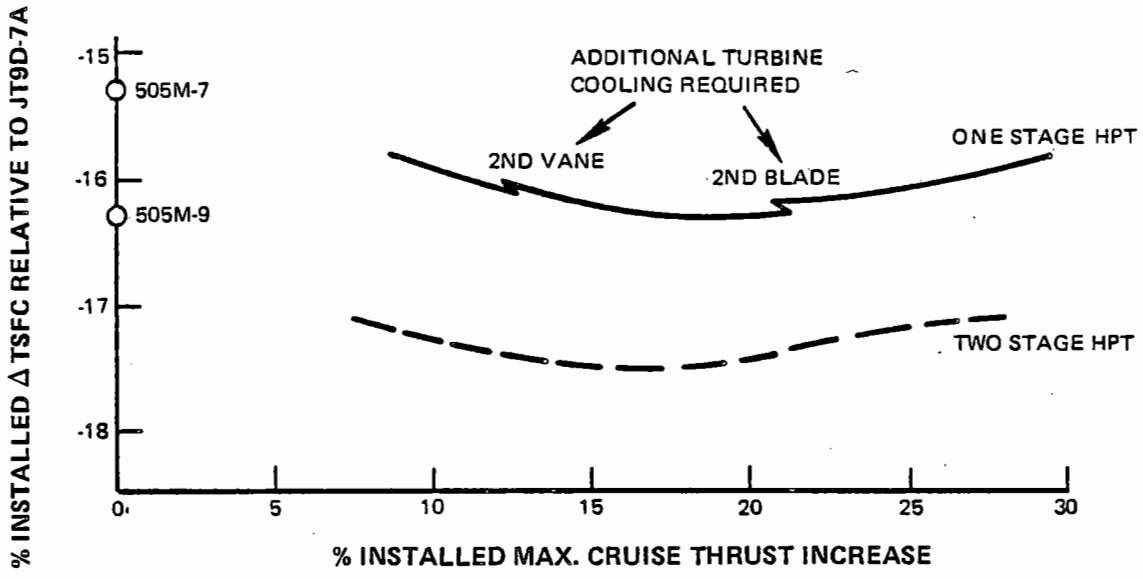

Figure C-101 Direct-Drive Engine Increased Fan Diameter Growth TSFC Trends

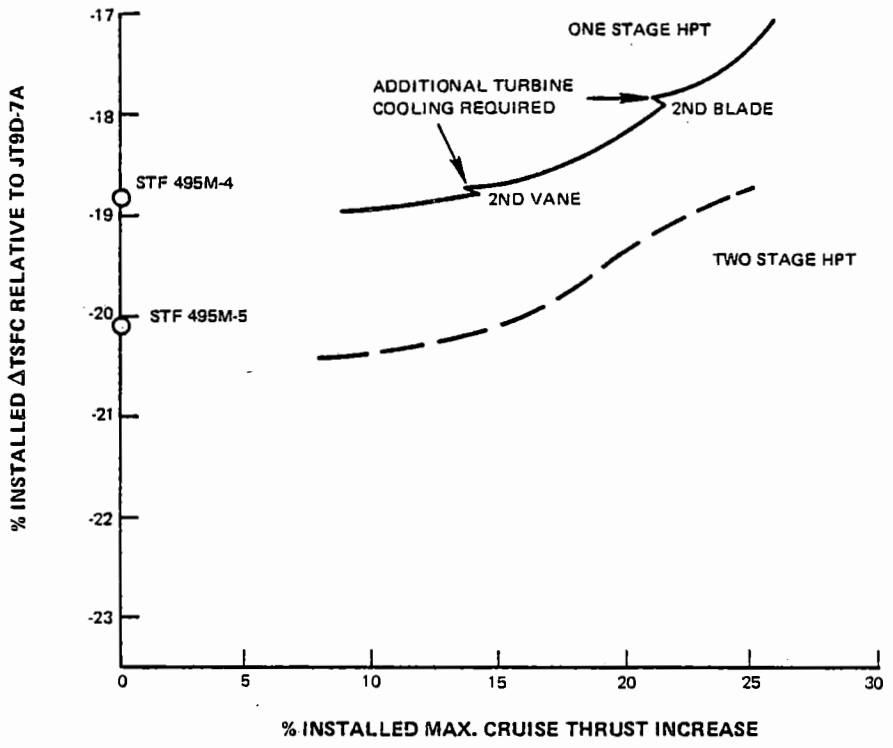

Figure C-102 Geared Engine Constant Fan Diameter Growth TSFC Trends

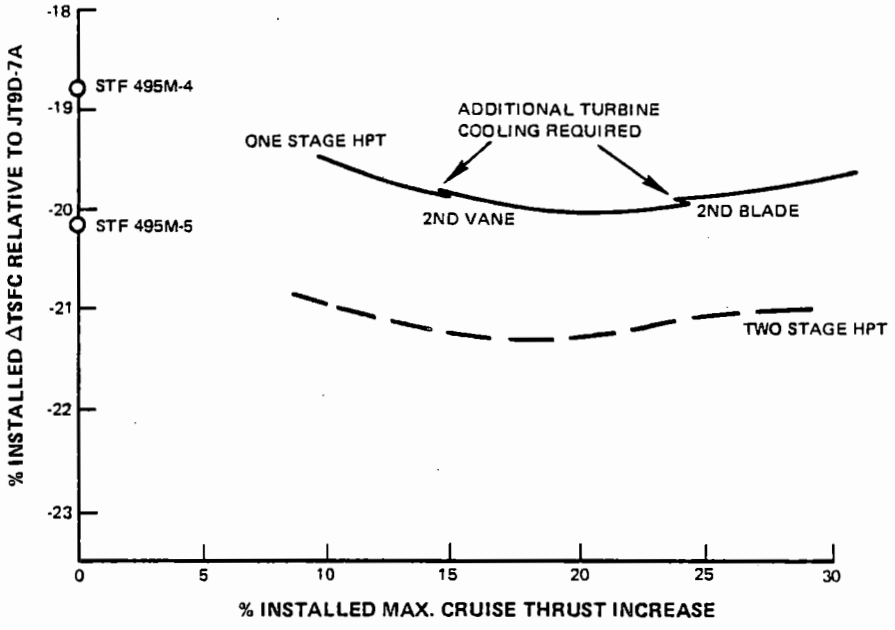

Figure C-103 Geared Engine Increased Fan Diameter Growth TSFC Trends

For the increased fan diameter approach, maximum thrust growths up to 30 percent were achieved for the maximum temperature considered. Thrust growth for the two-stage HPT engine again was slightly less than the one-stage for the same reason. TSFC trends were again similar for both engines, with fuel consumption maintained essentially constant beyond the initial supercharging step. As before, the one-stage HPT engine had less TSFC imporvement for the supercharging step, as a result of HPT efficiency penalty with increasing expansion ratio.

Comparison of the direct drive and geared engine thrust growth potentials showed both configurations to have equal capabilities.

Assessments were also made to measure the impact of the engine thrust growth approaches on noise and emission levels. Typical changes in engine noise calculated for the studied approaches are presented in Table C-LXXXIX .

These results show that both thrust growth approaches increase noise. However, it was apparent that the growth procedure normally followed initially in service, that of retaining the base fan diameter and achieving thrust increase with increased CET and FPR produces a significantly larger noise penalty. Only by increasing fan diameter would it be possible to achieve FAR 36 (1969)-10EPNdB with growth engines.

Growth effects on engine emissions were reviewed relative to those of Task I. The increased OPR was again found to cause changes to base engine emissions. NO_x EPAP was increased by about 1.0, while those for CO and HC were reduced by 0.2 and 0.05, respectively. As a result, NO_x goals most likely cannot be met by the growth engines, whereas the other emission parameters can be.

TABLE C-LXXXIX

GROWTH ENGINE STUDY NOISE SUMMARY – EPNdB
+ 18% T.O. THRUST

Engine:	1 Stage HPT, Direct Drive		1 Stage HPT, Geared	
Growth Approach:	Const. Fan Dia.	Incr. Fan Dia.	Const. Fan Dia.	Incr. Fan Dia.
Combustor Exit Temp. °C (°F)	+140(+250)	+70(+125)	+140(+250)	+70 (+4125)
PWA Trijet				
Approach	+1.2	+1.1	+2.0	+0.3
Takeoff	+2.1	+0.9	+2.7	+0.2
Sideline	+2.3	+1.1	+2.6	+0.1
PWA Quadjet				
Approach	+1.1	+0.8	+2.0	+0.5
Takeoff	+2.0	+0.9	+2.5	+0.1
Sideline	+2.4	+1.0	+2.6	+0.1

APPENDIX D

RISK ANALYSIS – TASK IV

LIST OF ILLUSTRATIONS
APPENDIX D

APPENDIX D

LIST OF TABLES

APPENDIX D

RISK ANALYSIS – TASK IV

1.0 INTRODUCTION

Task III cruise thrust specific fuel consumption (TSFC) and direct operating cost (DOC) reductions, relative to the JT9D-7A engine, were expanded into probability distributions to obtain comparisons at equal probabilities of achievement (POA). TSFC and DOC differences between one- and two-stage HPT engines remained unchanged by POA analysis. Task III direct-drive fan and geared-fan engine TSFC differences were narrowed by one-third. Lower domestic and international aircraft DOC's were estimated for the direct-drive fan engines at an equal POA, which reversed the Task III trends. All four Task III engine configurations were calculated to have a greater-than-95 percent probability of achieving the goals of a minimum cruise TSFC reduction of 12 percent and a minimum aircraft DOC reduction of five percent in international operation. Only the direct-drive fan, single-stage HPT engine was indicated to have a high probability (>80%) of providing at least a five percent DOC reduction relative to the JT9D-7A, in domestic aircraft operation.

The items considered in generating TSFC and DOC probability distribution are listed in Table D-I. Technology items included aerodynamic, structural, and material advancements. Test measurement accuracy was also considered. Many component areas were evaluated, including the turbomachinery, flow ducts, mixer, gear and heat exchanger, and nacelle. Pratt & Whitney Aircraft trade factors were used to convert the component information into TSFC and DOC probability distributions.

To determine the inherent level of difficulty associated with realization of the benefits in each of the component areas listed, the evaluation process was initiated with optimistic, most likely, and pessimistic estimates of individual technology improvements. Research, design and analysis, and study project personnel participated in this activity to obtain a concensus. Using these estimates, probability distributions were generated for each of the technology items and statistically summed to arrive at probability distributions for individual component areas.

Influence coefficients were applied to component efficiency, pressure loss, drag, and cooling air/leakage distributions to calculate the engine TSFC probability distribution. As the final step, using trade factors, TSFC was combined with weight, acquisition cost, and maintenance cost distributions derived from the last seven component areas listed on Table D-I to determine DOC. Higher fuel prices, 3¢ / liter (10¢ /gal.), were assumed in the DOC evaluation because of the uncertainty in cost projections. These calculations were obtained for direct drive fan, one- and two-stage HPT engines, and the geared fan, one-stage HPT engine. Geared fan, two-stage HPT engine capabilities were then estimated from the evaluation of the other three configurations.

A program risk assessment was also conducted as part of Task IV in order to identify potential problems which could affect a technology development program schedule or funding requirement. For each potential problem, a backup position and the magnitude of the impact on the overall program were identified. Results of this assessment are included in this appendix.

TABLE D-I

ITEMS CONSIDERED TO GENERATE TSFC AND DOC PROBABILITY DISTRIBUTIONS

Technology Item	Component Area	Engine TSFC	Aircraft DOC
Improved Airfoils Reduced Endwall Losses Reduced Windage	Fan Efficiency LPC Efficiency HPC Efficiency Combustor Pressure Loss	Influence Coefficients Applied to Component Data	Trade Factors Applied to TSFC, Component Weight, and Cost Data
Tighter Running Clearances Advanced Materials Smoother Acoustic Treatment Test Results Accuracy	HPT Efficiency LPT Efficiency HPT Airfoil Cooling HPT Outer Air Seal/ Rim Cavity Leakage Gear Efficiency Heat Exchanger Pressure Loss Ducting Pressure Losses Mixer Efficiency Nozzle Efficiency Nacelle Drag HPT Airfoil Material Cost and Life HPT Ceramic Outer Airseal Cost and Life Advanced Disk Material Cost and Properties HPT Airfoil Number Nacelle Weight Gearbox Weight, Cost and Life Heat Exchanger Effectiveness		

2.0 TSFC PROBABILITY DISTRIBUTIONS

Influence coefficients, listed in Table D-II, were used to convert the various component performance trends into engine TSFC probability distributions. The influence coefficients are at a 10,700 m (35,000 ft), Mach 0.8 maximum cruise flight condition and represent constant thrust operation.

2.1 Direct-Drive One-Stage Versus Two-Stage High-Pressure Turbine Engines

Figure D-1 shows the probability distribution of achieving various TSFC reductions, relative to the JT9D-7A, for direct-drive engines with one or two-stage HPT's. These curves were obtained by summing all the component efficiency and pressure loss effects on TSFC. The curve shapes are similar and equi-spaced, which is indicative of the same spread between optimistic and pessimistic performance values for all of the corresponding component areas.

The probability of achieving the TSFC reduction estimated in Task III for both of the direct drive engines was found to be approximately 40 percent. The respective components of both engines had the same probability of achieving Task III TSFC levels. Some components had a higher level of probability for achieving the Task III performance whereas other components had lower levels of probability in arriving at the final overall probability.

TABLE D-II

TASK IV TSFC INFLUENCE COEFFICIENTS
(10,700 m (35,000 ft), Mach 0.8 Max. Cruise)

Engine:	Direct-Drive 1 Stage HPT	Direct-Drive 2 Stage HPT	Geared 1 Stage HPT
a) Δ % TSFC Per 1 Percentage Point Efficiency			
Fan	0.64	0.64	0.66
LPC	0.15	0.09	0.23
HPC	0.54	0.57	0.59
HPT	0.65	0.67	0.69
LPT	0.83	0.77	0.87
Mixer	0.04	0.04	0.04
Gear	–	–	0.65
Nozzle Velocity Coefficient	2.3	2.3	3.0
b) Δ % TSFC Per 1 Percent Pressure Loss			
Core	0.36	0.36	0.36
Duct	0.74	0.74	1.15

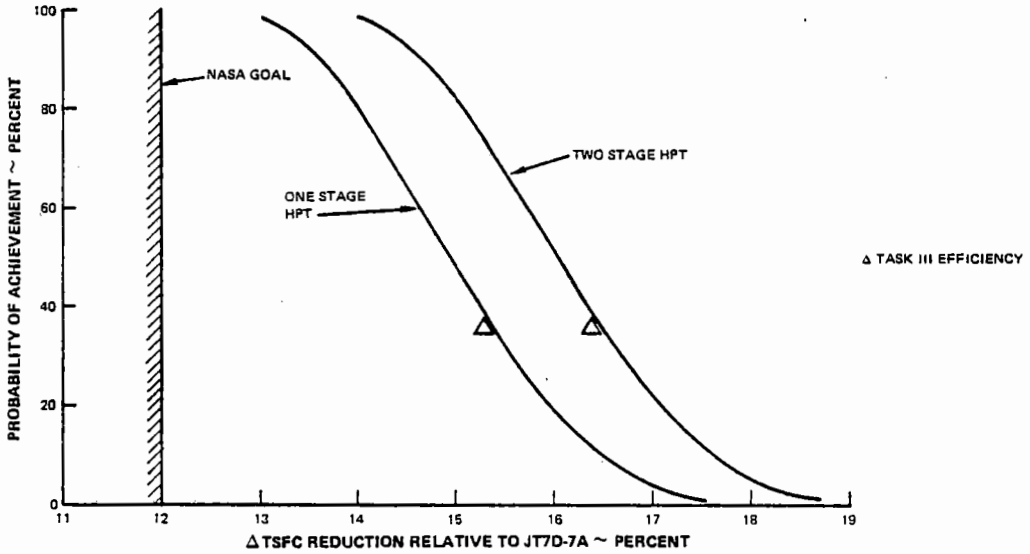

Figure D-1 Probability of Achieving Direct-Drive Engine TSFC with Mature Engines

A comparison of the probability distribution of the efficiency for the one and two-stage HPT's is shown in Figure D-2. The turbine is the only component having a major effect on the TSFC difference between the two engine configurations. The one-stage HPT is a high expansion ratio design requiring transonic blading velocities, resulting in the three percentage point efficiency difference between the two HPT's. The aerodynamic parameters affecting the performance of the one-stage HPT are well substantiated by a Pratt & Whitney Aircraft one-stage HPT rig. A 30 percent probability of achieving the efficiency used in Task III was calculated by statistically analyzing the probability of attaining the required performance levels in each technology area affected.

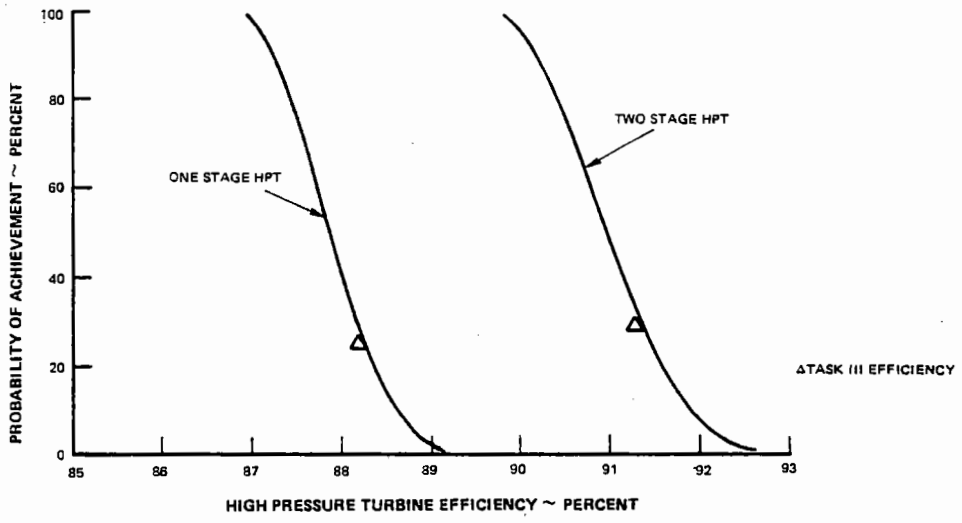

Figure D-2 Probability of Achieving High-Pressure Turbine Efficiency

The two-stage HPT also has aggressive aerodynamics, i.e., a significantly larger annulus area than the one-stage HPT, which resulted in similar gas velocity triangles and structural optimism. Maximum blade root centrifugal pull stresses were calculated to be 34.4 N/mm^2 (50 ksi) for both turbines. Disk attachment stresses were also calculated to be at the same percentage of the maximum allowables for the materials at their respective environmental temperature levels. As indicated in Figure D-2, the two-stage HPT also had a 30 percent probability of achieving the efficiency used in Task III.

2.2 Direct-Drive Versus Geared One-Stage High-Pressure Turbine Engines

The probability of achieving the TSFC for the direct drive and geared one-stage HPT engines is shown in Figure D-3. The two curves are similarly shaped with a constant difference between them. The significant difference shown on these curves is the lower probability of achieving the Task III TSFC estimate with the geared engine than with the direct drive engine.

The 30 percent difference in POA level represents a 1.2 percent difference in TSFC. This difference in level of probability of achieving the Task III TSFC levels was caused by optimistic projections in three geared engine components. These components are listed in Table D-III, along with a listing of the TSFC effects of providing a 40 percent TSFC POA with the geared engines.

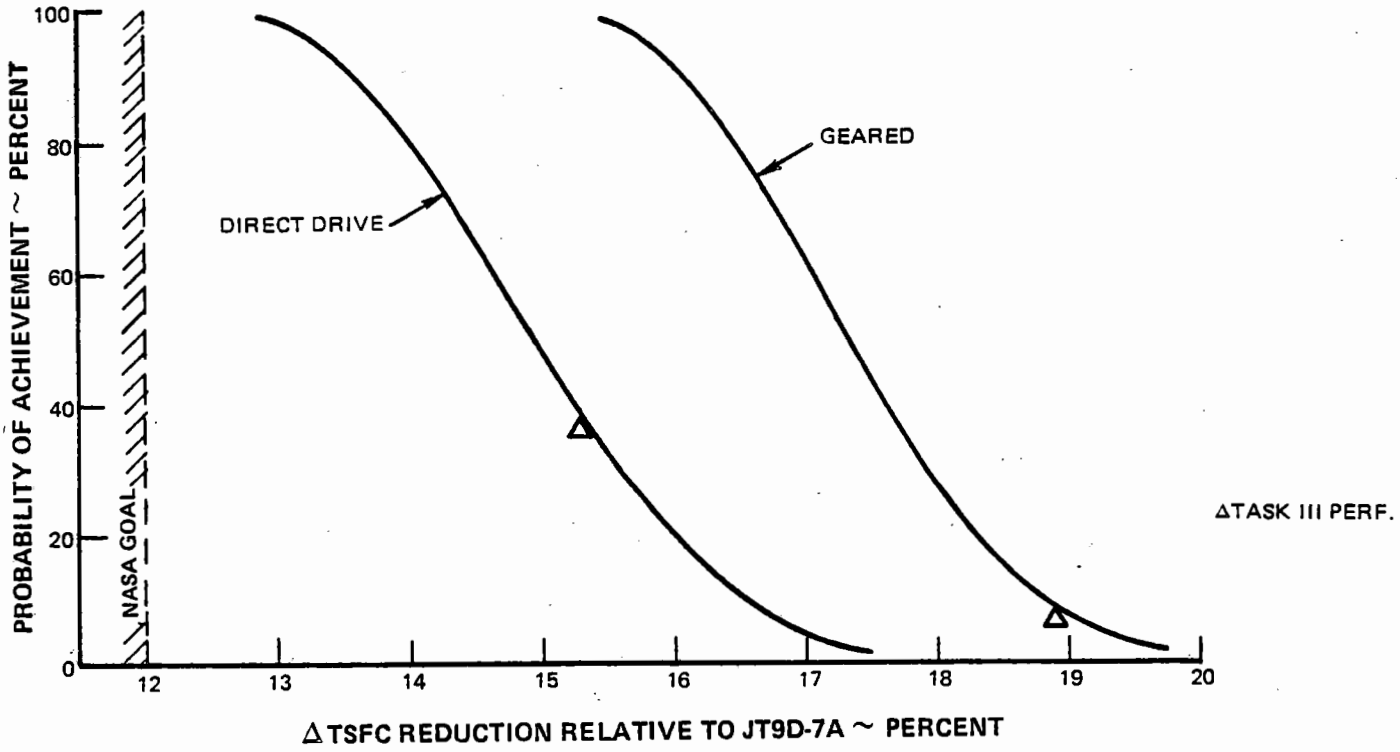

Figure D-3 Probability of Achieving One-Stage High-Pressure Turbine Engine TSFC

The probability of achieving the cruise gear efficiency is shown in Figure D-4. As indicated, the Task III gearbox efficiency was found to be highly optimistic.

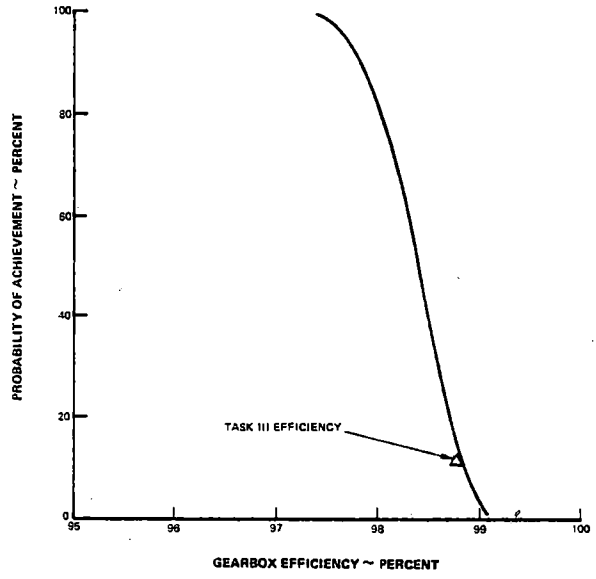

Figure D-4 Probability of Achieving Gearbox Efficiency at Cruise

The direct-drive engine LPC had a very high probability of achieving the Task III efficiency since only a modest step was required beyond the JT9D technology. In the geared engine, the LPC with its high rotative speed is aerodynamically similar to middle stages of HPC and the technology would be taken from the HPC program. However, the different environment and physical arrangement of these LPC stages would still not put their performance in a "very high" POA category.

In Task III, all engine accessories were located on the fan case for easy accessibility. This locally compromised the optimum cowl contour and increased the nacelle surface area, resulting in higher nacelle drag. While evaluating the probability of achieving the engine TSFC, the airframe accessories were relocated in the pylon area above the engine to minimize TSFC. Because of a smaller diameter nacelle, the direct-drive engine TSFC benefits exceeded those of the geared engine. Nacelle wetted area and friction drag were both reduced by a higher percentage through elimination of the airframe accessory bump. This accounts for the relative degradation in greared engine TSFC shown on Table D-III.

TABLE D-III

GEARED ENGINE COMPONENT PROBABILITY EFFECTS ON TSFC

	Percent Efficiency 10% to 40% POA	% Δ TSFC (10,700 m, 35,000 ft, Mach 0.8)
Gearbox	−0.3	+0.3
Low Pressure Compressor	−1.8	+0.3
Shift from fan case mounted to pylon mounted airframe accessories (relative to direct-drive engine)	–	+0.6
TOTAL	-2.1	+1.2

3.0 DIRECT OPERATING COST PROBABILITY DISTRIBUTION

3.1 Direct-Drive One-Stage Versus Two-Stage High-Pressure Turbine Engines

The DOC probability distributions for both the domestic and international mission aircraft are shown in Figure D-5, as applicable to the direct-drive one- and two-stage HPT engine configurations. These curves were obtained by combining the probability distributions

of TSFC, weight, acquisition cost, and maintenance costs. The probability of achieving the Task III level of DOC dropped, relative to TSFC, for both engines. This was caused primarily by optimistic maintenance cost calculations in Task III.

Increased maintenance costs in the four HPT technology areas reduced the probability of achieving the Task III DOC by about 20% relative to TSFC. The HPT airfoil material costs, ceramic outer airseal life, advanced disk material LCF properties, and the number of vanes and blades, as determined or used in Task III, were all found to be optimistic.

The probability of achieving full projected Task III single crystal airfoil material properties was rated low. The effect on spare parts replacement costs increased the maintenance costs, and reduced the probability of achieving the Task III DOC level by six percent. The probability of achieving the advanced disk material LCF properties was assessed at five percent, increasing maintenance costs, and netting a five percent reduction in the probability of achieving the Task III DOC. The probability of the HPT's having the low number of airfoils estimated in Task III was about 15%. Costs for spare parts replacement and maintenance were optimistic to the extent that the probability of achieving the Task III DOC was reduced about three percent.

Figure D-5 also shows the DOC probability distributions for 3¢ /liter (10¢ /gal.) higher fuel costs applicable to both mission aircraft. The DOC difference between the one- and (lower TSFC) two-stage HPT engines converged by 0.1 to 0.2 percent at the higher fuel cost.

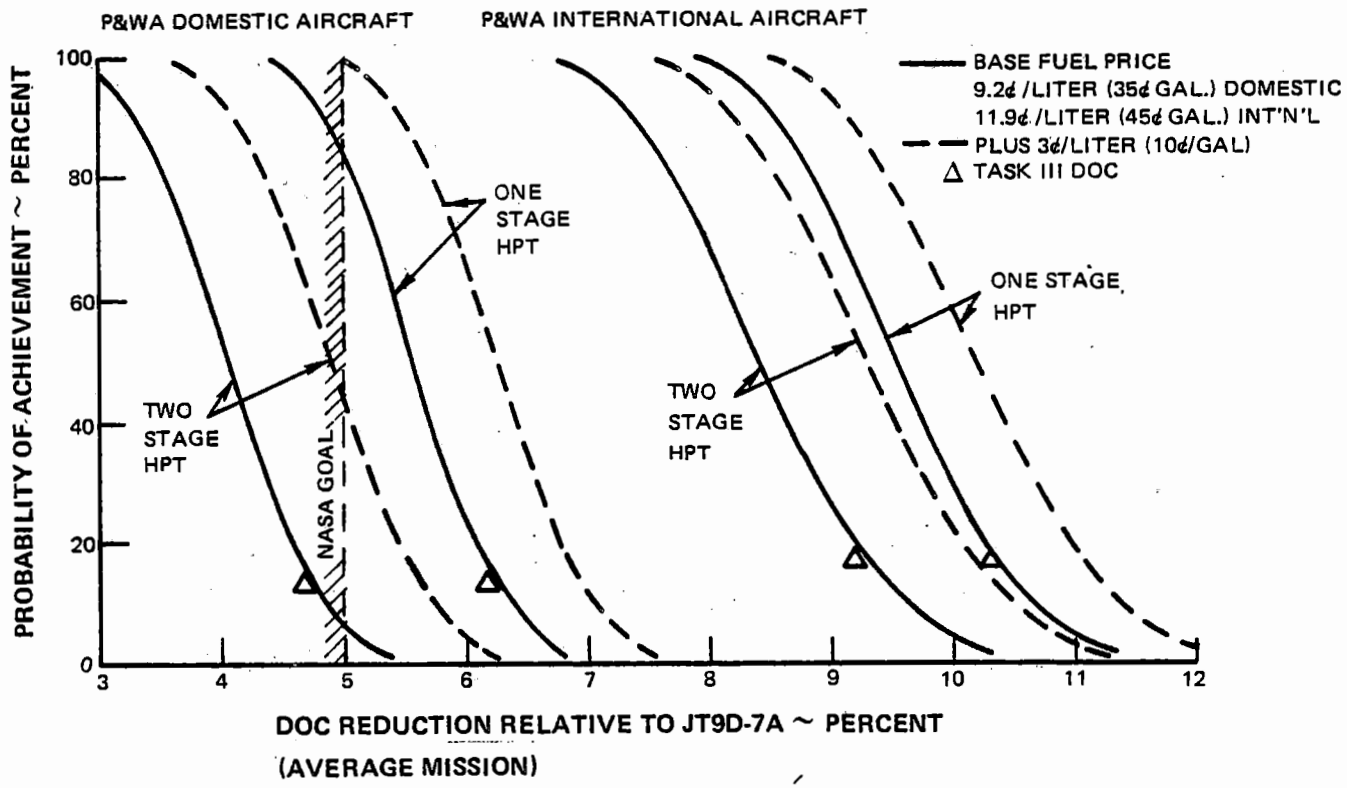

Figure D-5 Probability of Achieving Direct Drive Engine Aircraft Direct Operating Cost

3.2 Direct-Drive Versus Geared One-Stage High-Pressure Turbine Engines

A comparison of the DOC probability distributions for both the domestic and international mission aircraft with direct-drive and geared one stage HPT engine configurations is shown in Figure D-6. The probability of achieving the Task III level of DOC is very low, about one percent for the geared engine, primarily the result of the low probability of achieving the calculated Task III gearbox maintenance costs.

Using the POA level for the direct-drive engine as a base, the geared engine shows a DOC increase of 1.0 percent for the domestic aircraft, and 1.3 percent for the international aircraft. The lower TSFC POA of the geared engine accounted for an 0.4 and 0.7 percent increase in DOC for the domestic and international aircraft, respectively. Task III gearbox maintenance cost optimism represents about 0.4 percent DOC for both missions. Gearbox weight, acquisition cost, and air/oil heat exchanger effectiveness make up the remaining 0.2 percent DOC increase.

The higher gearbox maintenance costs are principally the result of optimistic Task III gearbox life and spare parts replacement rate projections. The gearbox probability assessment was based on Pratt & Whitney Aircraft experience with accessory gearbox drives. The experience was used to calibrate the results of a simplified failure analysis of the fan gearbox. This failure analysis used bearings and gears with 10,000 and 20,000-hour B-10 lives,

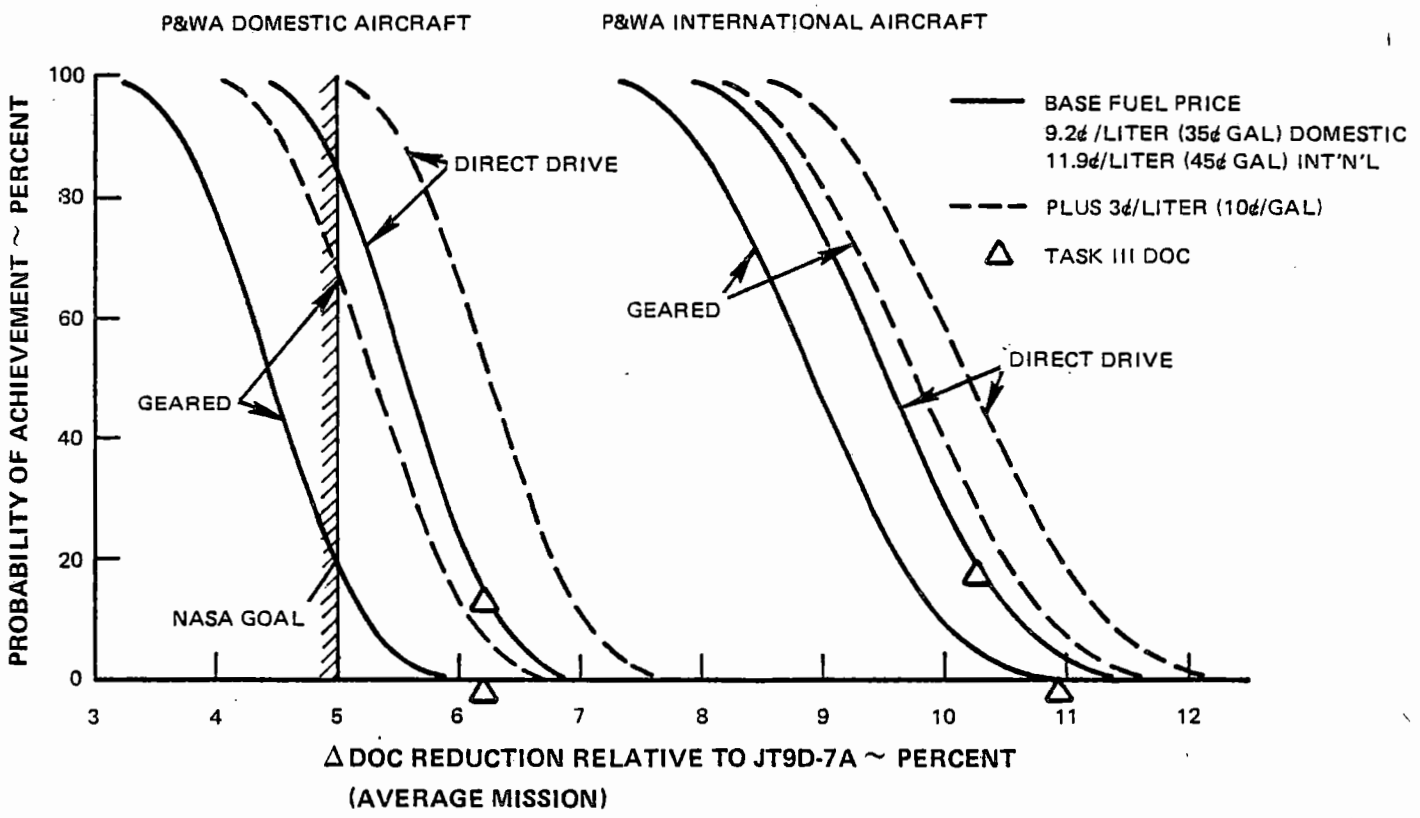

Figure D-6 Probability of Achieving One Stage High Pressure Turbine Engine Aircraft Direct Operating Cost

respectively. Mature fleet simulations were made, holding bearing and gear lives fixed, and varying the repair intervals to determine the number of expected failures over each interval. Failure rates were also controlled by a preventative maintenance schedule of refurbishing.

Based on JT8D and JT9D engine experience, it was necessary to replace 100 percent of the bearings and 50 percent of the gears at each shop visit to obtain an acceptable failure rate. This compares, respectively, to the 50 and 25 percent bearings and gear replacement used for the Task III engine with the same mean-time-between-repair period.

The lower TSFC and fuel costs of the geared engine resulted in a large variance in probability of achieving the five percent DOC reduction goal. Only the direct-drive one-stage HPT engine possessed a high probability of surpassing the NASA DOC goal.

4.0 PROGRAM RISK ASSESSMENT

Each potential problem area of a technology development program was categorized as having a minimal, moderate, or large impact on overall program schedule and/or budget. Minimal impact means an insignificant effect on either the schedule or funding. A moderate impact is interpreted as one that is mostly recoverable on an overall program basis, such that the end date and total funding are not significantly impacted. This would be achieved by adjusting individual programs or budgets within the overall program. A large program impact is one which calls for a major engine redesign with a significant impact on the overall schedule or funding. The results of this risk assessment are shown in Table D-IV, with each component area being described in the following paragraphs.

4.1 Fan Risk

The fan has a shroudless, hollow titanium blade incorporating advanced fabrication, structural, and aerodynamic technologies. If problems arise in the fabrication portion of the program that cannot be solved within the program timing and funding framework, then the shroudless blade aerodynamics, and hence the engine TSFC goal, could still be demonstrated by using a solid blade in the experimental engine. The weight penalty for the solid blade would then have to be addressed in a separate hollow fan fabrication program conducted in parallel with, or after, the base program, depending upon available funding. Structural problems such as flutter, bird strike, or resonance, which would show up during the analysis, structural test, or first fan rig test, would allow time to change to a part-span shroud configuration with a moderate program impact. Minor aerodynamic problems can be solved by removing the airfoils from the rig or experimental engine and recambering them, while major aerodynamic problems, which may prevent running of the experimental engine, would require a major fan redesign with significant program impact.

4.2 Low Pressure Compressor Risk

The main potential problem area in the LPC is in the aerodynamics which, similar to the fan, would require a recambering of the airfoils with minimum program impact, or a major redesign with significant program impact if severe stability or performance problems are encountered.

TABLE D-IV

E^3 PROGRAM RISK ASSESSMENT RESULTS

Component	Technology Feature	Potential Program	Component Program Redirection	Experimental Program Impact
Fan	Bonded Titanium Shroudless Blade	Fabrication	Solid	Minimal
	Bonded Titanium Shroudless Blade	Structural	Shrouded Blade	Moderate
	Aerodynamics	Aerodynamics	Recamber to Redesign Airfoils	Minimal to Large
LPC	Aerodynamics	Aerodynamics	Recamber to Redesign Airfoils	Minimal to Large
HPC	Aerodynamics	Aerodynamics	Recamber to Redesign Airfoils	Minimal to Large
	Active Clearance Control	Not Enough Movement	External Air Source	Minimal
Combustor	ODS Liner Material	Material	MERL 72 or Hast-X Material	Minimal
HPT	Active Clearance Control	Not Enough Movement	External Air Source	Minimal
	Single Crystal Airfoil Material	Material	MAR-509 Vane Material & DS Mod MAR-M-200 Blade Material	Moderate
	Aerodynamics	Moderate Aerodynamics	Rematch Engine (RIT, HPT Pressure Ratio) or Restagger Vanes	Moderate
	Aerodynamics	Severe Aerodynamics	Redesign	Large
LPT	Active Clearance Control	Not Enough Movement	External Air Source	Minimal
	Aerodynamics	Aerodynamics	Restagger to Redesign	Moderate to Large
Mixer	Aerodynamics	Aerodynamics	Redesign	Minimal
Bearings	High Speed	Durability	Monitor and Replace when Necessary	Minimal

4.3 High Pressure Compressor Risk

Two potential problem areas have been identified in the HPC. The first is aerodynamic which ranges from requiring an airfoil recambering to complete redesign, with minimal to significant program impacts, respectively. The other is failure of the active clearance control system to produce the desired clearances. This problem can be corrected with a minimal program impact by using an external air source to simulate redesign of the active clearance control system.

4.4 Combustor Risk

The ODS combustor liner material may present fabrication difficulties in which case MERL 72, or Hastelloy-X material backup positions have been identified. These backup positions would not achieve the same liner durability as the ODS material, but would be able to simulate the ODS liner design with minimal impact on the experimental program. An ODS fabrication program would be required at some point to complete the technological feasibility of the combustor.

4.5 High Pressure Turbine Risk

Several program risks have been identified in the HPT in the areas of the active clearance control system, materials, and aerodynamics. A failure of the active clearance control system to produce the desired clearances can be corrected by using an external air source to increase the system capabilities and to simulate redesign of the system with a minimal program impact. Current state-of-the-art airfoil materials could be utilized in the event that single crystal material is not available within the Energy Efficient Engine timing. This substitution would reduce airfoil life and, perhaps, maximum (RIT) capability, but would allow the general demonstrator program objectives to be met. The use of a current state-of-the-art airfoil material would have a moderate program impact, due to fabrication delays which would result from potential changes to the airfoil casting tooling and film cooling modifications. HPT aerodynamic problems such as flow capacity or efficiency misses in either the HPT or HPC could occur. These, in turn, may cause undesirable engine match shifts or overall performance misses which could be corrected by rematching the engine by adjustments to the RIT schedule and restaggering of the HPT airfoils. A moderate program impact would be incurred because of the additional machining time required to restagger the airfoils. Severe aerodynamic problems, which would require a complete HPT redesign,would have a major program impact.

4.6 Low Pressure Turbine Risk

The program risks associated with the LPT are in the active clearance control system and aerodynamics areas. An external air source would be utilized to correct active clearance control system problems. This would simulate redesign of the system with a minimal impact on the program. Aerodynamic problems could have a moderate to large program impact depending on the severity of the problem and whether restaggering of the airfoils or a complete LPT redesign is required.

4.7 Mixer Risk

The mixer aerodynamics may require redesign, but that would not prevent running the demonstration with the initial design. Therefore, program impact would be minimal.

4.8 Bearings Risk

The risk of the high speed bearing's durability is considered minimal since the bearings can be monitored and replaced, if necessary, during the experimental program.

APPENDIX E

AERODYNAMIC DESIGN OF HIGH PRESSURE COMPRESSOR – TASK V

LIST OF ILLUSTRATIONS
APPENDIX E

APPENDIX E

LIST OF TABLES

APPENDIX E

AERODYNAMIC DESIGN OF HIGH PRESSURE COMPRESSOR – TASK V

1.0 INTRODUCTION

The Task III high pressure compressor (HPC) flowpath and blading shapes were refined during Task V, prior to finalization of the preliminary design. The refinements were based on aerodynamic design analyses that utilized Pratt & Whitney Aircraft's meanline and streamline programs. The analyses considered the effects of interstage airbleeds, boundary-layer-flow blockage, and aerodynamic loading limits on HPC geometry. First-pass stage-vibration analyses were also conducted to establish structural design feasibility. The specific analyses and the resulting changes in the flowpath and airfoil shapes are summarized in Table E-I.

The net effects of the changes on geometry were a 0.76 cm (0.3 in.) reduction in the inlet-hub radius and a 2.5 cm (1.0 in.) increase in length. An addition of one hundred twenty-six airfoils was also required. The adiabatic efficiency was estimated to have decreased 0.3% from the 88.6% goal level. The drop in efficiency was primarily caused by increased losses resulting from the reduced gap-to-chord ratio in the midstage stator rows, which had been found necessary during the streamline analyses. The efficiency goals, however, remain unchanged. Additional design work will be performed to identify loss elements and to permit the efficiency calculations to be refined.

The meanline analysis program was also employed to identify an alternate HPC design. The alternate design has the same inlet dimensions as the Task III design, but the flowpath from stages 2 to 5 has been increased in flow area which reduced local Mach numbers. The alternate HPC required forty fewer airfoils than the shorter, 0.25 cm (0.10 in.) configuration (the Task V preliminary design) and has the same efficiency potential. Both Task V designs will be considered in finalizing the preliminary design.

2.0 MEANLINE ANALYSIS

Flowpath inner and outer radii were established with the meanline compressor analysis program. This program calculated the meanline aerodynamic conditions at each interblade axial location through the HPC. The meanline analysis program calculated velocity triangles based on effective areas with the actual flow areas calculated by assuming blockage factors at each axial station to account for the effects of wall and airfoil boundary layers.

The general blockage distribution used for the Task III parametric study was modified to reflect characteristics more representative of the advanced HPC's that have recently been tested at Pratt & Whitney Aircraft. Equivalent blockage factors were assigned to simulate customer, turbine cooling, and active clearance control bleeds. These factors simulated a 4.5 percent stator 3 exit bleed for cabin use and active clearance control, a 0.84 percent ID bleed at rotor 6 exit, and a 0.44 percent stator 7 exit bleed. The resulting Task V blockage distribution is compared with the Task III level in Figure E-1.

TABLE E-I

IMPACT OF INITIAL AERODYNAMIC DESIGN ON HIGH PRESSURE COMPRESSOR DEFINITION

Aerodynamic Design Analysis	Compressor Design Modification	
	Flowpath	Airfoils
Meanline Analysis		
• Boundary Layer Flow Blockage	Reduced Inlet Hub Diameter	
• Interstage Bleeds	Gaspath Height Adjustment	
	Longer Compressor	
Streamline Analysis		
• Stage Reaction		Midstage Stator Recamber and Lower Gap-to-Chord Ratio
Structural Analysis		
• Airfoil Flutter	Longer Compressor	Increased Chords and Thickness In Some Rotors and Stators
• 1st-Stage Blade 2E Resonance	No Change	No Change
• Blade Tip Mode Resonance		Minor Stage 2 and 10 Blade Tip Thickness Change
• Blade C Ratios		Increased L.E. and T.E. Radii In Several Stages

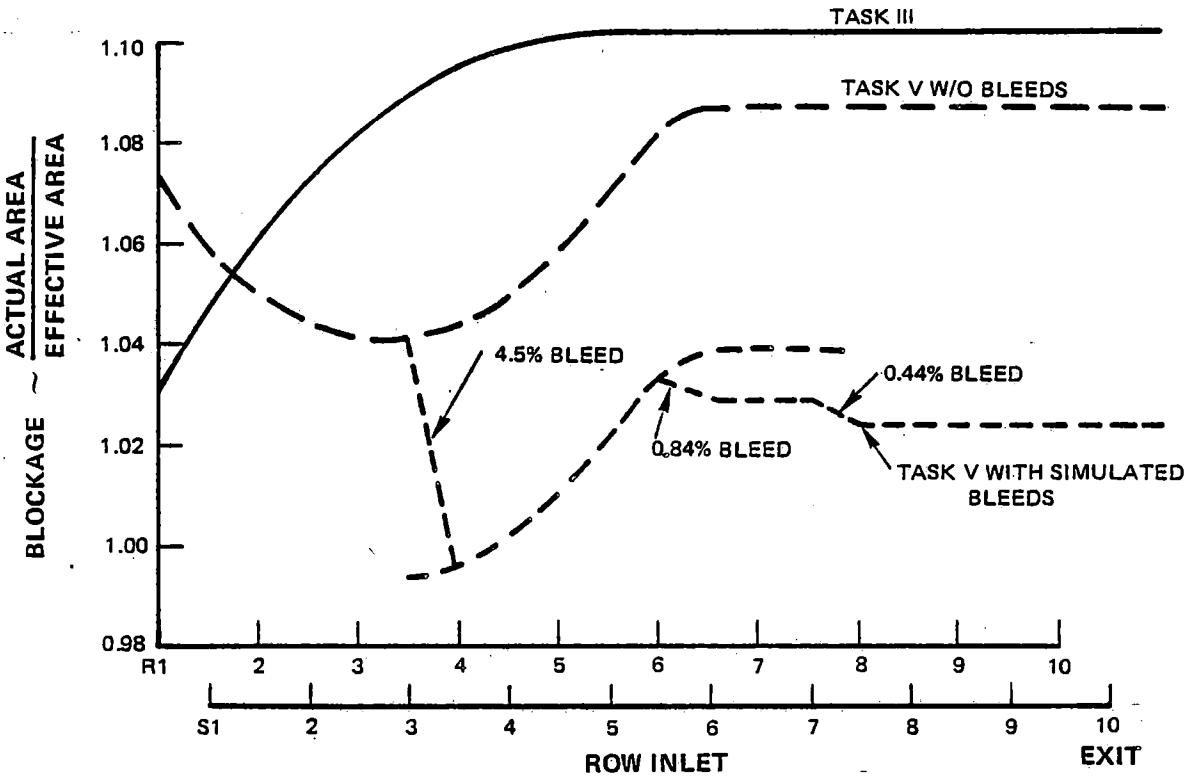

Figure E-1 Comparison of Task III and Task V Aerodynamic Flow Blockage Distribution. The Task V flow-blockage distribution is representative of advanced compressors recently tested at Pratt & Whitney Aircraft.

In general, the flow blockage was lower with the revised distribution, and less actual area was required to accommodate the flow. Front-end blockage increased, however, in accordance with the blockage effects observed in advanced-compressor intermediate cases at Pratt & Whitney Aircraft.

The flowpath inner and outer diameters were changed to provide the same approximate axial velocity distribution for Task III and Task V definitions. The inlet hub diameter was reduced to increase the area by 4.4%. The inlet tip diameter was held constant to maintain the same rotor inlet corrected tip speed. The remainder of the flowpath was also modified to account for the Task V blockage with bleeds. Resulting discontinuities in wall contours were faired to provide the final flowpath diameters. The flowpath length was increased 2.5 cm (1.0 in.) to provide sufficient axial gapping for bleed ports and to allow for the longer chord blading found necessary during structural analysis. Task III and Task V flowpaths are compared in Figure E-2.

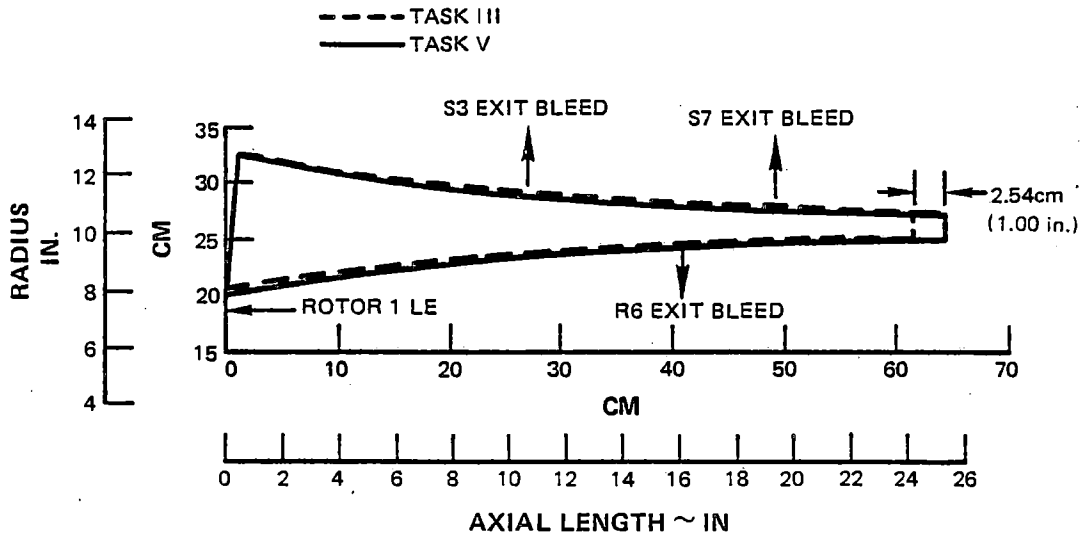

Figure E-2 *Comparison of Task III and Task V High Pressure Compressor Flowpath. The flowpath length was increased by 2.5 cm during Task V to provide axial gapping for bleed parts and to allow for longer chord blading.*

An alternate approach to the Task V baseline flowpath geometry was uncovered with additional meanline analysis. Inlet axial velocity was increased sufficiently to obtain the original Task III inlet dimensions and corrected specific airflow. Axial velocity was then redistributed as shown in Figure E-3. The higher inlet velocity was counterbalanced by velocity reduction in stages 2 through 5. A comparison of the two flowpath approaches is shown in Figure E-4.

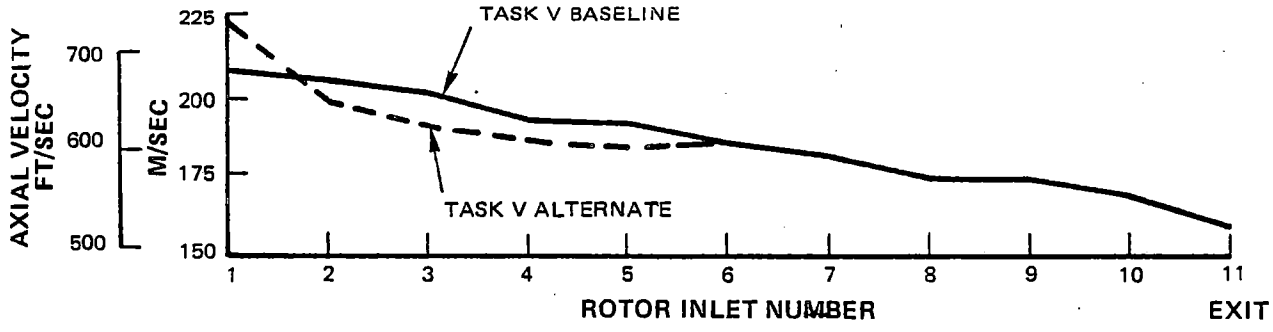

Figure E-3 *Task V Baseline and Alternate Core Compressor Axial Velocity Distribution. The Task V alternate core compressor has a larger inner-cavity volume which provides greater flexibility for arranging the front bearings.*

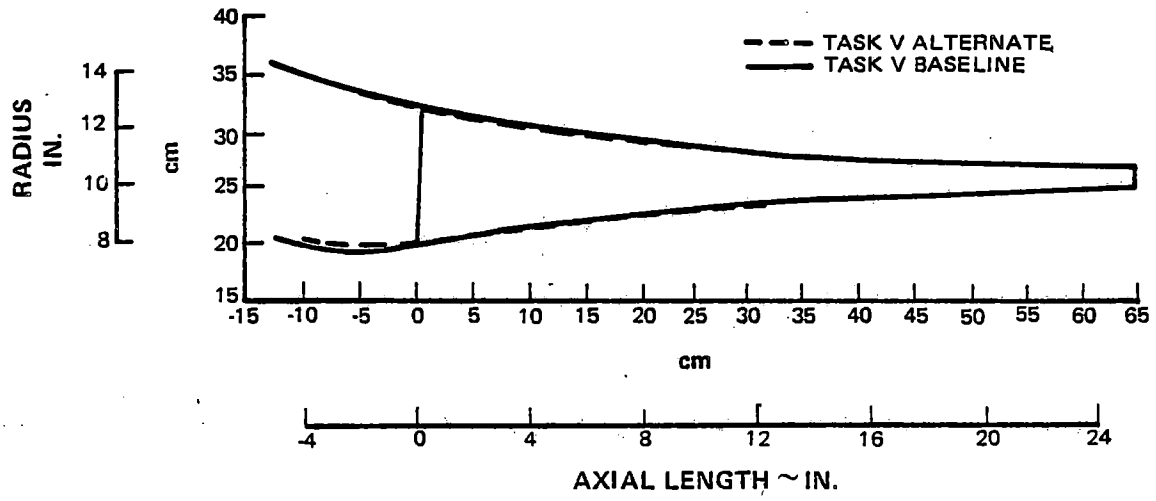

Figure E-4 Task V Baseline and Alternate Core-Compressor Flowpath. The Task V alternate core-compressor flowpath has the same inlet dimensions and corrected specific airflow as the Task III configuration.

The alternate approach requires a less tortuous intermediate section flowpath transition from the larger diameter low pressure compressor (LPC), and has a larger inner-cavity volume which provides greater flexibility for front-bearing arrangement. The adiabatic efficiency of both approaches was estimated to be 88.3%, assuming a 0.038 cm (0.015 in.) outer tip clearance in the first three stages and a 0.030 cm (0.012 in.) tip clearance in the remaining stages, consistent with preliminary estimates at the cruise design point and utilizing active clearance control. Streamline and structural analyses have yet to be conducted for the alternate design. Both analyses are necessary for choosing the final design approach.

3.0 STREAMLINE ANALYSIS

The selection of HPC blading consisted of establishing the flowfield by streamline analysis and then defining airfoil shapes using a design system based on cascade-tunnel data and rig and engine test experience obtained from other Pratt & Whitney Aircraft advanced designs. Multiple circular arc, circular arc, 65 series/circular arc with low loss leading edges, and 400 series airfoils were used for the various rows, depending on their specific flowfield requirements. In addition, supercritical airfoils will be considered for use in the second through sixth stages during the final design. The design system does not currently have supercritical airfoil capability. This capability will be available in time for the final design effort.

The high diffusion factors – 9% above current technology HPC's – and stage reaction levels assumed in Task III resulted in mid-compressor stator cambers that were excessive relative to available cascade design data and design experience with other advanced technology designs. To reduce stator cambers to acceptable levels, stator gap-to-chord ratios were reduced by 20% and stage reactions, by an average of 10%. The resultant circumferential airfoil gap-to-chord ratio and reaction level are compared

with Task III values in Figures E-5 and E-6. These changes by themselves increased the number of airfoils by 105 and reduced the estimated adiabatic efficiency by 0.2%. The average diffusion factor with these revisions is 5% higher than current state-of-the-art.

A takeoff surge margin of 16% was estimated based upon the diffusion factors and the endwall loading parameters. Experience with other HPC's and a preliminary stability audit indicate that this surge margin will be sufficient to ensure stable operation at take-off and all part power conditions.

4.0 STRUCTURAL ANALYSIS

The HPC airfoils were analyzed for flutter stability, 2E (two excitations per revolution) frequency margin, blade tip mode resonances, and airfoil C-ratios to determine the structural feasibility of the aerodynamic design. These studies indicated general structural design soundness. Only minor revisions to the airfoils were required to provide a design meeting all of the structural criteria.

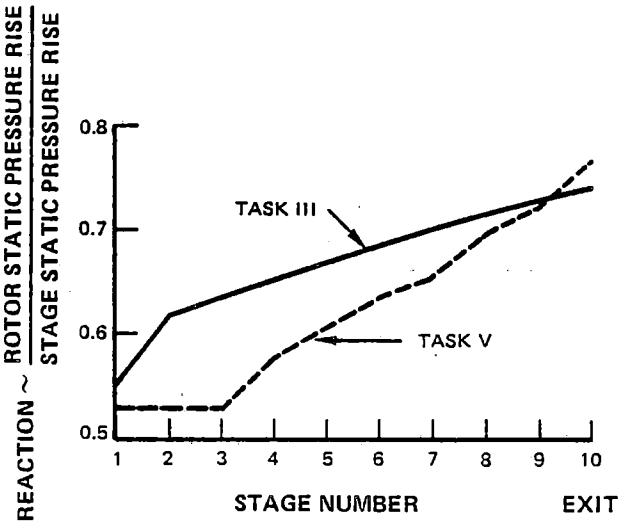

Figure E-6 Comparison of Task III and Task V Core-Compressor Reaction. The Task V reaction level is ten percent less than the Task III level.

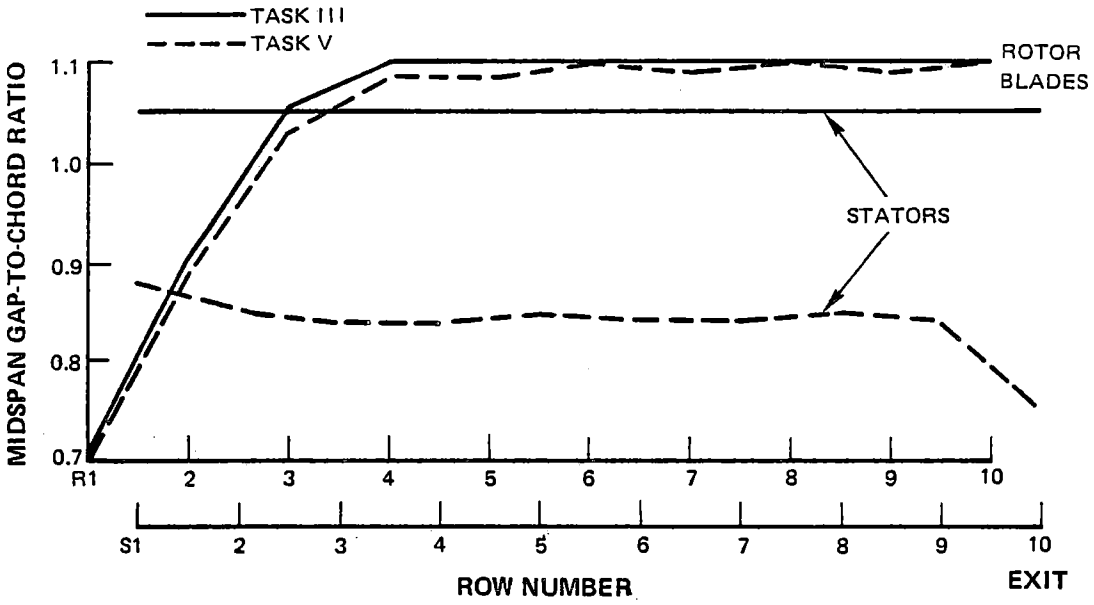

Figure E-5 Comparison of Task III and Task V High Pressure Compressor Gap-to-Chord Ratio. Stator gap-to-chord ratio of the Task V compressor is 20 percent less than for the Task III compressor.

Bending and torsional flutter stability calculations for all rotors and stators were compared with Pratt & Whitney Aircraft experience curves. The velocities and pressure ratios at the hot-day, sea-level takeoff operating condition were used for these calculations.

Rotors 5 through 10 were found to violate the experience criteria for bending flutter (see Figure E-7); rotors 5 and 6 also violated the torsional flutter criteria (see Figure E-8). A study of the thickness and chord changes required to meet the bending stability criteria was performed for the worst stage (rotor 6). The results of the rotor-6 study were used to estimate the changes necessary for rotors 7 and 8. The estimated change for rotor 5 was based on the required decrease in the torsional flutter parameter. These recommended changes are listed in Table E-II. The changes in the flutter parameters calculated for rotor 6 are shown in Figures E-7 and E-8. No specific recommendations were made for rotors 9 and 10 because the small decreases required for the bending flutter parameters should be easily obtained with only minor changes to thickness or chord.

All stator rows were found to have acceptable bending flutter stability margins. Stator rows 1 through 3 and 6 through 8 exceeded the experience limits for torsional flutter (see Figures E-9 and E-10.) Stator rows 6, 7, and 8 required only small thickness-or-chord changes to meet the criteria. These changes were not identified because the magnitude of the criteria violation was sufficiently small to be of no concern at this stage of blading definition. The variable stator rows (1, 2, and 3) required significant chord increases to meet torsional flutter stability criteria. An analysis determined the required changes for the first-stage stators. These results were used to estimate the changes required for the second and third stages. Chord changes needed for torsional flutter stability are listed in Table E-III. The change in stator 1 torsional flutter parameter in Task V is shown in Figure E-9.

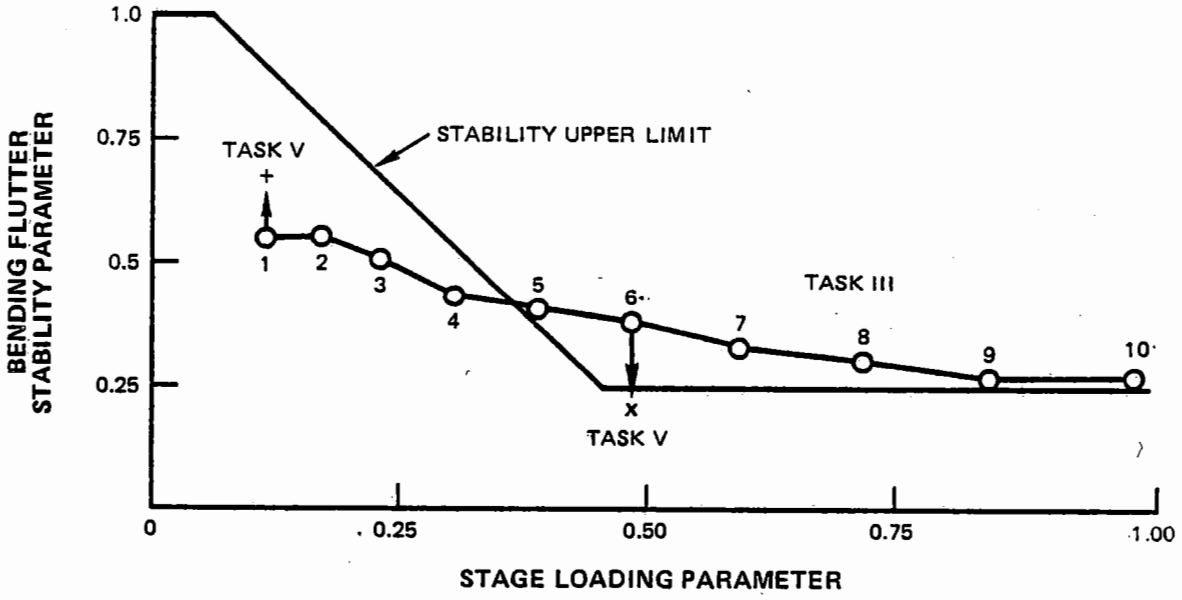

Figure E-7 *High Pressure Compressor Bending Flutter Criteria. The thickness and chord changes required for rotor-6 (the worst case) to meet bending stability criteria have been calculated.*

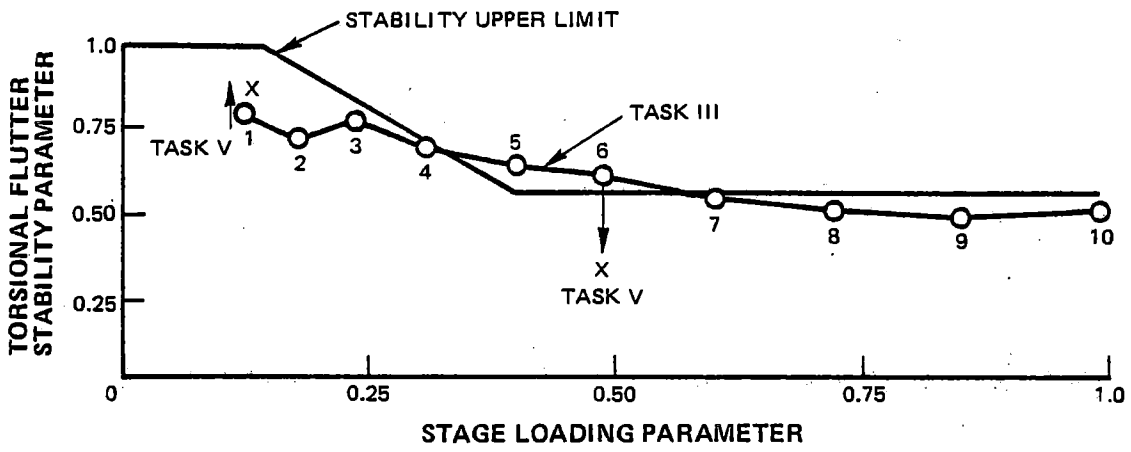

Figure E-8 *High Pressure Compressor Torsional Flutter Criteria. The estimated changes for rotor 5 are based on torsional flutter requirements; the changes required for rotor 6 are based on bending flutter criteria.*

TABLE E-II

BLADE GEOMETRY CHANGES REQUIRED TO MEET FLUTTER CRITERIA

Blade Row	Chord, cm (in.)	
	Original	Revised
5	2.50 (0.984)	2.60 (1.025)
6	2.31 (0.910)	2.95 (1.161)
7	2.19 (0.864)	2.46 (0.970)
8	2.11 (0.832)	2.24 (0.882)

The root thickness-to-chord ratio for the blade rows 5 to 8 were all originally 0.085 and were revised to 0.100.

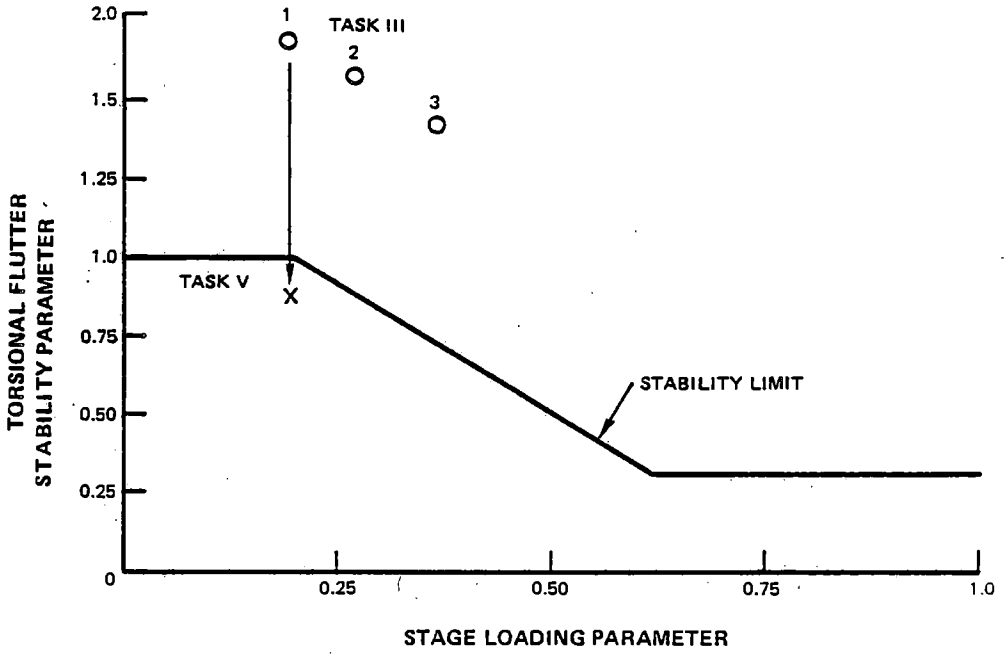

Figure E-9 *Variable Stator Torsional Flutter Criteria. Stators 1 through 3 exceed experience limits for torsional flutter and require significant chord increases to meet criteria.*

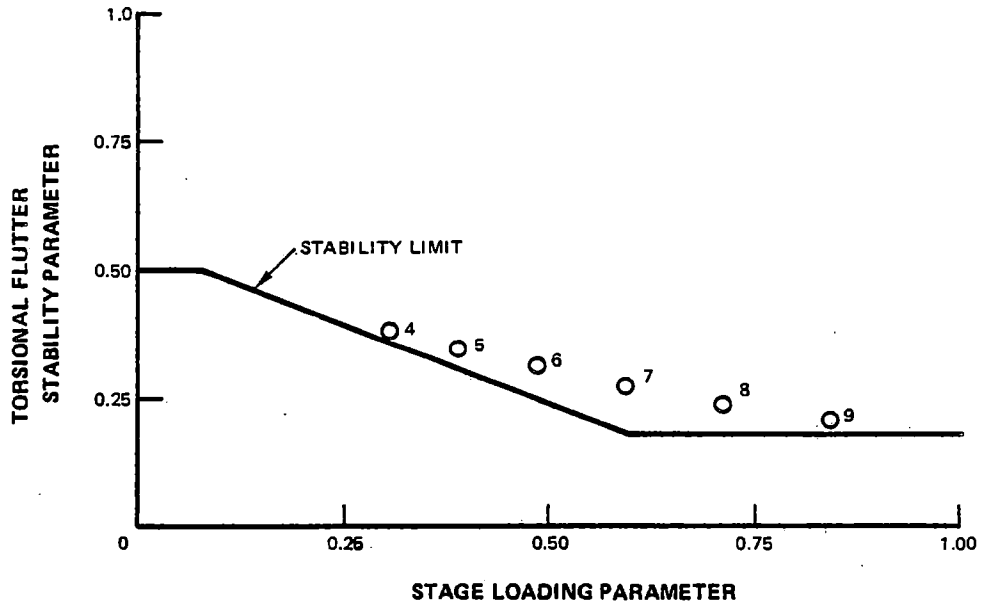

Figure E-10 *Shrouder Stator Torsion Flutter Criteria. Stators rows 6, 7, and 8 require only small thickness-to-chord ratio changes to meet criteria.*

TABLE E-III

STATOR GEOMETRY CHANGES TO MEET FLUTTER CRITERIA

Stator Row	Root Chord, cm (in.) Original	Root Chord, cm (in.) Revised	Tip Chord, cm (in.) Original	Tip Chord, cm (in.) Revised
1	4.382 (1.725)	4.613 (1.816)	4.382 (1.725)	5.766 (2.270)
2	3.416 (1.345)	3.597 (1.416)	3.416 (1.345)	4.496 (1.770)
3	2.934 (1.155)	3.089 (1.216)	2.934 (1.153)	3.861 (1.520)

The first stage blade-alone first mode resonant frequency was calculated to assure that the 2E resonance could be designed out of the operating speed range. At redline speed, 10.8% margin existed between the blade resonance frequency and engine 2E excitation. This margin provided the required disk-blade coupled frequency margin. Blade resonance calculations were also made for the chordwise bending tip modes. The design criteria for these blade sections required that the vane passing order tip mode resonances be kept out of the engine operating range. An examination of the Task V rotors indicated that all rotors except 2 and 10 met this criteria. Minor changes in tip thickness of these blades produced the required frequency margin.

Bending stress distribution and airfoil resistance to foreign object damage is controlled by a C-ratio criteria (C-ratio is defined in Figure E-11). Minimum axis bending stresses are compared between the maximum airfoil thickness location and the airfoil leading and trailing edge where airfoils are susceptible to foreign object damage. A design correlation relates the required C-ratios to the leading and trailing edge radii. The C-ratio was calculated for all blades and several were found to have exceeded the design criteria. But only small changes in edge radii were required to ameliorate this condition.

The incorporation of all the structural modifications resulted in an estimated 36 fewer airfoils and a 0.1% lower adiabatic efficiency.

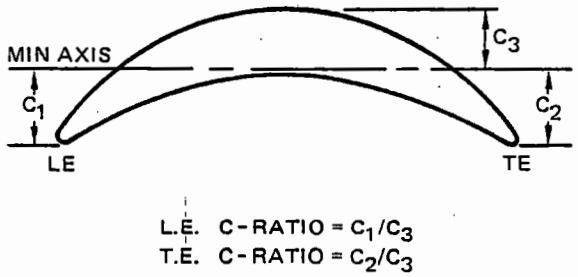

Figure E-11 Definition of C-Ratio Criteria. Bending stress distribution and airfoil resistance to foreign object damage are controlled by the C-ratio criteria.

5.0 COMPRESSOR INITIAL AERODYNAMIC DESIGN GEOMETRY

Blading geometric details of the initial Task V aerodynamic design are listed in Table E-IV. Both this geometry and the alternate mean-

line flowpath definition will be refined further during subsequent work to complete the preliminary design definition. The results of such structural changes as local thickening and aspect ratio changes have not been included in the table. These changes require additional streamline design and a cascade selection effort which will be accomplished after additional aerodynamic optimization has been performed during the on going preliminary design study.

TABLE E-IV

COMPRESSOR INITIAL AERODYNAMIC DESIGN AIRFOIL GEOMETRY
(Only the results of the meanline and streamline analyses are shown)

Row	Airfoils	Series	Chord b. cm R	Chord b. cm T	Chord b. in. R	Chord b. in. T	Av. Span cm	Av. Span in.	AR Ave. Span / Ave. b	Camber ~ degrees θ* R	Camber ~ degrees θ* M	Camber ~ degrees θ* T	t/b R	t/b T	r/b R	r/b T
R1	44	MCA	4.82	5.80	1.90	2.285	11.98	4.7175	2.254	66.1	28.3	8.3	0.090	0.024	0.593	0.788
S1	42	MCA	4.38		1.725		9.79	3.8525	2.233	45.3	39.9	51.7	0.050	0.090	0.719	1.053
R2	48	CA	2.81		1.50		8.36	3.290	2.193	58.6	27.2	19.2	0.085	0.045	0.746	1.033
S2	56	CA	3.42		1.345		7.28	2.865	2.130	50.1	38.4	48.6	0.050	0.090	0.730	0.970
R3	50	CA	3.15		1.240		6.45	2.540	2.048	50.5	31.0	28.2	0.085	0.045	0.904	1.161
S3	66	65/CAE[a]	2.93		1.155		5.75	2.265	1.961	41.0	36.6	52.9	0.050	0.090	0.745	0.932
R4	54	65/CAE[a]	2.77		1.090		5.05	1.990	1.826	53.1	33.4	33.6	0.085	0.045	0.978	1.191
S4	74	65/CAE[a]	2.62		1.032		4.63	1.8225	1.766	48.4	41.0	52.4	0.050	0.090	0.762	0.912
R5	60	65/CAE[a]	2.50		0.984		4.29	1.6875	1.715	52.9	32.7	33.8	0.085	0.045	0.993	1.172
S5	80	65/CAE[a]	2.40		0.944		4.01	1.5775	1.671	51.4	42.3	54.8	0.050	0.090	0.780	0.912
R6	64	65/CAE[a]	2.31		0.910		3.27	1.4825	1.629	50.2	30.8	22.0	0.085	0.045	1.017	1.177
S6	86	400	2.25		0.885		3.43	1.350	1.525	52.2	46.1	58.4	0.050	0.090	0.784	0.896
R7	68	400	2.19		0.864		3.23	1.270	1.470	51.9	33.4	33.5	0.085	0.045	1.020	1.156
S7	90	400	2.15		0.847		3.03	1.1925	1.408	53.4	47.6	61.2	0.050	0.090	0.789	0.887
R8	70	400	2.11		0.832		2.81	1.1075	1.331	47.4	30.5	32.4	0.085	0.045	1.037	1.156
S8	92	400	2.08		0.820		2.62	1.030	1.256	58.1	51.9	64.7	0.050	0.090	0.804	0.889
R9	72	400	2.07		0.814		2.47	0.9725	1.195	45.2	28.3	30.8	0.085	0.045	1.037	1.142
S9	94	400	2.06		0.810		2.34	0.920	1.136	65.3	59.0	73.2	0.050	0.090	0.808	0.876
R10	72	400	2.05		0.808		2.23	0.8775	1.086	32.2	21.5	28.0	0.085	0.045	1.050	1.145
S10	78	400	2.79		1.100		2.15	0.845	0.768	58.2	60.7	75.7	0.050	0.090	0.713	0.775

Note a) Circular Arc Elliptical Leading Edge

APPENDIX F

LIST OF ABBREVIATIONS

APPENDIX F

LIST OF ABBREVIATIONS

A - area
ACC - active clearance control
ADP - aerodynamic design point
amb. - ambient
AN^2 - product of turbine annulus area rotor speed squared
AR - aspect ratio
ATA - Airline Transport Association
atm. - atmosphere
avg., av. - average
b - airfoil chord
B - blade
BL, Bld - bleed extraction
BMOD - bill of material object damage
BPR - bypass ratio
BTU - British Thermal Units
C - wing chord
C - centrigrade
CD - flow coefficient
CET - combustor exit temperature
CF - friction coefficient
CFFC - counter flow film cooled
CL - lift coefficient
CM - centimeter
CMD - constant mean diameter
CNS - common nacelle system
CO - carbon monoxide
CR - cruise
CV - thrust coefficient
CX/U - absolute axial velocity divided by circumferential wheel speed
D - diameter
deg. - degrees
DF - diffusion factor
DOC - direct operating cost
Dom. - domestic
E - excitation
EFH - engine flight hour
EGV - exit guide vane
EI - emission index
EPA - Environmental Protection Agency
EPAP - EPA parameter
EPNL - effective perceived noise level
F - Fahrenheit
FAR - Federal Aviation Regulation
FAR Part 36 (1969)- Part 36 of 1969 published FAR
FG - gross thrust
FN - net thrust
FN/WAT - specific thrust (net thrust divided by total airflow)
FOD - foreign object damage
FPR - fan pressure ratio
FPS - feet per second
ft. - feet
gal. - gallon
h - enthalpy
hp - horsepower
HPC - high pressure compressor
HPT - high pressure turbine
HPX - horsepower extraction
hr. - hour
HZ - Hertz
ID - inner diameter
IGV - inlet guide vane
in. - inch
inter., intl.- international
IOC - indirect oeprating cost
Kg - Kilogram
Km - Kilometer
ksi - thousand pounds per square inch
kts - knots
kw - kilowatts
l - liter
lb - pound
LCF - low cycle fatigue
L/D - length divided by diameter ratio
LE - leading edge
L/H - length divided by height ratio
LPC - low pressure compressor
LPT - low pressure turbine
LTO - landing takeoff cycle
m - meter
max. - maximum
MCL - maximum climb
MCR - maximum cruise

MERL - Materials Engineering, Research Laboratory
min. - minimum, minute
mix. - mixed
mm - milimeter
M, Mn - Mach number
N - Newton, rotor or spool speed, number
Nm - nautical miles
No. - number
NO_x - nitrogen oxides
OD - outer diameter
ODS - oxide dispersion strengthened
OEW - operating empty weight
O/H - overhang
OPR - overall pressure ratio
p - pressure
pass. - passenger capacity
POA - probability of achievement
PR - pressure ratio
psi - pounds per squre inch
Q - dynamic pressure
R - rotor, root
RIT - rotor inlet temperature
ROI - return on investment
RPM - revolutions per minute
S - stator
SAE - Society of Automotive Engineers
S/C - single crystal
sec. - second
SOAPP - State-of-the-Art Performance Program
SPL - sound pressure level
Std. - standard
stg. - stage
t - thickness
T - temperature, tip
TE - trailing edge
THC - total hydrocarbons
T/O - takeoff
TOBI - tangential on board injection
TOGW - takeoff gross weight
TSFC - thrust specific fuel consumption
T/W - thrust loading (total thrust divided by total weight)
u - circumferential wheel speed
UHC - unburned hydrocarbons
V - vane
VJ - exhaust jet velocity
VM - mean velocity ratio
Vorbix - vortex burning and mixing
W/A - specific flow (airflow divided by annulus area)
WAE - engine (core) stream airflow
WAT - total propulsion system (fan) airflow
W/O - without
W/S - wing loading (total airplane weight divided by wing area)
α - vane air angle
β - blade air angle
Δ - change in
η - efficiency
θ - mean turning angle, camber
τ - circumferential gap between adjacent airfoils

APPENDIX G

APPENDIX G

DISTRIBUTION LIST

(One copy per addressee unless otherwise noted in parenthesis)

I. GOVERNMENT AGENCIES

1. NASA Headquarters
   600 Independence Ave., SW
   Washington, D. C. 20546
   Atten: RL/H. Johnson
   RI/F. Povinelli
   RJ/L. Harris
   Library

2. NASA-Lewis Research Center
   21000 Brookpark Road
   Cleveland, OH 44135
   Atten: D. L. Nored MS 301-2
   N. T. Saunders MS 301-4 (20)
   R. S. Colladay MS 301-4
   L. E. Macioce MS 301-4
   J. A. Ziemianski MS 301-4
   J. F. Dugan, Jr. MS 301-2
   E. W. Conrad MS 301-2
   N. T. Musial MS 500-311
   Library MS 60-3 (2)
   Report Control Office MS 5-5
   Technology Utilization Office
   MS 3-19
   W. L. Stewart MS 3-5
   M. A. Beheim MS 86-1
   R. W. Schroeder MS 500-207
   A. Ginsberg MS 5-3
   R. A. Rudey MS 60-4
   R. W. Hall MS 49-1
   D. J. Poferl MS 500-202
   R. J. Weber MS 500-307
   W. C. Strack MS 500-307
   R. J. Rulis MS 3-5
   T. P. Moffitt MS 77-2
   A. J. Glassman MS 77-2
   R. E. Jones MS 60-6
   L. P. Ludwig MS 23-2
   D. C. Mikkelson MS 86-1
   K. E. Skeels MS 500-313
   J. F. Groenewag MS 500-206
   W. M. Braithwaite MS 60-6
   R. L. Davies MS 105-1
   R. H. Johns MS 49-3
   L. J. Kaszubinski MS 21-4
   J. R. Mihaloew MS 100-1
   C. L. Ball MS 5-9
   R. W. Niedzweicki MS 60-6
   AFSC Liaison Office MS 501-3
   Army R&T Propulsion Lab MS 77-5

3. NASA Ames Research Center
   Moffett Field, CA 94035
   Atten: 202-7/M.H. Waters
   202-7/L. J. Williams
   Library

4. NASA Langley Research Center
   Langley Field, VA 23365
   Atten: R. Leonard
   D. Maiden
   Library

5. NASA Dryden Flight Research Center
   P.O. Box 273
   Edwards, CA 93523
   Atten: J. A. Albers
   Library

6. NASA Scientific and Technical Information
   Facility
   P.O. Box 33
   College Park, MD 20740
   Atten: Acquisition Branch (10)

7. Department of Defense
   Washington, D.C. 20301
   Atten: R. Standahar 3D1089 Pentagon

8. Wright-Patterson Air Force Base
   Dayton, OH 45433
   Atten: H.J.P. VonOhain AFAPL/CCN
   E. C. Simpson AFAPL/TB
   H. I. Bush AFAPL/TB
   E.E. Bailey (NASA Liaison)
   AFAPL/DO
   R. P. Carmichael ASD/XRHI
   R. Ellis ASD/YZN
   Col C. E. Painter ASD/EN

DISTRIBUTION LIST (Cont'd)

9. Eustis Directorate
U. S. Army Air Mobility
R&D Laboratory
Fort Eustis, VA 23604
Atten: J. Lane, SAVDL-EU-Tapp

10. Department of Transportation
NASA/DOT Joint Office of Noise
Abatement
Washington, D.C. 20590
Atten: C. Foster

11. Navy Department
Naval Air Systems Command
Washington, D.C. 20361
Atten: W. Koven AIR-O3E
J. L. Byers AIR-53602
E. A. Lichtman AIR-330E

12. Naval Air Propulsion Test Center
Trenton, NJ 08628
Atten: J. J. Curry
A. A. Martino

13. U. S. Naval Air Test Center
Code SY-53
Patuxent River, MD 20670
Atten: E. A. Lynch

14. Federal Aviation Administration
Noise Abatement Division
Washington, D.C. 20590
Atten: J. Woodhall

15. Environmental Protection Agency
1835 K Street, NW
Washington, D.C. 20460
Atten: J. Schettino

16. Environmental Protection Agency
2565 Plymouth Road
Ann Arbor, MI 48105
Atten: R. Munt

II. ENGINE MANUFACTURERS

1. Curtiss Wright Corporation
Woodridge, NJ 07075
Atten: S. Lombardo
S. Moskowitz

2. Detroit Diesel Allison Div. G.M.C.
P.O. Box 894
Indianapolis, IN 46206
Atten: W. L. McIntire
F. Walters

3. The Garrett Corporation
AiResearch Manufacturing Co.
Torrence, CA 90509
Atten: F. E. Faulkner

4. The Garrett Corporation
AiResearch Manufacturing Co.
402 S. 36 Street
Phoenix, AZ 85034
Atten: F. B. Wallace

5. General Electric Co./AEG
Neumann Way
Evandale, OH 45215
Atten: M. Hemsworth (3)
M. A. Zipkin

6. Cummins Engine Co.
Technical Center
500 S. Poplar
Columbus, IN 47201
Atten: J. R. Drake

7. AVCO/Lycoming
550 S. Main Street
Stratford, CN 06497
Atten: S. Deckeut

8. Williams Research Co.
P.O. Box 95
Walled Lake, MI 46088
Atten: K. J. Bremner

DISTRIBUTION LIST (Cont'd)

9. Teledyne CAE, Turbine Engines
   1330 Laskey Road
   Toledo, OH 43612
   Atten: W. Q. Wagner

10. General Electric Co./AEG
    1000 Western Ave.
    Lynn, MA 01910
    Atten: R. E. Neitzel

11. Pratt & Whitney Aircraft
    Florida R & D Center
    P.O. Box 2691
    West Palm Beach, FL 33402
    Atten: C. J. Peterson

12. Pratt & Whitney Aircraft
    Commercial Products Division
    East Hartford, CT 06108
    Atten: W. Gardner EB1M3 (3)
    W. H. Sens

III. AIRFRAME MANUFACTURERS

1. Boeing Commercial Airplane Co.
   P.O. Box 3707
   Seattle, WA 98124
   Atten: P. Johnson MS 40-53
   D. C. Nordstrom

2. The Boeing Co., Wichita Division
   Wichita, KS 67210
   Atten: D. Tarkelson

3. Douglas Aircraft Co.
   McDonnell Douglas Corp.
   3855 Lakewood Boulevard
   Long Beach, CA 90846
   Atten: R. T. Kawai Code 36-41
   M. Klotzsche

4. Lockheed California Co.
   Burbank, CA 91502
   Atten: J. F. Stroud, Dept. 75-42
   R. Tullis, Dept. 75-21
   J. I. Benson

5. General Dynamics Convair
   P.O. Box 80847
   San Diego, CA 92138
   Atten: S. Campbell, MS 632-00

6. Rockwell International
   International Airport
   Los Angeles Division
   Los Angeles, CA 90009
   Atten: A. W. Martin

7. Boeing Aerospace Co.
   P.O. Box 3999
   Seattle, WA 98124
   Atten: D. S. Miller MS 40-26
   H. Higgins

8. Gates Learjet Corp.
   P.O. Box 7707
   Wichita, KS 67277
   Atten: E. Schiller

9. McDonnell Aircraft Co.
   McDonnell Douglas Corp.
   P.O. Box 516
   St. Louis MO 63166
   Atten: F. C. Claser Dept. 243

10. Lockheed Georgia Co.
    Marietta, GA 30060
    Atten: H. S. Sweet

11. Grumman Aerospace Corp.
    South Oyster Bay Road
    Bethpage, NY 11714
    Atten: C. Hoeltzer

IV. AIRLINES

1. American Airlines
   Maint. & Engr. Center
   Tulsa, OK 74151
   Atten: W. R. Neeley

2. Eastern Airlines
   International Airport
   Miami, FL 33148
   Atten: A. E. Fishbein

DISTRIBUTION LIST (Cont'd)

3. Pan American World Airways, Inc.
   JFK International Airport
   Jamica, NY 11430
   Atten: J. G. Borger
   A. MacLarty

4. Delta Airlines, Inc.
   Hartsfield-Atlanta
   International Airport
   Atlanta, GA 30320
   Atten: C. C. Davis

5. Trans World Airlines
   605 Third Avenue
   New York, NY 10016
   Atten: A. E. Carrol

6. United Airlines
   San Francisco International Airport
   Maint. Operations Cntr.
   San Francisco, CA 94128
   Atten: J. J. Overton

V. OTHERS

1. Hamilton Standard
   Bradley Field
   Windsor Locks, CT 06096
   Atten: A. T. Reiff

2. FluiDyne Engineering Corp.
   5900 Olson Memorial Highway
   Minneapolis, MN 55422
   Atten: J. S. Holdhusen

3. Rohr Corporation
   P.O. Box 878
   Foot & H Street
   Chula Vista, CA 92012
   Atten: Library

4. Solar Division
   International Harvester
   2200 Pacific Highway
   San Diego, CA 92112
   Atten: Library

5. Westinghouse Electric Corporation
   R & D Center
   Beulah Road
   Pittsburgh, PA 15236
   Atten: Library

6. Martin Marietta Corp.
   P.O. Box 5837
   Orlando, FL 32805
   Atten: A. E. Walker

7. University of Tennessee Space Institute
   Tullahoma, TN 37388
   Atten: Dr. V. Smith

8. TRW Equipment Group
   TRW Inc.
   23555 Euclid Ave.
   Cleveland, OH 44117
   Atten: Library

9. Aerospace Corporation
   P.O. Box 95085
   Los Angeles, CA 90045
   Atten: Library

P163
20 mil clearance